frontiers | Research Topics

# Rearing, health, and disease management of special economic animals: paving the way for a sustainable special economy through animal agriculture

**Edited by**
Izhar Hyder Qazi and Ling Tian

**Published in**
Frontiers in Veterinary Science
Frontiers in Genetics
Frontiers in Plant Science

ISSN 1664-8714
ISBN 978-2-8325-6698-5
DOI 10.3389/978-2-8325-6698-5

**Generative AI statement**
Any alternative text (Alt text) provided alongside figures in the articles in this ebook has been generated by Frontiers with the support of artificial intelligence and reasonable efforts have been made to ensure accuracy, including review by the authors wherever possible. If you identify any issues, please contact us.

## About Frontiers

Frontiers is more than just an open access publisher of scholarly articles: it is a pioneering approach to the world of academia, radically improving the way scholarly research is managed. The grand vision of Frontiers is a world where all people have an equal opportunity to seek, share and generate knowledge. Frontiers provides immediate and permanent online open access to all its publications, but this alone is not enough to realize our grand goals.

## Frontiers journal series

The Frontiers journal series is a multi-tier and interdisciplinary set of open-access, online journals, promising a paradigm shift from the current review, selection and dissemination processes in academic publishing. All Frontiers journals are driven by researchers for researchers; therefore, they constitute a service to the scholarly community. At the same time, the *Frontiers journal series* operates on a revolutionary invention, the tiered publishing system, initially addressing specific communities of scholars, and gradually climbing up to broader public understanding, thus serving the interests of the lay society, too.

## Dedication to quality

Each Frontiers article is a landmark of the highest quality, thanks to genuinely collaborative interactions between authors and review editors, who include some of the world's best academicians. Research must be certified by peers before entering a stream of knowledge that may eventually reach the public - and shape society; therefore, Frontiers only applies the most rigorous and unbiased reviews. Frontiers revolutionizes research publishing by freely delivering the most outstanding research, evaluated with no bias from both the academic and social point of view. By applying the most advanced information technologies, Frontiers is catapulting scholarly publishing into a new generation.

## What are Frontiers Research Topics?

Frontiers Research Topics are very popular trademarks of the *Frontiers journals series*: they are collections of at least ten articles, all centered on a particular subject. With their unique mix of varied contributions from Original Research to Review Articles, Frontiers Research Topics unify the most influential researchers, the latest key findings and historical advances in a hot research area.

Find out more on how to host your own Frontiers Research Topic or contribute to one as an author by contacting the Frontiers editorial office: frontiersin.org/about/contact

# Rearing, health, and disease management of special economic animals: paving the way for a sustainable special economy through animal agriculture

**Topic editors**

Izhar Hyder Qazi — South China Agricultural University, China

Ling Tian — South China Agricultural University, China

**Citation**

Qazi, I. H., Tian, L., eds. (2025). *Rearing, health, and disease management of special economic animals: paving the way for a sustainable special economy through animal agriculture*. Lausanne: Frontiers Media SA. doi: 10.3389/978-2-8325-6698-5

# Table of contents

05 Editorial: Rearing, health, and disease management of special economic animals: paving the way for a sustainable special economy through animal agriculture
Izhar Hyder Qazi, Christiana Angel, Graeme B. Martin and Jiping Liu

08 Genome-wide association analysis of fleece traits in Northwest Xizang white cashmere goat
Xiaotian Lu, Langda Suo, Xiaochun Yan, Wenze Li, Yixin Su, Bohan Zhou, Can Liu, Lepu Yang, Jiayin Wang, De Ji, Renqing Cuomu, Awang Cuoji, Ba Gui, Zhiying Wang, Wei Jiang, Yujiang Wu and Rui Su

22 Effect of acute exposure of Hg on physiological parameters and transcriptome expression in silkworms (*Bombyx mori*)
Huanhuan Wen, Yanan Wang, Yongqiang Ji, Jing Chen, Yao Xiao, Qixiang Lu, Caiying Jiang, Qing Sheng, Zuoming Nie and Zhengying You

35 The first report of single nucleotide polymorphisms in the open reading frame of the prion-like protein gene in rabbits
Min-Ju Jeong, Yong-Chan Kim and Byung-Hoon Jeong

43 Lipidomic and transcriptomic profiles provide new insights into the triacylglycerol and glucose handling capacities of the Arctic fox
Yuhang Zhu, Yuan Yuan, Huazhe Si, Songze Li, Fei Zhao, Ruina Mu, Zihan Lin, Xiaoxu Wang, Qiang Qiu, Chao Xu, Lele Ji and Zhipeng Li

53 Molecular characterization and phylogenetic analyses of MetAP2 gene and protein of *Nosema bombycis* isolated from Guangdong, China
Izhar Hyder Qazi, Ting Yuan, Sijia Yang, Christiana Angel and Jiping Liu

69 Effects of dietary supplementation of *Enterococcus faecium* postbiotics on growth performance and intestinal health of growing male mink
Lin Cao, Fengxue Sun, Qifeng Ren, Ziyi Jiang, Jian Chen, Yalin Li and Lihua Wang

81 Identifying selection signatures for immune response and resilience to Aleutian disease in mink using genotype data
Guoyu Hu, Duy Ngoc Do, Ghader Manafiazar, Alyson A. Kelvin, Mehdi Sargolzaei, Graham Plastow, Zhiquan Wang, Pourya Davoudi and Younes Miar

101 Chicory supplementation improves growth performance in juvenile ostriches potentially by attenuating enteritis
Meng Li, Mahmoud M. Abouelfetouh, Eman Salah, Faisal Ayub Kiani, Sha Nan, Mingxing Ding and Yi Ding

114 Screening and expression validation of key proteins for secondary hair follicle growth in cashmere goats based on iTRAQ quantitative proteomics technology
Jiale Chang, Fanhua Meng, Ru Zhang, Juan Feng, Yujing Liu, Junjie Zhang, Zhaomin Liu, Jiayue Liang and Hongmei Xiao

130 Revisiting the role of pathogen diversity and microbial interactions in honeybee susceptibility and treatment of *Melissococcus plutonius* infection
Elizabeth Mallory, Gwendolyn Freeze, Brendan A. Daisley and Emma Allen-Vercoe

140 Effects of perinatal nutrition supplementation and early weaning on serum biochemistry, metabolomics, and reproduction in yaks
Kaiyuan Shang, Jiuqiang Guan, Tianwu An, Hongwen Zhao, Qin Bai, Huade Li, Quan Sha, Mingfeng Jiang, Xiangfei Zhang and Xiaolin Luo

157 Dietary supplementation with *Epimedium* contributes to the improvement of hormone levels, gut microbiota, and serum metabolite composition in the Chinese forest musk deer (*Moschus berezovskii*)
Shan Xie, Qinlin Yang, Zaixiang Ying, Mingcheng Cai, Wenqiao Fan, Hanyu Gao, Xiaolan Feng and Yongjiang Wu

172 Analysis of causal pathogens of mulberry bacterial blight in samples collected from eight provinces of China using culturomics and metagenomic sequencing methods
Xinpeng Huang, Ting Yuan, Yuxin Huang, Izhar Hyder Qazi and Jiping Liu

195 Effects of hemp-based polyunsaturated fatty acid supplementation on membrane lipid profiles and reproductive performance in Martina Franca jacks
Isa Fusaro, Salvatore Parrillo, Giovanni Buonaiuto, Paraskevi Prasinou, Alessandro Gramenzi, Roberta Bucci, Damiano Cavallini, Alessia Carosi, Augusto Carluccio and Ippolito De Amicis

frontiers | Frontiers in Veterinary Science

TYPE Editorial
PUBLISHED 28 July 2025
DOI 10.3389/fvets.2025.1651737



OPEN ACCESS

EDITED AND REVIEWED BY
Michael Ward,
The University of Sydney, Australia

*CORRESPONDENCE
Izhar Hyder Qazi
✉ vetdr_izhar@yahoo.com
Jiping Liu
✉ liujiping@scau.edu.cn

†These authors share first authorship

RECEIVED 22 June 2025
ACCEPTED 27 June 2025
PUBLISHED 28 July 2025

CITATION
Qazi IH, Angel C, Martin GB and Liu J (2025) Editorial: Rearing, health, and disease management of special economic animals: paving the way for a sustainable special economy through animal agriculture. *Front. Vet. Sci.* 12:1651737. doi: 10.3389/fvets.2025.1651737



# Editorial: Rearing, health, and disease management of special economic animals: paving the way for a sustainable special economy through animal agriculture

Izhar Hyder Qazi[1,2*†], Christiana Angel[3,4†], Graeme B. Martin[5] and Jiping Liu[1*]

[1]Guangdong Provincial Key Lab of Agro-Animal Genomics and Molecular Breeding, College of Animal Science, South China Agricultural University, Guangzhou, Guangdong, China, [2]Shaheed Benazir Bhutto University of Veterinary and Animal Sciences, Sakrand, Pakistan, [3]Key Laboratory for Agro-Ecological Processes in Subtropical Region, Institute of Subtropical Agriculture, The Chinese Academy of Sciences, Changsha, China, [4]University of Chinese Academy of Sciences, Beijing, China, [5]The UWA Institute of Agriculture and UWA School of Agriculture and Environment, The University of Western Australia, Crawley, WA, Australia

KEYWORDS

**silkworms, honeybee, mink, cashmere goat, ostrich, arctic fox, mulberry, animal agriculture**

Editorial on the Research Topic
Rearing, health, and disease management of special economic animals: paving the way for a sustainable special economy through animal agriculture

With the expanding demands of a growing human population, the concept of "Special Economy" has emerged in relation to animal agriculture. In that context, there is attention worldwide on the rearing and utilization of "special economic animals"—the 50 plus species that have been recently "domesticated" for commercial purposes, as a resource for food and fiber. Those developed to provide human food include livestock (e.g., sika deer, red deer, yak) and birds (e.g., silky chickens, pigeons, ostriches). Those developed to provide clothing for humans include fur animals (fox, raccoon dog, mink), and insects (e.g., silkworms). Another insect, the honeybee, provide human food as well as a pollination service (eg, honeybee).

However, the management of these "special economic animals" brings complex pressures and challenges, some of which we have addressed in this Research Topic where we explore a broad variety of topics, including rearing, production, health, and disease. We invited the submission of articles covering theoretical, basic, and applied research on any type of special economic animal and their habitats. We have thus been able to gather diverse insights that contribute to the development of more sustainable practices in this field of high significance to society. Here, we highlight those insights.

## Ruminants of special economic interest

In the Chinese forest musk deer, an endangered species, Xie et al. studied the effect of dietary supplementation of *Epimedium*, a traditional Chinese herb with aphrodisiac and anti-stress properties, on hormone levels, the gut microbiome, and metabolism. The supplement enhanced dry matter intake and feed-gain ratio, as well as the reproductive system. The analysis of the gut microbiota showed that the supplement increased abundance of beneficial bacteria, such as *Firmicutes*, and reduced the abundance of the potentially pathogenic *Proteobacteria*. Metabolomics analysis showed that several key pathways including lipid metabolism, hormone regulation (ovarian steroidogenesis) and antioxidation, were improved. Collectively, these findings indicate that *Epimedium* is beneficial for the rescue of the musk deer, might also be useful for other ruminant livestock.

In the yaks in the Qinghai-Tibet Plateau, the problem is that the transition period, an important determinant of female reproductive efficiency, usually falls in late winter and early spring, when the natural pasture is in very poor supply. Shang et al. therefore studied the effect of perinatal nutritional supplementation and early weaning on serum biochemistry, metabolites, and reproductive efficiency in transitioning yaks. They documented the limitations posed by the conventional grazing system and also report how a nutritional supplement has positive outcomes for glucose, nitrogen, and lipid metabolism, and increases the secretion of reproductive hormones. The outcome is an acceleration of postpartum recovery and therefore improved reproductive efficiency.

With respect to fiber production, the cashmere goat is of special interest. The animals are celebrated for their fine undercoat, produced by the secondary follicles in the skin and harvested to produce high-end textiles that command premium prices in global markets. We present below two papers that provide a molecular biological foundation for improving the yield and quality of cashmere. In the first, Chang et al. identified several key regulatory proteins in secondary follicles. Expression analysis has shown that these proteins were produced more in anagen and less in telogen, particularly in the outer root sheath. Lu et al. used a genome-wide association study to identify 107 candidate genes associated with fleece traits. Additionally, they detected 8 significant single-nucleotide polymorphisms (SNPs) at the genome level and 232 at the chromosome level, with several mutations being related to fleece traits and therefore potentially useful for genetic selection.

## Fur-producing animals of special economic interest

In addition to silk, the fashion industry makes use of high-quality fur produced by the mink and the arctic fox, and the rearing of these two animals has regional economic importance.

In the mink industry, Aleutian disease (mink plasmacytosis), causes spontaneous abortion and death, and thus inflicts huge economic losses. Hu et al. used genotype data to identify genetic markers associated with immune function and resistance to the virus that is responsible. Their work lays a reasonable foundation for a genetic framework based on biological processes that will contribute to improving resilience against the disease. Focussing on mink nutrition, Cao et al. showed that dietary supplementation with the postbiotic, *Enterococcus faecium*, can improve the health and productivity of growing males. They observed accelerated body weight gain, probably explained by improvements in the digestibility of crude protein and dry matter. In addition, *Enterococcus faecium* supplementation enhanced immunity and intestine development.

The Arctic fox exhibits a distinctive lipid metabolism, perhaps due to the extreme environment in which they evolved. The underlying mechanisms are poorly understood, so Zhu et al. used transcriptomics and lipidomics to investigate how the animal handles triacylglycerol and glucose. They found that that 40% dietary crude fat was used for body weight gain, primarily through an increase in accumulation of subcutaneous adipose tissue. Arctic foxes have high levels of triacylglycerol and phosphatidylethanolamine in their adipose tissue, as well as high levels of very-low-density lipoprotein in the liver. By contrast, the levels of free fatty-acids in adipose tissue were normal, so insulin resistance was not a problem. The authors emphasized that the higher fat accumulation capacity and distinct characteristics of hepatic and adipose lipid metabolism, and glucose metabolism, would facilitate glucose homeostasis and enhance fat accumulation.

## Insects of special economic interest

The honeybee is of special interest because it produces honey, and of massive general interest because it is responsible for pollinating food crops that supply up to 90% of the world's human nutrition. It is thus most disturbing that the worldwide honeybee population is under threat from a variety of factors, including diseases and parasites. Mallory et al. reviewed the status of European Foulbrood, a bacterial disease, caused by *Melissococcus plutonius*, that has already caused severe economic damage. They provide an overview on the diversity of causal pathogens, disease distribution, antibiotic resistance, and virulence determinants. They argue that the disease is made more severe by other microbial species that work alongside *M. plutonius*, although they also point out that more evidence is needed. Finally, they present alternative options for combatting the threat of European Foulbrood, hoping to stimulate a discussion on the use of honeybee symbionts and probiotics as therapeutic alternatives.

The silkworm has a long history as an insect of special economic importance and is the subject of three papers. First, focusing on the primary food source of the silkworm, the mulberry, Huang et al. reported on mulberry bacterial blight, a devastating disease that causes serious reduction in the yield and quality of mulberry. Using high-throughput culturomics and metagenomic sequencing technology, they identified 10 causal pathogens. Their study of the distribution patterns of the pathogens and changes in the microbiome community of mulberries revealed *Pseudomonas syringae* and *Pseudomonas fulva* to be most important causal pathogens in the eight provinces of China. Focussing on a serious disease that directly affects the silkworm, pebrine, Qazi et al. carried out an in-depth molecular and phylogenetic characterization of methionine aminopeptidase type 2 (MetAP2) in *Nosema*

*bombycis*, the causative microsporidian parasite. Phylogenetic analysis revealed that the MetAP2 gene and its protein sequence in *Nosema bombycis* were closely related to those of *Nosema* species infecting wild silkworms, but differ significantly from those in other insect microsporidia, fungi, yeasts, and higher organisms, including humans. These findings suggest that conservation of MetAP2 is closely aligned with evolution of the host species, and provide data that may support the improvement and development of diagnostic tools and therapeutic strategies to combat the disease in China's sericulture sector.

The third article on the silkworm, by Wen et al., concerned the potential toxic effects of mercury on growth, development, and antioxidant capacity in the larvae. Following mercury exposure, a histological analysis of both the midgut and fat body of silkworms showed signs of dose-dependent damage. Antioxidant enzyme activity and immune function were also disturbed. Several key genes that control oxidative phosphorylation, nutrient metabolism, hormone biosynthesis, lysosome activity, ribosome biogenesis in eukaryotes, and ribosome pathways, were found to be differentially expressed in the midgut or the fat body of mercury-exposed silkworms. These findings enhance our understanding of the impact of toxic elements on growth and development of the silkworm, and also provide a more general insight into the biological effects of mercury exposure in invertebrate organisms.

## The other species of special economic interest

For the rabbit, Jeong et al. studied a *prion-like protein* gene (*PRND*), a member of the prion protein family, and identified nine novel single-nucleotide polymorphisms (SNPs) that could affect protein function or structure and lead to potential harmful effects. This is preliminary evidence, but it indicates a direction for research into rabbits as partially resistant species.

In the Martina Franca breed of donkey, Fusaro et al. evaluated the effect of dietary supplementation of hemp-based polyunsaturated fatty acids (PUFAs) on the membrane lipid profiles and reproductive performance of males (jacks). The supplement improved sperm morphology, and reduced the peroxidation index and oxidative stress, suggesting improvements in membrane fluidity and oxidative stability, two measures of sperm function.

The only article on birds concerned the ostrich, an animal that provides quality meat, leather, and feathers, as well as other profitable by-products. Chick mortality, often resulting from enteritis, is a serious issue in the ostrich industry, leading to poor outcomes for farmers and breeders. In the search for a nutritional solution, Li et al. supplemented juvenile ostriches with chicory and found that it improved the growth rate and reduced early mortality, perhaps by modulating the intestinal microbiome and mitigating intestinal inflammation.

## Concluding remarks

Rearing, health, and disease management are as important for special economic animals as they are for mainstream livestock. Through proper care, monitoring, and preventive measures, farmers can enhance productivity, animal welfare, and economic returns, and lay a strong foundation for a resilient and sustainable special economy based on animal industries. Although many articles in this collection provide high-quality evidence on various animal species of special economic importance, there remains significant room for further discussion to raise awareness and interest in the rearing of these economically valuable animals.

## Author's note

GM has senior authorship for this article.

## Author contributions

IQ: Conceptualization, Writing – original draft, Writing – review & editing. CA: Writing – original draft. GM: Conceptualization, Supervision, Writing – original draft, Writing – review & editing. JL: Project administration, Resources, Writing – review & editing.

## Funding

The author(s) declare that financial support was received for the research and/or publication of this article. Izhar Hyder Qazi and Jiping Liu acknowledge the Earmarked Fund of the China Agriculture Research System (CARS-18-ZJ0304). The funder has no role in the conceptualization or writing of this manuscript.

## Conflict of interest

The authors declare that the research was conducted in the absence of any commercial or financial relationships that could be construed as a potential conflict of interest.

The authors declared that they were an editorial board member of Frontiers, at the time of submission. This had no impact on the peer review process and the final decision.

## Generative AI statement

The author(s) declare that no Gen AI was used in the creation of this manuscript.

## Publisher's note

frontiers | Frontiers in Veterinary Science

TYPE Original Research
PUBLISHED 30 May 2024
DOI 10.3389/fvets.2024.1409084



OPEN ACCESS

EDITED BY
Ran Di,
Chinese Academy of Agricultural Sciences, China

REVIEWED BY
Zeying Wang,
Shenyang Agricultural University, China
Yang Cao,
Jilin Academy of Agricultural Sciences (CAAS), China

*CORRESPONDENCE
Rui Su
✉ suruiyu@126.com
Yujiang Wu
✉ wuyujiang_1979@163.com

†These authors have contributed equally to this work and share first authorship

RECEIVED 29 March 2024
ACCEPTED 07 May 2024
PUBLISHED 30 May 2024

CITATION
Lu X, Suo L, Yan X, Li W, Su Y, Zhou B, Liu C, Yang L, Wang J, Ji D, Cuomu R, Cuoji A, Gui B, Wang Z, Jiang W, Wu Y and Su R (2024) Genome-wide association analysis of fleece traits in Northwest Xizang white cashmere goat.
*Front. Vet. Sci.* 11:1409084.
doi: 10.3389/fvets.2024.1409084



# Genome-wide association analysis of fleece traits in Northwest Xizang white cashmere goat

Xiaotian Lu[1,2†], Langda Suo[1,3†], Xiaochun Yan[2], Wenze Li[2], Yixin Su[2], Bohan Zhou[2], Can Liu[2], Lepu Yang[2], Jiayin Wang[2], De Ji[1,3], Renqing Cuomu[1,3], Awang Cuoji[1,3], Ba Gui[1,3], Zhiying Wang[2], Wei Jiang[2], Yujiang Wu[1,3]* and Rui Su[2,4]*

[1]Institute of Animal Science, Xizang Academy of Agricultural and Animal Husbandry Science, Lhasa, China, [2]College of Animal Science, Inner Mongolia Agricultural University, Hohhot, China, [3]Key Laboratory of Animal Genetics and Breeding on Xizang Plateau, Ministry of Agriculture and Rural Affairs, Lhasa, China, [4]Sino-Arabian Joint Laboratory of Sheep and Goat Germplasm Innovation, Hohhot, China

Northwest Xizang White Cashmere Goat (NXWCG) is the first new breed of cashmere goat in the Xizang Autonomous Region. It has significant characteristics of extremely high fineness, gloss, and softness. Genome-wide association analysis is an effective biological method used to measure the consistency and correlation of genotype changes between two molecular markers in the genome. In addition, it can screen out the key genes affecting the complex traits of biological individuals. The aim of this study was to analyze the genetic mechanism of cashmere trait variation in NXWCG and to discover SNP locus and key genes closely related to traits such as superfine cashmere. Additionally, the key genes near the obtained significant SNPs were analyzed by gene function annotation and biological function mining. In this study, the phenotype data of the four traits (cashmere length, fiber length, cashmere diameter, and cashmere production) were collected. GGP_Goat_70K SNP chip was used for genotyping the ear tissue DNA of the experimental group. Subsequently, the association of phenotype data and genotype data was performed using Gemma-0.98.1 software. A linear mixed model was used for the association study. The results showed that four fleece traits were associated with 18 significant SNPs at the genome level and 232 SNPs at the chromosome level, through gene annotated from *Capra hircus* genome using assembly ARS1. A total of 107 candidate genes related to fleece traits were obtained. Combined with Gene Ontology and Kyoto Encyclopedia of Genes and Genomes enrichment analysis, we can find that *CLNS1A*, *CCSER1*, *RPS6KC1*, *PRLR*, *KCNRG*, *KCNK9,* and *CLYBL* can be used as important candidate genes for fleece traits of NXWCG. We used Sanger sequencing and suitability chi-square test to further verify the significant loci and candidate genes screened by GWAS, and the results show that the base mutations loci on the five candidate genes, *CCSER1* (snp12579, 34,449,796, A → G), *RPS6KC1* (snp41503, 69,173,527, A → G), *KCNRG* (snp41082, 67,134,820, G → A), *KCNK9* (14:78472665, 78,472,665, G → A), and *CLYBL* (12: 9705753, 9,705,753, C → T), significantly affect the fleece traits of NXWCG. The results provide a valuable basis for future research and contribute to a better understanding of the genetic structure variation of the goat.

KEYWORDS

**Northwest Xizang white cashmere goat, genome-wide association analysis, cashmere trait, GGP_Goat_70K SNP chip, linear mixed model, Sanger sequencing**

# 1 Introduction

Cashmere goats, as a part of global biodiversity, have experienced a long process of natural selection and artificial breeding. Nowadays, they have become one of the breeds with the highest cashmere production and excellent cashmere quality in the world. The most important economic value of the cashmere goats derives from its cashmere. Cashmere has the characteristics of fine and soft, white color as snow, bright color, and delicate and smooth feel. Textiles made of cashmere are unique in lightness, comfort, warmth, and elegance. NXWCG is the first new breed of Cashmere Goat cultivation in Xizang Autonomous. Due to the particularity of its living environment, the NXWCG has the characteristics of hypoxia tolerance and high cold tolerance. NXWCG has the most pure blood, the finest cashmere, the largest hair follicle density, and the uniform thickness of a single fiber. Based on its significant characteristics of extremely high fineness, gloss, and softness, we selected this breed of cashmere goat as the experimental object for related genetic research.

The fleece traits are mostly one of the quantitative traits in the cashmere goats. Quantitative traits refer to traits that are controlled by a small number of major genes and gene networks, a large number of minor genes, and environmental modifications; there are interactions between genes and the environment, and gene expression is affected by other genes, biological small molecules, and gene methylation. The fleece quality traits are traits with continuous variation or non-Mendel intermittent variation (1, 2). In brief, the variation of cashmere quality is continuous, and the variation is easily affected by environmental conditions. The earliest genetic improvement method of quantitative traits is to select individual phenotype traits, including individual selection method, family selection method, and mixed selection method. With the introduction of the concept of quantitative genetics in the 1920s, quantitative genetics has undergone continuous development. It has achieved remarkable results in analyzing the genetic mechanism and biological evolution of quantitative traits (3, 4).

Molecular genetics is a branch of genetics that studies the mechanism of biological inheritance and variation at the molecular level. The main research contents of molecular genetics include the nature of the gene, the function of the gene, the change of the gene, and the structure and function of the protein. In the breeding of cashmere goats, the method of combining phenotype- and genotype-assisted selection is gradually improved, which provides theoretical support for improving the accuracy and efficiency of selection and shortening the generation interval. Duan et al. found that cashmere goats with curly fiber hair can produce higher production and finer fiber hair than straight cashmere goats by studying the cashmere characteristics of Yanshan cashmere goats, and this difference in fiber characteristics can be related to the mutation of *KRT1* and *KRT6A* genes (5). Li et al. used the iRTAQ-based method and identified that different protein abundances are associated with different fiber characteristics. Different protein abundances mainly refer to keratin or keratin-associated proteins (*KRTAP11-1*, *KRT6A*, and *KRT38*). Transcriptome sequencing confirmed that the *DSC2* gene was significantly associated with the fleece phenotype of goat (6). Purvis and Franklin found that keratin intermediate protein and keratin-associated protein play an important role in determining different fleece quality and production traits (7). These studies suggest that hair follicle and hair fiber-related genes are involved in skin structure and fleece development, and the diversity of these genes may have an impact on the structure and traits of fleece. DNA molecular marker is the genome roadmap. Molecular markers are widely used in genetic map construction, population genetic diversity analysis, marker-assisted selection breeding in animal breeding, gene mapping, and cloning. SNP marker is a single nucleotide polymorphism molecular marker based on PCR and sequencing technology. The mutation rate of SNP in the genome is very low, which can effectively distinguish different alleles and cover the whole genome with high density, low cost, and easy automation of high-throughput analysis (8, 9). Sun et al. reveal the potential genetic basis for litter size, coat color, and skin color by using genome-wide association analysis (GWAS), selection signature analysis, and ROH detection within the Youzhou dark goat population through GWAS; four SNPs were identified (10). Mukhina et al. evaluated the genetic risk of five Mongolian goat breeds (Buural, Ulgii Red, Gobi GS, Erchim, and Dorgon) using Illumina Goat SNP50 genotyping data and explored the phylogenetic relationship between these populations and other breeds (11).

Genome-wide association study (GWAS) is an analysis method based on the principle of linkage disequilibrium. By detecting the genetic variation polymorphism in the whole genome of the associated population composed of hundreds of individuals, tens of thousands or even millions of molecular markers are obtained, and then the relationship between the target traits and the molecular markers is identified, and the relationship between the genetic variation and the characteristics of the population samples is determined. GWAS is widely used in the genetic variation of non-disease quantitative trait variation such as height and weight (12–14). After several years of accumulation and summary of genomic association analysis theory, Klein et al. from Rockefeller University published a GWAS study on age-related macular degeneration in 2005 (15). The study by Klein et al. opened the prelude of GWAS in human, animal, and plant genetic research (16, 17).

In recent years, to accelerate the process of animal genetic improvement and overcome some difficulties in animal genetic breeding, genome-wide association analysis using genotype data obtained using genome resequencing and genotyping technology and animal phenotype trait data has become increasingly mature (18–20). GWAS technology is becoming more and more powerful with the development of next-generation and third-generation sequencing technology.

Sanger sequencing is the international gold standard for many gene detection technologies. This sequencing technology can well detect the accuracy of chip sequencing technology, second-generation sequencing technology, third-generation sequencing technology, and up-to-date fourth-generation sequencing technology. Takenaka quantified RNA editing efficiency by comparing base mutations in the Sanger sequencing chromatogram of RT-PCR products because its sequencing accuracy is superior to other sequencing methods (21). Studies show that Sanger sequencing can effectively and rapidly detect and quantify multiple low VAF BRAF mutations from FFPE samples (22). Danilov et al. compared Bead Chip and WGS/WES genotyping calls via Sanger sequencing, and the results showed that the average precision and accuracy of gene chip and WGS were more than 0.991 and 0.997, respectively (23). The Sanger sequencing method is widely used in the analysis of biological genetic mechanisms.

# 2 Materials and methods

## 2.1 Ethics statement

The feeding environment of this experiment is in line with the relevant standards of ordinary animal experimental facilities in the Chinese national standard "Laboratory Animal Environment and Facilities" (GB14925-2010). The feeding and experimental operation of animals meets the requirements of animal welfare. All the experimental procedures involving goats were reviewed and approved by the Experimental Animal Management Committee of Inner Mongolia Agricultural University, Hohhot, China.

## 2.2 Sample collection and obtaining phenotype data

In totally, 539 samples were collected from the NXWCG Original Breeding Farm in Ritu County, Ali Prefecture, Xizang Autonomous Region. Among them, 288 samples were used for the GWAS study and 251 samples were used for the validation test. It contains 335 breeding rams and 204 ewes. The production performance parameters, such as cashmere length and fiber length of the experimental group, were measured in the field of the Original Breeding Farm, and the cashmere and ear tissue samples of the experimental group were collected and brought back to the laboratory for further study.

Descriptive statistical analysis of phenotype data was performed using R software. The ggplot2 package of R software was used to draw the frequency distribution histogram and fitting curve of the phenotype, and the normal distribution law of each trait was judged by graphics.

## 2.3 Obtaining genotype data and quality control

The genotype data of this experiment were derived from the ear tissues of cashmere goats collected from the Original Breeding Farm of Northwest Xizang white cashmere goats. The ear tissues were collected and placed in a PE tube containing 75% anhydrous ethanol and stored in a refrigerator at −80°C. The DNA of ear tissues was extracted by phenol extraction method in the laboratory. The concentration of DNA was detected by NANODROP 2000c (Thermo, Waltham, MA, USA). The extracted genomic DNA was detected by agarose gel electrophoresis. There were clear bands with a length of more than 10 kb and no obvious degradation. The OD260/280 value of DNA samples should be between 1.7 and 2.1.

The DNA samples that met the requirements of phenotype data and DNA concentration were screened and placed in a 96-well PCR plate, and the genotype sequencing based on the goat 70 K chip was performed by Neogen Bio-Scientific Technology (Shanghai) Co., Ltd.

Plink1.90 software was used to control the quality of genotype data to eliminate unqualified samples and SNP loci. Quality control standards are as follows: (1) SNP deletion quality control: SNP genotype deletions greater than 10% (−geno0.1) were removed from the analysis; (2) Sample missing quality control: samples with a call rate lower than 90% (−mind0.1) were excluded from the analysis; (3) MAF deletion quality control: loci with a minimum allele frequency of less than 1% (−maf0.01) were excluded from the analysis; (4) Hardy–Weinberg equilibrium quality control: sites that did not meet the Hardy–Weinberg equilibrium test with a $p$-value of less than $10^{-6}$ were excluded from the analysis.

To determine whether the SNPs after quality control have sufficient coverage in the whole genome, Haploview4.1 software was used to calculate the LD coefficient between SNP markers and the distance between markers. Excel software is used to calculate the average value of the LD coefficient corresponding to each distance; finally, the average value is used to draw the LD attenuation diagram.

## 2.4 GWAS

In this study, the mixed linear model of GEMMA-0.98 software (Genome-wide Efficient Mixed Model Association algorithm) was used to perform genome-wide association analysis on the phenotype and genotype values of four fleece traits in the individuals after genotype quality control (24). Individual age is added to the mixed linear model as a fixed effect. In this study, $y = X\alpha + Z\beta + W\mu + e$ statistical analysis model was used, where y is the phenotype trait, X is the fixed effect matrix, α is the fixed effect estimation parameter, Z is the single nucleotide polymorphism matrix, β is the single nucleotide polymorphism effect, W is the random effect matrix, μ is the predicted random individual, e is the random error, and the distribution is $e \sim N\left(0, \sigma_e^2\right)$.

Through the principal component analysis of the population genotype data, the principal component of the population genetic variation is calculated, that is, the genetic variation of the population is compressed into several smaller dimensions, and then it is defined as the eigenvector of the inter-individual covariance matrix. The principal component is added as a covariate to the subsequent GWAS analysis model to correct the potential population stratification of the associated population. It is necessary to consider the interference factors caused by population stratification, and it is necessary to perform population stratification detection and parameter correction on the experiment population. In this study, the principal component analysis of the experiment population was carried out using Plink software. The first two principal components were extracted by R software, and the scatter plot of principal component analysis was drawn to observe whether there were differences in the genetic background of the population. Individual age and the first three principal components were added to the mixed linear model as covariates to correct the phenotype data.

The genome-wide association analysis of four phenotype traits (cashmere length, cashmere diameter, fiber length, and cashmere production of NXWCG) was carried out by Gemma-0.98.1 software under the Linux system. First, the population genome kinship matrix is calculated, and then the covariate and Kinship matrix are added to the model for data processing.

The output result files by Gemma software were sorted out, and the parameters used to draw the Q-Q diagram and Manhattan diagram were screened. R software was used to draw visual graphics of four trait variation sites. In order to eliminate the false negative caused by too strict Bonferroni correction, and to explore more significant SNPs loci and candidate genes affecting the fleece traits of NXWCG, combined with the results of association analysis in this study, when the potentially significant level threshold was $1 \times 10^{-3}$, that

correspond to 3 in -$\log_{10}$ ($p$-value) scale, it was determined that it was significantly associated with the traits studied (25, 26).

## 2.5 Gene annotation and bioinformatics analysis

The goat reference genome data (Genome assembly ARS1.2) was downloaded from the website of the National Center for Biotechnology Information[1]; the candidate genes within 50 kb upstream and downstream of the significant sites were annotated by bedtools software.

GO function annotation and KEGG signaling pathway analysis were performed using DAVID6.8[2] database. $p < 0.05$ is statistically significant in the results of enrichment analysis. GO and KEGG histograms and bubble plots were plotted using the ggplot2 package of R software.

## 2.6 Validation analysis of GWAS results

In this study, Sanger sequencing method was used to verify the results of GWAS analysis. The ear tissue DNA samples used for Sanger sequencing were all from NXWCG Original Breeding Farm. The DNA samples were different from the GWAS study. The ear tissue DNA of 96 individuals was screened for each fleece trait.

In this study, PCR primers were designed based on the 300 bp upstream and downstream chromosome fragments of 8 significant SNP loci obtained by GWAS (Table 1). Primer design and preparation were carried out by Sangon Biotech (Shanghai) Co., Ltd. (Table 2). PCR amplification was performed using the T100 Thermal Cycler (Bio-Rad), the Composition of conventional PCR reaction solution, and the PCR reaction conditions as follows (Tables 3, 4).

The unpurified samples, after PCR amplification, were sent to Sangon Biotech (Shanghai) Co., Ltd. for capillary electrophoresis sequencing (CE). The sequencing was performed using the 3730xl DNA Analyzer (Thermo Fisher). Finally, the peak color map in ab1 format and the sequence file in seq format were generated for genotyping statistics. The chisq.test function of R software was used to test the fitness of candidate genes, and the chi-square value and $p$-value value of each candidate gene were obtained.

# 3 Results

## 3.1 Basic statistical analysis of phenotype data

In this study, the fleece traits of 288 NXWCG for GWAS were measured, including cashmere length, cashmere diameter, fiber length, and cashmere production. The phenotype data were sorted out, and descriptive statistical analysis was performed on the four traits (Table 5). According to the frequency distribution histogram and fitting curve of each phenotype (Figure 1), it was judged that each trait tended to normal distribution and could be used for subsequent genome-wide association analysis.

TABLE 1 SNP locus verification table.

| Traits | Chr | SNP loci | SNP | $p$-value | Gene |
|---|---|---|---|---|---|
| CL | 6 | 34,449,796 | snp12579 | 1.16E-04 | *CCSER1* |
| CD | 16 | 69,173,527 | snp41503 | 4.50E-06 | *RPS6KC1* |
| FL | 12 | 67,134,820 | snp41082 | 2.84E-05 | KCNRG |
| CP | 14 | 78,472,665 | 14:78472665 | 3.83E-05 | KCNK9 |
| | 12 | 9,705,753 | 12:9705753 | 4.99E-05 | CLYBL |

CL, cashmere length; CD, cashmere diameter; FL, fiber length; CP, cashmere production.

## 3.2 Quality control of genotype data and analysis

A total of 67,088 SNP loci were obtained after genotyping 288 individual ear tissue DNA. Through genotype data quality control, 1,276 SNPs were excluded from the quality control of single nucleotide site deletion, two individuals were excluded from the sample missing quality control, 10,242 SNPs were excluded from MAF quality control, 1,890 SNPs were excluded from Hardy–Weinberg equilibrium, and 523 SNPs on sex chromosomes were removed. A total of 53,157 SNPs were obtained after quality control of raw data, which were uniformly distributed on 29 pairs of autosomes of goats (Figure 2). To reduce the false positive results of genome-wide association analysis, it is necessary to analyze the population structure of 286 individuals and add the first three principal components of the population as covariates to the GWAS model. The principal components analysis results showed that there was no obvious stratification in the group, indicating that there was almost no alien lineage between the samples (Figure 3).

The LD decay map is a two-dimensional curve to show the process that the average LD coefficient between SNP markers on the chromosome of the genome decreases linearly with the increase of the distance between markers. The linkage disequilibrium also measures the genotype synchronization and correlation index of the two molecular markers. In this study, the LD decay map showed that the LD correlation coefficient ($r^2$) decreased gradually after the physical distance reached 200 kb, indicating that the closer the distance between the two SNP loci on the chromosome, the stronger the correlation and the greater the LD coefficient (Figure 4).

## 3.3 GWAS

GWAS results of cashmere length showed that 77 SNPs were significant at the potentially significant level (Figure 5A). The calculation results of the expansion factor of the Q-Q diagram show that there was no genome expansion, indicating that the model used had a good fitting degree and was suitable for this trait. Through gene annotation, 18 candidate genes related to cashmere length traits were obtained. For the cashmere diameter trait, 71 SNPs were significant at the potentially significant level. The gene expansion factor was $\lambda = 1.027$ (Figure 5B); through gene annotation, 32 candidate genes related to the cashmere diameter trait were obtained. For the fiber length trait, 42 SNPs were significant at the potentially significant

1 http://www.ncbi.nlm.nih.gov

2 http://david.abcc.ncifcrf.gov

TABLE 2 The primer sequence information of PCR amplification.

| Gene | Primer Sequence | | Product size/bp |
|---|---|---|---|
| *CCSER1* | F | 5' GTGTTATCCCTAGAGAGCCTGTTTC 3' | 247 |
| | R | 5' AGCATGAACCTCAAAGACTGGAAG 3' | |
| *RPS6KC1* | F | 5' GCATCCACAGTTCCAGCAGAAG 3' | 263 |
| | R | 5' CAGAAGCCCAGCACTCGTTTG 3' | |
| *KCNRG* | F | 5' CTGTGGGAGATAAAGATAGGGCATC 3' | 283 |
| | R | 5' AAGTGTTAGTGACTGTAAGCCAAGG 3' | |
| *KCNK9* | F | 5' GCCTCTCTGGAATATCCTCCTATGG 3' | 214 |
| | R | 5' CATCGCCTTCTCTGGTTTGTTGG 3' | |
| *CLYBL* | F | 5' AACAAGAGAAACCAGCGAAAGGAG 3 | 218 |
| | R | 5' ACACGAGAGCCACTGGAATGAG 3' | |

level. The gene expansion factor was $\lambda = 0.983$ (Figure 5C); through gene annotation, 18 candidate genes related to fiber length trait were obtained. For the cashmere production trait, 60 SNPs were significant at the potentially significant level. The gene expansion factor was $\lambda = 1.023$ (Figure 5D); through gene annotation, 25 candidate genes related to cashmere production trait were obtained (Table 6). Table 6 lists some of the more significant loci and annotated genes in the GWAS results of four fleece traits, respectively.

## 3.4 GO and KEGG analysis

The GO and KEGG enrichment analysis of 107 candidate genes associated with fleece traits was performed by NCBI's DAVID 2021 Gene system (Table 7). Gene ontology was enriched to one biological process, five cellular components, and five molecular functions ($p < 0.05$). GO enrichment to the negative regulation of cell proliferation biological processes (GO: 0008285) includes *ALDH1A2*, *STAT3*, *CDH13,* and five other genes. It is enriched in cellular components such as cytoplasm (GO: 0005737), cell membrane surface (GO: 0009986), and endoplasmic reticulum (GO: 0005783), including genes such as *CREBBP*, *PRLR,* and *KCNRG*. The enriched molecular functions included ATP binding (GO: 0005524), calcium ion binding (GO: 0005509), and voltage-gated potassium channel activity (GO: 0005249), including *RPS6KC1*, *CAPNS1*, and *KCNK9* genes. KEGG was enriched to one signal pathway of motor protein (chx: 04814) ($p < 0.05$), and *MYO15A*, *KIF16B*, *MYO5C* and *MYO5A* were significantly enriched to this pathway (Figure 6).

## 3.5 Validation analysis of GWAS

The one or two most significant loci of each trait in GWAS results were selected for the verification test. In total, 5 pairs of primers for four fleece traits of NXWCG were pre-tested. Finally, 5 pairs of primers successfully amplified the target length fragment altogether. Based on 5 pairs of primers, PCR amplification was performed on 251 individual ear tissue DNA templates of NXWCG. Sanger sequencing was performed on 251 amplified sequences. The results of Sanger sequencing were analyzed using Chromas 2.6.6 software. Finally, 5 chromosome mutation sites were found (Figure 7). The candidate genes corresponding to the five chromosome mutation sites were genotyping statistics. The chi-square test was used to analyze the correlation between significant loci and phenotype traits (Table 8). Verification analysis results show that the mutation sites of *CCSER1* (snp12579,34,449,796, A → G), *RPS6KC1* (snp41503,69,173,527, A → G), *KCNRG* (snp41082, 67,134,820, G → A), *KCNK9* (14: 78472665,78,472,665, G → A), and *CLYBL* (12: 9705753,9,705,753, C → T) were consistent with the results of GWAS analysis and highly significant ($p < 0.01$). The accuracy of genome-wide association analysis of fleece traits of NXWCG was verified theoretically.

TABLE 3 Composition of the conventional PCR reaction solution.

| Reagent | Amount |
|---|---|
| *TaKaRa Ex Taq*®(5 U/μl) | 0.25 μL |
| 10 × *Ex Taq Buffer* ($Mg^{2+}$plus)(20 mM) | 5 μL |
| dNTP Mixture (2.5 mM each) | 4 μL |
| Template | 3 μL |
| Primer F | 3 μL |
| Primer R | 3 μL |
| $ddH_2O$ | 31.75 μL |

TABLE 4 Conventional PCR reaction conditions.

| Step | Temperature | Time | | Cycle |
|---|---|---|---|---|
| Degeneration | 98°C | 10s | } | 35 |
| Annealing | 58°C-62°C | 30s | | |
| Elongation | 72°C | 1 min | | |
| Elongation | 72°C | 5 min | | 1 |
| Preservation | 4°C | ∞ | | 1 |

# 4 Discussion

NXWCG has attracted much attention because of their excellent cashmere quality. To firmly implement the country's agricultural policy to promote the process of agricultural and rural modernization, science and technology have been on the road. To explore the important molecular markers and candidate genes related to the fleece traits of NXWCG, the research group collected the cashmere and ear tissue samples in the early stage to analyze the phenotype traits and

TABLE 5 Descriptive statistics of phenotype values of cashmere traits.

| Traits | Number | Mean | SD | Max | Min | CV |
|---|---|---|---|---|---|---|
| CL (cm) | 288 | 3.79 | 0.73 | 5.90 | 2.10 | 19.26% |
| CD (μm) | 288 | 13.75 | 0.91 | 16.41 | 11.68 | 6.62% |
| FL (cm) | 288 | 12.71 | 3.64 | 22.00 | 5.00 | 28.63% |
| CP (g) | 288 | 229.8 | 72.28 | 426.9 | 64.0 | 31.45% |

CL, cashmere length; CD, cashmere diameter; FL, fiber length; CP, cashmere production.

genotype data. By drawing the frequency distribution histogram and its fitting curve for the four phenotype traits of cashmere diameter, cashmere length, fiber length, and cashmere production, it can be seen that the phenotype data are in accordance with the normal distribution and can be used for subsequent genome-wide association analysis. A total of 288 ear tissue DNA samples shared by the four phenotype traits were selected for goat 70 K SNP chip sequencing. The results showed that 92% of the individuals were successfully genotyped, and the genotype detection rate was greater than 99%.

The basic principle of genome-wide association analysis is linkage disequilibrium. Linkage disequilibrium is a non-random association of alleles at different loci and a key indicator of population heritability (27–29). GWAS analysis does not completely rely on population pedigree information and can directly locate the target traits and SNP sites through genome-wide SNP linkage disequilibrium. GWAS analysis can also screen out the main genes that affect the complex traits of biological individuals (30, 31). The significant loci snp4438 of cashmere diameter traits is located at 38,993,710 bp on chromosome 20 of goats. This significant loci is located in the intron region of the prolactin receptor protein coding gene *PRLR*. The *PRLR* gene is the same as the candidate gene identified by the research group in Inner Mongolia Cashmere Goat. The *PRLR* gene has been confirmed to be related to the growth and development of hair follicles in cashmere goats (32). Wu et al. screened several candidate genes, such as *PRLR*, that are significantly related to hair follicle and hair growth in the study of revealing the driving factors of plateau adaptability of Jiangnan Cashmere Goat and Xizang Cashmere Goat by genome and transcriptome analysis. The finer cashmere traits of the Xizang Cashmere Goat make this breed better adapt to the cold environment of the Xizang Plateau (33).

To understand the application of candidate genes in the analysis of biological genetic mechanisms from a macro perspective, the information on key candidate genes that

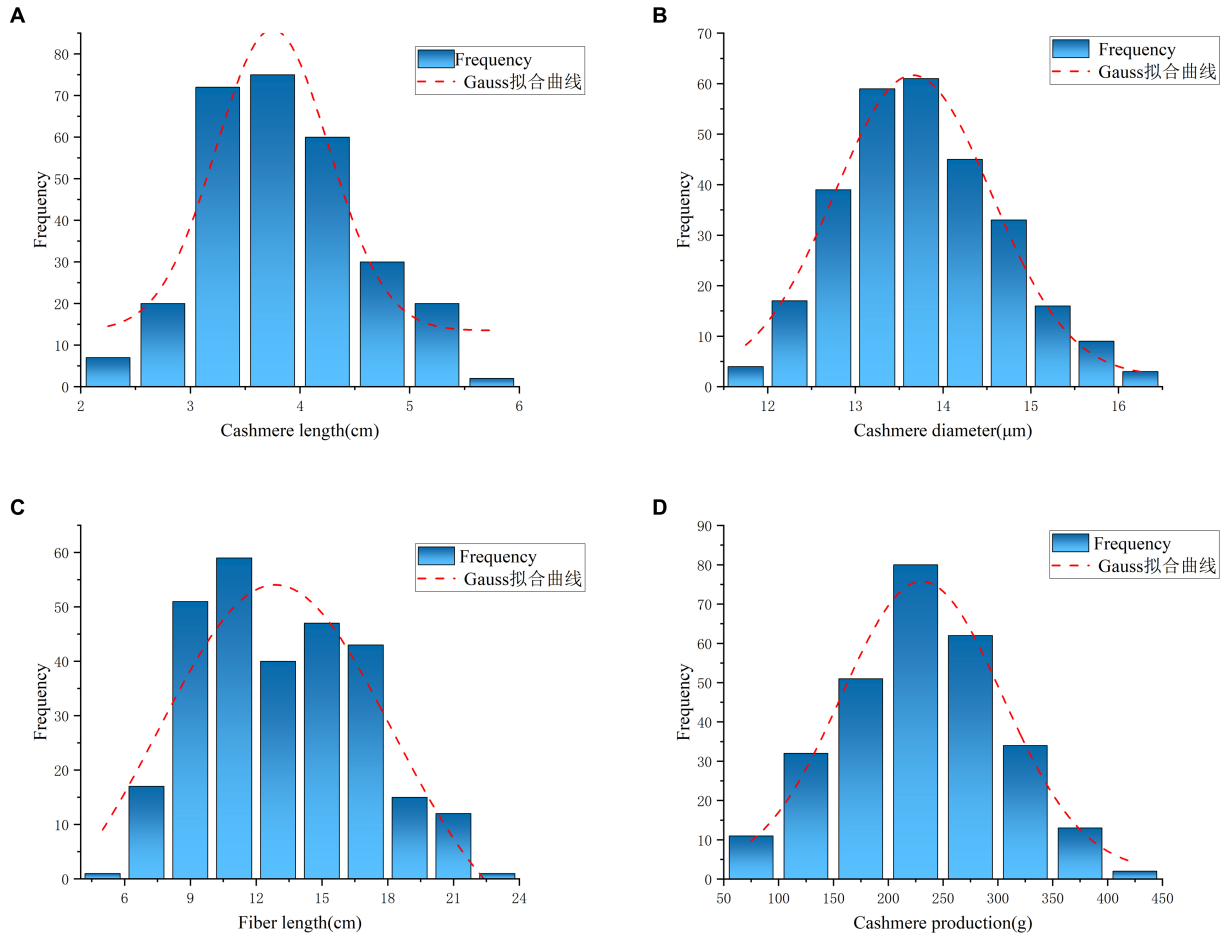


FIGURE 1
Frequency distribution histogram for fleece traits. **(A)** Indicate the frequency distribution and fitting curve of Cashmere length trait. **(B)** Indicate the frequency distribution and fitting curve of Cashmere diameter trait. **(C)** Indicate the frequency distribution and fitting curve of Fiber length trait. **(D)** Indicate the frequency distribution and fitting curve of Cashmere production trait.

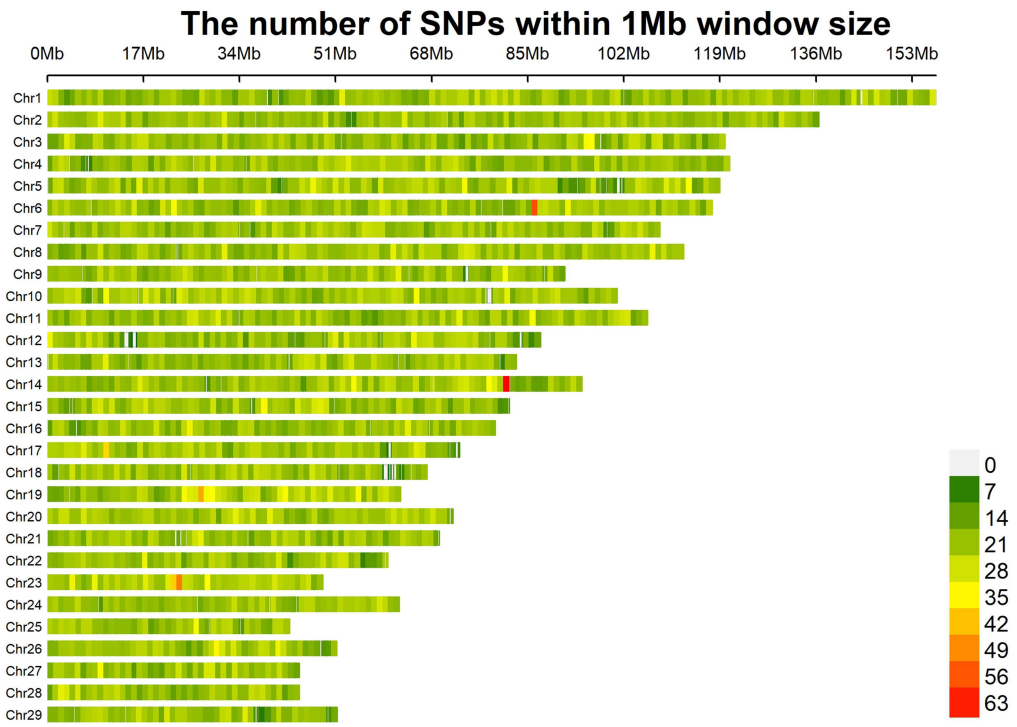


FIGURE 2
Distribution of SNPs in chromosome.

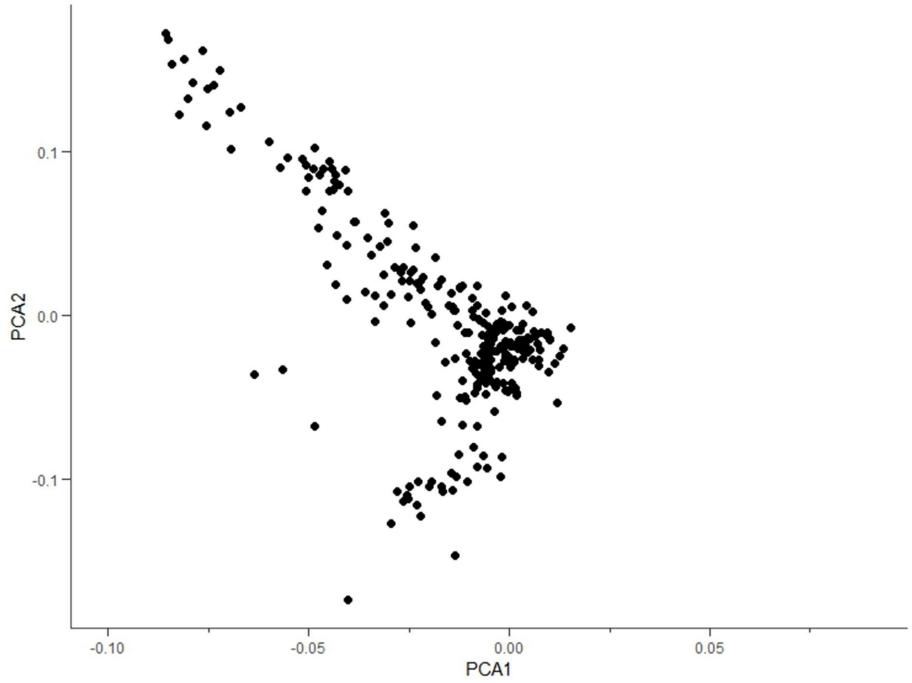


FIGURE 3
Principal component analysis.

significantly affect the fleece traits of NXWCG was retrieved through NCBI and PubMed databases. *CCSER1* is a gene encoding a coiled-coil serine-rich protein, which is located between 33,559,344 bp and 35,024,683 bp on chromosome 6 of the goat genome. Xu et al. detected the CNV of the *CCSER1* gene in 693 individuals of 6 goat breeds by q RT-PCR and analyzed the

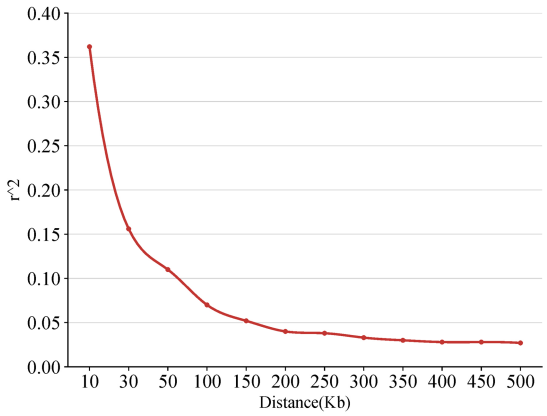


FIGURE 4
The diagram of the linkage disequilibrium.

correlation between CNV type and growth traits. The results showed that the CNV type of the *CCSER1* gene was significantly correlated with the body weight and chest circumference of GZW goats, and the expression profile showed that the *CCSER1* gene was highly expressed in the lung (34). Xue et al. used the Illumina PorcineSNP50 Bead Chip to perform genome-wide association analysis on the backfat thickness and lumbar muscle depth of 370 young eagle black pigs to detect the effects of QTL loci and candidate genes on growth traits. Finally, candidate genes related to backfat thickness, such as *CCSER1*, *GPHN*, and *MAGED1*, were screened (35). Yurchenko et al. carried out high-density genotyping and comprehensive scanning on the genomic marker selection of 15 indigenous sheep breeds in Russia. The scanning results showed that the region of the candidate gene *CCSER1* related to growth traits was consistent with the previous research results (36). *CLYBL* is a citramalyl-CoA lyase A protein, which is located between 9,645,150 bp and 9,878,794 bp on chromosome

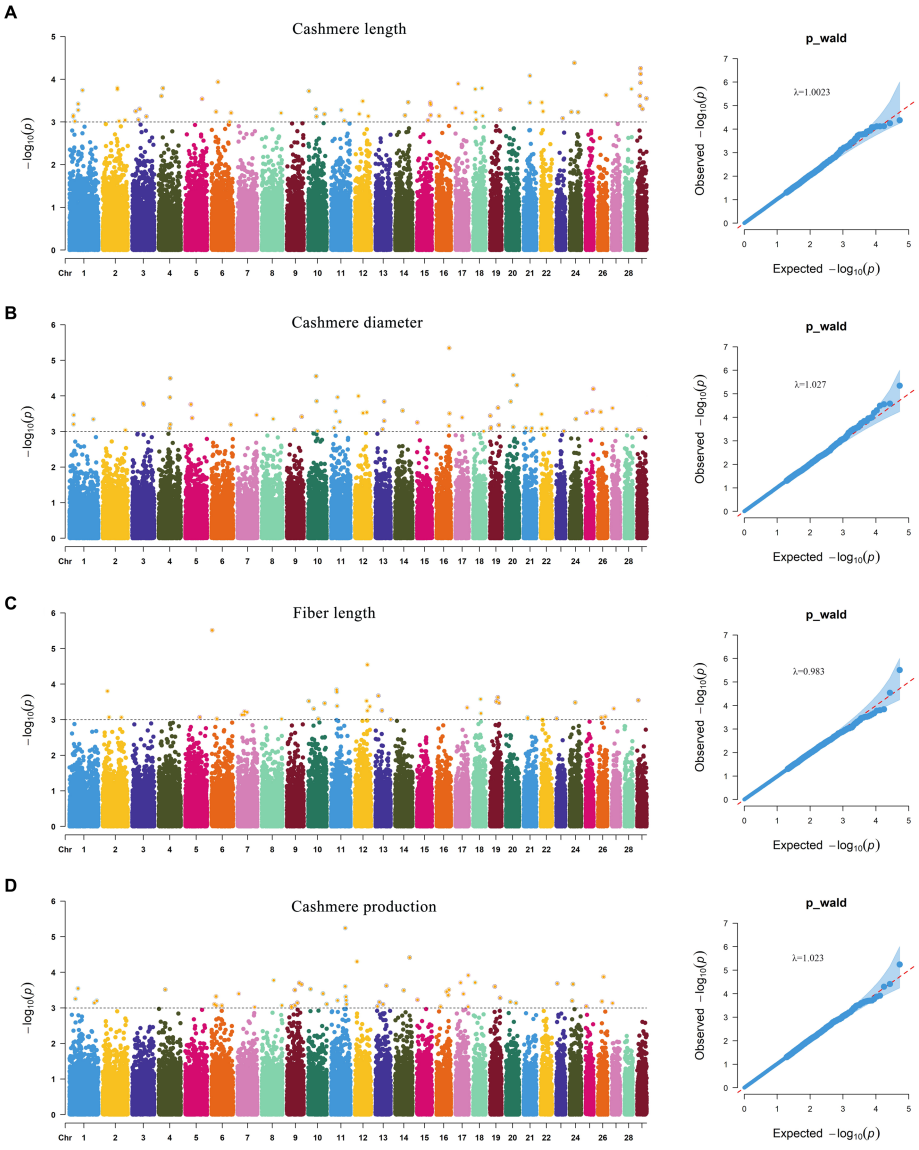


FIGURE 5
Manhattan and Q-Q plot of fleece trait. **(A)** Indicate the Manhattan and Q-Q plot of Cashmere length trait. **(B)** Indicate the Manhattan and Q-Q plot of Cashmere diameter trait. **(C)** Indicate the Manhattan and Q-Q plot of Fiber length trait. **(D)** Indicate the Manhattan and Q-Q plot of Cashmere production trait.

TABLE 6 Gene list of GWAS candidate genes of fleece traits.

| Traits | SNP | Chr | Position (bp) | Area | *p*-value | Gene |
|---|---|---|---|---|---|---|
| CL | NC_030836.1_17,791,205 | 29 | 17,791,205 | intron | 7.48E-05 | *CLNS1A* |
| | snp12579 | 6 | 34,449,796 | intron | 1.16E-04 | *CCSER1* |
| | 29:17721108 | 29 | 17,721,108 | intron | 1.20E-04 | *RSF1* |
| | snp57618 | 2 | 79,623,520 | intron | 1.60E-04 | *LRP1B* |
| | snp14053 | 4 | 22,588,864 | intron | 1.61E-04 | *EXOC4* |
| | snp33206 | 18 | 47,647,221 | cds | 1.62E-04 | *CAPNS1* |
| CD | snp41503 | 16 | 69,173,527 | intron | 4.50E-06 | *RPS6KC1* |
| | snp4438 | 20 | 38,993,710 | intron | 2.59E-05 | *PRLR* |
| | 10:42743991 | 10 | 42,743,991 | intron | 2.77E-05 | *ATP8B4* |
| | snp31138 | 4 | 62,616,471 | intron | 3.18E-05 | *IMMP2L* |
| | 12:17532273 | 12 | 17,532,273 | intron | 1.01E-04 | *GPC6* |
| | 10:45283375 | 10 | 45,283,375 | intron | 1.40E-04 | *MYO5A* |
| FL | snp41082 | 12 | 67,134,820 | intron | 2.84E-05 | *KCNRG* |
| | snp41082 | 12 | 67,134,820 | intron | 2.84E-05 | *LOC102188416* |
| | NC_030818.1_29,807,979 | 11 | 29,807,979 | intron | 1.43E-04 | *FBXO11* |
| | snp56066 | 13 | 15,313,527 | intron | 2.12E-04 | *CELF2* |
| | 19:42091591 | 19 | 42,091,591 | intron | 2.35E-04 | *STAT3* |
| | 18:39512710 | 18 | 39,512,710 | intron | 2.64E-04 | *ZFHX3* |
| CP | 14:78472665 | 14 | 78,472,665 | intron | 3.83E-05 | *KCNK9* |
| | 12:9705753 | 12 | 9,705,753 | intron | 4.99E-05 | *CLYBL* |
| | snp52367 | 17 | 69,328,879 | intron | 1.21E-04 | *CPE* |
| | NC_030825.1_9,378,797 | 18 | 9,378,797 | intron | 1.94E-04 | *LOC102181146* |
| | snp46857 | 17 | 27,541,955 | 3'-UTR | 1.95E-04 | *GUCY1A3* |
| | snp50516 | 9 | 66,936,671 | intron | 1.99E-04 | *ADGRG6* |

CL, cashmere length; CD, cashmere diameter; FL, fiber length; CP, cashmere production.

12 of the goat genome. The gene has the molecular function of activating citrate coenzyme A activity in the gene body and the biological process involved in regulating the cobalamin metabolic process, which is involved in the regulation of protein homotrimerization and cobalamin metabolism. *CLYBL* is a mitochondrial enzyme that exists in a variety of eukaryotes and is conserved in bacteria. It is expressed in the mitochondria of various organs such as brown fat and kidney in mammals (37).

Gene Ontology describes our understanding of biology from three aspects: biological processes, cellular components, and molecular functions. Biological processes refer to biological processes completed through a variety of molecular activities, such as DNA repair or signal transduction, in a broad sense. Cell components refer to the cellular structure where gene products perform functions, such as in the endoplasmic reticulum, ribosomes, and plasma membranes. Molecular function refers to the activity of a single gene product (including proteins and RNA) or a complex of multiple gene products at the molecular level, such as "response," "regulation," and "catabolic process." Gene Ontology has become one of the most popular frameworks to describe protein functions and their relationships (38–40).

The negative regulation process of cell population proliferation (GO: 0008285) enriched in this study refers to any process that can prevent or reduce the speed and degree of cell proliferation. It is a subtype of cell population proliferation regulation (GO: 0042127) and negative regulation of cell process (GO: 0048523)[3]. The genes enriched in this biological process are *ALDH1A2*, *STAT3*, *CDH13*, *NUDT6*, and *PTPN14*. Zhao et al. systematically studied the biological mechanism of hair follicle development and hair-related traits in Merino sheep based on the skin transcriptome and methylome data sets of Merino sheep and further predicted that transcription factors such as *STAT3* were involved in the morphogenesis of hair follicles during the special period of hair follicle development (41). *STAT3* has the molecular function of activating DNA binding transcription factor, RNA polymerase II specificity, and sequence-specific DNA binding in cis regulatory region of RNA polymerase II in gene ontology.

The KEGG-enriched motor protein (chx: 04814) signaling pathway ($p < 0.05$) belongs to the cell motor category in the cell process. This type of protein is involved in cell movements, such as rotational structures and structures that move along the cytoskeleton filaments. This signaling pathway was enriched in four genes: *MYO15A*, *KIF16B*, *MYO5C*, and *MYO5A*. The significant SNP loci 19: 34119983 on chromosome 19 is located in the CDS region of the *MYO15A* protein-coding gene, and

3 https://www.ebi.ac.uk/QuickGO

TABLE 7 GO function and KEGG signaling pathway enrichment table.

| Category | Term | Count | *p*-value | Gene |
|---|---|---|---|---|
| BP | negative regulation of cell proliferation | 5 | 0.0150 | *ALDH1A2, STAT3, CDH13*, etc |
| CC | cytoplasm | 17 | 0.0045 | *CREBBP, ZFHX3, DENND4A*, etc |
| CC | cell surface | 6 | 0.0082 | *ADGRG6, TNR, PRLR*, etc |
| CC | endoplasmic reticulum | 7 | 0.0088 | *KCNRG, HSPA13, CDS2*, etc |
| CC | myosin complex | 3 | 0.0128 | *MYO15A, MYO5C, MYO5A* |
| CC | neuron projection | 3 | 0.0293 | *GRM5, KCNQ1, CDH13* |
| MF | ATP binding | 13 | 0.0101 | *RPS6KC1, NARS2, MYO5C*, etc |
| MF | calcium ion binding | 8 | 0.0111 | *CAPNS1, PITPNM3, CDH13*, etc |
| MF | motor activity | 3 | 0.0116 | *MYO15A, MYO5C, MYO5A* |
| MF | receptor tyrosine kinase binding | 3 | 0.0139 | *PCNA, PITPNM3, PTPN14* |
| MF | voltage-gated potassium channel activity | 3 | 0.0186 | *KCND2, KCNK9, KCNH1* |
| KEGG | Motor proteins | 4 | 0.0429 | *MYO15A, KIF16B, MYO5A* |

BP, Biological process; CC, Cellular component; MF, Molecular function.

TABLE 8 Genotyping statistics and Chi-square test table.

| Traits | Genes | Genotype | Number | Mean | SD | CV | *p*-value |
|---|---|---|---|---|---|---|---|
| CL | *CCSER1* | AA | 29 (60.4%) | 3.77 | 1.22 | 32.36% | 0.00017 |
| | | AG | 13 (27.1%) | 3.46 | 1.10 | 31.79% | |
| | | GG | 6 (12.5%) | 3.80 | 1.13 | 29.74% | |
| CD | *RPS6KC1* | AA | 30 (83.3%) | 13.76 | 1.18 | 8.58% | 0.00006 |
| | | AG | 6 (16.7%) | 12.71 | 1.11 | 8.73% | |
| FL | *KCNRG* | AA | 3 (6.0%) | 13.50 | 4.33 | 32.07% | |
| | | AG | 22 (44.0%) | 12.50 | 4.93 | 39.44% | 0.00020 |
| | | GG | 25 (50.0%) | 11.82 | 5.37 | 45.43% | |
| CP | *KCNK9* | AA | 20 (30.8%) | 213.68 | 61.23 | 28.65% | |
| | | AG | 32 (49.2%) | 246.28 | 82.20 | 33.38% | 0.00113 |
| | | GG | 13 (20.0%) | 220.47 | 47.38 | 21.49% | |
| CP | *CLYBL* | CC | 40 (76.9%) | 207.41 | 62.27 | 30.02% | 0.00010 |
| | | CT | 12 (23.1%) | 203.93 | 66.92 | 32.82% | |

CL, cashmere length; CD, cashmere diameter; FL, fiber length; CP, cashmere production.

*MYO15A* encodes the Myosin-XVa protein. *MYO15A* has the molecular functions of ATP binding, protein binding, and cytoskeleton movement activation in the gene ontology. The cell components include the cytoskeleton and some myosin complexes. Hadi et al. used scanning electron microscopy to measure the number and diameter of stereocilia in auditory hair cells of shake-2 mice lacking long and short Myosin-XVa protein isoforms and found that Myosin-XVa protein short isoforms are critical for controlling the size of stereocilia (42). *KIF16B* is a kinesin family member 16B protein-coding gene, and the corresponding cashmere production trait significant locus NC _ 030820.1 _ 10,060,242 is located in the intron region of this gene. *KIF16B* has the molecular functions of ATP binding, microtubule binding, phosphatidylinositol binding, and microtubule movement activation and participates in microtubule-based motor biological processes. Based on the 50 K SNP chip, Wang et al. performed a GWAS study on five wool production traits of Chinese Merino sheep, including fiber diameter, fiber diameter coefficient of variation, and fineness dispersion. The 28 significant SNPs screened at the genomic level were annotated to several candidate genes related to wool traits, such as *KIF16B* and *TCF9* (43).

## 5 Conclusion

In summary, through genome-wide association analysis of four fleece traits of cashmere length, cashmere diameter, fiber length, and cashmere production of NXWCG, a total of 18 significant SNPs were associated at the genomic level, and 232 SNPs were associated at the chromosomal level. After gene annotation of significant loci, *CLNS1A*, *CCSER1*, *RPS6KC1*, *PRLR*, *KCNRG*, *FBXO11*, *KCNK9*, and

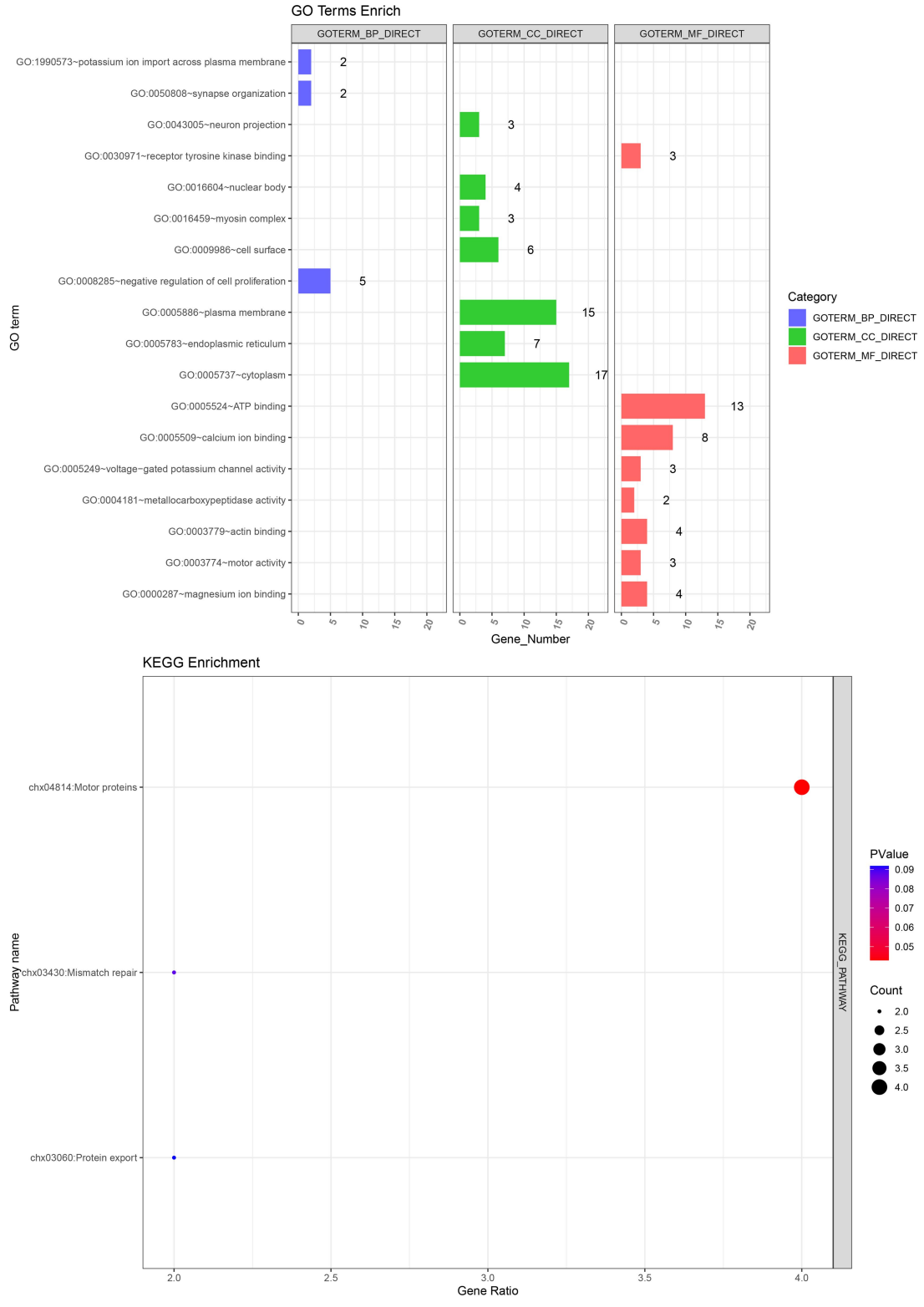


FIGURE 6
GO and KEGG enrichment analysis.

*CLYBL8* were screened as important candidate genes for fleece traits of NXWCG. Further verification of GWAS results through Sanger sequencing revealed that the mutation site of *CCSER1*, *RPS6KC1*, *KCNRG*, *KCNK9*, and *CLYBL8* genes significantly influence the fleece traits of NXWCG. The results of this study lay a theoretical foundation for further research and have extremely important scientific significance for analyzing the genetic mechanism of fleece traits.

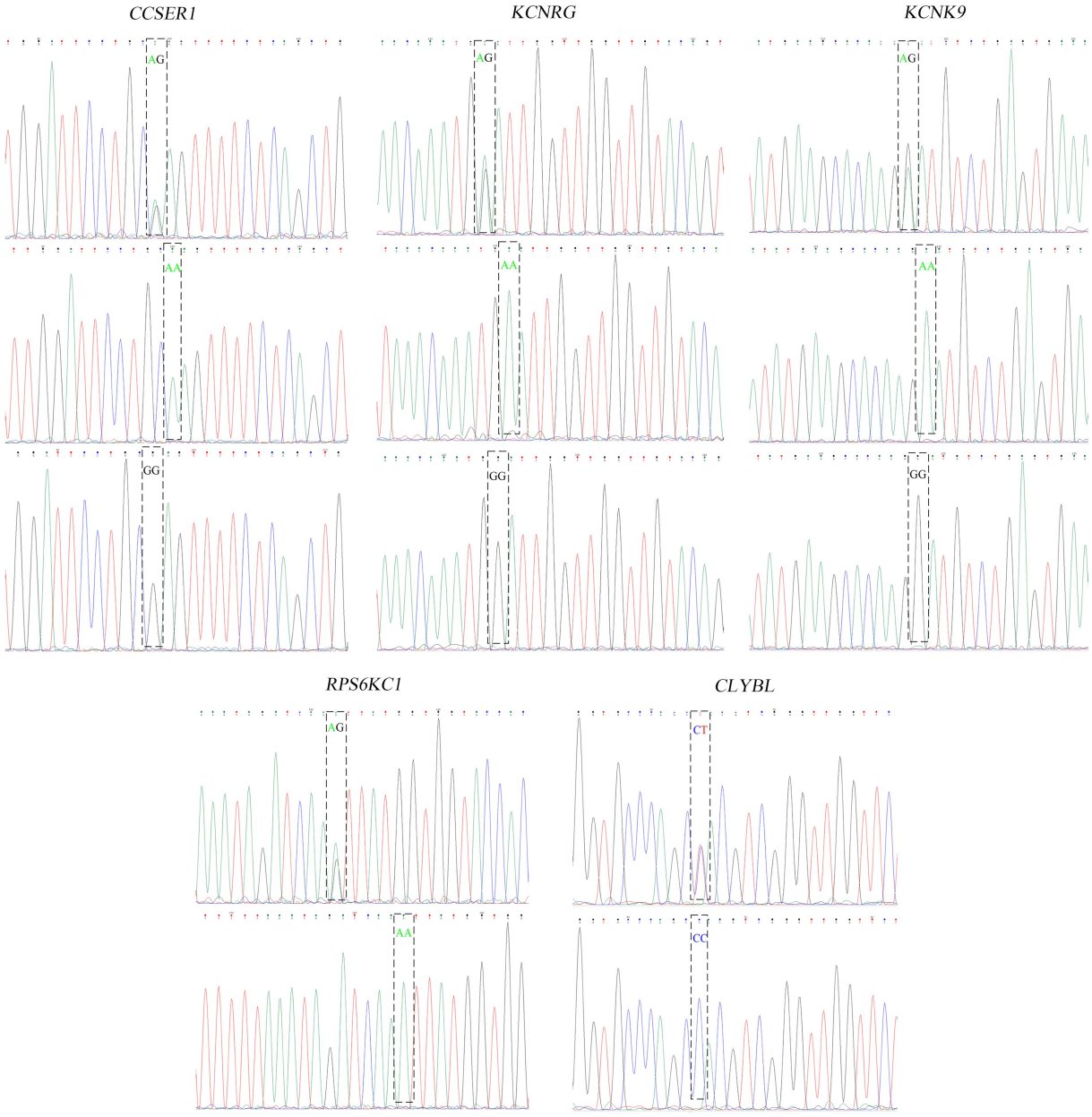


FIGURE 7
Peak color map of Sanger sequencing.

## Data availability statement

The original contributions presented in the study are included in the article/supplementary material, further inquiries can be directed to the corresponding authors.

## Ethics statement

The animal studies were approved by Experimental Animal Management Committee of Inner Mongolia Agricultural University. The studies were conducted in accordance with the local legislation and institutional requirements. Written informed consent was obtained from the owners for the participation of their animals in this study.

## Author contributions

XL: Data curation, Formal analysis, Investigation, Methodology, Software, Validation, Visualization, Writing – original draft, Writing – review & editing. LS: Data curation, Resources, Software, Writing – review & editing. XY: Conceptualization, Formal analysis, Visualization, Writing – original draft. WL: Methodology, Software, Visualization, Writing – original draft. YS: Formal analysis, Methodology, Writing – original draft. BZ: Investigation, Software,

Validation, Writing – original draft. CL: Formal analysis, Investigation, Methodology, Writing – original draft. LY: Formal analysis, Methodology, Writing – original draft. JW: Formal analysis, Investigation, Methodology, Writing – original draft. DJ: Investigation, Writing – original draft. RC: Investigation, Writing – original draft. AC: Investigation, Writing – original draft. BG: Data curation, Investigation, Writing – original draft. ZW: Methodology, Validation, Visualization, Writing – original draft. WJ: Formal analysis, Writing – original draft, Writing – review & editing. YW: Project administration, Resources, Writing – original draft, Writing – review & editing. RS: Funding acquisition, Methodology, Project administration, Writing – review & editing, Writing – original draft.

## Funding

The author(s) declare financial support was received for the research, authorship, and/or publication of this article. The authors are grateful for the grants supported by the National Key Research and Development Program of China [2022YFE0113300, 2022YFD1300204], Science and Technology project of the Xizang Autonomous Region: Breeding and healthy breeding of Xizang sheep [XZ202101ZD0001N], and China Agriculture Research System of MOF and MARA [No. CARS-39].

## Conflict of interest

The authors declare that the research was conducted in the absence of any commercial or financial relationships that could be construed as a potential conflict of interest.

## Publisher's note



## References

1. Doro S, Herman MA. On the Fourier transform of a quantitative trait: implications for compressive sensing. *J Theor Biol*. (2022) 540:110985. doi: 10.1016/j.jtbi.2021.110985

2. Togashi K, Lin CY. Theoretical efficiency of multiple-trait quantitative trait loci-assisted selection. *J Anim Breed Genet*. (2010) 127:53–63. doi: 10.1111/j.1439-0388.2009.00817.x

3. Norton B, Pearson ES. A note on the background to, and refereeing of, R. A. Fisher's 1918 paper 'On the correlation between relatives on the supposition of Mendelian inheritance. *Notes Rec R Soc Lond*. (1976) 31:151–62. doi: 10.1098/rsnr.1976.0005

4. Wright S. Evolution in Mendelian populations. *Genetics*. (1931) 16:97–159. doi: 10.1093/genetics/16.2.97

5. Duan C, Zhang L, Gao K, Guo Y, Liu Y, Zhang Y. Cashmere production, skin characteristics, and mutated genes in crimped cashmere fibre goats. *Animal*. (2022) 16:100565. doi: 10.1016/j.animal.2022.100565

6. Li Y, Zhou G, Zhang R, Guo J, Li C, Martin G, et al. Comparative proteomic analyses using itraq-labeling provides insights into fiber diversity in sheep and goats. *J Proteome*. (2018) 172:82–8. doi: 10.1016/j.jprot.2017.10.008

7. Purvis IW, Franklin IR. Major genes and Qtl influencing wool production and quality: a review. *Genet Sel Evol*. (2005) 37:S97–S107. doi: 10.1186/1297-9686-37-S1-S97

8. Kassa MT, You FM, Fetch TG, Fobert P, Sharpe A, Pozniak CJ, et al. Genetic mapping of SrCad and Snp marker development for marker-assisted selection of Ug99 stem rust resistance in wheat. *Theor Appl Genet*. (2016) 129:1373–82. doi: 10.1007/s00122-016-2709-z

9. Zhu H, Zhou X. Statistical methods for Snp heritability estimation and partition: a review. *Comput Struct Biotechnol J*. (2020) 18:1557–68. doi: 10.1016/j.csbj.2020.06.011

10. Xiaoyan S, Qunhao N, Jing J, et al. Identifying candidate genes for litter size and three morphological traits in Youzhou dark goats based on genome-wide Snp markers. *Genes*. (2023) 14:1183. doi: 10.3390/genes14061183

11. Vera M, Gulnara S, Valery V, et al. Genetic diversity, population structure and phylogeny of indigenous goats of Mongolia revealed by Snp genotyping. *Animals*. (2022) 12:221. doi: 10.3390/ani12030221

12. Flint J. GWAS. *Curr Biol*. (2013) 23:R265–6. doi: 10.1016/j.cub.2013.01.040

13. Portelli MA, Hodge E, Sayers I. Genetic risk factors for the development of allergic disease identified by genome-wide association. *Clin Exp Allergy*. (2015) 45:21–31. doi: 10.1111/cea.12327

14. Sun T, Wang J, Zheng M, Cai C, Yu J, Fu L, et al. Assessment of the relationship between genetic determinants of obesity, unhealthy eating habits and chronic obstructive pulmonary disease: a Mendelian randomisation study. *COPD*. (2024) 21:2309236. doi: 10.1080/15412555.2024.2309236

15. Klein RJ, Zeiss C, Chew EY, Tsai JY, Sackler RS, Haynes C, et al. Complement factor H polymorphism in age-related macular degeneration. *Science*. (2005) 308:385–9. doi: 10.1126/science.1109557

16. Duerr RH, Taylor KD, Brant SR, Rioux JD, Silverberg MS, Daly MJ, et al. A genome-wide association study identifies Il23R as an inflammatory bowel disease gene. *Science*. (2006) 314:1461–3. doi: 10.1126/science.1135245

17. Gail MH, Pfeiffer RM, Wheeler W, Pee D. Probability of detecting disease-associated single nucleotide polymorphisms in case-control genome-wide association studies. *Biostatistics*. (2008) 9:201–15. doi: 10.1093/biostatistics/kxm032

18. Heidaritabar M, Bink M, Dervishi E, et al. Genome-wide association studies for additive and dominance effects for body composition traits in commercial crossbred Piétrain pigs. *J Anim Breed Genet*. (2023) 140:413–30. doi: 10.1111/jbg.12768

19. Krivoruchko A, Likhovid A, Kanibolotskaya A, et al. Genome-wide search for associations with meat production parameters in Karachaevsky sheep breed using the Illumina bead Chip 600 K. *Genes*. (2023) 14:1288. doi: 10.3390/genes14061288

20. Sood V, Rodas-González A, Valente TS, Virtuoso MCS, Li C, Lam S, et al. Genome-wide association study for primal cut lean traits in Canadian beef cattle. *Meat Sci*. (2023) 204:109274. doi: 10.1016/j.meatsci.2023.109274

21. Takenaka M. Quantification of mitochondrial Rna editing efficiency using sanger sequencing data. *Methods Mol Biol*. (2022) 2363:263–78. doi: 10.1007/978-1-0716-1653-6_18

22. Cheng LY, Haydu LE, Song P, Nie J, Tetzlaff MT, Kwong LN, et al. High sensitivity Sanger sequencing detection of Braf mutations in metastatic melanoma Ffpe tissue specimens. *Sci Rep*. (2021) 11:9043. doi: 10.1038/s41598-021-88391-5

23. Danilov KA, Nikogosov DA, Musienko SV, Baranova AV. A comparison of bead Chip and Wgs genotyping outputs using partial validation by sanger sequencing. *BMC Genomics*. (2020) 21:528. doi: 10.1186/s12864-020-06919-x

24. Zhang Z, Ersoz E, Lai CQ, Todhunter RJ, Tiwari HK, Gore MA, et al. Mixed linear model approach adapted for genome-wide association studies. *Nat Genet*. (2010) 42:355–60. doi: 10.1038/ng.546

25. Ahn E, Prom LK, Park S, et al. Genome-wide association analysis uncovers genes associated with resistance to head smut Pathotype 5 in Senegalese Sorghum accessions. *Plants*. (2024) 13:977. doi: 10.3390/plants13070977

26. Sahana G, Guldbrandtsen B, Bendixen C, Lund MS. Genome-wide association mapping for female fertility traits in Danish and Swedish Holstein cattle. *Anim Genet*. (2010) 41:579–88. doi: 10.1111/j.1365-2052.2010.02064.x

27. Li H, Mazumder R, Lin X. Accurate and efficient estimation of local heritability using summary statistics and the linkage disequilibrium matrix. *Nat Commun*. (2023) 14:7954. doi: 10.1038/s41467-023-43565-9

28. Slatkin M. Linkage disequilibrium — understanding the evolutionary past and mapping the medical future. *Nat Rev Genet*. (2008) 9:477–85. doi: 10.1038/nrg2361

29. Waples RS. Practical application of the linkage disequilibrium method for estimating contemporary effective population size: a review. *Mol Ecol Resour*. (2024) 24:e13879. doi: 10.1111/1755-0998.13879

30. Qiao L, Gao X, Jia Z, Liu X, Wang H, Kong Y, et al. Identification of adult resistant genes to stripe rust in wheat from southwestern China based on Gwas and Wgcna analysis. *Plant Cell Rep*. (2024) 43:67. doi: 10.1007/s00299-024-03148-4

31. Sharma P, Senapati S, Goyal LD, Kaur B, Kamra P, Khetarpal P. Genome-wide association study (Gwas) identified Pcos susceptibility variants and replicates reported risk variants. *Arch Gynecol Obstet*. (2024) 309:2009–19. doi: 10.1007/s00404-024-07400-w

32. Ahlawat S, Arora R, Sharma R, Sharma U, Kaur M, Kumar A, et al. Skin transcriptome profiling of Changthangi goats highlights the relevance of genes involved in pashmina production. *Sci Rep*. (2020) 10:6050. doi: 10.1038/s41598-020-63023-6

33. Wu C, Ma S, Zhao B, Qin C, Wu Y, di J, et al. Drivers of plateau adaptability in cashmere goats revealed by genomic and transcriptomic analyses. *BMC Genomics*. (2023) 24:428. doi: 10.1186/s12864-023-09333-1

34. Xu Z, Wang X, Song X, An Q, Wang D, Zhang Z, et al. Association between the copy number variation of Ccser1 gene and growth traits in Chinese *Capra hircus* (goat) populations. *Anim Biotechnol*. (2023) 34:1377–83. doi: 10.1080/10495398.2022.2025818

35. Xue Y, Li C, Duan D, Wang M, Han X, Wang K, et al. Genome-wide association studies for growth-related traits in a crossbreed pig population. *Anim Genet*. (2021) 52:217–22. doi: 10.1111/age.13032

36. Yurchenko AA, Deniskova TE, Yudin NS, Dotsev AV, Khamiruev TN, Selionova MI, et al. High-density genotyping reveals signatures of selection related to acclimation and economically important traits in 15 local sheep breeds from Russia. *BMC Genomics*. (2019) 20:294. doi: 10.1186/s12864-019-5537-0

37. Strittmatter L, Li Y, Nakatsuka NJ, Calvo SE, Grabarek Z, Mootha VK. Clybl is a polymorphic human enzyme with malate synthase and β-methylmalate synthase activity. *Hum Mol Genet*. (2014) 23:2313–23. doi: 10.1093/hmg/ddt624

38. Li W, Wang B, Dai J, Kou Y, Chen X, Pan Y, et al. Partial order relation-based gene ontology embedding improves protein function prediction. *Brief Bioinform*. (2024) 25:77. doi: 10.1093/bib/bbae077

39. Zhang YH, Huang F, Li J, Shen WF, Chen L, Feng KY, et al. Identification of protein-protein interaction associated functions based on gene ontology. *Protein J*. (2024). doi: 10.1007/s10930-024-10180-6

40. Zhao Y, Yang Z, Hong Y, Yang Y, Wang L, Zhang Y, et al. Protein function prediction with functional and topological knowledge of gene ontology. *IEEE Trans Nanobioscience*. (2023) 22:755–62. doi: 10.1109/TNB.2023.3278033

41. Zhao B, Luo H, He J, Huang X, Chen S, Fu X, et al. Comprehensive transcriptome and methylome analysis delineates the biological basis of hair follicle development and wool-related traits in merino sheep. *BMC Biol*. (2021) 19:197. doi: 10.1186/s12915-021-01127-9

42. Hadi S, Alexander AJ, Vélez-Ortega AC, Frolenkov GI. Myosin-Xva controls both staircase architecture and diameter gradation of Stereocilia rows in the auditory hair cell bundles. *J Assoc Res Otolaryngol*. (2020) 21:121–35. doi: 10.1007/s10162-020-00745-4

43. Wang Z, Zhang H, Yang H, Wang S, Rong E, Pei W, et al. Genome-wide association study for wool production traits in a Chinese merino sheep population. *PLoS One*. (2014) 9:e107101. doi: 10.1371/journal.pone.0107101

frontiers | Frontiers in Veterinary Science

TYPE Original Research
PUBLISHED 11 June 2024
DOI 10.3389/fvets.2024.1405541



OPEN ACCESS

EDITED BY
Izhar Hyder Qazi,
Shaheed Benazir Bhutto University of Veterinary & Animal Sciences, Pakistan

REVIEWED BY
Feng Wang,
Southwest University, China
Qiaoling Zhao,
Jiangsu University of Science and Technology, China

*CORRESPONDENCE
Zhengying You
✉ zyyou@zstu.edu.cn

RECEIVED 25 March 2024
ACCEPTED 23 May 2024
PUBLISHED 11 June 2024

CITATION
Wen H, Wang Y, Ji Y, Chen J, Xiao Y, Lu Q, Jiang C, Sheng Q, Nie Z and You Z (2024) Effect of acute exposure of Hg on physiological parameters and transcriptome expression in silkworms (*Bombyx mori*). *Front. Vet. Sci.* 11:1405541. doi: 10.3389/fvets.2024.1405541



# Effect of acute exposure of Hg on physiological parameters and transcriptome expression in silkworms (*Bombyx mori*)

Huanhuan Wen[1,2], Yanan Wang[1,2], Yongqiang Ji[1,2], Jing Chen[1,2], Yao Xiao[1,2], Qixiang Lu[1], Caiying Jiang[1,2], Qing Sheng[1,2], Zuoming Nie[1,2] and Zhengying You[1,2]*

[1]College of Life Sciences and Medicine, Zhejiang Sci-Tech University, Hangzhou, China, [2]Zhejiang Provincial Key Laboratory of Silkworm Bioreactor and Biomedicine, Zhejiang Sci-Tech University, Hangzhou, China

Mercury (Hg) contamination poses a global threat to the environment, given its elevated ecotoxicity. Herein, we employed the lepidopteran model insect, silkworm (*Bombyx mori*), to systematically investigate the toxic effects of Hg-stress across its growth and development, histomorphology, antioxidant enzyme activities, and transcriptome responses. High doses of Hg exposure induced evident poisoning symptoms, markedly impeding the growth of silkworm larvae and escalating mortality in a dose-dependent manner. Under Hg exposure, the histomorphology of both the midgut and fat body exhibited impairments. Carboxylesterase (CarE) activity was increased in both midgut and fat body tissues responding to Hg treatment. Conversely, glutathione S-transferase (GST) levels increased in the fat body but decreased in the midgut. The transcriptomic analysis revealed that the response induced by Hg stress involved multiple metabolism processes. Significantly differently expressed genes (DEGs) exhibited strong associations with oxidative phosphorylation, nutrient metabolisms, insect hormone biosynthesis, lysosome, ribosome biogenesis in eukaryotes, and ribosome pathways in the midgut or the fat body. The findings implied that exposure to Hg might induce the oxidative stress response, attempting to compensate for impaired metabolism. Concurrently, disruptions in nutrient metabolism and insect hormone activity might hinder growth and development, leading to immune dysfunction in silkworms. These insights significantly advance our theoretical understanding of the potential mechanisms underlying Hg toxicity in invertebrate organisms.

KEYWORDS

***Bombyx mori*, mercury-stress, toxicity effect, transcriptome, oxidative stress**

## 1 Introduction

Mercury (Hg) is one of the highly toxic heavy metals prevalent in our environment, and its substantial accumulation via the food chain poses severe adverse effects on human health (1, 2). The historical Minamata mass epidemic in Iraq and Japan vividly showcased the profound toxicity of Hg (3, 4). Pollution by Hg stems primarily from a range of natural and anthropogenic activities, including volcanic eruptions, rock weathering, and diverse industrial processes (5). Hg exists in different forms in the environment. Elemental Hg can undergo

oxidation, forming soluble species ($Hg^{2+}$), which, through natural processes, may further convert into the highly toxic methylmercury (MeHg) species (6). Human exposure to Hg has been associated with multiple adverse effects on the gastrointestinal system, kidneys, central nervous system, and the developing fetus (7, 8). Consequently, it is imperative to thoroughly investigate the responses and mechanisms of Hg exposure on organisms.

The primary toxicity mechanism of Hg lies in its capacity to bind sulfhydryl groups in biomolecules and inhibit specific antioxidant factors, leading to the overproduction of reactive oxygen species (ROS) and triggering oxidative stress. Consequently, enzymes, lipids, and nucleic acids suffer damage, ultimately resulting in cell death (9). In response to Hg-induced oxidative stress, the induction of antioxidant defense systems becomes paramount (10). Crucial players in this defense include glutathione S-transferases (GSTs), carboxylesterases (CarEs), superoxide dismutase (SOD), catalase (CAT), cytochrome P450 monooxygenases (CYP450s), glutathione peroxidase (GPX), thioredoxin reductase (TrXR), and glutathione reductase (GR) which play pivotal roles in mitigating the adverse effects of ROS and are commonly employed as indicators of xenobiotic-mediated oxidative damage (11, 12). Another critical defense against potential environmental pollutants is associated with immune response, which poses potential threats to the host's health, making it more susceptible to various pathogens, and elevating the risk of death from infectious diseases (13). Previous studies have suggested that the Toll and immune deficiency (IMD) signaling pathways, along with the JAK/STAT pathway and the steroid hormone 20-hydroxyecdysone (20E), play regulatory roles in the innate immunity of the silkworm (*Bombyx mori*) (14). Disruption of these signaling pathways may disturb the expression of antimicrobial peptides (AMP), resulting in immune system dysfunction. Despite the existing estimations of Hg toxicity from various perspectives, there is a scarcity of research exploring the mechanisms of damage in invertebrate animals.

Silkworm is an extensively domesticated, silk-producing, oligophagous insect primarily nourished by fresh mulberry leaves. Mulberry trees tend to accumulate heavy metal ions from soil and atmosphere, which are subsequently stored in their leaves. Silkworms feeding on these contaminated leaves exhibit diminished growth, development, and cocoon silk production, thereby posing a significant challenge to the silk industry (15). Consequently, there is a pressing need to investigate the toxicological impacts of heavy metals and elucidate detoxification mechanisms in silkworms, given the substantial environmental accumulation of heavy metals (16). Owing to its remarkable characteristics and longstanding history of artificial domestication, the silkworm has obtained considerable attention from scientists across various fields, particularly in recent years, encompassing environmental pollution, nanomaterial toxicity assessment, pesticides, and medicine (17–20). The Chinese Oak silkworm (*Antheraea pernyi*) among the best-known species of wild silkworms has been used as a well-known wild silk moth in sericultural and medicine industry for hundreds of years. Notably, they have seen increased utilization in studies involving heavy metals, with research focusing on the potential toxicity effects of cadmium (21), silver (22), uranium (23), and lead (24) *in vivo*. However, there remains a paucity of research specifically addressing Hg exposure processes, which could be pivotal in elucidating the underlying mechanisms of Hg toxicity and tracking out the vital targets for Hg tolerance.

To better understand the underlying mechanisms of Hg exposure in *B. mori*, we focused on the larval midgut and fat body. As the two pivotal organs of the silkworms, the midgut functions as the primary surface and barrier, crucial in preventing the absorption of diverse toxins into the body; the fat body, a functionally diverse tissue involved in storage, metabolism, and protein synthesis, facilitates nutrition metabolism and accommodates variable physiological demands throughout its life cycle (25, 26). Therefore, these two organs were chosen as model systems in this study to investigate the effects of Hg exposure comprehensively. In the present study, we evaluated the sensitivity of *B. mori* exposed to varying concentrations of Hg stress. Our assessment examined growth status, developmental changes, and antioxidant enzyme activities. Furthermore, we conducted a transcriptomic analysis in the midgut and fat body tissues to elucidate key genes and pathways associated with the silkworm's response to Hg exposure. These findings aim to provide the potential toxicological effects of Hg responses at biochemical and molecular levels and offer a holistic perspective on the risk assessment of Hg exposure in the environment.

## 2 Materials and methods

### 2.1 Insect rearing and chemicals

*Nistari*, a multivoltine silkworm strain used in our experiment was sourced from the Zhejiang Academy of Agricultural Sciences (China). Silkworm larvae were reared at a temperature of 25 ± 2°C and 75% relative humidity as described in previous research (27). Larvae on the 2nd day of the 5th instar were chosen, and then randomly divided into six groups (90 larvae for each group) in each treatment, and each group was triplicated. The standard Hg liquid, containing 5% $HNO_3$, was procured from Solarbio (Beijing, China).

### 2.2 Hg treatment

To examine the impact of Hg stress on silkworms, we employed five concentrations of Hg (20, 40, 60, 80, and 100 mg/L). Solutions with these Hg concentrations were used to briefly soak mulberry leaves for approximately 1 min, naturally dried, and then provided to the larvae. The mulberry leaves were dipped in deionized water and used as the untreated group. Each group was supplied with the equivalent weight of mulberry leaves. Body weight and survival rate were recorded on 1-, 2-, 3-, 4-, 5-, and 6-day treatment. After 72 h Hg exposure, silkworm midgut and fat body samples were collected from each group in triplicates. Samples were kept at −80°C for RNA extraction and enzyme activity assay.

### 2.3 Tissue processing and H and E staining

Following exposure to Hg treatment, the midgut and fat body were collected for hematoxylin-eosin (HE) staining, as described in prior studies (28, 29). Briefly, the collected samples were initially fixed in 4% paraformaldehyde at 25°C no more than 24 h, and then dehydrated using a series of gradient ethanol baths ranging from 70 to 100% to displace water, vitrified with dimethylbenzene, infiltrated by paraffin

wax, and cut into sections (5 μm). The obtained tissue sections were dyed using 2% Mayer's hematoxylin and 1% eosin. Slides were observed and the light microscope (SOPTOP, CX40) was used to capture the images.

## 2.4 Antioxidant enzyme activities assay

To detect the effects of oxidative stress under different concentrations of Hg exposure on silkworms, the enzyme activities of carboxylesterase (CarE) and glutathione S-transferases (GSTs) were determined after 72 h Hg exposure. The silkworm midgut and fat body samples were extracted from each group in triplicates. The homogenates of midgut and fat body in tissue lysate were centrifuged at 12,000 rpm at 4°C for 15 min. The supernatants were obtained and used for enzyme activity measurement. The BCA Protein Assay Kit (P0010, Beyotime, China) was chosen for the protein content measurement. The enzyme activities of GST and CarE were determined by glutathione S-transferase (GST) Assay Kit (Serial No: BC0355) and carboxylesterase (CarE) Assay Kit (Serial No: BC0845) from Solarbio Life Sciences (Beijing, China) by the instruction for use. At least three replications were performed for enzyme assay.

## 2.5 Total RNA preparation, library construction, and transcriptome sequencing (RNA-seq)

The total RNA of midgut and fat bodies from the group exposed with 80 mg/L Hg was obtained using TRIzol reagent (Invitrogen, Carlsbad, CA, United States) as described previously (30), and used for the transcriptome sequencing. The Hg concentration of 80 mg/L was determined by a series of preliminary experiments and relevant literature was used for the following experiments (21). Library preparation, clustering, and RNA-Seq techniques of 12 samples (with three biological replicates) were carried out at Beijing Novogene (Beijing, China). The total RNA quality and quantity were analyzed with RNA Nano 6000 Assay Kit by Agilent Technologies 2100 Bioanalyzer (Agilent Technologies, CA, United States). RIN (RNA integrity number) of the RNA samples of more than 8.5 were prepared for RNA-seq. Libraries were created with the NEB Next Ultra RNA Library Prep Kit for Illumina (NEB, United States) according to the Kit's instructions. Using an Illumina HiSeq 2000 platform (Illumina, United States), sequencing of the 12 samples was conducted, and the paired-end reads between 125 to 150 bp were generated. After sequencing, adapter sequences, and low-quality reads were deleted, and then clean reads were generated from raw reads. GC content, Q20, and Q30 of clean reads were adopted to estimate the reliability of data. The clean data were mapped to the SilkBase (31) and KAIKObase (32) to get read information using HISAT2 (33). The expression levels of the identified genes were evaluated by fragments per kilobase of transcript per million mapped reads (FPKM) (34).

## 2.6 Bioinformatic analysis

The DEGs analysis between Hg and ultrapure water treatment was performed by DESeq2 (35). The standard of $|\log2FoldChange| \geq 1.0$ & $p_{adj} \leq 0.05$ was carried out to identify the DEGs. Gene Ontology (GO) and Kyoto Encyclopedia of Genes and Genomes (KEGG) were performed for classification and pathway enrichment analysis, respectively, with $p_{adj} \leq 0.05$.

## 2.7 Expression analysis of DEGs by quantitative real-time PCR

The real-time PCR (RT-qPCR) was performed to further confirm the reliability of RNA-Seq data. The total RNA of the midgut and fat body were extracted from the larvae treated with Hg exposure for 72 h and the control group using TRIzol reagent (Invitrogen, United States) as described above. PCR primers (Supplementary Table S1) were designed and then synthesized via Sangon Biotech (Shanghai, China). The Prime Script kit including the gDNA Eraser (Takara, China) was used to synthesize the first cDNA based on the instructions. The RT-qPCR was performed on an ABI 7500 Real-Time PCR system (Applied Biosystems, CA) using a SYBR®Premix Ex TaqTM II kit (Takara). The amplification reaction was carried out in a 20.0 μL reaction mixture as follows: denaturation at 95°C for 30 s followed by 40 cycles of 95°C for 5 s and 60°C for 30 s, and melting curves were constructed. The *BmRp49* (accession number: NM_001098282) was adopted as a reference and the ΔΔCt method (36) was employed to calculate the relative expression. At least three independent replicates were conducted.

## 2.8 Statistical analysis

Statistical analyses and graphs were performed using OriginPro (version 2022b). One-way ANOVA analysis (Tukey's *post hoc* test) was used to compare variance between the experimental and control groups. The $p < 0.05$ represented the significance of the data compared to the control group.

# 3 Results

## 3.1 Impact of Hg treatment on the growth and development of *Bombyx mori*

To assess the effects of Hg stress on silkworms, we exposed them to different concentrations of Hg-treated mulberry leaves for 144 h (6 days). The body weights of the low-concentration groups (20 mg/L, 40 mg/L, 60 mg/L) exhibited a slight increase compared with the control group, while the high-concentration groups (80 mg/L and 100 mg/L) experienced a reduction during Hg treatment (Figure 1A and Supplementary Table S2). Although almost all larvae successfully formed cocoons, some in the high-concentration groups, particularly at 100 mg/L, produced thinner cocoons and even succumbed (Figure 1B). Additionally, histological staining was performed to further clarify histomorphology and structure variations in midguts and fat bodies exposed to 100 mg/L Hg for 72 h. As shown in Figure 2, midgut cell morphology changed with the emergence of bubble-like structure under Hg stress. Histopathological observation of fat bodies also revealed noticeable nuclear pyknosis. These results collectively indicate that exposure to a high concentration of Hg induces morphological and structural alterations in midguts and fat bodies, significantly hindering the normal growth and development of fifth-instar silkworm larvae in a dose-dependent manner.

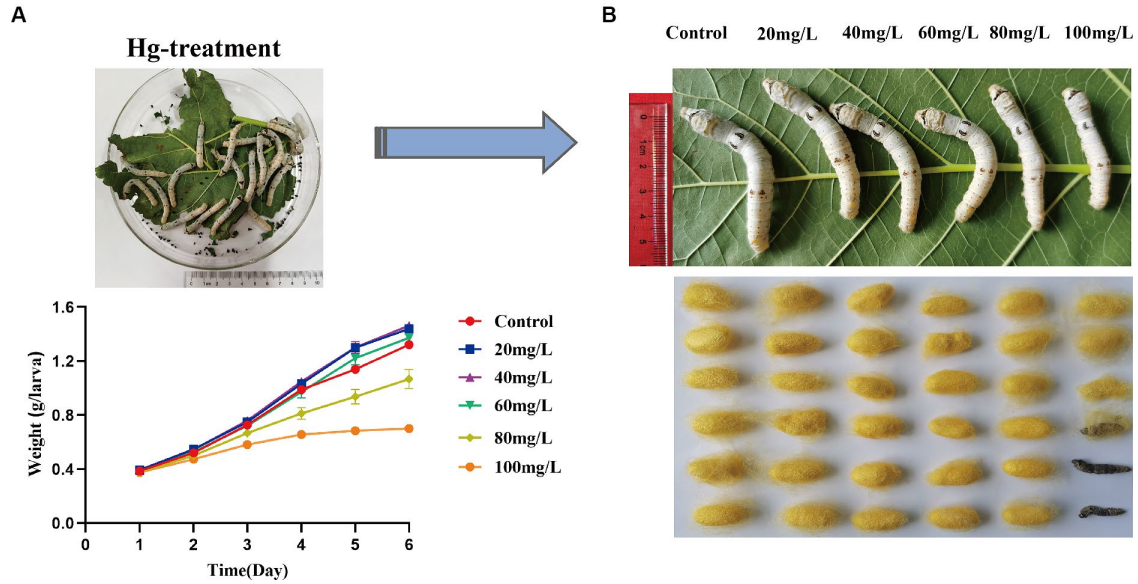


FIGURE 1
Symptoms and toxicological characteristics of silkworms caused by Hg exposure. **(A)** The trend of silkworm larvae body weight changes after 1, 2, 3, 4, 5, and 6 days of Hg exposure. **(B)** The larvae and cocoon features of 20 mg/L, 40 mg/L, 60 mg/L, 80 mg/L, and 100 mg/L Hg treatment, respectively.

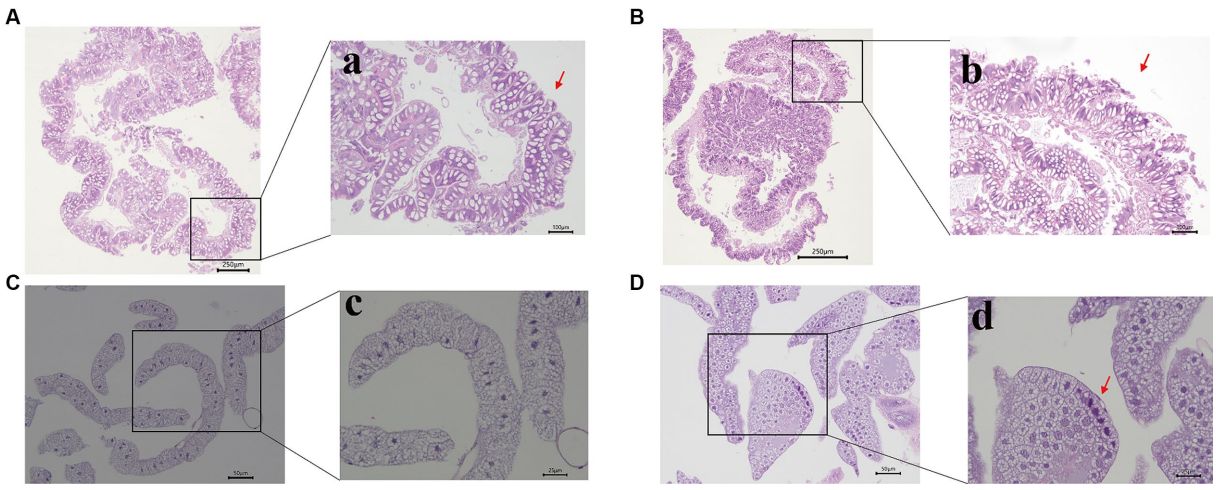


FIGURE 2
Morphological changes of the midgut and fat bodies with different treatments. **(A,B)** are the pictures of the midgut of the control and experimental group; **a,b** are pictures with high magnification. The bubble-like structure was generated in the midgut (indicated by the red arrowhead). **(C,D)** are the pictures of the fat bodies of the control and treatment group; **c,d** are pictures with high magnification. Nuclear pyknosis emerged in the fat body (indicated by the red arrowhead). Bars: **A,B**: 250 μm; **a,b**: 100 μm; **C,D**: 50 μm; **c,d**: 25 μm.

## 3.2 Analysis of antioxidant enzyme activity in response to Hg stress

In this investigation, we observed changes in antioxidant enzyme activities between experimental and the control group after 72 h of Hg exposure. Carboxylesterase (CarE) enzyme activity exhibited a gradual increase with increased concentrations of Hg exposure both in the midgut and fat body, and then followed by a gradual decline with further concentration increase (Figures 3A,B). Conversely, Glutathione S-transferase (GST) activity in the midgut (Figure 3C) showed a significant decrease. In contrast, the fat body demonstrated a gradual increase in GST enzyme activity, and subsequently declining with further concentration (Figure 3D) increase.

## 3.3 RNA-sequencing and DEGs analysis in response to Hg exposure

Data quality from transcriptome sequencing is presented in Supplementary Table S3. Following the removal of redundant and low-quality reads, each group yielded more than 40 million clean reads, representing almost 99% of the raw reads. The values of Q20 and Q30 were 97 and 93% for all quality scores, respectively, and the

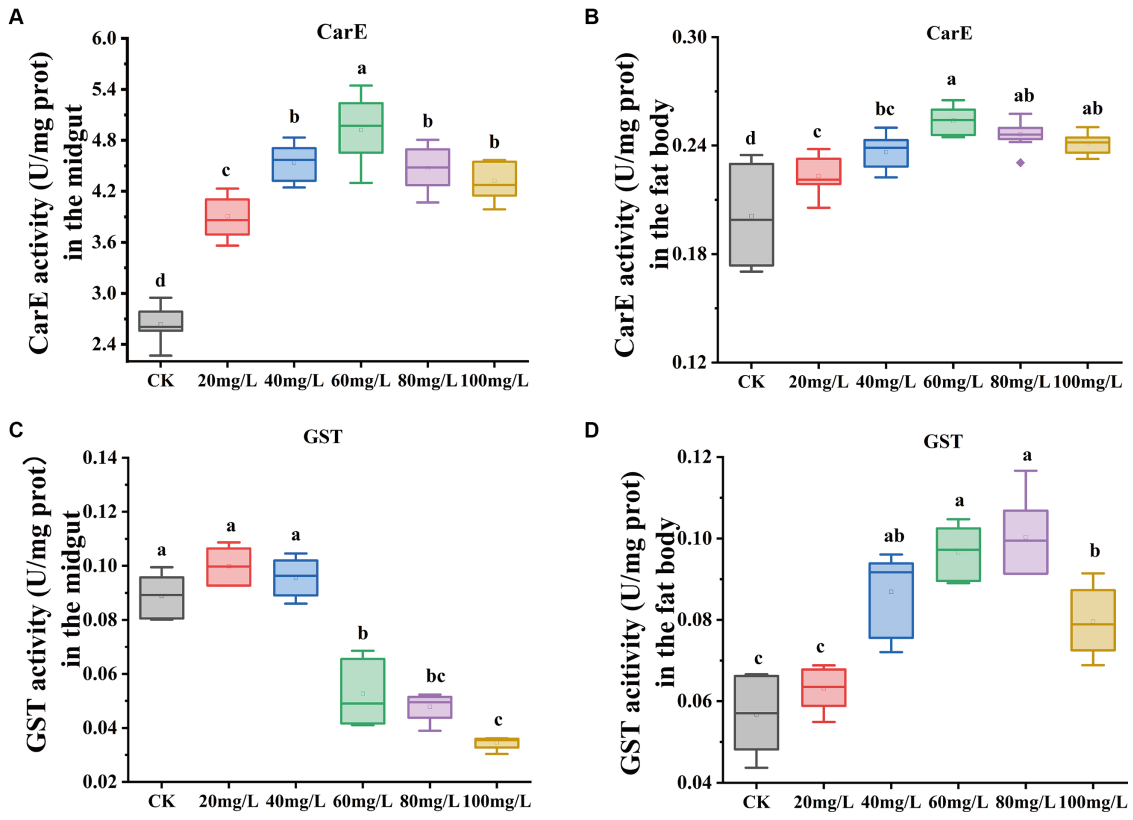


FIGURE 3
Effect on antioxidant enzyme activities in the midgut and fat body under exposure at different concentrations of Hg. **(A)** The CarE enzyme activity in the midgut. **(B)** The CarE enzyme activity in the fat body. **(C)** The GST enzyme activity in the midgut. **(D)** The GST enzyme activity in the fat body. Data are shown as the mean ± SD. Significant differences across the treatments at $p < 0.05$ were indicated using different letters (one-way ANOVA with Tukey's *post hoc* test).

range of GC contents was from 44.23 to 47.55%. High consistency across different sample replicates (Figure 4A) was indicated by the Pearson correlation coefficient. Subsequently, a principal component analysis (PCA) model was established based on the expression of unigenes, revealing differences among the four groups (Supplementary Figure S1). These findings indicated that the quality of sequencing data was relatively high, and the subsequent annotation analysis could be performed.

To further assess the impact of Hg treatment on different tissues, we identified DEGs in both the midgut and fat body, comparing them with the reference groups using the DESeq2 method (Figure 4B). In the Hg_MG (80 mg/L) vs. CK_MG analysis, among the 1,142 identified DEGs, 482 were upregulated, and 660 were downregulated (Figure 4B; Supplementary Figure S2A and Supplementary Table S4). Similarly, in the analysis of Hg_FB (80 mg/L) vs. CK_FB, 805 DEGs showed increased expression, while 801 DEGs exhibited decreased expression out of the 1,606 identified DEGs (Figure 4B; Supplementary Figure S2B and Supplementary Table S5). Additionally, we found 809 and 1,273 DEGs specifically expressed in the midgut and fat body, respectively, with 333 DEGs common to both tissues, as illustrated in the Venn diagram (Figure 4C). Furthermore, for a comprehensive view of these DEGs, we conducted hierarchical clustering based on normalized FPKM values across the 12 samples (Figure 4D), offering a global understanding of gene expression changes.

## 3.4 Gene Ontology functional annotation of DEGs

We conducted GO enrichment analysis to elucidate the correlations between DEGs and biological functions (Figure 5). In the Hg_MG vs. CK_MG group, the highest percentages of GO terms in the biological process (BP) category were associated with "transmembrane transport" (82 DEGs). Within the cellular component (CC) class, the focus was on the "extracellular region" (26 DEGs). Notably, we found that GO terms were mainly grouped into "molecular function," with extensive assignments. The most prevalent "molecular function" assignment was "oxidoreductase activity" (61 DEGs). Additionally, crucial assignments like "peptidase activity" and "transporter activity" exhibited high enrichment levels, suggesting a widespread alteration in the molecular function of the midgut following Hg exposure (Figure 5A).

In the Hg_FB vs. CK_FB group, the most abundant category within the biological process was the "oxidation-reduction process" (82 DEGs). Cellular component categories featured prominently with DEGs distributed in the "extracellular region" (40 DEGs), "ribonucleoprotein complex" (30 DEGs), and "ribosome" (26 DEGs). Among the molecular functions, "oxidoreductase activity" (97 DEGs), "cofactor binding" (61 DEGs), and "structural molecular activity" (40 DEGs) were the predominant groups (Figure 5B). The GO analysis of DEGs in Hg_MG vs. CK_MG and Hg_MG vs. CK_MG groups are available in Supplementary Tables S6, S7, respectively.

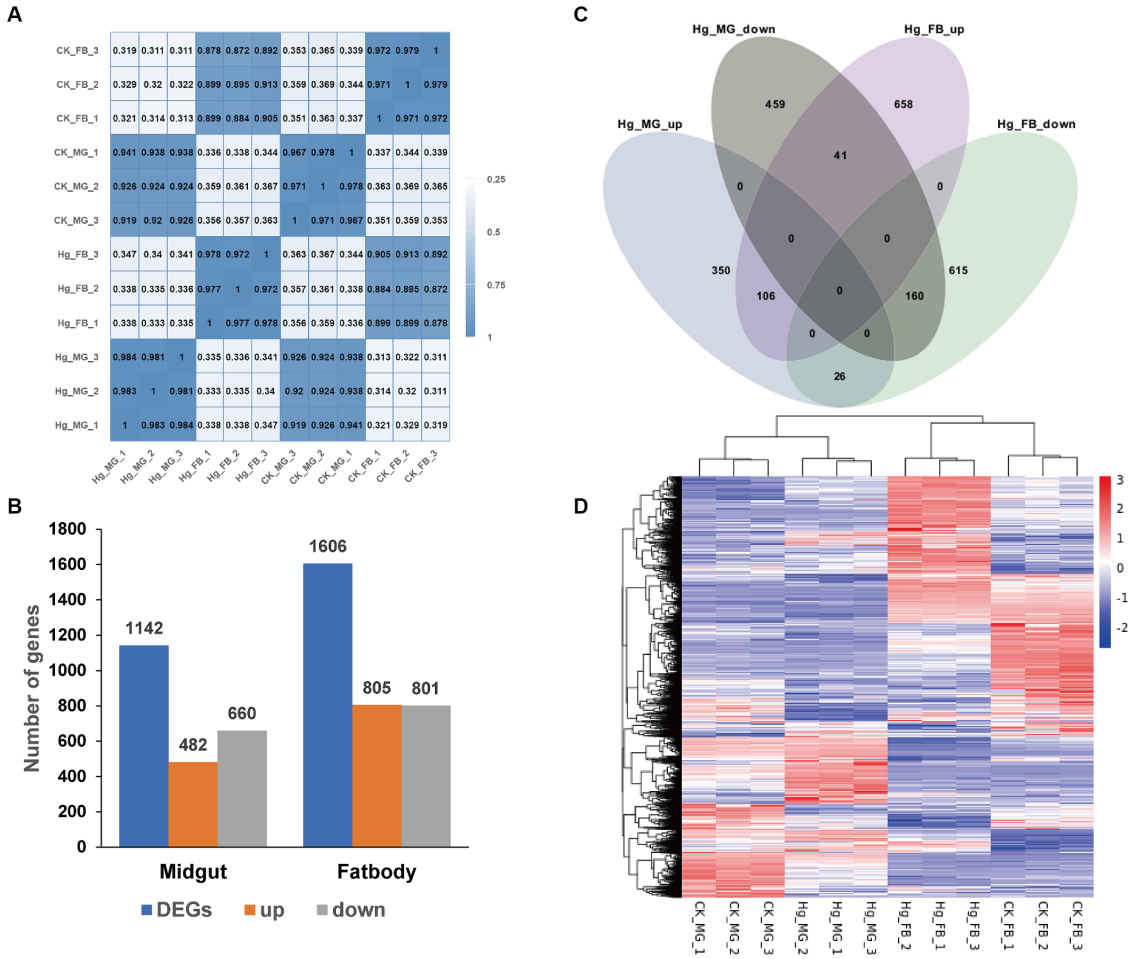


FIGURE 4
Comparative analysis of DEGs in the midgut and fat body after Hg stress. **(A)** Pearson's correlation analysis among the 12 samples. The color of the heat map is on behalf of the degree of correlation among samples. **(B)** The overview of DEGs (the up-regulated and down-regulated genes) in the midgut and fat body. **(C)** Venn diagram analysis for DEGs in the midgut and fat body. MG, midgut; FB, fat body; up, up-regulated DEGs; down, down-regulated DEGs. **(D)** The global changes of DEGs across the 12 samples. Hierarchical clustering of DEGs was generated after Hg treatment. The color scale represents the log2 transformed FPKM value based on the row scale. Their phylogenetic relationships were shown on the left tree. The top tree showed the cluster relationship of the samples.

These findings underscore the involvement of numerous metabolic processes and organelle functions in response to Hg exposure in the midgut and fat body of silkworms.

## 3.5 KEGG pathway functional annotation of DEGs

Following annotation, the enrichment analysis unveiled that a substantial number of DEGs were predominantly associated with Metabolism, Genetic information processing, Environmental information processing, Cellular processes, or Organismal systems. Notably, metabolism-related pathways exhibited a high clustering of DEGs in both the midgut and fat body organs (Figure 6). A total of 277 DEGs were allocated to 98 known pathways, with 26 pathways significantly enriched ($p < 0.05$) in the Hg_MG vs. CK_MG group, distributed across five categories (Figure 6A and Supplementary Table S8). Twenty pathways were implicated in diverse metabolic processes, with one dedicated to genetic information processing, another linked to environmental information processing, two involved in cellular processes, and one relevant to organismal systems. The highest number of DEGs was associated with the "lysosome," followed by "metabolism of xenobiotics by cytochrome P450," "drug metabolism-other enzymes," and "drug metabolism-cytochrome P450," indicating their crucial roles in the context of Hg exposure. Additionally, certain pathways demonstrated a connection between metabolism and antioxidant defense, such as "retinol metabolism," "ascorbate and aldarate metabolism," "carbon metabolism," and "apoptosis-fly." Notably, "ribosome biogenesis in eukaryotes" was linked to protein synthesis. While the "ECM-receptor interaction" pathway was associated with environmental concentrations.

In the Hg_FB vs. CK_FB group, 458 DEGs were assigned to 107 known pathways (Supplementary Table S9), which were categorized into four distinct groups. Figure 6B illustrated the 26 significant pathways ($p < 0.05$) with 19 pathways linked to metabolism, three to genetic information processing, and one to environmental information processing, one to organismal systems. As depicted in Figure 6B and detailed in Supplementary Table S9, DEGs were notably enriched in key signaling pathways, including "oxidative phosphorylation,"

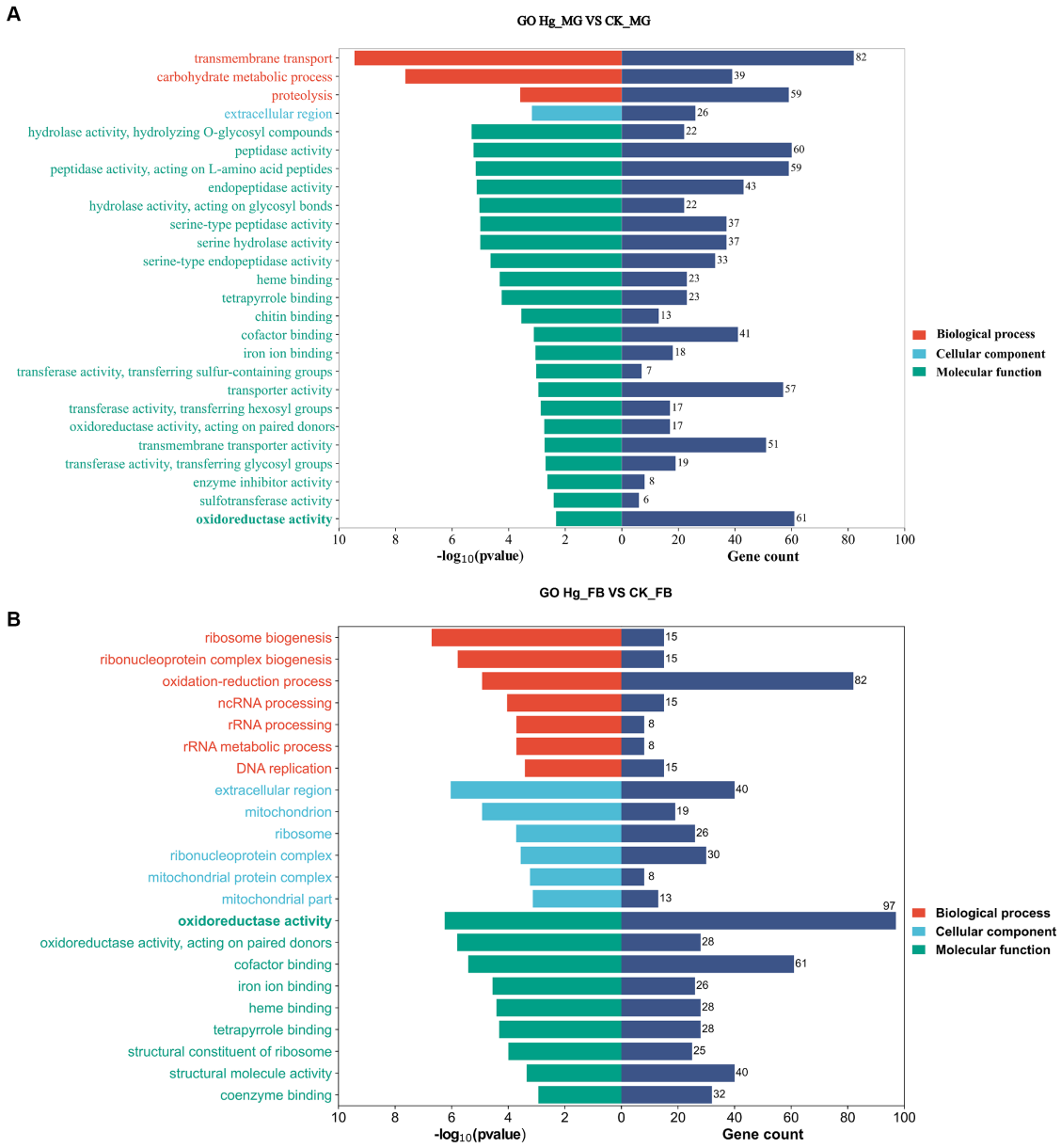


FIGURE 5
GO enrichment analysis in responsive DEGs caused by Hg stress. GO enrichment analysis of the DEGs after Hg exposure in groups **(A)** Hg_MG vs. CK_MG, and **(B)** Hg_FB vs. CK_FB. The *X*-axis is on behalf of the number of DEGs and -$\log_{10}$(*p*-value), and the *Y*-axis depicts various gene functions.

"ribosome biogenesis in eukaryotes," "ribosome," and "drug metabolism-other enzymes." Additionally, pathways such as "biosynthesis of amino acids," "metabolism of xenobiotics by cytochrome P450," "drug metabolism-cytochrome P450," "glycine, serine and threonine metabolism," and "ascorbate and aldarate metabolism" demonstrated associations with antioxidant defense and protein metabolism.

## 3.6 Key genes involved in the insect hormone metabolism signal pathway

This investigation reveals a noteworthy down-regulation of the ecdysone oxidase gene, *Cyp314a1*, in both the midgut and fat body following exposure to Hg (Figures 7A,B). Consequently, the ecdysone receptor complex EcR/USP and several downstream transcription factor genes, including *E74*, *E75*, *Rack1*, and *Hr3*, displayed reduced expression levels. Genes associated with the juvenile hormone biosynthesis and degradation pathway, such as *ALDH*, *JHAMT*, *P450*, *JHEH*, and *JHDH*, exhibited significant upregulation in the fat body, while JHAMT experienced decreased expression in the midgut. Moreover, juvenile hormone (JH) receptor *Met* and *USP*, *Kruppel homolog 1* (*Kr-h1*), *$Na^+/K+$-ATPase*, and *Lp-c* demonstrated reduced expression (Figure 7C). Additionally, alterations were observed in the expressions of *AKH2/3 and ILP*. 20-hydroxyecdysone (20E) and Insulin/insulin-like growth factor (IGF) signaling (IIS) are recognized as the two major factors regulating growth period and growth rate, respectively. These findings suggest significant perturbations in the

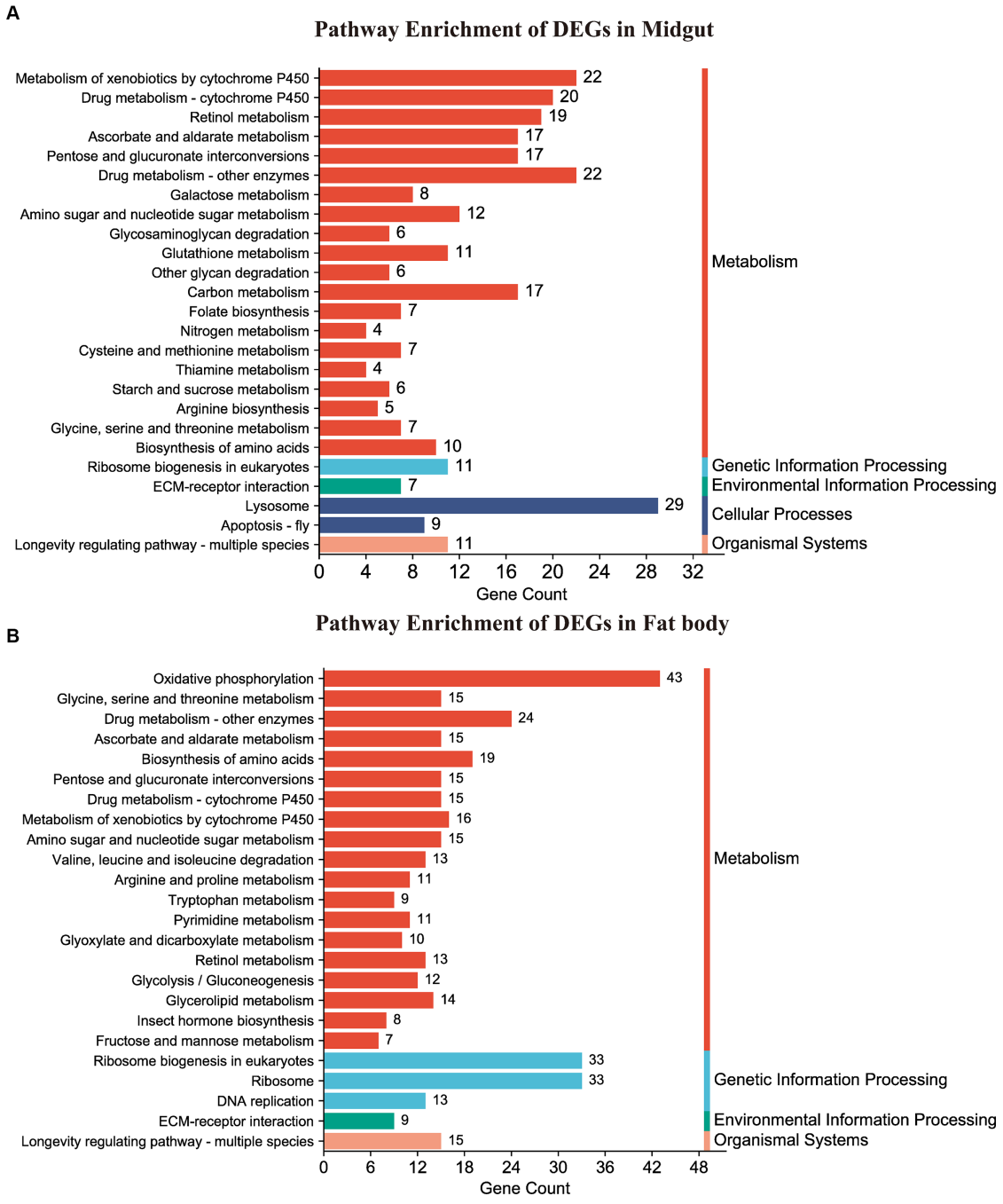


FIGURE 6
KEGG pathway enrichment analysis of DEGs. **(A,B)** Represented the DEG-enriched KEGG pathways in the midgut and fat body, respectively.

20E-JH biosynthesis and metabolism pathways due to Hg exposure, likely contributing to a decrease in body weight (Figure 7D).

## 3.7 RT-qPCR verification of the DEGs

To assess the reliability of the RNA-seq data, we conducted an RT-qPCR experiment on a set of 10 DEGs. The expression tendency of these DEGs was highly similar to the results of RNA-Seq, demonstrating the validity of RNA-Seq data for genes with different expression levels (Figure 8 and Supplementary Table S10).

# 4 Discussion

Hg contamination poses a significant global threat to both the environment and human health, exhibiting potent neurotoxic properties and instigating a range of adverse health effects (7, 37). In this study, we investigated the detrimental effects of acute Hg exposure on silkworms under varying concentrations, examining aspects such as development, histomorphology, antioxidant enzyme activities, and transcriptome of the larval midgut and fat body. The form, dose, and duration of Hg exposure determine the toxic effects, with even trace amounts capable of causing harm in the atmosphere (8). Lower

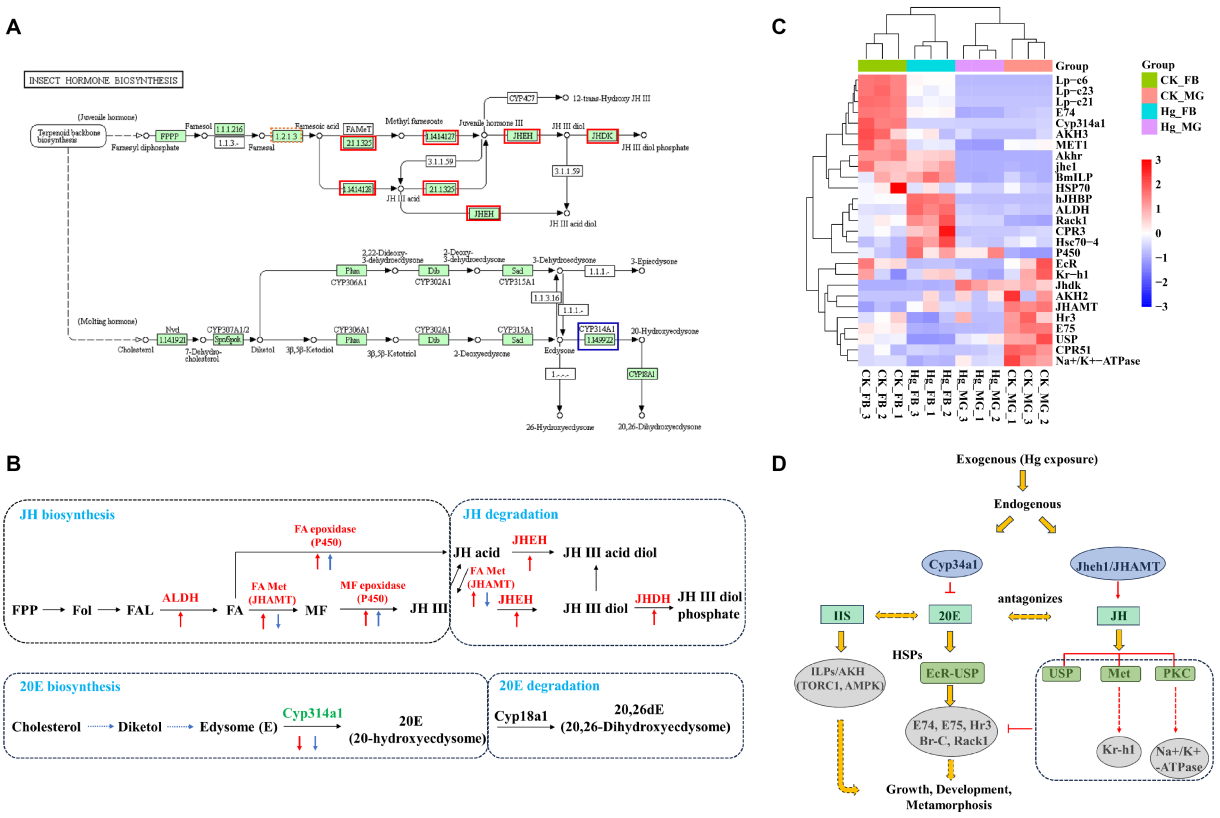


FIGURE 7
Expression pattern analysis of key genes associated with JH-20E metabolism pathway. **(A)** KEGG pathways of the insect hormone biosynthesis in the Hg_FB vs. CK_FB group. The increased DEGs were labeled with the red box, blue box represents decreased DEGs. **(B)** The DEGs are involved in the JH-20E metabolism pathway both in the midgut and fat body. The red arrow is associated with DEGs in the tissue of the fat body, the blue arrow represents DEGs in the midgut. The Up and down arrows mean up-regulated and down-regulated DEGs, respectively. **(C)** The heatmap of the important genes related to the JH-20E metabolism pathway. **(D)** Potential mechanisms of JH-20E regulated growth and development of silkworm after mercury exposure.

concentrations of Hg, upon acute exposure, did not induce any decline in body weight or fatality in larvae compared to the control group; in fact, there was a modest increase in body weight to a certain extent. Conversely, silkworms exposed to higher concentrations of Hg exhibited evident poisoning symptoms, significantly inhibiting their growth in a dose-dependent manner. Previous studies have noted alterations in silkworm weight following treatment with heavy metals (21, 38). In summary, the findings indicate that exposure of silkworms to high concentrations of Hg adversely influences their growth and development and interferes with fundamental metabolic processes.

Insects rely on a detoxification defense system to eliminate ROS and counteract oxidative damage (39). Essential antioxidant enzymes, including GSTs, SOD, CAT, GR, and GSHPX, serve as primary defenders against the adverse impacts of ROS and are established biomarkers for xenobiotic-mediated oxidative stress (40, 41). Our investigation revealed an up-regulation of CAT expression in the midgut, whereas a down-regulation was observed in the fat body. CAT plays a pivotal role in cellular defense against ROS damage by breaking down hydrogen peroxide ($H_2O_2$) into oxygen and water (42). Contrarily, increased GST activity was observed in the fat body, while it was inhibited in the midgut. A parallel increase in GST activity in the fat body has been documented in previous studies involving dinotefuran exposure (19), suggesting a potential association of GSTs with primary detoxification mechanisms in the fat body. Carboxylesterase (CarE) activity exhibited a gradual rise and then gradually declined with increasing concentration in both the midgut and fat body. Additionally, our results highlighted the enrichment of glutathione metabolism in the midgut. Functioning as the intracellular dominant antioxidant defense buffer, glutathione plays a pivotal role in numerous metabolic activities, sustaining intracellular glutathione homeostasis and redox balance (43). Cytochrome P450s, heme-thiolate enzymes crucial for primary defenses against various xenobiotics (44), are essential detoxification enzymes in insects, serving diverse physiological functions (45). Notably, the pathways "drug metabolism-cytochrome P450" and "metabolism of xenobiotics by cytochrome P450" were significantly enriched in both the midgut and fat body, underscoring their vital role in detoxification processes.

The DEGs were mainly involved in the poisoning process of Hg exposure, and KEGG and GO enrichment analysis identified several pivotal pathways, inducing the antioxidant defense system, the basal metabolic processes, development regulation, and immune dysfunction responses. Physiological concentrations of ROS play a crucial role in maintaining intracellular homeostasis (9). Conversely, serious oxidative stress can lead to damage to DNA, lipids, and proteins, when it exceeds the cell's antioxidant capacity (43). Our data indicate significant enrichment of pathways related to genetic information processing, including "Ribosome biogenesis in eukaryotes" in both the midgut and fat body, and "ribosome" and "DNA replication" in the fat body. Exposure to heavy metals can induce DNA damage through ROS production, resulting in increased DNA attacks and reduced repair

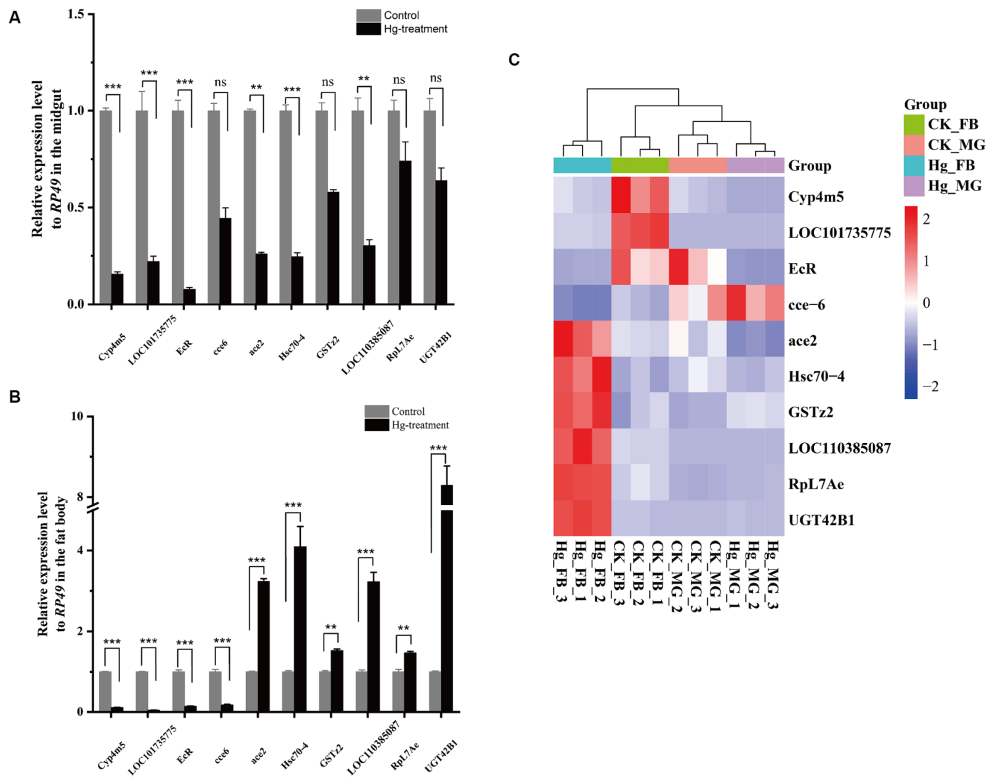


FIGURE 8
RT-qPCR analysis was carried out to confirm the DEGs identified by RNA-Seq. **(A)** The 10 DEGs in the Hg_MG vs CK_MG group were quantified by RT-qPCR. **(B)** The 10 DEGs in the Hg_FB vs CK_FB group were quantified by RT-qPCR. **(C)** The 10 DEGs in the Hg_MG vs CK_MG and Hg_FB vs CK_FB groups were quantified by RNA-seq. Data are shown as the mean ± SD of three biological replicates per treatment. The variance of DEGs between the treatment and control groups was determined by pairwise comparison (ns means no significance, $*p < 0.05$, $**p < 0.01$, and $***p < 0.001$).

processes (46). Additionally, pathways associated with cellular processes such as "lysosome" and "apoptosis-fly" were enriched in the midgut. Lysosomes, acting as degradation centers and signaling hubs, play vital roles in cellular homeostasis, growth, development, and aging (47). These findings suggest a shift towards apoptotic events following Hg exposure. Therefore, elevated ROS concentrations could impede cellular proliferation and differentiation, potentially triggering apoptosis in associated cells.

Oxidoreductases constitute a diverse class of enzymes that frequently catalyze oxidation-reduction reactions, playing a crucial role in maintaining cellular redox homeostasis; aberrant expression of these enzymes can lead to the onset of various disorders (48, 49). In our study, GO analysis revealed significant enrichment of the molecular function "oxidoreductase activity" in both the midgut and fat body, while the biological process "oxidation–reduction process" was notably enriched in the fat body. Additionally, KEGG enrichment analysis of the Hg-exposed fat body versus the control fat body group demonstrated a remarkable enrichment of the "oxidative phosphorylation" pathway. Oxidative phosphorylation (OXPHOS), a central process in nearly all eukaryotic cells, occurs in the mitochondria and directly contributes to cellular adenosine triphosphate (ATP) production (50). It is well-established that mitochondria, with their highly dynamic nature, play a key role in regulating cellular homeostasis by sustaining ATP levels and generating appropriate levels of reactive oxygen species (ROS); disruption in either of these processes can lead to pathological conditions (51). Thus, these results indicate that the energy metabolism and oxidative status of silkworms were significantly affected following exposure to Hg.

Consistent with previous research, a decrease in average insect weight emerged as a common response to heavy metal treatment, attributed to elevated protein, glycogen, and lipid consumption (52), or a reduction in the anti-damage and self-repair mechanisms (21, 22, 53). In this study, the basal metabolic processes, including "amino sugar and nucleotide sugar metabolism," "biosynthesis of amino acids," "glycine, serine and threonine metabolism," "pentose and glucuronate interconversions," "ascorbate and aldarate metabolism," and "retinol metabolism" were significantly affected both in the midgut and fat body. Additionally, alterations in "carbon metabolism" and "nitrogen metabolism" were observed specifically in the midgut, while changes in "oxidative phosphorylation," "glycolysis/gluconeogenesis," and "glycerolipid metabolism" were exclusive to the fat body. These changed metabolism pathways control the production, maintenance, and destruction of biomolecular, and energy balance (54). Notably, processes related to genetic information processing, such as "ribosome" and "ribosome biogenesis in eukaryotes" (55), were also enriched in the midgut or fat body following exposure to Hg. Consistent and distinct metabolic shifts were observed in both the midgut and fat body in response to Hg treatment. Carbohydrates, lipids, and proteins represent crucial energy sources for organisms, undergoing catabolism through specific biochemical cascades necessitating enzymes, cofactors, and energy (56, 57). Disruptions in these potential pathways might lead to diverse cellular disorders and

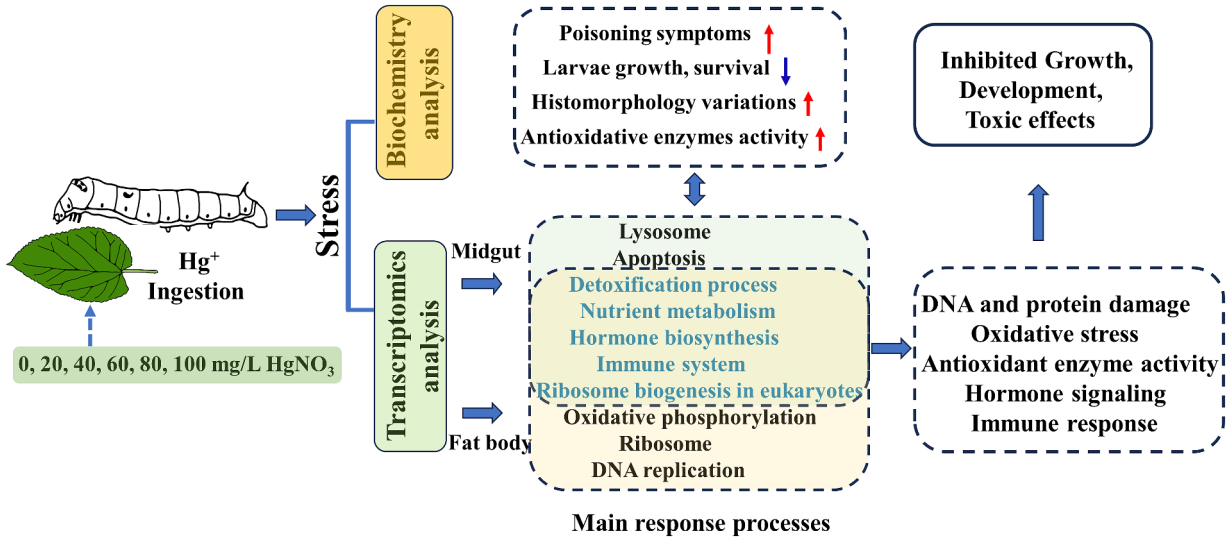


FIGURE 9
Schematic summary of Hg-stress on the biological functions of the silkworm.

metabolic diseases, which finally impact the growth and development of the larval and subsequent weight loss under high concentrations of Hg stress.

The heat shock proteins (HSPs) family plays a pivotal role in enabling organisms to shield themselves from cellular damage induced by environmental stressors, and it is crucial in regulating apoptosis and activating the innate immune system across various organisms (58). In our investigation, there was a decrease in the transcription levels of small *HSPs*, specifically *Hsp21.4*, *Hsp19.9*, *Hsp20.8*, and *Hsp20.1* in the midgut, and *Hsp19.9*, *Hsp20.8*, and *Hsp20.4* in the fat body. Within the Hsp70 family, both *Hsp70A* in the midgut and fat body, and *Hsp68* in the fat body exhibited down-regulated expressions. Notably, *Hsc70-4* demonstrated an up-regulated expression in the fat body, a phenomenon associated with *Bombyx mori* nucleopolyhedrovirus (BmNPV) infection, as reported previously (59–61). In our previous research, we observed an induction in the translational level of *BmGRP78* (also known as *Hsc70-3*) and its translocation into the cell nucleus following Hg exposure (62). These results demonstrated that these HSP proteins may be functionally related to Hg exposure. The underlying molecular mechanisms are needed to elucidate in further study.

Insects rely on the innate immune system response to defend against external invaders by producing humoral response molecules, notably antimicrobial peptides (AMPs), which can induce apoptosis or expression of antioxidant enzymes (63). Primary immune response indicators in lepidopteran insects, such as Cecropin, Attacin, and Lysozyme, were examined in the silkworm (64). Our data revealed an increase in the expression of *cecropin-D*, while *attacin1* and *enb3* exhibited decreased expression in the fat body. Additionally, *Lysozyme* showed down-regulated expression in the midgut. Exposure to Hg induced downregulated expression of *attacin1* and *enb3* in the fat body, and *Lysozyme* in the midgut, suggesting that immunotoxicity was induced in the silkworm and could be linked to the observed instances of diseased silkworms in the higher concentration exposure group. Previous studies also reported that the immunosuppressed state in the silkworms was produced by xenobiotics invaders, including insecticide (19), nanoplastics (12, 17), antibiotics (64), and silver (22). In our study, *serpin-15* exhibited up-regulated expression in the midgut, while *serpin-13*, *serpin-5*, *serpin-7*, and *serpin-3* displayed up-regulated expression, and *serpin-6* was down-regulated in the fat body. The innate immune response in invertebrate animals involves a serine protease cascade (65). Serpins, a widely distributed family of serine protease (SP) inhibitors, primarily regulate the Toll pathway, promoting the synthesis of antimicrobial peptides (AMPs) and activating the prophenoloxidase (proPO) system by inhibiting cascades of serine proteinase (66). Negative regulators such as *serpin-5*, *serpin-3*, and *serpin-15* control insect innate immunity by inhibiting clip proteinase cascades, which trigger immune responses, including the Toll pathway and melanization (67–70). In this study, the up-regulation of these serpins in the midgut or fat body suggests their potential role in the innate immune response to Hg exposure.

## 5 Conclusion

In our study, the silkworms as a lepidopteran model organism were employed to assess the potential adverse effect of Hg exposure. Our results showed that higher doses of Hg exposure induced evident poisoning symptoms, decreased weight body, impaired histomorphology, and changed antioxidant enzyme activity. Transcriptomic data analysis of these tissues suggested that Hg exposure impaired fundamental metabolic processes, elicited an oxidative stress response, and induced hormone and immune dysfunction in silkworms (Figure 9). These results facilitate the knowledge of the biological effects of Hg exposure on invertebrate organisms.

## Data availability statement

The data presented in the study are deposited in the Sequence Read Archive (SRA) repository, accession number PRJNA999381.

## Ethics statement

The manuscript presents research on animals that do not require ethical approval for their study.

## Author contributions

HW: Writing – original draft, Visualization, Data curation. YW: Writing – original draft, Formal analysis, Data curation. YJ: Writing – original draft, Visualization, Investigation. JC: Writing – original draft, Software, Data curation. YX: Writing – original draft, Formal analysis, Data curation. QL: Writing – review & editing, Validation, Project administration. CJ: Writing – review & editing, Validation, Supervision. QS: Writing – review & editing, Supervision. ZN: Writing – review & editing, Supervision, Resources. ZY: Writing – review & editing, Supervision, Resources, Funding acquisition, Conceptualization.

## Funding

The author(s) declare that financial support was received for the research, authorship, and/or publication of this article. This work was supported by the National Natural Science Foundation of China (Grant No. 31702183), and the Science Foundation of Zhejiang Sci-Tech University (Grant Nos. 18042138-Y and 19042144-Y).

## Conflict of interest

The authors declare that the research was conducted in the absence of any commercial or financial relationships that could be construed as a potential conflict of interest.

## Publisher's note



## Supplementary material

The Supplementary material for this article can be found online at: https://www.frontiersin.org/articles/10.3389/fvets.2024.1405541/full#supplementary-material

## References

1. Omara T, Karungi S, Kalukusu R, Nakabuye B, Kagoya S, Musau B. Mercuric pollution of surface water, superficial sediments, Nile tilapia (*Oreochromis nilotica* Linnaeus 1758 [Cichlidae]) and yams (*Dioscorea alata*) in auriferous areas of Namukombe stream, Syanyonja, Busia, Uganda. *PeerJ*. (2019) 7:e7919. doi: 10.7717/peerj.7919

2. Wang X, Wang WX. The three 'B' of fish mercury in China: bioaccumulation, biodynamics and biotransformation. *Environ Pollut*. (2019) 250:216–32. doi: 10.1016/j.envpol.2019.04.034

3. Natasha M, Shahid S, Khalid I, Bibi J, Bundschuh NK, Khan Niazi N, et al. A critical review of mercury speciation, bioavailability, toxicity and detoxification in soil-plant environment: ecotoxicology and health risk assessment. *Sci Total Environ*. (2020) 711:134749. doi: 10.1016/j.scitotenv.2019.134749

4. Yang L, Zhang Y, Wang F, Luo Z, Guo S, Strähle U. Toxicity of mercury: molecular evidence. *Chemosphere*. (2020) 245:125586. doi: 10.1016/j.chemosphere.2019.125586

5. Finster ME, Raymond MR, Scofield MA, Smith KP. Mercury-impacted scrap metal: source and nature of the mercury. *J Environ Manag*. (2015) 161:303–8. doi: 10.1016/j.jenvman.2015.05.041

6. Zheng J, Liang JL, Jia P, Feng SW, Lu JL, Luo ZH, et al. Diverse methylmercury (MeHg) producers and degraders inhabit acid mine drainage sediments, but few taxa correlate with MeHg accumulation. *mSystems*. (2023) 8:e0073622. doi: 10.1128/msystems.00736-22

7. Cariccio VL, Samà A, Bramanti P, Mazzon E. Mercury involvement in neuronal damage and in neurodegenerative diseases. *Biol Trace Elem Res*. (2019) 187:341–56. doi: 10.1007/s12011-018-1380-4

8. Azar J, Yousef MH, El-Fawal HAN, Abdelnaser A. Mercury and Alzheimer's disease: a look at the links and evidence. *Metab Brain Dis*. (2021) 36:361–74. doi: 10.1007/s11011-020-00649-5

9. Li X, Pan J, Wei Y, Ni L, Xu B, Deng Y, et al. Mechanisms of oxidative stress in methylmercury-induced neurodevelopmental toxicity. *Neurotoxicology*. (2021) 85:33–46. doi: 10.1016/j.neuro.2021.05.002

10. Teleanu DM, Niculescu A-G, Lungu II, Radu CI, Vladâcenco O, Roza E, et al. An overview of oxidative stress, neuroinflammation, and neurodegenerative diseases. *Int J Mol Sci*. (2022) 23:5938. doi: 10.3390/ijms23115938

11. Xu L, Xu X, Kuang H, Liu Y, Xu C, Wu X. Transcriptomics and metabolomics for co-exposure to a cocktail of neonicotinoids and the synergist piperonyl butoxide. *Anal Chem*. (2023) 95:3108–18. doi: 10.1021/acs.analchem.2c05754

12. Muhammad A, He J, Yu T, Sun C, Shi D, Jiang Y, et al. Dietary exposure of copper and zinc oxides nanoparticles affect the fitness, enzyme activity, and microbial community of the model insect, silkworm *Bombyx mori*. *Sci Total Environ*. (2022) 813:152608. doi: 10.1016/j.scitotenv.2021.152608

13. Hou J, Yu J, Qin Z, Liu X, Zhao X, Hu X, et al. Guadipyr, a new insecticide, induces microbiota dysbiosis and immune disorders in the midgut of silkworms (*Bombyx mori*). *Environ Pollut*. (2021) 286:117531. doi: 10.1016/j.envpol.2021.117531

14. Hu Z, Zhu F, Chen K. The mechanisms of silkworm resistance to the baculovirus and antiviral breeding. *Annu Rev Entomol*. (2023) 68:381–99. doi: 10.1146/annurev-ento-120220-112317

15. Fan W, Kong Q, Chen Y, Lu F, Wang S, Zhao A. Safe utilization and remediation potential of the mulberry-silkworm system in heavy metal-contaminated lands: a review. *Sci Total Environ*. (2024) 927:172352. doi: 10.1016/j.scitotenv.2024.172352

16. Ali H, Khan E, Ilahi I. Environmental chemistry and ecotoxicology of hazardous heavy metals: environmental persistence, toxicity, and bioaccumulation. *J Chem*. (2019) 2019:6730305. doi: 10.1155/2019/6730305

17. Muhammad A, Zhou X, He J, Zhang N, Shen X, Sun C, et al. Toxic effects of acute exposure to polystyrene microplastics and nanoplastics on the model insect, silkworm *Bombyx mori*. *Environ Pollut*. (2021) 285:117255. doi: 10.1016/j.envpol.2021.117255

18. Andoh V, Chen L, Zhu F, Ge Q, Ma L, Wang Q, et al. The evaluation of the biological effects of melanin by using silkworm as a model animal. *Toxins*. (2022) 14:421. doi: 10.3390/toxins14070421

19. Xu S, Hao Z, Li Y, Zhou Y, Shao R, Chen R, et al. Biochemical toxicity and transcriptome aberration induced by dinotefuran in *Bombyx mori*. *Environ Pollut*. (2022) 307:119562. doi: 10.1016/j.envpol.2022.119562

20. Abdelli N, Peng L, Keping C. Silkworm, *Bombyx mori*, as an alternative model organism in toxicological research. *Environ Sci Pollut Res Int*. (2018) 25:35048–54. doi: 10.1007/s11356-018-3442-8

21. Liu Y, Yang C, Sun L, Wang A, Lan X, Xu W, et al. In-depth transcriptome unveils the cadmium toxicology and a novel metallothionein in silkworm. *Chemosphere*. (2021) 273:128522. doi: 10.1016/j.chemosphere.2020.128522

22. Nouara A, Lü P, Chen L, Pan Y, Yang Y, Chen K. Silver effects on silkworm, *Bombyx mori*. *J Toxicol Sci*. (2018) 43:697–709. doi: 10.2131/jts.43.697

23. Zhang C, Liu Y, He L, Shi F, Yao W, Luo X. Effects of uranium on the antioxidant responses of Chinese oak silkworm, *Antheraea pernyi*. *Pak J Zool*. (2021) 54:339–46. doi: 10.17582/journal.pjz/20190715000752

24. Xin Z-Z, Liu Q-N, Liu Y, Zhang D-Z, Wang Z-F, Zhang H-B, et al. Transcriptome-wide identification of differentially expressed genes in Chinese oak silkworm *Antheraea*

*pernyi* in response to lead challenge. *J Agric Food Chem*. (2017) 65:9305–14. doi: 10.1021/acs.jafc.7b03391

25. Attardo GM, Hansen IA, Raikhel AS. Nutritional regulation of vitellogenesis in mosquitoes: implications for anautogeny. *Insect Biochem Mol Biol*. (2005) 35:661–75. doi: 10.1016/j.ibmb.2005.02.013

26. Li S, Yu X, Feng Q. Fat body biology in the last decade. *Annu Rev Entomol*. (2019) 64:315–33. doi: 10.1146/annurev-ento-011118-112007

27. Li S, Fei J, Cheng D, Jin Y, Zhang W, Zhang Y, et al. Bioinformatics, tissue distribution, and subcellular localization analyses of Fk506 binding protein 12b from silkworms. *Arch Insect Biochem Physiol*. (2016) 91:109–23. doi: 10.1002/arch.21312

28. Liu Y, Su H, Li R, Li X, Xu Y, Dai X, et al. Comparative transcriptome analysis of *Glyphodes pyloalis* Walker (Lepidoptera: Pyralidae) reveals novel insights into heat stress tolerance in insects. *BMC Genomics*. (2017) 18:974. doi: 10.1186/s12864-017-4355-5

29. Shen Y, Zeng X, Chen G, Wu X. Comparative transcriptome analysis reveals regional specialization of gene expression in larval silkworm (*Bombyx mori*) midgut. *Insect Sci*. (2022) 29:1329–45. doi: 10.1111/1744-7917.13001

30. Liu Y, Liang Y, Yang C, Shi R, Lu W, Wang X, et al. A deep insight into the transcriptome of midgut and fat body reveals the toxic mechanism of fluoride exposure in silkworm. *Chemosphere*. (2021) 262:127891. doi: 10.1016/j.chemosphere.2020.127891

31. Lu F, Wei Z, Luo Y, Guo H, Zhang G, Xia Q, et al. Silk DB 3.0: visualizing and exploring multiple levels of data for silkworm. *Nucleic Acids Res*. (2020) 48:D749–55. doi: 10.1093/nar/gkz919

32. Yang CC, Yokoi K, Yamamoto K, Jouraku A. An update of KAIKObase, the silkworm genome database. *Database*. (2021) 2021:baaa099. doi: 10.1093/database/baaa099

33. Kim D, Langmead B, Salzberg SL. HISAT: a fast spliced aligner with low memory requirements. *Nat Methods*. (2015) 12:357–60. doi: 10.1038/nmeth.3317

34. Trapnell C, Williams BA, Pertea G, Mortazavi A, Kwan G, van Baren MJ, et al. Transcript assembly and quantification by RNA-Seq reveals unannotated transcripts and isoform switching during cell differentiation. *Nat Biotechnol*. (2010) 28:511–5. doi: 10.1038/nbt.1621

35. Love MI, Huber W, Anders S. Moderated estimation of fold change and dispersion for RNA-seq data with DESeq2. *Genome Biol*. (2014) 15:550. doi: 10.1186/s13059-014-0550-8

36. Livak KJ, Schmittgen TD. Analysis of relative gene expression data using real-time quantitative PCR and the $2^{-\Delta\Delta C_T}$ method. *Methods*. (2001) 25:402–8. doi: 10.1006/meth.2001.1262

37. Lei HL, Wei HJ, Chen PH, Hsi HC, Chien LC. Preliminary study of blood methylmercury effects on reproductive hormones and relevant factors among infertile and pregnant women in Taiwan. *Chemosphere*. (2015) 135:411–7. doi: 10.1016/j.chemosphere.2015.05.006

38. Jiang L, Peng LL, Cao YY, Thakur K, Hu F, Tang SM, et al. Transcriptome analysis reveals gene expression changes of the fat body of silkworm (*Bombyx mori* L.) in response to selenium treatment. *Chemosphere*. (2020) 245:125660. doi: 10.1016/j.chemosphere.2019.125660

39. Mittapalli O, Neal JJ, Shukle RH. Antioxidant defense response in a galling insect. *Proc Natl Acad Sci USA*. (2007) 104:1889–94. doi: 10.1073/pnas.0604722104

40. Hu M, Palić D. Micro- and nano-plastics activation of oxidative and inflammatory adverse outcome pathways. *Redox Biol*. (2020) 37:101620. doi: 10.1016/j.redox.2020.101620

41. Xu Y, Wang W, Ma L, Cui X, Lynch I, Wu G. Acute toxicity of zinc oxide nanoparticles to silkworm (*Bombyx mori* L.). *Chemosphere*. (2020) 259:127481. doi: 10.1016/j.chemosphere.2020.127481

42. Gu ZY, Li FC, Wang BB, Xu KZ, Ni M, Zhang H, et al. Differentially expressed genes in the fat body of *Bombyx mori* in response to phoxim insecticide. *Pestic Biochem Physiol*. (2015) 117:47–53. doi: 10.1016/j.pestbp.2014.10.007

43. Lv H, Zhen C, Liu J, Yang P, Hu L, Shang P. Unraveling the potential role of glutathione in multiple forms of cell death in cancer therapy. *Oxid Med Cell Longev*. (2019) 2019:3150145. doi: 10.1155/2019/3150145

44. Meng S, Ji Y, Zhu L, Dhoke GV, Davari MD, Schwaneberg U. The molecular basis and enzyme engineering strategies for improvement of coupling efficiency in cytochrome P450s. *Biotechnol Adv*. (2022) 61:108051. doi: 10.1016/j.biotechadv.2022.108051

45. Nauen R, Bass C, Feyereisen R, Vontas J. The role of cytochrome P450s in insect toxicology and resistance. *Annu Rev Entomol*. (2022) 67:105–24. doi: 10.1146/annurev-ento-070621-061328

46. Hattab S, Boughattas I, Cappello T, Zitouni N, Touil G, Romdhani I, et al. Heavy metal accumulation, biochemical and transcriptomic biomarkers in earthworms *Eisenia andrei* exposed to industrially contaminated soils from South-Eastern Tunisia (Gabes Governorate). *Sci Total Environ*. (2023) 887:163950. doi: 10.1016/j.scitotenv.2023.163950

47. Yang C, Wang X. Lysosome biogenesis: regulation and functions. *J Cell Biol*. (2021) 220:e202102001. doi: 10.1083/jcb.202102001

48. Sidhu JS, Kaur N, Singh N. Trends in small organic fluorescent scaffolds for detection of oxidoreductase. *Biosens Bioelectron*. (2021) 191:113441. doi: 10.1016/j.bios.2021.113441

49. Hommes G, Gasser CA, Ammann EM, Corvini PFX. Determination of oxidoreductase activity using a high-throughput microplate respiratory measurement. *Anal Chem*. (2013) 85:283–91. doi: 10.1021/ac302716j

50. Braun HP. The oxidative phosphorylation system of the mitochondria in plants. *Mitochondrion*. (2020) 53:66–75. doi: 10.1016/j.mito.2020.04.007

51. Nolfi-Donegan D, Braganza A, Shiva S. Mitochondrial electron transport chain: oxidative phosphorylation, oxidant production, and methods of measurement. *Redox Biol*. (2020) 37:101674. doi: 10.1016/j.redox.2020.101674

52. Li X, Wang M, Jiang R, Zheng L, Chen W. Evaluation of joint toxicity of heavy metals and herbicide mixtures in soils to earthworms (*Eisenia fetida*). *J Environ Sci*. (2020) 94:137–46. doi: 10.1016/j.jes.2020.03.055

53. Meng X, Abdlli N, Wang N, Lü P, Nie Z, Dong X, et al. Effects of ag nanoparticles on growth and fat body proteins in silkworms (*Bombyx mori*). *Biol Trace Elem Res*. (2017) 180:327–37. doi: 10.1007/s12011-017-1001-7

54. Matarese G, La Cava A. The intricate interface between immune system and metabolism. *Trends Immunol*. (2004) 25:193–200. doi: 10.1016/j.it.2004.02.009

55. Wang S, You Z, Feng M, Che J, Zhang Y, Qian Q, et al. Analyses of the molecular mechanisms associated with silk production in silkworm by iTRAQ-based proteomics and RNA-sequencing-based transcriptomics. *J Proteome Res*. (2016) 15:15–28. doi: 10.1021/acs.jproteome.5b00821

56. Croom E. Chapter three—metabolism of xenobiotics of human environments In: E Hodgson, editor. *Progress in molecular biology and translational science*: Academic Press (2012). 31–88. doi: 10.1016/B978-0-12-415813-9.00003-9

57. Suzuki A, Minamide M, Iwaya C, Ogata K, Iwata J. Role of metabolism in bone development and homeostasis. *Int J Mol Sci*. (2020) 21:8992. doi: 10.3390/ijms21238992

58. Wallin RP, Lundqvist A, Moré SH, von Bonin A, Kiessling R, Ljunggren HG. Heat-shock proteins as activators of the innate immune system. *Trends Immunol*. (2002) 23:130–5. doi: 10.1016/S1471-4906(01)02168-8

59. Mao F, Zhu Y, Gao X, Chen X, Ngowo J, Miao M, et al. HSP/HSC70 activity is required for *Bombyx mori* nucleopolyhedrovirus replication at the early infectious phase. *Microb Pathog*. (2021) 153:104647. doi: 10.1016/j.micpath.2020.104647

60. Zhang X, Yu W. Heat shock proteins and viral infection. *Front Immunol*. (2022) 13:947789. doi: 10.3389/fimmu.2022.947789

61. Mao F, Chen X, Ngowo J, Zhu Y, Lei J, Gao X, et al. Deacetylation of HSC70-4 promotes *Bombyx mori* nucleopolyhedrovirus proliferation via proteasome-mediated nuclear import. *Front Physiol*. (2021) 12:609674. doi: 10.3389/fphys.2021.609674

62. Xiao Y, Ren L, Wang Y, Wen H, Ji Y, Li C, et al. Biochemical characterization and functional analysis of glucose regulated protein 78 from the silkworm *Bombyx mori*. *Int J Mol Sci*. (2023) 24:3964. doi: 10.3390/ijms24043964

63. Cheng T, Zhao P, Liu C, Xu P, Gao Z, Xia Q, et al. Structures, regulatory regions, and inductive expression patterns of antimicrobial peptide genes in the silkworm *Bombyx mori*. *Genomics*. (2006) 87:356–65. doi: 10.1016/j.ygeno.2005.11.018

64. Li G, Shi M, Zhao S, Long Y, Zhu Y. Toxicity response of silkworm intestine to *Bacillus cereus* SW7-1 pathogen. *Sci Total Environ*. (2019) 692:1282–90. doi: 10.1016/j.scitotenv.2019.07.349

65. Iwanaga S, Lee BL. Recent advances in the innate immunity of invertebrate animals. *J Biochem Mol Biol*. (2005) 38:128–50. doi: 10.5483/bmbrep.2005.38.2.128

66. Meekins DA, Kanost MR, Michel K. Serpins in arthropod biology. *Semin Cell Dev Biol*. (2017) 62:105–19. doi: 10.1016/j.semcdb.2016.09.001

67. Liu D, Wang L, Yang L, Qian C, Wei G, Dai L, et al. Serpin-15 from *Bombyx mori* inhibits prophenoloxidase activation and expression of antimicrobial peptides. *Dev Comp Immunol*. (2015) 51:22–8. doi: 10.1016/j.dci.2015.02.013

68. Chu Y, Zhou F, Liu Y, Hong F, Wang G, An C. Ostrinia furnacalis serpin-3 regulates melanization cascade by inhibiting a prophenoloxidase-activating protease. *Insect Biochem Mol Biol*. (2015) 61:53–61. doi: 10.1016/j.ibmb.2015.03.007

69. Wang X, Wang K, He Y, Lu X, Wen D, Wu C, et al. The functions of serpin-3, a negative-regulator involved in prophenoloxidase activation and antimicrobial peptides expression of Chinese oak silkworm, *Antheraea pernyi*. *Dev Comp Immunol*. (2017) 69:1–11. doi: 10.1016/j.dci.2016.11.022

70. Liu H, Xu J, Wang L, Guo P, Tang Z, Sun X, et al. Serpin-1a and serpin-6 regulate the toll pathway immune homeostasis by synergistically inhibiting the Spätzle-processing enzyme CLIP2 in silkworm, *Bombyx mori*. *PLoS Pathog*. (2023) 19:e1011740. doi: 10.1371/journal.ppat.1011740

frontiers | Frontiers in Veterinary Science

TYPE Original Research
PUBLISHED 17 June 2024
DOI 10.3389/fvets.2024.1388339



OPEN ACCESS

EDITED BY
Jesus R. Requena,
University of Santiago de Compostela, Spain

REVIEWED BY
Christopher J. Silva,
United States Department of Agriculture (USDA), United States
Alba Marín Moreno,
Ministry of Agriculture, Fisheries and Food, Spain

*CORRESPONDENCE
Byung-Hoon Jeong
✉ bhjeong@jbnu.ac.kr

†These authors have contributed equally to this work

RECEIVED 15 March 2024
ACCEPTED 29 April 2024
PUBLISHED 17 June 2024

CITATION
Jeong M-J, Kim Y-C and Jeong B-H (2024) The first report of single nucleotide polymorphisms in the open reading frame of the prion-like protein gene in rabbits. *Front. Vet. Sci.* 11:1388339. doi: 10.3389/fvets.2024.1388339



# The first report of single nucleotide polymorphisms in the open reading frame of the prion-like protein gene in rabbits

Min-Ju Jeong[1,2†], Yong-Chan Kim[3†] and Byung-Hoon Jeong[1,2*]

[1]Korea Zoonosis Research Institute, Jeonbuk National University, Iksan, Jeonbuk, Republic of Korea, [2]Department of Bioactive Material Sciences, Jeonbuk National University, Jeonju, Jeonbuk, Republic of Korea, [3]Department of Biological Sciences, Andong National University, Andong, Republic of Korea

**Background:** Natural cases of prion disease have not been reported in rabbits, and prior attempts to identify a prion conversion agent have been unsuccessful. However, recent applications of prion seed amplifying experimental techniques have sparked renewed interest in the potential susceptibility of rabbits to prion disease infections. Among several factors related to prion disease, polymorphisms within the prion-like protein gene (*PRND*), a member of the prion protein family, have been reported as significantly associated with disease susceptibility in various species. Therefore, our study aimed to investigate polymorphisms in the *PRND* gene of rabbits and analyze their genetic characteristics.

**Methods:** Genomic DNA was extracted from 207 rabbit samples to investigate leporine *PRND* polymorphisms. Subsequently, amplicon sequencing targeting the coding region of the leporine *PRND* gene was conducted. Additionally, linkage disequilibrium (LD) analysis was employed to assess the connection within and between loci. The impact of non-synonymous single nucleotide polymorphisms (SNPs) on the Doppel protein was evaluated using PolyPhen-2.

**Results:** We found nine novel SNPs in the leporine *PRND* gene: c.18A > G, c.76G > C, c.128C > T, c.146C > T, c.315A > G, c.488G > A, c.525G > C, c.544G > A, and c.579A > G. Notably, seven of these *PRND* SNPs, excluding c.525G > C and c.579A > G, exhibited strong LD values exceeding 0.3. In addition, LD analysis confirmed a robust link between *PRNP* SNP c.234C > T and *PRND* SNPs at c.525G > C and c.579A > G. Furthermore, according to PolyPhen-2 and SIFT analyses, the four non-synonymous SNPs were predicted to have deleterious effects on the function or structure of the Doppel protein. However, PANTHER and Missense3D did not indicate such effects.

**Conclusion:** In this paper, we have identified novel SNPs in the rabbit *PRND* gene and predicted their potential detrimental effects on protein function or structure through four non-synonymous SNPs. Additionally, we observed a genetic linkage between SNPs in the *PRND* and *PRNP* genes. These findings may provide insights into understanding the characteristics of rabbits as partially resistant species. To the best of our knowledge, this study is the first to genetically characterize *PRND* SNPs in rabbits.

KEYWORDS

**prion, rabbit, Doppel, prion-like protein gene, *PRND*, polymorphism, SNP**

## Introduction

Prion diseases are lethal neurodegenerative disorders characterized by aberrant misfolding of the cellular form of prion protein ($PrP^{C}$) into the pathogenic, protease-resistant isoform of prion protein ($PrP^{Sc}$), resulting in their accumulation within the brain (1, 2). Host species exhibiting high susceptibility to prion diseases include humans (Creutzfeldt-Jakob disease, CJD), deer and elk (chronic wasting disease, CWD), cattle (bovine spongiform encephalopathy, BSE), and sheep and goats (scrapie), whereas dogs, horses, and chickens are resistant to prion diseases (3, 4). Occurrences of prion disease have not been reported in these resistant species in natural environments, and experimental infections have also failed to induce the disease (4, 5).

To date, there have been no reported cases of natural prion disease infection in rabbits (4, 6). Despite experimental attempts involving infection with the human kuru and CJD agents, as well as the scrapie agent isolated from sheep and mouse (Me7 strain), rabbits have proven to be resistant (7, 8). Further supporting this resistance, *in vitro* experiments demonstrated that rabbit $PrP^{C}$ did not convert to rabbit $PrP^{Sc}$ in mouse neuroblastoma cells persistently infected with the mouse scrapie agent (RML strain) (9). Notably, a recent application of serial automated protein misfolding cyclic amplification (saPMCA) aimed to confirm protein misfolding and potential infection in rabbits, challenging the previous notion of rabbit resistance to prion diseases (10). The report indicated that rabbit brain homogenates, when amplified *in vitro* by saPMCA, exhibited resistance to proteinase K digestion. Upon injection into other rabbits, clinical symptoms emerged, leading to fatality. In brief, rabbits show prion resistance in natural transmission condition without extreme artificial replication techniques. Interestingly, rabbits exhibited a reduced propensity to transition to the β-structured state, which is believed to be associated with the mechanism of prion diseases, compared to susceptible species. However, they showed a higher propensity than dogs and horses (11). To further understand this partial resistance trait in rabbits, our investigation will focus on genetic factors associated with susceptibility to prion diseases.

Recent research has reported an association between the susceptibility to prion diseases and polymorphisms within the prion gene family (12–22). The prion protein gene family comprises the prion protein gene (*PRNP*), prion-like protein gene (*PRND*), prion-related protein gene (*PRNT*), and the shadow of prion protein gene (*SPRN*) (23). Among them, special attention is being given to *PRND* as a notable candidate gene. The *PRND* gene is located most closely to the *PRNP* gene, and the Doppel protein, encoded by *PRND*, shares biochemical and structural similarities with PrP (24, 25).

Previous studies propose an association between *PRND* polymorphisms and prion disease susceptibility in several species (26–30). In humans, significant differences in the frequencies of polymorphisms at codon 174 and the 3′ untranslated region (UTR) +28 of human *PRND* were observed in sporadic CJD patients compared to healthy controls (26, 27). In cattle, the genotype distributions of polymorphisms at codons 95 and 132 of the bovine *PRND* gene were significantly different between BSE-affected and healthy German Fleckvieh cattle (28). In sheep, linkage disequilibrium (LD) analysis revealed a significant linkage between the G allele of codon 26 of the ovine *PRND* gene and the ARR allele of the ovine *PRNP* gene, known to confer genetic resistance to scrapie (29). Even in goats, caprine *PRND* single nucleotide polymorphisms (SNPs) c.28 T > C, c.151A > G, and c.385G > C are strongly linked to caprine *PRNP* c.428A > G (H143R) (30). Consequently, the major homozygote genotype of caprine *PRND* SNPs is genetically associated with the caprine *PRNP* HH genotype, which is related to scrapie progression.

The exploration of polymorphisms in the *PRND* gene of prion disease-resistant species has yielded intriguing findings. In the canine *PRND* gene, four polymorphisms were identified, and researchers attempted to validate the association between *PRNP* and *PRND* through LD analysis (31). Despite the relatively shorter genetic distances in dogs compared to sheep and goats, no strong LD was observed between *PRNP* and *PRND*. In the equine *PRND* gene, SNPs were either absent or rare, depending on the breed (32, 33). Even in cases where they were rarely present, weak LD was confirmed between *PRNP* and *PRND* (33). Moreover, the *PRND* gene has not been identified in birds (34).

To date, studies on *PRND* polymorphisms in rabbits have not yet been performed, and this area is considered worth exploring. In this study, we investigated the genotype and allele frequencies of *PRND* polymorphisms in a group of 207 rabbits. In addition, we performed an LD analysis between *PRNP* and *PRND* to identify genetic linkage. Furthermore, we assessed the possible impact of non-synonymous SNPs on the structure and function of the Doppel protein using *in silico* prediction tools.

## Materials and methods

### Sample preparation

All 207 rabbit samples of hybrid breeding rabbits (New Zealand white and Flemish Giant FG) were provided by a slaughterhouse located in the Republic of Korea. Genomic DNA was isolated from 20 mg brain tissue following the manufacturer's manuals using the Labopass Tissue Genomic DNA Isolation Kit (Cosmo Genetech Co., Ltd., Seoul). The overall experimental processes were approved by the Jeonbuk National University Institutional Animal Care and Use Committee (CBNU 2019-058). All experiments were performed in accordance with the Korea Experimental Animal Protection Act.

### Genetic analysis in the leporine *PRND* gene

Primers were designed based on the leporine *PRND* gene sequence (*Oryctolagus cuniculus*) available in GenBank at the National Center for Biotechnology Information (NCBI) (Gene ID: 100347890). The gene-specific forward and reverse primer sequences were GGGTAGACCGGTTGGGAAAT and TGAGCACTGAAGCACT GAGG, respectively. Polymerase chain reaction (PCR) was performed targeting the coding region of the leporine *PRND* gene by an S-1000 Thermal Cycler (Bio-Rad, Hercules, CA, United States). The PCR conditions followed the manual guide of BioFACT™ Taq DNA Polymerase (BioFACT Co., Ltd., Daejeon, Korea) with an annealing temperature of 65°C. The amplified products were purified using the FavorPrep™ GEL/PCR Purification Kit (Favorgen Biotech Corp., Kaohsiung, Taiwan), and then sequenced by an ABI PRISM 3730XL Analyzer (ABI, Foster City, CA, United States). These sequencing

results for each sample were analyzed using Finch TV software (Geospiza Inc., Seattle, WA, United States).

## Statistical analysis

The Hardy–Weinberg Equilibrium (HWE) test was conducted to assess the genotyping errors of the collected individual samples for this study. In HWE testing, a *p*-value lower than 0.05 indicates that the observed genotype or allele frequencies are not consistent with HWE (35, 36). The HWE test was conducted by the Michael H. Court's calculator.

Additionally, LD analysis was performed to examine the statistical relationship between SNPs at each locus of the genes. LD, a measure of the correlation between two genetic loci (or SNPs), was assessed using the $r^2$ value (37). The $r^2$ value ranges from 0 to 1. Higher values indicate strong linkage between two genetic loci, suggesting the presence of associated genetic regions. Conversely, lower $r^2$ values indicate that the variations at two genetic loci are independent or weakly correlated. The LD and haplotype distribution were estimated using the Haploview version 4.2 (Broad Institute, Cambridge, MA, United States).

## *In silico* prediction of the impact of non-synonymous SNPs in leporine *PRND*

PolyPhen-2 determines the effect of non-synonymous SNPs on the structure or function of a protein according to a position-specific independent counts (PSIC) score difference. The results are assigned as "probably damaging," "possibly damaging" or "benign," depending on the degree of risk. SIFT predicts the impact of amino acid substitutions on protein function based on sequence homology, assuming that alignment correlates well with evolution to maintain protein function. The SIFT score ranges from 0 to 1, where values below 0.05 are considered deleterious. PANTHER assesses the effect of non-synonymous SNPs on function using PANTHER-PSEP (position-specific evolutionary preservation). Positions conserved over longer periods are expected to have more detrimental effects. These effects are quantitatively scored as Pdel (probability of deleterious effect), and the results are classified as "probably damaging," "possibly damaging," and "probably benign." Missense3D predicts structural changes resulting from deleterious variants that affect protein stability. It identifies structural damage through comprehensive analysis, which includes examining factors such as disruption of buried salt bridges and alterations in secondary structure.

## Analysis of the genetic linkage among SNPs of *PRNP* and *PRND* genes

To investigate the genetic linkage between *PRNP* and *PRND* SNPs, we conducted LD analysis between the loci of these two genes. Initially, we obtained the dataset of *PRNP* genotypes from rabbits, which included results from previously reported 203 samples. Subsequently, we performed preprocessing to match the *PRNP* genotype data with the individuals analyzed for *PRND*. Of the total genotype datasets examined, 201 matched, and these were used to analyze the LD scores between *PRNP* and *PRND* SNPs.

# Results

## Investigation of leporine *PRND* polymorphisms

To investigate the leporine *PRND* polymorphisms, we analyzed DNA sequences targeting the open reading frame (ORF) of leporine *PRND* in 207 rabbits. The leporine *PRND* gene comprises two exons, with the ORF (537 bp) located in exon 2 (Figure 1A). PCR and sequencing were performed using a pair of primers designed in this study, and the sequencing results were identical to the leporine *PRND* gene registered in GenBank (Gene ID: 100347890). We found nine novel SNPs in leporine *PRND*: c.18A > G, c.76G > C, c.128C > T, c.146C > T, c.315A > G, c.488G > A, c.525G > C, c.544G > A, and c.579A > G (Figure 1B). Among them, four SNPs at c.76G > C (A26P), c.128C > T (T43M), c.146C > T (A49V), and c.488G > A (R163Q) are nonsynonymous SNPs within the ORF region, and two SNPs at c.544G > A and c.579A > G are located in the 3′ untranslated region (Figure 1A). Detailed information about the genotype and allele frequencies of the leporine *PRND* SNPs is described in Table 1.

We investigated the extent of LD among the leporine *PRND* SNPs by calculating the $r^2$ values (Table 2). Seven of the *PRND* SNPs, excluding c.525G > C and c.579A > G, exhibited strong linkage with values greater than 0.3. In addition, we examined the haplotype frequency of the leporine *PRND* SNPs (Table 3). The most frequently observed haplotype was GCCCAGGGA (46.9%), followed by AGTTGAGAA (46.6%), AGCCAGCGG (6%), AGTTGAGGA (0.2%), and AGCCGGGAA (0.2%).

## *In silico* prediction of the functional effect of non-synonymous leporine *PRND* SNPs

We evaluated the potential effect of non-synonymous SNPs on leporine *PRND* using *in silico* prediction tools (Table 4). Both PolyPhen-2 and SIFT predicted that all four non-synonymous SNPs would have deleterious effects on protein function and structure. In Polyphen-2, the three SNPs at c.76G > C (A26P), c.128C > T (T43M), and c.488G > A (R163Q) were predicted as "Possibly damaging" with scores of 0.895, 0.924, and 0.816, respectively. Interestingly, the SNP at c.146C > T (A49V) was predicted as "Probably damaging" with a score of 0.991. In SIFT, all non-synonymous SNPs were predicted to impact protein function with a score of 0.00. However, both PANTHER and Missense3D classified all non-synonymous SNPs as benign.

## Investigation of genetic linkage between leporine *PRNP* and *PRND* SNPs

A previous study reported a synonymous SNP (c.234C > T) identified in the ORF of the leporine *PRNP* gene (38). To investigate whether leporine *PRND* SNPs have strong genetic linkage with this leporine *PRNP* SNP, we performed LD analysis between *PRNP* and

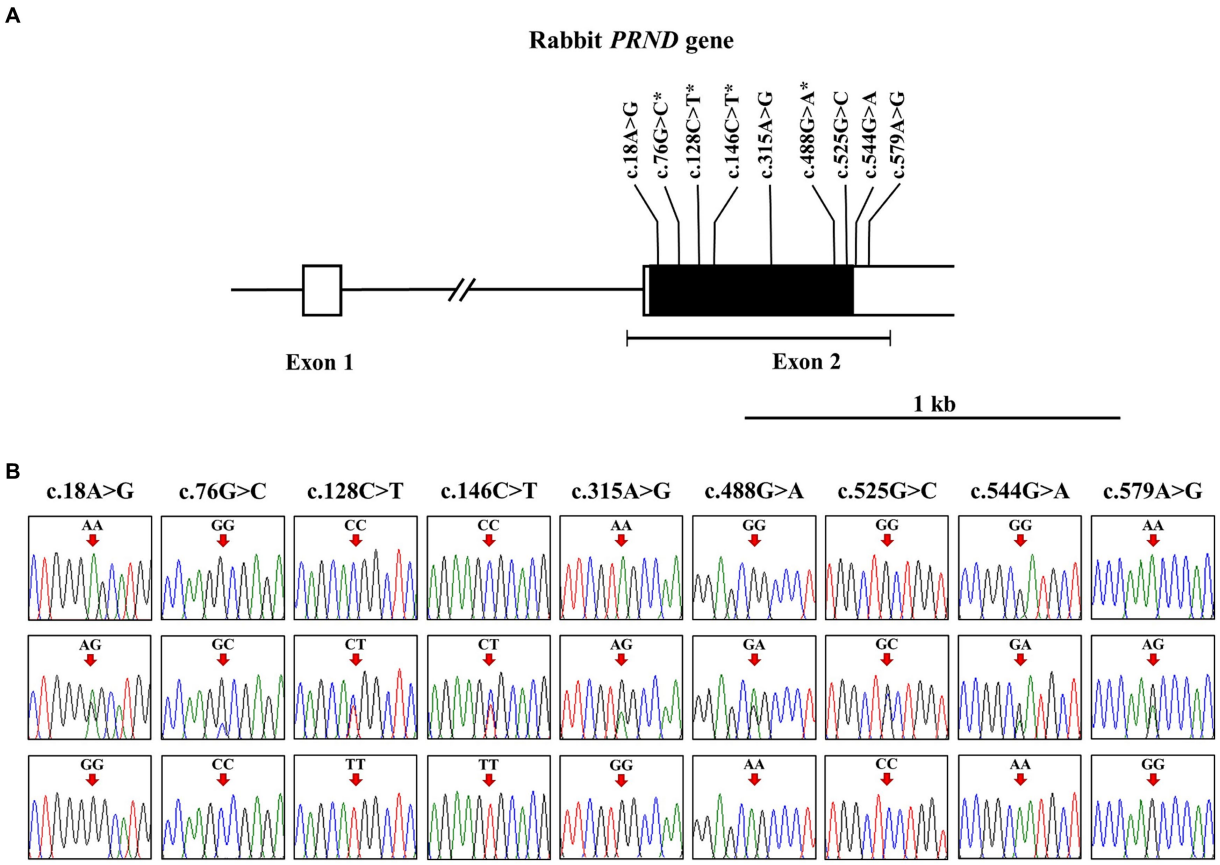


FIGURE 1
Identification of single nucleotide polymorphisms (SNPs) in the leporine prion-like protein gene (*PRND*). **(A)** The schematic diagram illustrates the genomic structure of the leporine *PRND*. The open reading frame (ORF) within exon 2 is represented by the black box, and the 5′ and 3′ untranslated regions (UTRs) from exon 1 to 2 are shown by the white boxes. The edged horizontal bar indicates the length of PCR products in this study. The positions of the polymorphisms identified in this study are shown in bold, with an asterisk denoting the non-synonymous SNP. **(B)** Electropherograms displaying nine novel SNPs discovered in the leporine *PRND* gene are presented. The electropherograms show three genotypes at c.18A > G, c.76G > C, c.128C > T, c.146C > T, c.315A > G, c.488G > A, c.525G > C, c.544G > A, and c.579A > G. The colors of the peaks represent each base of the DNA sequence as follows: green for adenine; red for thymine; blue for cytosine; black for guanine. Arrows indicate the position of the polymorphisms identified in this study. Upper panel, homozygote of the major allele; middle panel, heterozygote; lower panel, homozygote of the minor allele.

*PRND* SNPs using $r^2$ values. LD scores were estimated in 201 animals after excluding 6 animals that did not have genotyping data for the *PRNP* gene. As shown in Table 5, *PRND* SNPs at c.525G > C and c.579A > G were strongly linked with *PRNP* SNP c.234C > T ($r^2$ value of 0.912). The remaining seven *PRND* SNPs were weakly linked with $r^2$ scores of less than 0.3.

## Discussion

Since the pathological mechanisms of prion diseases remain elusive, investigating the genetic characteristics of prion disease-susceptible species is crucial for understanding this disease. However, exploring the genetic characteristic of resistant species offers a novel avenue to unravel the mysteries of prion diseases, providing valuable perspective (4). Previous research has suggested that resistance to prion diseases may be attributed to a specific structural stability unique to PrP in species resistant to such disease. For instance, the presence of an aspartic acid (Asp) residue at codon 163 of canine PrP enhances protein stability by forming an additional salt bridge compared to asparagine (Asn), the amino acid found at that position in prion disease-susceptible animal PrP (39, 40). This structural stabilization contributes to the resistance properties. Similarly, the Asp residue at codon 167 in equine PrP plays a crucial role in maintaining the well-defined structure of PrP, particularly within the β2–α2 loop, thereby contributing to disease resistance (41–44). While the amino acid structure of rabbit PrP shares similarities with that of prion disease-susceptible species, a detailed examination revealed that the β-sheet of rabbit PrP is shorter than that of human PrP (6). Notably, the β2–α2 loop of rabbit PrP spanning residues 165–175 exhibits a well-defined structure, contributing to the structural stability of rabbit PrP (11, 45). The V166 residue establishes hydrophobic contacts with the Y218 residue of helix 3 in rabbit PrP, potentially influencing the structural stability of the β2–α2 loop (11, 45). Furthermore, the S174 residue in rabbit PrP forms a robust hydrogen bond with the N171 residue, a key interaction believed to play a role in the observed resistance to prion susceptibility when serine replaces asparagine at codon 174 in mouse PrP (9, 11).

Given the influence of rabbit PrP-specific residues on structural stability, our attention may be directed towards exploring alterations in the rabbit PrP sequence and the potential influencing factors. In a

TABLE 1 Genotype and allele frequencies of the leporine prion-like protein gene (*PRND*) single nucleotide polymorphisms (SNPs).

| Polymorphism | Genotype frequency, *n* (%) | | | Total, *n* (%) | Allele frequency, *n* (%) | | Total, *n* (%) | HWE |
|---|---|---|---|---|---|---|---|---|
| c.18A > G | **AA** | **AG** | **GG** | | **A** | **G** | | |
| (G6G) | 57 | 106 | 44 | 207 | 220 | 194 | 414 | 0.68 |
| | (27.54) | (51.21) | (21.26) | (100) | (53.14) | (46.86) | (100) | |
| c.76G > C | **GG** | **GC** | **CC** | | **G** | **C** | | |
| (A26P) | 57 | 106 | 44 | 207 | 220 | 194 | 414 | 0.68 |
| | (27.54) | (51.21) | (21.26) | (100) | (53.14) | (46.86) | (100) | |
| c.128C > T | **CC** | **CT** | **TT** | | **C** | **T** | | |
| (T43M) | 55 | 110 | 42 | 207 | 220 | 194 | 414 | 0.33 |
| | (26.57) | (53.14) | (20.29) | (100) | (53.14) | (46.86) | (100) | |
| c.146C > T | **CC** | **CT** | **TT** | | **C** | **T** | | |
| (A49V) | 55 | 110 | 42 | 207 | 220 | 194 | 414 | 0.33 |
| | (26.57) | (53.14) | (20.29) | (100) | (53.14) | (46.86) | (100) | |
| c.315A > G | **AA** | **AG** | **GG** | | **A** | **G** | | |
| (V105V) | 55 | 109 | 43 | 207 | 219 | 195 | 414 | 0.41 |
| | (26.57) | (52.66) | (20.77) | (100) | (52.90) | (47.10) | (100) | |
| c.488G > A | **GG** | **GA** | **AA** | | **G** | **A** | | |
| (R163Q) | 55 | 110 | 42 | 207 | 220 | 194 | 414 | 0.33 |
| | (26.57) | (53.14) | (20.29) | (100) | (53.14) | (46.86) | (100) | |
| c.525G > C | **GG** | **GC** | **CC** | | **G** | **C** | | |
| (L175L) | 183 | 23 | 1 | 207 | 389 | 25 | 414 | 0.76 |
| | (88.41) | (11.11) | (0.48) | (100) | (93.96) | (6.04) | (100) | |
| c.544G > A | **GG** | **GA** | **AA** | | **G** | **A** | | |
| | 56 | 108 | 43 | 207 | 220 | 194 | 414 | 0.49 |
| | (27.05) | (52.17) | (20.77) | (100) | (53.14) | (46.86) | (100) | |
| c.579A > G | **AA** | **AG** | **GG** | | **A** | **G** | | |
| | 183 | 23 | 1 | 207 | 389 | 25 | 414 | 0.76 |
| | (88.41) | (11.11) | (0.48) | (100) | (93.96) | (6.04) | (100) | |

TABLE 2 Linkage disequilibrium (LD) scores of the leporine prion-like protein gene (*PRND*) single nucleotide polymorphisms (SNPs).

| $r^2$ | c.18A > G | c.76G > C | c.128C > T | c.146C > T | c.315A > G | c.488G > A | c.525G > C | c.544G > A | c.579A > G |
|---|---|---|---|---|---|---|---|---|---|
| c.18A>G | – | **1.0** | **0.778** | **0.778** | **0.758** | **0.778** | 0.057 | **0.778** | 0.057 |
| c.76G>C | – | – | **0.778** | **0.778** | **0.758** | **0.778** | 0.057 | **0.778** | 0.057 |
| c.128C>T | – | – | – | **1.0** | **0.99** | **1.0** | 0.057 | **0.981** | 0.057 |
| c.146C>T | – | – | – | – | **0.99** | **1.0** | 0.057 | **0.981** | 0.057 |
| c.315A>G | – | – | – | – | – | **0.99** | 0.057 | **0.99** | 0.057 |
| c.488G>A | – | – | – | – | – | – | 0.057 | **0.981** | 0.057 |
| c.525G>C | – | – | – | – | – | – | – | 0.057 | **0.1** |
| c.544G>A | – | – | – | – | – | – | – | – | 0.057 |
| c.579A>G | – | – | – | – | – | – | – | – | – |

Bold indicates strong LD with $r^2 > 0.3$.

recent study investigating polymorphisms within rabbit *PRNP*, a single SNP within the ORF region was identified. The study assessed the impact of substitutions in amino acids unique to rabbit compared to those conserved in other prion disease-susceptible species (38). While *in silico* analysis predicted benign effects on protein function and structure for amino acid substitutions in the unique residues of rabbit PrP (38), 3D structure predictions revealed weakened hydrogen bonds in residues such as S175, Q221, A226, and A230 of rabbit PrP resulting from these substitutions (38). However, the sensitivity to prion diseases cannot be fully explained by analyzing the sequence

characteristics of *PRNP* alone. Recent studies have reported that the genetic profile of polymorphisms in the *PRND* gene, a member of the prion protein family, serves as an important cofactor associated with susceptibility to various types of prion diseases (12–22, 26–33, 46–53).

Recent case-controlled studies have suggested that susceptibility to prion diseases is associated with *PRND* polymorphisms at codon 174 and 3′ untranslated region (UTR) +28 in humans (12, 26, 27), codons 95 and 132 in cattle (28), codon 26 in sheep (29), and codon 10 in goats (54). Moreover, significant associations have been observed between polymorphisms of the *PRNP* and *PRND* genes in sheep and goats (29, 30). This suggests that *PRND* SNPs may indirectly contribute to susceptibility to prion diseases across various species. In our study, we investigated polymorphisms within the ORF region of the leporine *PRND* gene, which is located proximal to the *PRNP* gene and observed a strong linkage between *PRNP* (c.234C > T) and *PRND* (c.525G > C and c.579A > G) polymorphisms in rabbits. These results align with prion disease-susceptible species such as goats and sheep (strong LD between *PRNP* and *PRND* SNPs). Interestingly, weak LD values were observed for seven *PRND* SNPs (c.18A > G, c.76G > C, c.128C > T, c.146C > T, c.315A > G, c.488G > A, and c.544G > A). Particularly, weak linkage between *PRNP* and *PRND* SNPs was observed in dogs and horses, which can be interpreted as a characteristic of prion disease-resistant species. Although natural infections have not been reported in rabbits, they are considered partially resistant species with confirmed experimental infection potential. Therefore, further research is needed to explore various characteristics related to genetic diversity in rabbits. Additional research on the association of intergenic polymorphisms in rabbits, considering the observed weak LD in resistant species and strong LD in susceptible species, will require in depth exploration.

In addition, we identified several SNPs, and four non-synonymous SNPs showed a potent effect on leporine Doppel (Figure 1; Table 4). All non-synonymous SNPs were predicted to impact protein function by PolyPhen-2 and SIFT, whereas PANTHER and Missense3D did not indicate any effect. Since *in silico* prediction tools employ algorithms based on their specific criteria, further research is needed to validate these predictions using cellular or animal models in the future. Interestingly, since the Doppel protein is predominantly expressed in the testis, the impact induced by the *PRND* SNP may affect male fertility (55, 56). In the previous study, researchers investigated the influence of a single SNP, c.78G.A (A26A), identified in the *PRND* gene of sheep, on sperm reproductive ability (29, 57). Semen from sheep carrying the A allele exhibited a higher proportion of the F pattern in spermatozoa compared to those carrying the G allele. Additionally, there was an improvement in cleavage rate and enhanced embryo rates at 6 and 8 days. Consequently, the A allele at codon 26 of the *PRND* gene has been suggested to correlate with male reproductive performance. Although individuals carrying SNPs that may significantly impact reproductive capacity could have been culled from the breeding population, the degree of variation in reproductive ability may depend on the extent to which *PRND* SNPs affect the functional characteristics of Doppel protein. Therefore, further functional studies in natural rabbit populations, which lack the artificial selection present in the breeding population used in this study, are needed to elucidate the relationship between *PRND* polymorphism and reproductive capacity.

In this study, we investigated the polymorphism of the leporine *PRND* gene and analyzed its characteristics. The hybrid breeding rabbits we utilized are primarily consumed breeds in Korea. All individuals included in this study were sourced from rabbits slaughtered at regional abattoirs of the Korea Rabbit & Deer Farmers National Agricultural Cooperative Federation during sample collection. To determine whether rabbits from different breeds exhibit genotype distributions or novel polymorphisms distinct from those observed in this study, future genetic analysis studies on various rabbit breeds, particularly native breeds, will be necessary.

TABLE 3 Haplotype frequencies of the leporine prion-like protein gene (*PRND*) single nucleotide polymorphisms (SNPs).

| Haplotype | Frequency, *n* (%) |
|---|---|
| GCCCAGGGA | 194 (46.9) |
| AGTTGAGAA | 192 (46.6) |
| AGCCAGCGG | 24 (6) |
| AGTTGAGGA | 2 (0.2) |
| AGCCGGGAA | 2 (0.2) |

## Conclusion

In the present study, we found nine novel SNPs in the leporine *PRND* gene, including four deleterious non-synonymous SNPs. In addition, we performed LD analysis between *PRNP* and *PRND* polymorphisms and found strong LD between *PRNP* (c.234C > T) and *PRND* SNPs (c.525G > C and c.579A > G). The remaining seven *PRND* SNPs (c.18A > G, c.76G > C, c.128C > T, c.146C > T, c.315A > G, c.488G > A, and c.544G > A) showed weak linkage with *PRNP* SNP. To the best of our knowledge, this study is the first to present a genetic characterization of *PRND* SNPs in rabbits.

TABLE 4 *In silico* prediction of the functional effect of non-synonymous single nucleotide polymorphisms (SNPs) in the leporine prion-like protein gene (*PRND*).

| Variation | PolyPhen-2 | | SIFT | | PANTHER | | Missense3D |
|---|---|---|---|---|---|---|---|
| | Score | Prediction | Score | Prediction | Score | Prediction | Prediction |
| c.76G > C (A26P) | 0.895 | Possibly damaging | 0 | Damaging | – | Not scored | No structural damage detected |
| c.128C > T (T43M) | 0.924 | Possibly damaging | 0 | Damaging | 0.19 | Probably benign | No structural damage detected |
| c.146C > T (A49V) | 0.991 | Probably damaging | 0 | Damaging | 0.27 | Probably benign | No structural damage detected |
| c.488G > A (R163Q) | 0.816 | Possibly damaging | 0 | Damaging | 0.27 | Probably benign | No structural damage detected |

TABLE 5 Linkage disequilibrium (LD) scores between leporine prion protein gene (*PRNP*) and prion-like protein gene (*PRND*) single nucleotide polymorphisms (SNPs).

| $r^2$ | *PRND* | | | | | | | | |
|---|---|---|---|---|---|---|---|---|---|
| | c.18A > G | c.76G > C | c.128C > T | c.146C > T | c.315A > G | c.488G > A | c.525G > C | c.544G > A | c.579A > G |
| *PRNP* c.234C>T | 0.052 | 0.052 | 0.05 | 0.05 | 0.051 | 0.05 | **0.912** | 0.05 | **0.912** |

Bold indicates strong LD with $r^2 > 0.3$.

## Data availability statement

The data presented in the study are deposited in the DRYAD repository (https://datadryad.org/stash/share/3gw51vGYS1FWIFzOBEC5JEfIhPxygvyC9eAgSh3SwKI).

## Ethics statement

The animal study was approved by the overall experimental processes were approved by the Jeonbuk National University Institutional Animal Care and Use Committee (CBNU 2019-058). All experiments were performed in accordance with the Korea Experimental Animal Protection Act. The study was conducted in accordance with the local legislation and institutional requirements.

## Author contributions

M-JJ: Conceptualization, Formal analysis, Writing – original draft, Writing – review & editing. Y-CK: Conceptualization, Formal analysis, Writing – review & editing. B-HJ: Conceptualization, Formal analysis, Writing – review & editing.

## Funding

The author(s) declare financial support was received for the research, authorship, and/or publication of this article. This research was supported by the Basic Science Research Program through the National Research Foundation (NRF) of Korea funded by the Ministry of Education (grant Nos. 2017R1A6A1A03015876 and 2021R1A6A3A01086488), National Research Foundation of Korea (NRF) grant funded by the Korean government (MSIT) (grant Nos. 2021R1A2C1013213 and 2022R1C1C2004792), and Korea Basic Science Institute (National research Facilities and Equipment Center) grant funded by the Ministry of Education (grant No. 2021R1A6C101C369). M-JJ was supported by the BK21 Four Program in the Department of Bioactive Material Sciences, Jeonbuk National University.

## Conflict of interest

The authors declare that the research was conducted in the absence of any commercial or financial relationships that could be construed as a potential conflict of interest.

## Publisher's note



## References

1. Prusiner SB. Prions. *Proc Natl Acad Sci USA*. (1998) 95:13363–83. doi: 10.1073/pnas.95.23.13363

2. Collins SJ, Lawson VA, Masters CL. Transmissible spongiform encephalopathies. *Lancet*. (2004) 363:51–61. doi: 10.1016/S0140-6736(03)15171-9

3. Mead S, Lloyd S, Collinge J. Genetic factors in mammalian prion diseases. *Annu Rev Genet*. (2019) 53:117–47. doi: 10.1146/annurev-genet-120213-092352

4. Qing LL, Zhao H, Liu LL. Progress on low susceptibility mechanisms of transmissible spongiform encephalopathies. *Dongwuxue Yanjiu*. (2014) 35:436–45. doi: 10.13918/j.issn.2095-8137.2014.5.436

5. Moore J, Hawkins SA, Austin AR, Konold T, Green RB, Blamire IW, et al. Studies of the transmissibility of the agent of bovine spongiform encephalopathy to the domestic chicken. *BMC Res Notes*. (2011) 4:501. doi: 10.1186/1756-0500-4-501

6. Myers R, Cembran A, Fernandez-Funez P. Insight from animals resistant to prion diseases: deciphering the genotype-Morphotype-phenotype code for the prion protein. *Front Cell Neurosci*. (2020) 14:254. doi: 10.3389/fncel.2020.00254

7. Barlow RM, Rennie JC. The fate of Me7 scrapie infection in rats, guinea-pigs and rabbits. *Res Vet Sci*. (1976) 21:110–1. doi: 10.1016/S0034-5288(18)33406-4

8. Gibbs CJ Jr, Gajdusek DC. Experimental subacute spongiform virus encephalopathies in Primates and other laboratory animals. *Science*. (1973) 182:67–8. doi: 10.1126/science.182.4107.67

9. Vorberg I, Groschup MH, Pfaff E, Priola SA. Multiple amino acid residues within the rabbit prion protein inhibit formation of its abnormal isoform. *J Virol*. (2003) 77:2003–9. doi: 10.1128/jvi.77.3.2003-2009.2003

10. Chianini F, Fernandez-Borges N, Vidal E, Gibbard L, Pintado B, de Castro J, et al. Rabbits are not resistant to prion infection. *Proc Natl Acad Sci USA*. (2012) 109:5080–5. doi: 10.1073/pnas.1120076109

11. Khan MQ, Sweeting B, Mulligan VK, Arslan PE, Cashman NR, Pai EF, et al. Prion disease susceptibility is affected by Beta-structure folding propensity and local side-chain interactions in Prp. *Proc Natl Acad Sci USA*. (2010) 107:19808–13. doi: 10.1073/pnas.1005267107

12. Peoc'h K, Guerin C, Brandel JP, Launay JM, Laplanche JL. First report of polymorphisms in the prion-like protein gene (PRND): implications for human prion diseases. *Neurosci Lett*. (2000) 286:144–8. doi: 10.1016/s0304-3940(00)01100-9

13. Won SY, Kim YC, Do K, Jeong BH. The first report of genetic polymorphisms of the equine Sprn gene in outbred horses, Jeju and Halla horses. *Animals (Basel)*. (2021) 11:2574. doi: 10.3390/ani11092574

14. Kim YC, Kim HH, Kim AD, Jeong BH. Novel insertion/deletion polymorphisms and genetic features of the shadow of prion protein gene (Sprn) in dogs, a prion-resistant animal. *Front Vet Sci*. (2022) 9:942289. doi: 10.3389/fvets.2022.942289

15. Kim YC, Kim HH, Kim K, Kim AD, Jeong BH. Novel polymorphisms and genetic characteristics of the shadow of prion protein gene (Sprn) in cats, hosts of feline spongiform encephalopathy. *Viruses*. (2022) 14:981. doi: 10.3390/v14050981

16. Roh IS, Kim YC, Kim HJ, Won SY, Jeong MJ, Hwang JY, et al. Polymorphisms of the prion-related protein gene are strongly associated with Cervids' susceptibility to chronic wasting disease. *Vet Rec*. (2022) 190:e940. doi: 10.1002/vetr.940

17. Kim YC, Kim HH, Jeong BH. The first report of polymorphisms and genetic characteristics of the shadow of prion protein (Sprn) in prion disease-resistant animal, chickens. *Front Vet Sci*. (2022) 9:904305. doi: 10.3389/fvets.2022.904305

18. Jeong BH, Kim NH, Kim JI, Carp RI, Kim YS. Polymorphisms at codons 56 and 174 of the prion-like protein gene (PRND) are not associated with sporadic Creutzfeldt-Jakob disease. *J Hum Genet*. (2005) 50:311–4. doi: 10.1007/s10038-005-0254-8

19. Kim YC, Jeong BH. First report of prion-related protein gene (Prnt) polymorphisms in cattle. *Vet Rec*. (2018) 182:717. doi: 10.1136/vr.104123

20. Roh IS, Kim YC, Kim HJ, Won SY, Jeong MJ, Kang HE, et al. Identification of the prion-related protein gene (Prnt) sequences in various species of the Cervidae Family. *Mol Biol Rep*. (2020) 47:6155–64. doi: 10.1007/s11033-020-05697-9

21. Kim YC, Jeong BH. The first report of prion-related protein gene (Prnt) polymorphisms in goat. *Acta Vet Hung*. (2017) 65:291–300. doi: 10.1556/004.2017.028

22. Kim YC, Kim SK, Jeong BH. Scrapie susceptibility-associated Indel polymorphism of shadow of prion protein gene (Sprn) in Korean native black goats. *Sci Rep*. (2019) 9:15261. doi: 10.1038/s41598-019-51625-8

23. Jeong BH, Kim YS. Genetic studies in human prion diseases. *J Korean Med Sci*. (2014) 29:623–32. doi: 10.3346/jkms.2014.29.5.623

24. Benvegnu S, Franciotta D, Sussman J, Bachi A, Zardini E, Torreri P, et al. Prion protein paralog Doppel protein interacts with Alpha-2-macroglobulin: a plausible mechanism for Doppel-mediated neurodegeneration. *PLoS One*. (2009) 4:e5968. doi: 10.1371/journal.pone.0005968

25. Moore RC, Lee IY, Silverman GL, Harrison PM, Strome R, Heinrich C, et al. Ataxia in prion protein (Prp)-deficient mice is associated with upregulation of the novel Prp-like protein Doppel. *J Mol Biol*. (1999) 292:797–817. doi: 10.1006/jmbi.1999.3108

26. Croes EA, Alizadeh BZ, Bertoli-Avella AM, Rademaker T, Vergeer-Drop J, Dermaut B, et al. Polymorphisms in the prion protein gene and in the Doppel gene increase susceptibility for Creutzfeldt-Jakob disease. *Eur J Hum Genet*. (2004) 12:389–94. doi: 10.1038/sj.ejhg.5201161

27. Jeong BH, Kim NH, Choi EK, Lee C, Song YH, Kim JI, et al. Polymorphism at 3' Utr +28 of the prion-like protein gene is associated with sporadic Creutzfeldt-Jakob disease. *Eur J Hum Genet*. (2005) 13:1094–7. doi: 10.1038/sj.ejhg.5201460

28. Kim YC, Jeong BH. Bovine spongiform encephalopathy (Bse) associated polymorphisms of the prion-like protein gene (PRND) in Korean dairy cattle and Hanwoo. *J Dairy Res*. (2018) 85:7–11. doi: 10.1017/S0022029917000814

29. Mesquita P, Batista M, Marques MR, Santos IC, Pimenta J, Silva Pereira M, et al. Prion-like Doppel gene polymorphisms and scrapie susceptibility in Portuguese sheep breeds. *Anim Genet*. (2010) 41:311–4. doi: 10.1111/j.1365-2052.2009.01992.x

30. Jeong MJ, Kim YC, Jeong BH. Prion-like protein gene (PRND) polymorphisms associated with scrapie susceptibility in Korean native black goats. *PLoS One*. (2018) 13:e0206209. doi: 10.1371/journal.pone.0206209

31. Won SY, Kim YC, Kim K, Kim AD, Jeong BH. The first report of polymorphisms and genetic features of the prion-like protein gene (PRND) in a prion disease-resistant animal, dog. *Int J Mol Sci*. (2019) 20:1404. doi: 10.3390/ijms20061404

32. Jeong MJ, Jeong BH. No polymorphisms in the coding region of the prion-like protein gene in thoroughbred racehorses. *Acta Vet Hung*. (2019) 67:174–82. doi: 10.1556/004.2019.019

33. Won SY, Kim YC, Do K, Jeong BH. Absence of strong genetic linkage disequilibrium between single nucleotide polymorphisms (Snps) in the prion protein gene (Prnp) and the prion-like protein gene (PRND) in the horse, a prion-resistant species. *Genes (Basel)*. (2020) 11:518. doi: 10.3390/genes11050518

34. Premzl M, Gamulin V. Comparative genomic analysis of prion genes. *BMC Genomics*. (2007) 8:1. doi: 10.1186/1471-2164-8-1

35. Hosking L, Lumsden S, Lewis K, Yeo A, McCarthy L, Bansal A, et al. Detection of genotyping errors by hardy-Weinberg equilibrium testing. *Eur J Hum Genet*. (2004) 12:395–9. doi: 10.1038/sj.ejhg.5201164

36. Gomes I, Collins A, Lonjou C, Thomas NS, Wilkinson J, Watson M, et al. Hardy-Weinberg quality control. *Ann Hum Genet*. (1999) 63:535–8. doi: 10.1046/j.1469-1809.1999.6360535.x

37. Gabriel SB, Schaffner SF, Nguyen H, Moore JM, Roy J, Blumenstiel B, et al. The structure of haplotype blocks in the human genome. *Science*. (2002) 296:2225–9. doi: 10.1126/science.1069424

38. Kim DJ, Kim YC, Jeong BH. First report of a novel polymorphism and genetic characteristics of the leporine prion protein (Prnp) gene. *Front Vet Sci*. (2023) 10:1229369. doi: 10.3389/fvets.2023.1229369

39. Fernandez-Borges N, Parra B, Vidal E, Erana H, Sanchez-Martin MA, de Castro J, et al. Unraveling the key to the resistance of canids to prion diseases. *PLoS Pathog*. (2017) 13:e1006716. doi: 10.1371/journal.ppat.1006716

40. Otero A, Bolea R, Hedman C, Fernandez-Borges N, Marin B, Lopez-Perez O, et al. An amino acid substitution found in animals with low susceptibility to prion diseases confers a protective dominant-negative effect in prion-infected transgenic mice. *Mol Neurobiol*. (2018) 55:6182–92. doi: 10.1007/s12035-017-0832-8

41. Sanchez-Garcia J, Fernandez-Funez P. D159 and S167 are protective residues in the prion protein from dog and horse, two prion-resistant animals. *Neurobiol Dis*. (2018) 119:1–12. doi: 10.1016/j.nbd.2018.07.011

42. Perez DR, Damberger FF, Wuthrich K. Horse prion protein Nmr structure and comparisons with related variants of the mouse prion protein. *J Mol Biol*. (2010) 400:121–8. doi: 10.1016/j.jmb.2010.04.066

43. Kurt TD, Bett C, Fernandez-Borges N, Joshi-Barr S, Hornemann S, Rulicke T, et al. Prion transmission prevented by modifying the Beta2-Alpha2 loop structure of host Prpc. *J Neurosci*. (2014) 34:1022–7. doi: 10.1523/JNEUROSCI.4636-13.2014

44. Zhang J. The structural stability of wild-type horse prion protein. *J Biomol Struct Dyn*. (2011) 29:369–77. doi: 10.1080/07391102.2011.10507391

45. Wen Y, Li J, Yao W, Xiong M, Hong J, Peng Y, et al. Unique structural characteristics of the rabbit prion protein. *J Biol Chem*. (2010) 285:31682–93. doi: 10.1074/jbc.M110.118844

46. Won SY, Kim YC, Kim SK, Jeong BH. The first report of genetic and structural diversities in the SPRN gene in the horse, an animal resistant to prion disease. *Genes (Basel)*. (2019) 11:39. doi: 10.3390/genes11010039

47. Lee YR, Kim YC, Won SY, Jeong MJ, Park KJ, Park HC, et al. Identification of a novel risk factor for chronic wasting disease (Cwd) in elk: S100g single nucleotide polymorphism (Snp) of the prion protein gene (Prnp). *Vet Res*. (2023) 54:48. doi: 10.1186/s13567-023-01177-7

48. Jo WS, Kim YC, Oem JK, Jeong BH. First report of structural characteristics and polymorphisms of the prion protein gene in raccoon dogs: the possibility of prion disease-resistance. *Front Vet Sci*. (2022) 9:989352. doi: 10.3389/fvets.2022.989352

49. Kim KH, Kim YC, Jeong BH. Novel polymorphisms and genetic characteristics of the prion protein gene in pheasants. *Front Vet Sci*. (2022) 9:935476. doi: 10.3389/fvets.2022.935476

50. Kim YC, Kim SK, Won SY, Jeong BH. Polymorphisms of shadow of prion protein gene (Sprn) in Korean native cattle (Hanwoo) and Holstein cattle. *Sci Rep*. (2020) 10:15272. doi: 10.1038/s41598-020-72225-x

51. Kim Y, Kim YC, Jeong BH. Novel single nucleotide polymorphisms (Snps) and genetic features of the prion protein gene (Prnp) in quail (*Coturnix Japonica*). *Front Vet Sci*. (2022) 9:870735. doi: 10.3389/fvets.2022.870735

52. Kim HH, Kim YC, Kim K, Kim AD, Jeong BH. Novel polymorphisms and genetic features of the prion protein gene (Prnp) in cats, hosts of feline spongiform encephalopathy. *Genes (Basel)*. (2020) 12:13. doi: 10.3390/genes12010013

53. Jeong MJ, Wang Z, Zou WQ, Kim YC, Jeong BH. The first report of polymorphisms of the prion protein gene (Prnp) in Pekin ducks (*Anas Platyrhynchos* Domestica). *Front Vet Sci*. (2023) 10:1273050. doi: 10.3389/fvets.2023.1273050

54. Uboldi C, Del Vecchio I, Foti MG, Azzalin A, Paulis M, Raimondi E, et al. Prion-like Doppel gene (PRND) in the goat: genomic structure, Cdna, and polymorphisms. *Mamm Genome*. (2005) 16:963–71. doi: 10.1007/s00335-005-0084-1

55. Behrens A, Genoud N, Naumann H, Rulicke T, Janett F, Heppner FL, et al. Absence of the prion protein homologue Doppel causes male sterility. *EMBO J*. (2002) 21:3652–8. doi: 10.1093/emboj/cdf386

56. Paisley D, Banks S, Selfridge J, McLennan NF, Ritchie AM, McEwan C, et al. Male infertility and DNA damage in Doppel knockout and prion protein/Doppel double-knockout mice. *Am J Pathol*. (2004) 164:2279–88. doi: 10.1016/S0002-9440(10)63784-4

57. Ferreira LM, Garcia-Herreros M, Domingos A, Marques CC, Mesquita P, Barbas JP, et al. Prion protein 2 (Dublet) gene (PRND): role in ovine semen capacitation, cryopreservation and fertility. *Reprod Fertil Dev*. (2017) 29:985–97. doi: 10.1071/RD15214

frontiers | Frontiers in Veterinary Science

TYPE Original Research
PUBLISHED 26 June 2024
DOI 10.3389/fvets.2024.1388532



OPEN ACCESS

EDITED BY
Izhar Hyder Qazi,
Shaheed Benazir Bhutto University of Veterinary &Animal Sciences, Pakistan

REVIEWED BY
Lihua Wang,
Qingdao Agricultural University, China
Grant B. McClelland,
McMaster University, Canada

*CORRESPONDENCE
Zhipeng Li
✉ zhplicaas@163.com
Lele Ji
✉ jilele@fmmu.edu.cn
Chao Xu
✉ xcjlau@163.com

†These authors have contributed equally to this work and share first authorship

RECEIVED 04 April 2024
ACCEPTED 10 June 2024
PUBLISHED 26 June 2024

CITATION
Zhu Y, Yuan Y, Si H, Li S, Zhao F, Mu R, Lin Z, Wang X, Qiu Q, Xu C, Ji L and Li Z (2024) Lipidomic and transcriptomic profiles provide new insights into the triacylglycerol and glucose handling capacities of the Arctic fox. *Front. Vet. Sci.* 11:1388532. doi: 10.3389/fvets.2024.1388532



# Lipidomic and transcriptomic profiles provide new insights into the triacylglycerol and glucose handling capacities of the Arctic fox

Yuhang Zhu[1†], Yuan Yuan[2†], Huazhe Si[1,3], Songze Li[1], Fei Zhao[1], Ruina Mu[1], Zihan Lin[4], Xiaoxu Wang[5], Qiang Qiu[2], Chao Xu[1*], Lele Ji[6*] and Zhipeng Li[1,3*]

[1]College of Animal Science and Technology, Jilin Agricultural University, Changchun, China, [2]School of Ecology and Environment, Northwestern Polytechnical University, Xi'an, China, [3]Key Lab of Animal Production, Product Quality and Security, Ministry of Education, Jilin Agricultural University, Changchun, China, [4]College of Plant Protection, Jilin Agricultural University, Changchun, China, [5]Department of Special Animal Nutrition and Feed Science, Institute of Special Animal and Plant Sciences, Chinese Academy of Agricultural Sciences, Changchun, China, [6]National Demonstration Center for Experimental Preclinical Medicine Education, The Fourth Military Medical University, Xi'an, China

The Arctic fox (*Vulpes lagopus*) is a species indigenous to the Arctic and has developed unique lipid metabolism, but the mechanisms remain unclear. Here, the significantly increased body weight of Arctic foxes was consistent with the significantly increased serum very-low-density lipoprotein (VLDL), and the 40% crude fat diet further increased the Arctic fox body weight. The enhanced body weight gain stems primarily from increased subcutaneous adipose tissue accumulation. The adipose triacylglycerol and phosphatidylethanolamine were significantly greater in Arctic foxes. The adipose fatty-acid synthase content was significantly lower in Arctic foxes, highlighting the main role of exogenous fatty-acids in fat accumulation. Considering the same diet, liver-derived fat dominates adipose expansion in Arctic foxes. Liver transcriptome analysis revealed greater fat and VLDL synthesis in Arctic foxes, consistent with the greater VLDL. Glucose homeostasis wasn't impacted in Arctic foxes. And the free fatty-acids in adipose, which promote insulin resistance, also did not differ between groups. However, the hepatic glycogen was greater in Arctic foxes and transcriptome analysis revealed upregulated glycogen synthesis, improving glucose homeostasis. These results suggest that the superior fat accumulation capacity and distinct characteristics of hepatic and adipose lipid and glucose metabolism facilitate glucose homeostasis and massive fat accumulation in Arctic foxes.

KEYWORDS

**fatty acid oxidation, insulin-like growth factor 1, lipid droplets, uridine, VLDL, glycogen**

## 1 Introduction

The Arctic fox (*Vulpes lagopus*), the smallest nonhibernating carnivore in Arctic regions, has developed notable adaptations to increase its survival rate and withstand extreme winter temperatures (1). These adaptations include a dietary preference for seabirds, eggs and animal carcasses (2), which leads to a significant increase in body mass through the accumulation of

adipose tissue during autumn (3). The increased dietary fat consumption is usually associated with nonalcoholic fatty liver disease (NAFLD), diabetes and hyperlipidemia in humans and rodents (4, 5). However, the intake of a diet containing 40% crude fat does not have adverse effects on hepatic fat accumulation or serum triacylglycerol (TAG) levels in the Arctic fox (6). In contrast, the silver fox (*Vulpes vulpes*), a species evolutionary close to the Arctic fox, displays a significantly increased serum TAG level upon consumption of a diet containing 26.11% crude fat in comparison with a 14.71% crude fat diet (7). This stark discrepancy suggests that the Arctic fox possesses unique adaptations for lipid metabolism.

To better understand these advantageous characteristics of the Arctic fox, comparative genomic analyses have been performed and have highlighted several positively selected genes related to lipid metabolism and pyrimidine metabolism (8, 9), identified a single-nucleotide polymorphism of Insulin induced gene 2 (*Insig2*) in the Arctic fox, and increased expression of this gene reduced hepatic lipogenesis in rats (10). Moreover, comparative transcriptomic analysis of the liver, brain and kidney in the Arctic fox revealed that *Gltpd1* and *Akt2*, genes associated with fatty acid metabolism, were under positive selection (11). *Akt2*, in particular, promotes anabolic lipid metabolism in the liver through the insulin signaling pathway (12). These findings collectively underscore the significance of the genetic basis of lipid metabolism in the Arctic fox and the interconnection between fatty acid and glucose metabolism.

The liver is the central organ that controls lipid and glucose homeostasis (13). TAG can be packaged into very-low-density lipoprotein (VLDL) particles and exported from the liver, with increased VLDL assembly ameliorating NAFLD caused by hepatic lipid droplet accumulation (14, 15). Additionally, the liver maintains blood glucose homeostasis through glycogen synthesis and breakdown (16). Moreover, insulin-like growth factor 1 (IGF-1) produced in the liver not only mediates glycogen synthesis (17) but also functions as a critical hormone for fuel metabolism, increasing glucose tolerance and insulin sensitivity in mice (18). Further evidence for the role of IGF-1 in lipid metabolism includes the significant increase in plasma IGF-1 during the period of rapid weight gain in the reindeer (19) and brown bear during the nonhibernation period when fat depots accumulate (20).

In this study, we investigated the body weight gain rate, serum biochemical parameters, and glucose tolerance of the Arctic fox and silver fox. Moreover, we compared the hepatic gene expression profiles using bulk RNA sequencing and further validated these profiles by determining the concentrations of metabolites or proteins. Finally, we determined the differences in lipidomic component and key enzyme concentrations in adipose tissue (Figure 1A).

# 2 Materials and methods

## 2.1 Animals, experimental design, and sample collection

Sixteen healthy male captive Arctic foxes [body weight (BW) = 5.74 ± 0.10 kg] and 7 healthy male captive silver foxes (BW = 7.08 ± 0.43 kg) that were maintained in the research farm of Jilin Agricultural University were included in this study. The Arctic foxes were randomly assigned to either a 15% crude fat diet group ($n = 8$, LFA group) or a 40% crude fat diet group ($n = 8$, HFA group). Silver foxes were fed a 15% crude fat diet ($n = 7$, LFS group). The dietary components and composition are shown in Supplementary Table S1. Each animal was individually housed, and following a one-week adaptation period, then they were fed each diet for 11 weeks, respectively. The body weight was recorded weekly. All animal procedures were approved and authorized by the Animal Ethics Committee of Jilin Agricultural University (No.20210314002) and used the ARRIVE guidelines 2.0 (21).

At the end of the study, blood samples were collected from the hindlimb vein, and centrifuged at 3,500 g for 10 min at 4°C to obtain serum. Animals were then intravenously injected with 5 mL of succinylcholine (0.4 mg/mL), and subcutaneously adipose tissue and liver tissue were collected. Tissue samples were cut into small pieces (approximately 0.5 × 0.5 cm) and immediately frozen in liquid nitrogen for further analysis. Liver samples were also cut into small pieces (1.0 × 1.0 cm) and fixed in 10% neutral buffered formalin for histological assessment.

## 2.2 Glucose homeostasis test

The intraperitoneal glucose tolerance test (IPGTT) was performed according to previous established methods (22). Briefly, 3 animals from each group at 9 weeks were selected to conduct the IPGTT. Following a 14 h overnight fast, animals were received intraperitoneal administration glucose (1 g/kg). Whole blood samples were collected from the hindlimb vein before administration (0 min) and at time points (15, 30, 60, 90, 120, 150, and 180 min) after administration, and blood glucose levels were measured using an Accu-Chek glucometer (Roche Diagnostics Shanghai Ltd., China).

## 2.3 Assessment of metabolites, enzymes, hormones, and liver histology

Serum samples was used to determine the concentrations of glucose, aspartate transaminase (AST), alanine transaminase (ALT), TAG, total cholesterol (CHO), high-density lipoprotein cholesterol (HDL-C) and low-density lipoprotein cholesterol (LDL-C) using the commercial kits (Jiancheng Bioengineering Institute, Nanjing, China) with an automatic biochemical analyzer (Vitalab Selectra E, Vitalab, Dieren, Netherlands). The concentrations of growth hormone (GH), IGF-1, insulin and VLDL in serum were measured using the commercial ELISA kits (MLbio, Shanghai, China).

The liver samples fixed in 10% neutral buffered formalin were embedded in paraffin, cut to 5 μm sections, and stained using H&E (23), and then were visualized using an Olympus AX80 microscope (Olympus Optical, Tokyo, Japan) equipped with Nikon D2X high-resolution camera (Nikon, Tokyo, Japan). The lipid droplet areas were quantified by Image J 1.53a software, and the lipid droplet areas were divided by the area of image to calculate the percentage of lipid droplet areas (24). The concentrations of glucose, TAG, adenosine 3′, 5′-phosphate (cAMP), uridine, glycogen, insulin-like growth factor 1 receptor (IGF1R) and insulin receptor substrate 1 (IRS1) in the liver were measured by the commercial kits (Jiancheng Bioengineering Institute, Nanjing, China) according to the manufacturer's instructions.

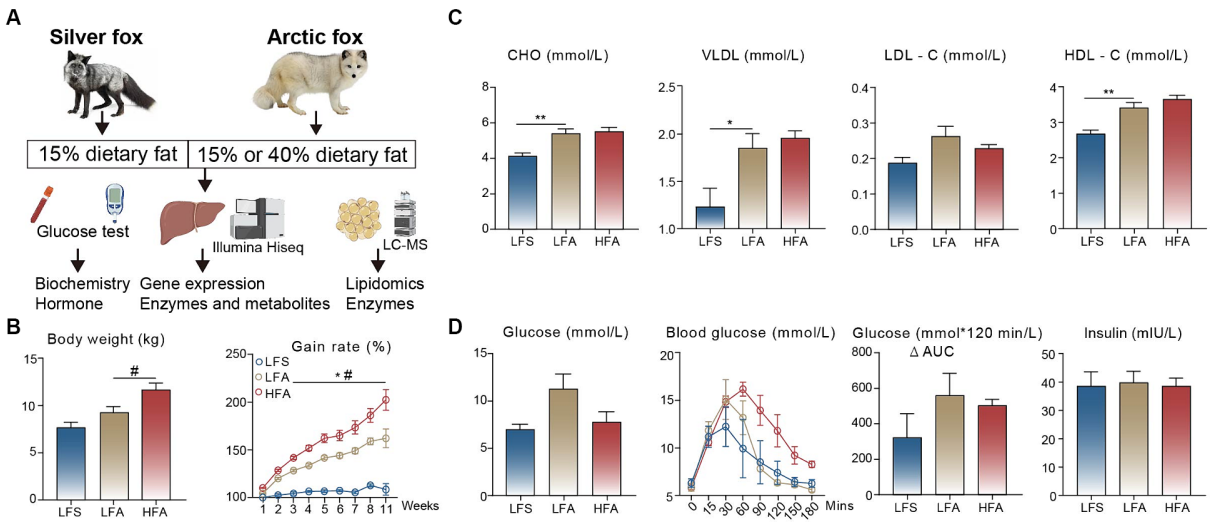


FIGURE 1
Comparison of serum biochemical analysis and glucose tolerance. **(A)** The experimental design of this study. **(B)** Final body weights and body weight gain rate (% of initial) and **(C)** serum levels of total cholesterol (CHO), very-low-density lipoprotein (VLDL), low-density lipoprotein cholesterol (LDL-C) and high-density lipoprotein cholesterol (HDL-C) among the three groups. The number of animals in the LFS, LFA, and HFA groups were 4, 5, and 5, respectively. **(D)** Assessment of glucose tolerance between arctic fox ($n$ = 3) and silver fox ($n$ = 3). Results showed as mean ± standard error of the mean (SEM). * indicates significant differences between the LFA group and the LFS group ($p < 0.05$), # indicates significant differences between the HFA group and the LFA group ($p < 0.05$). * $p < 0.05$, ** $p < 0.01$.

## 2.4 Liver bulk-RNA sequencing and bioinformatics analysis

Total RNA from liver samples was extracted using the RNeasy Mini Kit (QIAGEN, CA, United States). RNA purity, concentration and integrity were determined using a NanoPhotometer® (IMPLEN, CA, United States), an Agilent 2,100 bioanalyzer in combination with the RNA Nano 6,000 assay kit (Agilent Technologies, CA, United States). A total of 1–3 μg of RNA from each sample with an integrity number greater than 7.0 was used to construct the RNA-Seq library using the VAHTS Universal V6 RNA-seq Library Prep Kit for Illumina®. The cDNA concentration of constructed library was measured using the Qubit® RNA Assay Kit in Qubit® 3.0. Each library was then sequenced on a Novaseq 6000 platform, producing 150 bp paired-end reads.

Trimmomatic (25) was used to remove low quality and adapter sequences, and HISAT2 was employed to align the remaining clean reads to the reference genomes of the Arctic fox and silver fox, respectively (8, 26, 27). Gene expression level was calculated using the raw count data. Differentially expressed genes (DEGs) were determined using the DeSeq2 package (28) based on the threshold $|\log_2 FC| > 0.5$ and Benjamini-Hochberg adjusted $p$ value <0.05. The weighted gene coexpression network analysis (WGCNA) was conducted to explore the correlation between DEGs and serum biochemical indices using the WGCNA package (29). The clusterProfiler package was utilized to conduct Gene Ontology (GO) term and Kyoto Encyclopedia of Gene and Genomics (KEGG) pathway enrichment analyses (30).

## 2.5 Adipose lipidomic analysis and enzyme examination

A total of 20 mg adipose tissue from each animal in the LFA and LFS groups was dissolved in 400 μL water, vortexed for 60 s, and homogenized at 45 Hz for 4 min, and sonicated for 5 min in ice-water bath. The homogenization and sonication circle were repeated for 3 times. A 20 μL portion of the homogenate was mixed with 180 μL water, and then 480 μL extract solution (MTBE: MeOH = 5:1) containing internal standard (Supplementary Table S2) was added. After vortexing for 60 s, the samples were sonicated for 10 min in ice-water bath. The samples were then centrifuged at 3,000 rpm for 15 min at 4°C. A 250 μL supernatant was transferred to a fresh tube. The remaining sample was mixed with 250 μL of MTBE, followed with vortex, sonication and centrifugation, and another 250 μL supernatant was collected. The supernatants were combined and dried in a vacuum concentrator at 37°C and were reconstituted in 200 μL resuspension buffer (DCM: MeOH: $H_2O$ = 60: 30: 4.5). The samples were vortexed for 30 s and sonicated for 10 min in ice-water bath. The mixture was then centrifuged at 12,000 rpm for 15 min at 4°C, and 35 μL of supernatant was transferred to a fresh glass vial for LC/MS analysis.

The ultra-high-performance liquid chromatography (UHPLC) separation was performed using a SCIEX ExionLC series UHPLC System. The mobile phase A consisted of 40% water, 60% acetonitrile, and 10 mmol/L ammonium formate. The mobile phase B consisted of 10% acetonitrile and 90% isopropanol, and 10 mmol/L ammonium formate. The column temperature was set to 45°C, while the auto-sampler temperature was set to 6°C. The injection volume was 2 μL. The Biobud-v2.1.4.1 Software (Biotree Biotech Co., Ltd., Shanghai, China) was used to quantify the metabolites. The absolute content of individuals lipids corresponding to the internal standard was calculated based on peak area and the actual concentration of the identical lipid class internal standard. Principal component analysis (PCA) was applied to reveal the differences of lipids. The value of variable importance in the projection (VIP) of the first principal component in orthogonal projections to latent structures discriminant analysis (OPLS-DA) was determined. Metabolites with VIP > 1 and a

Benjamini-Hochberg adjusted $p$ value <0.05 (student's $t$-test) were considered as significantly changed metabolites (31).

The concentrations of LPCAT4 and FAS were measured by commercial kits from Jiancheng Bioengineering Institute (Nanjing, China) and BiotechPack (Beijing, China), respectively, according to the manufacturer's instructions.

## 2.6 Statistical analysis

One-way ANOVA was utilized to determine the statistical significance of final body weights, serum biochemical indices and hormones, areas under curves of IPGTT, liver lipid droplets areas, metabolites and proteins among the LFA, HFA, and LFS groups. The unpaired $t$-test was performed to identify the statistical significance of adipose metabolites and proteins between the LFS and LFA groups. The statistical analysis was performed using Graphpad Prism (version 9.0.0, GraphPad Software Inc., San Diego, CA, United States). All $p$ value < 0.05 were considered to indicate statistical significance.

# 3 Results

## 3.1 Comparison of the growth, biochemical indices, and IPGTT among the three groups

We monitored body weight of Arctic and silver foxes fed a 15% crude fat diet and found that the body weight gain rate of Arctic foxes was significantly greater than that of silver foxes over the 11-week monitoring period. In addition, consumption of a 40% crude fat diet led to further increases in the body weight and the body weight gain rate of Arctic foxes (Figure 1B). Consequently, the thickness of subcutaneous adipose tissue in Arctic foxes was approximately 3 times greater than that in silver foxes (Supplementary Figure S1), indicating that the weight gain observed in Arctic foxes was due primarily to fat deposition. We measured serum biochemical parameters and found that the serum concentrations of CHO, VLDL and HDL-C in Arctic foxes were significantly greater than those in silver foxes fed a 15% crude fat diet ($p < 0.05$; Figure 1C). Notably, no differences were observed in these serum biochemical parameters between Arctic foxes fed a 15% crude fat diet and those fed a 40% crude fat diet, indicating that Arctic foxes can maintain normal blood lipid levels on a 40% crude fat diet. The serum glucose and insulin levels did not differ significantly among the three experimental groups (Figure 1D). In addition, we conducted an IPGTT and found that the glucose metabolism capacity did not differ significantly among the groups (Figure 1D), suggesting that liver function and glucose homeostasis remained largely unaffected.

## 3.2 Significant differences in gene expression, the concentrations of protein and metabolite in the liver

Histopathological analysis indicated that even upon consumption of a 40% crude fat diet, the lipid droplet area within the liver remained lower in Arctic foxes than in silver foxes (Figure 2A). Accordingly, consumption of a 40% crude fat diet did not increase the hepatic TAG content in the Arctic fox, nor did it result in elevated serum levels of AST and ALT (Supplementary Figure S2A). Transcriptomic analysis revealed significant differences in global gene expression profiles between LFA and LFS groups as well as between the LFA and HFA groups ($p < 0.01$; Figure 2B). This analysis led to the identification of DEGs in the following comparisons: LFA versus LFS and HFA versus LFA. A total of 5,504 DEGs were significantly upregulated and 1,719 DEGs were downregulated between the LFA and LFS groups (Figure 2C). In contrast, the comparison between the HFA and LFA groups revealed 30 DEGs, 15 of which were upregulated and 15 of which were downregulated (Supplementary Figure S2B), suggesting that consumption of a 40% crude fat diet does not induce substantial alterations in the liver function of Arctic foxes.

The upregulated DEGs in LFA versus LFS were significantly enriched in the PI3K-Akt signaling pathway (*Igf1*, *Igf1r*, *Irs1*), purine metabolism pathway (*Nme2*, *Cant1*, and *Adcy6*), insulin signaling pathway and pyrimidine metabolism pathway (*Nme3*, *Cant1*, and *Nt5e*) (Figure 2D; Supplementary Figure S2C). These DEGs were also significantly enriched in the following biological process terms: purine-containing compound metabolic process, glucose homeostasis, fatty acid oxidation (*Acox1*, *Acadm*, *Ppara*), pyrimidine-containing compound metabolic process and neutral lipid biosynthetic process (*Gpat3*, *Lpin3*, *Dgat1*, Figure 2E; Supplementary Figure S2C). In addition, insulin-like growth factor binding and insulin receptor substrate binding were noted as enriched molecular function terms (Figure 2E). The downregulated DEGs were enriched in the biosynthesis of cofactors, carbon metabolism, and amino sugar and nucleotide sugar metabolism pathways (Figure 2D); the biological process terms positive regulation of proteolysis and cellular amino acid metabolic process; the cellular component terms organelle outer membrane and sarcoplasmic reticulum; and the molecular function terms structural constituent of ribosome and catalytic activity (Figure 2E).

WGCNA was used to explore the associations between the DEGs and serum biochemical parameters, and 17 modules containing between 45 and 3,084 genes per module were identified (Figure 2F). Module 13 showed a significant positive correlation with the serum concentrations of CHO, HDL-C and VLDL (Figure 2F). The genes within module 13 were enriched in pathways such as ABC transporters, pyrimidine metabolism, PPAR signaling pathway and purine metabolism (Figure 2G). Triglyceride biosynthetic process, pyrimidine-containing compound metabolic process, lipid oxidation, regulation of glucose metabolic process, and response to purine-containing compound were identified as enriched biological process terms. Insulin-like growth factor 1 binding and UDP-xylosyltransferase activity were identified as enriched molecular function terms (Figure 2G). Taken together, these findings suggest that pyrimidine, purine, and glucose metabolism, along with insulin-like growth factor and insulin receptor responses, are likely enhanced in the liver of Arctic foxes. Further analysis revealed significantly greater hepatic concentrations of glycogen, cAMP, uridine, IGF1R and IRS1 in Arctic foxes than in silver foxes ($p < 0.05$); in contrast, the hepatic concentration of glucose was lower in Arctic foxes than in silver foxes, although the difference was nonsignificant (Figures 3A–C). Additionally, the serum concentration of IGF-1 was significantly greater in Arctic foxes than in silver foxes, although the serum concentration of GH was not significantly different between Arctic and silver foxes (Figure 3D).

10.3389/fvets.2024.1388532

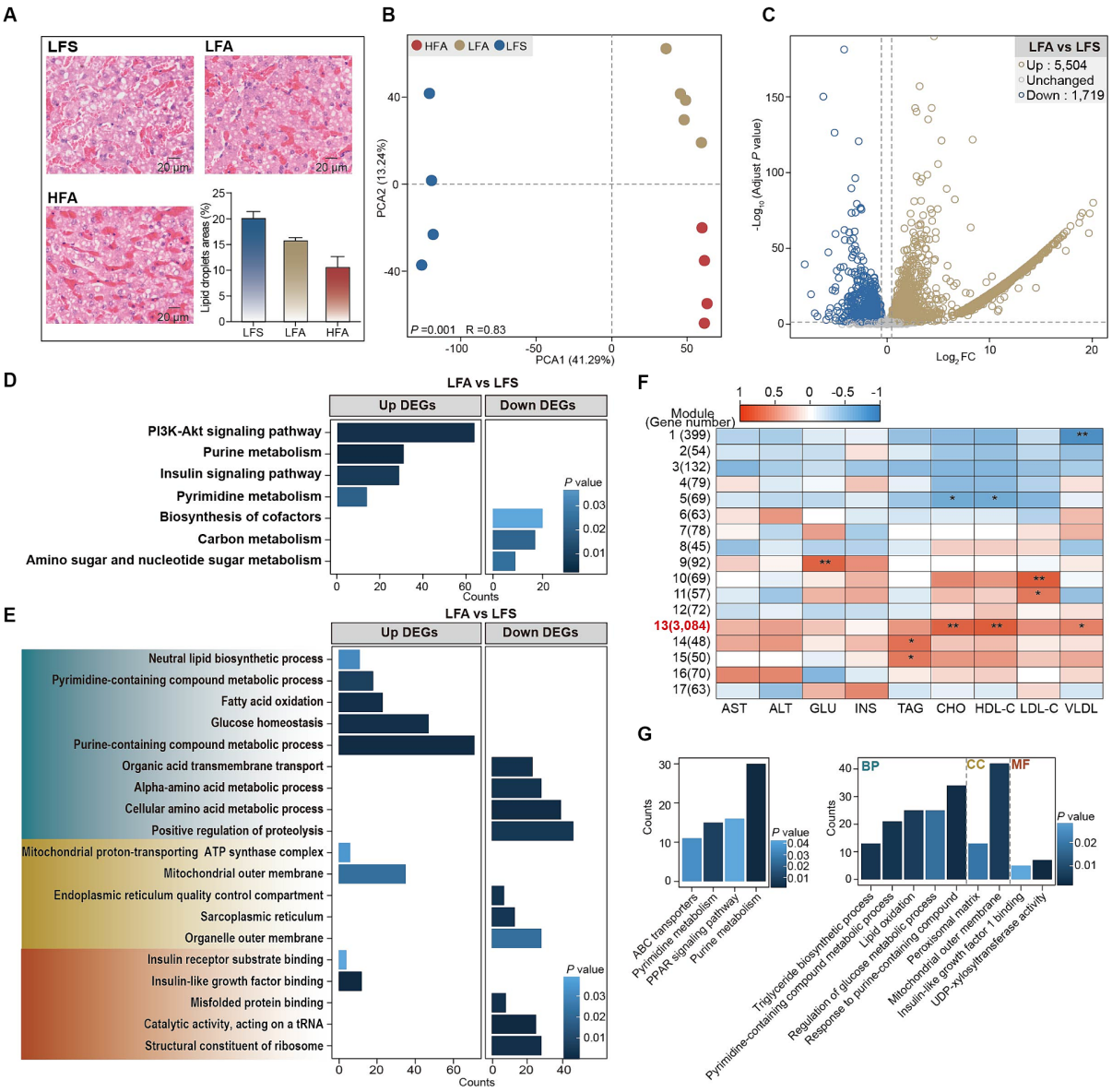


FIGURE 2
The results of histological analysis and transcriptome analysis of liver. **(A)** Liver H&E staining (scale bar, 20 μm) and lipid droplet area in liver ($n$ = 3 in each group). Results showed as mean ± SEM. **(B)** The PCA plot based on the gene count to reveal the expression profiles in liver among 3 groups. **(C)** Volcano plot to show the up- and down- differentially expressed genes (DEGs) in the comparison between LFA versus LFS. **(D)** Kyoto Encyclopedia of Gene and Genomics (KEGG) enrichment analysis of DEGs. **(E)** Gene Ontology (GO) enrichment analysis of DEGs. GO terms in green, yellow and red regions belonging to biological process, cell component and molecular function, respectively. **(F)** Correlation between the identified weighted gene coexpression network analysis (WGCNA) modules and the serum biochemical parameters. **(G)** KEGG and GO enrichment analysis of genes in the module 13. Up, significantly upregulated DEGs; Down, significantly downregulated DEGs. * $p < 0.05$, ** $p < 0.01$. GLU, glucose; INS, insulin.

## 3.3 Significantly increased TAG and PE concentrations in the adipose tissue of Arctic foxes

Given the significant changes in body mass, serum cholesterol and liver transcriptome profiles in Arctic foxes (LFA group) compared with silver foxes (LFS group), we explored the lipid composition and concentration in adipose tissue and identified 443 TAGs, 46 diacylglycerols (DAGs) and 26 phosphatidylethanolamines (PEs) (Supplementary Figure S3). TAGs constituted more than 99% of the lipid content in all the samples (Figure 4A). The total concentrations of TAG ($p < 0.05$) and PE ($p < 0.01$) in Arctic foxes were significantly greater than those in silver foxes, while the total concentration of free fatty acids (FFAs) was not significantly different (Figure 4B). The PCA results revealed that the lipid profiles were significantly different between the LFA and LFS groups ($p < 0.05$; Figure 4C). The abundances of 215 lipids were significantly increased in Arctic foxes compared with silver foxes, and the numbers of significantly increased TAGs, PEs and DAGs were 160, 14 and 12, respectively (Figure 4D; Supplementary Tables S3, S4). Further comparison revealed that 8 of the 10 lipids with the greatest $\log_2$ fold change (FC) values were TAGs and the other 2 were PEs (Figure 4E), indicating likely increases in

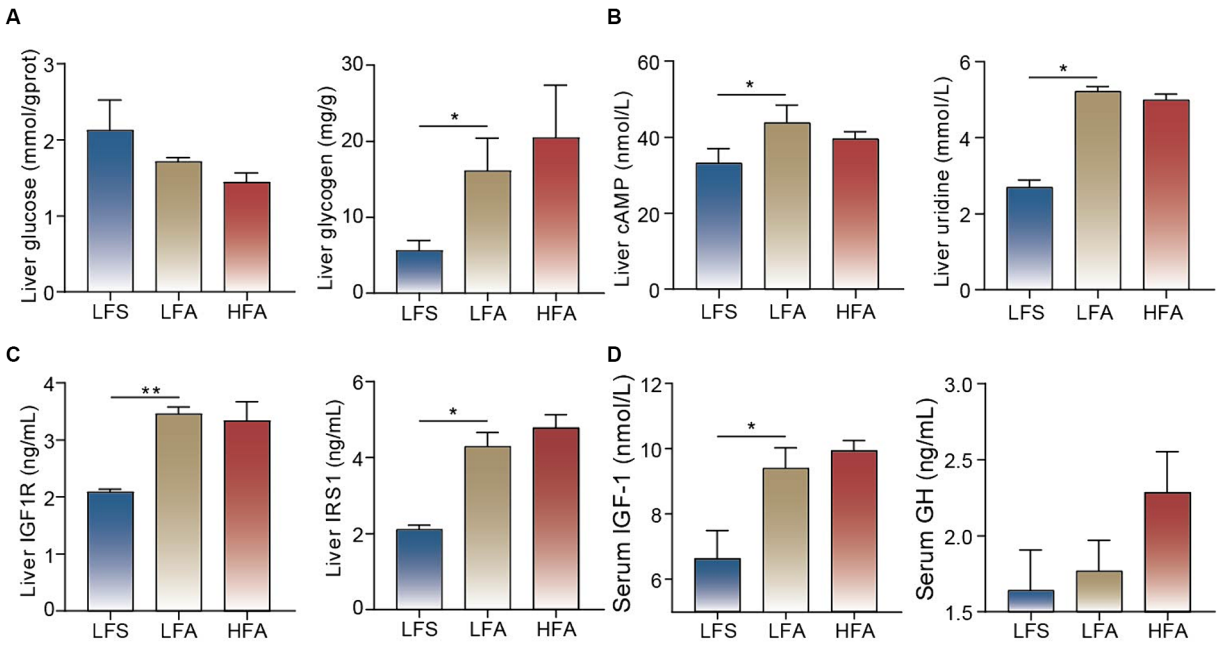


FIGURE 3
Measurement of key metabolites and hormones. **(A)** Glucose and glycogen concentrations in liver. **(B)** cAMP and uridine concentrations in liver. **(C)** Insulin like growth factor 1 receptor (IGF1R) and insulin receptor substrate 1 (IRS1) concentrations in liver among the three groups. **(D)** The concentrations of insulin-like growth factor 1 (IGF-1) and growth hormone (GH) in serum among the three groups. Results showed as mean ± SEM. * $p < 0.05$, ** $p < 0.01$.

TAG and PE synthesis. We thus measured the concentrations of LPCAT4 and FAS that catalyze the synthesis of PEs and fatty acids in adipose tissue. The concentration of LPCAT4 ($p < 0.01$) in Arctic foxes was significantly greater than that in silver foxes, while the concentration of FAS in Arctic foxes was significantly less than that in silver foxes ($p < 0.05$) (Figure 4F), suggesting the PE synthesis is increased and fatty acid synthesis is decreased in Arctic foxes.

## 4 Discussion

Our results revealed greater subcutaneous adipose deposition and body weight gain in Arctic foxes when fed a 15% or 40% crude fat diet than in silver foxes when fed a 15% crude fat diet. Previous studies revealed dramatic fat deposition in the Arctic fox and brown bear in autumn (3, 32). These findings confirmed the notable ability for fat accumulation in Arctic animals. We also found that the TAG and PE concentrations in the adipose tissue of Arctic foxes were significantly greater than those in the adipose tissue of silver foxes. This finding is consistent with the observation that the TAG and PE concentrations in adipose tissue of brown bears were greater during hibernation than during the active state (33). When the concentration of TAGs between the leaflets of the endoplasmic reticulum bilayer increases, TAGs coalesce and eventually form lipid droplets (34). It has also been reported that PE is involved in lipid droplet formation and stability (35). Moreover, the concentration of LPCAT4, the key enzyme in PE biosynthesis (36), was also significantly greater in Arctic foxes than in silver foxes. These results suggest that increased PE biosynthesis likely contributes to fat accumulation in Arctic foxes by promoting TAG storage in lipid droplets. We also found that the serum IGF-1 level was significantly higher in Arctic foxes than in silver foxes. This finding is in line with previous findings that plasma IGF-1 is increased in the reindeer and brown bear during the accumulation of fat depots (19, 20). IGF-1 can also induce lipid synthesis through the PI3K-Akt signaling pathway (37, 38). Therefore, the increased amount of IGF-1 is likely responsible for TAG and PE synthesis in the adipose tissue of Arctic foxes. Hepatic synthesis and release of IGF-1 are primarily affected by GH (39). However, the serum GH level was not significantly different between Arctic foxes and silver foxes. The expression of *Igf1r* in the liver regulates the serum IGF-1 level through a negative feedback mechanism (40). Our results showed that *Igf1r* was significantly upregulated in Arctic foxes and that the IGF1R concentration in the liver was significantly greater in Arctic foxes than in silver foxes. Therefore, the increased IGF-1 production in Arctic foxes is likely associated with IGF1R-mediated negative feedback.

Interestingly, we found that the FFA content in adipose tissue, the insulin level in serum and glucose tolerance were not significantly different between Arctic foxes and silver foxes. The brown bear also remains insulin sensitive during the fat accumulation period (32). Our results thus indicated the key role of FFA metabolism homeostasis in maintaining insulin sensitivity in the Arctic fox. However, the concentration of the crucial enzyme of *de novo* lipogenesis, FAS (41), was significantly lower in Arctic foxes than in silver foxes, leading to decreased *de novo* lipogenesis. Dietary and liver-derived FFAs can also be transported into adipose tissue. FFAs can be esterified by diglyceride acyltransferase on the surface of lipid droplets and stored in lipid droplets in the form of TAGs (42). The TAG concentration in adipose tissue was significantly greater in Arctic foxes than in silver foxes; considering the consumption of the same diet and the decreased *de novo* lipogenesis in Arctic foxes, liver-derived FFAs could be the main

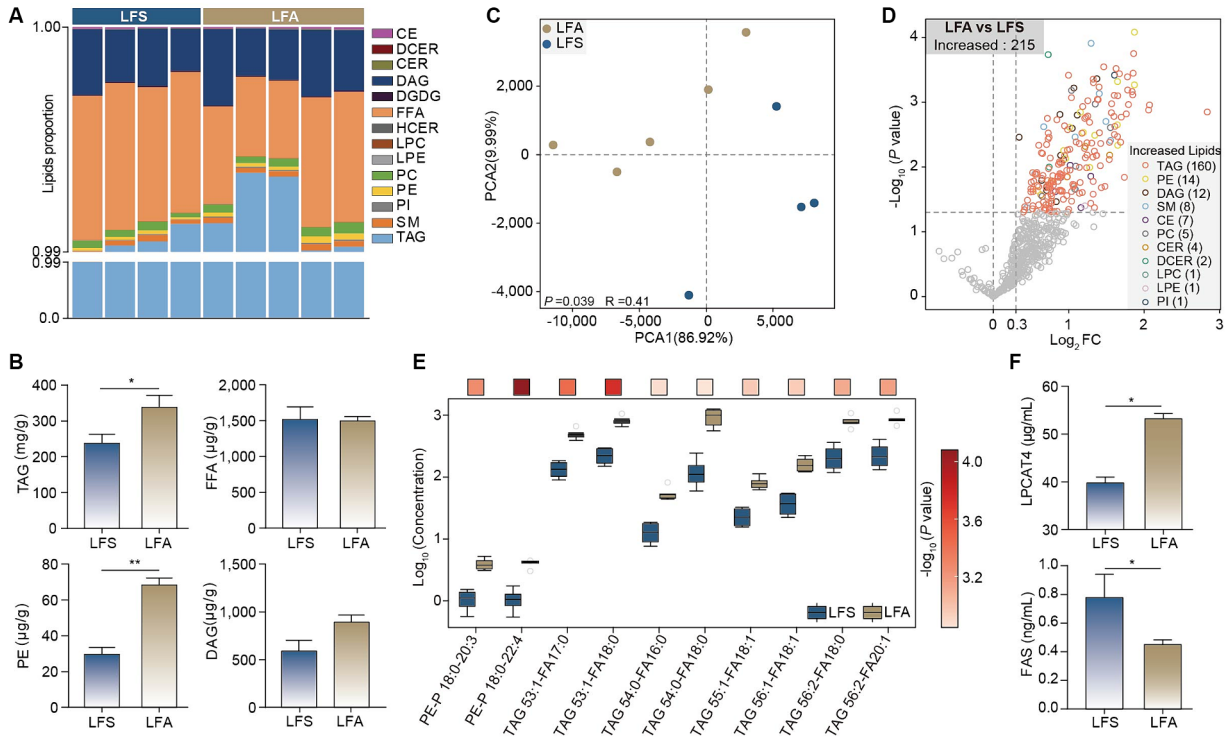


FIGURE 4
Lipidomic analysis and enzymes of adipose tissue. **(A)** The composition and proportion of the identified lipids in adipose tissue. **(B)** Differences in total concentrations of TAG, FFA, PE and DAG in adipose tissue. **(C,D)** PCA and volcano plot revealing the differences of lipid components between arctic fox and silver fox. **(E)** The top 10 different lipids in adipose tissue between arctic fox and silver fox. The color of the square indicates the significance of the different lipids from maximum (red) to minimum. **(F)** The concentrations of LPCAT4 and FAS in adipose tissue. Results showed as mean ± SEM. PE, phosphatidylethanolamines; DAG, diacylglycerols; SM, sphingomyelins; CE, cholesterol esters; PC, phosphatidylcholines; CER, ceramides; DCER, dihydroceramides; LPC, lysophosphatidylcholine; PI, phosphatidylglycerol; LPE, lysophosphatidylethanolamines; FFA, free fatty acids. * $p < 0.05$, ** $p < 0.01$.

source for TAG accumulation in Arctic foxes. Therefore, the esterification of FFAs to TAGs likely plays a role in maintaining FFA homeostasis, and liver-derived FFAs can dominate fat accumulation in the adipose tissue of Arctic foxes. Moreover, a previous study demonstrated that IGF-1 can promote adipogenesis (43), resulting in increased lipid storage and decreased insulin resistance (44). Therefore, the increased IGF-1 expression in Arctic foxes also likely promotes lipid accumulation in adipose tissue and prevents insulin resistance.

Lipid droplets are ubiquitous intracellular storage organelles specialized for the storage of excess energy in the form of neutral lipids. Surprisingly, we found that the lipid droplet area and TAG concentration in the livers of Arctic foxes were less than those in the livers of silver foxes. However, body weight gain is usually associated with an increased risk of abnormal lipid accumulation in the liver (45). Liver transcriptome analysis revealed greater differences in lipid metabolism-related genes than in other types of genes between Arctic foxes and silver foxes, and the genes upregulated in Arctic foxes were enriched in the neutral lipid biosynthesis process and pyrimidine metabolism, which involves *Dgat1* and *Nt5e*. Moreover, the genes positively correlated with the serum concentrations of CHO, HDL-C and VLDL were significantly enriched in the triglyceride biosynthetic process and pyrimidine metabolism. These findings are consistent with those of a comparative genomic analysis revealing that the positively selected genes in the Arctic fox were also significantly enriched for lipid metabolism and pyrimidine metabolism (8). The lipid metabolism and pyrimidine metabolism pathways have been reported to play important roles in hepatic lipid metabolism (46). *Dgat1* encodes a crucial enzyme involved in TAG synthesis (47), and *Nt5e* is essential for uridine synthesis during pyrimidine metabolism (48). These results indicate the crucial roles of lipid and pyrimidine metabolism in hepatic lipid homeostasis in Arctic foxes. The uridine concentration in the liver and the VLDL concentration in the serum of Arctic foxes were significantly greater than those in silver foxes. TAGs synthesized in the endoplasmic reticulum can be used for the synthesis of lipid droplets or VLDL (49). An increase in VLDL was reported to ameliorate lipid accumulation in liver (14). Previous studies revealed a role for uridine in inhibiting lipid droplet synthesis in the liver (50). *Dgat1* is also involved in VLDL synthesis and can increase the plasma VLDL concentration, while *Dgat2* (downregulated in Arctic foxes) is associated with liver steatosis (51). These results revealed that the Arctic fox may prevent abnormal lipid droplet accumulation by increasing uridine and VLDL synthesis.

Purine metabolism and fatty acid oxidation, which involve *Adcy6*, *Ppara, Acadm*, and *Acox1*, were also identified as significantly enriched in the liver of Arctic foxes. The proliferator-activated receptor alpha (PPARα) protein encoded by *Ppara* promotes the expression of *Acadm* and *Acox1*, inducing fatty acid oxidation in mitochondria and peroxisomes (52, 53). cAMP, a product of purine metabolism, can activate PPARα through the cAMP/PKA pathway (54), and *Adcy6* is the crucial gene for cAMP production (55). Moreover, the liver cAMP concentration was significantly greater in Arctic foxes than in silver foxes. These results reveal that fatty acid oxidation is likely promoted in the

10.3389/fvets.2024.1388532

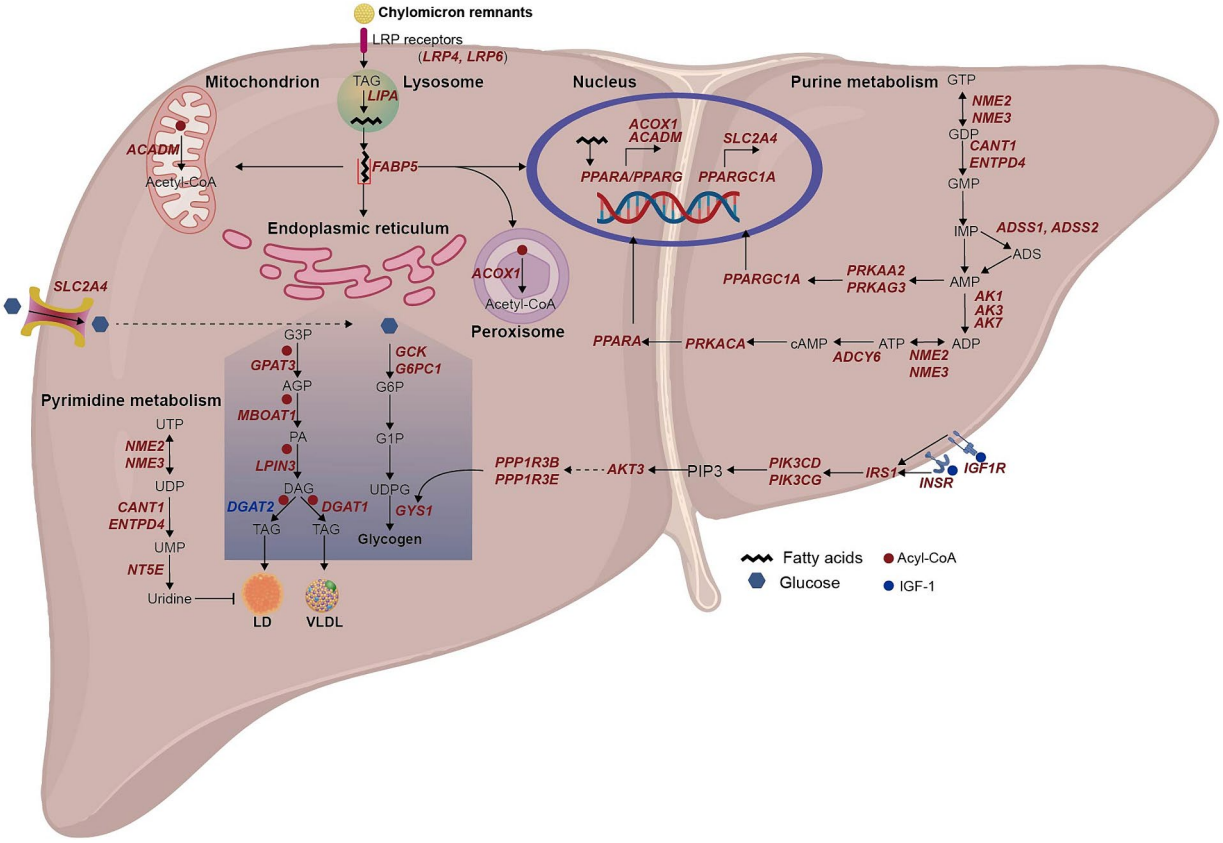


FIGURE 5
Schematic summary of lipid and glucose metabolism in hepatocyte of arctic fox. The italic red and blue texts indicate up-and down-regulated DEGs in LFA group compared to LFS group. We manually reconstructed the metabolic pathways in liver of Arctic foxes based on the significantly enriched GO terms and KEGG pathways, and the significantly different metabolites, enzymes and hormones. Then the figure was drawn using Adobe Illustrator. UTP, uridine triphosphate; UDP, uridine 5′-diphosphate; UMP, uridine monophosphate; G3P, glycerol 3-phosphate; AGP, 1-Acyl-glycerol 3-phosphate; PA, phosphatidate; DAG, diacylglycerols; TAG, triacylglycerol; LD, lipid droplet; G6P, glucose 6-phosphate; G1P, glucose 1-phosphate; UDPG, uracil-diphosphate glucose; GTP, guanosine 5′-triphosphate; GDP, guanosine 5′-diphosphate; GMP, guanosine 5′-phosphate; IMP, inosine monophosphate; ADS, adenylosuccinate; AMP, adenosine 5′-monophosphate; ADP, adenosine 5′-diphosphate; ATP, adenosine 5′-triphosphate; cAMP, adenosine 3′, 5′-phosphate; PIP3, Phosphatidylinositol-3,4,5-triphosphate.

Arctic fox through the cAMP/PKA pathway. The PI3K-AKT signaling pathway, insulin signaling pathway and the expression of *Slc2a4*, which encodes glucose transporter type 4 (GLUT4), were significantly upregulated in Arctic foxes. The PI3K-AKT signaling pathway and insulin signaling pathway are important for glucose homeostasis (56) and GLUT4 transports glucose into the liver (57). However, the liver glycogen concentration in Arctic foxes was significantly greater than that in silver foxes, while the glucose concentration was not significantly different between the two species. The key gene involved in glycogen synthesis, *Gys1* (58), was significantly upregulated in Arctic foxes. In addition, IGF-1 can promote *Gys1* expression through the PI3K-AKT signaling pathway (59). These results indicate that the Arctic fox may maintain glucose homeostasis by increasing liver glycogen synthesis.

In this study, we confirmed that the Arctic fox adapts to its diet through unique alterations in lipid and glucose metabolism in liver tissue (Figure 5). The Arctic fox can increase TAG storage from liver-derived fat by increasing PE synthesis in adipose tissue. Additionally, it can prevent aberrant lipid droplet accumulation in the liver by increasing uridine and VLDL synthesis and cAMP/PKA pathway-mediated fatty acid oxidation. Moreover, the Arctic fox can maintain glucose homeostasis by increasing liver glycogen synthesis.

## Data availability statement

The data presented in the study are deposited in the NCBI repository, accession number PRJNA1028137.

## Ethics statement

The animal study was approved by Ethical Committee of Jilin Agricultural University. The study was conducted in accordance with the local legislation and institutional requirements.

## Author contributions

YZ: Formal analysis, Investigation, Writing – original draft, Software, Visualization. YY: Formal analysis, Data curation, Software, Writing – review & editing. HS: Investigation, Writing – review & editing. SL: Investigation, Writing – review & editing. FZ: Investigation, Writing – review & editing. RM: Investigation, Writing – review & editing. ZhL: Investigation, Writing – review & editing.

XW: Investigation, Writing – review & editing. QQ: Writing – review & editing. CX: Writing – review & editing. LJ: Conceptualization, Methodology, Supervision, Writing – review & editing. ZpL: Conceptualization, Formal analysis, Funding acquisition, Methodology, Project administration, Supervision, Writing – review & editing.

## Funding

The author(s) declare financial support was received for the research, authorship, and/or publication of this article. This work was supported by the Key Research and Development Program Projects (2023YFD1302000) and Innovation and Entrepreneurship Talent Program from Jilin Province (2023QN02) to ZpL.

## Acknowledgments

We would like to thank Qianlong Yang for the assistance on sample collection.

## Conflict of interest

The authors declare that the research was conducted in the absence of any commercial or financial relationships that could be construed as a potential conflict of interest.

## Publisher's note



## Supplementary material

The Supplementary material for this article can be found online at: https://www.frontiersin.org/articles/10.3389/fvets.2024.1388532/full#supplementary-material

SUPPLEMENTARY FIGURE S1
The thickness of subcutaneous adipose tissue among the LFS, LFA and HFA groups.

SUPPLEMENTARY FIGURE S2
Comparison of metabolites, enzymes and gene expression between Arctic foxes and silver foxes. **(A)** The concentrations of liver TAG and serum AST and ALT among the LFS, LFA and HFA groups. **(B)** Volcano plot to show the up- and down- differentially expressed genes (DEGs) in liver between HFA and LFA. **(C)** Heatmap showing the DEGs in liver between Arctic foxes and silver foxes, which are involved in glucose and lipid metabolism. TAG: triacylglycerol; AST: aspartate transaminase; ALT: alanine transaminase.

SUPPLEMENTARY FIGURE S3
The composition of lipids in the subcutaneous adipose tissue based on the lipidomic analysis. The percentage in the brackets of pie chart means the proportion of lipids, and the numbers in the brackets of legend means the numbers of lipids. CE: cholesterol esters; CER: ceramides; DAG: diacylglycerols; DCER: dihydroceramides; DGDG: digalactosyldiacylglycerol; FFA: free fatty acids; HCER: hexosylceramides; LPC: lysophosphatidylcholines; LPE: lysophosphatidylethanolamines; PC: phosphatidylcholines; PE: phosphatidylethanolamines; PI: phosphatidylinositol; SM: sphingomyelins; TAG: triacylglycerols.

SUPPLEMENTARY TABLE S1
Ingredients of diets (DM basis).

SUPPLEMENTARY TABLE S2
The information of internal standard in lipidomic analysis.

SUPPLEMENTARY TABLE S3
The identified lipids in the subcutaneous adipose tissue of the LFA and LFS groups.

SUPPLEMENTARY TABLE S4
Significantly different lipids between the LFA and LFS groups.

## References

1. Fuglei E, Øritsland NA. Seasonal trends in body mass, food intake and resting metabolic rate, and induction of metabolic depression in arctic foxes (*Alopex Lagopus*) at Svalbard. *J Comp Physiol B*. (1999) 169:361–9. doi: 10.1007/s003600050232

2. Frafjord K. Food habits of arctic foxes (*Alopex Lagopus*) on the western coast of Svalbard. *Arctic*. (1993) 46:49–54. doi: 10.14430/arctic1321

3. Prestrud P, Nilssen K. Fat deposition and seasonal variation in body composition of Arctic foxes in Svalbard. *J Wildl Manag*. (1992) 56:221–33. doi: 10.2307/3808816

4. Gérard P. Gut microbiota and obesity. *Cell Mol Life Sci*. (2016) 73:147–62. doi: 10.1007/s00018-015-2061-5

5. Ong JP, Younossi ZM. Epidemiology and natural history of NAFLD and NASH. *Clin Liver Dis*. (2007) 11:1–16. doi: 10.1016/j.cld.2007.02.009

6. Geng Y, Zhang T, Zhang Z, Gao X, Yang F, Xing X. Dietary fat levels affect growth performance, body fat deposition and serum biochemical parameters of growing blue foxes (*Alopex Lagopus*). *Chin J Anim Nutr*. (2011) 23:1637–46.

7. Zhang T, Zhong W, Sun WL, Wang Z, Sun H, Fan Y, et al. Effects of dietary fat: carbohydrate ratio on nutrient digestibility, serum parameters, and production performance in male silver foxes (*Vulpes Vulpes*) during the winter fur-growing period. *Can J Anim Sci*. (2016) 97:199–206. doi: 10.1139/cjas-2015-0167

8. Peng Y, Li H, Liu Z, Zhang C, Li K, Gong Y, et al. Chromosome-level genome assembly of the Arctic fox (*Vulpes Lagopus*) using pacbio sequencing and hi-c technology. *Mol Ecol Resour*. (2021) 21:2093–108. doi: 10.1111/1755-0998.13397

9. Grzes M, Szczerbal I, Fijak-Nowak H, Szydlowski M, Switonski M. Two candidate genes (*Fto* and *Insig2*) for fat accumulation in four canids: chromosome mapping, gene polymorphisms and association studies of body and skin weight of red foxes. *Cytogenet Genome Res*. (2011) 135:25–32. doi: 10.1159/000330457

10. Takaishi K, Duplomb L, Wang M-Y, Li J, Unger RH. Hepatic Insig-1 or −2 overexpression reduces lipogenesis in obese zucker diabetic fatty rats and in fasted/refed normal rats. *Proc Natl Acad Sci USA*. (2004) 101:7106–11. doi: 10.1073/pnas.0401715101

11. Kumar V, Kutschera VE, Nilsson MA, Janke A. Genetic signatures of adaptation revealed from transcriptome sequencing of Arctic and red foxes. *BMC Genomics*. (2015) 16:585. doi: 10.1186/s12864-015-1724-9

12. Wan M, Leavens KF, Saleh D, Easton RM, Guertin DA, Peterson TR, et al. Postprandial hepatic lipid metabolism requires signaling through Akt2 independent of the transcription factors Foxa2, Foxo1, and Srebp1c. *Cell Metab*. (2011) 14:516–27. doi: 10.1016/j.cmet.2011.09.001

13. Zhang H, Ren G, Qiao A. Editorial: hepatic glucose and lipid metabolism. *Front Physiol*. (2022) 13:1009566. doi: 10.3389/fphys.2022.1009566

14. Zhu X, Xiong T, Liu P, Guo X, Xiao L, Zhou F, et al. Quercetin ameliorates HFD-induced NAFLD by promoting hepatic VLDL assembly and lipophagy via the Ire1a/Xbp1s pathway. *Food Chem Toxicol*. (2018) 114:52–60. doi: 10.1016/j.fct.2018.02.019

15. Rui L. Energy metabolism in the liver. *Compr Physiol*. (2014) 4:177–97. doi: 10.1002/cphy.c130024

16. Sharabi K, Tavares CD, Rines AK, Puigserver P. Molecular pathophysiology of hepatic glucose production. *Mol Asp Med*. (2015) 46:21–33. doi: 10.1016/j.mam.2015.09.003

17. Wang J, Zhu X, Chen C, Li X, Gao Y, Li P, et al. Effect of insulin-like growth factor-1 (IGF-1) on the gluconeogenesis in calf hepatocytes cultured in vitro. *Mol Cell Biochem*. (2012) 362:87–91. doi: 10.1007/s11010-011-1130-9

18. Hong H, Cui Z-Z, Zhu L, Fu S-P, Rossi M, Cui Y-H, et al. Central Igf1 improves glucose tolerance and insulin sensitivity in mice. *Nutr Diabetes*. (2017) 7:2. doi: 10.1038/s41387-017-0002-0

19. Bubenik GA, Schams D, White RG, Rowell J, Blake J, Bartos L. Seasonal levels of metabolic hormones and substrates in male and female reindeer (*Rangifer Tarandus*). *Comp Biochem Physiol C Pharmacol Toxicol Endocrinol*. (1998) 120:307–15. doi: 10.1016/S0742-8413(98)10010-5

20. Frøbert AM, Brohus M, Roesen TS, Kindberg J, Fröbert O, Conover CA, et al. Circulating insulin-like growth factor system adaptations in hibernating brown bears indicate increased tissue igf availability. *Am J Physiol Endocrinol Metab*. (2022) 323:E307–18. doi: 10.1152/ajpendo.00429.2021

21. Percie S, Nathalie A, Amrita A, Sabina A, Marc TB, Monya B, et al. Reporting animal research: explanation and elaboration for the ARRIVE guidelines 2.0. *PLoS Biol*. (2020) 18:e3000411. doi: 10.1371/journal.pbio.3000411

22. Schneider S, Feilen PJ, Brunnenmeier F, Minnemann T, Zimmermann H, Zimmermann U, et al. Long-term graft function of adult rat and human islets encapsulated in novel alginate-based microcapsules after transplantation in immunocompetent diabetic mice. *Diabetes*. (2005) 54:687–93. doi: 10.2337/diabetes.54.3.687

23. Baptista PM, Siddiqui MM, Lozier G, Rodriguez SR, Atala A, Soker S. The use of whole organ decellularization for the generation of a vascularized liver organoid. *Hepatology*. (2011) 53:604–17. doi: 10.1002/hep.24067

24. Abràmoff MD, Magalhães PJ, Ram SJ. Image processing with image j. *Biophoton Int*. (2004) 11:36–42.

25. Bolger AM, Lohse M, Usadel B. Trimmomatic: a flexible trimmer for illumina sequence data. *Bioinformatics*. (2014) 30:2114–20. doi: 10.1093/bioinformatics/btu170

26. Kim D, Langmead B, Salzberg SL. Hisat: a fast spliced aligner with low memory requirements. *Nat Methods*. (2015) 12:357–60. doi: 10.1038/nmeth.3317

27. Kukekova AV, Johnson JL, Xiang X, Feng S, Liu S, Rando HM, et al. Red fox genome assembly identifies genomic regions associated with tame and aggressive behaviours. *Nat Ecol Evol*. (2018) 2:1479–91. doi: 10.1038/s41559-018-0611-6

28. Love MI, Huber W, Anders S. Moderated estimation of fold change and dispersion for RNA-Seq data with Deseq2. *Genome Biol*. (2014) 15:550. doi: 10.1186/s13059-014-0550-8

29. Langfelder P, Horvath S. Wgcna: an R package for weighted correlation network analysis. *BMC Bioinformatics*. (2008) 9:559. doi: 10.1186/1471-2105-9-559

30. Yu G, Wang L-G, Han Y, He Q-Y. Clusterprofiler: an R package for comparing biological themes among gene clusters. *OMICS*. (2012) 16:284–7. doi: 10.1089/omi.2011.0118

31. Chen H, Cao G, Chen D-Q, Wang M, Vaziri ND, Zhang Z-H, et al. Metabolomics insights into activated redox signaling and lipid metabolism dysfunction in chronic kidney disease progression. *Redox Biol*. (2016) 10:168–78. doi: 10.1016/j.redox.2016.09.014

32. Rigano KS, Gehring JL, Evans Hutzenbiler BD, Chen AV, Nelson OL, Vella CA, et al. Life in the fat lane: seasonal regulation of insulin sensitivity, food intake, and adipose biology in brown bears. *J Comp Physiol B*. (2017) 187:649–76. doi: 10.1007/s00360-016-1050-9

33. Giroud S, Chery I, Bertile F, Bertrand-Michel J, Tascher G, Gauquelin-Koch G, et al. Lipidomics reveals seasonal shifts in a large-bodied hibernator, the brown bear. *Front Physiol*. (2019) 10:389. doi: 10.3389/fphys.2019.00389

34. Olzmann JA, Carvalho P. Dynamics and functions of lipid droplets. *Nat Rev Mol Cell Biol*. (2019) 20:137–55. doi: 10.1038/s41580-018-0085-z

35. Hörl G, Wagner A, Cole LK, Malli R, Reicher H, Kotzbeck P, et al. Sequential synthesis and methylation of phosphatidylethanolamine promote lipid droplet biosynthesis and stability in tissue culture and in vivo. *J Biol Chem*. (2011) 286:17338–50. doi: 10.1074/jbc.M111.234534

36. Hishikawa D, Shindou H, Kobayashi S, Nakanishi H, Taguchi R, Shimizu T. Discovery of a lysophospholipid acyltransferase family essential for membrane asymmetry and diversity. *Proc Natl Acad Sci USA*. (2008) 105:2830–5. doi: 10.1073/pnas.0712245105

37. Hoxhaj G, Manning BD. The PI3K–AKT network at the interface of oncogenic signalling and cancer metabolism. *Nat Rev Cancer*. (2020) 20:74–88. doi: 10.1038/s41568-019-0216-7

38. Ma X, Bai Y. IGF-1 activates the PI3K/AKT signaling pathway via upregulation of secretory clusterin. *Mol Med Rep*. (2012) 6:1433–7. doi: 10.3892/mmr.2012.1110

39. Jones JI, Clemmons DR. Insulin-like growth factors and their binding proteins: biological actions. *Endocr Rev*. (1995) 16:3–4. doi: 10.1210/edrv-16-1-3

40. Romero CJ, Ng Y, Luque RM, Kineman RD, Koch L, Bruning JC, et al. Targeted deletion of somatotroph insulin-like growth factor-i signaling in a cell-specific knockout mouse model. *Mol Endocrinol*. (2010) 24:1077–89. doi: 10.1210/me.2009-0393

41. Jensen-Urstad APL, Semenkovich CF. Fatty acid synthase and liver triglyceride metabolism: housekeeper or messenger? *Biochim Biophys Acta*. (2012) 1821:747–53. doi: 10.1016/j.bbalip.2011.09.017

42. Chitraju C, Mejhert N, Haas JT, Diaz-Ramirez LG, Grueter CA, Imbriglio JE, et al. Triglyceride synthesis by Dgat1 protects adipocytes from lipid-induced ER stress during lipolysis. *Cell Metab*. (2017) 26:407–418.e3. doi: 10.1016/j.cmet.2017.07.012

43. Wabitsch M, Hauner H, Heinze E, Teller WM. The role of growth hormone/insulin-like growth factors in adipocyte differentiation. *Metabolism*. (1995) 44:45–9. doi: 10.1016/0026-0495(95)90220-1

44. Medina-Gomez G, Gray S, Vidal-Puig A. Adipogenesis and lipotoxicity: role of peroxisome proliferator-activated receptor γ (PPARγ) and PPARγcoactivator-1 (PGC1). *Public Health Nutr*. (2007) 10:1132–7. Epub 2007/10/01. doi: 10.1017/S1368980007000614

45. Cho EJ, Yu SJ, Jung GC, Kwak M-S, Yang JI, Yim JY, et al. Body weight gain rather than body weight variability is associated with increased risk of nonalcoholic fatty liver disease. *Sci Rep*. (2021) 11:14428. doi: 10.1038/s41598-021-93883-5

46. Huang X, Yuan Z, Liu X, Wang Z, Lu J, Wu L, et al. Integrative multi-omics unravels the amelioration effects of zanthoxylum bungeanum maxim on non-alcoholic fatty liver disease. *Phytomedicine*. (2023) 109:154576. doi: 10.1016/j.phymed.2022.154576

47. Harris CA, Haas JT, Streeper RS, Stone SJ, Kumari M, Yang K, et al. Dgat enzymes are required for triacylglycerol synthesis and lipid droplets in adipocytes. *J Lipid Res*. (2011) 52:657–67. doi: 10.1194/jlr.M013003

48. Che X, Liu P, Wu C, Song W, An N, Yu L, et al. Potential role of the ecto-5′-nucleotidase in morphine-induced uridine release and neurobehavioral changes. *Neuropharmacology*. (2018) 141:1–10. doi: 10.1016/j.neuropharm.2018.07.035

49. Gluchowski NL, Becuwe M, Walther TC, Farese RV. Lipid droplets and liver disease: from basic biology to clinical implications. *Nat Rev Gastroenterol Hepatol*. (2017) 14:343–55. doi: 10.1038/nrgastro.2017.32

50. Liu Y, Xie C, Zhai Z, Deng Z-Y, De Jonge HR, Wu X, et al. Uridine attenuates obesity, ameliorates hepatic lipid accumulation and modifies the gut microbiota composition in mice fed with a high-fat diet. *Food Funct*. (2021) 12:1829–40. doi: 10.1039/D0FO02533J

51. Yamazaki T, Sasaki E, Kakinuma C, Yano T, Miura S, Ezaki O. Increased very low density lipoprotein secretion and gonadal fat mass in mice overexpressing liver Dgat1. *J Biol Chem*. (2005) 280:21506–14. doi: 10.1074/jbc.M412989200

52. Rakhshandehroo M, Hooiveld G, Müller M, Kersten S. Comparative analysis of gene regulation by the transcription factor pparα between mouse and human. *PLoS One*. (2009) 4:e6796. doi: 10.1371/journal.pone.0006796

53. Gulick T, Cresci S, Caira T, Moore DD, Kelly DP. The peroxisome proliferator-activated receptor regulates mitochondrial fatty acid oxidative enzyme gene expression. *Proc Natl Acad Sci USA*. (1994) 91:11012–6. doi: 10.1073/pnas.91.23.11012

54. Pawlak M, Lefebvre P, Staels B. Molecular mechanism of pparα action and its impact on lipid metabolism, inflammation and fibrosis in non-alcoholic fatty liver disease. *J Hepatol*. (2015) 62:720–33. doi: 10.1016/j.jhep.2014.10.039

55. Simko V, Iuliano F, Sevcikova A, Labudova M, Barathova M, Radvak P, et al. Hypoxia induces cancer-associated cAMP/PKA signalling through HIF-mediated transcriptional control of adenylyl cyclases VI and VII. *Sci Rep*. (2017) 7:10121. doi: 10.1038/s41598-017-09549-8

56. Gao Y-F, Zhang M-N, Wang T-X, Wu T-C, Ai R-D, Zhang Z-S. Hypoglycemic effect of d-chiro-inositol in type 2 diabetes mellitus rats through the PI3K/AKT signaling pathway. *Mol Cell Endocrinol*. (2016) 433:26–34. doi: 10.1016/j.mce.2016.05.013

57. Zhao P, Tian D, Song G, Ming Q, Liu J, Shen J, et al. Neferine promotes Glut4 expression and fusion with the plasma membrane to induce glucose uptake in L6 cells. *Front Pharmacol*. (2019) 10:999. doi: 10.3389/fphar.2019.00999

58. McCorvie TJ, Loria PM, Tu M, Han S, Shrestha L, Froese DS, et al. Molecular basis for the regulation of human glycogen synthase by phosphorylation and glucose-6-phosphate. *Nat Struct Mol Biol*. (2022) 29:628–38. doi: 10.1038/s41594-022-00799-3

59. Zhang Y, Liu X, Han L, Gao X, Liu E, Wang T. Regulation of lipid and glucose homeostasis by mango tree leaf extract is mediated by AMPK and PI3K/AKT signaling pathways. *Food Chem*. (2013) 141:2896–905. doi: 10.1016/j.foodchem.2013.05.121

frontiers | Frontiers in Veterinary Science

TYPE Original Research
PUBLISHED 28 June 2024
DOI 10.3389/fvets.2024.1429169



OPEN ACCESS

EDITED BY
Mian Muhammad Awais,
Bahauddin Zakariya University, Pakistan

REVIEWED BY
Rao Zahid Abbas,
University of Agriculture, Pakistan
Salvatore Massa,
University of Foggia, Italy

*CORRESPONDENCE
Jiping Liu
✉ liujiping@scau.edu.cn

†These authors have contributed equally to this work

RECEIVED 07 May 2024
ACCEPTED 10 June 2024
PUBLISHED 28 June 2024

CITATION
Qazi IH, Yuan T, Yang S, Angel C and Liu J (2024) Molecular characterization and phylogenetic analyses of MetAP2 gene and protein of *Nosema bombycis* isolated from Guangdong, China.
*Front. Vet. Sci.* 11:1429169.
doi: 10.3389/fvets.2024.1429169



# Molecular characterization and phylogenetic analyses of MetAP2 gene and protein of *Nosema bombycis* isolated from Guangdong, China

Izhar Hyder Qazi[1†], Ting Yuan[1†], Sijia Yang[1], Christiana Angel[2] and Jiping Liu[1*]

[1]Guangdong Provincial Key Lab of Agro-Animal Genomics and Molecular Breeding, College of Animal Science, South China Agricultural University, Guangzhou, China, [2]Shaheed Benazir Bhutto University of Veterinary and Animal Sciences, Sakrand, Pakistan

**Background:** Pebrine, caused by microsporidium *Nosema bombycis*, is a devastating disease that causes serious economic damages to the sericulture industry. Studies on development of therapeutic and diagnostic options for managing pebrine in silkworms are very limited. *Methionine aminopeptidase type 2* (*MetAP2*) of microsporidia is an essential gene for their survival and has been exploited as the cellular target of drugs such as fumagillin and its analogues in several microsporidia spp., including Nosema of honeybees.

**Methods:** In the present study, using molecular and bioinformatics tools, we performed in-depth characterization and phylogenetic analyses of MetAP2 of *Nosema bombycis* isolated from Guangdong province of China.

**Results:** The full length of *MetAP2* gene sequence of *Nosema bombycis* (Guangdong isolate) was found to be 1278 base pairs (bp), including an open reading frame of 1,077 bp, encoding a total of 358 amino acids. The bioinformatics analyses predicted the presence of typical alpha-helix structural elements, and absence of transmembrane domains and signal peptides. Additionally, other characteristics of a stable protein were also predicted. The homology-based 3D models of MetAP2 of *Nosema bombycis* (Guangdong isolate) with high accuracy and reliability were developed. The MetAP2 protein was expressed and purified. The observed molecular weight of MetAP2 protein was found to be ~43–45 kDa. The phylogenetic analyses showed that MetAP2 gene and amino acids sequences of *Nosema bombycis* (Guangdong isolate) shared a close evolutionary relationship with *Nosema* spp. of wild silkworms, but it was divergent from microsporidian spp. of other insects, *Aspergillus* spp., *Saccharomyces cerevisiae*, and higher animals including humans. These analyses indicated that the conservation and evolutionary relationships of MetAP2 are closely linked to the species relationships.

**Conclusion:** This study provides solid foundational information that could be helpful in optimization and development of diagnostic and treatment options for managing the threat of *Nosema bombycis* infection in sericulture industry of China.

KEYWORDS

***Bombyx mori*, microsporidia, *Nosema*, pebrine, sericulture**

## Introduction

Sericulture has been practiced since millennia and today holds a cultural legacy integral to the ancient history of China (1). Sericulture has not only provided subsistence to local rural economies, but it has been practiced at mechanized and industrial levels in recent times, particularly in China. Although sericulture, as a low-capital, high yield industry, has now moved into the global market (2), its sustainable and healthy development is facing several challenges including economic losses due to poor management practices and inadequate disease control measures in mulberry and silkworm production systems (3, 4).

The domesticated *Bombyx mori* L., the only truly domesticated insect species (5), is largely reared by silk producers to produce high quality silk threads of commercial importance. However, since many decades, silkworm production has been affected by many pathogens (6) causing serious economic damages to the industry.

Microsporidia are a fascinating and hyper-diverse group of obligate spore-forming intracellular parasites infecting a wide range of vertebrate and invertebrate hosts, including human and virtually all major animal taxa in all global biomes (7–10). To date, over 1,700 microsporidian species belonging to over 200 genera have been identified (9, 10). Many of these microsporidian parasites have been reported to infect several agriculturally important animal species including honeybees, shrimps, fish, and silkworms (11). However, despite their widespread occurrence and distribution, our understanding of their complex biology, pathogenic mechanisms, diagnosis, and treatment remains limited. The good news is that these areas have emerged as hot topics of research in recent times (12–16).

In 1857, microsporidium *Nosema bombycis* was identified as a causal pathogen of pebrine, a destructive disease of silkworms (17). *Nosema bombycis* has the ability to infect silkworms through fecal-oral (horizontal) and transovarial (vertical) routes (11), the latter causing a significant economic threat to sericulture production systems in major sericulture-intensive countries. At present, the precise mechanistic basis of the transovarial transmission and how *Nosema bombycis* parasite penetrates the host barrier system and enter into the oocytes remain poorly understood (11). However, recently it was shown that *Nosema bombycis* initially infects the follicular and nurse cells of the silkworm ovariole sheath, ultimately getting entry into the oocytes. Additionally, *Bombyx mori* vitellogenin and specific spore wall proteins of *Nosema bombycis* were shown to be key factors involved in the transovarial transmission (11).

When infected with *Nosema bombycis*, the silkworm larvae exhibit signs of delayed growth, molting problems, pustular milky white patches attached to the silk glands, and black spots on the entire body, eventually leading to death (18–21). Given that the obvious symptoms appear late in the infection, asymptomatic and mild infections are extremely deceptive, making the prevention, diagnosis and treatment of pebrine very challenging. Due to these reasons, pebrine remains the only disease with a mandatory quarantine (22) in the sericulture industry.

Previously, efforts were made to identify possible therapeutic targets and to develop treatment options to cure microsporidia infections, unfortunately results have ranged from disappointing to promising so far (21). We now know that methionine aminopeptidase type 2 (*MetAP2*) of microsporidia is an essential gene for their survival and has been exploited as the cellular target of drugs such as fumagillin, ovalicin, and TNP-470 (23). Fumagillin, the only approved veterinary drug for the treatment of *Nosema* infections in honey bees (21), can irreversibly inhibit *MetAP2* of microsporidia, blocking the essential enzymes and interfering the protein homeostasis necessary for pathogen survival (24, 25). However, it has also been shown that, despite its broader antimicrosporidial activity, fumagillin was not found to be effective against all microsporidia spp. (21, 24).

Given that the reports on therapeutic effects of drugs for treating *Nosema bombycis* infection in silkworms are very limited, it would be a timely effort to identify and characterize select genes that could be utilized as potential targets for specifically diagnosing and treating *Nosema bombycis* infection in silkworms [e.g., as argued in (26)]. Therefore, in the present study, building on our pioneering work (Qazi and Liu, 2024; unpublished results) on *de novo* transcriptome sequencing of *Nosema bombycis* (Guangdong isolate), we performed an in-depth study on identification, expression, and characterization of MetAP2 gene and protein using molecular and bioinformatics tools. Meanwhile, *MetAP2* gene of *Nosema antheraeae*, a microsporidium infecting the Chinese oak (Tussah) silkworms (27), was also sequenced and annotated for phylogenetic comparison. This study provides solid foundational information based on the local isolate of *Nosema bombycis*, and will pave a way for optimization and development of diagnostic and treatment options for managing the threat of *Nosema bombycis* infection in sericulture industry of China.

## Materials and methods

### Ethics statement

This work was conducted in accordance with the institutional ethical guidelines of South China Agricultural University, and other relevant International guidelines. No specific approval was needed, as currently research on insects including the silkworms does not require ethical approvals (28).

### Collection and purification of parasites and DNA extraction

*Nosema bombycis* spores were propagated and purified from silkworms (*Bombyx mori*) maintained in our laboratory as described previously (29). The pure suspension of *Nosema bombycis* spores was prepared at a concentration of $1 \times 10^{\wedge 8}$ spores/mL. This suspension was uniformly spread on the back of mulberry leaves and fed to the fourth-instar silkworms. The confirmation of *Nosema bombycis* infection was done by the light microscopic examination of the dead silkworms. The dead silkworms were placed in a tissue homogenizer for homogenization, and the pure *Nosema bombycis* were recovered. Briefly, the homogenate was filtered through four layers of gauze and one layer of absorbent cotton. The filtrate was put into a 15 mL centrifuge tube and centrifuged at 500 r/min for 2 min to remove the silkworm body and sediment. Then, it was centrifuged at 3000 r/min for 15 min and the supernatant was discarded. The pellet was resuspended in $ddH_2O$ and centrifugation was continued three times until a clear supernatant was obtained. Finally, a relatively pure white spore pellet was obtained and stored at 4°C for further use.

Meanwhile, other microsporidia, including *Nosema antheraeae* (Host: *Antheraea pernyi;* Oak Silkworm), *Endoreticulatus* sp. Zhejiang (Host: *Bombyx mori;* Mulberry Silkworm), and *Nosema pyraustae* GZ (Host: *Pyrausta nubilalis,* Hubern; Corn Borer) were utilized from our laboratory-maintained collection. The genomic DNA of these microsporidia was extracted using the DNeasy Mini Kit (Qiagen, Germany) following the manufacturer's instructions.

## PCR amplification of *MetAP2* gene

*MetAP2* gene of *Nosema bombycis* was annotated using *Nosema bombycis* (Guangdong isolate) transcriptome (Qazi and Liu, 2024; unpublished data), the MicrosporidiaDB[1] and the National Center for Biotechnology Information (NCBI) (30) databases. The primers were designed using Primer 5.0 software (31) as follows: MC-F (5'-ATGA GGCCTATTGTTTTATCAGAAG-3′)/MC-R (5'-TTAAAAATCAT TCCTTTTGTAAGA-3′), with an amplification length of 1,077 bp. *MetAP2* genes of three other species of insect microsporidia were amplified. These included *Nosema antheraeae*, *Endoreticulatus* sp. Zhejiang, and *Nosema pyraustae* GZ.

For PCR validation of *MetAP2* gene, DNA of other common pathogenic microorganisms of silkworms including *Bacillus bombysepticus*, *Bacillus thuringiensis*, *Beauveria bassiana*, *Bombyx mori* cytoplasmic polyhedrosis virus (BmCPV) polyhedron, and *Bombyx mori* nuclear polyhedrosis virus (BmNPV) was used as template. The DNA of these microorganisms was extracted using the DNeasy Mini Kit (Qiagen, Germany) following the manufacturer's instructions. Sterilized water was used as a negative control.

The PCR reaction system comprised 12.5 μL of 2 × Taq PCR Master Mix, 1 μL each of 10 μmol/L primers MC-F/R, 2 μL of 10 ng/μL DNA template, and sterilized ddH2O up to a total volume of 25 μL. Amplification conditions were as follows: pre-denaturation at 94°C for 5 min; denaturation at 94°C for 30 s, annealing at 50°C for 40 s, extension at 72°C for 1 min for 32 cycles; final extension at 72°C for 8 min, and storage at 4°C. 5 μL of PCR amplification products were subjected to 1.2% agarose gel electrophoresis for detection.

## Construction and sequence analysis of *MetAP2* gene recombinant plasmid

The PCR amplification product was subjected to agarose gel electrophoresis, and recovered using the TaKaRa MiniBEST DNA Gel Recovery Kit (Takara Bio Inc.) as per the manufacturer's instructions. The recovered DNA fragment was ligated into the pMD™19-T vector and transformed into DH5α competent cells. The desired bacterial strains were selected, and plasmids were extracted according to the instructions of the TaKaRa MiniBEST Plasmid Purification Kit (Takara Bio Inc.). Following PCR verification using the primers MC-F/R, the samples were sent to Sangon Biotech (Shanghai) Co., Ltd. for sequencing using the dideoxy method. The cloned sequencing results were analyzed using MegAlign Pro sequence alignment software (version 17.6) of DNASTAR Lasergene for multiple sequence alignment to assess the similarity of *MetAP2* gene across species. The sequence of *Nosema bombycis MetAP2* gene generated in the present study was submitted to the NCBI database with accession number KX185053.1.

## Annotation and functional prediction of *Nosema bombycis* MetAP2

The ORF finder[2] (32) was used to identify protein encoding sequence. The predicted MetAP2 protein sequence of *Nosema bombycis* was verified using the Basic Local Alignment Search Tool (BLAST) on NCBI[3] (33).

The predicted *Nosema bombycis* MetAP2 protein sequence was subjected to conserved domain prediction using CD-search[4] on NCBI (34–36). The physico-chemical properties, molecular weight, and isoelectric point of MetAP2 protein were predicted using ProtParam online software of EXPASY[5] (37). Transmembrane regions of amino acids were predicted using the DeepTMHMM (v.1.0.24)[6] (38). The presence of signal peptides in amino acid sequence was predicted using the SignalP 6.0 Server[7] (39). The secondary structure of protein was predicted using the Multivariate Linear Regression Combination (MLRC) method of online prediction software Network Protein Sequence Analysis[8] (40), and protein sub-localization was predicted using Protein Subcellular Localization Prediction Tool (PSORT II)[9] (41) and DeepLoc-2.0[10] software (42).

## Homology and phylogenetic analyses of MetAP2 of *Nosema bombycis*

*MetAP2* gene and protein sequences of *Nosema bombycis* were BLAST-searched to retrieve similar sequences of other species on NCBI. Meanwhile, MetAP2 sequences were also retrieved manually using the MicrosporidiaDB (see text footnote 1) database. After filtering, sequences with high similarity to the *Nosema bombycis* MetAP2 were downloaded for homology and phylogenetic analyses. MetAP2 gene and protein sequences from different species including humans, animals, *Bombyx mori*, and *Aspergillus* spp., as well as MetAP2 sequences of *Nosema antheraeae* obtained in the present study, were aligned using the Clustal W. method (43) using MegAlign Pro sequence alignment software (version 17.6) of DNASTAR Lasergene. The phylogenetic analysis (molecular evolutionary trees) was performed using the latest Randomized Axelerated Maximum Likelihood (RAxML; version 8.2.12) method (44), which is based on the rapid bootstrapping algorithm. The bootstrap value was set to 100 replicates. The homology comparisons (percent identity and

1 http://microsporidiadb.org/micro/

2 https://www.ncbi.nlm.nih.gov/orffinder/
3 https://blast.ncbi.nlm.nih.gov/Blast.cgi
4 https://www.ncbi.nlm.nih.gov/Structure/cdd/cdd.shtml
5 https://web.expasy.org/protparam/
6 https://dtu.biolib.com/DeepTMHMM
7 https://services.healthtech.dtu.dk/services/SignalP-6.0/
8 https://npsa-prabi.ibcp.fr
9 https://www.genscript.com/psort.html
10 https://services.healthtech.dtu.dk/services/DeepLoc-2.0/

divergence) of MetAP2 with other species were also carried out using MegAlign Pro sequence alignment software (version 17.6) of DNASTAR Lasergene.

## Homology modelling

Homology modelling of 3D protein structure of MetAP2 was performed using the SWISS-MODEL software[11] (45). This method uses template search which is performed against the SWISS-MODEL template library (SMTL, last update: 2024-02-21, last included PDB release: 2024-02-16). Models are built based on the target-template alignment using ProMod3 (46, 47). The global and per-residue model quality was assessed using the QMEAN scoring function (46, 47). Briefly, the protein sequence of MetAP2 of *Nosema bombycis* generated in the present study was used as target sequence to develop its 3D homology model. The search retrieved overall 662 templates, out of which 50 templates with high similarity were auto selected for model development. The templates which were considered to be less suitable for modelling were auto removed and the top 50 filtered templates were retained. In this case, we selected two best matching templates with higher quality estimation scores. These included: (1) A0A3G6ILP9.1.A methionine aminopeptidase 2 AlphaFold DB model of A0A3G6ILP9_9MICR (*MetAP2* of *Nosema assamensis*); (2) 3 fm3.1.A (X-ray Crystal structure of *MetAP2* of *Encephalitozoon cuniculi*).

## Prokaryotic expression of *Nosema bombycis* MetAP2

### Construction of expression vector

The Primer Premier 5.0 software was used to analyze the restriction sites of *MetAP2* gene and to design primers incorporating dual restriction sites NdeI/XhoI (Supplementary Figure S1). Primers Pmet-F (F: 5'-GACACCATATGTTAGAAGCGAGGCGTGCAG CTG-3′) and Pmet-R (5'-GTGTCCTCGAGCTATTAAAAATCAT CTCCTTTTG-3′) were designed for PCR amplification of *Nosema bombycis* DNA, yielding a product of 871 bp in length. The PCR amplification system and program were the same as described in sub-section "PCR Amplification of *MetAP2* Gene." The PCR products were recovered using TaKaRa MiniBEST DNA Gel Recovery Kit (Takara Bio Inc.).

### Ligation of target gene and vector

The recovered target fragment and vector pET-28a were digested with NdeI and XhoI, followed by ligation using T4 ligase. The transformation of the ligation products and extraction of recombinant plasmids were the same as detailed in sub-section "Construction and Sequencing Analysis of *MetAP2* Gene Recombinant Plasmid." The PCR-verified positive bacterial culture was incubated at 37°C with shaking overnight for plasmid extraction, followed by restriction digestion with NdeI and XhoI. The positive cultures were sent to Sangon Biotech (Shanghai) Co., Ltd. for sequencing. The correctly sequenced recombinant plasmid was named pET-28A–met.

### Transformation into *Rosetta* (DE3) strain

One µl of pET-28A–met was added to *Rosetta* (DE3) strain suspension and subjected to heat shock at 42°C for 90 s. After two min of rest on ice, the suspension was spread on plates (34 µg/mL chloramphenicol and 30 µg/mL kanamycin) and incubated overnight at 37°C. After transformation, the colonies were picked up aseptically for PCR verification.

### Prokaryotic expression

Colonies containing pET-28A–met were picked and cultured in 2.5 mL LB medium (containing 34 µg/mL chloramphenicol and 30 µg/mL kanamycin) at 37°C and 220 rpm for approximately three h. When the OD value reached about 0.6, IPTG was added to a final concentration of 0.5 mM, and incubation was continued at 20°C overnight with shaking at 220 rpm. The cell pellets were collected by centrifugation, with non-IPTG-induced samples serving as the negative controls. The collected bacteria were resuspended in lysis buffer (1 × PBS, pH 7.4). The cell lysis was achieved through ultrasonication in an ice bath at 400 W power for 20 min. The suspension was centrifuged at 12000 rpm at 4°C for 20 min, and the supernatant was collected.

A five mL Ni-IDA column was equilibrated with 10 column volumes of binding buffer at a flow rate of 5 mL/min. The sample was then loaded onto the column at a flow rate of 2 mL/min, and the flow-through was collected. The column was washed with 10 column volumes of binding buffer at a flow rate of 5 mL/min. Washing with a wash buffer was performed at the same flow rate, and wash fractions were collected. Elution was done using an elution buffer at a flow rate of 2 mL/min, and eluate was collected. The fractions were analyzed by the SDS-PAGE, and the fraction with the highest purity was dialyzed in 1 × PBS, 0.1% SKL, 2 mM DTT, pH 8.8. The dialysis was conducted overnight, followed by filtration through a 0.45 µm filter, concentration, and aliquoting into 2 mL/tube, and stored at −80°C. A 12% SDS-PAGE was prepared in Tris-Gly electrophoresis buffer. The samples (10 µL) were loaded, initially run on stacking gel at 80 V for 20 min, followed by separation on resolving gel at 120 V for 60 min. Following electrophoresis, the gel was stained with Coomassie Brilliant Blue for 20 min and destained.

## Western blot analysis

After the completion of the SDS-PAGE, the gel was removed, and a nitrocellulose membrane and six pieces of 3 mm filter paper of the same size of the gel were prepared. Both the membrane and the filter papers were pre-equilibrated in chilled transfer buffer for 15 min. The transfer assembly was arranged in the following order from bottom to top: three layers of filter paper, nitrocellulose membrane, gel, and three layers of filter paper, ensuring no contact between the upper and lower filter papers. The transfer was carried out on a semi-dry electrophoretic transfer device at 15 V for 15 min to transfer the corresponding bands from the gel to the nitrocellulose membrane. After transfer, the membrane was processed for blocking, washing, incubation with primary antibody (rabbit anti-his), washing, incubation with secondary antibody (goat

11 https://swissmodel.expasy.org/

anti-rabbit), and washing. Finally, the nitrocellulose membrane was scanned in the Odyssey dual-color laser scanning system to obtain results.

# Results

## Confirmation of symptoms of *Nosema bombycis* infection in silkworms

Upon microscopic examination, the disease symptoms were quite evidently observed in infected silkworms. The representative images of the apparent symptoms observed in different parts of *Bombyx mori* infected with *Nosema bombycis* are shown in Figure 1.

## Verification and PCR amplification of *Nosema bombycis MetAP2* gene

The *MetAP2* gene from transcriptome database of *Nosema bombycis* (Guangdong isolate was) was targeted for verification. The amplification was performed using primers MC-F/R, and the results are presented in Figure 2. The absence of band in lane 7, which served as a negative control, suggested no contamination in the reaction system. Lane 1 shows specific amplification band of *MetAP2* of *Nosema bombycis*. Lanes 2 to 6 correspond to *Bacillus bombysepticus*, *Bacillus thuringiensis*, *Beauveria bassiana*, BmCPV, and BmNPV, respectively. The PCR product of the target band (1,077 bp) was subjected to bidirectional sequencing. For determining consistency, the sequencing result was compared with the transcriptome data of *Nosema bombycis* (Guangdong isolate). The comparison showed a

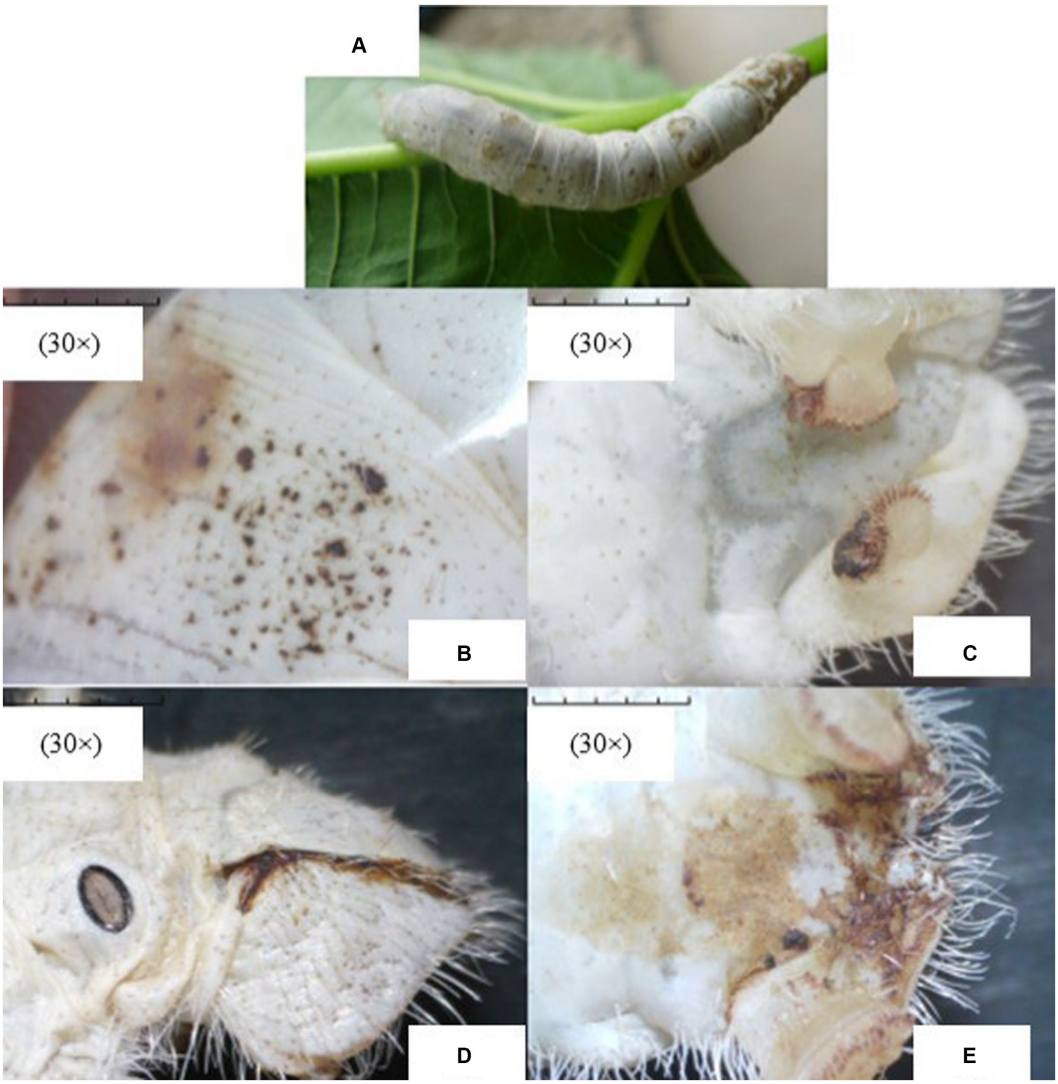


FIGURE 1
The representative images of apparent symptoms of *Nosema bombycis* infection in fifth-instar silkworms. **(A)** represents the fifth-instar silkworm infected with *Nosema bombycis*. **(B–E)** depict different symptoms of pebrine disease in the fifth-instar infected silkworms observed under the stereomicroscope. **(A)** the fifth-instar silkworm infected with *Nosema bombycis* showed many pepper-like spots on its entire body. **(B)** zoomed-in image showing pepper-like spots on the body of a fifth-instar silkworm infected with *Nosema bombycis*. **(C)** shows the tail end of a fifth-instar silkworm infected with *Nosema bombycis*, characterized by a charred black appearance and some signs of rot. **(D,E)** depict the brown secretions at the tail of a fifth-instar silkworm infected with *Nosema bombycis*.

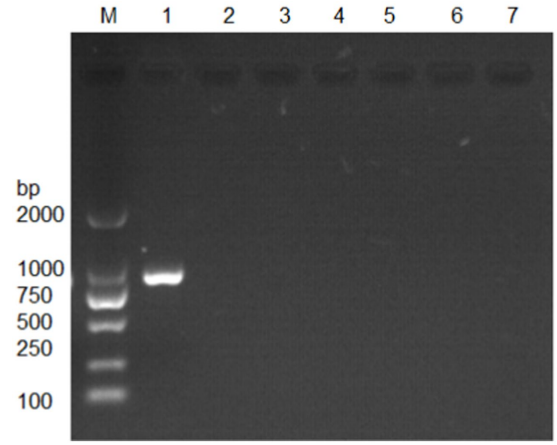


FIGURE 2
Electrophoretic gel showing amplification of *MetAP2* gene of *Nosema bombycis* (Guangdong isolate) using MC-F/R primers. Lane 1. *MetAP2* gene of *Nosema bombycis* (Guangdong isolate); Lane 2. *Bacillus bombysepticus*; Lane 3. *Bacillus thuringiensis*; Lane 4. *Beauveria bassiana*; Lane 5. BmCPV; Lane 6. BmNPV; 7. Sterilized water (negative control); M: DL2000 marker.

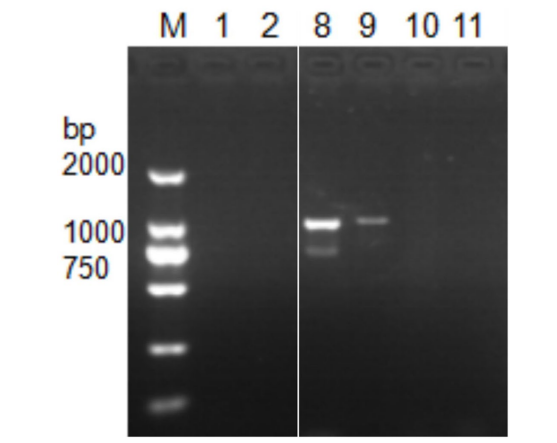


FIGURE 3
Electrophoretic gel showing PCR amplification of DNA templates of *Nosema bombycis* (Guangdong isolate) and other insect microsporidia spp., using MC-F/R primers. 1. *Endoreticulatus* sp. Zhejiang; 2. *Nosema pyraustae*; 8. *Nosema antheraeae*; 9. *Nosema bombycis*; 10. Midgut of silkworm; 11. Sterilized water; M: DL2000 Marker. Lanes 3 to 7 in this gel represented *MetAP2* genes of other microsporidia spp. of mulberry pests. These lanes were removed, as they were not part of the current manuscript. White border separates the two cropped segments of gel.

high consistency (99.9%). This finding confirmed that the primers MC-F/R specifically amplified *MetAP2* gene of *Nosema bombycis*.

Next, DNA of *Nosema bombycis*, *Nosema antheraeae*, *Endoreticulatus* sp. Zhejiang, and *Nosema pyraustae* were used for amplification of *MetAP2* gene. DNA of healthy silkworm midgut was used as a template. The electrophoresis results are shown in Figure 3. No bands were observed in Lanes 1 (*Endoreticulatus* sp. Zhejiang) and 2 (*Nosema pyraustae*), indicating that *MetAP2* gene of these microsporidia spp. was not amplified with the primers used in the present study. Lanes 10 and 11, DNA of the midgut of a healthy silkworm and sterile water did not show amplification bands, indicating that the system was free of contamination. Lanes 8 and 9, representing *MetAP2* genes *of Nosema bombycis* and *Nosema antheraeae*, respectively yielded corresponding bands (Figure 3). The PCR products were recovered and bidirectional sequencing was performed. The sequencing results were compared for consistency with the transcriptome data of *Nosema bombycis* and *Nosema antheraeae* (Qazi and Liu, 2024; unpublished results). The comparison results of GC content are shown in Table 1.

## Homology and phylogenetic analyses of MetAP2 of *Nosema bombycis*

### Analysis of *MetAP2* gene sequences of *Nosema bombycis* and other insect microsporidia spp.

The sequenced *MetAP2* gene *of Nosema bombycis*, along with *MetAP2* genes from other select microsporidia spp. were analyzed for homology and used to construct RAxML phylogenetic tree. The homology comparisons (Figure 4) revealed that the homology (%identity) between *MetAP2* genes of different microsporidia spp. ranged from 54.13 to 99%. Specifically, the homology between *Nosema bombycis* (Guangdong isolate) and other microsporidia spp. ranged from 61.25 to 99%. *Nosema bombycis* (Guangdong isolate) sequenced in the present study had the closest %identity with *Nosema bombycis* (Indian isolate; 99%) and *Nosema bombycis* (CQ1; 98.50%). Meanwhile, %identity with Nosema spp. infecting wild silkworm spp. ranged between 94 to 94.38%. From these, the closest relative to *Nosema bombycis* (Guangdong isolate) was found to be the Chinese oak silkworm microsporidium (*Nosema antheraeae*; sequenced in the present study), with a %identity of 94.38% (Figure 4).

Meanwhile, the phylogenetic analysis based on RAxML tree showed that *Nosema bombycis* sp. including the Guangdong isolate clustered together, with Nosema sp. of the domestic and wild silkworms forming separate branches (Figure 5). The microsporidia spp. *Nosema ceranae* (honeybees) *and Nosema bombi* (bumblebees) clustered on the same branch and had a distant relationship with the *Nosema bombycis* (Guangdong isolate) and *Nosema antheraeae* sequenced in the present study.

In addition, microsporidia of *Nosema* spp. showed a more distant relationship with members of Encephalitozoon genus, in which many spp. infecting humans formed a separate major branch (Figure 5). Within the Encephalitozoon genus, *Encephalitozoon cuniculi*, *Encephalitozoon intestinalis*, *Encephalitozoon hellem*, and *Encephalitozoon romaleae* showed a close relationship between them (Figure 5). *Anncaliia algerae* (human isolate) and *Spraguea lophii* (Monkfish microsporidium),

TABLE 1 Sequencing length (bp) and GC content (%) of *MetAP2* genes of *Nosema bombycis* (Guangdong isolate) and *Nosema antheraeae* amplified in the present study.

| *Nosema* species | Length (bp) | GC content (%) |
|---|---|---|
| *Nosema bombycis* | 1,077 | 33.24 |
| *Nosema antheraeae* | 1,068 | 32.21 |

DNA templates of *Endoreticulatus* sp. Zhejiang and *Nosema pyraustae* were not amplified.

| | | A | B | C | D | E | F | G | H | I | J | K | L | M | N | O |
|---|---|---|---|---|---|---|---|---|---|---|---|---|---|---|---|---|
| A | *Encephalitozoon cuniculi EC2 (AEWQ_100660)* | | 59.75 | 54.13 | 79.63 | 81.13 | 79.75 | 54.50 | 57.13 | 63.25 | 63.13 | 62.88 | 63.63 | 63.25 | 63.25 | 63.00 |
| B | *Nosema ceranae BRL01 (NCER_100348)* | 0.40 | | 64.75 | 64.13 | 63.75 | 64.00 | 62.13 | 61.25 | 70.25 | 70.38 | 68.25 | 74.75 | 68.50 | 70.50 | 68.50 |
| C | *Encephalitozoon bieneusi H348 (EBI_27249)* | 0.46 | 0.35 | | 56.25 | 57.75 | 57.38 | 64.25 | 64.00 | 63.38 | 63.63 | 62.38 | 61.00 | 62.50 | 63.50 | 62.38 |
| D | *Encephalitozoon hellem Swiss (KMI_100660)* | 0.20 | 0.36 | 0.44 | | 79.38 | 85.75 | 56.38 | 57.75 | 64.50 | 64.50 | 63.00 | 64.25 | 63.50 | 64.63 | 63.38 |
| E | *Encephalitozoon intestinalis (Eint_100700)* | 0.19 | 0.36 | 0.42 | 0.21 | | 80.13 | 56.25 | 60.88 | 63.75 | 63.75 | 63.63 | 65.25 | 64.50 | 63.88 | 63.50 |
| F | *Encephalitozoon romaleae SJ-2008 (EROM_100620)* | 0.20 | 0.36 | 0.43 | 0.14 | 0.20 | | 56.25 | 59.75 | 65.63 | 65.63 | 64.38 | 65.75 | 64.63 | 65.75 | 64.63 |
| G | *Anncalia algerae (H311_00215)* | 0.46 | 0.38 | 0.36 | 0.44 | 0.44 | 0.44 | | 67.75 | 61.38 | 61.75 | 61.38 | 59.63 | 61.50 | 61.50 | 61.50 |
| H | *Spraguea lophii (SLOPH_1347)* | 0.43 | 0.39 | 0.36 | 0.42 | 0.39 | 0.40 | 0.32 | | 61.38 | 61.50 | 61.63 | 60.38 | 61.38 | 61.63 | 61.25 |
| I | *Nosema assamensis isolate AA1 (MG926528.1)* | 0.37 | 0.30 | 0.37 | 0.35 | 0.36 | 0.34 | 0.39 | 0.39 | | 99.38 | 94.00 | 68.13 | 95.75 | 99.25 | 94.00 |
| J | *Nosema mylitta (MG926526.1)* | 0.37 | 0.30 | 0.36 | 0.35 | 0.36 | 0.34 | 0.38 | 0.38 | 0.01 | | 94.25 | 68.38 | 94.00 | 99.63 | 94.25 |
| K | *Nosema bombycis [Indian Isolate] (KX820249.1)* | 0.37 | 0.32 | 0.38 | 0.37 | 0.36 | 0.36 | 0.39 | 0.38 | 0.06 | 0.06 | | 69.50 | 98.88 | 94.13 | 99.00 |
| L | *Nosema bombi (JQ927011.1)* | 0.36 | 0.25 | 0.39 | 0.36 | 0.35 | 0.34 | 0.40 | 0.40 | 0.32 | 0.32 | 0.31 | | 69.38 | 68.50 | 69.50 |
| M | *Nosema bombycis CQ1 (NBO_1166g0001)* | 0.37 | 0.31 | 0.38 | 0.37 | 0.35 | 0.35 | 0.38 | 0.39 | 0.06 | 0.06 | 0.01 | 0.31 | | 94.13 | 98.50 |
| N | *Nosema antheraeae [Chinese Isolate Na01] (PP576694)* | 0.37 | 0.29 | 0.37 | 0.35 | 0.36 | 0.34 | 0.38 | 0.38 | 0.01 | 0.00 | 0.06 | 0.31 | 0.06 | | 94.38 |
| O | *Nosema bombycis [Guangdong Isolate] (KX185055)* | 0.37 | 0.31 | 0.38 | 0.37 | 0.37 | 0.35 | 0.38 | 0.39 | 0.06 | 0.06 | 0.01 | 0.31 | 0.01 | 0.06 | |

FIGURE 4
Homology comparison of *MetAP2* genes between *Nosema bombycis* (Guangdong isolate) and other microsporidia spp. Values in turquoise colored boxes denote the percent (%) identity, and values in red colored boxes denote the divergence. Color gradient highlights the values (%identity and divergence) from higher (dark) to lower (light) range. *MetAP2* genes of *Nosema bombycis* (Guangdong isolate) and *Nosema antheraeae* (Chinese isolate) were sequenced in the present study.

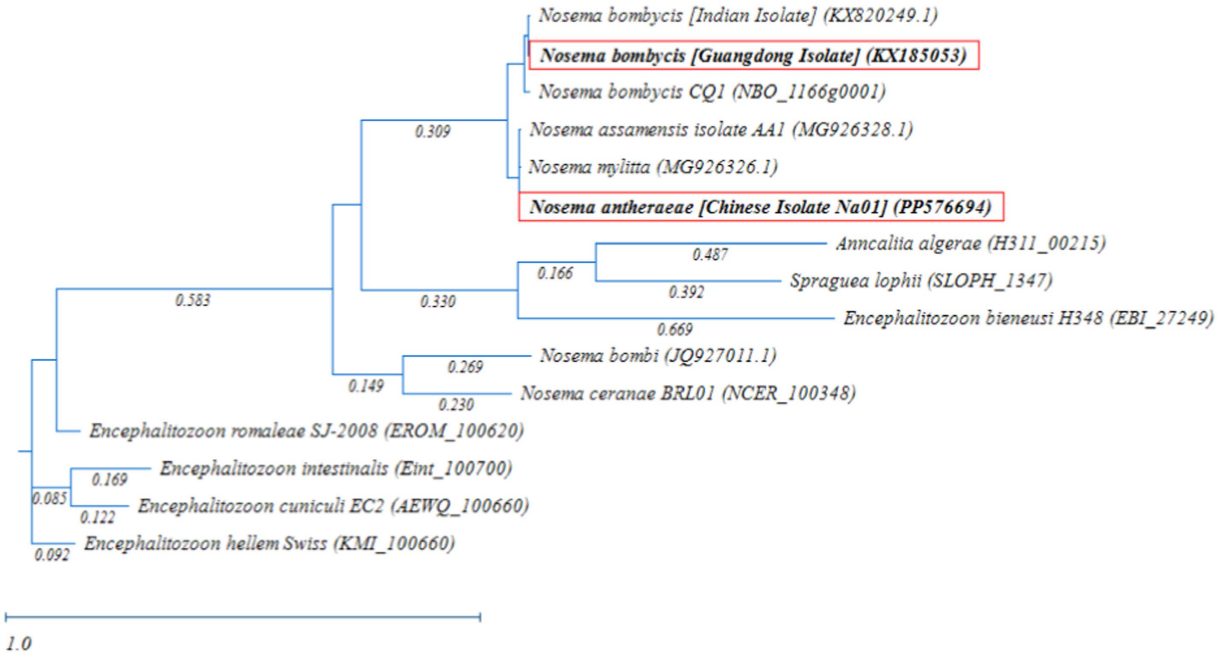


FIGURE 5
Randomized Axelerated Maximum Likelihood (RAxML) phylogenetic tree of *MetAP2* gene sequences of *Nosema bombycis* (Guangdong isolate) and other microsporidia spp. Red boxes highlight *MetAP2* genes of *Nosema bombycis* (Guangdong isolate) and *Nosema antheraeae* (Chinese isolate) that were sequenced in the present study. The scale bar indicates sequence divergence.

formed a separate branch and showed more distant relationship with other species (Figure 5). The results of the homology comparisons were consistent with the outcomes of the phylogenetic analysis.

## Homology and phylogenetic analyses of MetAP2 amino acids sequences of different species

The homology comparisons revealed that the homology (%identity) between MetAP2 of *Nosema bombycis* (Guangdong isolate) and other spp. ranged from 40.18 to 96.93% (Supplementary Figure S2).

The phylogenetic comparison of MetAP2 protein of different species was carried out by constructing a RAxML tree. As shown in Figure 6, the MetAP2 amino acids of chordates clustered in one group, with mammals showing close evolutionary proximity. The MetAP2 amino acids of insects and microorganisms were found to be relatively close. Specifically, insects (*Bombyx mori* and *Drosophila melanogaster*) clustered on the same branch and formed a distinct group, while *Saccharomyces cerevisiae*, *Nosema bombycis*, *Nosema antheraeae*, and *Trypanosoma brucei* did not form a single group, but they were relatively close in the distance.

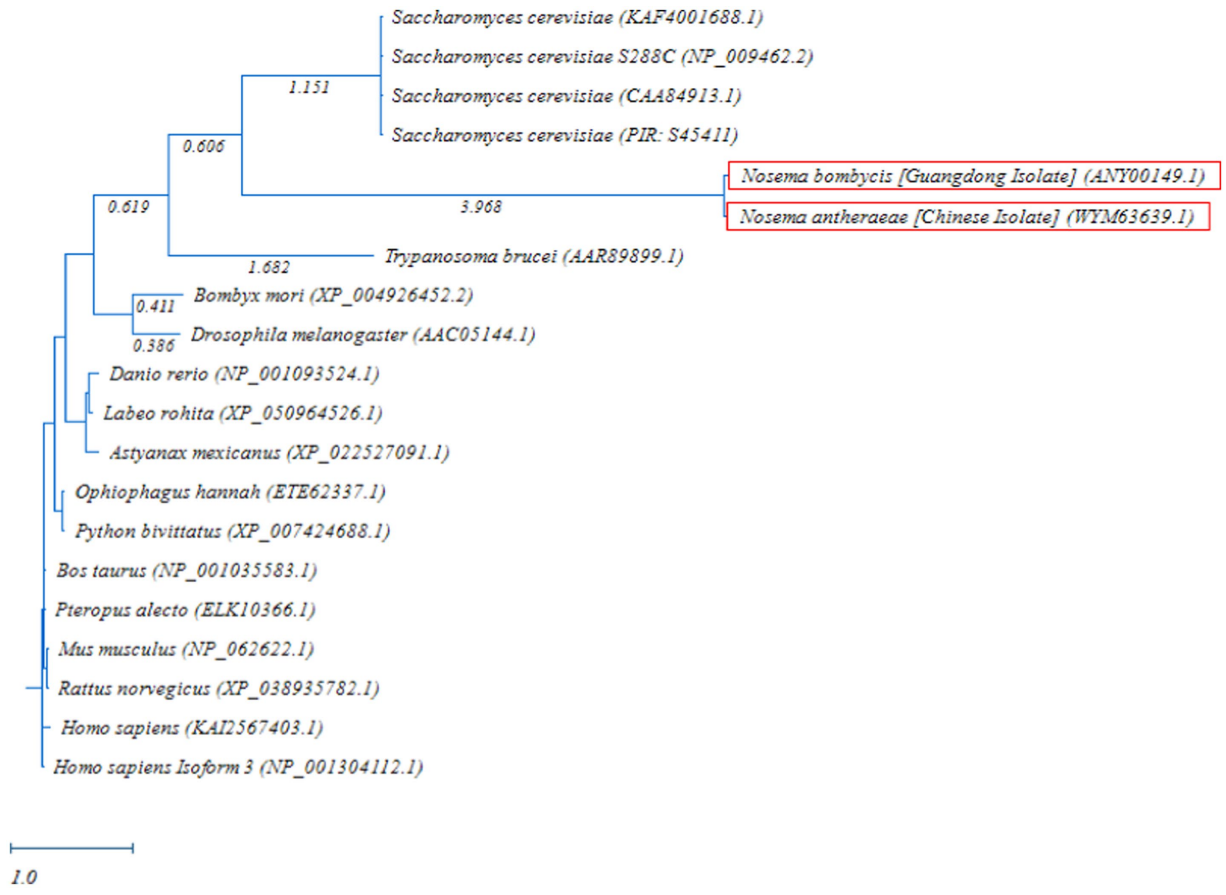


FIGURE 6
Randomized Axelerated Maximum Likelihood (RAxML) phylogenetic tree of *MetAP2* amino acids sequences of *Nosema bombycis* (Guangdong isolate) and other species. Red boxes highlight amino acid sequences of *MetAP2* of *Nosema bombycis* (Guangdong isolate) and *Nosema antheraeae* (Chinese isolate) that were generated in the present study. The scale bar indicates sequence divergence (i.e., amino acid substitution per site).

## Homology and phylogenetic analyses of MetAP2 amino acid sequences between *Nosema bombycis* (Guangdong isolate) and its relatives Aspergillus spp., and *Saccharomyces cerevisiae*

The homology of MetAP2 amino acid sequences between *Nosema bombycis*, *Nosema antheraeae*, *Aspergillus* spp., and *Saccharomyces cerevisiae* was analyzed. As shown in Figure 7, the percent identity of MetAP2 amino acids ranged between 38.04 and 96.74%, with the percent identity between *Nosema bombycis* and different *Aspergillus* spp. not being particularly high (38.04 to 43.12%).

Next, the RAxML phylogenetic tree was constructed using the MetAP2 amino acid sequences of *Nosema bombycis* (Guangdong isolate), *Nosema antheraeae*, *Aspergillus* spp., and *Saccharomyces cerevisiae*. As shown in Figure 8, as expected, MetAP2 of *Nosema bombycis* and *Nosema antheraeae* clustered together and formed a distinct branch, which was separated from the branches of *Aspergillus* and *Saccharomyces cerevisiae* spp. In summary, the distant relationship as seen in these molecular evolutionary (phylogenetic) analyses altogether signifies that the conservation and evolutionary relationships of MetAP2 gene and amino acids sequences are closely linked to the species relationships.

## Bioinformatics analysis of *Nosema bombycis* MetAP2 gene and protein

The full length of *Nosema bombycis MetAP2* DNA sequence was found to be 1278 base pairs (bp). This included a 5′ non-coding region of 49 bp, a 3′ non-coding region of 152 bp, and an open reading frame of 1,077 bp, encoding a total of 358 amino acids. The predicted molecular weight of MetAP2 protein was found to be 40.51 kDa approximately, with a molecular formula of $C_{1816}H_{2845}N_{479}O_{542}S_{14}$. The theoretical isoelectric point was 5.91, with an Aliphatic index of 88.24, instability index of 31.64, and the Grand average hydropathicity (GRAVY) index of −0.337, all indicating characteristics of a stable protein.

The conserved structural domain of MetAP2 protein is depicted in Supplementary Figure S3. Briefly, the predicted conserved region of *Nosema bombycis* MetAP2 protein spanned approximately 60–355 amino acids, with predicted active sites located at positions 110, 130, 140, 210, 241, and 340.

The results of predictions of transmembrane domains and signal peptides in *Nosema bombycis* (Guangdong isolate) MetAP2 protein are shown in Supplementary Figures S4, S5, respectively. Briefly, these analyses showed absence of transmembrane domains and signal peptides in predicted *Nosema bombycis* MetAP2 protein.

| | | A | B | C | D | E | F | G | H | I | J | K |
|---|---|---|---|---|---|---|---|---|---|---|---|---|
| A | *Aspergillus fumigatus Z5 (KMK54421.1)* | | 68.12 | 67.39 | 60.51 | 93.48 | 64.49 | 94.57 | 61.96 | 61.96 | 41.30 | 40.58 |
| B | *Aspergillus fumigatus Z5 [1] (KMK57018.1)* | 0.32 | | 98.91 | 56.16 | 68.48 | 60.87 | 68.48 | 57.61 | 57.61 | 40.22 | 40.58 |
| C | *Aspergillus fumigatus (KEY82946.1)* | 0.33 | 0.01 | | 56.16 | 67.75 | 60.87 | 68.12 | 57.25 | 57.25 | 40.22 | 40.58 |
| D | *Aspergillus terreus NIH2624 [2023] (XP_001209448.1)* | 0.39 | 0.44 | 0.44 | | 60.51 | 84.06 | 61.23 | 52.17 | 52.54 | 38.41 | 38.04 |
| E | *Aspergillus oryzae (OOO14416.1)* | 0.07 | 0.32 | 0.32 | 0.39 | | 65.22 | 97.83 | 63.04 | 63.04 | 42.39 | 42.39 |
| F | *Aspergillus niger CBS 101883 (XP_025450073.1)* | 0.36 | 0.39 | 0.39 | 0.16 | 0.35 | | 65.58 | 56.88 | 57.25 | 39.86 | 39.86 |
| G | *Aspergillus nomiae NRRL 13137 (XP_015406780.1)* | 0.05 | 0.32 | 0.32 | 0.39 | 0.02 | 0.34 | | 62.68 | 62.68 | 43.12 | 43.12 |
| H | *Saccharomyces cerevisiae (PIR: S45411 )* | 0.38 | 0.42 | 0.43 | 0.48 | 0.37 | 0.43 | 0.37 | | 99.64 | 42.39 | 42.39 |
| I | *Saccharomyces cerevisiae (KAF4001688.1)* | 0.38 | 0.42 | 0.43 | 0.47 | 0.37 | 0.43 | 0.37 | 0.00 | | 42.39 | 42.39 |
| J | *Nosema antheraeae [Chinese Isolate] (WYM63639.1)* | 0.59 | 0.60 | 0.60 | 0.62 | 0.58 | 0.60 | 0.57 | 0.58 | 0.58 | | 96.74 |
| K | *Nosema bombycis [Guangdong Isolate] (ANY00149.1)* | 0.59 | 0.59 | 0.59 | 0.62 | 0.58 | 0.60 | 0.57 | 0.58 | 0.58 | 0.03 | |

FIGURE 7
MetAP2 amino acid sequence alignment results of *Nosema bombycis* (Guangdong isolate), *Aspergillus* spp., and *Saccharomyces cerevisiae*. Values in turquoise colored boxes denote the percent (%) identity, and values in red colored boxes denote the divergence. Color gradient highlights the values (%identity and divergence) from higher (dark) to lower (light) range.

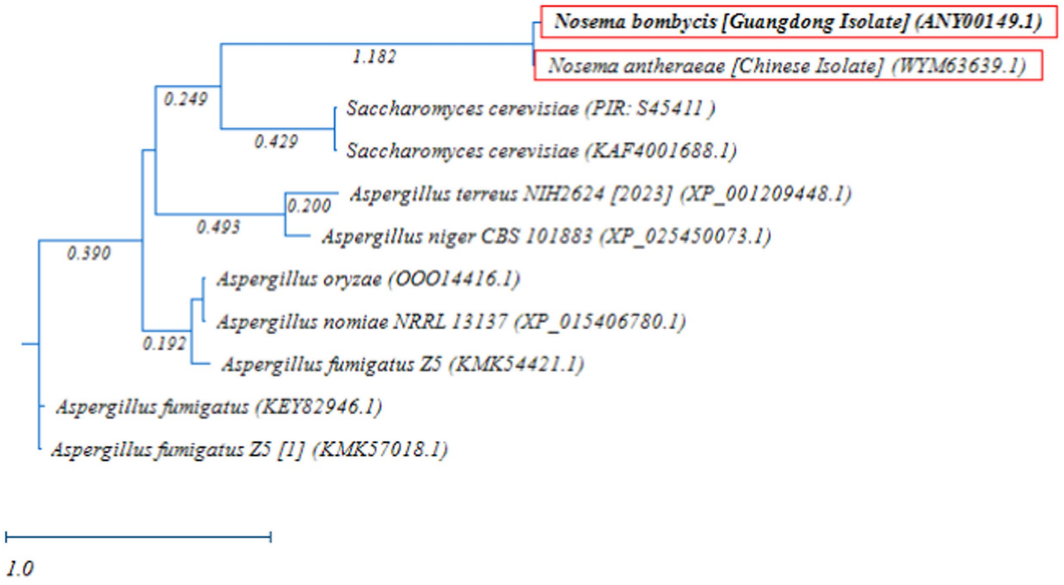


FIGURE 8
Randomized Axelerated Maximum Likelihood (RAxML) phylogenetic tree of MetAP2 amino acids sequences of *Nosema bombycis* (Guangdong isolate), *Nosema antheraeae, Aspergillus* spp., and *Saccharomyces cerevisiae*. Red boxes highlight amino acid sequences of MetAP2 of *Nosema bombycis* (Guangdong isolate) and *Nosema antheraeae* (Chinese isolate) that were generated in the present study. The scale bar indicates sequence divergence (i.e., amino acid substitution per site).

## Prediction of secondary structural domains of MetAP2 protein

The prediction of secondary structural domain of MetAP2 protein is shown in Supplementary Figure S6. The predicted protein had a predominance of alpha-helix (Alphahelix) structural elements, consisting of 115 amino acids. Additionally, random coil structural elements consisting of 181 amino acids were also present. Given the presence of typical alpha-helix structural elements in MetAP2 protein structure, it can be hypothesized that the *Nosema bombycis* MetAP2 protein may form certain structural or functional domains.

## Prediction of subcellular localization of MetAP2 protein

Based on online prediction software PSORT II, the prediction of subcellular localization of MetAP2 protein revealed the following descriptions: 1. the sequence has a potential cleavage site between positions 54 and 55. R-2 motif at 12 MRP|IV was found at mitochondrial presequence cleavage sites. No prenylation modification motifs were present. 2. The sequence lacks an N-terminal signal peptide and N-myristoylation patterns. There were no C-terminal retention motifs and C-terminal glycosylation signals like SKL, SKL2, or peroxisomal targeting signals. 3. No endoplasmic reticulum (ER) retention motif was present in the C-terminus. There were two motifs (XXRR-like motif in the N-terminus: RPIV and KKXX-like motif in the C-terminus: KGDD) in the ER membrane retention signals were predicted. No predicted vacuolar targeting motifs were present in the sequence. Additionally, there were no motifs for transport from the cell surface to the Golgi apparatus, and the tail end of the sequence lacked tyrosine and Dileucine motifs. 4. The sequence did not contain RNA-binding motifs, and either type of

Actinin-type actin-binding motifs. No DNA binding and ribosomal protein motifs were present. 5. Lupas's algorithm detected no coiled-coil regions, suggesting a cytoplasmic/nuclear localization. NUCDISC, which identifies nuclear localization signals, found no binding or free pat4 and pat7 motifs, with virtually zero residual content and an NLS index of −0.47. Reinhardt's method predicted that the MetAP2 was located in the cytoplasm, with a reliability sore of 76.7. The sub-cellular localization results retrieved through DeepLoc - 2.0 were consistent with PSORT II and showed a probability value of 0.7329 for cytoplasmic localization.

## Homology modeling-based 3D structure of MetAP2 protein of *Nosema bombycis*

Based on target-template alignment, two homology models (models 1 and 2) were built. The 3D structures of models 1 and 2 are presented in confidence scheme view (Figure 9A; Supplementary Figure S7A). The overall model quality measurement evaluation showed that the Global Model Quality Estimate (QMQE) value for models 1 and 2 was 0.97 and 0.89 respectively, indicating the high accuracy and reliability of the developed models. The QMEANDisCo global score of model 2 was 0.86 ± 0.05. The QMEANDisCo local score, QMEAN Z-score and comparison plot for model 2 are shown in Figures 9B–D. These analyses were not computed for model 1, as its template (A0A3G6ILP9.1.A) itself was built using AlphaFold2 database. The Ramachandran Favoured value for models 1 and 2 were 95.48 (Supplementary Figure S7B) and 97.47% (Supplementary Figure S7C), respectively. The target-template sequence alignments for models 1 and 2 are presented in Supplementary Figures S7D,E. Overall, model 2 (Figure 9A) was considered as practically more reliable structure, as it was based on template sequence of experimentally produced MetAP2 of *Encephalitozoon cuniculi* (ID: 3 fm3.1.A).

## Prokaryotic expression of MetAP2 protein

### Construction of cloning vector

After the PCR amplification of *Nosema bombycis* DNA using primers MC-F/R, the product was subjected to agarose gel electrophoresis and subsequent gel recovery (Supplementary Figure S8). The lane 3, representing sterile water, displayed no band amplification, indicating no contamination in the reaction system. The MC-F/R primers also did not produce any nonspecific dimer amplification. Bands in lanes 1 and 2 were approximately 1,000 bp, clear and bright, making them suitable for further cloning and expression experiments.

Following PCR amplification and purification of *MetAP2* gene, the cloning was performed. The PCR identification of bacterial liquid cultures from individual colonies is depicted in Supplementary Figure S9. The lane 4, representing sterile water, showed no amplification band, confirming no contamination in the reaction system. Although Lane 3 showed nonspecific amplification in the midgut of silkworm but did not affect the results of this experiment. Lane 1, representing *Nosema bombycis* DNA, showed a specific amplification band at around 1,100 bp, indicating a well-functioning reaction system. Lane 2 showed a specific amplification band at the corresponding position for the post-cloning bacterial liquid, suggesting the successful construction of *MetAP2* gene cloning vector.

Then, the recovered target fragment was ligated with pMD19-T vector and transformed into DH5α cells. Positive clones were sent to Sangon Biotech (Shanghai) Co., Ltd. for sequencing verification. The correct pMD19-T recombinant plasmids were selected after nucleotide sequence comparison.

## Construction of pET-28A–met

The correctly sequenced pMD19-T recombinant plasmid was subjected to double digestion, and the digested fragment was ligated with the prokaryotic expression vector pET-28A(+). This construct was then transformed into *Rosetta* (DE3) cells to obtain positive recombinant plasmids. The PCR and double digestion with NdeI and XhoI for verification are presented in Supplementary Figure S10. The results indicate that the size of the enzyme-digested bands corresponds to *MetAP2* gene, demonstrating the successful construction of prokaryotic recombinant plasmid pET-28A–met. This allowed for the subsequent expression of protein.

## Induction of protein expression

Next, the SDS-PAGE analysis was conducted which showed the presence of a specific target band at ~43–45 kDa (Supplementary Figure S11). Although, this observed size was slightly higher than the predicted size, it was sufficient to indicate the successful expression.

## Nickel nitrilotriacetic acid (Ni-NTA) agarose affinity chromatography purification of protein

The SDS-PAGE results after purification using Ni-NTA agarose affinity chromatography are depicted in Supplementary Figure S12. After ultrasonic disruption, the expressed protein was present both in the supernatant and the pellet, with a higher concentration in the supernatant. This allowed for the use of the supernatant from the induced expression of the recombinant bacteria for affinity purification. A volume of 1 mL of the protein supernatant was subjected to purification through a nickel affinity column. The subsequent 12% SDS-PAGE electrophoresis demonstrated a high purity of the purified protein (Supplementary Figure S12: lanes 4 and 5). The results indicated a significant increase in the expression of the soluble protein. The purified product, analyzed through SDS-PAGE, showed a single protein band around ~43–45 kDa, indicating the effectiveness of the purification method in yielding a high-purity protein (Supplementary Figure S12: lanes 4 and 5).

## Identification, purification and expression of protein

The SDS-PAGE of the protein is shown in Figure 10, and the Western blot analysis result are presented in Figure 11. The purified protein showed a clear band at the corresponding position on

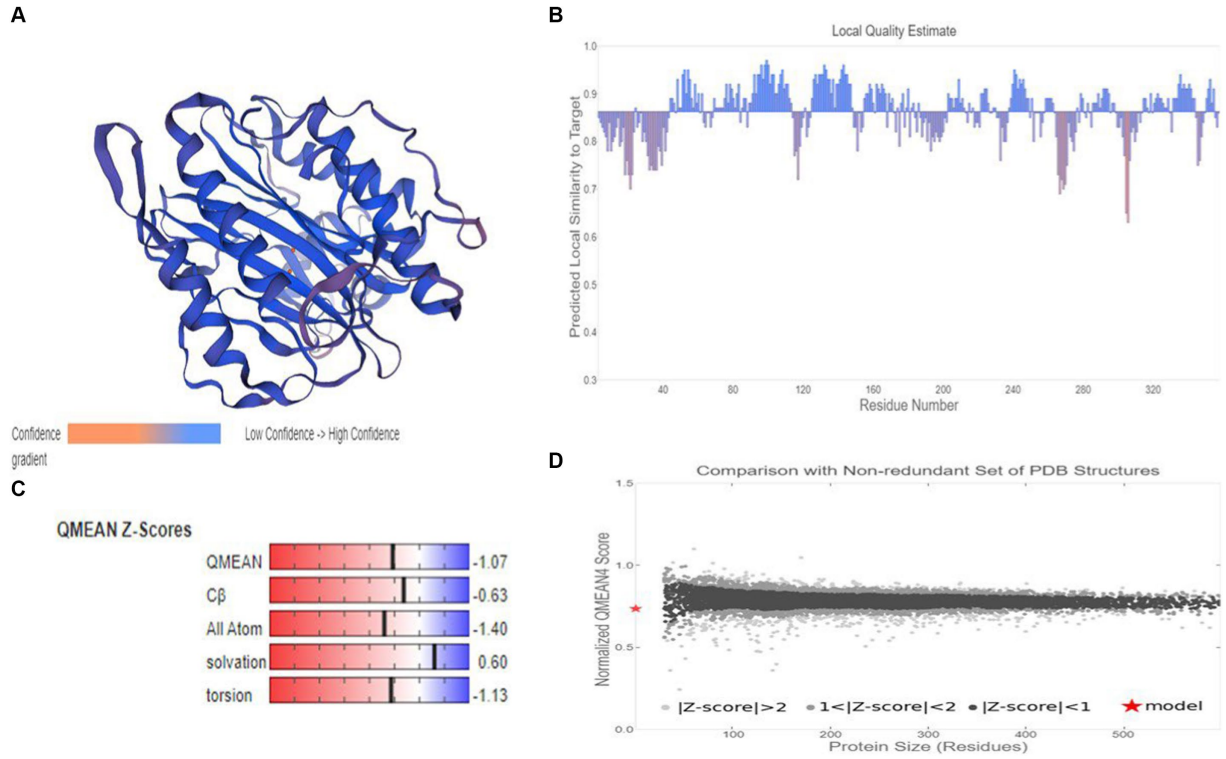


FIGURE 9
Homology modelling of MetAP2 protein of *Nosema bombycis* (Guangdong isolate). **(A)** 3D structure of MetAP2 protein of *Nosema bombycis*. This model was developed based on template 3 fm3.1 (MetAP2 *Encephalitozoon cuniculi*). Color scheme of ribbon represents the confidence gradient (key shown). Two orange spheres represent ligand [metal ions; FE (III)] coordinated within the active site. **(B)** QMEAND is local score: this shows, for each residue of the model (reported on the x-axis), the expected similarity to the native structure (y-axis). Typically, residues showing a score below 0.6 are expected to be of low quality. Different model chains are shown in different colors. **(C)** QMEAN Z-score: Z-scores around 0.0 therefore reflect a "native-like" structure and, as a rule of thumb, a "QMEAN" Z-score below −4.0 indicates a model with low quality. **(D)** Comparison plot: the x-axis shows protein length (number of residues). The y-axis is the "QMEAN" score. Every dot represents one experimental protein structure. Black dots are experimental structures with a "QMEAN" score within 1 standard deviation of the mean (|Z-score| between 0 and 1), experimental structures with a |Z-score| between 1 and 2 are grey. Experimental structure that are even further from the mean are light grey. The actual model is represented as a red star.

SDS-PAGE (Figure 10), indicating the successful purification. As shown in Figure 11, the Western Blot analysis showed a target band at around ~43–45 kDa. The Western blot identification indicated that the protein can specifically bind with the anti-His tag antibody, demonstrating good immunoreactivity, and confirming that the protein was successfully expressed in *E. coli* Rosetta (DE3).

## Discussion

It has been argued that, a thorough understanding of essential genes related to the survival of a given pathogen is critical in devising a viable control strategy (26). This becomes increasingly important while determining therapeutic options and diagnostic tools for fascinating pathogens like microsporidia. Pebrine, the only disease with a mandatory quarantine (22), is a devastating disease of domesticated silkworms with a huge economic impact on sericulture industry in countries like China. This disease is caused by *Nosema bombycis*, for which currently there are no established therapeutic and control options available. Although, our understanding of the mechanisms of high infectious ability and the broad host range of *Nosema bombycis* is limited so far, it has been previously argued that certain factors such as gene duplication, transposable element expansion, and horizontal gene transfer are the likely contributors to high pathogenicity of this mysterious parasite (48). Based on genomic evidence, it was suggested that the specific essential genes of *Nosema bombycis* maybe utilized as primary targets while devising therapeutic (48) and diagnostic (26) options for this deadly disease.

Historically, MetAP2 is known as a bifunctional protein (49). It has been known for its peptidase activity and involvement in inhibition of phosphorylation of eukaryotic initiation factor 2α in yeast and mammals (49, 50). But given the fact that polylysine stretch was found to be missing from the NH2-terminus in MetAP2 of microsporidia spp., it lacked the ability to inhibit phosphorylation of initiation factor2α (50). However, it was argued that this lack of N-terminal extension (polylysine rich region) was not associated with enzyme activity of MetAP2 (51). It was reported that MetAP2-dependent yeast *Saccharomyces cervisiae* was killed by ovalicin, an analogue of fumagillin, whereas MetAP1-dependent yeasts were not killed (49, 52). This evidence indicated that MetAP2 is a selective cellular target of fumagillin and its analogues (23, 51). We know that both *MetAp1* and *MetAP2* are present in higher eukaryotes and yeasts (51). But as with the other microsporidian spp. (50), our transcriptome data (Qazi and Liu, 2024; unpublished results) returned only *MetAP2*

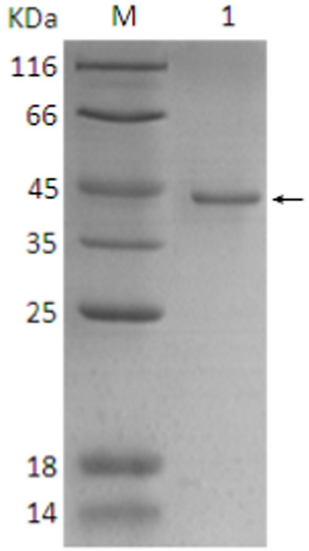


FIGURE 10
SDS-PAGE analysis of final protein purification. 1. Target protein (pointing arrow); M: Protein marker.

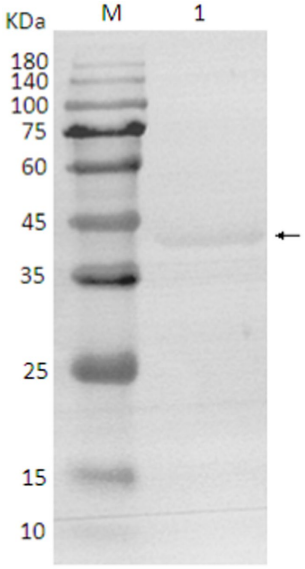


FIGURE 11
Western blot analysis of protein. 1. target protein (pointing arrow); M: pre-stained marker.

both in *Nosema bombycis* (Guangdong isolate) and *Nosema antheraeae*. Given that *MetAP2* gene is currently the only known cellular target of fumagillin and its analogues (23, 50, 51), in the present study we performed an in-depth molecular and phylogenetic characterization of MetAP2 gene and protein of the Guangdong isolate of *Nosema bombycis*. Meanwhile, MetAP2 of *Nosema antheraeae* was also sequenced and annotated for phylogenetic comparison.

To our knowledge, this is the first report of identification, expression, characterization, and phylogenetic analysis of MetAP2 gene and its protein in the Chinese (Guangdong) isolate of *Nosema bombycis*. Utilizing the transcriptome data (Qazi and Liu, 2024; unpublished results) of Guangdong isolate of *Nosema bombycis* and the sequence resources generated in this study, it was observed that the full length of the DNA sequence of *MetAP2* gene was 1,278 bp, including a 5′ non-coding region of 49 bp, a 3′ non-coding region of 152 bp. Specifically, a large open reading frame of 1,077 bp, encoding 358 amino acids, was found. The predicted molecular weight of MetAP2 protein was 40.5 kDa, but the observed molecular weight obtained through prokaryotic expression and purification was about ~43–45 kDa, which was slightly higher than the predicted value in the present study. This phenomenon is not uncommon and has been reported for several proteins studied previously [Guan et al. (53) and references therein]. The GC content (35.48%) of *MetAP2* gene of *Nosema bombycis* was comparable with the lower GC% as observed for its wild relative *Nosema antheraeae* studied in the present study. Tellingly, the overall GC content of *Nosema bombycis* (Guangdong isolate) and *Nosema antheraeae* (Chinese isolate) transcriptome was also observed to be 31 and 28%, respectively (Qazi and Liu, 2024; unpublished results). This is particularly relevant because the lower GC content has been linked to a larger proportion of repetitive sequences relative to the total assembled sequence and longer intergenic regions (54). Additionally, there is an evidence by Pan et al., in their landmark paper (48), where they have shown that *Nosema bombycis* genome is composed of over 38% repetitive elements.

Although, limited work has been done on *MetAP2* gene of *Nosema bombycis*, there is a recent report (55) on characterization of *MetAP2* gene of the Indian isolate of *Nosema bombycis*. To compare the sequence identity between the Guangdong and the Indian isolates of *Nosema bombycis*, we performed the BLAST search analysis using the NCBI (see text footnote 3), and observed a high sequence identity (99%) between the two isolates, with a difference only at 10 bp (1,067/1077) in the open reading frame. Similarly, we also compared sequence identity between *Nosema bombycis* (Guangdong isolate) and uncharacterized *MetAP2* sequence of *Nosema bombycis CQ 1* (Chongqing, China) isolate that was retrieved from its genome sequence data set (48). Interestingly, BLAST search analysis revealed a difference of 27 bp (1,050/1077) in the open reading frames of the two sequences. In keeping with these differences, we currently do not know whether these subtle variations in *MetAP2* gene sequences between *Nosema bombycis* isolated from geographically different locations have any biological significance. But, in keeping with the local context, due consideration is still required while designing of therapeutic or diagnostic options. In any case, further in-depth molecular studies are still required to gain more insight in this regard.

Previously, it was shown that indeed intraspecies polymorphism does exist between four different isolates of *Nosema bombycis* recovered from different geographical regions of China, including one from Guangdong province (56). These authors further reported that the obvious polymorphic differences between analogous sequences were seen both in terms of length and composition of sequence. In a study on *Nosema* spp. of honeybees in Saudi Arabia (57), it was reported that 16S rRNA gene sequence analysis of two geographically different isolates (*ksuNC4* and *ksuNC6*) showed a high identity 99% (217/218) between sequences. In this case, the difference was only found at one position, i.e., the 18th bp was polymorphic with one gap. In the same study, a 100% sequence identity of the Saudi isolate

(*ksuNC4*) of *Nosema ceranae* with the 16S rDNA of other previously reported isolates from different parts of the world was reported (57). It was argued that this identity in sequences can be attributed to the evolutionary relationship between different isolates and species (57). Previously, two putative isolates of *Nosema* sp. (PX1 and PX2) that were recovered from the diamondback moths in Taiwan also showed high divergence in the sequences of the ITS and IGS regions (58). Recently, based on the IGS sequence analysis, 12% average sequence variation was reported in 20 isolates of *Nosema mylitta* collected from different geographic locations in India (59). Based on the genetic and phylogenetic analysis, it was reported that the evolutionary divergence in *Nosema mylitta* was potentially associated with adaptation of pathogen, host defense response, and the geographic conditions in which the host lives (59). This molecular evidence augments the argument that the variation in gene sequences in microsporidian spp. is indeed a result of evolutionary process (59).

Due to the complex silkworm rearing environment and management practices of mulberry orchards, it is reasonable to argue that the cross-infection [e.g., as reported in Huang et al. (60)] of pathogenic insect microsporidian spp. is difficult to control in sericulture production settings. In keeping with the context of the present study, it is pertinent to mention here that the biological evolutionary relationship between *MetAP2* of *Nosema bombycis* of silkworms and other microsporidian spp. carried by different mulberry orchard pests has not been reported yet. It is therefore desirable that the future studies should cover this caveat.

In the present study, homology comparisons showed a varied percent identity between *MetAP2* gene of *Nosema bombycis* and that of other insect and human microsporidian spp. Tellingly, *Nosema bombycis MetAP2* showed a close relationship (%identity) with *MetAP2* of *Nosema antheraeae* of *the* Chinese oak silkworms, and *Nosema mylitta* and *Nosema assamensis*, both infecting the Indian wild silkworms (59, 61). Consistent with the homology comparison, the phylogenetic analysis showed that *MetAP2* of *Nosema bombycis* clustered together and formed a separate branch, with a close evolutionary relationship with *Nosema* spp. of wild silkworms *Nosema antheraeae*, *Nosema mylitta* and *Nosema assamensis*. *Nosema ceranae* and *Nosema bombi* clustered together and showed a distant relationship with *MetAP2* gene of *Nosema bombycis* in the phylogenetic tree. Understandably, *MetAP2* of human microsporidia spp. clustered on the same branch, showing a close relationship between them, but showed a distant evolutionary relationship with *Nosema* spp. of domestic and wild silkworms. Previously, it was argued that *Nosema* spp. infecting domestic and wild silkworms are regarded as "True *Nosema* group/clade," whereas those infecting Lepidoptera and other insects such as honeybees and bumblebees are regarded as "*Nosema*/Vairimorpha group/clade" (9, 61). In the present study, *MetAP2* of *Nosema* spp. of domestic and wild silkworms showed a close phylogenetic relationship between them, but were placed distantly from *Nosema ceranae* (honeybees) and *Nosema bombi* (bumblebees).

The phylogenetic analysis of MetAP2 proteins of various species revealed that amino acids sequences of MetAP2 of *Nosema* spp. did not cluster with any other organisms, but they were placed closer in distance to *Saccharomyces cerevisiae* and *Trypanosoma brucei*. Similarly, further homology and phylogenetic analyses of MetAP2 amino acid sequences between *Nosema* spp., and its ancestral fungal relatives *Aspergillus* spp., and *Saccharomyces cerevisiae* returned consistent results.

Due to lack of available sequences, there has been a limited use of protein coding genes in phylogenetic reconstruction of microsporidian spp. (62). It has been said that *MetAP2* genes of microsporidian spp. do not show any stronger relationship to fungal *MetAP2* than that of other eukaryotes (51). Based on phylogeny of *MetAP2*, it was previously shown that human microsporidia lineage did not cluster with fungi *Aspergillus* and *Saccharomyces* spp. (62). These findings indicate that the conservation and evolutionary relationships of MetAP2 amino acids are closely linked to the species relationships. The molecular weight of MetAP2 protein of *Nosema bombycis* observed in the present study was also closer (~43–45 kDa) to the molecular weights of *Encephalitozoon* spp. of microsporidians (48 to 49 kDa) and *Bruchiolu algerae* (47 kDa) reported previously (50, 63). To put this in the context, the molecular masses of MetAP2 proteins of fungi *Saccharomyces cerevisiae* and humans were reported to be much higher, i.e., 65 and 67 kDa, respectively (50).

It has been said that "*any level of physical characterization of a protein, as opposed to its absence, is valuable*" (64). In recent times, 3D structure modelling of proteins is seen as a focal point where diverse research efforts can combine to provide a detailed view of the underlying mechanistic basis (65). Homology modeling is now seen as important utility in biomedical research, particularly making the targeted drug discovery research faster, easier, cheaper and more practical (66, 67). The selection of an appropriate structural template is a prerequisite in successful application of 3D model of protein. However, templates with the highest sequence identity to the target protein does not necessarily mean that they are appropriate choices (65). It is usually believed that close homologue structures can produce accurate models; however, templates with lower sequence similarity (~20%) can still produce suitable models (68, 69). In keeping with this notion, we developed two 3D structures models of MetAp2 protein. Model 1 was based on template of MetAp2 of *Nosema assamensis* (ID: A0A3G6ILP9.1.A) and had high quality estimate values. But, the template itself was prepared using a prediction (AlphaFold2) database. We therefore prepared a second model based on template of MetAp2 of *Encephalitozoon cuniculi* (ID: 3 fm3.1.A). Although, template used in model 2 had a lower sequence identity with the target sequence, it was considered more reliable, as it was experimentally produced using x-ray crystallography (23).

At present our understanding of precise molecular and physiological roles of MetAP2 of insect microsporidia spp. is very limited. We therefore envision that the results of the present study could be utilized as a reasonable foundation, as we look ahead for the rational drug design, development of improved and highly specific anti-microsporidian agents, and field friendly diagnostic tools. The encouraging news is that MetAP2 is now seen as an extremely logical therapeutic target[12] for microsporidia spp. For instance, it was reported that human microsporadian *Enterocytozoon bieneusi* (MetAP2c) and human MetAP2b structures have small amino acid differences in the active sites (S1 subsite). It was argued that these differences can be exploited to design fumagillin analogues that are

12 https://einsteinmed.edu/departments/pathology/research/microsporidia

specific for MetAP2 of microsporidian spp. (23). Although new inhibitors of this pathway hold great promise as therapeutic agents, drugs such as fumagillin and its derivatives were shown to have inhibitory effect on *MetAP2* of human microsporidia (70) and *Nosema ceranae* of honeybees (71).

Given that currently there is no established therapeutic agent to control "pebrine," a deadly disease of silkworms caused by *Nosema bombycis*, it is important to utilize therapeutic agents like fumagillin and its analogues which are already tested on other microsporidia spp. This argument is reinforced by the fact that fumagillin still holds great promise in controlling Nosema infection in honeybees in the field conditions (72).

## Data availability statement

The datasets presented in this study can be found in online repositories. The names of the repository/repositories and accession number(s) can be found at: https://www.ncbi.nlm.nih.gov/genbank/, KX185053.1; https://www.ncbi.nlm.nih.gov/genbank/, PP576694.1.

## Ethics statement

The manuscript presents research on animals that do not require ethical approval for their study.

## Author contributions

IQ: Conceptualization, Data curation, Formal analysis, Investigation, Methodology, Software, Validation, Writing – original draft. TY: Data curation, Investigation, Methodology, Writing – review & editing. SY: Conceptualization, Data curation, Investigation, Methodology, Writing – review & editing. CA: Formal analysis, Software, Writing – review & editing. JL: Funding acquisition, Project administration, Resources, Supervision, Validation, Writing – review & editing.

## Funding

The author(s) declare financial support was received for the research, authorship, and/or publication of this article. The research was financially supported by the China Agriculture Research System (CARS-18-ZJ0304).

## Acknowledgments

We thank all lab mates who supported during this project.

## Conflict of interest

JL is inventor on a patent on *MetAP2* of *Nosema bombycis*, which is held by the South China Agricultural University.

The remaining authors declare that the research was conducted in the absence of any commercial or financial relationships that could be construed as a potential conflict of interest.

## Publisher's note



## Supplementary material

The Supplementary material for this article can be found online at: https://www.frontiersin.org/articles/10.3389/fvets.2024.1429169/full#supplementary-material

## References

1. Jiang L, Peng L-L, Cao Y-Y, Thakur K, Hu F, Tang S-M, et al. Transcriptome analysis reveals gene expression changes of the fat body of silkworm (Bombyx mori L.) in response to selenium treatment. *Chemosphere*. (2020) 245:125660. doi: 10.1016/j.chemosphere.2019.125660

2. Altman GH, Farrell BD. Sericulture as a sustainable agroindustry. *Clean Circ Bioecon*. (2022) 2:100011. doi: 10.1016/j.clcb.2022.100011

3. Jiang L, Xia Q. The progress and future of enhancing antiviral capacity by transgenic technology in the silkworm Bombyx mori. *Insect Biochem Mol Biol*. (2014) 48:1–7. doi: 10.1016/j.ibmb.2014.02.003

4. Walia SS, Kaur T. (eds.). Sericulture. In: *Basics of integrated farming systems*. Singapore: Springer (2023). p. 105–108.

5. Zhu Y-N, Wang L-Z, Li C-C, Cui Y, Wang M, Lin Y-J, et al. Artificial selection on storage protein 1 possibly contributes to increase of hatchability during silkworm domestication. *PLoS Genet*. (2019) 15:e1007616. doi: 10.1371/journal.pgen.1007616

6. Li K, Dong Z, Pan M. Common strategies in silkworm disease resistance breeding research. *Pest Manag Sci*. (2023) 79:2287–98. doi: 10.1002/ps.7454

7. Didier ES. Microsporidiosis: an emerging and opportunistic infection in humans and animals. *Acta Trop*. (2005) 94:61–76. doi: 10.1016/j.actatropica.2005.01.010

8. Han B, Pan G, Weiss LM. Microsporidiosis in humans. *Clin Microbiol Rev*. (2021) 34:e00010–20. doi: 10.1128/CMR.00010-20

9. Stentiford G, Becnel J, Weiss L, Keeling P, Didier E, Bjornson S, et al. Microsporidia–emergent pathogens in the global food chain. *Trends Parasitol*. (2016) 32:336–48. doi: 10.1016/j.pt.2015.12.004

10. Weyer E, Weiss LM. Microsporidian spores contain hibernating dimeric ribosomes. *Nat Microbiol*. (2023) 8:1762–3. doi: 10.1038/s41564-023-01481-0

11. Wang C, Yu B, Meng X, Xia D, Pei B, Tang X, et al. Microsporidian Nosema bombycis hijacks host vitellogenin and restructures ovariole cells for transovarial transmission. *PLoS Pathog*. (2023) 19:e1011859. doi: 10.1371/journal.ppat.1011859

12. Chen Y, Lv Q, Liao H, Xie Z, Hong L, Qi L, et al. The microsporidian polar tube: origin, structure, composition, function, and application. *Parasit Vectors*. (2023) 16:305. doi: 10.1186/s13071-023-05908-9

13. De La Mora A, Morfin N, Tapia-Rivera JC, Macías-Macías JO, Tapia-González JM, Contreras-Escareño F, et al. The fungus Nosema ceranae and a sublethal dose of the neonicotinoid insecticide Thiamethoxam differentially affected the health and immunity of Africanized honey bees. *Microorganisms*. (2023) 11:1258. doi: 10.3390/microorganisms11051258

14. Han B, Polonais V, Sugi T, Yakubu R, Takvorian PM, Cali A, et al. The role of microsporidian polar tube protein 4 (Ptp4) in host cell infection. *PLoS Pathog*. (2017) 13:e1006341. doi: 10.1371/journal.ppat.1006341

15. Han B, Takvorian PM, Weiss LM. The function and structure of the microsporidia polar tube. *Exp Suppl*. (2022) 114:179–213. doi: 10.1007/978-3-030-93306-7_8

16. Lv Q, Hong L, Qi L, Chen Y, Xie Z, Liao H, et al. Microsporidia dressing up: the spore polaroplast transport through the polar tube and transformation into the sporoplasm membrane. *MBio*. (2024) 15:e02749–23. doi: 10.1128/mbio.02749-23

17. Nageli C. uber die neue Krankheit der Seidenraupe und verwandte Organismen. [Abstract of report before 33. Versamml. Deutsch. Naturf. u. Aerzte. Bonn, 21 Sept.]. *Bot Ztg*. (1857) 15:760–1.

18. Gupta SK, Hossain Z, Nanu MM, Mondal K. Impact of microsporidian infection on growth and development of silkworm Bombyx mori L.(Lepidoptera: Bombycidae). *Agric Nat Res*. (2016) 50:388–95. doi: 10.1016/j.anres.2016.02.005

19. Hu N, Dong Z-Q, Long J-Q, Zheng N, Hu C-W, Wu Q, et al. Transcriptome analysis reveals changes in silkworm energy metabolism during Nosema bombycis infection. *Pesticide Biochem*. (2021) 174:104809. doi: 10.1016/j.pestbp.2021.104809

20. Szumowski SC, Troemel ER. Microsporidia–host interactions. *Curr Opin Microbiol*. (2015) 26:10–6. doi: 10.1016/j.mib.2015.03.006

21. Wei J, Fei Z, Pan G, Weiss LM, Zhou Z. Current therapy and therapeutic targets for microsporidiosis. *Front Microbiol*. (2022) 13:835390. doi: 10.3389/fmicb.2022.835390

22. Fu Z, He X, Cai S, Liu H, He X, Li M, et al. Quantitative Pcr for detection of Nosema bombycis in single silkworm eggs and newly hatched larvae. *J Microbiol Methods*. (2016) 120:72–8. doi: 10.1016/j.mimet.2015.12.003

23. Alvarado JJ, Nemkal A, Sauder JM, Russell M, Akiyoshi DE, Shi W, et al. Structure of a microsporidian methionine aminopeptidase type 2 complexed with fumagillin and Tnp-470. *Mol Biochem Parasitol*. (2009) 168:158–67. doi: 10.1016/j.molbiopara.2009.07.008

24. Huang W-F, Solter LF, Yau PM, Imai BS. Nosema ceranae escapes fumagillin control in honey bees. *PLoS Pathog*. (2013) 9:e1003185. doi: 10.1371/journal.ppat.1003185

25. Huntsman EM, Cho RM, Kogan HV, Mcnamara-Bordewick NK, Tomko RJ Jr, Snow JW. Proteasome inhibition is an effective treatment strategy for microsporidia infection in honey bees. *Biomol Ther*. (2021) 11:1600. doi: 10.3390/biom11111600

26. Esvaran V, Jagadish A, Terenius O, Suraporn S, Mishra RK, Ponnuvel KM. Targeting essential genes of Nosema for the diagnosis of pebrine disease in silkworms. *Ann Parasitol*. (2020) 66:303–10. doi: 10.17420/ap6603.268

27. Wang LL, Chen KP, Zhang Z, Yao Q, Gao GT, Zhao Y. Phylogenetic analysis of Nosema antheraeae (microsporidia) isolated from Chinese oak silkworm, Antheraea pernyi. *J Eukaryot Microbiol*. (2006) 53:310–3. doi: 10.1111/j.1550-7408.2006.00106.x

28. Panthee S, Paudel A, Hamamoto H, Sekimizu K. Advantages of the silkworm as an animal model for developing novel antimicrobial agents. *Front Microbiol*. (2017) 8:242960. doi: 10.3389/fmicb.2017.00373

29. Zhang F, Lu X, Kumar V, Zhu H, Chen H, Chen Z, et al. Effects of a novel anti-exospore monoclonal antibody on microsporidial Nosema bombycis germination and reproduction in vitro. *Parasitology*. (2007) 134:1551–8. doi: 10.1017/S0031182007002934

30. Sayers EW, Bolton EE, Brister JR, Canese K, Chan J, Comeau DC, et al. Database resources of the national center for biotechnology information. *Nucleic Acids Res*. (2022) 50:D20–6. doi: 10.1093/nar/gkab1112

31. Lalitha S. Primer premier 5. *Biotech Softw Int Rep*. (2000) 1:270–2. doi: 10.1089/152791600459894

32. Wheeler DL, Church DM, Federhen S, Lash AE, Madden TL, Pontius JU, et al. Database resources of the National Center for biotechnology. *Nucleic Acids Res*. (2003) 31:28–33. doi: 10.1093/nar/gkg033

33. Altschul SF, Gish W, Miller W, Myers EW, Lipman DJ. Basic local alignment search tool. *J Mol Biol*. (1990) 215:403–10. doi: 10.1016/S0022-2836(05)80360-2

34. Lu S, Wang J, Chitsaz F, Derbyshire MK, Geer RC, Gonzales NR, et al. Cdd/Sparcle: the conserved domain database in 2020. *Nucleic Acids Res*. (2020) 48:D265–8. doi: 10.1093/nar/gkz991

35. Marchler-Bauer A, Bo Y, Han L, He J, Lanczycki CJ, Lu S, et al. Cdd/Sparcle: functional classification of proteins via subfamily domain architectures. *Nucleic Acids Res*. (2017) 45:D200–3. doi: 10.1093/nar/gkw1129

36. Wang J, Chitsaz F, Derbyshire MK, Gonzales NR, Gwadz M, Lu S, et al. The conserved domain database in 2023. *Nucleic Acids Res*. (2023) 51:D384–8. doi: 10.1093/nar/gkac1096

37. Gasteiger E, Hoogland C, Gattiker A, Duvaud SE, Wilkins MR, Appel RD, et al. Protein identification and analysis tools on the ExPASy Server. In: Walker JM, editor. *The proteomics protocols handbook. Springer protocols handbooks*. Humana Totowa, NJ: Humana Press (2005).

38. Hallgren J, Tsirigos KD, Pedersen MD, Almagro Armenteros JJ, Marcatili P, Nielsen H, et al. Deeptmhmm predicts alpha and beta transmembrane proteins using deep neural networks. *BioRxiv*. (2022) 2022:08.487609. doi: 10.1101/2022.04.08.487609

39. Teufel F, Almagro Armenteros JJ, Johansen AR, Gíslason MH, Pihl SI, Tsirigos KD, et al. SignalP 6.0 predicts all five types of signal peptides using protein language models. *Nat Biotechnol*. (2022) 40:1023–5. doi: 10.1038/s41587-021-01156-3

40. Combet C, Blanchet C, Geourjon C, Deléage G. Nps@: network protein sequence analysis. *Trends Biochem Sci*. (2000) 25:147–50. doi: 10.1016/S0968-0004(99)01540-6

41. Nakai K, Horton P. Psort: a program for detecting sorting signals in proteins and predicting their subcellular localization. *Trends Biochem Sci*. (1999) 24:34–5. doi: 10.1016/S0968-0004(98)01336-X

42. Thumuluri V, Almagro Armenteros JJ, Johansen AR, Nielsen H, Winther O. DeepLoc 2.0: multi-label subcellular localization prediction using protein language models. *Nucleic Acids Res*. (2022) 50:W228–34. doi: 10.1093/nar/gkac278

43. Thompson JD, Higgins DG, Gibson TJ. Clustal W: improving the sensitivity of progressive multiple sequence alignment through sequence weighting, position-specific gap penalties and weight matrix choice. *Nucleic Acids Res*. (1994) 22:4673–80. doi: 10.1093/nar/22.22.4673

44. Stamatakis A. Raxml version 8: a tool for phylogenetic analysis and post-analysis of large phylogenies. *Bioinformatics*. (2014) 30:1312–3. doi: 10.1093/bioinformatics/btu033

45. Waterhouse A, Bertoni M, Bienert S, Studer G, Tauriello G, Gumienny R, et al. Swiss-model: homology modelling of protein structures and complexes. *Nucleic Acids Res*. (2018) 46:W296–303. doi: 10.1093/nar/gky427

46. Studer G, Rempfer C, Waterhouse AM, Gumienny R, Haas J, Schwede T. QmeandisCo—distance constraints applied on model quality estimation. *Bioinformatics*. (2020) 36:1765–71. doi: 10.1093/bioinformatics/btz828

47. Studer G, Tauriello G, Bienert S, Biasini M, Johner N, Schwede T. ProMod3—a versatile homology modelling toolbox. *PLoS Comput Biol*. (2021) 17:e1008667. doi: 10.1371/journal.pcbi.1008667

48. Pan G, Xu J, Li T, Xia Q, Liu S-L, Zhang G, et al. Comparative genomics of parasitic silkworm microsporidia reveal an association between genome expansion and host adaptation. *BMC Genomics*. (2013) 14:1–14. doi: 10.1186/1471-2164-14-186

49. Griffith EC, Su Z, Turk BE, Chen S, Chang Y-H, Wu Z, et al. Methionine aminopeptidase (type 2) is the common target for angiogenesis inhibitors Agm-1470 and ovalicin. *Chem Biol*. (1997) 4:461–71. doi: 10.1016/S1074-5521(97)90198-8

50. Pandrea I, Mittleider D, Brindley PJ, Didier ES, Robertson DL. Phylogenetic relationships of methionine aminopeptidase 2 among Encephalitozoon species and genotypes of microsporidia. *Mol Biochem Parasitol*. (2005) 140:141–52. doi: 10.1016/j.molbiopara.2004.12.006

51. Zhang H, Huang H, Cali A, Takvorian PM, Feng X, Zhou G, et al. Investigations into microsporidian methionine aminopeptidase type 2: a therapeutic target for microsporidiosis. *Folia Parasitol*. (2005) 52:182–92. doi: 10.14411/fp.2005.023

52. Sin N, Meng L, Wang MQ, Wen JJ, Bornmann WG, Crews CM. The anti-angiogenic agent fumagillin covalently binds and inhibits the methionine aminopeptidase, Metap-2. *Proc Natl Acad Sci*. (1997) 94:6099–103. doi: 10.1073/pnas.94.12.6099

53. Guan Y, Zhu Q, Huang D, Zhao S, Jan Lo L, Peng J. An equation to estimate the difference between theoretically predicted and Sds Page-displayed molecular weights for an acidic peptide. *Sci Rep*. (2015) 5:13370. doi: 10.1038/srep13370

54. Haag KL, Pombert J-F, Sun Y, De Albuquerque NRM, Batliner B, Fields P, et al. Microsporidia with vertical transmission were likely shaped by nonadaptive processes. *Genome Biol Evol*. (2020) 12:3599–614. doi: 10.1093/gbe/evz270

55. Esvaran VG, Gupta T, Nayaka AN, Sivaprasad V, Ponnuvel KM. Molecular characterization of Nosema bombycis methionine aminopeptidase 2 (*MetAP2*) gene and evaluation of anti-microsporidian activity of Fumagilin-B in silkworm Bombyx mori. *3 Biotech*. (2018) 8:386. doi: 10.1007/s13205-018-1411-z

56. Liu H, Pan G, Luo B, Li T, Yang Q, Vossbrinck CR, et al. Intraspecific polymorphism of rdna among five Nosema bombycis isolates from different geographic regions in China. *J Invertebr Pathol*. (2013) 113:63–9. doi: 10.1016/j.jip.2013.01.008

57. Ansari MJ, Al-Ghamdi A, Nuru A, Khan KA, Alattal Y. Geographical distribution and molecular detection of Nosema ceranae from indigenous honey bees of Saudi Arabia. *Saudi J Biolog Sci*. (2017) 24:983–91. doi: 10.1016/j.sjbs.2017.01.054

58. Ku C-T, Wang C-Y, Tsai Y-C, Tzeng C-C, Wang C-H. Phylogenetic analysis of two putative Nosema isolates from cruciferous lepidopteran pests in Taiwan. *J Invertebr Pathol*. (2007) 95:71–6. doi: 10.1016/j.jip.2006.11.008

59. Hassan W, Nath BS, Ponnuvel KM, Mishra RK, Pradeep ANR. Evolutionary diversity in the intracellular microsporidian parasite Nosema sp. infecting wild silkworm revealed by Igs nucleotide sequence diversity. *J Mol Evol*. (2020) 88:345–60. doi: 10.1007/s00239-020-09936-2

60. Huang X, Tang Q, Luo M, Huang S, Jiang S, Xia Q, et al. Investigation on resource of insect microsporidan in Guangxi and its characters. *J Southern Agric*. (2018) 49:1541–7. doi: 10.5555/20183334264

61. Subrahmanyam G, Esvaran VG, Ponnuvel KM, Hassan W, Chutia M, Das R. Isolation and molecular identification of microsporidian pathogen causing nosemosis in Muga silkworm, Antheraea assamensis Helfer (Lepidoptera: Saturniidae). *Indian J Microbiol*. (2019) 59:525–9. doi: 10.1007/s12088-019-00822-0

62. Johny S, Larson TM, Solter LF, Edwards KA, Whitman DW. Phylogenetic characterization of Encephalitozoon romaleae (microsporidia) from a grasshopper host: relationship to Encephalitozoon spp. infecting humans. *Infect Genet Evol*. (2009) 9:189–95. doi: 10.1016/j.meegid.2008.10.010

63. Weiss LM. Microsporidia 2003: Iwop-8. *J Eukaryot Microbiol*. (2003) 50:566–8. doi: 10.1111/j.1550-7408.2003.tb00631.x

64. Vakser IA. Low-resolution structural modeling of protein interactome. *Curr Opin Struct Biol*. (2013) 23:198–205. doi: 10.1016/j.sbi.2012.12.003

65. Schmidt T, Bergner A, Schwede T. Modelling three-dimensional protein structures for applications in drug design. *Drug Discov Today*. (2014) 19:890–7. doi: 10.1016/j.drudis.2013.10.027

66. Haddad Y, Adam V, Heger Z. Ten quick tips for homology modeling of high-resolution protein 3D structures. *PLoS Comput Biol*. (2020) 16:e1007449. doi: 10.1371/journal.pcbi.1007449

67. Muhammed MT, Aki-Yalcin E. Homology modeling in drug discovery: overview, current applications, and future perspectives. *Chem Biol Drug Des*. (2019) 93:12–20. doi: 10.1111/cbdd.13388

68. Maccallum JL, Pérez A, Schnieders MJ, Hua L, Jacobson MP, Dill KA. Assessment of protein structure refinement in Casp9. *Proteins*. (2011) 79:74–90. doi: 10.1002/prot.23131

69. Mariani V, Kiefer F, Schmidt T, Haas J, Schwede T. Assessment of template based protein structure predictions in Casp9. *Proteins*. (2011) 79:37–58. doi: 10.1002/prot.23177

70. Han B, Weiss LM. Therapeutic targets for the treatment of microsporidiosis in humans. *Expert Opin Ther Targets*. (2018) 22:903–15. doi: 10.1080/14728222.2018.1538360

71. Higes M, Nozal MJ, Alvaro A, Barrios L, Meana A, Martín-Hernández R, et al. The stability and effectiveness of fumagillin in controlling Nosema ceranae (microsporidia) infection in honey bees (Apis mellifera) under laboratory and field conditions. *Apidologie*. (2011) 42:364–77. doi: 10.1007/s13592-011-0003-2

72. Peirson M, Pernal SF. A systematic review of Fumagillin field trials for the treatment of Nosema disease in honeybee colonies. *Insects*. (2024) 15:29. doi: 10.3390/insects15010029

frontiers | Frontiers in Veterinary Science

TYPE Original Research
PUBLISHED 10 July 2024
DOI 10.3389/fvets.2024.1409127



OPEN ACCESS

EDITED BY
Izhar Hyder Qazi,
Shaheed Benazir Bhutto University of Veterinary and Animal Sciences, Pakistan

REVIEWED BY
Yanzhu Zhu,
Jilin Agricultural Science and Technology College, China
Chao Xu,
Jilin Agricultural University, China
Zheng Ruan,
Nanchang University, China

*CORRESPONDENCE
Lihua Wang
✉ lhwang@qau.edu.cn

RECEIVED 29 March 2024
ACCEPTED 18 June 2024
PUBLISHED 10 July 2024

CITATION
Cao L, Sun F, Ren Q, Jiang Z, Chen J, Li Y and Wang L (2024) Effects of dietary supplementation of *Enterococcus faecium* postbiotics on growth performance and intestinal health of growing male mink. *Front. Vet. Sci.* 11:1409127. doi: 10.3389/fvets.2024.1409127



# Effects of dietary supplementation of *Enterococcus faecium* postbiotics on growth performance and intestinal health of growing male mink

Lin Cao, Fengxue Sun, Qifeng Ren, Ziyi Jiang, Jian Chen, Yalin Li and Lihua Wang*

College of Animal Science and Technology, Qingdao Agricultural University, Qingdao, China

Recent studies have demonstrated that postbiotics possess bioactivities comparable to those of probiotics. Therefore, our experiment aimed to evaluate the effects of postbiotics derived from *Enterococcus faecium* on the growth performance and intestinal health of growing male minks. A total of 120 growing male minks were randomly assigned to 4 groups, each with 15 replicates of 2 minks. The minks in the 4 groups were fed a basal diet supplemented with 0 (control), 0.05, 0.1, and 0.15% postbiotics derived from *E. faecium* (PEF), respectively. Compared to the control, PEF improved feed/gain (F/G) during the first 4 weeks and the entire 8 weeks of the study ($p < 0.05$); in addition, 0.1% PEF improved average daily gain (ADG) during the first 4 weeks and the entire 8 weeks of the study ($p < 0.05$), while 0.15% PEF improved ADG during the first 4 weeks of the study ($p < 0.05$). Consequently, 0.1% PEF minks displayed greater body weight (BW) at weeks 4 and 8 ($p < 0.05$), and 0.15% PEF minks had greater BW at week 4 ($p < 0.05$) than minks in the control. Furthermore, compared to the control, both 0.05 and 0.1% PEF enhanced the apparent digestibility of crude protein (CP) and ether extract (EE) ($p < 0.05$) in the initial 4 weeks, while both 0.1 and 0.15% PEF enhanced the apparent digestibility of CP and DM in the final 4 weeks ($p < 0.05$). Additionally, trypsin activity was elevated in the 0.1 and 0.15% PEF groups compared to the control ($p < 0.05$). In terms of intestinal morphology, PEF increased the villus height and villus/crypt (V/C) in the jejunum ($p < 0.05$), and both 0.1 and 0.15% PEF decreased the crypt depth and increased the villus height and V/C in the duodenum ($p < 0.05$) compared to the control group. Supplementation with 0.1% PEF increased the SIgA levels but decreased the IL-2, IL-8, and TNF-α levels in the jejunum ($p < 0.05$). Compared to the control, *E. faecium* postbiotics decreased the relative abundances of *Serratia* and *Fusobacterium* ($p < 0.05$). In conclusion, the results indicate that the growth performance, digestibility, immunity, and intestine development of minks are considerably affected by *E. faecium* postbiotics. In particular, dietary supplementation with 0.1% *E. faecium* postbiotics provides greater benefits than supplementation with 0.05 and 0.15%.

KEYWORDS

**mink, postbiotics, *Enterococcus faecium*, nutrients digestibility, intestinal morphology, immune status, intestinal microbiota**

# 1 Introduction

Minks have been domesticated for approximately 100 years (1). On commercial mink farms, intestinal diseases such as enteritis and diarrhea are a considerable threat to the health, growth, and survival of minks during their developing period (2). Traditionally, antibiotics have been widely used to prevent these intestinal diseases (3), which promote the growth of the animals. However, the misuse of antibiotics has resulted in the emergence of antibiotic-resistant bacteria and genes, reducing their therapeutic efficacy against diseases in both humans and animals (4). Consequently, many countries have prohibited the use of antibiotics for growth promotion in animal feed (5). With the implementation of this ban, the search for viable alternatives to antibiotics has increasingly attracted attention.

*Enterococcus faecium* is a lactic acid bacterium recognized and approved for use as a direct-fed microbial by the Ministry of Agriculture (MOA) in China (6). Some studies have demonstrated that *E. faecium* is beneficial as a feed additive for improving growth performance (7), digestibility (8), and immunity (9), while reducing diarrhea occurrence (7) and alleviating salmonella infection (9, 10). However, some strains of *E. faecium* have been identified as opportunistic pathogens with resistance to many antibiotics (11, 12). Consequently, concerns have been raised regarding the safety of *E. faecium* as a probiotic. Furthermore, ensuring the stringent storage and transportation conditions necessary for lactic acid bacteria presents a significant challenge (13). As some studies have demonstrated that the viability of bacteria is not essential for all probiotic effects, the inactivated microorganisms and their derived fractions, termed postbiotics by the International Scientific Association for Probiotics and Prebiotics (ISAPP) (14), possess bioactivities comparable to those of live probiotic bacteria (15, 16). The beneficial impact of the probiotic is partly due to the various metabolites generated by viable probiotics (17). Therefore, it is reasonable to expect that *E. faecium* postbiotics may offer more advantages than *E. faecium* probiotics due to their higher safety and stability (18).

At present, the probiotic effects of *E. faecium* on livestock and poultry production have been extensively documented (19–21). However, there is limited research on postbiotics derived from *E. faecium*, especially in mink. The present experiment was conducted to evaluate the effects of the postbiotics derived from mink-origin *E. faecium* on male minks by analyzing growth performance, nutrient apparent digestibility, digestive enzyme activity, intestinal morphology, intestinal mucosal immunity, and gut microbiota composition.

# 2 Materials and methods

## 2.1 Ethics approval

The Animal Care and Use Committee of Animal Science and Technology at Qingdao Agricultural University reviewed and approved the experimental protocol (DKY20230524-2). This study was conducted in accordance with the ARRIVE 2.0 guidelines.

## 2.2 *Enterococcus faecium* postbiotics

The strain of *E. faecium* was previously isolated from the rectal contents of mink, identified by 16S rRNA gene sequence analysis, and preserved in the China General Microbiological Culture Collection Center (No. 29262). The 16S rRNA gene sequence was deposited in the National Center for Biotechnology Information (NCBI) database under the accession number PP886227. The isolated strain of *E. faecium* was inoculated in MRS medium and cultured at 37°C for 24 h. The viable *E. faecium* in the suspension was more than $10^7$ cfu/mL by colony count. The *E. faecium* in suspension was inactivated by heat, and then the postbiotics derived from *E. faecium* were obtained. The *E. faecium* postbiotic sample was subjected to chromatographic separation using a SHIMADZU-LC30 ultra-high-performance liquid chromatography (UHPLC) system, equipped with an ACQUITY UPLC® HSS T3 (2.1 × 150 mm, 1.8 μm) (Waters, Milford, MA, United States) column. Following the UHPLC separation, the sample was analyzed using mass spectrometry with a QE Plus mass spectrometer (Thermo Scientific). Metabolomic analysis indicated that *E. faecium* postbiotics contained 28.71% organic acids and their derivatives as well as 19.01% lipids and lipid-like molecules.

## 2.3 Animals and experimental design

The experiment was carried out on a commercial mink farm in Haiyang, Yantai. A total of 120 male minks (Regal White) at 12 weeks of age with an initial body weight (IBW) of 1281.52 ± 5.98 g were randomly assigned to 4 numerically equal groups. Each group consisted of 15 replicates with 2 minks in each replicate. The minks in the 4 groups were fed a basal diet with *E. faecium* postbiotics at 0, 0.05, 0.1, and 0.15% of the diet, respectively. Our previous study (22) has demonstrated that postbiotics derived from another *Lactobacillus* species exhibit probiotic effects in minks at comparable levels of supplementation. So, similar levels of *E. faecium* postbiotics supplementation were adopted in this study. The experiment lasted 8 weeks following a 1-week adaptation period.

## 2.4 Diet and management

All minks were housed in a two-row shelter with two open sides. Two minks were kept in a cage with the dimensions of 30 × 75 × 45 $cm^3$ (width × depth × height). Each cage was equipped with a wooden nest box (30 cm × 30 cm × 30 cm, L × W × H) with a metal mesh ceiling. Minks had free access to the home cage and nest box via the entrance. During the trial period, the health status of the minks was checked twice daily, and any minks with poor health or compromised welfare were promptly removed from the study. During the period of the study, minks were fed twice per day. The paste diets were formulated from sea fishes and byproducts, chicken byproducts, and egg products. The composition of the experimental diets and the nutrient levels are presented in Table 1. Each cage was equipped with one drinker, and minks had *ad libitum* access to drinking water by the drinker. The ambient temperature was maintained at 26.24°C (± 0.05), relative humidity was 65.27% (± 0.05), and the light schedule was natural light regime throughout the study.

TABLE 1 Ingredients and nutrient composition of the basal diet (air-dry basis, %).

| Items | 0–4 weeks | 5–8 weeks |
|---|---|---|
| Sea fishes and byproducts | 32 | 32 |
| Unhatched fertilized egg | 32 | 32 |
| Chicken head | 20 | 20 |
| Extruded corn | 10 | 10 |
| Lard | 1 | 2 |
| Soybean meal | 2 | 2 |
| Premix[1] | 3 | 2 |
| Total | 100 | 100 |
| *Nutrient levels* | | |
| ME (MJ/kg)[2] | 15.98 | 17.04 |
| Ether extract | 16.65 | 19.85 |
| Crude protein | 31.81 | 31.26 |
| Calcium | 2.47 | 2.59 |
| Phosphorus | 1.59 | 1.64 |

[1]The premix provided the following per kg of the diets: VA 9,000 IU, VC 40 mg, VE 20 mg, VK30.5 mg, VB15 mg, VB23 mg, VB6 2.5 mg, VB121 mg, VD3 2,000 IU, nicotinic acid 20 mg, pantothenic acid 6 mg, folic acid 0.5 mg, biotin 0.5 mg, Fe 30 mg, Zn 25 mg, Mn 10 mg, Cu 5 mg, I 0.25 mg, Se 0.2 mg. [2]The metabolizable energy is the calculated value, and the other value is the measured value. ME is calculated using the equation ME = (0.85 × CP% × 4.5 + 0.90 × EE% × 9.5 + 0.75 × NFE% × 4.0) × 4.184, NFE (%) = 100%-CP (%)-EE (%)-ash (%).

## 2.5 Samples and data collection

### 2.5.1 Evaluation of growth performance

Animals were individually weighed at the beginning (week 0), week 4, and week 8 of the study to determine the initial (week 0), week 4, and final (week 8) body weight. The average daily gain (ADG) of minks was calculated. During the experimental period, the feed supplied and leftovers were accurately weighed and recorded over 3 days per week. The average daily feed intake (ADFI) and feed/gain (F/G) of minks were calculated for each mink individually.

### 2.5.2 Digestive experiment

A digestive experiment using the endogenous indicator method was performed to evaluate the apparent digestibility of nutrients at weeks 3 and 7 of the experiment. Fecal samples were collected via an inclined stainless steel plate hung under the cage. A total of 24 uncontaminated fecal samples in the four groups (with six replicates in each group) were sampled to approximately 200 g over 3 days, respectively. The 3-day fecal samples were mixed and then kept at −20°C until analysis. Meanwhile, the diets of each group were sampled daily during the 3 days before feeding the minks, then pooled to obtain representative samples, and stored at −20°C until analysis. The diet and fecal samples were air-dried at 65°C to obtain the initial moisture content. All air-dried samples were ground and passed through a 40-mesh sieve. Ground diet and fecal samples were analyzed for dry matter (DM) (GB/T 6435–2014), crude ash (GB/T 6438–2007), hydrochloric acid insoluble ash (GB/T 23742–2009), crude protein (CP) (GB/T 6432–2018), and ether extract (EE) (GB/T 6433–2006).

$$\text{Nutrient apparent digestibility}\,(\%) = 100\% - (A1 / A2) \times (B2 / B1)$$

Where A1 is the content of hydrochloric acid-insoluble ash in the diet, A2 is the content of hydrochloric acid-insoluble ash in the fecal samples, B1 is the content of a certain nutrient in the diet, and B2 is the content of a certain nutrient in the fecal sample.

### 2.5.3 Collection and detection of intestinal samples

At the end of the study (week 8), minks ($n = 8$) from each group were randomly selected and euthanized. Approximately 2–5 g of contents of the duodenum, 5 cm sections of the duodenum and jejunum, 2–5 g of the jejunum mucosal tissue, and a rectal mucosal swab were sampled per mink.

The contents of the duodenum were centrifuged at 3500 ×*g* at 4°C for 10 min. The supernatant was used to measure the activity of α-amylase, trypsin, and lipase using assay kits (Jiancheng Bioengineering Research Institute, Nanjing, China).

The duodenum and jejunum samples were rinsed with saline and then placed into 4% paraformaldehyde fixative. After rinsing with flowing water for 24 h, the samples were dehydrated through a graded series of ethanol solutions, cleared with xylene, and embedded in paraffin wax. The samples were sectioned into 5-μm-thick sections, stained with hematoxylin and eosin (H&E), mounted with coverslips, and sealed with neutral resin for subsequent histological evaluation. The villus height and crypt depth were visualized under a light microscope (Carl Zeiss, Germany), and the images captured were analyzed using the software ZEN 2011 (Blue version). The villus height was determined from the tip of the villus to the villus–crypt junction, while the crypt depth was measured from the base of the crypt to the same junction. For each sample, the average of villus heights and crypt depths was calculated from 9 measurements taken at 3 discontinuous fields (50×), with 3 measuring points per field (23). Subsequently, the villus height to crypt depth ratio (V/C) was calculated (24).

The jejunum mucosal tissue of the mink was taken, diluted with 0.9% saline (1:9 w/v), and homogenized. The homogenate was centrifuged at 3500 ×*g* at 4°C for 10 min to obtain the supernatant, which was then analyzed for immune components, including SIgA and cytokines (IL-1β, IL-8, IL-10, IL-2, IL-6, IL-12, TNF-α, and

IFN-γ). These indicators were detected using the Enzyme-Linked Immunosorbent Assay (ELISA) Kit (Jiancheng Bioengineering Research Institute, Nanjing, China), and the OD values were measured at a wavelength of 450 nm using a full-spectrum microplate reader (Tecan Austria GmbH, Grodig, Austria).

The total DNA of the rectal mucosa samples of mink was extracted using the Fast DNA Spin Kit for Soil (MP, Santa Ana, CA, United States) (22). The extracted genomic DNA was detected by 1% agarose gel electrophoresis. The primers 338F (5'-ACTCCTACGGGAGGCAGCAG-3') and 806R (5'-GGACTACHVGGGTWTCTAAT-3') were used to amplify the V3-V4 region of the 16S rRNA gene. PCR amplification was performed on an ABI Gene Amp PCR system 9,700 thermal cycler with a program consisting of an initial denaturation at 95°C for 3 min, followed by 27 cycles of denaturation at 95°C for 30 s, annealing at 55°C for 30 s, and extension at 72°C for 30 s, concluding with a final extension at 72°C for 10 min (25). The amplicons were excised from the 2% agarose gel, purified using the AxyPrep DNA Gel Extraction Kit (Axygen, Union City, CA, United States), and tested by 2% agarose gel electrophoresis. Quantification was performed using the QuantiFluor™-ST Blue fluorescence quantification system (Promega, Madison, WI, United States). A PE 300 library was constructed based on the Illumina MiSeq platform and sequenced using the Illumina MiSeq PE 300 platform (26).

## 2.6 Statistical analysis

The data on growth performance, nutrient digestibility, digestive enzyme activity, intestinal morphology, and jejunum mucosal immune components were expressed as means ± standard error (SE) and were analyzed using one-way ANOVA with SPSS 25.0 (SPSS Institute Inc., Chicago, USA). A $p < 0.05$ means a significant difference. Duncan's tests were used to analyze differences between groups.

The intestinal flora data were analyzed on the I-Sanger cloud platform. FLASH 1.2.11 software was used for pair-end double-ended sequence splicing. The Spearman correlation coefficient was adopted to analyze the correlation between the intestinal flora and the immunity of minks.

# 3 Results

## 3.1 Effect of PEF on growth performance

The postbiotics of *E. faecium* had significant effects on BW, ADG, and F/G of minks during the study ($p < 0.05$; Table 2). Compared to the control minks, the minks in the 0.15% PEF group were heavier ($p < 0.05$) at week 4 of the study and had greater ADG ($p < 0.05$) during the initial 4 weeks, while the minks in the 0.1% PEF group were heavier ($p < 0.05$) at weeks 4 and 8 of the study and had greater ADG ($p < 0.05$) during the initial 4 weeks and the entire 8 weeks of the study. The minks in the PEF groups had less F/G ($p < 0.05$) than the minks in the control group during the initial 4 weeks and the entire 8-week period of the study.

## 3.2 Effect of PEF on nutrient apparent digestibility

*Enterococcus faecium* postbiotics had significant effects on the apparent digestibility of CP, EE, and DM ($p < 0.05$, Table 3). Compared to the control, 0.05% PEF significantly improved digestibility of CP ($p < 0.05$) and EE ($p < 0.05$) during the initial 4 weeks, 0.1% PEF increased digestibility of CP ($p < 0.05$) and EE ($p < 0.05$) during the

TABLE 2 Effect of *Enterococcus faecium* postbiotics on growth performance ($n = 15$).

| Item | Groups | | | | *p* |
|---|---|---|---|---|---|
| | Control | 0.05% PEF | 0.10% PEF | 0.15% PEF | |
| *BW* | | | | | |
| Week 0, g | 1283.21 ± 11.89 | 1278.57 ± 12.50 | 1,290 ± 13.40 | 1274.29 ± 10.85 | 0.822 |
| Week 4, g | 1742.14 ± 29.36$^{b}$ | 1800.36 ± 19.62$^{ab}$ | 1846.79 ± 20.47$^{a}$ | 1836.79 ± 25.54$^{a}$ | 0.014 |
| Week 8, g | 2181.07 ± 44.04$^{b}$ | 2272.86 ± 39.15$^{ab}$ | 2366.43 ± 31.03$^{a}$ | 2288.00 ± 36.19$^{ab}$ | 0.012 |
| *ADG, g* | | | | | |
| 0–4 week | 16.39 ± 0.95$^{b}$ | 18.64 ± 0.66$^{ab}$ | 19.89 ± 0.73$^{a}$ | 20.09 ± 0.94$^{a}$ | 0.010 |
| 5–8 week | 15.68 ± 0.98 | 16.88 ± 1.23 | 18.56 ± 0.87 | 16.11 ± 0.78 | 0.183 |
| 0–8 week | 16.03 ± 0.75$^{b}$ | 17.76 ± 0.80$^{ab}$ | 19.22 ± 0.59$^{a}$ | 18.10 ± 0.62$^{ab}$ | 0.019 |
| *ADFI, g* | | | | | |
| 0–4 week | 268.35 ± 3.28 | 258.64 ± 4.24 | 259.68 ± 3.64 | 263.42 ± 3.96 | 0.272 |
| 5–8 week | 302.09 ± 6.16 | 281.86 ± 6.65 | 279.82 ± 8.14 | 287.23 ± 4.8 | 0.082 |
| 0–8 week | 285.23 ± 3.95 | 270.25 ± 3.97 | 269.75 ± 5.37 | 275.33 ± 3.79 | 0.051 |
| *F/G* | | | | | |
| 0–4 week | 17.16 ± 1.11$^{a}$ | 14.11 ± 0.55$^{b}$ | 13.23 ± 0.38$^{b}$ | 13.46 ± 0.60$^{b}$ | 0.001 |
| 5–8 week | 20.34 ± 1.39 | 18.23 ± 1.74 | 15.41 ± 0.67 | 18.26 ± 0.79 | 0.054 |
| 0–8 week | 18.34 ± 0.95$^{a}$ | 15.59 ± 0.68$^{b}$ | 14.14 ± 0.34$^{b}$ | 15.38 ± 0.43$^{b}$ | <0.001 |

$^{a,b,c}$Means in the same row with different superscripts differ significantly ($p < 0.05$).

TABLE 3 Effects of *Enterococcus faecium* postbiotics on nutrient apparent digestibility ($n = 6$).

| Item | Groups | | | | *p* |
|---|---|---|---|---|---|
| | Control | 0.05% PEF | 0.10% PEF | 0.15% PEF | |
| *0–4 weeks* | | | | | |
| DM, % | 74.22 ± 0.79 | 76.02 ± 0.90 | 75.70 ± 1.18 | 74.02 ± 1.12 | 0.416 |
| CP, % | 86.91 ± 0.59$^{b}$ | 88.62 ± 0.38$^{a}$ | 89.24 ± 0.39$^{a}$ | 88.11 ± 0.55$^{ab}$ | 0.024 |
| EE, % | 91.18 ± 1.29$^{b}$ | 95.06 ± 0.33$^{a}$ | 94.95 ± 0.40$^{a}$ | 93.48 ± 0.88$^{ab}$ | 0.014 |
| Ash, % | 29.62 ± 3.14 | 35.45 ± 4.17 | 37.32 ± 4.33 | 29.63 ± 3.37 | 0.376 |
| *5–8 weeks* | | | | | |
| DM, % | 74.72 ± 0.64$^{c}$ | 75.34 ± 0.97$^{bc}$ | 77.34 ± 0.28$^{ab}$ | 77.93 ± 0.67$^{a}$ | 0.012 |
| CP, % | 85.99 ± 0.19$^{b}$ | 86.92 ± 0.61$^{ab}$ | 88.71 ± 0.65$^{a}$ | 88.43 ± 0.94$^{a}$ | 0.030 |
| EE, % | 96.55 ± 0.33 | 97.07 ± 0.60 | 97.13 ± 0.40 | 97.36 ± 0.32 | 0.601 |
| Ash, % | 19.26 ± 1.98 | 21.16 ± 3.19 | 28.76 ± 2.56 | 27.62 ± 2.90 | 0.060 |

DM, dry matter; CP, crude protein; EE, ether extract. $^{a,b,c}$Means in the same row with different superscripts differ significantly ($p < 0.05$).

TABLE 4 Effects of *Enterococcus faecium* postbiotics on digestive enzyme activity ($n = 8$).

| Item | Groups | | | | *p* |
|---|---|---|---|---|---|
| | Control | 0.05% PEF | 0.10% PEF | 0.15% PEF | |
| Trypsin, U/mgprot | 270.16 ± 34.26$^{b}$ | 359.56 ± 26.34$^{ab}$ | 403.36 ± 41.75$^{a}$ | 449.60 ± 38.86$^{a}$ | 0.014 |
| Lipase, U/gprot | 39.35 ± 6.74 | 38.82 ± 6.67 | 43.38 ± 8.55 | 39.00 ± 6.37 | 0.963 |
| Alpha-amylase, U/mgprot | 2.02 ± 0.10 | 1.96 ± 0.12 | 2.31 ± 0.17 | 2.10 ± 0.09 | 0.239 |

$^{a,b,c}$Means in the same row with different superscripts differ significantly ($p < 0.05$).

TABLE 5 Effects of *Enterococcus faecium* postbiotics on intestinal morphology ($n = 8$).

| Item | Groups | | | | *p* |
|---|---|---|---|---|---|
| | Control | 0.05% PEF | 0.10% PEF | 0.15% PEF | |
| *Duodenum* | | | | | |
| Villus height, μm | 1132.26 ± 35.87$^{b}$ | 1334.21 ± 89.41$^{ab}$ | 1477.76 ± 56.81$^{a}$ | 1322.97 ± 115.54$^{ab}$ | 0.042 |
| Crypt depth, μm | 766.25 ± 31.15$^{a}$ | 757.19 ± 11.98$^{a}$ | 682.68 ± 19.33$^{b}$ | 653.54 ± 25.88$^{b}$ | 0.004 |
| V:C ratio | 1.49 ± 0.07$^{b}$ | 1.77 ± 0.13$^{ab}$ | 2.18 ± 0.12$^{a}$ | 2.06 ± 0.21$^{a}$ | 0.008 |
| *Jejunum* | | | | | |
| Villus height, μm | 1124.78 ± 34.84$^{b}$ | 1324.69 ± 46.75$^{a}$ | 1383.37 ± 43.73$^{a}$ | 1368.31 ± 43.77$^{a}$ | 0.001 |
| Crypt depth, μm | 704.84 ± 35.04 | 690.65 ± 14.18 | 716.47 ± 19.90 | 704.09 ± 22.65 | 0.902 |
| V:C ratio | 1.62 ± 0.10$^{b}$ | 1.92 ± 0.07$^{a}$ | 1.94 ± 0.09$^{a}$ | 1.95 ± 0.07$^{a}$ | 0.024 |

$^{a,b,c}$Means in the same row with different superscripts differ significantly ($p < 0.05$).

first 4 weeks as well as increased digestibility of CP ($p < 0.05$) during the final 4 weeks, and 0.15% PEF increased digestibility of CP ($p < 0.05$) and DM ($p < 0.05$) during the final 4 weeks. In addition, the 0.15% PEF group had greater digestibility of DM ($p < 0.05$) than the 0.05% PEF group during the final 4 weeks.

## 3.3 Effect of PEF on digestive enzyme activities

*Enterococcus faecium* postbiotics had significant effects on trypsin activity ($p < 0.05$, Table 4). Compared to the control, both 0.1 and 0.15% PEF significantly increased trypsin activity ($p < 0.05$).

## 3.4 Effect of PEF on intestinal morphology

*Enterococcus faecium* postbiotics had significant effects on intestinal morphology indicators ($p < 0.05$; Table 5; Figure 1). Compared to the control, 0.1% PEF increased the villus height and V/C in both the duodenum and jejunum ($p < 0.05$) and decreased the crypt depth ($p < 0.05$) in the duodenum, 0.15% PEF increased the villus height of jejunum and the V/C in both the duodenum and jejunum ($p < 0.05$) and similarly decreased the crypt depth in the duodenum ($p < 0.05$), and 0.05% PEF increased the villus height and the V/C in the jejunum ($p < 0.05$). In addition, the 0.1 and 0.15% PEF minks had less crypt depth of duodenum than the minks in the 0.05% PEF group ($p < 0.05$).

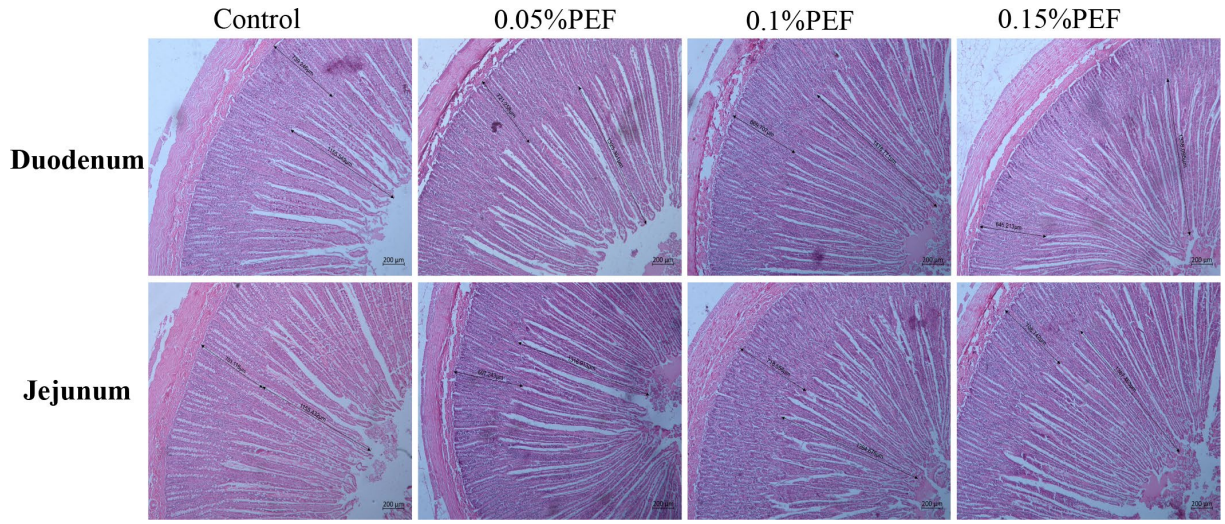


FIGURE 1
Effect of *Enterococcus faecium* postbiotics on duodenum and jejunum tissue sections of growing male minks ($n = 8$). Pictures were observed at 50 × magnification. The villus height was measured from the tip of the villus to the villus–crypt junction. The crypt depth was measured from the base of the crypt to villus–crypt junction.

TABLE 6 Effects of *Enterococcus faecium* postbiotics on jejunum mucosal immunity ($n = 6$).

| Item | Groups | | | | *p* |
|---|---|---|---|---|---|
| | Control | 0.05% PEF | 0.10% PEF | 0.15% PEF | |
| IL-2, pg/ml | $332.49 \pm 10.50^{a}$ | $278.84 \pm 6.24^{b}$ | $242.57 \pm 7.40^{c}$ | $270.45 \pm 8.83^{b}$ | <0.001 |
| IL-6, pg/ml | $31.38 \pm 1.87$ | $31.17 \pm 2.55$ | $29.17 \pm 1.79$ | $28.61 \pm 1.99$ | 0.717 |
| IL-8, pg/ml | $115.36 \pm 1.72^{a}$ | $108.87 \pm 1.03^{ab}$ | $104.02 \pm 3.97^{b}$ | $112.66 \pm 1.84^{a}$ | 0.019 |
| SIgA, pg/ml | $2439.30 \pm 36.55^{b}$ | $2716.97 \pm 109.07^{ab}$ | $2848.48 \pm 122.37^{a}$ | $2420.78 \pm 95.75^{b}$ | 0.015 |
| IL-10, pg/ml | $83.14 \pm 2.79^{ab}$ | $70.07 \pm 3.99^{b}$ | $93.51 \pm 5.36^{a}$ | $82.61 \pm 5.65^{ab}$ | 0.026 |
| IL-1β, pg/ml | $326.83 \pm 11.94$ | $288.61 \pm 14.31$ | $346.60 \pm 26.73$ | $297.56 \pm 13.04$ | 0.107 |
| IFN-γ, pg/ml | $1251.79 \pm 120.67$ | $1055.60 \pm 69.36$ | $1166.08 \pm 111.35$ | $1099.56 \pm 156.53$ | 0.674 |
| TNF-α, pg/ml | $774.09 \pm 15.28^{a}$ | $684.02 \pm 23.28^{b}$ | $693.13 \pm 14.40^{b}$ | $730.32 \pm 16.17^{ab}$ | 0.009 |

[a,b,c]Means in the same row with different superscripts differ significantly ($p < 0.05$).

## 3.5 Effect of PEF on jejunum mucosal immunity indexes

*Enterococcus faecium* postbiotics had significant effects on the levels of SIgA, IL-2, IL-8, IL-10, and TNF-α in the jejunum mucosa ($p < 0.05$, Table 6). Compared to the control, 0.05% PEF decreased IL-2 ($p < 0.05$) and TNF-α ($p < 0.05$) levels, 0.1% PEF increased SIgA levels ($p < 0.05$) and decreased IL-2 ($p < 0.05$), IL-8 ($p < 0.05$), and TNF-α levels ($p < 0.05$), and 0.15% PEF decreased IL-2 levels ($p < 0.05$). Compared to the 0.1% PEF minks, the 0.05% PEF minks had less IL-10 levels ($p < 0.05$), and the 0.15% PEF minks had greater IL-8 levels ($p < 0.05$).

## 3.6 Effect of PEF on intestinal flora

The 16S rRNA sequence was assigned as an OTU with at least 97% sequence similarity. As shown in Figure 2, the end of the curve tends to be flat, indicating that the amount of sequencing data is reasonable, and all samples have sufficient sequencing depth. There were no differences among the four groups in the ACE, Chao, Shannon, Simpson, and Sobs indexes ($p > 0.05$, Figure 3).

At the phylum level, Firmicutes, Proteobacteria, and unclassified_k__norank_d__Bacteria were consistently the most abundant phyla in the four groups, which together constituted more than 96.00% of the gut microbiota (Figure 4A). At the genus level, the data obtained confirmed that *Mycoplasma*, unclassified_k__norank_d__Bacteria, *Lactococcus*, *Sphingobium*, and *Acinetobacter* were the top five dominant genera in the control group and the 0.15% PEF group (Figure 4B). *Paeniclostridium*, unclassified_k__norank_d__Bacteria, *Candidatus_Arthromitus*, *Sphingobium*, and *Acinetobacter* were the top five dominant genera in the 0.05% PEF group. *Mycoplasma*, unclassified unclassified_k__norank_d__Bacteria, *Candidatus_Arthromitus*, *Acinetobacter*, and *Sphingobium* were the top five dominant genera in the 0.1% PEF group. Further analysis of bacterial taxa among the groups indicated that the control group had a significantly higher abundance of *Serratia* than the other groups ($p < 0.05$, Figure 4C). In addition, the 0.15% PEF group displayed the highest richness of *Fusobacterium* than other groups ($p < 0.05$).

## 3.7 Correlation analysis of gut microbiota and immunity

The Spearman correlation heatmap results showed that *Acinetobacter* had negative correlations with IL-1β, IL-10, TNF-α, and IFN-γ ($p < 0.05$, Figure 5). *Sphingobium* had a negative correlation with IL-1β ($p < 0.05$). *Sphingomonas* had negative correlations with IL-1β and IL-10 ($p < 0.05$). *Clostridium_sensu_stricto_1* had a negative correlation with SIgA ($p < 0.05$). *Staphylococcus* correlated positively with IL-2 ($p < 0.05$). *Lactococcus* correlated positively with TNF-α and negatively with SIgA ($p < 0.05$).

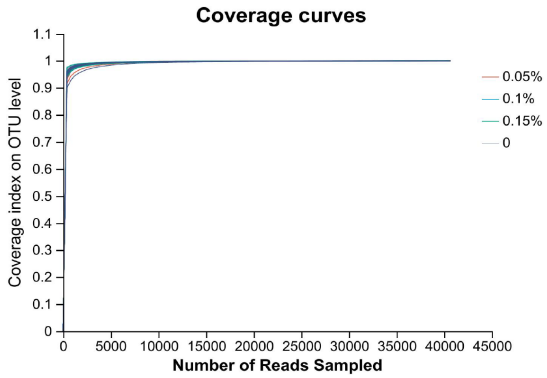


FIGURE 2
Assessment of coverage index for OUT of gut microbiota across four groups ($n = 8$).

## 4 Discussion

The objective of this study was to investigate whether postbiotics derived from *E. faecium* could have potential probiotic effects on growing minks. This study demonstrated that *E. faecium* postbiotics improved the growth performance of male minks. The results were consistent with previous studies of *E. faecium* on piglets (24, 27) and broilers (28). In the current study, the increased ADG was associated with improvement of F/G, indicating that the minks in the *E. faecium* postbiotics groups were efficient in utilizing dietary nutrients for growth. This could be due to the *E. faecium* postbiotics containing many functional compounds such as short-chain fatty acids (SCFA), microbial fractions, functional proteins, secreted polysaccharides, extracellular polysaccharides (EPSs), cell lysates, and teichoic acid (29), which could improve immune function (30), inhibit pathogenic bacteria (31), promote the development of intestinal villi (32), enhance the activities of intestinal digestive enzymes (33), and improve the efficiency of nutrient utilization (24). Consequently, the growth performance of the animals was improved. The study findings confirmed that postbiotics derived from *E. faecium* at 0.1 and 0.15% were effective in enhancing both the ADG and feed efficiency of minks. In contrast, 0.05% *E. faecium* postbiotics improved feed efficiency without effect on ADG, thereby

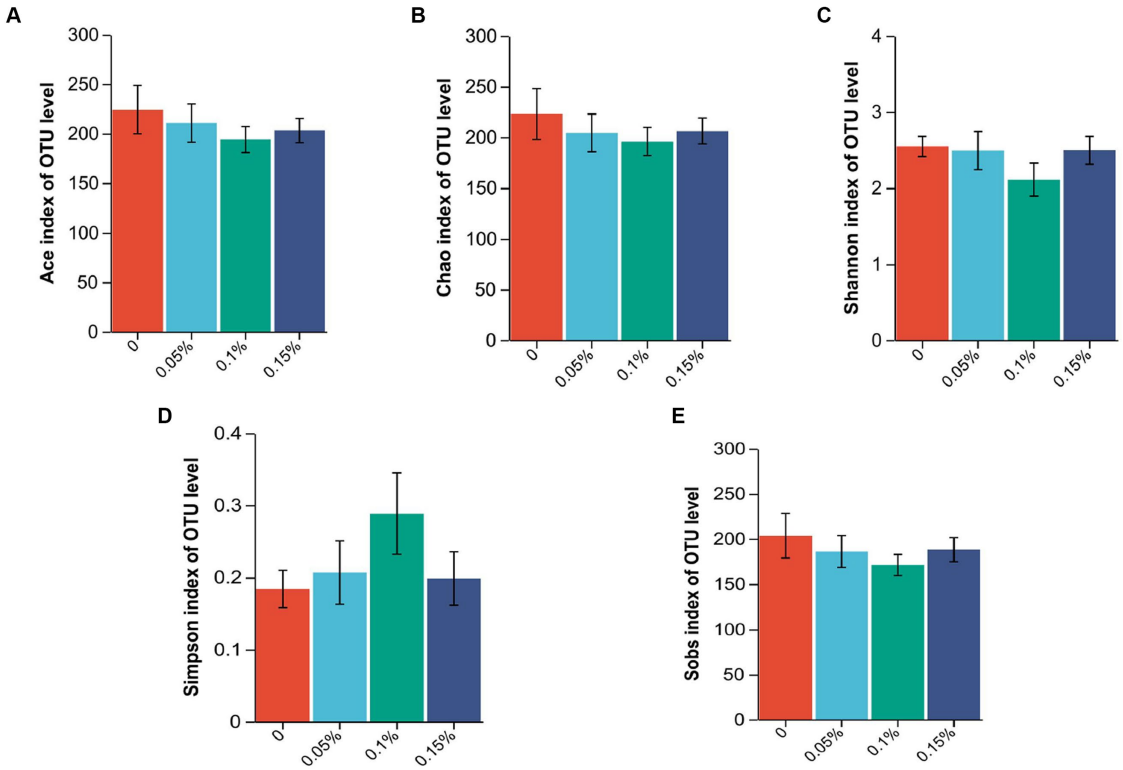


FIGURE 3
Effect of *Enterococcus faecium* postbiotics on alpha diversity indices of the growing male minks in different groups ($n = 8$). **(A)** Ace index, **(B)** Chao index, **(C)** Shannon index, **(D)** Simpson index, and **(E)** Sobs index.

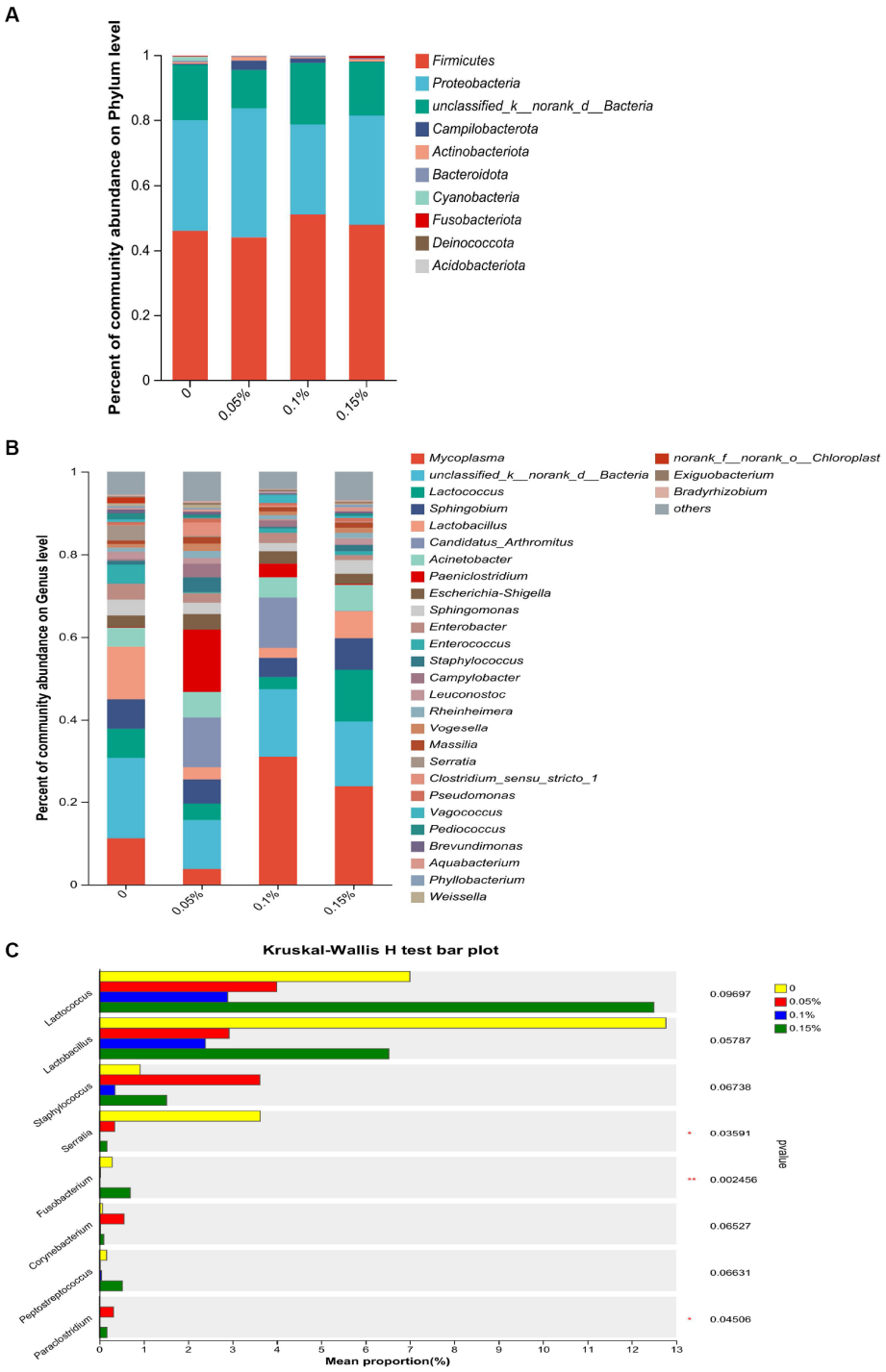


FIGURE 4
Effect of *Enterococcus faecium* postbiotics on gut microbiota composition of growing male minks. **(A)** Distribution of bacterial community structure at the phylum level ($n = 8$). **(B)** Distribution of bacterial community structure at the genus level ($n = 8$). **(C)** The significance of differences among the four groups of the same species (*represents $p < 0.05$, and ** represents $p < 0.01$). The result was statistically analyzed through non-parametric Kruskal–Wallis tests ($n = 8$).

demonstrating a dose-dependent effect of the postbiotics. These results suggest that a higher dosage of postbiotic supplementation is necessary to achieve improvements in ADG. However, these improvements were only evident in the initial 4 weeks. The findings indicate that *E. faecium* postbiotics may have short-term effects on growth performance.

In the current study, *E. faecium* postbiotics increased the apparent digestibility of CP, EE, and DM. The results were consistent with previous studies on pigs, which showed that *E. faecium* improved nutrient digestibility (34, 35). Chen et al. (36) also found that *E. faecium* could improve the digestibility of DM in pigs. However, it is interesting to note that 0.05 and 0.15%

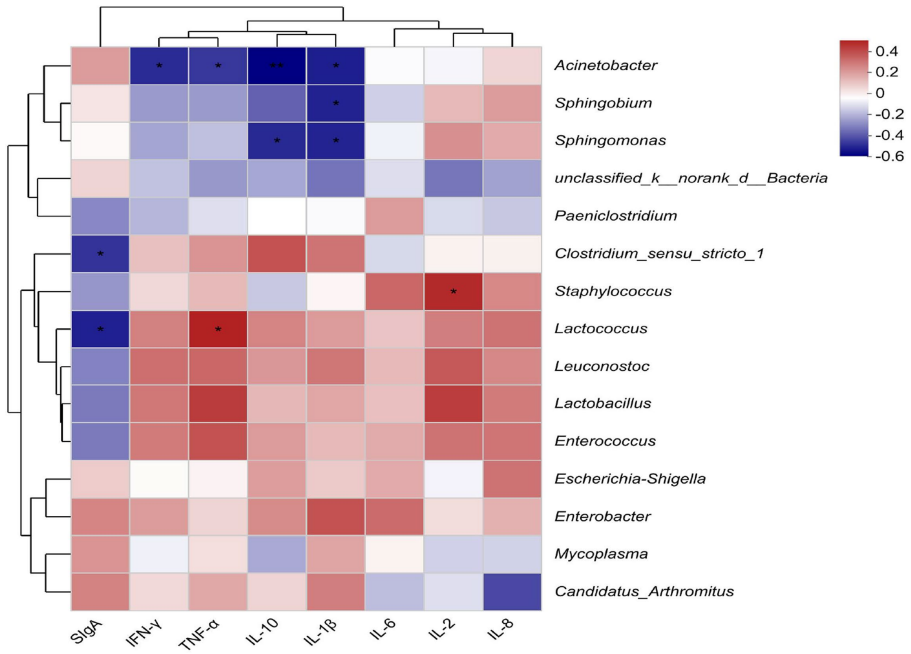


FIGURE 5
Heatmap shows the correlation between intestinal flora (genus level) and intestinal immune indicators ($n = 8$). The X-axis and Y-axis are intestinal immune indicators and species, respectively, and the correlation R-values and $p$-values are obtained through calculation. R-values are displayed in different colors in the figure. If the $p < 0.05$, they are marked with *. The legend on the right is the color range of different $R$-values; the left and upper sides present the species and immune indicator cluster trees; *represents $p < 0.05$, and **represents $p < 0.01$.

*E. faecium* postbiotics only improved the apparent digestibility of CP in minks during the initial and last 4 weeks of the study, respectively. In contrast, 0.1% *E. faecium* postbiotics enhanced the apparent digestibility of CP throughout the study period. This suggests that 0.1% *E. faecium* postbiotics are the optimal dosage for improving the apparent digestibility of CP in growing minks. Omar et al. (37) suggested that the digestive enzyme activities contributed to feed utilization associated with the growth performance of animals. This may be due to the enhancement of digestive enzyme activity. Digestive enzymes break down nutrients into smaller molecules, facilitating their absorption by the animal (38). Lipases hydrolyze triglycerides into glycerol and long-chain fatty acids (39), amylase breaks down starches into monosaccharides such as glucose, and protease degrades proteins into peptides and amino acids (40). As a carnivore, the mink has a high capacity for fat digestion but a limited capacity for carbohydrate digestion due to the low activity of α-amylase (41). Furthermore, the mink has a higher protein requirement than other domestic animals (42). The increased activity of trypsin likely facilitated protein digestibility in this study. The results were consistent with the findings of previous research on fish (43) and broilers (44, 45), which showed that dietary supplementation with probiotics could increase digestive enzyme activity. It is probable that short-chain fatty acids (SCFAs) present in *E. faecium* postbiotics help maintain a healthy intestinal environment conducive to the optimal functioning of digestive enzymes. Consequently, this enhancement in nutrient digestibility improves the growth performance of the animal (46).

Furthermore, the study revealed that 0.1% *E. faecium* postbiotics increased the villus height and the V/C in both the duodenum and jejunum of minks and decreased the crypt depth in the duodenum. Several previous studies have reported that *E. faecium* probiotic or heat-killed *E. faecium* significantly increased the villus height (19, 47) and V/C (24) and decreased the crypt depth (48). The measurements of the villus height and crypt depth are indicative of gut health and function (49). To a certain extent, increases in the villus height and reductions in the crypt depth enhance digestibility and absorptivity (50). The V/C indicates the integrity of the intestinal mucosa and is associated with digestion and absorption capacity (51). These findings further elucidate that *E. faecium* postbiotics contribute to the promotion of intestinal development, thereby improving the digestibility of nutrients in minks.

In this study, 0.1% *E. faecium* postbiotics was observed to reduce IL-8, IL-2, and TNF-α levels and increase sigma levels in jejunum mucosa. However, 0.05 and 0.15% *E. faecium* postbiotics had no significant effect on the levels of IL-8 and sigma. The findings suggest that 0.1% *E. faecium* postbiotics are more effective in modulating intestinal immunity compared to the 0.05 and 0.15% supplementation. The intestinal mucosal immune system comprises lymph nodes, lamina propria, and epithelial cells, which constitute a protective barrier for maintaining intestinal integrity (52). M cells secrete SIgA through the polymeric immunoglobulin receptor in the crypts, effectively defending against the invasion of pathogens and commensal microorganisms (53, 54). As the predominant immunoglobulin in the intestine, Shiga provides immune protection to prevent the penetration

of microorganisms and mucosal antigens into the mucosal barrier through immune exclusion (55). The experimental results indicated that the SIgA levels initially increased and subsequently declined with the increasing supplementation of *E. faecium* postbiotics. This suggests that *E. faecium* postbiotics may stimulate polymeric immunoglobulin receptor expression by activating pattern recognition receptors on intestinal epithelial and immune cells and increasing the concentration of SIgA in the intestinal lumen (53). While postbiotics can stimulate the immune system of the host and enhance SIgA production within an optimal dosage range, excessively high supplementation might trigger an immune suppressive or resistance, potentially resulting in a reduction of SIgA levels (56).

The intestinal epithelium can generate cytokines including IL-2, IL-8, and TNF-α, which are closely involved in triggering the inflammatory response (57). Maintaining the balance between pro-inflammatory and anti-inflammatory cytokines is essential for regulating intestinal inflammation (58). A previous study on piglets confirmed that supplementation with *E. faecium* reduced the relative expression of the IL-8 gene and the level of TNF-α in the jejunum mucosa and increased the relative expression of the IL-10 and TGF-β genes in the ileum mucosa (59). Similar results in macrophage have been reported, indicating that both live and heat-killed *E. faecium* promote IL-10 secretion and inhibit TNF-α release, respectively (60). In this study, the results indicated that *E. faecium* postbiotics could regulate immunity and inflammatory responses. A previous study confirmed that postbiotics derived from *E. faecium* SF68 could reversibly inhibit the activation of the NF-κB and JNK signaling pathway in intestinal epithelial cells and counteract the effects of bacterial and other toll-like receptors (TLRs) (61). Therefore, it is suggested that the *E. faecium* postbiotics likely regulate the immune functions of male minks by inhibiting the activation of the NF-κB and JNK signaling pathways.

The gut microbiota is associated with the metabolism, immunity, digestibility, and health of the host (62). Establishing and maintaining beneficial interactions between the host and microbiota is important to maintain host health (63). However, the results of alpha diversity in the current study did not show any effect of *E. faecium* postbiotics on the enrichment and diversity of the gut microbiota. In contrast, a previous study on piglets demonstrated that probiotic *E. faecium* increased the Sobs, Chao, ACE, and Shannon indexes and decreased the Simpson index from days 1 to 14 (20). This may be due to colonization of viable *E. faecium* on the intestinal mucosa, which contributed to the enhancement of community richness (64). In agreement with previous studies on mink, Firmicutes and Proteobacteria were identified as the most dominant phyla on the rectal mucosa in male minks, consistent with observations in the colon (65) and feces (66) of mink. In fact, Firmicutes and Proteobacteria are widely found in the gastrointestinal tract of carnivores such as otters and raccoon dogs (67). At the genus level, we observed changes in the abundance of flora. The relative abundance of *Serratia* was reduced in all PEF groups, and *Fusobacterium* showed a decrease in 0.05 and 0.1% PEF groups, respectively. *Serratia marcescens*, a member of the *Serratia* (68), is an opportunistic pathogen related to respiratory, urinary, and digestive tract infections (69). *Fusobacterium* is a gram-negative anaerobic bacterium that is typically found as part of the normal flora in the oral cavity and gastrointestinal tract (70). Several members of the *Fusobacterium* genus are opportunistic pathogens that can cause bacteremia and acute infections (71). These results illustrate that *E. faecium* postbiotics may prevent harmful bacteria from adhering to the intestinal mucosa and reduce the occurrence of inflammation.

The interaction between the intestinal microbial flora and immunity has been extensively described in many published reports (22, 72, 73). Our study specifically investigated the interaction between specific intestinal microbiota genera and gut immune indicators. We discovered a positive association between the genus *Lactococcus* and the inflammatory marker TNF-α, and an inverse relationship with SIgA. These findings suggest that *Lactococcus* may not contribute positively to mink health. The intestinal microbiome can protect the integrity of the mucosal barrier by acting on the host immune system (72), thus inhibiting the occurrence of intestinal inflammation. In addition, several previous studies suggested that alterations in microbiota may lead to immune-mediated diseases because microbial communities affect barrier surfaces as well as remote organs, including the lungs and skin (74, 75).

## 5 Conclusion

The study findings confirm that postbiotics derived from *E. faecium* exhibit probiotic effects on growing male minks. In particular, dietary supplementation with 0.1% *E. faecium* postbiotics improves growth performance (ADG and F/G during the initial 4 weeks and the entire 8 weeks of the study), the apparent digestibility of nutrients (CP, EE, and DM), and impacts immune status and intestinal morphology in the minks. Therefore, it can be concluded that supplementation with 0.1% provides greater benefits than supplementation with 0.05 and 0.15%.

## Data availability statement

The data presented in the study are deposited in the National Center for Biotechnology Information (NCBI) repository, accession number PP886227.

## Ethics statement

The animal study was approved by the Animal Care and Use Committee of Animal Science and Technology at Qingdao Agricultural University. The study was conducted in accordance with the local legislation and institutional requirements.

## Author contributions

LC: Data curation, Writing – original draft, Writing – review & editing. FS: Investigation, Writing – original draft. QR: Formal analysis, Investigation, Writing – review & editing. ZJ: Formal analysis, Writing – review & editing. JC: Conceptualization, Methodology, Writing – review & editing. YL: Conceptualization, Methodology,

Writing – review & editing. LW: Funding acquisition, Supervision, Writing – review & editing.

## Funding

The author(s) declare financial support was received for the research, authorship, and/or publication of this article. This research was funded by the Shandong Province Agricultural Innovation Team (SDAIT-21).

## Acknowledgments

The authors thank the Shandong Province Agricultural Innovation Team (SDAIT-21) for supporting this study.

## Conflict of interest

The authors declare that the research was conducted in the absence of any commercial or financial relationships that could be construed as a potential conflict of interest.

## Publisher's note

All claims expressed in this article are solely those of the authors and do not necessarily represent those of their affiliated organizations, or those of the publisher, the editors and the reviewers. Any product that may be evaluated in this article, or claim that may be made by its manufacturer, is not guaranteed or endorsed by the publisher.

## References

1. Hänninen S, Mononen J, Harjunpää S, Pyykönen T, Sepponen J, Ahola L. Effects of family housing on some behavioural and physiological parameters of juvenile farmed mink (*Mustela vison*). *Appl Anim Behav Sci*. (2008) 109:384–95. doi: 10.1016/j.applanim.2007.03.002

2. Birch JM, Ullman K, Struve T, Agger JF, Hammer AS, Leijon M, et al. Investigation of the viral and bacterial microbiota in intestinal samples from mink (*Neovison vison*) with pre-weaning diarrhea syndrome using next generation sequencing. *PLoS One*. (2018) 13:e0205890. doi: 10.1371/journal.pone.0205890

3. Bahl MI, Honoré AL, Skønager ST, Honoré OL, Clausen T, Andresen L, et al. The microbiota of farmed mink (*Neovison vison*) follows a successional development and is affected by early life antibiotic exposure. *Sci Rep*. (2020) 10:20434. doi: 10.1038/s41598-020-77417-z

4. Qiao M, Ying G-G, Singer AC, Zhu Y-G. Review of antibiotic resistance in China and its environment. *Environ Int*. (2018) 110:160–72. doi: 10.1016/j.envint.2017.10.016

5. Buonavoglia A, Leone P, Solimando AG, Fasano R, Malerba E, Prete M, et al. Antibiotics or no antibiotics, that is the question: An update on efficient and effective use of antibiotics in dental practice. *Antibiotics*. (2021) 10:550. doi: 10.3390/ANTIBIOTICS10050550

6. Zl L, Yj C, Ql M, Zhang X, Xl W. Progress in the application of *Enterococcus faecium* in animal husbandry. *Front Cell Infect Microbiol*. (2023) 13:1168189. doi: 10.3389/FCIMB.2023.1168189

7. Biricik H, Brav FC, Çetin E, Aydin L, Fantinati P, Cappellozza BI. Effects of supplementing a direct-fed microbial containing *Enterococcus faecium* 669 on performance, health, and metabolic responses of pre-weaning Holstein dairy calves. *J Dairy Sci*. (2023) 106:8684–93. doi: 10.3168/JDS.2023-23581

8. Lan RX, Kim JK, Liu YH, Yun HM, Kim IH. Effects of dietary supplementation with a probiotic (*Enterococcus faecium*) on growth performance, nutrient digestibility, fecal microbiota, and fecal score in weanling pigs. *J Anim Sci*. (2017) 95:80. doi: 10.2527/asasmw.2017.12.169

9. Khalifa A, Ibrahim HIM. *Enterococcus faecium* from chicken feces improves chicken immune response and alleviates Salmonella infections: a pilot study. *J Anim Sci*. (2023) 101:skad016. doi: 10.1093/JAS/SKAD016

10. Olsen MSR, Thøfner I, Sandvang D, Poulsen LL. Research note: the effect of a probiotic *E. faecium* 669 mitigating *Salmonella Enteritidis* colonization of broiler chickens by improved gut integrity. *Poultry Sci*. (2022) 101:102029. doi: 10.1016/J.PSJ.2022.102029

11. Moon BY, Ali MS, Choi JH, Heo YE, Lee YH, Kang HS, et al. Antimicrobial resistance profiles of *Enterococcus faecium* and *Enterococcus faecalis* isolated from healthy dogs and cats in South Korea. *Microorganisms*. (2023) 11:2991. doi: 10.3390/MICROORGANISMS11122991

12. Zelaya C, Arriagada G, Galarce N, Sanchez F, Escobar B, Miranda M, et al. A preliminary report on critical antimicrobial resistance in *Escherichia coli*, *enterococcus faecalis*, and *Enterococcus faecium* strains isolated from healthy dogs in Chile during 2021-2022. *Prev Vet Med*. (2024) 224:106139. doi: 10.1016/J.PREVETMED.2024.106139

13. Derunets AS, Selimzyanova AI, Rykov SV, Kuznetsov AE, Berezina OV. Strategies to enhance stress tolerance in lactic acid bacteria across diverse stress conditions. *World J Microb Biot*. (2024) 40:126. doi: 10.1007/S11274-024-03905-3

14. Salminen S, Collado MC, Endo A, Hill C, Lebeer S, Quigley EMM, et al. The international scientific Association of Probiotics and Prebiotics (ISAPP) consensus statement on the definition and scope of postbiotics. *Nat Rev Gastro Hepat*. (2021) 18:649–67. doi: 10.1038/S41575-021-00440-6

15. Aguilar-Toalá JE, Garcia-Varela R, Garcia HS, Mata-Haro V, González-Córdova AF, Vallejo-Cordoba B, et al. Postbiotics: An evolving term within the functional foods field. *Trends Food Sci Tech*. (2018) 75:105–14. doi: 10.1016/j.tifs.2018.03.009

16. Gao J, Li Y, Wan Y, Hu T, Liu L, Yang S, et al. A novel Postbiotic from *Lactobacillus rhamnosus* GG with a beneficial effect on intestinal barrier function. *Front Microbiol*. (2019) 10:477. doi: 10.3389/fmicb.2019.00477

17. Żółkiewicz J, Marzec A, Ruszczyński M, Feleszko W. Postbiotics—a step beyond pre-and probiotics. *Nutrients*. (2020) 12:2189. doi: 10.3390/nu12082189

18. Heniedy AM, Mahdy DM, Elenien WIA, Mourad S, Kadi RAE. Postbiotics as a health-promoting technique: a review article on scientific and commercial interest. *Process Biochem*. (2024) 144:6–19. doi: 10.1016/J.PROCBIO.2024.05.010

19. Shin S, Yasuhiro I, Kaoruko Y, Shengbin R, Kentaro O, Fumihiro A, et al. Effects of oral administration of heat-killed *Enterococcus faecium* strain NHRD IHARA in post-weaning piglets. *Anim Sci J*. (2014) 85:454–60. doi: 10.1111/asj.12163

20. Hu C, Xing W, Liu X, Zhang X, Li K, Liu J, et al. Effects of dietary supplementation of probiotic *Enterococcus faecium* on growth performance and gut microbiota in weaned piglets. *AMB Express*. (2019) 9:33–12. doi: 10.1186/s13568-019-0755-z

21. Castañeda CD, Dittoe DK, Wamsley KK, McDaniel CD, Blanch A, Sandvang D, et al. Discovering the optimal concentration of an *Enterococcus faecium*–based product to enhance broiler hatchability, live performance, and intestinal morphology. *Poultry Sci*. (2020) 99:6163–72. doi: 10.1016/j.psj.2020.08.002

22. Li Y, Zhen S, Cao L, Sun F, Wang L. Effects of *Lactobacillus plantarum* Postbiotics on growth performance, immune status, and intestinal microflora of growing minks. *Animals*. (2023) 13:2958. doi: 10.3390/ANI13182958

23. Shuai C, Chen D, Yu B, Luo Y, Zheng P, Huang Z, et al. Effect of fermented rapeseed meal on growth performance, nutrient digestibility, and intestinal health in growing pigs. *Anim Nutr*. (2023) 15:420–9. doi: 10.1016/J.ANINU.2023.06.011

24. Xie YH, Zhang CY, Wang LX, Shang QH, Zhang GG, Yang WR. Effects of dietary supplementation of *Enterococcus faecium* on growth performance, intestinal morphology, and selected microbial populations of piglets. *Livest Sci*. (2018) 210:111–7. doi: 10.1016/j.livsci.2018.02.010

25. Nan W, Si H, Yang Q, Shi H, Zhang T, Shi Q, et al. Effect of vitamin a supplementation on growth performance, serum biochemical parameters, intestinal immunity response and gut microbiota in American mink (*Neovison vison*). *Animals*. (2021) 11:1577. doi: 10.3390/ani11061577

26. Xu Y, Yu Y, Shen Y, Li Q, Lan J, Wu Y, et al. Effects of *Bacillus subtilis* and *Bacillus licheniformis* on growth performance, immunity, short chain fatty acid production, antioxidant capacity, and cecal microflora in broilers. *Poultry Sci*. (2021) 100:101358. doi: 10.1016/J.PSJ.2021.101358

27. Giang HH, Viet TQ, Ogle B, Lindberg JE. Effects of different probiotic complexes of lactic acid bacteria on growth performance and gut environment of weaned piglets. *Livest Sci*. (2010) 133:182–4. doi: 10.1016/j.livsci.2010.06.059

28. Suvorov A, Zhao S, Leontieva G, Alekhina G, Yang J, Tsapieva A, et al. Evaluation of the efficacy of *Enterococcus faecium* L3 as a feed probiotic additive in chicken. *Probiotics Antimicro*. (2022) 15:1169–79. doi: 10.1007/S12602-022-09970-0

29. Izuddin WI, Humam AM, Loh TC, Foo HL, Samsudin AA. Dietary Postbiotic *Lactobacillus plantarum* improves serum and ruminal antioxidant activity and upregulates hepatic antioxidant enzymes and ruminal barrier function in post-weaning lambs. *Antioxidants*. (2020) 9:250. doi: 10.3390/antiox9030250

30. Pimentel TC, Cruz AG, Pereira E, Costa WKA, Rocha RS, Pedrosa GTS, et al. Postbiotics: An overview of concepts, inactivation technologies, health effects, and driver trends. *Trends Food Sci Tech.* (2023) 138:199–214. doi: 10.1016/J.TIFS.2023.06.009

31. Teame T, Wang A, Xie M, Zhang Z, Yang Y, Ding Q, et al. Paraprobiotics and Postbiotics of probiotic *lactobacilli*, their positive effects on the host and action mechanisms: a review. *Front Nutr*. (2020) 7:570344. doi: 10.3389/fnut.2020.570344

32. Zhang Y, Wu T, Chen Z, Meng Y, Zhu Z, Wang Q, et al. Dietary supplementation with *Enterococcus faecium* R1 attenuates intestinal and liver injury in piglets challenged by lipopolysaccharide. *Animals*. (2021) 11:1424. doi: 10.3390/ANI11051424

33. Liu J, Cao SC, Liu J, Xie YN, Zhang HF. Effect of probiotics and xylo-oligosaccharide supplementation on nutrient digestibility, intestinal health and noxious gas emission in weanling pigs. *Asian Austral J Anim.* (2018) 31:1660–9. doi: 10.5713/ajas.17.0908

34. Zhang ZF, Lee JM, Kim IH. Effects of *Enterococcus faecium* DSM 7134 on weanling pigs were influenced by dietary energy and crude protein density. *Livest Sci.* (2014) 169:106–11. doi: 10.1016/j.livsci.2014.09.022

35. Xin JL, Sang IL, Kwang YL, Dinh HN, In HK. Effects of a blend of organic acids and medium-chain fatty acids with and without *Enterococcus faecium* on growth performance, nutrient digestibility, blood parameters, and meat quality in finishing pigs. *Can J Anim Sci*. (2018) 98:852–9. doi: 10.1139/cjas-2017-0126

36. Chen YJ, Min BJ, Cho JH, Kwon OS, Son KS, Kim IH, et al. Effects of dietary *Enterococcus faecium* SF68 on growth performance, nutrient digestibility, blood characteristics and Faecal noxious gas content in finishing pigs. *Asian Austral J Anim*. (2006) 19:406–11. doi: 10.5713/ajas.2006.406

37. Omar AE, Al-Khalaifah HS, Ismail TA, Abd El-Aziz RM, El-Mandrawy SAM, Shalaby SI, et al. Performance, serum biochemical and immunological parameters, and digestive enzyme and intestinal barrier-related gene expression of broiler chickens fed fermented fava bean by-products as a substitute for conventional feed. *Front Vet Sci*. (2021) 8:696841. doi: 10.3389/fvets.2021.696841

38. Liu X, Ju Y, Huang L, Liu M, Bo J, Zhou T, et al. Effects of a new fermented soya bean meal on growth performance, serum biochemistry profile, intestinal immune status and digestive enzyme activities in piglets. *J Anim Physiol An N*. (2021) 106:1046–59. doi: 10.1111/JPN.13649

39. Kozan DW, Derrick JT, Ludington WB, Farber SA. From worms to humans: understanding intestinal lipid metabolism via model organisms. *BBA-Mol Cell Biol L*. (2023) 1868:159290. doi: 10.1016/J.BBALIP.2023.159290

40. Ehrmann M, Clausen T. PROTEOLYSIS AS A REGULATORY MECHANISM. *Annu Rev Genet*. (2004) 38:709–24. doi: 10.1146/annurev.genet.38.072902.093416

41. Jensen K, Simpson SJ, Nielsen VH, Hunt J, Raubenheimer D, Mayntz D. Nutrient-specific compensatory feeding in a mammalian carnivore, the mink, *Neovison vison*. *Br J Nutr*. (2014) 112:1226–33. doi: 10.1017/S0007114514001664

42. Jiang Q, Li G, Zhang T, Zhang H, Gao X, Xing X, et al. Effects of dietary protein level on nutrients digestibility and reproductive performance of female mink (*Neovison vison*) during gestation. *Anim Nutr.* (2015) 1:65–9. doi: 10.1016/j.aninu.2015.05.002

43. Sun YZ, Yang HL, Ma RL, Song K, Li JS. Effect of *Lactococcus lactis* and *Enterococcus faecium* on growth performance, digestive enzymes and immune response of grouper *Epinephelus coioides*. *Aquac Nutr*. (2012) 18:281–9. doi: 10.1111/j.1365-2095.2011.00894.x

44. Gong L, Wang B, Mei X, Xu H, Qin Y, Li W, et al. Effects of three probiotic *Bacillus* on growth performance, digestive enzyme activities, antioxidative capacity, serum immunity, and biochemical parameters in broilers. *Anim Sci J*. (2018) 89:1561–71. doi: 10.1111/asj.13089

45. Sun Y, Zhang Y, Liu M, Li J, Lai W, Geng S, et al. Effects of dietary *Bacillus amyloliquefaciens* CECT 5940 supplementation on growth performance, antioxidant status, immunity, and digestive enzyme activity of broilers fed corn-wheat-soybean meal diets. *Poultry Sci.* (2021) 101:101585. doi: 10.1016/J.PSJ.2021.101585

46. Blaak EE, Canfora EE, Theis S, Frost G, Groen AK, Mithieux G, et al. Short chain fatty acids in human gut and metabolic health. *Benef Microbes*. (2020) 11:411–55. doi: 10.3920/bm2020.0057

47. Samli HE, Senkoylu N, Koc F, Kanter M, Agma A. Effects of *Enterococcus faecium* and dried whey on broiler performance, gut histomorphology and intestinal microbiota. *Arch Anim Nutr*. (2007) 61:42–9. doi: 10.1080/17450390601106655

48. Cao GT, Zeng XF, Chen AG, Zhou L, Zhang L, Xiao YP, et al. Effects of a probiotic, *Enterococcus faecium*, on growth performance, intestinal morphology, immune response, and cecal microflora in broiler chickens challenged with *Escherichia coli* K88. *Poultry Sci.* (2013) 92:2949–55. doi: 10.3382/ps.2013-03366

49. Wang JX, Peng KM. Developmental morphology of the small intestine of African ostrich chicks. *Poultry Sci.* (2008) 87:2629–35. doi: 10.3382/ps.2008-00163

50. Sansonetti PJ. War and peace at mucosal surfaces. *Nat Rev Immunol.* (2004) 4:953–64. doi: 10.1038/nri1499

51. Wang J, Liu S, Ma J, Dong X, Long S, Piao X. Growth performance, serum parameters, inflammatory responses, intestinal morphology and microbiota of weaned piglets fed 18% crude protein diets with different ratios of standardized ileal digestible isoleucine to lysine. *Anim Nutr*. (2024) 16:313–25. doi: 10.1016/J.ANINU.2023.11.008

52. Shi N, Li N, Duan X, Niu H. Interaction between the gut microbiome and mucosal immune system. *Military Med Res*. (2017) 4:14. doi: 10.1186/s40779-017-0122-9

53. Kaetzel CS. Cooperativity among secretory IgA, the polymeric immunoglobulin receptor, and the gut microbiota promotes host–microbial mutualism. *Immunol Lett*. (2014) 162:10–21. doi: 10.1016/j.imlet.2014.05.008

54. Lin Z, Yang G, Zhang M, Yang R, Wang Y, Guo P, et al. Dietary supplementation of mixed organic acids improves growth performance, immunity, and antioxidant capacity and maintains the intestinal barrier of Ira rabbits. *Animals*. (2023) 13:3140. doi: 10.3390/ANI13193140

55. Corthésy B. Multi-faceted functions of secretory IgA at mucosal surfaces. *Front Immunol*. (2013) 4:185. doi: 10.3389/fimmu.2013.00185

56. Hezaveh K, Shinde RS, Klötgen A, Halaby MJ, Lamorte S, Ciudad MT, et al. Tryptophan-derived microbial metabolites activate the aryl hydrocarbon receptor in tumor-associated macrophages to suppress anti-tumor immunity. *Immunity*. (2022) 55:324–340.e8. doi: 10.1016/J.IMMUNI.2022.01.006

57. Wu QJ, Zhu DD, Wang DD, Zhang BB, Ren A, Zhang ZB. Effects of dietary supplementation with glutamine on the lymphocyte proliferation and intestinal immune gene expression in broiler chickens infected with *Salmonella Enteritidis*. *Res Vet Sci*. (2021) 139:18–24. doi: 10.1016/J.RVSC.2021.06.018

58. Chen P, Lv H, Liu W, Wang Y, Zhang K, Che C, et al. Effects of *Lactobacillus plantarum* HW1 on growth performance, intestinal immune response, barrier function, and Cecal microflora of broilers with necrotic enteritis. *Animals*. (2023) 13:3810. doi: 10.3390/ANI13243810

59. Cui B, Wang L, Guo Q, Huang Y, Hu S. Effects of *Enterococcus faecium* on expression of intestinal tight junction proteins, cytokine responses and toll-like receptors genes in piglets. *Chin. J. Animal Nutr.* (2022) 34:7616–27. (in chinese). doi: 10.3969/j.issn.1006-267x.2022.12.015

60. Ren Y, Guo Q, Li Y, Xiang M, Huang Y. Effect of live *Enterococcus faecium* and heat-inactivated bacteria on TNF-c/IL-10 balance and mitogen-activated protein kinase signaling in RAW264.7 cells. *Chin. J. Animal Nutr.* (2020) 32:4345–57. doi: 10.3969/j.issn.1006-267x.2020.09.045

61. Ghazisaeedi F, Meens J, Hansche B, Maurischat S, Schwerk P, Goethe R, et al. A virulence factor as a therapeutic: the probiotic *Enterococcus faecium* SF68 arginine deiminase inhibits innate immune signaling pathways. *Gut Microbes*. (2022) 14:2106105. doi: 10.1080/19490976.2022.2106105

62. Gratiela GP, Janie L, Ozan G, Nicolae C, Iuliana I, Luciana O, et al. Effects of the lipid profile, type 2 diabetes and medication on the metabolic syndrome—associated gut microbiome. *Int J Mol Sci*. (2022) 23:7509. doi: 10.3390/IJMS23147509

63. Sommer F, Bäckhed F. The gut microbiota--masters of host development and physiology. *Nat Rev Microbiol*. (2013) 11:227–38. doi: 10.1038/nrmicro2974

64. Li Q, Chen S, Zhu K, Huang X, Huang Y, Shen Z, et al. Collateral sensitivity to pleuromutilins in vancomycin-resistant *Enterococcus faecium*. *Nat Commun*. (2022) 13:1888. doi: 10.1038/S41467-022-29493-0

65. Bahl MI, Hammer AS, Clausen T, Jakobsen A, Skov S, Andresen L. The gastrointestinal tract of farmed mink (*Neovison vison*) maintains a diverse mucosa-associated microbiota following a 3-day fasting period. *Microbiology Open*. (2017) 6:e00434. doi: 10.1002/mbo3.434

66. Compo NR, Gomez DE, Tapscott B, Weese SJ, Turner PV. Fecal bacterial microbiota of Canadian commercial mink (*Neovison vison*): yearly, life stage, and seasonal comparisons. *PLoS One*. (2018) 13:e0207111. doi: 10.1371/journal.pone.0207111

67. An C, Okamoto Y, Xu S, Eo KY, Kimura J, Yamamoto N. Comparison of fecal microbiota of three captive carnivore species inhabiting Korea. *J Vet Med Sci*. (2017) 79:542–6. doi: 10.1292/jvms.16-0472

68. Ludueña LM, Anzuay MS, Angelini JG, McIntosh M, Becker A, Rupp O, et al. Strain Serratia sp. S119: a potential biofertilizer for peanut and maize and a model bacterium to study phosphate solubilization mechanisms. *Appl Soil Ecol*. (2018) 126:107–12. doi: 10.1016/j.apsoil.2017.12.024

69. Deorukhkar AA, Chander R, Ghosh SB, Sainis KB. Identification of a red-pigmented bacterium producing a potent anti-tumor N-alkylated prodigiosin as *Serratia marcescens*. *Res Microbiol*. (2007) 158:399–404. doi: 10.1016/j.resmic.2007.02.010

70. Lee SJ, Baek YJ, Kim JN, Lee KH, Lee EH, Yeom JS, et al. Increasing *Fusobacterium* infections with *Fusobacterium varium*, an emerging pathogen. *PLoS One*. (2022) 17:e0266610. doi: 10.1371/JOURNAL.PONE.0266610

71. Stokowa-Sołtys K, Wojtkowiak K, Jagiełło K. *Fusobacterium nucleatum* – friend or foe? *J Inorg Biochem*. (2021) 224:111586. doi: 10.1016/J.JINORGBIO.2021.111586

72. Hirano T, Nakase H. The multifaceted effects of gut microbiota on the immune system of the intestinal mucosa. *Immuno*. (2021) 1:583–94. doi: 10.3390/IMMUNO1040041

73. Xu X, Duarte ME, Kim SW. Postbiotics effects of *Lactobacillus* fermentate on intestinal health, mucosa-associated microbiota, and growth efficiency of nursery pigs challenged with F18 + *Escherichia coli*. *J Anim Sci*. (2022) 100:skac210. doi: 10.1093/JAS/SKAC210

74. Dehner C, Fine R, Kriegel MA. The microbiome in systemic autoimmune disease: mechanistic insights from recent studies. *Curr Opin Rheumatol*. (2019) 31:201–7. doi: 10.1097/BOR.0000000000000574

75. Ruff WE, Kriegel MA. Autoimmune host–microbiota interactions at barrier sites and beyond. *Trends Mol Med*. (2015) 21:233–44. doi: 10.1016/j.molmed.2015.02.006

frontiers | Frontiers in Genetics

TYPE Original Research
PUBLISHED 12 July 2024
DOI 10.3389/fgene.2024.1370891



OPEN ACCESS

EDITED BY
Izhar Hyder Qazi,
Shaheed Benazir Bhutto University of Veterinary & Animal Sciences, Pakistan

REVIEWED BY
Anna Szczerba-Turek,
University of Warmia and Mazury in Olsztyn, Poland
Chao Xu,
Jilin Agricultural University, China

*CORRESPONDENCE
Younes Miar,
miar@dal.ca

RECEIVED 15 January 2024
ACCEPTED 17 June 2024
PUBLISHED 12 July 2024

CITATION
Hu G, Do DN, Manafiazar G, Kelvin AA, Sargolzaei M, Plastow G, Wang Z, Davoudi P and Miar Y (2024), Identifying selection signatures for immune response and resilience to Aleutian disease in mink using genotype data. *Front. Genet.* 15:1370891. doi: 10.3389/fgene.2024.1370891



# Identifying selection signatures for immune response and resilience to Aleutian disease in mink using genotype data

Guoyu Hu[1], Duy Ngoc Do[1], Ghader Manafiazar[1], Alyson A. Kelvin[2], Mehdi Sargolzaei[3,4], Graham Plastow[5], Zhiquan Wang[5], Pourya Davoudi[1] and Younes Miar[1]*

[1]Department of Animal Science and Aquaculture, Dalhousie University, Truro, Canada, [2]Vaccine and Infectious Disease Organization (VIDO), University of Saskatchewan, Saskatoon, Canada, [3]Department of Pathobiology, University of Guelph, Guelph, Canada, [4]Select Sires Inc., Plain City, OH, United States, [5]Livestock Gentec, Department of Agricultural, Food and Nutritional Science, University of Alberta, Edmonton, Canada

Aleutian disease (AD) brings tremendous financial losses to the mink industry. Selecting AD-resilient mink has been conducted to control AD. Such selections could have altered the patterns of genetic variation responding to selection pressures. This study aimed to identify selection signatures for immune response (IRE) and resilience to AD. A total of 1,411 mink from an AD-positive facility were used. For IRE, 264 animals were categorized according to the combined results of enzyme-linked immunosorbent assay (ELISA) and counterimmunoelectrophoresis (CIEP). For resilience, two grouping methods were used: 1) general resilience performance (GRP, n = 30) was evaluated based on the feed conversion ratio, Kleiber ratio, and pelt quality; and 2) female reproductive performance (FRP, n = 36) was measured based on the number of kits alive 24 h after birth. Detection methods were the pairwise fixation index, nucleotide diversity, and cross-population extended haplotype homozygosity. A total of 619, 569, and 526 SNPs were identified as candidates for IRE, GRP, and FRP, respectively. The annotated genes were involved in immune system process, growth, reproduction, and pigmentation. Two olfactory-related Gene Ontology (GO) terms were significant ($q < 0.05$) for all traits, suggesting the impact of AD on the sense of smell of infected mink. Differences in detected genes and GO terms among different color types for IRE indicated variations in immune response to AD among color types. The mitogen-activated protein kinase (MAPK) signaling pathway was significant ($q < 0.05$) for FRP, suggesting that AD may disrupt MAPK signaling and affect FRP. The findings of this research contribute to our knowledge of the genomic architecture and biological mechanisms underlying AD resilience in mink.

KEYWORDS

**Aleutian disease resilience, American mink, selection signatures, genotypes, immune response**

# 1 Introduction

Aleutian disease (AD) is one of the most severe diseases in mink farming, leading to significant financial losses to the mink industry due to its adverse influences on several economically important traits (Henson et al., 1962; Porter et al., 1982; Farid and Ferns, 2011; Reichert and Kostro, 2014). This disease is caused by the Aleutian mink disease virus (AMDV) and is defined as an immune-complex disease. Specific antibodies produced against AMDV fail to neutralize the virus and instead form complexes with the infectious virus, resulting in damage to the mink's glomerular and arterial systems (Porter et al., 1969; Cho and Ingram, 1973; Porter et al., 1973; Stolze and Kaaden, 1987). Thus, the higher the levels of anti-AMDV antibodies produced, the more severe the infection caused by AMDV (Porter et al., 1972; Kanno et al., 1993; Bloom et al., 1994; Aasted et al., 1998; Bloom et al., 2001). Meanwhile, AMDV infection was also found to cause adverse influences on body weight growth (Porter et al., 1982), feed intake (Elzhov et al., 2016; Jensen et al., 2016), pelt quality (Farid and Ferns, 2011), and female reproductive performance (Henson et al., 1962; Reichert and Kostro, 2014). Thus, the anti-AMDV antibody level, growth, feed efficiency, and female reproductive performance were suggested as AD-resilience indicator traits in previous studies (Hu et al., 2021; Hu et al., 2022). Several methods, including vaccination, medicine, and culling strategy, have been attempted to control AD, but these methods have been largely ineffective. Consequently, mink farmers have resorted to selecting AD-resilient mink based on AD tests and/or AD-resilience indicator traits, such as body size, pelt quality, and reproductive performance, in AD-positive farms. Several mink farms in the Canadian province of Nova Scotia select AD-resilient mink using the iodine agglutination test and assessments of the productive performance (Farid and Ferns, 2017). Similarly, some findings indicated that some AD-positive mink farms in North America and Europe have applied enzyme-linked immunosorbent assay tests (ELISA) to select AD-resilient mink (Knuuttila et al., 2009; Farid and Rupasinghe, 2016; Farid et al., 2018).

Selection could cause changes in the patterns of genetic variation among selected loci and linked neutral loci (Kreitman, 2000; Qanbari and Simianer, 2014; Ma et al., 2015). These patterns are termed selection signatures, and they can be used to identify loci subject to the selection (Kreitman, 2000; Qanbari and Simianer, 2014; Ma et al., 2015). Therefore, identifying the signatures would be helpful in detecting genes and biological processes related to AD resilience. Characterizing the genomic regions associated with mink response to AD could aid in the development of breeding programs focusing on improving AD-resilience in mink farms. Several statistical methods have been proposed for detecting selection signatures in livestock. The pairwise fixation index (Fst) (Weir and Cockerham, 1984), nucleotide diversity ($\theta\pi$) (Nei and Li, 1979), and cross-population extended haplotype homozygosity (XP-EHH) (Sabeti et al., 2007) are the three methods commonly used to detect selection signatures, where Fst and $\theta\pi$ are based on the genetic diversity and genetic differentiation, and XP-EHH is based on the frequency of extended haplotypes between two subpopulations.

Advancements in next-generation sequencing (NGS) technologies, high-density single-nucleotide polymorphism (SNP) arrays, and bioinformatics tools have now significantly improved the detection of selection signatures in livestock species (Bertolini et al., 2018). For example, studies using selection signatures have identified several genes associated with disease resistance/susceptibility in cattle (Li et al., 2020; Saravanan et al., 2021). Xu et al. (2020) conducted a signature of selection study and detected several genes related to the susceptibility of swine to respiratory disease. For AD in American mink, Karimi et al. (2021) detected 99 genomic regions associated with the response to AMDV infection using genotyping by sequencing (GBS) data and five phenotypes (the anti-AMDV antibody titer, mortality, AD symptoms in the kidneys, and virus clearance at two different times) from 225 experimental black American mink that were inoculated with AMDV. These regions encompassed 63 genes involved in immune response, liver development, and reproduction (Karimi et al., 2021).

The ineffectiveness of vaccination, medication, and culling strategies in controlling AD has compelled farmers to select AD-resilient mink (Knuuttila et al., 2009; Farid and Rupasinghe, 2016; Farid and Ferns, 2017; Farid et al., 2018). However, the absence of a comprehensive understanding of the genetic/genomic architecture of AD resilience hinders breeders from incorporating this innovative trait into their breeding programs. In previous studies (Hu et al., 2021; Hu et al., 2022), the genetic and phenotypic parameters for various AD tests and other AD-resilient or economically important traits in mink, including reproductive performance, growth, feed intake, and pelt quality, were elucidated. The findings delineated the heritabilities of AD tests and other AD-resilient traits and genetic relationships among them. The outcomes also emphasized the antigen-based enzyme-linked immunosorbent assay test (ELISA-G) as the most reliable and practical indicator trait for selecting AD-resilient mink among all AD tests (Hu et al., 2021; Hu et al., 2022). The population genomic study conducted by Hu et al. (2023) investigated the genetic structures of farmed mink in Canada with diverse color types using the genotypes. The findings updated the linkage disequilibrium patterns and the effective population size of studied populations and revealed genetic distance, genetic diversity, and the admixture pattern of studied populations. The population genomic information from the study provided the essential information to implement the SNP panel in genomic studies of American mink. However, the signature of selection study focusing on the response of mink to AD had not been conducted using genotype data in conjunction with AD-resilience indicator traits (e.g., growth, feed efficiency, pelt quality, and reproduction) for mink reared in AD-positive commercial farms. It has been reported that mink with darker color types seem to be more resilient to AMDV than lighter color types (Ellis, 1996). A signature of the selection study is a potential approach to study the performances of different color types of mink against AMDV infection. Therefore, the objectives of this study were to use genotype data and different color types of American mink to 1) detect the selection signatures associated with immune response, general resilience, and female reproductive performance resilience to AD; 2) identify the genes related to immune response, general resilience, and female reproductive performance resilience to AD; and 3) investigate whether mink of different color types exhibit distinct respond to AD and explore potential differences in AD resilience mechanisms among color variations.

# 2 Materials and methods

This study was approved by the Dalhousie University Animal Care and Use Committee (certification#: 2018-009 and 2019-012). All the mink were farmed following the Code of Practice for the Care and Handling of Farmed Mink guidelines from the Canada Mink Breeders Association (Turner P et al., 2013). The study was carried out in compliance with the ARRIVE 2.0 guidelines (Percie du Sert et al., 2020).

## 2.1 Animals and sampling

All the individuals (n = 1,411) studied in this research were from the Canadian Center for Fur Animal Research (CCFAR) at Dalhousie University, Faculty of Agriculture (Truro, Nova Scotia, Canada), from 2013 to 2021. In 2013, an outbreak of AD occurred at CCFAR, resulting in most of the mink being dead or culled in the barn. The exact source of the outbreak was not determined definitively, but it was suspected that AMDV-contaminated feed and contact with wild animals carrying AMDV were the most likely causes. Thus, within 3 years of the disease outbreak, approximately 150 mink (120 dam and 30 sires) from six AD-positive farms in Nova Scotia (Canada), which were believed to be resilient to AD and have been phenotypically selected for AD-resilient mink for many years, were introduced and used as breeders at CCFAR. AD was first identified in the province of Nova Scotia in Canada in 1941 (Agriculture_and_Marketing_of_Nova_Scotia_Government, 1998), and many mink farms in the province started selecting AD-resilient mink based on specific AD-resilient traits (Farid and Ferns, 2017). The studied mink included five different color types: black (n = 177), demi (n = 542), mahogany (n = 527), pastel (n = 152), and stardust (n = 13). The color type was identified by experienced technicians at CCFAR at weaning.

## 2.2 Aleutian disease test

Counterimmunoelectrophoresis (CIEP) and antigen-based enzyme-linked immunosorbent assay tests (ELISA-G) were used to measure the immune response of the studied mink to AMDV exposure. The tests were conducted using established protocols described by Hu et al. (2021). In brief, blood samples of the studied mink were collected in mid-November before selecting breeders and in mid-February before mating from 2013 to 2021. The blood samples were sent to the Animal Health Laboratory at the University of Guelph (Ontario, Canada) and Middleton Veterinary Services (Nova Scotia, Canada) for CIEP and ELISA-G tests, respectively. The CIEP tests were used to detect the existence of anti-AMDV antibodies, and the results were recorded as 0 (negative: none or extremely low antibody level detected) or 1 (positive: detectable antibody level). The ELISA-G tests were applied to measure amounts of antibodies against AMDV using optical density, and the test results included eight categories with 1-point increments from 0 (none or an extremely low level of antibodies) to 7 (extremely high antibody level).

## 2.3 Growth and measurement

The Kleiber ratio (KR) and feed conversion ratio (FCR) were used to measure the growth and feed efficiency of the studied mink, respectively. The body weights of the studied individuals were collected using the established protocols described by Do et al. (2021). In brief, the body weight (BW) of the mink was measured at both birth and weaning (around 6 weeks after birth) and every 3 weeks from 13 to 28 weeks after birth. The average daily gain (ADG) and mid-test metabolic BW ($BW^{0.75}$) were calculated by the following equations, respectively:

$$ADG = \frac{Final\ BW - Initial\ BW}{\text{Number of days on the test}},$$

$$BW^{0.75} = \left(\frac{Initial\ BW + Final\ BW}{2}\right)^{0.75},$$

where final BW was the BW on the last day of the feeding trial and the initial BW was the BW at 13 weeks of age. The Kleiber ratio (KR) was calculated using the following equation:

$$KR = \frac{ADG}{BW^{0.75}}.$$

The feed intake data on the studied mink were collected using the established protocols described by Davoudi et al. (2022). In brief, mink were raised individually in separate cages, and feed was distributed daily to cages. The daily feed intake (DFI) of each mink was measured by calculating the difference between the amount of feed left over and the feed provided. The individual DFI records obtained during the experiment were averaged to obtain the individual average daily feed intake (ADFI). The FCR was calculated using the following equation:

$$FCR = \frac{ADFI}{ADG}.$$

## 2.4 Pelt quality evaluation

The pelt quality tests were conducted using the same method described by Hu et al. (2021). The live grading of overall pelt quality (QUA) was performed to measure the qualities of the mink pelt when they were alive. The grading was conducted based on the North American Fur Auctions live animal grading procedure by a skilled technician. The grading focused on checking the color consistency, fur roughness, and overall gloss. The QUA was scored into three categories from 1 (poor) to 3 (best).

## 2.5 Female reproductive performance measurement

The female reproductive performance was measured using the same approach described by Hu et al. (2021). Female reproductive performance was measured and recorded by the technicians in CCFAR during each annual reproduction cycle from 2006 to 2021. In this study, the number of newborn kits that survived

TABLE 1 Number of individuals from different color types in each subgroup in different Aleutian disease tests and the final dataset for detecting selection signatures for immune response to Aleutian mink disease virus infection in American mink.

| Color type | ELISA-G[a] (0-7) | | CIEP[b] | | Immune response[c] | |
|---|---|---|---|---|---|---|
| | Negative (0) | Positive (5-7) | Negative | Positive | Low | High |
| Black | 67 | 23 | 12 | 78 | 10 | 19 |
| Demi | 264 | 57 | 87 | 329 | 70 | 51 |
| Mahogany | 244 | 40 | 50 | 258 | 39 | 37 |
| Pastel | 42 | 31 | 14 | 70 | 11 | 25 |
| Stardust | 5 | 3 | 1 | 8 | 1[d] | 1[d] |
| All | 622 | 154 | 164 | 743 | 131 | 133 |

[a]ELISA-G = AMDV-G-based enzyme-linked immunosorbent assay test.
[b]CIEP = counterimmunoelectrophoresis test.
[c]The individuals were used in the final dataset for detecting selection signatures for immune response to Aleutian mink disease virus infection.
[d]No independent analysis was conducted for stardust color-type individuals due to the small sample size.

TABLE 2 Number of individuals with positive counterimmunoelectrophoresis test results in each subgroup of the feed conversion ratio, Kleiber ratio, live pelt quality, general resilience performance, and female reproductive performance traits.

| Feed conversion ratio | | Kleiber ratio | | Pelt quality | | General resilience performance[a] | | Female reproductive performance[b] | |
|---|---|---|---|---|---|---|---|---|---|
| Bottom 20% (14.38–22.49) | Top 20% (41.46–72.28) | Bottom 20% (2.19–4.41) | Top 20% (7.14–9.17) | Score 1 | Score 3 | Resilient | Susceptible | Low litter size (1–4) | High litter size (9–11) |
| 78 | 78 | 78 | 78 | 83 | 120 | 19 | 11 | 20 | 16 |

[a]The evaluation of individual general resilience performance based on the feed conversion ratio, Kleiber ratio, and pelt quality.
[b]The measurement of female reproductive performance resilience (dams with a positive counterimmunoelectrophoresis test only) based on the number of kits alive 24 h after birth.

24 h after birth was used to quantify the reproduction performance of dams under AMDV exposure.

## 2.6 Animal grouping

Studied individuals were grouped into pairwise subgroups based on their immune response, general resilience, and female reproductive performance. Studied individuals with both CIEP and ELISA-G test results were grouped into low- or high-immune response subgroups based on their CIEP and ELISA-G test results. Individuals with zero ELISA-G scores and negative CIEP results were grouped into low-immune response subgroups, and individuals with 5–7 ELISA-G scores and positive CIEP results were grouped into the high-immune response subgroup (Table 1). In this study, we not only grouped the entire populations of individuals into low- or high-immune response subgroups but also the individuals within the same color type, which included black, demi, mahogany, and pastel color types (Table 1). For resilience indicator traits, two methods were used to group CIEP-positive individuals into pairwise groups (Table 2). Studied individuals with positive CIEP results that had BW, feed intake, and pelt quality records were grouped into resilient or susceptible subgroups. The CIEP-positive individuals, which had bottom 20% FCR (14.38–22.49), top 20% KR (7.14–9.17), and score 3 (high pelt quality) for QUA were grouped into the resilient subgroup, and the CIEP-positive individuals, which had top 20% FCR (41.46–72.28), bottom 20% KR (2.19–4.41), and score 1 (low pelt quality) for QUA, were grouped into the susceptible subgroup (Table 2). Meanwhile, studied CIEP-positive dams, which had records for the number of newborn kits that survived 24 h after birth, were grouped into low- or high-female reproductive performance subgroups. The CIEP-positive dams with less than four newborn kits that survived 24 h after birth were grouped into the low-reproductive performance subgroup, and the CIEP-positive dams that had more than nine newborn kits that survived 24 h after birth were grouped into the high-reproductive performance subgroup (Table 2).

## 2.7 Sample collection and genotype detection

Tongue tissues from studied individuals were collected before pelting. The DNeasy Blood and Tissue Kit (QIAGEN, Hilden, Germany) was used to extract the DNA from the tongue tissue based on the manufacturer's instructions. The NanoDrop ND-1000 spectrophotometer (NanoDrop Technologies Inc., Wilmington, DE) was applied to measure the quantity and quality of the extracted DNA samples. The 260/280-nm readings for all samples ranged from 1.7 to 2.0. All samples had a final concentration of 20 ng and were finally genotyped by an Axiom

Affymetrix Mink 70K SNP panel (Neogen, Lincoln, Nebraska, USA) (Do et al., 2024).

## 2.8 Animals and SNP quality control

PLINK (Purcell et al., 2007) was used to conduct animal and SNP data quality control. SNPs which had a minor allele frequency lower than 1%, call rate lower than 90%, excess of heterozygosity higher than 15%, Mendelian error frequency larger than 5%, and were out of Hardy–Weinberg equilibrium with a very low probability ($1 \times 10^{-5}$) were excluded from the analyses. Meanwhile, mink, which had a call rate lower than 90%, were also removed from the dataset. After quality control, 26,406 SNPs and 1,411 animals remained for further analyses.

## 2.9 Methods for the detection of selection signatures

Three methods, including the pairwise fixation index (Fst) (Weir and Cockerham, 1984), nucleotide diversity (θπ) (Nei and Li, 1979), and cross-population extended haplotype homozygosity (XP-EHH) (Sabeti et al., 2007), were performed to detect the selection signatures. The Fst and θπ methods directly utilize the SNP genotype, while the XP-EHH method uses phased data. The Fst analysis was conducted for each SNP based on the method proposed by Weir and Cockerham (1984) using VCFtools software (Danecek et al., 2011). The Z-transformation was performed using the *scale* function in the R program (Team, 2022) to normalize the Fst values. All negative Fst values were set to zero. The Fst values of all SNPs were ranked, and the SNPs with the top 5% Fst values were considered candidate selection signatures. The θπ analysis was conducted for each SNP based on the method proposed by Nei and Li (1979) using VCFtools software (Danecek et al., 2011). The θπ ratios were computed as θπ (subgroup1)/θπ (subgroup2) for all pairs of groups and were then log2-transformed (log2 (θπ ratios)). The SNPs with the top 5% θπ ratio values were considered candidate selection signatures. The XP-EHH approach was calculated for each SNP using selscan software (Torres et al., 2018). The missing genotypes were removed using VCFtools software (Danecek et al., 2011), and the genotypes were phased using Beagle software (Browning et al., 2018) because selscan software can only handle the phased genotypes without missing genotypes. The original obtained XP-EHH values were normalized using the norm function within the selscan software program. Then, the *pnorm* function in the R program was applied to calculate the *p*-values of the normalized XP-EHH values. The *p*-values of the normalized XP-EHH values were log-transformed, and the SNPs with -log (*p*-value) more than two were considered candidate selection signatures. Only the SNPs detected as candidate selection signatures by at least two methods were used for genome annotation, Gene Ontology, and functional analysis.

## 2.10 Genome annotation, Gene Ontology, and functional analysis

The potential selection regions were defined by extending 350 kb both upstream and downstream of the candidate selection signatures. The regions were defined based on the previous study that suggested that linkage disequilibrium ($r^2 < 0.2$) in the current studied American mink population did not exceed 350 kb (Hu et al., 2023). Genome annotation was conducted using bedtools software (Quinlan, 2014) referring to the genome assembly of *Neogale vison* (Karimi et al., 2022). The Gene Ontology (GO) terms, including biological process (GO:BP), cellular component (GO:CC), and molecular function (GO:MF), were assigned to annotated genes using PANTHER 14.1 (Thomas et al., 2003). The overrepresentation tests of annotated genes were conducted using Fisher's exact test and adjusted by the false discovery rate (FDR) correction, and the terms with the FDR-adjusted *p*-value (q-value) <0.05 were considered the overrepresented terms. Meanwhile, the Kyoto Encyclopedia of Genes and Genomes (KEGG) pathway analyses were conducted using the *clusterProfiler* package (Yu et al., 2012) in the R program with FDR control.

# 3 Results

## 3.1 Selection signatures for the immune response trait

The genome-wide distribution of selection signatures associated with the immune response trait is presented in Figure 1. Additionally, Figure 2 illustrates the selection signatures that overlap across the three methods. Supplementary Material S1 presents the candidate selection signatures (chromosome number and location on the chromosome) detected by each method. When considering the entire population of individuals, a total of 619 SNPs were detected as candidate selection signatures by at least two methods. Notably, 33 SNPs were detected by all three methods and were considered strongly selected candidates (Figure 2). Furthermore, when analyzing individuals within specific color types, 444, 512, 385, and 335 were detected as candidate selection signatures for black, demi, mahogany, and pastel color-type mink, respectively. In addition, 57, 31, 32, and 45 SNPs were detected by all three methods for black, demi, mahogany, and pastel color-type mink, respectively, highlighting strong selection signature candidates specific to the immune response trait within each color type (Figure 2).

The candidate genes annotated from the selection signatures in the whole population and different color types are listed in Supplementary Material S1. Figure 3 shows the overlapped annotated candidate genes among the whole population and different color types. A total of 1,611 candidate genes were annotated from the selection signatures detected from the whole population (Figure 3 and Supplementary Material S2A). For black, demi, mahogany, and pastel color-type individuals, 1,355, 1,645, 1,436, and 1,042 candidate genes were annotated, respectively (Figure 3). Among the candidate genes annotated from the whole population and different color types, many genes were found to be associated with the AD-characterized phenotypes, including the immune system process, growth, pigmentation (except for the black color-type), reproduction, and response to stimulus (Supplementary Material S2, Figures 3, 4). Table 3 provides a list of genes for all color types. However, no common gene was detected among all color types for immune response traits (Figure 3).

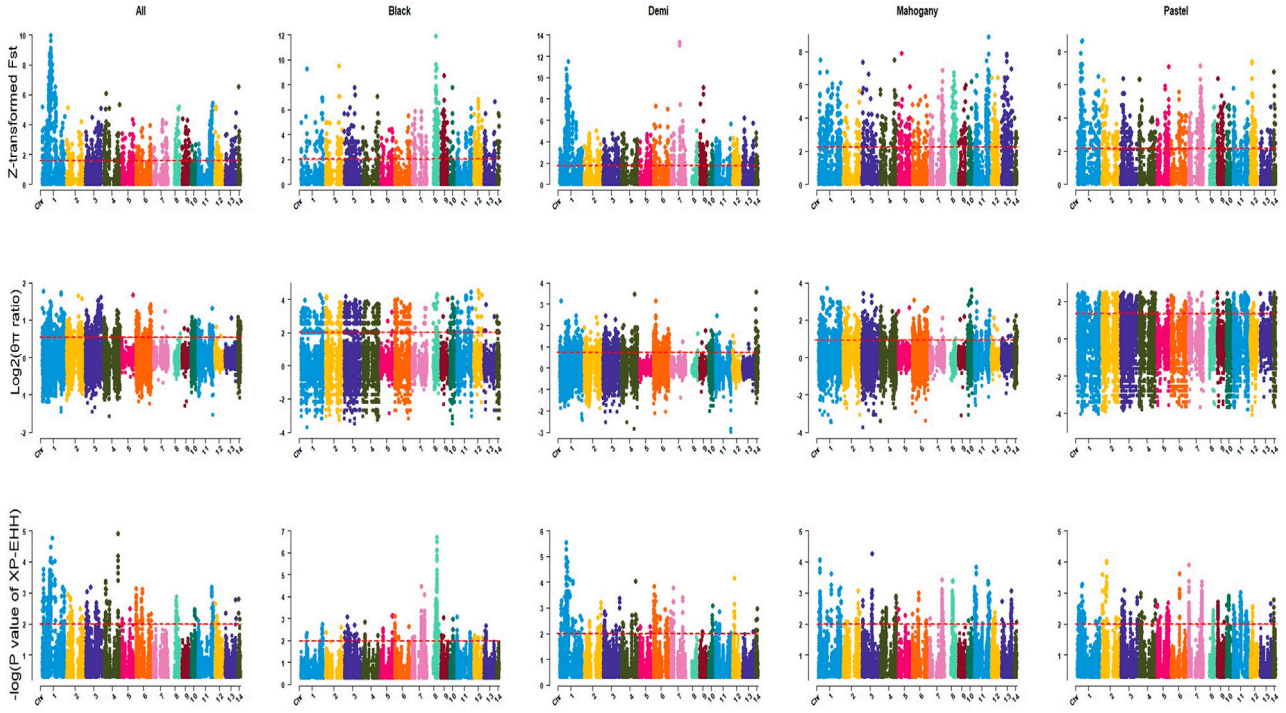


FIGURE 1
Genome-wide distribution of detected selection signatures for immune response trait across all autosomes in the whole population and different color types of individuals. The red lines of Z-transformed Fst and log2 (θπ ratio) plots display the threshold levels of 5%. The red lines of XP-EHH plots display the threshold levels of -log (*p*-value)>2.

Figure 4 presents the functional classifications of candidate genes related to the immune response trait. The genes annotated from the whole population, black, demi, mahogany, and pastel color-type individuals were classified into 17, 18, 17, 20, and 18 GO:BP categories, respectively, where the top four biological processes were the cellular process, metabolic process, biological regulation, and response to stimulus in all cases (Figure 4). The cellular anatomical entity and protein-containing complex were the two cellular components detected from the whole population and all color types. Regarding the GO:MF classifications, both analyses for whole population individuals and black color-type individuals detected 11 GO:MF, while analyses for demi, mahogany, and pastel color-type individuals detected 12 GO:MF. The top four GO:MF categories for the whole population and all color types were binding activity, catalytic activity, transcription regulator activity, and molecular transducer activity (Figure 4).

Table 4 (GO:BP) and Table 5 (GO:CC and GO:MF) present the overrepresentations of candidate genes. A total of 27, 18, 50, 26, and 18 significant (q-value<0.05) overrepresented GO enrichment terms were detected from the whole population, black, demi, mahogany, and pastel color-type individuals, respectively (Tables 4 and 5). Among all detected significant (q-value<0.05) overrepresented GO enrichment terms, some of them were commonly detected in the whole population and all color types (Tables 4 and 5), including two GO:BP (detection of chemical stimulus involved in sensory perception of smell (GO:0050911) and sensory perception of smell (GO:0007608)), three GO:CC (cytoplasm (GO:0005737), intracellular anatomical structure (GO:0005622), and organelle (GO:0043226)), and one molecular function (olfactory receptor activity (GO:0004984)). However, some were only detected in a certain color type of mink or the entire population. For example, the biological processes of adaptive immune response (GO:0002250) and system development (GO:0048731) were only detected for the whole population. Several metabolism-related GO:BP (e.g., heterocycle metabolic process (GO:0046483), macromolecule metabolic process (GO:0043170), and nitrogen compound metabolic process (GO:0006807)) and several GO:CC (e.g., envelope (GO:0031975), protein-containing complex (GO:0032991), and synapse (GO:0045202)) were only detected in demi color-type mink. Two unique GO:MF, namely, catalytic activity (GO:0003824) and hydrolase activity (GO:0016787), were only detected in mahogany color-type mink.

## 3.2 Selection signatures for general resilience and female reproductive performance traits

The genome-wide distribution of selection signatures for general resilience and female reproductive performance traits are presented in Figure 5, and the overlapped selection signatures are presented in Figure 6. Supplementary Material S3 presents the SNPs detected as candidate selection signatures by each method and the SNPs detected as candidate selection signatures by at least two methods. For general resilience traits, 569 SNPs were detected as candidate selection signatures by at least two

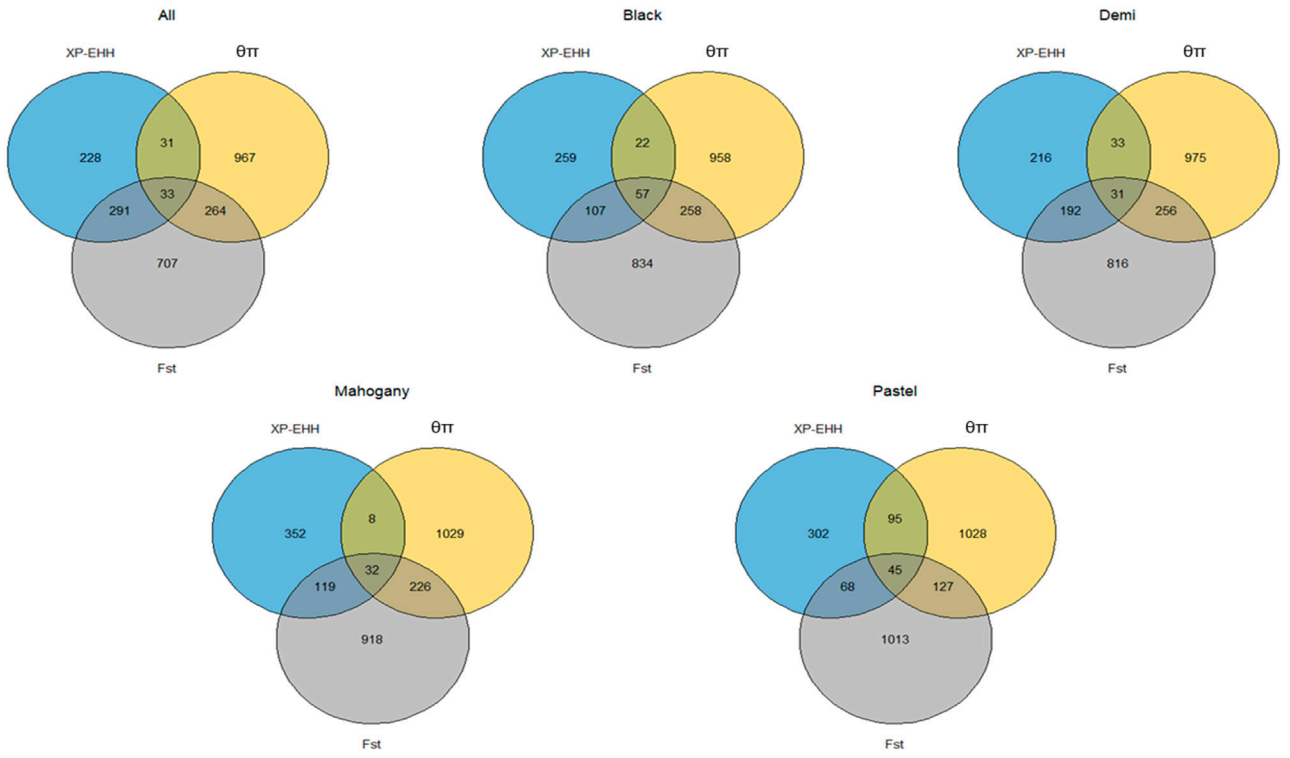


FIGURE 2
Overlapped selection signatures detected in the whole population and different color types of individuals among three detection methods for the immune response trait.

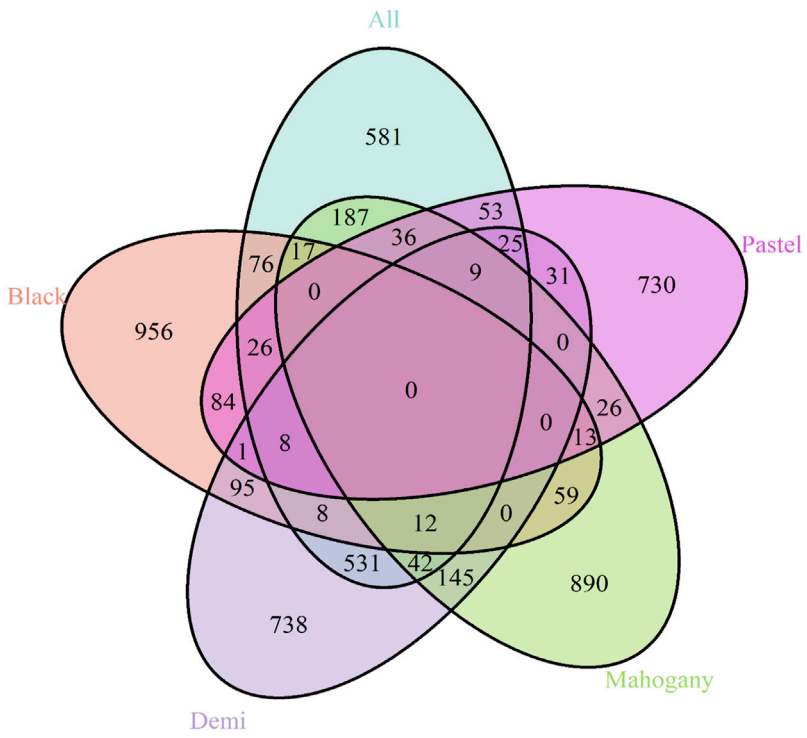


FIGURE 3
Venn diagram shows the genes overlapping among the whole population and different color types for the immune response trait.

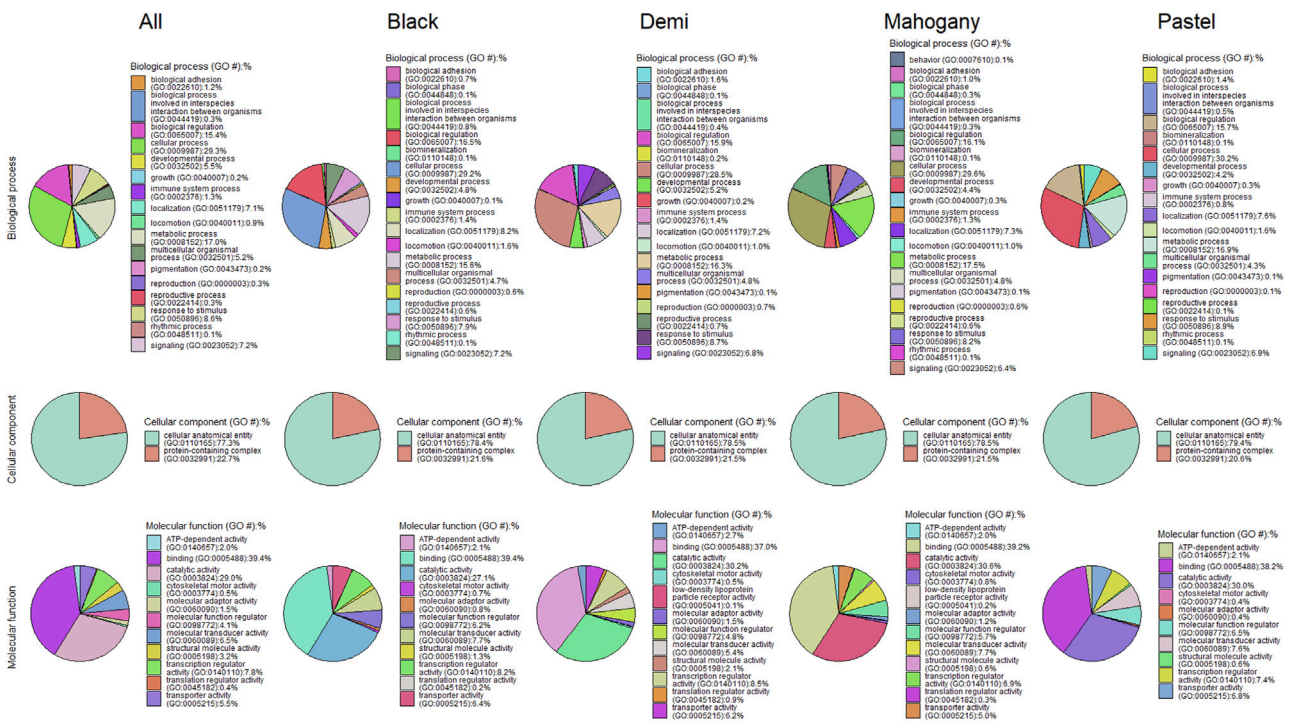


FIGURE 4
Pie charts of functional classifications of candidate genes under selection pressure in the whole population and different color types of individuals for immune response traits.

**TABLE 3** Immune response-related genes annotated from selection signatures detected from different color types.

| Color type | Genes |
|---|---|
| Black | *ANKRD17*, *CEBPA*, *CTSH*, *CXCL6*, *CXCL8*, *FYB1*, *GAL*, *HAVCR1*, *IL1A*, *IL1F10*, *IL1RN*, *IL36RN*, *ITK*, *MARCHF1*, *MTURN*, *PATZ1*, *SIGLEC15*, *TMEM178A*, *TNFRSF1B*, and *UBASH3A* |
| Demi | *C4A*, *CACTIN*, *CCL26*, *CCR9*, *CEBPA*, *CGAS*, *CTLA4*, *CXCR6*, *DEF6*, *FYN*, *HIC2*, *HSPD1*, *MPIG6B*, *NFAM1*, *RUNX1*, *RUNX2*, *SH2B2*, *SHFL*, *TNFRSF21*, *TRAF3IP2*, *TYK2*, *VEGFA*, *XCR1*, *YES1*, *ZBTB12*, and *ZBTB37* |
| Mahogany | *ANKRD17*, *C4A*, *CASP3*, *CXCL6*, *CXCL8*, *EPOR*, *FYB2*, *HSPD1*, *MEIS1*, *MPIG6B*, *NFAM1*, *PLA2G2D*, *PLA2G2F*, *PLA2G5*, *RAG2*, *REL*, *TNFRSF11A*, *TNFRSF13C*, and *ZBTB12* |
| Pastel | *AKIRIN1*, *BANK1*, *BCL10*, *UBASH3A*, *FGR*, *LPXN*, *SEC14L1*, *THEMIS2*, and *TNFRSF1B* |

methods, and 57 SNPs were detected as candidate selection signatures by all three methods (Figure 6). For female reproductive performance traits, 526 SNPs were detected as candidate selection signatures by at least two methods, and 16 SNPs were detected as candidate selection signatures by all three methods (Figure 6).

The candidate genes annotated from the candidate selection are listed in Supplementary Material S3, and the functional classifications of candidate genes are shown in Figure 7. A total of 1,933 genes were annotated from the selection signatures for the general resilience trait (Supplementary Material S2B). Several annotated genes were related to AD resilient traits, including growth, immune system process, pigmentation, and reproduction. The functional classifications of the annotated genes resulted in 18 GO:BP, 2 GO:CC, and 11 GO:MF. The annotation of selection signatures related to the female reproductive performance trait resulted in a total of 1,538 genes (Supplementary Material S2B). Except for 10 genes related to reproduction, several other genes were related to some AD-resilience indicator traits, including growth, immune system process, and pigmentation. The annotated genes were classified into 18 GO:BP, 2 GO:CC, and 11 GO:MF.

The overrepresentations of candidate genes are presented in Table 6. For general resilience traits, nine significant (q-value<0.05) overrepresented GO:BP were detected, and they were involved primarily in development, cellular process, and sensory perception of smell. Meanwhile, nine GO:CC (mostly related to organelle) and three GO:MF (related to olfactory receptor activity or binding) were significant (q-value<0.05) in the overrepresentation tests of candidate genes related to the general resilience. The overrepresentation tests of candidate

TABLE 4 Significant (q-value<0.05) biological processes detected from overrepresentation tests of candidate genes from the whole studied population and different color types of mink for immune response traits.

| Biological process (GO ID) | All | Black | Demi | Mahogany | Pastel |
|---|---|---|---|---|---|
| Adaptive immune response (GO:0002250) | a | b | b | b | b |
| Anatomical structure development (GO:0048856) | a | b | a | a | a |
| Anatomical structure morphogenesis (GO:0009653) | a | b | b | a | b |
| Bicellular tight junction assembly (GO:0070830) | b | b | a | b | b |
| Cell development (GO:0048468) | a | b | a | a | b |
| Cell differentiation (GO:0030154) | a | b | a | a | b |
| Cellular aromatic compound metabolic process (GO:0006725) | b | b | a | b | b |
| Cellular component morphogenesis (GO:0032989) | b | b | b | a | b |
| Cellular component organization (GO:0016043) | b | b | a | a | b |
| Cellular component organization or biogenesis (GO:0071840) | b | b | a | a | b |
| Cellular developmental process (GO:0048869) | a | b | a | a | b |
| Cellular metabolic process (GO:0044237) | b | b | a | b | b |
| Cellular nitrogen compound metabolic process (GO:0034641) | b | b | a | b | b |
| Detection of chemical stimulus (GO:0009593) | a | a | a | b | a |
| Detection of chemical stimulus involved in sensory perception (GO:0050907) | a | a | a | b | a |
| Detection of chemical stimulus involved in sensory perception of smell (GO:0050911) | a | a | a | a | a |
| Detection of stimulus (GO:0051606) | a | b | b | b | b |
| Detection of stimulus involved in sensory perception (GO:0050906) | a | a | b | b | b |
| Developmental process (GO:0032502) | a | b | a | a | b |
| Heterocycle metabolic process (GO:0046483) | b | b | a | b | b |
| Macromolecule metabolic process (GO:0043170) | b | b | a | a | b |
| Metabolic process (GO:0008152) | b | b | a | b | b |
| Mitochondrial gene expression (GO:0140053) | b | b | a | b | a |
| Multicellular organism development (GO:0007275) | a | b | b | a | a |
| Multicellular organismal process (GO:0032501) | a | b | b | b | b |
| Nitrogen compound metabolic process (GO:0006807) | b | b | a | b | b |
| Nucleobase-containing compound metabolic process (GO:0006139) | b | b | a | b | b |
| Organelle organization (GO:0006996) | b | b | b | a | b |
| Organic substance metabolic process (GO:0071704) | b | a | a | a | b |
| Positive regulation of the multicellular organismal process (GO:0051240) | b | b | b | b | a |
| Primary metabolic process (GO:0044238) | b | b | a | a | b |
| Regulation of the multicellular organismal process (GO:0051239) | b | b | b | b | a |
| Sensory perception of chemical stimulus (GO:0007606) | a | a | a | b | a |
| Sensory perception of smell (GO:0007608) | a | a | a | a | a |
| Small-molecule catabolic process (GO:0044282) | b | a | b | b | b |
| System development (GO:0048731) | a | b | b | b | b |
| Tight junction organization (GO:0120193) | b | b | a | b | b |

[a]The biological process was detected in this color type/population.
[b]The biological process was not detected in this color type/population.

10.3389/fgene.2024.1370891

TABLE 5 Significant (q-value<0.05) cellular components and molecular functions detected from overrepresentation tests of candidate genes from the whole studied population and different color types of mink for immune response traits.

| Functional enrichment item | All | Black | Demi | Mahogany | Pastel |
|---|---|---|---|---|---|
| Cellular component (GO ID) | | | | | |
| Bicellular tight junction (GO:0005923) | b | b | a | b | b |
| Cell junction (GO:0030054) | a | b | a | b | b |
| Cellular anatomical entity (GO:0110165) | b | a | a | b | a |
| Collagen type IV trimer (GO:0005587) | b | b | b | b | a |
| Cytoplasm (GO:0005737) | a | a | a | a | a |
| Cytosol (GO:0005829) | b | a | a | b | b |
| Endomembrane system (GO:0012505) | b | b | b | b | a |
| Envelope (GO:0031975) | b | b | a | b | b |
| Intracellular anatomical structure (GO:0005622) | a | a | a | a | a |
| Intracellular membrane-bounded organelle (GO:0043231) | b | a | a | a | b |
| Intracellular organelle (GO:0043229) | b | a | a | a | a |
| Intracellular organelle lumen (GO:0070013) | b | b | a | b | b |
| Membrane-bounded organelle (GO:0043227) | b | a | a | a | a |
| Membrane-enclosed lumen (GO:0031974) | b | b | a | b | b |
| Mitochondrial matrix (GO:0005759) | b | b | a | b | b |
| Mitochondrion (GO:0005739) | b | b | a | b | b |
| Organelle (GO:0043226) | a | a | a | a | a |
| Organelle envelope (GO:0031967) | b | b | a | b | b |
| Organelle lumen (GO:0043233) | b | b | a | b | b |
| Protein-containing complex (GO:0032991) | b | b | a | b | b |
| Synapse (GO:0045202) | b | b | a | b | b |
| Tight junction (GO:0070160) | b | b | a | b | b |
| Molecular function (GO ID) | | | | | |
| Actin binding (GO:0003779) | a | b | b | b | b |
| Binding (GO:0005488) | a | a | a | a | b |
| Catalytic activity (GO:0003824) | b | b | b | a | b |
| Hydrolase activity (GO:0016787) | b | b | b | a | b |
| Identical protein binding (GO:0042802) | b | b | a | b | b |
| Olfactory receptor activity (GO:0004984) | a | a | a | a | a |
| Protein binding (GO:0005515) | a | a | a | a | b |
| Protein-containing complex binding (GO:0044877) | a | b | b | b | b |
| RNA binding (GO:0003723) | b | b | a | b | b |
| RNA polymerase II-specific DNA-binding transcription factor binding (GO:0061629) | a | b | b | b | b |

[a]The cellular component or molecular function was detected in this color type/population.
[b]The cellular component or molecular function was not detected in this color type/population.

genes from female reproductive performance traits resulted in 10 significant (q-value<0.05) overrepresented GO:BP (mostly related to development and detection of stimulus), 6 significant overrepresented GO:CC (mostly related organelle), and 4 significant overrepresented GO:MF (related to olfactory receptor activity or binding).

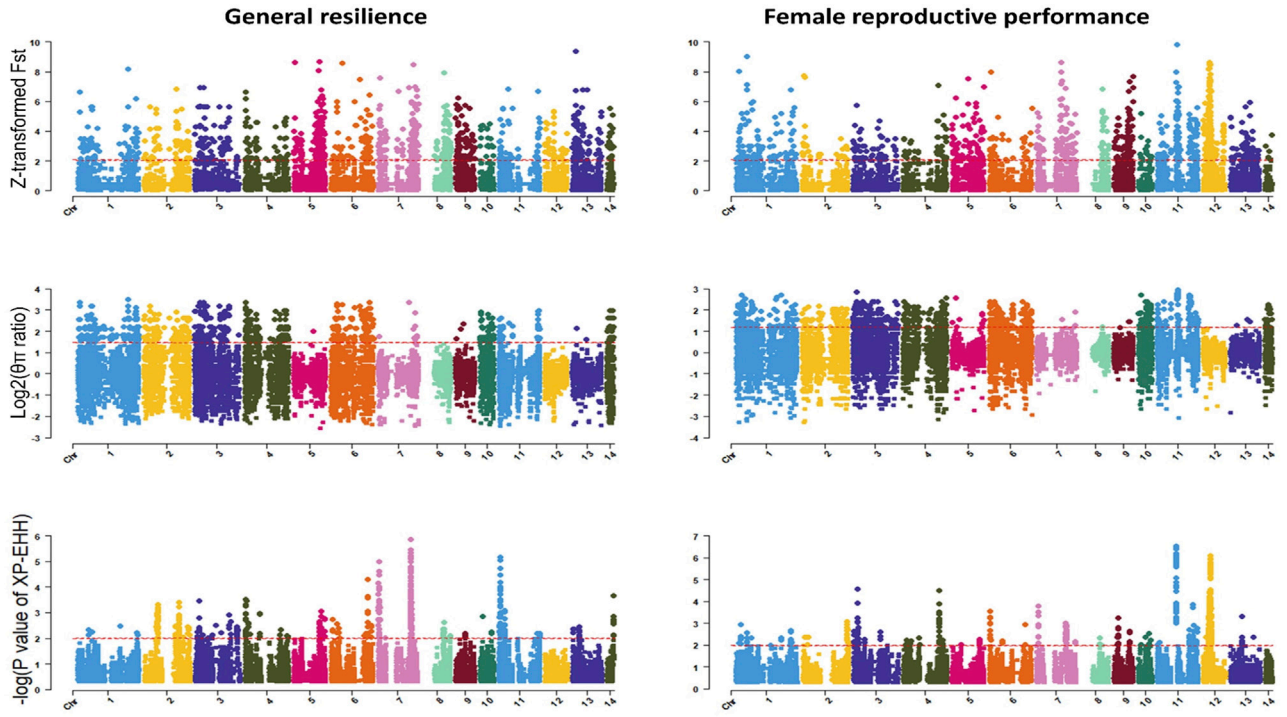


FIGURE 5
Genome-wide distribution of detected selection signatures for general resilience and female reproductive performance traits across all autosomes from the whole population. The red lines of Z-transformed Fst and log2 (θπ ratio) plots display the threshold levels of 5%. The red lines of XP-EHH plots display the threshold levels of -log (*p*-value)>2.

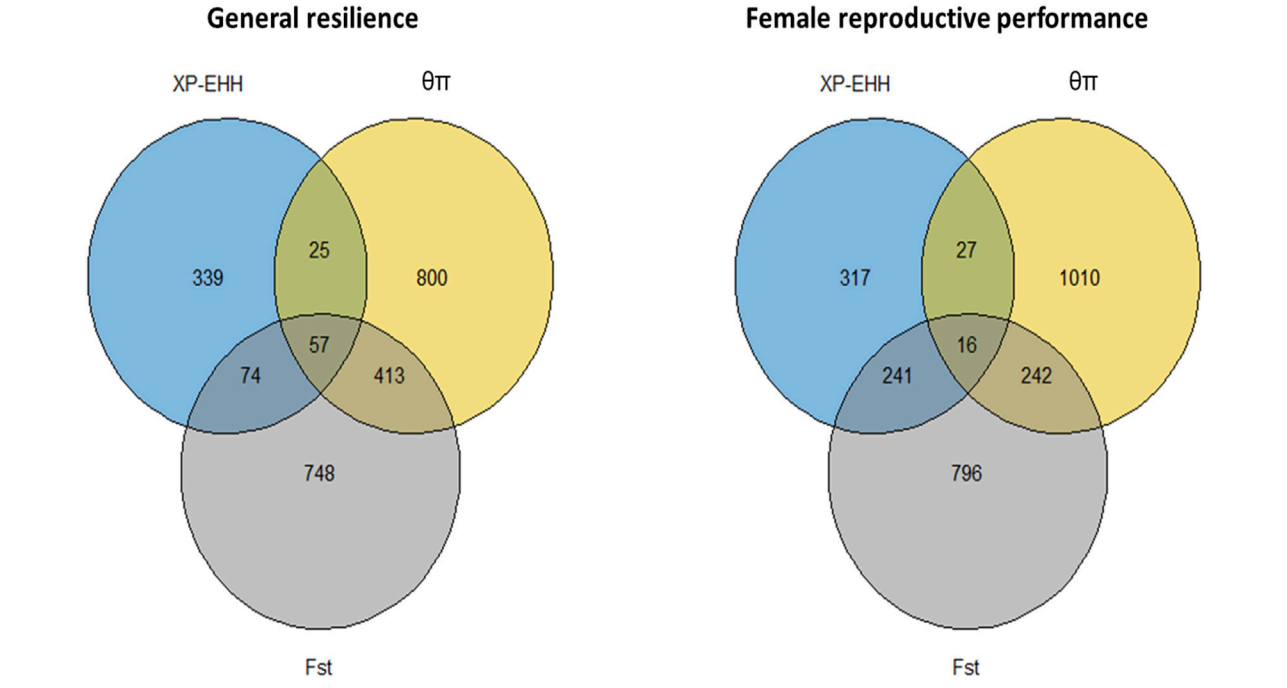


FIGURE 6
Overlapped selection signatures detected from the whole population individuals for general resilience and female reproductive performance traits.

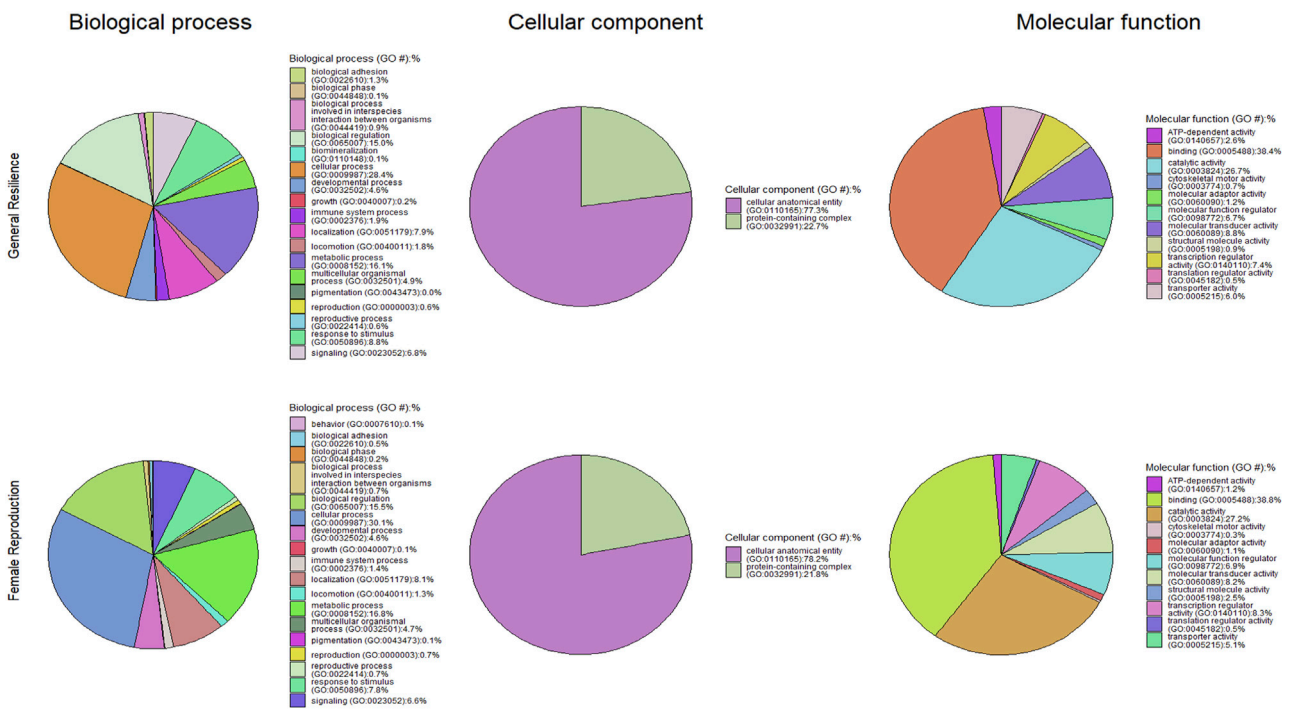


FIGURE 7
Pie charts of functional classifications of candidate genes under selection pressure in the whole population individuals for general resilience and female reproductive performance traits.

## 3.3 Common genes among studied traits and KEGG pathways

The overlapped genes among immune response, general resilience, and female reproductive performance traits are presented in Figure 8. In brief, 1,347, 1,680, and 1,277 unique genes were annotated from the selection signatures related to immune response, general resilience, and female reproductive performance traits, respectively. Sixteen genes, namely, *ARHGAP19* (chr2: 209,800,177–209,812,754 bp), *COL14A1* (chr4: 19,536,084–19,755,397 bp), *DEPTOR* (chr4: 19,803,040–19,933,557 bp), *EXOSC1* (chr2: 209,917,603–209,928,479 bp), *FAM135B* (chr4: 4,922,384–4,961,329 bp), *FRAT1* (chr2: 209,829,018–209,831,565 bp), *FRAT2* (chr2: 209,839,939–209,842,216 bp), *LOC122905718* (chr4: 5,215,903–5,216,010 bp), *MMS19* (chr2: 209,938,058-209,971,536 bp), *MRPL13* (chr4: 19,501,767–19,518,965 bp), *PGAM1* (chr2: 209,910,223–209,917,518 bp), *PTCHD4* (chr1: 94,047,590–94,230,349 bp), *RRP12* (chr2: 209,866,295–209,895,940 bp), *TBX18* (chr1: 44,912,005–44,922,875 bp), *UBTD1* (chr2: 209,972,082–210,024,677 bp), and *ZDHHC16* (chr2: 209,928,631–209,937,825 bp), were detected from all three studied traits.

The significant ($q < 0.05$) KEGG pathways of candidate genes from immune response, general resilience, and female reproductive performance traits are listed in Table 7. For immune response traits, only one significant ($q < 0.05$) pathway, the longevity regulating pathway, was detected. For female reproductive performance traits, one significant ($q < 0.05$) pathway, the mitogen-activated protein kinase (MAPK) signaling pathway, was detected. No significant ($q < 0.05$) KEGG pathway was detected for the general resilience trait.

# 4 Discussion

The failure to control AD by the culling strategy, immunoprophylaxis, and medical treatment resulted in the selection of AD-resilient mink based on the diagnostic tests or individual production performances (Knuuttila et al., 2009; Farid and Rupasinghe, 2016; Farid and Ferns, 2017; Farid et al., 2018). Although the phenotypic selection of AD-resilient mink is conducted in many AD-positive mink farms, the genomic architecture of AD resilience is still unclear, which might influence the effectiveness of selecting AD-resilient mink. In this study, genotypes from the Axiom Affymetrix Mink 70K panel and three methods were applied to detect the selection signatures related to immune response, general resilience, and female reproductive performance of farmed American mink under AMDV exposure. In brief, 1,611, 1,933, and 1,538 genes were annotated from the 619, 569, and 526 selection signatures detected from immune response, general resilience, and female reproductive performance traits, respectively. Although more than a thousand genes have been annotated as potential candidates for these traits, many genes, such as the identified *LOC122904335*, *LOC122905665*, and *LOC122904336* genes, were novel genes of unknown function in mink; thus, the discussions were focused on the genes with available information in the existing literature. Functional enrichment analyses revealed that some annotated genes might play an important role in the immune system process, growth, reproduction, pigmentation, sensory perception, and detection of smell.

10.3389/fgene.2024.1370891

TABLE 6 Significant (q-value<0.05) biological processes, cellular components, and molecular functions detected from overrepresentation tests of candidate genes for general resilience and female reproductive performance traits.

| Trait | Term (GO ID) | Annotation set |
|---|---|---|
| General resilience | Anatomical structure morphogenesis (GO:0009653) | Biological process |
| | Cell migration (GO:0016477) | Biological process |
| | Cell motility (GO:0048870) | Biological process |
| | Cellular process (GO:0009987) | Biological process |
| | Chemotaxis (GO:0006935) | Biological process |
| | Detection of chemical stimulus involved in sensory perception of smell (GO:0050911) | Biological process |
| | Locomotion (GO:0040011) | Biological process |
| | Sensory perception of smell (GO:0007608) | Biological process |
| | Taxis (GO:0042330) | Biological process |
| | Cell projection (GO:0042995) | Cellular component |
| | Cellular anatomical entity (GO:0110165) | Cellular component |
| | Cytoplasm (GO:0005737) | Cellular component |
| | Intracellular anatomical structure (GO:0005622) | Cellular component |
| | Intracellular membrane-bounded organelle (GO:0043231) | Cellular component |
| | Intracellular organelle (GO:0043229) | Cellular component |
| | Membrane-bounded organelle (GO:0043227) | Cellular component |
| | Organelle (GO:0043226) | Cellular component |
| | Plasma membrane-bounded cell projection (GO:0120025) | Cellular component |
| | Binding (GO:0005488) | Molecular function |
| | Olfactory receptor activity (GO:0004984) | Molecular function |
| | Protein binding (GO:0005515) | Molecular function |
| Female reproductive performance | Adaptive immune response (GO:0002250) | Biological process |
| | Anatomical structure development (GO:0048856) | Biological process |
| | Cellular process (GO:0009987) | Biological process |
| | Detection of chemical stimulus (GO:0009593) | Biological process |
| | Detection of chemical stimulus involved in sensory perception (GO:0050907) | Biological process |
| | Detection of chemical stimulus involved in sensory perception of smell (GO:0050911) | Biological process |
| | Developmental process (GO:0032502) | Biological process |
| | Protein metabolic process (GO:0019538) | Biological process |
| | Sensory perception of chemical stimulus (GO:0007606) | Biological process |
| | Sensory perception of smell (GO:0007608) | Biological process |
| | Cellular anatomical entity (GO:0110165) | Cellular component |
| | Cytoplasm (GO:0005737) | Cellular component |
| | Intracellular anatomical structure (GO:0005622) | Cellular component |
| | Intracellular membrane-bounded organelle (GO:0043231) | Cellular component |
| | Membrane-bounded organelle (GO:0043227) | Cellular component |
| | Organelle (GO:0043226) | Cellular component |
| | Binding (GO:0005488) | Molecular function |

(Continued on following page)

TABLE 6 (*Continued*) Significant (q-value<0.05) biological processes, cellular components, and molecular functions detected from overrepresentation tests of candidate genes for general resilience and female reproductive performance traits.

| Trait | Term (GO ID) | Annotation set |
|---|---|---|
| | Olfactory receptor activity (GO:0004984) | Molecular function |
| | Protein binding (GO:0005515) | Molecular function |
| | Protein–arginine deiminase activity (GO:0004668) | Molecular function |

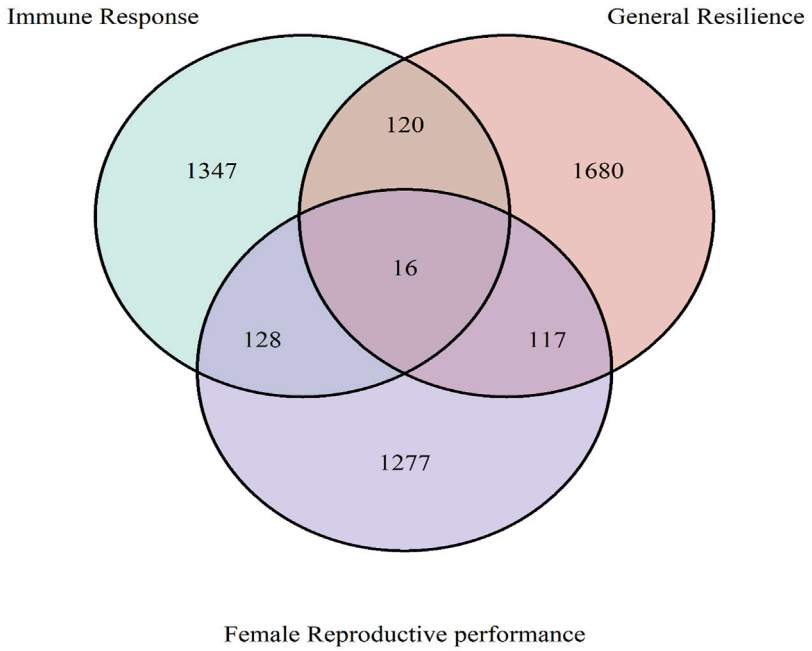


FIGURE 8
Overlapped genes among immune response, general resilience, and female reproductive performance traits. The common 16 genes among all traits were *ARHGAP19*, *COL14A1*, *DEPTOR*, *EXOSC1*, *FAM135B*, *FRAT1*, *FRAT2*, *LOC122905718*, *MMS19*, *MRPL13*, *PGAM1*, *PTCHD4*, *RRP12*, *TBX18*, *UBTD1*, and *ZDHHC16*.

TABLE 7 Significantly (q-value<0.05) presented Kyoto Encyclopedia of Genes and Genomes (KEGG) pathways of genes detected from signature selection analyses of the immune response, general resilience, and female reproductive performance traits.

| Trait | Pathway | Genes | q-value |
|---|---|---|---|
| Immune response (mahogany color-type mink only) | Longevity regulating pathway | *AKT3*, *ATF6B*, *CAMK4*, *CAT*, *CREB5*, *EHMT2*, *IGF1R*, *IRS1*, *PRKAA1*, *PRKAA2*, *RPTOR*, and *SOD2* | 0.049 |
| Female reproductive performance | MAPK signaling pathway | *AKT3*, *ATF2*, *BRAF*, *CACNB1*, *CACNB4*, *CASP3*, *DUSP3*, *DUSP6*, *EGF*, *ERBB4*, *FGF17*, *FGF18*, *FGFR2*, *FLNB*, *IKBKB*, *KIT*, *KITLG*, *MAP2K5*, *MAP3K11*, *MAP3K2*, *MYC*, *NFKB1*, *PDGFRA*, *PPP3CA*, *PPP3CC*, *RELA*, and *STK3* | 0.015 |

## 4.1 Immune responses

A total of 1,611 annotated genes were related to the immune response trait by considering the whole population (Supplementary Material S2A). Some of these annotated genes were related to the immune system process (Figure 4; Tables 4 and 5). A total of 23 genes, namely, *CCL26*, *CD28*, *CGAS*, *DEF6*, *EPOR*, *FAS*, *FYB1*, *GGT1*, *HIC2*, *IL16*, *JAK3*, *MEIS1*, *MFAP3*, *PATZ1*, *RUNX2*, *SHFL*, *SIGLEC15*, *THEMIS*, *TNFRSF21*, *TOX*, *TREM2*, *YES1*, and *ZNF572*, were related to the immune system process, which might play important roles in immune-mediated responses to AMDV infection. Three genes, namely, *TNFRSF21* (chr1: 93,535,621-93,549,929 bp), *CCL26* (chr4: 10,918,021-10,922,028 bp), and *TREM2* (chr1: 87,946,316-87,950,960 bp), are related to inflammatory processes (Stubbs et al., 2010; Santer et al., 2012; Liu et al., 2020). This may be due to several inflammations, which include interstitial nephritis, myocarditis, hepatitis, splenitis, meningoencephalitis, pneumonia, glomerulonephritis, and arteritis, caused by AD infection (Jepsen et al., 2009). Four genes, *SIGLEC15* (chr3:

151,209,875–151,221,497 bp), *JAK3* (chr6: 213,007,629–213,025,411 bp), *DEF6* (ch1: 117,504,375-117,525,807 bp), and *FAS* (chr2: 164,464,382-164,489,036 bp), were related to autoimmune disorders in humans (Hsu et al., 2012; García-Bermúdez et al., 2015; Serwas et al., 2019; Läubli and Varki, 2020), and AD is defined as an immune complex-mediated disorder disease in mink (Bloom et al., 1988). Three genes, *IL16* (chr13: 150,353,853-150,448,017 bp), *THEMIS* (chr1: 73,061,569-73,141,431 bp), and *CD28* (chr3: 15,437,373-15,465,940 bp), were related to T-cell proliferation (June et al., 1987; Wilson et al., 2004; Fu et al., 2009), and the *TOX* (chr4: 75,470,800-75,728,160 bp) gene was detected to be a crucial transcription factor involved in the exhaustion of $CD8^+$ T cells (Seo et al., 2019). The detection of those genes might be related to the proliferation of $CD8^+$ T cells after AD infection as $CD8^+$ T cells were found to double in numbers during the development of AD (Aasted, 1989). The *EPOR* (chr6: 216,150,503–216,156,409 bp) gene was discovered to be associated with the production of red blood cells, and severe anemia was observed in AD-infected mink few months after infection (McGuire et al., 1979). The *FYB1* (chr1: 286,138,312–286,169,159 bp) gene was found to be related to thrombocytopenia (Levin et al., 2015), which is one of the typical symptoms of AD infection (Gordon et al., 1967). The *CGAS* (chr1: 114,736,330–114,760,223 bp) gene was related to the production of the type I interferons and activation of inflammasomes (Wang et al., 2017; Decout et al., 2021), and the increase in the number of type I interferons was observed in the host during AD infection (Jensen et al., 2003). Meanwhile, the overrepresentation tests on the annotated genes detected one significant ($q < 0.05$) GO:BP, adaptive immune response (GO: 0002250), related to immune response, where eight genes (*IL12B*, *TNFRSF21*, *TAP1*, *JAK3*, *TAP2*, *C7*, *THEMIS*, and *C6*) were involved.

The immune-response-related genes detected in this study were different from the genes detected by a previous study (Karimi et al., 2021). Seven genes, namely, *TRAF3IP2*, *WDR7*, *SWAP70*, *TNFRSF11A*, *CBFB*, *IGF2R*, and *GPR65*, were detected and related to the immune system process, as explained by Karimi et al. (2021), and none of these genes were detected in the current study. Several potential reasons could lead to these discrepancies: 1) the use of different types of genomic data (GBS in their study vs genotypes in this study); 2) the use of different grouping methods, where kidney lesion levels and virus loads were also considered in grouping animals in their study in addition to antibody titer; 3) the different ways the animal contracted AMDV (intranasal inoculation in their study vs natural exposure in this study); and 4) the color types of studied mink (only black in their study vs multiple colors in this study).

A total of 20, 26, 19, and 9 genes were related to the immune response in black, demi, mahogany, and pastel color types, respectively (Table 3). Most of the genes detected from a single-color type were unique from the rest of the color types. For black, demi, and mahogany color types, there were few genes in common between the two color types, but no common gene was detected among all of them. For pastel, eight of nine detected genes (only *TNFRSF1B* gene was common with the black color type) were unique from the rest of the three darker color types, which might indicate that pastel color-type mink has different immune responses to AD infection compared with the other three darker color types of mink. This could be a potential reason to explain the previous finding by Ellis (1996), where the mink with lighter color types were observed to be more susceptible to the AMDV than darker mink.

The KEGG pathway analysis of annotated genes from the whole population or different color types only detected one significant KEGG pathway, the longevity regulation pathway, in mahogany color-type mink. The relationship between longevity and immune response is complex. A strong and well-functioning immune system is crucial for protecting an organism from infections and other threats, and therefore, may contribute to increased longevity (Xia et al., 2019). Furthermore, chronic inflammation and overactivation of the immune system have been linked to aging and age-related diseases, which can shorten lifespan (Rea et al., 2018). Aleutian disease is defined as an immune complex disease and can cause persistent and chronic infection in mink (Porter and Cho, 1980; Stolze and Kaaden, 1987). Thus, the detection of the longevity regulation pathway may be related to chronic infection and autoimmune disorders caused by AD.

## 4.2 General resilience

Since the general response trait used in this study was a combination of three AD resilient traits, which include growth, feeding efficiency, and pelt quality, we focused on genomic regions containing genes related to these traits. A total of 1,933 genes were related to the general resilience trait (Supplementary Material S3B). From these, several annotated genes were related to body growth. For example, *PRKAG3* (chr3: 29,115,382–29,120,999 bp), a regulatory subunit of the AMP-activated protein kinase, was detected in this study and found to be related to body growth in several livestock species including swine (Ryan et al., 2012), sheep (Ibrahim, 2015), and beef cattle (Li et al., 2012). The *PLAG1* (chr1: 58,588,578–58,696,784 bp) gene was also detected in this study. This gene is a positive regulator of insulin-like growth factor 2 (Voz et al., 2000; Van Dyck et al., 2007) that is known to affect body weight in both livestock (e.g., swine (Van Laere et al., 2003) and beef cattle (Huang et al., 2013)) and humans (Sandhu et al., 2003). The *TMEM18* (chr1: 8,940,691–9,011,524 bp) gene detected in this study has been reported to be associated with growth traits and obesity in rats (Rask-Andersen et al., 2012), cattle (Ma et al., 2012), and humans (Almén et al., 2010; Haupt et al., 2010). Meanwhile, three genes, *TPRA1* (chr6: 165,580,535-165,594,267 bp), *MCM2* (chr6: 165,600,097-165,621,492 bp), and *Tbx18* (chr1: 44,894,084-44,922,875 bp), which were all found to be related to embryo development in mice (Aki et al., 2008; Wehn and Chapman, 2010; Xu et al., 2022), were also detected in this study indicating that AD may influence the early stages of mink development, and therefore, influence growth. Meanwhile, several genes related to feed efficiency were also detected, for example, *MRAP2* (chr1: 45,464,087-45,513,205 bp) and *GLP1R* (chr1: 85,852,947-85,884,385 bp). *MRAP2* (Berruien and Smith, 2020) and *GLP1R* (Dailey and Moran, 2013) were found to play important roles in regulating appetite, and AD has been reported to cause adverse influences on the appetite of infected mink (Jensen et al., 2016). The annotated gene, *HCRTR2* (chr1: 101,039,715-101,147,858 bp), is an orexin receptor and plays an important role in feeding behavior and balance of energy metabolism (Spinazzi et al., 2006; Belkina and

Denis, 2012). In addition, several annotated genes, including *ESRRG* (chr10: 14,353,012-14,953,383 bp), *LZTFL1* (chr6: 208,512,050-208,525,767 bp), and *ELOVL4* (chr1: 49,176,236-49,208,238 bp), were reported to play key roles in regulating metabolism processes (Zhang et al., 2001; Alaynick et al., 2007; Wei et al., 2018). In addition to the genes related to growth and feed efficiency, the *DCT* gene (chr5: 151,495,518-151,529,776 bp), related to pigmentation (Guyonneau et al., 2004), was also detected in this study, and this might be related to the hair depigmentation, which causes single white hairs in the fur (sprinklers) impacting the pelt quality of AD infected mink (Farid and Ferns, 2011).

## 4.3 Female reproductive performance

A total of 1,538 genes were detected from female reproductive performance traits (Figure 7; Table 6). From these, several genes, including *SLX4* (chr14: 18,318,274-18,338,014 bp), *TDRD6* (chr1: 92,984,166-92,997,290 bp), *TACR3* (chr11: 104,943,216-105,013,153 bp), *SHOC1* (chr9: 21,365,597-21,443,498 bp), *FBXW11* (chr1: 255,864,225-255,951,567 bp), *EPC2* (chr3: 82,648,215- 82,734,211 bp), GSC (chr13: 10,120,630-10,122,701 bp), and *DICER1* (chr3: 9,803,946-9,876,750 bp), were related to reproduction. *SLX4* (Hamer and de Rooij, 2018), *TDRD6* (Vasileva et al., 2009), *SHOC1* (Zhang Q. et al., 2019), and *FBXW11* (O'Doherty et al., 2018) play important roles in the development of germ cells. The gene *TACR3* plays a key role in reproductive functions, and loss-of-function mutations in this gene can lead to hypogonadotropic hypogonadism and infertility in humans (Guran et al., 2009; Topaloglu et al., 2009; Young et al., 2010). *EPC2*, *GSC*, and *DICER1* genes are all important for the development of early embryos in animals and have been related to the reproduction traits (e.g., litter size) in swine and cattle (Kaczmarek et al., 2020; Chen J. et al., 2022; Chen Z. et al., 2022; Wang et al., 2022). The reproduction-related genes detected in this study were different from the genes detected in the signature selection study for response to Aleutian disease by Karimi et al. (2021). In that study, the genes *FBXO5*, *CATSPER4*, *GOT2*, and *CatSperβ* were annotated from the candidate selection regions and related to reproductive performance, which were not detected in our study. The different genomic data, grouping methods, and population structures could be the potential reasons that lead to the differences between these studies.

The KEGG pathway analyses of annotated genes detected only one significant ($q < 0.05$) pathway, the MAPK signaling pathway. The MAPK signaling pathway is involved in female reproductive performance by regulating the proliferation, differentiation, and apoptosis of granulosa cells in the follicle, ultimately affecting folliculogenesis and oocyte maturation (Zhang and Liu, 2002; Sun et al., 2016; Huang et al., 2022). The MAPK pathway also plays a role in regulating luteinizing hormone secretion, which stimulates ovulation and formation of the corpus luteum (Kahnamouyi et al., 2018). Additionally, MAPK signaling has been implicated in regulating the menstrual cycle and endometrial function (Zhou et al., 2010; Makieva et al., 2018). Meanwhile, previous studies found that abnormal MAPK signaling can cause reproductive disorders (e.g., infertility and embryonic death) in swine (Prochazka et al., 2012; Prochazka and Nemcova, 2019) and cattle (Sigdel et al., 2021; Tahir et al., 2021). The detection of the MAPK signaling pathway in this study may indicate that AD infection may lead to the disorder of the MAPK signaling pathway, therefore influencing female reproductive performance.

## 4.4 Common genes and ontology terms among all three traits

A total of 16 genes, *ARHGAP19*, *COL14A1*, *DEPTOR*, *EXOSC1*, *FAM135B*, *FRAT1*, *FRAT2*, *LOC122905718*, *MMS19*, *MRPL13*, *PGAM1*, *PTCHD4*, *RRP12*, *TBX18*, *UBTD1*, and *ZDHHC16*, were common to all three studied traits. From these, five genes were related to growth in livestock species in previous studies. For example, the gene *ARHGAP19* was found to be related to body weight in yak (Jiang et al., 2022); the gene *FAM135B* was related to body weight growth in cattle (Serão et al., 2013; Seabury et al., 2017), the genes *COL14A1* (Cardoso et al., 2018) and *PTCHD4* (Doyle et al., 2020) were found to play important roles in muscle development in cattle and swine, the gene *EXOSC1* (Dall'Olio et al., 2020; Ropka-Molik et al., 2018) has been related to muscle growth, and *PGAM1* was found to relate to the development of adipose tissue (Xing et al., 2019). Meanwhile, two genes, *FAM135B* (Serão et al., 2013; Seabury et al., 2017) and *COL14A1* (de Lima et al., 2020), were also found to be related to feed efficiency in cattle. In addition, several genes were found to be related to reproduction in previous studies. *UBTD1* (Kongmanas et al., 2015), *ZDHHC16* (Uzbekova et al., 2021; Caetano et al., 2023), *RRP12* (Tiensuu et al., 2019), *MMS19* (Tsai et al., 2017), and *PGAM1* (Zhang et al., 2015) genes were found to be associated with the development of germ cells. The genes *FAM135B* and *FRAT1* were detected to be associated with the reproductive performance in swine (Zhang Z. et al., 2019) and cows (Melo et al., 2017), respectively. The Tbx18 gene was related to mouse embryonic development (Wehn and Chapman, 2010).

Two GO terms, olfactory receptor activity (GO:0004984) and detection of chemical stimulus involved in sensory perception of smell (GO:0050911), were significant ($q < 0.05$) among all three studied traits. This may indicate that AD may influence the sense of smell in mink, although the relationship between AD and smell has not been reported in the literature. However, reduced appetite of infected mink seems to corroborate the loss of their sense of smell because the smell is vital for mink feeding behavior (Saunders, 1988). In American mink, Adney et al. (2022) speculated that individuals experimentally infected with SARS-CoV-2 may have altered sense of smell because they observed neutrophilic infiltrate in the olfactory epithelium. Thus, future studies could assess the condition of the olfactory epithelium of AD-infected mink to determine if infection could influence their sense of smell.

# 5 Conclusion

The detection of potential signatures of selection related to the response of American mink to AD provides valuable insights into

the genetic factors associated with the mink's immune response. The genes and GO terms detected from this study would enhance the understanding of genomic architecture underlying mink's resilience to AD and shed light on the underlying biological mechanisms involved. Meanwhile, the detection of numerous potential loci underlying the selection for responses to AD infection in this study indicated that genomic selection could be a feasible approach to reduce the adverse influence caused by AD. By incorporating the detected loci with the availability of the first Axiom Affymetrix Mink 70K panel, the mink industry could eradicate the adverse influences caused by AD by increasing the resilience of American mink to AMDV infection through genomic selection.

## Data availability statement

Due to confidentiality agreements with participating farms and industries, the datasets presented in this article are not suitable for public deposition. To access the dataset used in this research, the request should be directed to the corresponding author, YM.

## Ethics statement

The animal study was approved by the Dalhousie University Animal Care and Use Committee (certification#: 2018-009 and 2019-012). The study was conducted in accordance with the local legislation and institutional requirements.

## Author contributions

GH: conceptualization, data curation, formal analysis, methodology, validation, visualization, writing–original draft, and writing–review and editing. DD: data curation, formal analysis, methodology, validation, and writing–review and editing. GM: supervision and writing–review and editing. AK: supervision and writing–review and editing. MS: conceptualization, funding acquisition, software, and writing–review and editing. GP: conceptualization, funding acquisition, and writing–review and editing. ZW: conceptualization, funding acquisition and writing–review and editing. PD: data curation, validation, and writing–review and editing. YM: conceptualization, data curation, funding acquisition, methodology, project administration, resources, supervision, validation, and writing–review and editing.

## Funding

The author(s) declare financial support was received for the research, authorship, and/or publication of this article. Financial support was received from the Natural Sciences and Engineering Research Council of Canada (NSERC), Mitacs, Joint Mink Research Committee, Canada Mink Breeders Association, Nova Scotia Mink Breeders Association, Nova Scotia Department of Agriculture, Fur Commission USA, and Mink Veterinary Consulting Research and Services.

## Acknowledgments

The authors gratefully acknowledge the financial support from the Natural Sciences and Engineering Research Council of Canada (NSERC), Mitacs, Joint Mink Research Committee, Canada Mink Breeders Association, Nova Scotia Mink Breeders Association, Nova Scotia Department of Agriculture, Fur Commission USA, and Mink Veterinary Consulting Research and Services. They would also like to thank the Canadian Center for Fur Animal Research and Millbank Fur Farm staff for collecting and providing the data, and the members of Miar Lab (https://miarlab.ca/personnel) who helped in field data collection and molecular laboratory.

## Conflict of interest

MS is employed by Select Sires Inc. This organization did not play any role in the study design, data collection and analysis, decision to publish, or preparation of the manuscript.

The remaining authors declare that the research was conducted in the absence of any commercial or financial relationships that could be construed as a potential conflict of interest.

## Publisher's note



## Supplementary material

The Supplementary Material for this article can be found online at: https://www.frontiersin.org/articles/10.3389/fgene.2024.1370891/full#supplementary-material

## References

Aasted, B. (1989). Mink infected with Aleutian disease virus have an elevated level of CD8-positive T-lymphocytes. *Vet. Immunol. Immunopathol.* 20 (4), 375–385. doi:10.1016/0165-2427(89)90082-2

Aasted, B., Alexandersen, S., and Christensen, J. (1998). Vaccination with Aleutian mink disease parvovirus (AMDV) capsid proteins enhances disease, while vaccination with the major non-structural AMDV protein causes partial protection from disease. *Vaccine* 16 (11-12), 1158–1165. doi:10.1016/s0264-410x(98)80114-x

Adney, D. R., Lovaglio, J., Schulz, J. E., Yinda, C. K., Avanzato, V. A., Haddock, E., et al. (2022). Severe acute respiratory disease in American mink experimentally infected with SARS-CoV-2. *JCI Insight* 7 (22), e159573. doi:10.1172/jci.insight.159573

Agriculture_and_Marketing_of_Nova_Scotia_Government (1998). *Agriculture and marketing of Nova Scotia government, testing for aleutian disease in minks, 1998*. Halifax, Nova Scotia: Agriculture and Marketing of Nova Scotia Government. Available at: https://novascotia.ca/news/release/?id=19980120008.

Aki, T., Funakoshi, T., Nishida-Kitayama, J., and Mizukami, Y. (2008). TPRA40/GPR175 regulates early mouse embryogenesis through functional membrane transport by Sjögren's syndrome-associated protein NA14. *J. Cell. Physiol.* 217 (1), 194–206. doi:10.1002/jcp.21492

Alaynick, W. A., Kondo, R. P., Xie, W., He, W., Dufour, C. R., Downes, M., et al. (2007). ERRgamma directs and maintains the transition to oxidative metabolism in the postnatal heart. *Cell Metab.* 6 (1), 13–24. doi:10.1016/j.cmet.2007.06.007

Almén, M. S., Jacobsson, J. A., Shaik, J. H. A., Olszewski, P. K., Cedernaes, J., Alsiö, J., et al. (2010). The obesity gene, TMEM18, is of ancient origin, found in majority of neuronal cells in all major brain regions and associated with obesity in severely obese children. *BMC Med. Genet.* 11 (1), 58. doi:10.1186/1471-2350-11-58

Belkina, A. C., and Denis, G. V. (2012). BET domain co-regulators in obesity, inflammation and cancer. *Nat. Rev. Cancer* 12 (7), 465–477. doi:10.1038/nrc3256

Berruien, N. N. A., and Smith, C. L. (2020). Emerging roles of melanocortin receptor accessory proteins (MRAP and MRAP2) in physiology and pathophysiology. *Gene* 757, 144949. doi:10.1016/j.gene.2020.144949

Bertolini, F., Servin, B., Talenti, A., Rochat, E., Kim, E. S., Oget, C., et al. (2018). Signatures of selection and environmental adaptation across the goat genome post-domestication. *Genet. Sel. Evol.* 50 (1), 57–24. doi:10.1186/s12711-018-0421-y

Bloom, M. E., Alexandersen, S., Perryman, S., Lechner, D., and Wolfinbarger, J. B. (1988). Nucleotide sequence and genomic organization of Aleutian mink disease parvovirus (ADV): sequence comparisons between a nonpathogenic and a pathogenic strain of ADV. *J. Virology* 62 (8), 2903–2915. doi:10.1128/JVI.62.8.2903-2915.1988

Bloom, M. E., Best, S. M., Hayes, S. F., Wells, R. D., Wolfinbarger, J. B., McKenna, R., et al. (2001). Identification of Aleutian mink disease parvovirus capsid sequences mediating antibody-dependent enhancement of infection, virus neutralization, and immune complex formation. *J. Virol.* 75 (22), 11116–11127. doi:10.1128/JVI.75.22.11116-11127.2001

Bloom, M. E., Kanno, H., Mori, S., and Wolfinbarger, J. B. (1994). Aleutian mink disease: puzzles and paradigms. *Infect. Agents Dis.* 3 (6), 279–301.

Browning, B. L., Zhou, Y., and Browning, S. R. (2018). A one-penny imputed genome from next-generation reference panels. *Am. J. Hum. Genet.* 103 (3), 338–348. doi:10.1016/j.ajhg.2018.07.015

Caetano, L. C., Verruma, C. G., Pinaffi, F. L. V., Jardim, I. B., Furtado, G. P., Silva, L. A., et al. (2023). *In vivo* and *in vitro* matured bovine oocytes present a distinct pattern of single-cell gene expression. *Zygote* 31 (1), 31–43. doi:10.1017/S0967199422000478

Cardoso, D. F., de Albuquerque, L. G., Reimer, C., Qanbari, S., Erbe, M., do Nascimento, A. V., et al. (2018). Genome-wide scan reveals population stratification and footprints of recent selection in Nelore cattle. *Genet. Sel. Evol.* 50 (1), 22. doi:10.1186/s12711-018-0381-2

Chen, J., Wu, Z., Chen, R., Huang, Z., Han, X., Qiao, R., et al. (2022a). Identification of genomic regions and candidate genes for litter traits in French large white pigs using genome-wide association studies. *Animals* 12 (12), 1584. doi:10.3390/ani12121584

Chen, Z., Zhang, Z., Wang, Z., Zhang, Z., Wang, Q., and Pan, Y. (2022b). Heterozygosity and homozygosity regions affect reproductive success and the loss of reproduction: a case study with litter traits in pigs. *Comput. Struct. Biotechnol. J.* 20, 4060–4071. doi:10.1016/j.csbj.2022.07.039

Cho, H. J., and Ingram, D. G. (1973). Pathogenesis of aleutian disease of mink: nature of the antiglobulin reaction and elution of antibody from erythrocytes and glomeruli of infected mink. *Infect. Immun.* 8 (2), 264–271. doi:10.1128/iai.8.2.264-271.1973

Dailey, M. J., and Moran, T. H. (2013). Glucagon-like peptide 1 and appetite. *Trends Endocrinol. Metab.* 24 (2), 85–91. doi:10.1016/j.tem.2012.11.008

Dall'Olio, S., Schiavo, G., Gallo, M., Bovo, S., Bertolini, F., Buttazzoni, L., et al. (2020). Candidate gene markers associated with production, carcass and meat quality traits in Italian Large White pigs identified using a selective genotyping approach. *Livest. Sci.* 240, 104145. doi:10.1016/j.livsci.2020.104145

Danecek, P., Auton, A., Abecasis, G., Albers, C., Banks, E., DePristo, M., et al. (2011). The variant call format and VCFtools. *Bioinformatics* 27 (15), 2156–2158. doi:10.1093/bioinformatics/btr330

Davoudi, P., Do, D. N., Colombo, S., Rathgeber, B., Hu, G., Sargolzaei, M., et al. (2022). Genetic and phenotypic parameters for feed efficiency and component traits in American mink. *J. Anim. Sci.* 100 (8), skac216. doi:10.1093/jas/skac216

Decout, A., Katz, J. D., Venkatraman, S., and Ablasser, A. (2021). The cGAS–STING pathway as a therapeutic target in inflammatory diseases. *Nat. Rev. Immunol.* 21 (9), 548–569. doi:10.1038/s41577-021-00524-z

de Lima, A. O., Koltes, J. E., Diniz, W. J. S., de Oliveira, P. S. N., Cesar, A. S. M., Tizioto, P. C., et al. (2020). Potential biomarkers for feed efficiency-related traits in nelore cattle identified by Co-expression network and integrative genomics analyses. *Front. Genet.* 11, 189. doi:10.3389/fgene.2020.00189

Do, D. N., Karimi, K., Sargolzaei, M., Plastow, G., Wang, Z., and Miar, Y. (2023). PSXII-10 development of a 70k snp genotyping array for American mink (neogale vison). *J. Anim. Sci.* 101 (3), 350–351. doi:10.1093/jas/skad281.416

Do, D. N., Karimi, K., Sargolzaei, M., Plastow, G., Wang, Z., and Miar, Y. (2024). *Development of a 70K SNP genotyping array for American mink (Neogale vison)*. Under preparation.

Doyle, J. L., Berry, D. P., Veerkamp, R. F., Carthy, T. R., Evans, R. D., Walsh, S. W., et al. (2020). Genomic regions associated with muscularity in beef cattle differ in five contrasting cattle breeds. *Genet. Sel. Evol.* 52 (1), 2. doi:10.1186/s12711-020-0523-1

Ellis, L. C. (1996). Melatonin reduces mortality from Aleutian disease in mink (Mustela vison). *J. Pineal Res.* 21 (4), 214–217. doi:10.1111/j.1600-079x.1996.tb00288.x

Elzhov, T. V., Mullen, K. M., Spiess, A., and Bolker, B. (2016). Package 'minpack. Lm'. Title R interface to the levenberg-marquardt nonlinear least-squares algorithm found in MINPACK. *Plus support bounds* 1, 2–1.

Farid, A., Daftarian, P., and Fatehi, J. (2018). Transmission dynamics of Aleutian mink disease virus on a farm under test and removal scheme. *J. Vet. Sci. Med. Diagn.* 7 (2). doi:10.4172/2325-9590.1000253

Farid, A., and Ferns, L. (2011). Aleutian mink disease virus infection may cause hair depigmentation. *Scientifur* 35 (3/4), 55–59.

Farid, A., and Ferns, L. (2017). Reduced severity of histopathological lesions in mink selected for tolerance to Aleutian mink disease virus infection. *Res. Vet. Sci.* 111, 127–134. doi:10.1016/j.rvsc.2017.02.009

Farid, A., and Rupasinghe, P. P. (2016). Accuracy of enzyme-linked immunosorbent assays for quantification of antibodies against Aleutian mink disease virus. *J. Virol. Methods* 235, 144–151. doi:10.1016/j.jviromet.2016.06.004

Fu, G., Vallée, S., Rybakin, V., McGuire, M. V., Ampudia, J., Brockmeyer, C., et al. (2009). Themis controls thymocyte selection through regulation of T cell antigen receptor-mediated signaling. *Nat. Immunol.* 10 (8), 848–856. doi:10.1038/ni.1766

García-Bermúdez, M., López-Mejías, R., Genre, F., Castañeda, S., Corrales, A., Llorca, J., et al. (2015). Lack of association between JAK3 gene polymorphisms and cardiovascular disease in Spanish patients with rheumatoid arthritis. *Biomed. Res. Int.* 2015, 318364. doi:10.1155/2015/318364

Gordon, D. A., Franklin, A. E., and Karstad, L. (1967). Viral plasmacytosis (Aleutian disease) of mink resembling human collagen disease. *Can. Med. Assoc. J.* 96 (18), 1245–1251.

Guran, T., Tolhurst, G., Bereket, A., Rocha, N., Porter, K., Turan, S., et al. (2009). Hypogonadotropic hypogonadism due to a novel missense mutation in the first extracellular loop of the neurokinin B receptor. *J. Clin. Endocrinol. Metab.* 94 (10), 3633–3639. doi:10.1210/jc.2009-0551

Guyonneau, L., Murisier, F., Rossier, A., Moulin, A., and Beermann, F. (2004). Melanocytes and pigmentation are affected in dopachrome tautomerase knockout mice. *Mol. Cell Biol.* 24 (8), 3396–3403. doi:10.1128/mcb.24.8.3396-3403.2004

Hamer, G., and de Rooij, D. G. (2018). Mutations causing specific arrests in the development of mouse primordial germ cells and gonocytes. *Biol. Reprod.* 99 (1), 75–86. doi:10.1093/biolre/ioy075

Haupt, A., Thamer, C., Heni, M., Machicao, F., Machann, J., Schick, F., et al. (2010). Novel obesity risk loci do not determine distribution of body fat depots: a whole-body MRI/MRS study. *Obesity* 18 (6), 1212–1217. doi:10.1038/oby.2009.413

Henson, J., Gorham, J., and Leader, R. (1962). Field test for Aleutian disease. *Natl. Fur News* 34 (2), 8–9.

Hsu, A. P., Dowdell, K. C., Davis, J., Niemela, J. E., Anderson, S. M., Shaw, P. A., et al. (2012). Autoimmune lymphoproliferative syndrome due to FAS mutations outside the signal-transducing death domain: molecular mechanisms and clinical penetrance. *Genet. Med.* 14 (1), 81–89. doi:10.1038/gim.0b013e3182310b7d

Hu, G., Do, D. N., Davoudi, P., Manafiazar, G., Kelvin, A. A., Plastow, G., et al. (2022). Genetic and phenotypic correlations between Aleutian disease tests with body weight, growth, and feed efficiency traits in mink. *J. Anim. Sci.* 100 (12), skac346. doi:10.1093/jas/skac346

Hu, G., Do, D. N., Karimi, K., and Miar, Y. (2021). Genetic and phenotypic parameters for Aleutian disease tests and their correlations with pelt quality, reproductive performance, packed-cell volume, and harvest length in mink. *J. Anim. Sci.* 99 (8), skab216–12. doi:10.1093/jas/skab216

Hu, G., Do, D. N., Manafiazar, G., Kelvin, A. A., Sargolzaei, M., Plastow, G., et al. (2023). Population genomics of American mink using genotype data. *Front. Genet.* 14, 1175408. doi:10.3389/fgene.2023.1175408

Huang, Y., Wang, J., Zhan, Z., Cao, X., Sun, Y., Lan, X., et al. (2013). Assessment of association between variants and haplotypes of the IGF2 gene in beef cattle. *Gene* 528 (2), 139–145. doi:10.1016/j.gene.2013.07.035

Huang, Z., Tian, Z., Zhao, Y., Zhu, F., Liu, W., and Wang, X. (2022). MAPK signaling pathway is essential for female reproductive regulation in the cabbage beetle, colaphellus bowringi. *Cells* 11 (10), 1602. doi:10.3390/cells11101602

Ibrahim, A. H. M. (2015). The prkag3 gene polymorphisms and their associtations with growth performance and body indices in barki lambs. *Egypt. J. Sheep Goat Sci.* 10 (3), 1–14. doi:10.12816/0025811

Jensen, P. V., Castelruiz, Y., and Aasted, B. (2003). Cytokine profiles in adult mink infected with aleutian mink disease parvovirus. *J. Virol.* 77 (13), 7444–7451. doi:10.1128/jvi.77.13.7444-7451.2003

Jensen, T. H., Chriél, M., and Hansen, M. S. (2016). Progression of experimental chronic Aleutian mink disease virus infection. *Acta Vet. Scand.* 58 (1), 35. doi:10.1186/s13028-016-0214-7

Jepsen, J. R., d'Amore, F., Baandrup, U., Clausen, M. R., Gottschalck, E., and Aasted, B. (2009). Aleutian mink disease virus and humans. *Emerg. Infect. Dis.* 15 (12), 2040–2042. doi:10.3201/eid1512.090514

Jiang, H., Chai, Z., Cao, H., Zhang, C., Zhu, Y., Zhang, Q., et al. (2022). Genome-wide identification of SNPs associated with body weight in yak. *BMC Genom* 23 (1), 833. doi:10.1186/s12864-022-09077-4

June, C. H., Ledbetter, J. A., Gillespie, M. M., Lindsten, T., and Thompson, C. B. (1987). T-cell proliferation involving the CD28 pathway is associated with cyclosporine-resistant interleukin 2 gene expression. *Mol. Cell Biol.* 7 (12), 4472–4481. doi:10.1128/mcb.7.12.4472

Kaczmarek, M. M., Najmula, J., Guzewska, M. M., and Przygrodzka, E. (2020). MiRNAs in the peri-implantation period: contribution to embryo-maternal communication in pigs. *Int. J. Mol. Sci.* 21 (6), 2229. doi:10.3390/ijms21062229

Kahnamouyi, S., Nouri, M., Farzadi, L., Darabi, M., Hosseini, V., and Mehdizadeh, A. (2018). The role of mitogen-activated protein kinase-extracellular receptor kinase pathway in female fertility outcomes: a focus on pituitary gonadotropins regulation. *Ther. Adv. Endocrinol. Metab.* 9 (7), 209–215. doi:10.1177/2042018818772775

Kanno, H., Wolfinbarger, J. B., and Bloom, M. E. (1993). Aleutian mink disease parvovirus infection of mink macrophages and human macrophage cell line U937: demonstration of antibody-dependent enhancement of infection. *J. Virol.* 67 (12), 7017–7024. doi:10.1128/JVI.67.12.7017-7024.1993

Karimi, K., Do, D. N., Wang, J., Easley, J., Borzouie, S., Sargolzaei, M., et al. (2022). A chromosome-level genome assembly reveals genomic characteristics of the American mink (Neogale vison). *Commun. Biol.* 5 (1), 1381. doi:10.1038/s42003-022-04341-5

Karimi, K., Farid, A. H., Myles, S., and Miar, Y. (2021). Detection of selection signatures for response to Aleutian mink disease virus infection in American mink. *Sci. Rep.* 11 (1), 2944. doi:10.1038/s41598-021-82522-8

Knuuttila, A., Aronen, P., Saarinen, A., and Vapalahti, O. (2009). Development and evaluation of an enzyme-linked immunosorbent assay based on recombinant VP2 capsids for the detection of antibodies to aleutian mink disease virus. *Clin. Vaccine Immunol.* 16 (9), 1360–1365. doi:10.1128/CVI.00148-09

Kongmanas, K., Kruevaisayawan, H., Saewu, A., Sugeng, C., Fernandes, J., Souda, P., et al. (2015). Proteomic characterization of pig sperm anterior head plasma membrane reveals roles of acrosomal proteins in ZP3 binding. *J. Cell. Physiol.* 230 (2), 449–463. doi:10.1002/jcp.24728

Kreitman, M. (2000). Methods to detect selection in populations with applications to the human. *Annu. Rev. Genomics Hum. Genet.* 1, 539–559. doi:10.1146/annurev.genom.1.1.539

Läubli, H., and Varki, A. (2020). Sialic acid–binding immunoglobulin-like lectins (Siglecs) detect self-associated molecular patterns to regulate immune responses. *Cell. Mol. Life Sci.* 77 (4), 593–605. doi:10.1007/s00018-019-03288-x

Levin, C., Koren, A., Pretorius, E., Rosenberg, N., Shenkman, B., Hauschner, H., et al. (2015). Deleterious mutation in the FYB gene is associated with congenital autosomal recessive small-platelet thrombocytopenia. *J. Thromb. Haemost.* 13 (7), 1285–1292. doi:10.1111/jth.12966

Li, R., Li, C., Chen, H., Li, R., Chong, Q., Xiao, H., et al. (2020). Genome-wide scan of selection signatures in Dehong humped cattle for heat tolerance and disease resistance. *Anim. Genet.* 51 (2), 292–299. doi:10.1111/age.12896

Li, W., Li, J., Gao, X., Xu, S., and Yue, W. (2012). Association analysis of PRKAG3 gene variants with carcass and meat quality traits in beef cattle. *Afr. J. Biotechnol.* 11 (8), 1855–1861. doi:10.5897/ajb11.2454

Liu, W., Taso, O., Wang, R., Bayram, S., Graham, A. C., Garcia-Reitboeck, P., et al. (2020). Trem2 promotes anti-inflammatory responses in microglia and is suppressed under pro-inflammatory conditions. *Hum. Mol. Genet.* 29 (19), 3224–3248. doi:10.1093/hmg/ddaa209

Ma, W., Ma, Y., Liu, D., Gao, Y., Sun, X. m., Li, A. M., et al. (2012). Novel SNPs in the bovine Transmembrane protein 18 gene, their linkage and their associations with growth traits in Nanyang cattle. *Genes & Genomics* 34 (6), 591–597. doi:10.1007/s13258-012-0034-8

Ma, Y., Ding, X., Qanbari, S., Weigend, S., Zhang, Q., and Simianer, H. (2015). Properties of different selection signature statistics and a new strategy for combining them. *Heredity* 115 (5), 426–436. doi:10.1038/hdy.2015.42

Makieva, S., Giacomini, E., Ottolina, J., Sanchez, A. M., Papaleo, E., and Viganò, P. (2018). Inside the endometrial cell signaling subway: mind the gap(s). *Int. J. Mol. Sci.* 19 (9), 2477. doi:10.3390/ijms19092477

McGuire, T. C., Perryman, L. E., and Gorham, J. R. (1979). Mechanisms of anemia in Aleutian disease viral infection of mink. *Vet. Microbiol.* 4 (1), 17–27. doi:10.1016/0378-1135(79)90026-9

Melo, T. P. d., de Camargo, G. M. F., de Albuquerque, L. G., and Carvalheiro, R. (2017). Genome-wide association study provides strong evidence of genes affecting the reproductive performance of Nellore beef cows. *PLOS ONE* 12 (5), e0178551. doi:10.1371/journal.pone.0178551

Nei, M., and Li, W. (1979). Mathematical model for studying genetic variation in terms of restriction endonucleases. *Proc. Natl. Acad. Sci.* 76 (10), 5269–5273. doi:10.1073/pnas.76.10.5269

O'Doherty, A. M., O'Brien, Y. M., Browne, J. A., Wingfield, M., and O'Shea, L. C. (2018). Expression of granulosa cell microRNAs, AVEN and ATRX are associated with human blastocyst development. *Mol. Reprod. Dev.* 85 (11), 836–848. doi:10.1002/mrd.22990

Percie du Sert, N., Hurst, V., Ahluwalia, A., Alam, S., Avey, M. T., Baker, M., et al. (2020). The ARRIVE guidelines 2.0: updated guidelines for reporting animal research. *PLOS Biol.* 18 (7), e3000410. doi:10.1371/journal.pbio.3000410

Porter, D. D., and Cho, H. J. (1980). "Aleutian disease of mink: a model for persistent infection," in *Comprehensive virology: vol. 16: virus-host interactions: viral invasion, persistence, and disease*. Editors H. Fraenkael-Conrat and R. R. Wagner (Boston, MA: Springer US).

Porter, D. D., Larsen, A. E., and Porter, H. G. (1969). The pathogenesis of Aleutian disease of mink: I. *in vivo* viral replication and the host antibody response to viral antigen. *J. Exp. Med.* 130 (3), 575–593. doi:10.1084/jem.130.3.575

Porter, D. D., Larsen, A. E., and Porter, H. G. (1972). The pathogenesis of aleutian disease of mink. *J. Immunol.* 109 (1), 1–7. doi:10.4049/jimmunol.109.1.1

Porter, D. D., Larsen, A. E., and Porter, H. G. (1973). The pathogenesis of Aleutian disease of mink. 3. Immune complex arteritis. *Am. J. Pathol.* 71 (2), 331–344.

Porter, H. G., Porter, D. D., and Larsen, A. E. (1982). Aleutian disease in ferrets. *Infect. Immun.* 36 (1), 379–386. doi:10.1128/IAI.36.1.379-386.1982

Prochazka, R., Blaha, M., and Nemcova, L. (2012). Signaling pathways regulating FSH- and amphiregulin-induced meiotic resumption and cumulus cell expansion in the pig. *Reproduction* 144 (5), 535–546. doi:10.1530/REP-12-0191

Prochazka, R., and Nemcova, L. (2019). Mechanisms of FSH- and amphiregulin-induced MAP kinase 3/1 activation in pig cumulus-oocyte complexes during maturation *in vitro*. *Int. J. Mol. Sci.* 20 (5), 1179. doi:10.3390/ijms20051179

Purcell, S., Neale, B., Todd-Brown, K., Thomas, L., Ferreira, M. A. R., Bender, D., et al. (2007). PLINK: a tool set for whole-genome association and population-based linkage analyses. *Am. J. Hum. Genet.* 81 (3), 559–575. doi:10.1086/519795

Qanbari, S., and Simianer, H. (2014). Mapping signatures of positive selection in the genome of livestock. *Livest. Sci.* 166, 133–143. doi:10.1016/j.livsci.2014.05.003

Quinlan, A. R. (2014). BEDTools: the Swiss-army tool for genome feature analysis. *Curr. Protoc. Bioinform.* 47, 11–34. doi:10.1002/0471250953.bi1112s47

Rask-Andersen, M., Jacobsson, J. A., Moschonis, G., Chavan, R. A., Sikder, M. A. N., Allzén, E., et al. (2012). Association of TMEM18 variants with BMI and waist circumference in children and correlation of mRNA expression in the PFC with body weight in rats. *Eur. J. Hum. Genet.* 20 (2), 192–197. doi:10.1038/ejhg.2011.176

Rea, I. M., Gibson, D. S., McGilligan, V., McNerlan, S. E., Alexander, H. D., and Ross, O. A. (2018). Age and age-related diseases: role of inflammation triggers and cytokines. *Front. Immunol.* 9, 586. doi:10.3389/fimmu.2018.00586

Reichert, M., and Kostro, K. (2014). Effect of persistent infection of mink with Aleutian mink disease virus on reproductive failure. *Bull. Vet. Inst. Pulawy.* 58 (3), 369–373. doi:10.2478/bvip-2014-0057

Ropka-Molik, K., Bereta, A., Żukowski, K., Tyra, M., Piórkowska, K., Żak, G., et al. (2018). Screening for candidate genes related with histological microstructure, meat quality and carcass characteristic in pig based on RNA-seq data. *Asian-Australas J. Anim. Sci.* 31 (10), 1565–1574. doi:10.5713/ajas.17.0714

Ryan, M. T., Hamill, R. M., O'Halloran, A. M., Davey, G. C., McBryan, J., Mullen, A. M., et al. (2012). SNP variation in the promoter of the PRKAG3 gene and association with meat quality traits in pig. *BMC Genet.* 13, 66. doi:10.1186/1471-2156-13-66

Sabeti, P. C., Varilly, P., Fry, B., Lohmueller, J., Hostetter, E., Cotsapas, C., et al. (2007). Genome-wide detection and characterization of positive selection in human populations. *Nature* 449, 913–918. doi:10.1038/nature06250

Sandhu, M. S., Gibson, J. M., Heald, A. H., Dunger, D. B., and Wareham, N. J. (2003). Low circulating IGF-II concentrations predict weight gain and obesity in humans. *Diabetes* 52 (6), 1403–1408. doi:10.2337/diabetes.52.6.1403

Santer, D. M., Wiedeman, A. E., Teal, T. H., Ghosh, P., and Elkon, K. B. (2012). Plasmacytoid dendritic cells and C1q differentially regulate inflammatory gene induction by lupus immune complexes. *J. Immunol.* 188 (2), 902–915. doi:10.4049/jimmunol.1102797

Saravanan, K. A., Panigrahi, M., Kumar, H., Parida, S., Bhushan, B., Gaur, G. K., et al. (2021). Genomic scans for selection signatures revealed candidate genes for adaptation and production traits in a variety of cattle breeds. *Genomics* 113 (3), 955–963. doi:10.1016/j.ygeno.2021.02.009

Saunders, D. A. (1988). *Adirondack mammals*. Syracuse, New York: State University of New York, College of Environmental Science and Forestry.

Seabury, C. M., Oldeschulte, D. L., Saatchi, M., Beever, J. E., Decker, J. E., Halley, Y. A., et al. (2017). Genome-wide association study for feed efficiency and growth traits in U.S. beef cattle. *BMC Genom* 18 (1), 386. doi:10.1186/s12864-017-3754-y

Seo, H., Chen, J., González-Avalos, E., Samaniego-Castruita, D., Das, A., Wang, Y. H., et al. (2019). TOX and TOX2 transcription factors cooperate with NR4A transcription factors to impose CD8+ T cell exhaustion. *Proc. Natl. Acad. Sci.* 116 (25), 12410–12415. doi:10.1073/pnas.1905675116

Serão, N. V. L., González-Peña, D., Beever, J. E., Faulkner, D. B., Southey, B. R., and Rodriguez-Zas, S. L. (2013). Single nucleotide polymorphisms and haplotypes associated with feed efficiency in beef cattle. *BMC Genet.* 14 (1), 94. doi:10.1186/1471-2156-14-94

Serwas, N. K., Hoeger, B., Ardy, R. C., Stulz, S. V., Sui, Z., Memaran, N., et al. (2019). Human DEF6 deficiency underlies an immunodeficiency syndrome with systemic autoimmunity and aberrant CTLA-4 homeostasis. *Nat. Commun.* 10 (1), 3106. doi:10.1038/s41467-019-10812-x

Sigdel, A., Bisinotto, R. S., and Peñagaricano, F. (2021). Genes and pathways associated with pregnancy loss in dairy cattle. *Sci. Rep.* 11 (1), 13329. doi:10.1038/s41598-021-92525-0

Spinazzi, R., Andreis, P. G., Rossi, G. P., and Nussdorfer, G. G. (2006). Orexins in the regulation of the hypothalamic-pituitary-adrenal Axis. *Pharmacol. Rev.* 58 (1), 46–57. doi:10.1124/pr.58.1.4

Stolze, B., and Kaaden, O. (1987). Apparent lack of neutralizing antibodies in aleutian disease is due to masking of antigenic sites by phospholipids. *Virology* 158 (1), 174–180. doi:10.1016/0042-6822(87)90251-0

Stubbs, V. E., Power, C., and Patel, K. D. (2010). Regulation of eotaxin-3/CCL26 expression in human monocytic cells. *Immunology* 130 (1), 74–82. doi:10.1111/j.1365-2567.2009.03214.x

Sun, M. J., Zhu, S., Li, Y. W., Lin, J., Gong, S., Jiao, G. Z., et al. (2016). An essential role for the intra-oocyte MAPK activity in the NSN-to-SN transition of germinal vesicle chromatin configuration in porcine oocytes. *Sci. Rep.* 6, 23555. doi:10.1038/srep23555

Tahir, M. S., Porto-Neto, L. R., Gondro, C., Shittu, O. B., Wockner, K., Tan, A. W. L., et al. (2021). Meta-analysis of heifer traits identified reproductive pathways in *Bos indicus* cattle. *Genes (Basel)* 12 (5), 768. doi:10.3390/genes12050768

Team, R. C. (2022). *R: a language and environment for statistical computing*. Vienna, Austria: R Foundation for Statistical Computing.

Thomas, P. D., Campbell, M. J., Kejariwal, A., Mi, H., Karlak, B., Daverman, R., et al. (2003). PANTHER: a library of protein families and subfamilies indexed by function. *Genome. Res.* 13 (9), 2129–2141. doi:10.1101/gr.772403

Tiensuu, H., Haapalainen, A. M., Karjalainen, M. K., Pasanen, A., Huusko, J. M., Marttila, R., et al. (2019). Risk of spontaneous preterm birth and fetal growth associates with fetal SLIT2. *PLoS Genet.* 15 (6), e1008107. doi:10.1371/journal.pgen.1008107

Topaloglu, A. K., Reimann, F., Guclu, M., Yalin, A. S., Kotan, L. D., Porter, K. M., et al. (2009). TAC3 and TACR3 mutations in familial hypogonadotropic hypogonadism reveal a key role for Neurokinin B in the central control of reproduction. *Nat. Genet.* 41 (3), 354–358. doi:10.1038/ng.306

Torres, R., Szpiech, Z. A., and Hernandez, R. D. (2018). Human demographic history has amplified the effects of background selection across the genome. *PLoS Genet.* 14 (6), e1007387. doi:10.1371/journal.pgen.1007387

Tsai, T. S., Johnson, J., White, Y., and John, J. C. (2017). The molecular characterization of porcine egg precursor cells. *Oncotarget* 8 (38), 63484–63505. doi:10.18632/oncotarget.18833

Turner, P., Buijs, S., Rommers, J. M., and M, T. (2013). *The code of practice for the care and handling of farmed mink, vol. 58*. Rexdale: The National Farm Animal Care Council.

Uzbekova, S., Teixeira-Gomes, A.-P., Marestaing, A., Jarrier-Gaillard, P., Papillier, P., Shedova, E. N., et al. (2021). Protein palmitoylation in bovine ovarian follicle. *Int. J. Mol. Sci.* 22 (21), 11757. doi:10.3390/ijms222111757

Van Dyck, F., Declercq, J., Braem, C. V., and Van de Ven, W. J. (2007). PLAG1, the prototype of the PLAG gene family: versatility in tumour development (review). *Int. J. Oncol.* 30 (4), 765–774. doi:10.3892/ijo.30.4.765

Van Laere, A. S., Nguyen, M., Braunschweig, M., Nezer, C., Collette, C., Moreau, L., et al. (2003). A regulatory mutation in IGF2 causes a major QTL effect on muscle growth in the pig. *Nature* 425 (6960), 832–836. doi:10.1038/nature02064

Vasileva, A., Tiedau, D., Firooznia, A., Müller-Reichert, T., and Jessberger, R. (2009). Tdrd6 is required for spermiogenesis, chromatoid body architecture, and regulation of miRNA expression. *Curr. Biol.* 19 (8), 630–639. doi:10.1016/j.cub.2009.02.047

Voz, M. L., Agten, N. S., Van de Ven, W. J., and Kas, K. (2000). PLAG1, the main translocation target in pleomorphic adenoma of the salivary glands, is a positive regulator of IGF-II. *Cancer Res.* 60 (1), 106–113.

Wang, X., Wang, L., Shi, L., Zhang, P., Li, Y., Li, M., et al. (2022). GWAS of reproductive traits in large white pigs on chip and imputed whole-genome sequencing data. *Int. J. Mol. Sci.* 23 (21), 13338. doi:10.3390/ijms232113338

Wang, Y., Ning, X., Gao, P., Wu, S., Sha, M., Lv, M., et al. (2017). Inflammasome activation triggers caspase-1-mediated cleavage of cGAS to regulate responses to DNA virus infection. *Immunity* 46 (3), 393–404. doi:10.1016/j.immuni.2017.02.011

Wehn, A. K., and Chapman, D. L. (2010). Tbx18 and Tbx15 null-like phenotypes in mouse embryos expressing Tbx6 in somitic and lateral plate mesoderm. *Dev. Biol.* 347 (2), 404–413. doi:10.1016/j.ydbio.2010.09.001

Wei, Q., Gu, Y. F., Zhang, Q. J., Yu, H., Peng, Y., Williams, K. W., et al. (2018). Lztfl1/BBS17 controls energy homeostasis by regulating the leptin signaling in the hypothalamic neurons. *J. Mol. Cell Biol.* 10 (5), 402–410. doi:10.1093/jmcb/mjy022

Weir, B. S., and Cockerham, C. C. (1984). Estimating F-statistics for the analysis of population structure. *Evolution* 38, 1358–1370. doi:10.1111/j.1558-5646.1984.tb05657.x

Wilson, K. C., Center, D. M., and Cruikshank, W. W. (2004). The effect of interleukin-16 and its precursor on T lymphocyte activation and growth. *Growth factors.* 22 (2), 97–104. doi:10.1080/08977190410001704679

Xia, J., Gravato-Nobre, M., and Ligoxygakis, P. (2019). Convergence of longevity and immunity: lessons from animal models. *Biogerontology* 20 (3), 271–278. doi:10.1007/s10522-019-09801-w

Xing, K., Wang, K., Ao, H., Chen, S., Tan, Z., Wang, Y., et al. (2019). Comparative adipose transcriptome analysis digs out genes related to fat deposition in two pig breeds. *Sci. Rep.* 9 (1), 12925. doi:10.1038/s41598-019-49548-5

Xu, X., Hua, X., Brown, K., Ren, X., and Zhang, Z. (2022). Mcm2 promotes stem cell differentiation via its ability to bind H3-H4. *eLife* 11, e80917. doi:10.7554/eLife.80917

Xu, Z., Sun, H., Zhang, Z., Zhang, C. Y., Zhao, Q. B., Xiao, Q., et al. (2020). Selection signature reveals genes associated with susceptibility loci affecting respiratory disease due to pleiotropic and hitchhiking effect in Chinese indigenous pigs. *Asian-Australas J. Anim. Sci.* 33 (2), 187–196. doi:10.5713/ajas.18.0658

Young, J., Bouligand, J., Francou, B., Raffin-Sanson, M. L., Gaillez, S., Jeanpierre, M., et al. (2010). TAC3 and TACR3 defects cause hypothalamic congenital hypogonadotropic hypogonadism in humans. *J. Clin. Endocrinol. Metab.* 95 (5), 2287–2295. doi:10.1210/jc.2009-2600

Yu, G., Wang, L.-G., Han, Y., and He, Q.-Y. (2012). clusterProfiler: an R Package for comparing biological themes among gene clusters. *OMICS J. Integr. Biol.* 16 (5), 284–287. doi:10.1089/omi.2011.0118

Zhang, K., Kniazeva, M., Han, M., Li, W., Yu, Z., Yang, Z., et al. (2001). A 5-bp deletion in ELOVL4 is associated with two related forms of autosomal dominant macular dystrophy. *Nat. Genet.* 27 (1), 89–93. doi:10.1038/83817

Zhang, Q., Ji, S., Busayavalasa, K., and Yu, C. (2019a). SPO16 binds SHOC1 to promote homologous recombination and crossing-over in meiotic prophase I. *Sci. Adv.* 5 (1), eaau9780. doi:10.1126/sciadv.aau9780

Zhang, S., Zhao, Y., Lei, B., Li, C., and Mao, X. (2015). PGAM1 is involved in spermatogenic dysfunction and affects cell proliferation, apoptosis, and migration. *Reprod. Sci.* 22 (10), 1236–1242. doi:10.1177/1933719115572485

Zhang, W., and Liu, H. T. (2002). MAPK signal pathways in the regulation of cell proliferation in mammalian cells. *Cell Res.* 12 (1), 9–18. doi:10.1038/sj.cr.7290105

Zhang, Z., Chen, Z., Ye, S., He, Y., Huang, S., Yuan, X., et al. (2019b). Genome-wide association study for reproductive traits in a duroc pig population. *Animals* 9 (10), 732. doi:10.3390/ani9100732

Zhou, W. D., Chen, Q. H., and Chen, Q. X. (2010). The action of p38 MAP kinase and its inhibitors on endometriosis. *Yao Xue Xue Bao* 45 (5), 548–554.

frontiers | Frontiers in Veterinary Science

TYPE Original Research
PUBLISHED 23 September 2024
DOI 10.3389/fvets.2024.1432269



OPEN ACCESS

EDITED BY
Izhar Hyder Qazi,
Shaheed Benazir Bhutto University of Veterinary & Animal Sciences, Pakistan

REVIEWED BY
Nikolai Kolba,
Cornell University, United States
Sarah C. Pearce,
United States Department of Agriculture, United States

*CORRESPONDENCE
Yi Ding
dingyi@mail.hzau.edu.cn

RECEIVED 16 May 2024
ACCEPTED 03 September 2024
PUBLISHED 23 September 2024

CITATION
Li M, Abouelfetouh MM, Salah E, Kiani FA, Nan S, Ding M and Ding Y (2024) Chicory supplementation improves growth performance in juvenile ostriches potentially by attenuating enteritis.
*Front. Vet. Sci.* 11:1432269.
doi: 10.3389/fvets.2024.1432269



# Chicory supplementation improves growth performance in juvenile ostriches potentially by attenuating enteritis

Meng Li[1,2], Mahmoud M. Abouelfetouh[1,3], Eman Salah[4], Faisal Ayub Kiani[1,5], Sha Nan[1], Mingxing Ding[1] and Yi Ding[1]*

[1]College of Veterinary Medicine, Huazhong Agricultural University, Wuhan, China, [2]Henan Jinlu Special Breeding Farm, Zhengzhou, China, [3]Department of Surgery, Anesthesiology, and Radiology, Faculty of Veterinary Medicine, Benha University, Moshtohor, Egypt, [4]Department of Pharmacology, Faculty of Veterinary Medicine, Benha University, Moshtohor, Egypt, [5]Department of Clinical Sciences, Faculty of Veterinary Medicine, Bahauddin Zakariyah University, Multan, Pakistan

**Introduction:** Enteritis and dysbiosis are the major causes of high morbidity and mortality of juvenile ostriches. Chicory (CC) has been proven to have excellent antioxidant, anti-inflammatory, and antibacterial activities. However, it's unclear whether CC could improve the survival rate of juvenile ostriches by relieving enteritis and correcting dysbiosis.

**Materials and methods:** South African ostrich hatchlings (*Struthio camelus domesticus*) were fed with and without a CC-supplemented diet, and the body weight gain and mortality were compared over 4 months of age. Fresh fecal samples of clinically healthy ostriches were collected, and 16S DNAs were analyzed. Moreover, ostrich chicks with LPS-induced enteritis were fed with different dosages (0, 20, 40, and 80 mg/kg) of chicoric acid (CA), a major bioactive component of CC, for five consecutive days. The expression levels of tight junction (TJ)-related proteins and inflammatory mediators in the ilea were detected with western blot and immunofluorescence.

**Results:** The ostrich chicks fed on the CC-supplemented diet began to increase in weight at the 1st month of age and became remarkably heavier at the fourth month ($p < 0.01$) compared with those fed on the non-CC-supplemented diet. Additionally, the mortality percentage was lower in the chicks fed on the CC-supplemented diet than those fed on the non-CC-supplemented diet (19% vs. 36%, respectively). The diet with the CC supplementation significantly increased the abundance of *Phascolactobacteria* (linear discriminant analysis; LDA >4) and *Bacteroidota* (26.7% vs. 17.7%, respectively) as well as decreased the enrichment of *Clostridium* (5.0% vs. 9.1%, respectively) in the ostrich ilea compared to the diet without CC. The supplementation of CA at a dose of 80 mg/kg significantly increased the expression level of ZO-1 and claudin-3 ($p < 0.0001$) and suppressed the levels of IL-1β, IL-6, and TNF-α ($p < 0.0001$) in ostriches with LPS-induced ileitis.

**Conclusion:** Our results substantiate that CC or CA supplementation in a diet could effectively improve growth performance and reduce mortality in juvenile ostriches via modulating the gut microbiota and attenuating enteritis.

KEYWORDS

**chicory, chicoric acid, intestinal inflammation, mortality rate, ostriches, microbiota**

# 1 Introduction

The ostrich industry is gaining much attention worldwide due to the high market value of its products and byproducts (1). However, the high prevalence of juvenile mortality has a negative influence on ostrich farming as well as the breeders' enthusiasm (2). Ostrich hatchlings appear to have structural and functional deficiencies in the intestinal mucosa that lead to inadequacy in the digestive function (3). Additionally, the inherent coprophagy behavior of ostriches contributes to a high incidence of intestinal ailments and mortality in ostrich chicks (4, 5). The mortality rate in the young population (up to 3 months of age) is reported to be 30–40%, primarily due to intestinal tract diseases and/or an imbalance of the gut microbiota (dysbiosis) (2, 6). Dysbiosis is characterized by a reduction of beneficial bacteria and an overgrowth of pathogenic bacteria (2). Bacterial enteritis has been recognized as the main cause of mortality in ostrich chicks (7). The diversity of microbes and disease response vary markedly across the length of the intestinal tract. Among gut regions, the ileum is more sensitive to enterocolitis in ostriches, showing a higher degree of inflammation and conspicuous evidence of dysbiosis (2). A vast variety of antimicrobial agents were extensively used to prevent and/or treat bacterial enteritis in the poultry industry. These communal practices result in the emergence of drug-resistant pathogens, gut dysbiosis, delayed growth, and increased drug residues in animal products with a potential public health hazard (8–10). The discovery of new therapeutic agents and the evolution of biologically active substances as safe substitutes have received significant attention in this regard (11–13). Herbal products offer a vast resource of new medicinal agents for the protection and/or remedy of various diseases in various animal species (14–16). Therefore, it's important to look for alternatives that could attenuate enteritis in ostrich chicks, improve gut health and growth performance, and limit the use of antimicrobials.

Chicory (CC) (*Cichorium intybus*), a highly palatable perennial plant grown worldwide, is well-known for its numerous nutritional and medicinal properties (17). Due to its versatile bioactive ingredients, CC could be used in livestock production as a sustainable, beneficial forage-based nutrient (18). Various *in-vivo* trials have demonstrated intriguing consequences regarding CC supplementation in various livestock. CC could amend the gut microbiota and improve digestibility and development of the gastrointestinal tract in growing pigs (19, 20) and sheep (21). Dietary inclusion of CC in a forage-dependent diet is helpful to enhance feed intake, feed conversion efficiency, and growth performance in beef steers (22). In addition, CC has been reported to modify intestinal structure and enhance gut microbial diversity in broiler chickens (23). Supplementation of CC for broilers could also enhance growth performance with an improved immune status and blood lipid profile, such as cholesterol, triglycerides, and low-density lipoprotein levels (24). Chicoric acid (CA), a major biological constituent of CC, is considered a bioactive component with potent anti-oxidant, anti-inflammatory, and anti-bacterial bioactivities (17, 25, 26). CA has been reported to effectively lessen inflammation and oxidative stress induced by lipopolysaccharide (LPS) in acute liver injury (27), acute lung injury (28), and BV-2 microglia cell models (25). However, the beneficial effect of CC or CA on the enteritis of juvenile ostriches has not yet been investigated.

Up to date, CC supplements have not yet been extensively used in ostrich production. The objective of this current study was to elucidate the influence of CC on growth performance and mortality rate associated with enteritis in juvenile ostriches. We hypothesized that CC supplementation could improve growth performance, attenuate enteritis, and decrease the incidence of mortality by modulating the gut microbiota and relieving intestinal inflammation.

# 2 Materials and methods

## 2.1 Animals

South African black-necked ostrich hatchlings (*Struthio camelus domesticus*) at Henan Jinlu Special Breeding Co., Ltd., (Zhengzhou, Henan Province, China) were selected for the present study. The ostrich hatchlings were kept in a warm, dry, and draft-free environment with sufficient space to move around and allowed to have free access to water and food. The brooding temperature (BT) of the hatchlings was set at 33.5°C during the 1st week of age and then gradually decreased to reach 25°C at the end of the 4th week of age. The BT was further reduced to 20°C at the end of the 8th week, then adjusted to 18°C from the 9th week to the end of the experiment. Dehumidifiers were used to reduce the ambient moisture during brooding. The level of humidity was between 25 and 55% during the entire period of the experiment. This study was approved by the Animal Protection and Utilization Committee of Huazhong Agricultural University (ID number: HZAUBI-2023-0003).

## 2.2 Study design

### 2.2.1 Effect of chicory forage on enteritis and mortality in juvenile ostriches

To determine the effect of CC forage on growth performance, 200 zero-day-old healthy ostrich hatchlings with weights (828.9 ± 24.2 grams) from a newly hatched batch were enrolled in this prospective randomized design. All experimental hatchlings were initially allocated into five allocations (A, B, C, D, and E) ($n = 40$ each). These allocations were selected in a random order to assign two equal-sized groups (non-chicory control (NC) and chicory group (CC); $n = 100$) using computer software.[1] The chicks were kept in an outdoor enclosure (9 × 30 m) with soil substrate during the daytime and in an indoor pen of approximately 3.5 × 4 m during the night. Both NC and CC chicks were fed concentrate and green forage at a consistent weight ratio of 1:1. The green forage in the NC group was composed of amaranth, cabbage, and *Ipomoea aquatica*, which was replaced by CC fodder in the CC group. The nutritional composition of the supplied concentrate is shown in Table 1. The chicks were allowed *ad libitum* access to water. Body weights were recorded monthly in both groups up to 4 months of age. The chicks' clinical manifestations were monitored daily, and the deceased chicks were autopsied for gross and histological examination. The mortalities with enteritis in both the NC and CC groups were calculated.

1 www.randomizer.org

TABLE 1 Nutritional composition of the supplied concentrate.

| Component | Value | Component | Value | Component | Value |
|---|---|---|---|---|---|
| Metabolizable energy (MJ/kg) | 11.3 MJ | Vit A | 12,000 IU | Vit B12 | 0.1 mg |
| Crude protein (%) | 21 | Vit D | 3,000 IU | Pantothenic acid | 18 mg |
| L-Lysine (%) | 1.1 | Vit E | 30 mg | Niacin | 80 mg |
| Methionine (%) | 0.45 | Vit K | 3 mg | Biotin | 0.3 mg |
| Ca (%) | 1.5 | Vit B1 | 4 mg | Folic acid | 2 mg |
| Available P (%) | 0.75 | Vit B2 | 12 mg | Choline | 500 mg |
| NaCl (%) | 0.25 | Vit B6 | 8 mg | Fe | 160 mg |
| Cu | 20 mg | Mn | 120 mg | I | 0.6 mg |
| Se | 0.3 mg | Zn | 80 mg | Co | 0.5 mg |
| Corn (g) | 598 | Soybean (g) | 270 | Fish meal | 15 g |

All elements were supplied per kilogram concentrate and provided in accordance with China Ostrich Breeding and Development Association.

### 2.2.2 Gut microbiota analysis

To investigate the effect of CC on the gut microbial community, we collected six fresh fecal samples of one-month-old clinically healthy ostriches from each of the CC and NC groups in the experiment above. The total microbial DNA was extracted using the OMEGA Mag-Bind Soil DNA Kit (M5635-02) (Omega Bio-Tek, Norcross, GA, United States) according to the manufacturer's instructions. The quantity of the extracted DNA was determined using an ultraviolet-visible spectrophotometer (NanoDrop 2000, United States), and its integrity was assessed using agarose gel electrophoresis. DNA samples were uniformly diluted to 20 ng/μL. The DNA of the 16S V3V4 region was PCR amplified using specific primers (341F, 5′-CCTAYGGGRBGCASCAG-3′; and 806R, 5′-GGACTACNNGGGTATCTAAT-3′). The PCR amplification conditions were as follows: initial denaturation at 98°C for 2 min, denaturation at 98°C for 15 s, annealing at 55°C for 30 s, extension at 72°C for 30 s, final extension at 72°C for 5 min, 10°C hold, 25–30 cycles. PCR amplification products were subjected to fluorescent quantification using the Quant-iT PicoGreen dsDNA Assay (Thermo Fisher Scientific Inc., China). According to the fluorescent quantification results, the samples were mixed in the appropriate proportions to meet the sequencing requirements. The microbial DNA was processed to construct metagenome sequencing libraries using TruSeq Nano DNA LT Library Preparation Kit (Illumina, Inc. CA, United States). The library DNA fragments were PCR amplified to enrich the sequencing library template. The amplified products were then purified using AMPure XP system (Beckman, Coulter, Beverly, CA, United States). The enriched library was further purified, and the final fragment selection was performed using 2% agarose gel electrophoresis. Before sequencing, the library was subjected to quality control using an Agilent Bioanalyzer system with the Agilent High Sensitivity DNA Kit (Agilent, CA, United States). Sequencing was performed on the MiSeq platform using 2 × 300 bp paired-end reads with the MiSeq Reagent Kit V3 (600 cycles) (Illumina, Inc. CA, United States). To ensure high sequencing quality, the optimal sequencing length for target fragments was between 200–450 bp. Sequences were denoised or clustered into Operational Taxonomic Units (OTUs) using the QIIME2 (2019.4) DADA2 software. Based on the distribution of ASVs/OTUs in different samples, the α diversity level of each sample was assessed. Various unsupervised ordination, clustering methods, and statistical tests were employed to measure and determine the significance of β diversity differences and assess the differences in species abundance between samples. Based on the bacterial metagenomic data, the predicted functional pathways of the bacterial communities were extracted from the Kyoto Encyclopedia of Genes and Genomes (KEGG) database.

### 2.2.3 Effect of chicoric acid on intestinal inflammation induced by LPS in juvenile ostriches

To determine whether CC could relieve enteritis via its bioactive component CA, clinically healthy 42 ten-day-old South African ostrich chicks (1130.83 ± 34.3 grams) were selected and randomly allocated into seven groups ($n = 6$ each): non-treatment control (NC), CA control (CAC, 80 mg/kg of CA was supplemented in diet), LPS + CA (LC, 1.5 mg/kg LPS intraperitoneally injected, and 0, 20, 40, and 80 mg/kg of CA were supplemented in diet), and LPS + amoxicillin (LA, 1.5 mg/kg LPS intraperitoneally injected, and 20 mg/kg of amoxicillin was supplemented in diet). LPS (Sigma Aldrich, Germany) was administered on day 0 of the experiment. The ostrich chicks were fed with the same ratio of concentrate and green forage (amaranth, cabbage, and *Ipomoea aquatica*) as in the above experiment. CA (Shanxi Qinling Biological Engineering Company, China) or amoxicillin (CSPC Pharmaceutical Group Limited, China) were supplemented in the diet, starting at day 0, for five consecutive days. The chicks were weighed on days 1, 3, and 5. On day 5, the chicks were anesthetized with Zoletil 50 (0.1 mg/kg; IM; Virbac, France), and the ilea were harvested. The ileal samples were then divided into two parts: one stored at −80°C for protein analysis, and the other was fixed in a 10% neutral formalin solution for histopathological examination.

## 2.3 Histopathological examination

The harvested ileal samples were fixed in 10% neutral-buffered formalin, dehydrated in serial dilutions of ethanol concentrations ranging from 50 to 100%, cleared in xylene, and embedded in paraffin. The paraffin-embedded tissues were cut into 5 μm thick sections. The intact slices were chosen for conventional H&E staining protocol. For staining, the tissue sections were deparaffinized in three xylene baths, and hydrated by passing through decreasing concentrations of alcohols (100, 95, 80, 75%) and water. The tissue was stained with

hematoxylin for three to 5 min, followed by a water wash for 5 min. Then, the tissue was dipped in 1% acid alcohol for few seconds, followed by ammonia water bathing. After a tap water wash, the tissue slices were stained with 1% eosin for one to 2 min. Next, the sections were dehydrated in increasing concentrations of alcohol baths and cleared in two xylene baths. Finally, the slides were mounted and examined by a professional pathologist under a Leica DM4B light microscope (Leica Microsystems, Germany). Tissue evaluation was based on a modified histological scoring [none (0), mild (1), moderate (2), and severe (3)] (29), describing the severity and degrees of villous inflammation, cellular infiltration, congestion, and epithelial cell shedding. Additionally, the average villus heights of fifteen well-oriented villi with intact lamina propria were measured from the crypt opening to the end of the villi (30) using Aperio ImageScope software x64 (Leica Biosystem Imaging, Inc., Germany).

## 2.4 Western blot

Protein extraction from the ileum tissue was performed using RIPA Lysate Buffer (Merck Ltd., Darmstadt, Germany), and the concentrations were measured by the BCA Protein Assay Kit in accordance with the manufacturer's procedure, and then diluted to the same concentration. Proteins were separated by SDS-PAGE and transferred to a PVDF membrane with a Trans-Blot® TurboTM transfer system (Bio-Rad, Hercules, CA, United States). Then, the membrane was blocked with 5% skim milk in Tris-buffered saline (TBS) at 37°C for 2 h, and immunolabeled with TBS-diluted primary antibodies at 4°C overnight. Primary antibodies used in this study were rabbit polyclonal anti-TLR4 (1:1,000 dilution) (ABclonal, Inc., Wuhan, China), rabbit polyclonal anti-P-P65 (1:1,000 dilution) (Cell Signaling Technology, Inc., United States), rabbit polyclonal P65 (1:1,000 dilution) (AbMart Pharmaceutical Technology Co., Ltd., Shanghai, China), rabbit polyclonal anti-IL-1β (1:1,000 dilution), rabbit polyclonal anti-IL-6 (1:1,000 dilution) (ABclonal, Inc., Wuhan, China), anti-TNF-α (1:1,000 dilution) (Boaosen Biotechnology Co., Ltd., Beijing, China), rabbit polyclonal anti-ZO-1 (1:1,000 dilution), anti-claudin-3 (1:1,000 dilution) (Wanlei Biotechnology Co., Ltd., Shenyang, China) and rabbit polyclonal anti-GAPDH (1:10,000 dilution) (ABclonal, Inc., Wuhan, China). Following TBST wash for 3 × 5 min, the blots were then incubated together with horseradish peroxidase (HRP)-conjugated donkey anti-rabbit (1:50,000 dilution) (Servicebio Technology Co., Ltd., Wuhan, China) as secondary antibodies at 37°C for 1 h. The antigen-antibody complex was visualized by a Clarity Max™ Western ECL Substrate (Bio-Rad) and the imaging of immunoreactive proteins was taken using the Bio-Rad ChemiDoc™ MP imaging system. The protein bands were scrutinized by Image J 1.46r (National Institutes of Health, United States). The target protein values were denoted as the proportion of the optical density of the protein bands in treatment groups to the density of the corresponding control band in the negative control group.

## 2.5 Immunofluorescence of ZO-1 and claudin-3 proteins

To determine the effect of CA on the intestinal barrier of ostrich chicks with enteritis, the main TJ proteins were measured with immunofluorescence. The harvested ilea were fixed in 10% neutral-buffered formalin, dehydrated in serial dilutions of ethanol concentrations (50–100%), cleared in xylene, and embedded in paraffin. The paraffin-embedded tissues were sectioned into 5 μm-thick sections. The sections were treated with 5% BSA at room temperature for 30 min before being incubated with the primary antibody at 4°C for 12 h. The sections were washed with PBS, incubated with the secondary antibody at room temperature for 30 min, and stained with 4,6-diamidino-2-phenylindole (DAPI; 1:5,000, Beyotime, SH, China) for 5 min at room temperature. Primary antibodies were rabbit polyclonal anti-ZO-1 (1:500 dilution) and anti-claudin-3 (1:500 dilution) (Wanlei Biotechnology Co., Ltd., Shenyang, China), and secondary antibodies were HRP-conjugated Cy3 labeled goat anti-rabbit (1:500), and FITC-conjugated goat anti-rabbit antibodies (1:500 dilution) (Servicebio Technology Co., Ltd., Wuhan, China). The stained sections were examined using flourescence microscope (Olympus cellsens Entry, Japan). The fluorescence signal was analyzed using Image J 1.46r (National Institutes of Health, United States).

## 2.6 Statistical analysis

Sequencing data analysis was performed using QIIME2 (v2.0) software. The DADA2 method was employed to filter, denoise, merge, and remove chimeric and singleton sequences from the original data. ASVs (equivalent to representative operational taxonomic units (OTU) sequences) were obtained through 100% similarity clustering. Species annotation, taxonomic composition, α diversity, and β diversity analyses were conducted using custom scripts in QIIME2 and the R programming language. Corresponding charts were generated to visualize the results. The assumption of normality in α diversity indices was tested using the Kolmogorov–Smirnov (KS) analysis. The variables of the α diversity did not meet the basic assumption and were therefore analyzed by non-parametric tests (31). Kruskal–Wallis rank sum test with post-hoc Dunn's tests were used to compare α diversity indices (Chao 1, Good's coverage, Shannon, and Pielou) and the data were expressed as median (IQR). Principal coordinates analysis (PCoA) was performed in R using scripts to output the PCoA coordinates of sample points and plot them into a two-dimensional scatter plot. The discrimination of distance metrics between groups was based on the ordination method and verified to ensure consistency (31, 32). Permutational multivariate analysis of variance (PERMANOVA) was used to analyze Bray–Curtis and weighted UniFrac distances to confirm the dissimilarity. LEfSe [linear discriminant analysis (LDA) effect size] analysis using Kruskal–Wallis and Wilcoxon rank sum tests was used to analyze the differences in the microbial community compositions. LDA score >4 was considered statistically significant. Phylogenetic Investigation of Communities by Reconstruction of Unobserved States (PICRUSt2) method was used to predict microbial metabolic functions. Abundance values for metabolic pathways based on the metabolic pathway KEGG database were calculated. Weight gain, mortality, and numerical data of western blot and immunofluorescence were compared using one-way ANOVA analysis with least significance difference (LSD) using SPSS software

10.3389/fvets.2024.1432269

(IBM statistics 26). Data are presented as mean ± SD. A statistical significance was defined as $p$-value <0.05.

# 3 Results

## 3.1 Chicory forage improved growth and reduced enteritis-associated mortality in juvenile ostriches

The CC-supplemented chicks showed an increase in weight compared to the NC chicks ($p < 0.05$) at day 30 to 120 of the experiment (Figure 1A). There was a death proportion of ostriches in both CC and NC, but the mortality percentage in the NC group was far greater than that in the CC group at day 120 (36% vs. 19%; Figure 1B). The autopsy showed that enteritis contributes to 25% of the mortality in the NC group and 9% in the CC group. In both groups, post-mortem inspection of the deceased chicks with enteritis revealed an inflamed red gut characterized by a varying degree of congestion, bleeding, abnormal coloration, and thinning of the intestinal wall (Figure 1C right; Figure 1D) compared to those in the clinically healthy ostrich chicks (Figure 1C left; Figure 1D). Histologically, the deceased chicks with enteritis showed a loose arrangement of small intestinal villi, accompanied by necrosis and the shedding of villous epithelial cells. As well, the ileal villi showed a varying degree of congestion with substantial lymphocytic infiltration (Figure 1E).

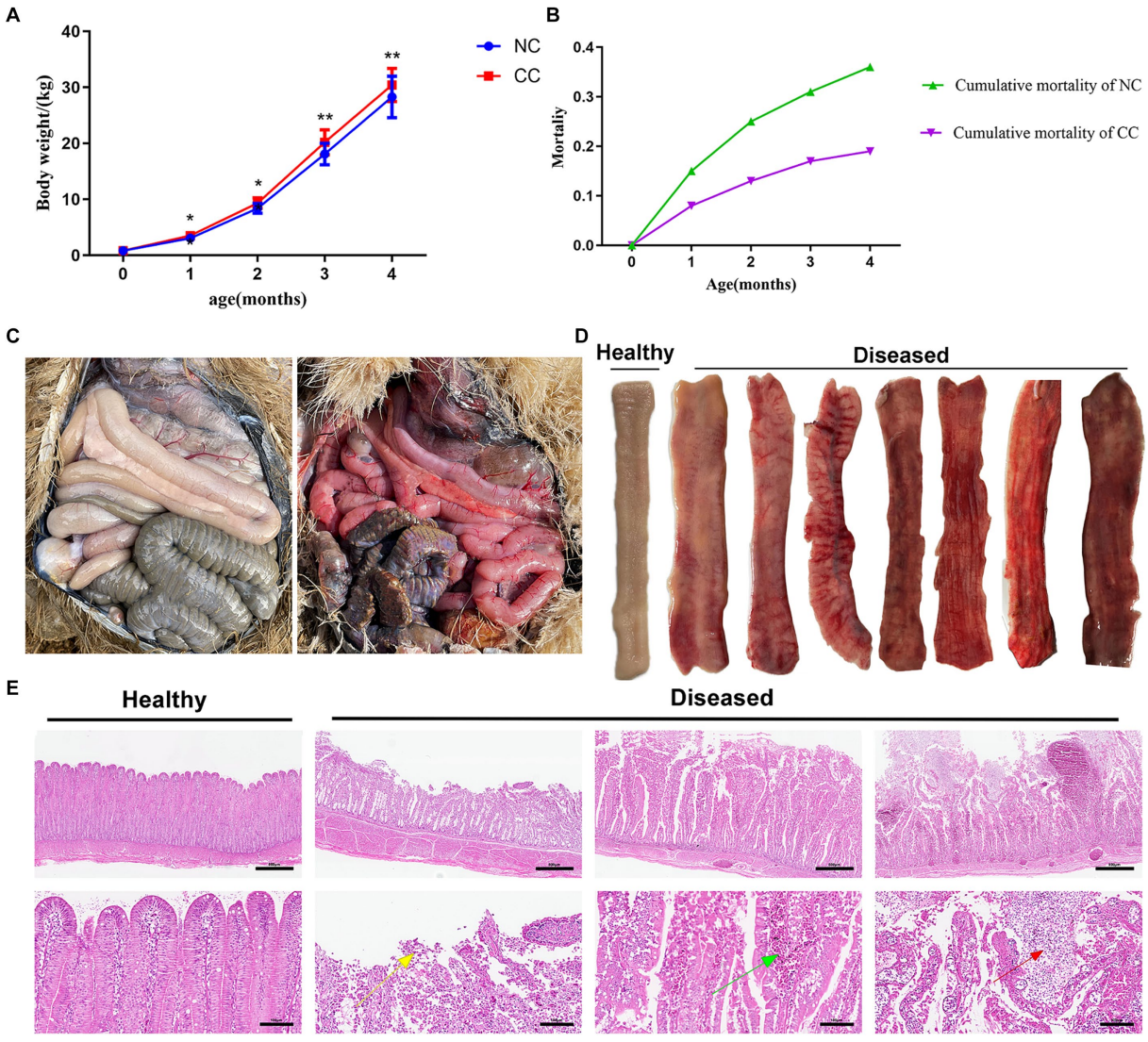


FIGURE 1
Effect of chicory supplementation on body weight and mortalities due to intestinal inflammation in ostrich chicks. **(A)** Weight changes in the non-chicory group (NC; $n = 100$) and chicory group (CC; $n = 100$) during the experiment. **(B)** Cumulative mortality in the ostriches throughout the entire period of the experiment (4 months). **(C)** Left: guts of clinically healthy ostriches; right: generalized gut inflammation in deceased ostriches. **(D)** Gross appearance of ileal mucosa in healthy and diseased ostriches with enteritis. **(E)** Representative H&E histopathological examination of the ilea of healthy ostriches and diseased ostriches with enteritis shows the shedding of villous epithelial cells (yellow arrow), congestion in the intestinal villi (green arrow), and substantial lymphocytic infiltration (red arrow). Image magnification is 40× and 200× and scale bar = 500 and 100 μm. The asterisk symbol * indicates $p < 0.05$; ** indicates $p < 0.01$.

## 3.2 Chicory forage modified gut microbiota of juvenile ostriches

A total of 770 common operational taxonomic units (OTUs) was identified between the NC and CC groups, representing approximately 17.3% of the total OTUs. The rarefaction curves and species accumulation curves in both groups revealed that almost all bacteria in the fecal samples were detected. Furthermore, the rank abundance curves showed a commendable level of uniformity and ASV/OTUs abundance in the samples (Supplementary Figure S1). Good's coverage ranged from 99.71 to 99.95% in the NC and CC groups ($p = 0.34$), indicating the vast majority of bacteria was recognized. The CC group exhibited a significant increase in Chao1 (829.347 ± 61.452; $p = 0.037$) and Shannon indices (0.985 ± 0.006; $p = 0.025$) as compared to the NC group (701.918 ± 121.335 and 0.975 ± 0.011 respectively). The Chao1 and Shannon indices of the CC group indicated a higher species richness compared with the NC group. Additionally, Pielou's evenness in the CC group was significantly higher compared with the NC group (0.794 ± 0.028 vs. 0.754 ± 0.030, respectively) ($p = 0.037$) (Figure 2A). Based on Bray–Curtis and weighted UniFrac distance methods, PCoA plots demonstrated a substantial distance between the NC and CC groups on the coordinate axes. The discrimination between the groups was distinct, and the intra-variability between the samples in the NC group is much lower than the intra-variability between the samples in the CC group, indicating changes in the composition and structure of the gut microbiota between the two groups (Figures 2B,C). The pairwise PERMANOVA displayed a statistically significant difference between the distance metrics observed for the NC group and the CC group ($p < 0.005$).

The top species at the phylum level of the samples of both the NC and CC groups are shown in Figure 2D, with *Bacillota*, *Bacteroidota*, and *Spirochaetota* constituting the major phylum and making up more than 70% of the total. The average abundances of these phyla in the NC and CC groups were 47.2, and 41.7% for *Bacillota*, 17.7, and 26.7% for *Bacteroidota*, and 5.7, and 2.8% for *Spirochaetota*, respectively. The top species at the genus level were displayed in Figure 2E, the relative abundances for *Clostridium* were 9.1, 5.0%, *Treponema* were 5.6, 2.8%, *Bacteroides* were 3.8, 4.1%, *Desulfotomaculum* were 4.4, 3.3%, *Duncaniella* were 3.3, 3.2%, in the NC and CC groups, respectively. LEfSe analysis (LDA score >4) demonstrated differential microbiota-based biomarkers with higher abundances of *Christensenellaceae*, *Clostridium*, and *Christensenella* found in the NC group, and *Acidaminococcales*, *Acidaminococcaceae*, *Phascolarctobacterium*, and *Oscillibacter* in the CC group (Figure 2F). Four species at the genus level, two upregulated and two downregulated in each group, are depicted in Supplementary Figure S2, which provides a thorough explanation of these differential variations. On the basis of KEGG pathway analysis, the predicted metabolic pathways for microbial communities were significantly influenced by the supplementation of CC. The metabolic pathways of amino acid biosynthesis and nucleoside and nucleotide biosynthesis were significantly increased in the CC group compared to the NC group ($p = 0.034$; $p = 0.013$, respectively). However, the CC group showed a decreased level of fatty acid and lipid biosynthesis pathway compared to the NC group ($p = 0.019$) (Supplementary Figure S3).

## 3.3 Chicoric acid alleviated LPS-induced intestinal inflammation in juvenile ostriches

Chicks treated with LC-0 mg/kg exhibited a decrease in body weight compared with those in the NC and CAC groups on day 3 and 5 ($p < 0.0001$). Chicks received LC-(40 and 80) mg/kg and LA-20 mg/kg became heavier on day 3 and their weight gain was remarkably increased on day 5 as compared to those given LC-0 mg/kg ($p < 0.05$). The LC-80 and LA-20 mg/kg treatments showed non-significant difference in body weight during the entire period of the experiment (Figure 3A).

Both the LC-80 and LA-20 mg/kg treatments showed a significant increase ($p = 0.043$; $p = 0.007$, respectively) in ileal villus length on day 5 compared with the LC-0 mg/kg treatment (Figure 3B). Histologically, the LC-0 mg/kg treatment caused moderate to severe epithelial cell shedding, lymphocyte infiltration, and bleeding on day 5. There was no pathological change observed in the villous morphology of ostrich chicks supplemented with LC-80 and LA-20 mg/kg, while the ilea of ostrich chicks treated with LC-(20 and 40) mg/kg showed mild hemorrhagic congestion in the villi infiltrated with lymphocytes at day 5 (Figure 3C).

## 3.4 Chicoric acid downregulated expression levels of TLR4/NF-κBp65 pathway-related proteins and upregulated TJ-related proteins

The effect of CA treatment on the intestinal inflammation in ostrich chicks was evaluated by measuring the expression biomarkers of toll-like receptor 4 (TLR4)-dependent nuclear factor kappa B (TLR4/NF-κB) pathway-related proteins and TJ-related proteins on day 5 (Figure 4). The levels of TLR4, P-P65, IL-1β, IL-6, and TNF-α were increased ($p < 0.0001$) in the LC-0 mg/kg group compared with the NC and CAC groups. However, the levels of these inflammatory factors were reduced ($p < 0.05$) in chicks receiving LC-(20, 40, and 80 mg/kg) and LA-20 mg/kg compared with those treated with LC-0 mg/kg. The LC-80 mg/kg caused a significant decrease ($p < 0.001$) in IL-1β, IL-6, and TNF-α compared with the LC-20 mg/kg and LC-40 mg/kg. There was no difference in the levels of TLR4, P-P65, IL-1β, and TNF-α between the LC-80 mg/kg treatment and the NC or CAC group.

Chicks treated with LC-0 mg/kg resulted in a significant decrease in the levels of ZO-1 and claudin-3 proteins compared with the NC and CA groups ($p < 0.0001$). These proteins in the LC-(20, 40, and 80) mg/kg and LA-20 mg/kg-treated chicks were upregulated compared with those administered LC-0 mg/kg ($p < 0.05$). There was no difference in the levels of claudin-3 between LC-80 and LA-20 mg/kg treatments.

The fluorescence detection of ZO-1 and claudin-3 in the ileum tissue on day 5 is shown in Figure 5. The fluorescence intensity of ZO-1 and claudin-3 in the LC-0 mg/kg group was significantly decreased ($p = 0.0001$; $p = 0.0002$, respectively) compared to the NC group. The LC-(20, 40, and 80 mg/kg) and LA-20 mg/kg treatments significantly increased the fluorescence intensity of ZO-1 and claudin-3 as compared to the LC-0 mg/kg ($p < 0.05$). Interestingly, the LC-80 mg/kg and

10.3389/fvets.2024.1432269

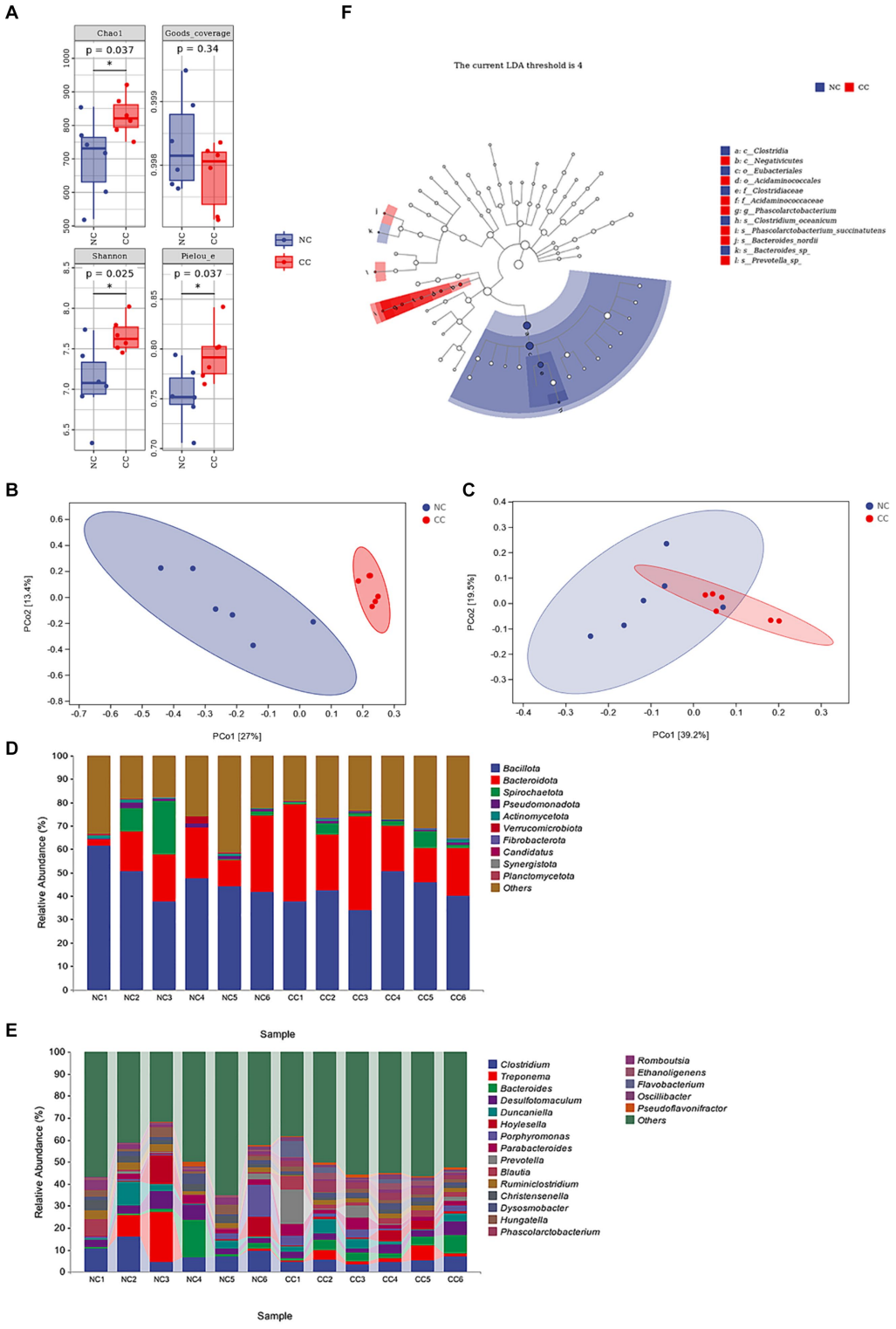


FIGURE 2
Effect of chicory supplementation on gut microbiota screened from fecal specimens of non-chicory group (NC, $n$ = 6) and chicory group (CC, $n$ = 6) in ostriches. **(A)** Alpha diversity (Chao 1, Good's coverage, Shannon, and Pielou indices) in both NC and CC groups; **(B,C)** Principal coordinates analysis (PCoA) plots of Bray–Curtis distance and weighted UniFrac distance between the two groups. Ellipses denote 95% confidence intervals. **(D)** Abundance of the fecal microbiota at the phylum level (top 10) in samples of both groups. **(E)** Abundance of intestinal microbiota at the genus level (top 20). **(F)** LEfSe analysis integrated with LDA scores revealed differential biomarkers, LDA scores >4 was considered statistically significant. The symbol * indicates $p$<0.05.

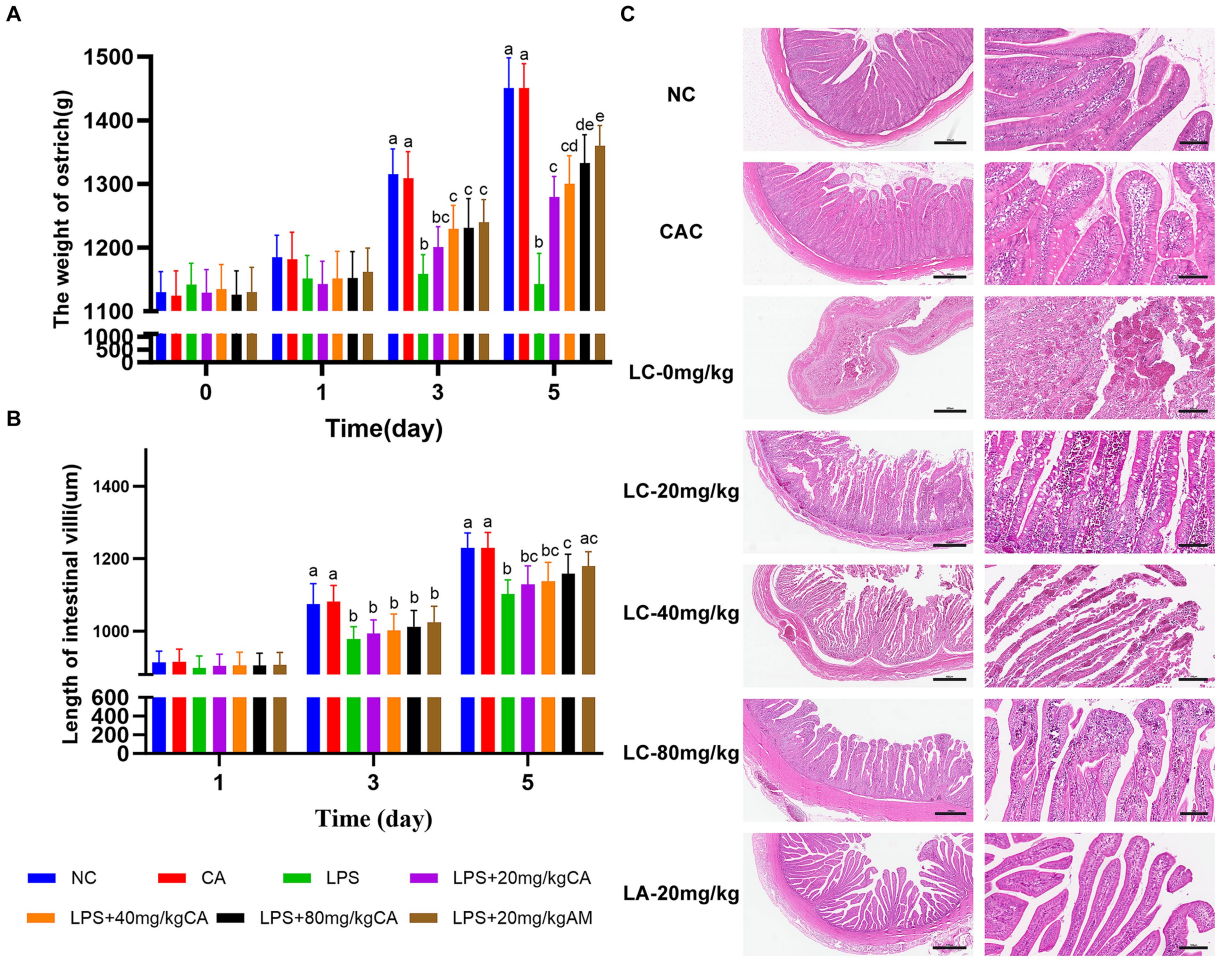


FIGURE 3
Effect of chicoric acid (CA) on body weight and ilea histology of lipopolysaccharide (LPS)-challenged ostriches. **(A)** Body weight of ostrich chicks (g) on days 1, 3, and 5. **(B)** Length of ileal villi (μm) on days 1, 3, and 5. **(C)** H&E microscopic pictures of ilea of ostrich chicks on day 5 after being challenged with LPS and fed with CA (20, 40, and 80 mg/kg) and amoxicillin (AM; 20 mg/kg) ($n = 6$). NC, non-CA supplementation; CAC, 80 mg/kg CA supplementation; LC-0 mg/kg, LC-20 mg/kg, LC-40 mg/kg and LC-80 mg/kg indicate LPS 1.5 mg/kg, IP, and 0, 20, 40, and 80 mg/kg CA were supplemented in the diet, respectively, and LA-20 mg/kg indicates LPS 1.5 mg/kg, IP, and 20 mg/kg AM was supplemented in the diet. Data were presented as mean ± SD. Different superscript letters indicate a significant difference ($p < 0.05$). H&E image magnification is 40× and 200× and scale bar = 500 and 100 μm.

LA-20 mg/kg treatments obviously reversed the LPS-induced decrease in fluorescence signal intensity of ZO-1 and claudin-3 ($p < 0.0001$).

## 4 Discussion

Worldwide, the high mortality rate in the juvenile ostrich population has greatly influenced the ostrich industry. Up to 50% of ostrich chicks all over the world are lost during the first 3 months (33). In Europe, the average mortality of chicks under 4 weeks old exceeds 50% (34). In South Africa, chicks were deceased, with a mortality rate reaching up to 46.7% before 28 days of age, and an extra 30.7% was seen between 28 and 90 days after hatching (35). According to previous reports, intestinal tract diseases and gut microbiota imbalances are the leading causes of death in juvenile ostriches (6, 36). Modulating the gut microbiota has been reported to lower the mortality associated with intestinal tract disorders (36). Common pathogens responsible for enteritis in ostriches include *Escherichia coli*, *Clostridium* spp., *Campylobacter jejuni*, *Pseudomonas aeruginosa*, *Salmonella* spp., and *Klebsiella* spp. (6, 37, 38). Postmortem inspection of deceased individuals revealed widespread inflammation and hemorrhage in the gut mucosa (2). In this current study, CC supplements enhanced growth rate and shifted gut microbiota in growing ostrich chicks. Furthermore, CC attenuated gut inflammation and improved the histological architecture of the gut epithelium. Our current findings appear to be well substantiated by other studies on ostriches (39), growing pigs (20), sheep (21), and broiler chickens (23). The CC supplementation could improve the palatability of the forage-based diet in sheep and subsequently increase their daily dry matter intake and digestibility aptitude (21). Moreover, the mean weight gain observed in the ostriches during the first 4 months of life is in accordance with previous studies (40, 41). Adding CC forage to the cereal diet increased daily feed intake, growth performance, and feed conversion ratio in growing pigs (19) and broiler chickens (42). The highest level of mortality in ostrich chicks has been found to occur in the first month of life (2, 35, 43). Hence, in this current study, the fecal microbiota of

10.3389/fvets.2024.1432269

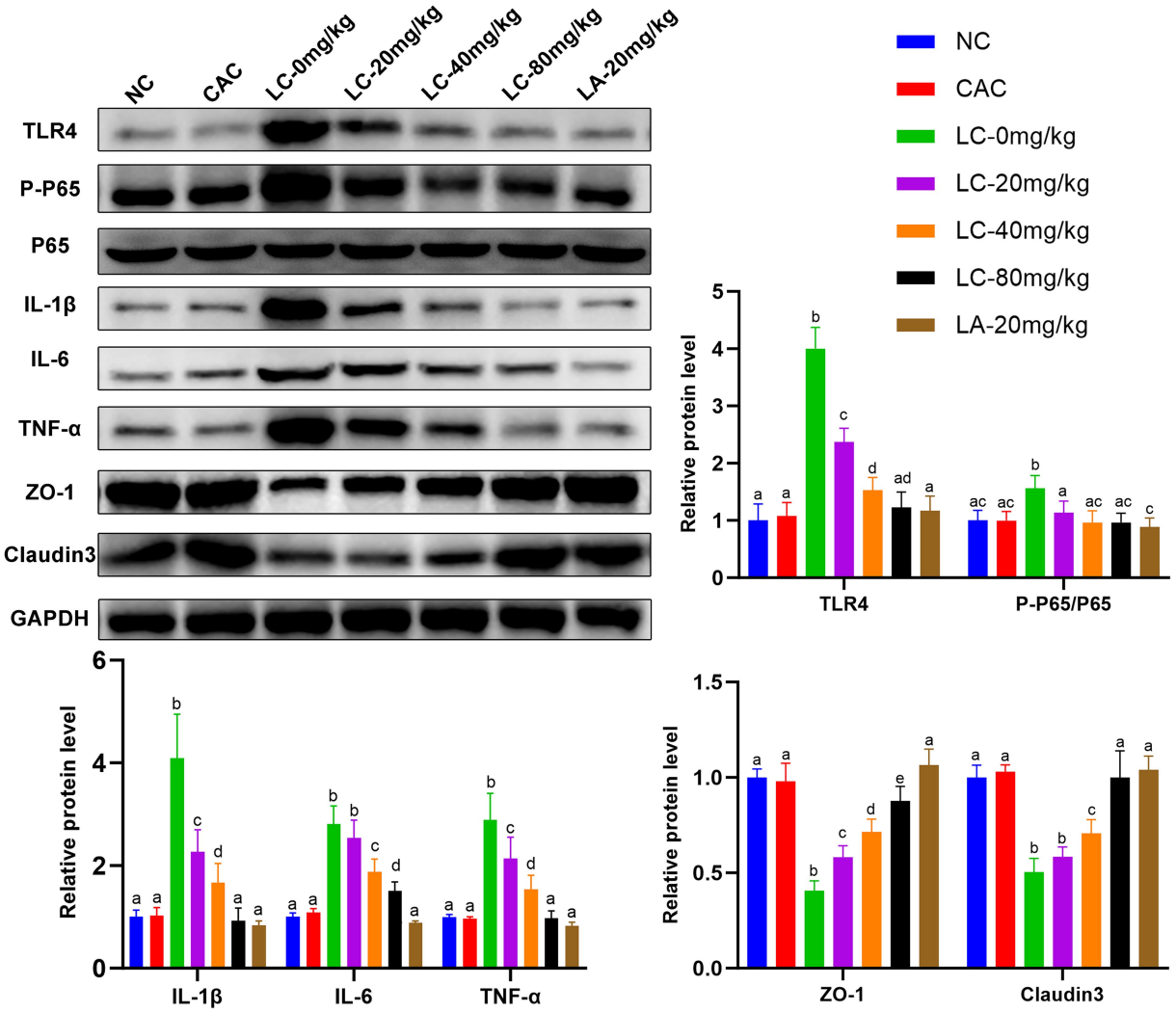


FIGURE 4
Effect of CA on expression levels of TLR4/NF-κBp65 pathway-related proteins and tight junction (TJ) proteins in the ileal tissues of lipopolysaccharide (LPS)-challenged ostrich chicks on day 5 after being challenged with LPS and fed with CA (20, 40, and 80 mg/kg) and amoxicillin (AM; 20 mg/kg) ($n = 6$). NC, non-CA supplementation; CAC, 80 mg/kg CA supplementation; LC-0 mg/kg, LC-20 mg/kg, LC-40 mg/kg and LC-80 mg/kg indicate LPS 1.5 mg/kg, IP, and 0, 20, 40, and 80 mg/kg CA were supplemented in the diet, respectively, and LA-20 mg/kg indicates LPS 1.5 mg/kg, IP, and 20 mg/kg AM was supplemented in the diet. Data were presented as mean ± SD. Different superscript letters indicate a significant difference ($p < 0.05$).

one-month-old chicks was sequenced to help identify disparities in the gut microbial composition. Our findings were in line with a prior study (39), showing a positive correlation between ileal microbial diversity and the ostrich's growth rate. Additionally, the abundance of the phylum *Bacteroidota* was mostly enriched in the ostrich ilea, which mainly ferments the dietary carbohydrate and produces a pool of short chain fatty acids as energy sources (44). Furthermore, CC significantly increased the population levels of the genus *Phascolarctobacterium* and *Phascolarctobacterium succinatutens* spp. while simultaneously decreasing the levels of the family *Clostridiaceae* and the genus *Clostridium*. Beneficial taxa are well known to enhance gut barrier integrity and decrease metabolic endotoxemia (39, 45). *Phascolarctobacterium succinatutens* can effectively utilize succinate, a stress-induced signaling mediator produced by other pathobionts, and in turn decrease gut inflammation (46, 47). Conversely, *Clostridiaceae* showed more conspicuous taxonomic patterns, including a tremendous rise in the genus *Clostridium*. *Clostridium* spp. has been reported to induce extensive intestinal damage, gut inflammation, and enterotoxaemia in ostriches, resulting in high morbidity and mortality (2, 6). Our findings revealed drastically higher microbial α and β diversity with CC supplementation, suggesting that CC could improve the composition of gut microorganisms. The functional microbial species identified in this study coincide with various reports at various taxonomic levels (2, 36, 39). The impact of gut microbiota on health and metabolic processes is widely documented (48), and the variation of the gut microbiota could regulate most of the biological processes in the body, thereby affecting health and growth performance (49). In this current study, the outcome of the KEGG pathway analysis revealed that gut taxonomic compositions associated with the CC supplementation were closely related to functional biosynthesis pathways, such as amino acid biosynthesis and fatty acid and lipid biosynthesis. In agreement with our findings, CC supplementation in growing-finishing pigs could increase the amino acid concentrations, such as threonine, aspartic acid, phenylalanine, histidine, alanine, and glycine (50). Additionally,

10.3389/fvets.2024.1432269

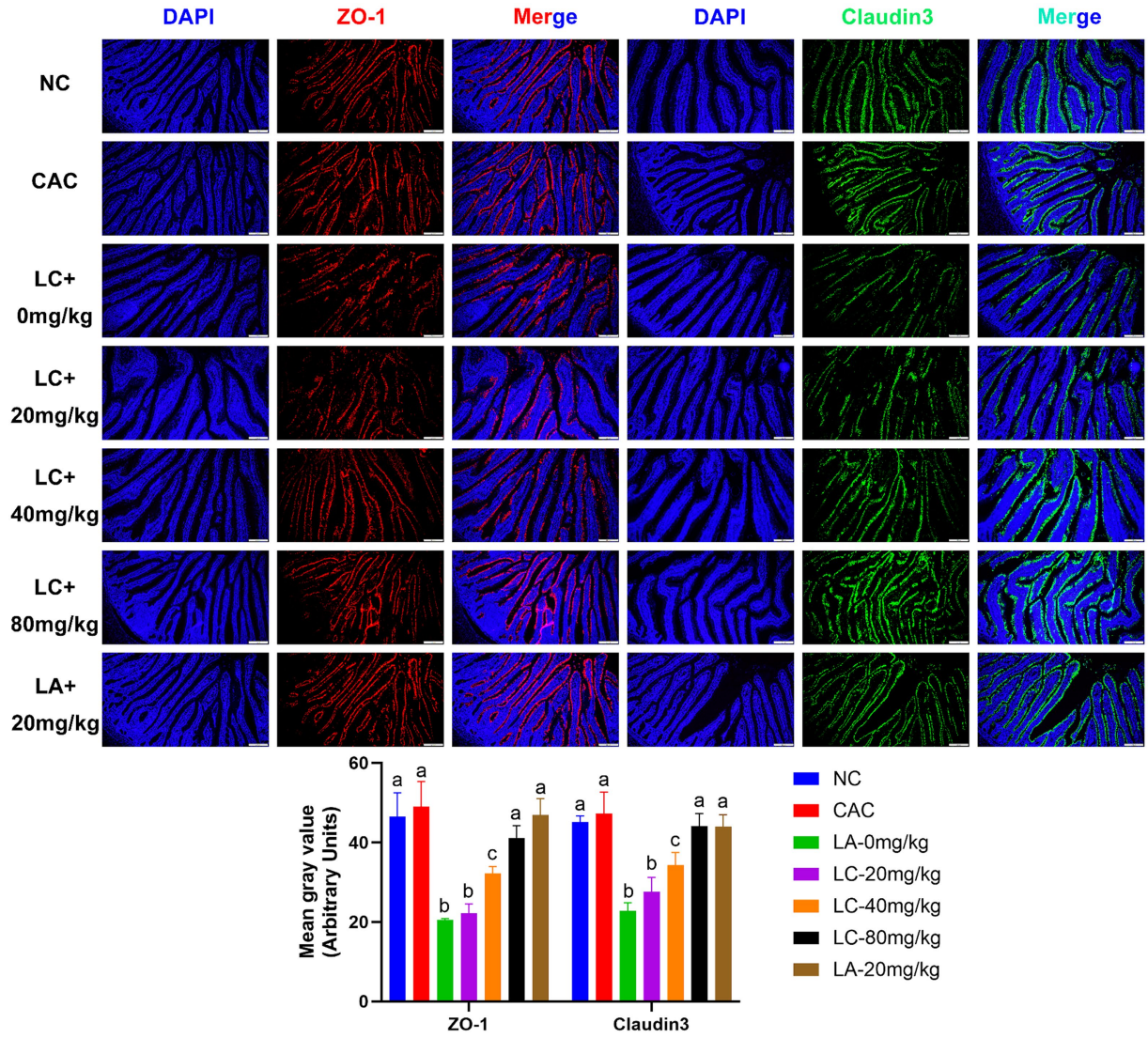


FIGURE 5
Effect of chicoric acid (CA) on immunofluorescence density of tight junctions (TJs) in the ileal tissues of lipopolysaccharide (LPS)-challenged ostrich chicks on day 5 after being challenged with LPS and fed with CA (20, 40, and 80 mg/kg) and amoxicillin (AM; 20 mg/kg) ($n = 6$). NC, non-CA supplementation; CAC, 80 mg/kg CA supplementation; LC-0 mg/kg, LC-20 mg/kg, LC-40 mg/kg and LC-80 mg/kg indicate LPS 1.5 mg/kg, IP, and 0, 20, 40, and 80 mg/kg CA were supplemented in the diet, respectively, and LA-20 mg/kg indicates LPS 1.5 mg/kg, IP, and 20 mg/kg AM was supplemented in the diet. Data were presented as mean ± SD. Different superscript letters indicate a significant difference ($p < 0.05$). Image magnification is 100× and scale bar = 200 μm.

CC supplementation could improve the systemic lipid profile, as indicated by decreased levels of cholesterol, triglyceride, and low-density lipoprotein levels (50, 51).

The TLR4/NF-κBp65 signaling pathway is a key regulator of intestinal inflammation (52, 53), and also plays a vital role in maintaining gut barrier integrity (54). LPS, a major endotoxin derived from gut gram-negative bacteria, acts on TLR4/NF-κBp65, causing overproduction of pro-inflammatory cytokines that disrupt intestinal TJs and eventually lead to intestinal permeability (55, 56). In this current study, CA markedly downregulated proinflammatory cytokines and subsequently alleviated intestinal inflammation induced by LPS in juvenile ostriches via the inactivating TLR4/NF-κBp65 signaling pathway (Figure 4). The TLR4 transduction cascade has been involved in the regulation of LPS-induced TJ permeability and mucosal damage (55). Managing gut leakage is crucial to improving the health and performance of the birds (57). In a variety of LPS-induced inflammatory models, CA has been evaluated and evidenced for its anti-inflammatory and antioxidant effects in acute liver injury (27), nerve injury (25), and acute lung damage (28). Additionally, CA supplementation enhanced the growth performance of the juvenile ostriches, which could be attributable to the modifications in the intestinal histomorphology with increasing villus height. Inclusion of CC forage in the basal diet resulted in increased villus length in growing pigs (20) and broiler chickens (23). The height of the intestinal villi are positively correlated with absorption surface area, nutrient bioavailability, and better utilization of dietary energy

(58, 59). Using natural medicinal plants as potential alternatives to antibiotic growth promoters in animal husbandry provides ubiquitous advantages, such as solving the drug residue issue, as well as improving the quality and quantity of meat production (60). For instance, herbal dietary supplementation was evidenced to improve growth performance and feed conversion ratios in broiler chickens (61, 62) and promote lean mutton quality and production in sheep (63). Our findings revealed that the supplementation of CA at a dose of 80 mg for 5 consecutive days could decrease the gut inflammatory process, improving the ostrich's growth performance to a level comparable to the effect of AM treatment at a dose of 20 mg/kg. Therefore, our findings prompt antibiotic-free production cycles and open the doors for animal farming to adopt CA as a therapeutic and/or growth promoter substitute.

The current study provides valuable information about CC and CA supplementation, either on the gut microbial diversity or the growth performance of juvenile ostriches. However, the small sample size for sequencing data analysis in this study may have limited the value of observations as a true representation of gut microbial diversity in the ostrich population. In addition, the outdoor access of ostriches was occasionally limited by some inclimental environmental conditions, and the outside temperature and humidity were uncontrollable, which may have had a certain impact on the experiment's repeatability. In the future, it will be a vital issue for further studies with larger sample sizes to investigate the long-term impact of CC and CA supplementation in a controlled environment. As well, *in vitro* research using the ostrich's intestinal cell culture model is needed to fully authenticate the effect of CA in ostriches.

## 5 Conclusion

The CC forage supplementation could enhance body weight and lower the incidence of fatal enteritis in juvenile ostriches. These enthralling findings were probably due to pivotal shifts in the gut microbiota by increasing the abundance of *Phascolactobacteria* and decreasing the enrichment of *Clostridium*. Additionally, CA could efficiently mitigate the gut inflammation and maintain intestinal barrier function by suppressing the IL-1β/IL-6/TNF-α-driven inflammatory response and enhancing the expression of ZO-1 and claudin-3 TJ proteins. This current study indicates that the use of CC as a feed supplement might be a potential therapeutic and/or growth promotor alternative or complement to antimicrobials in the animal industry.

## Data availability statement

Sequencing data presented in this study can be found in online repository. The name of the repository and accession number can be found below: https://www.ncbi.nlm.nih.gov/sra/PRJNA1082686.

## Ethics statement

The animal study was approved by Animal Protection and Utilization Committee of Huazhong Agricultural University (ID number: HZAUBI-2023-0003). The study was conducted in accordance with the local legislation and institutional requirements.

## Author contributions

ML: Data curation, Formal analysis, Investigation, Methodology, Software, Validation, Visualization, Writing – original draft, Writing – review & editing. MA: Data curation, Formal analysis, Investigation, Methodology, Software, Validation, Visualization, Writing – original draft, Writing – review & editing. ES: Data curation, Formal analysis, Investigation, Writing – review & editing. FK: Investigation, Software, Writing – review & editing. SN: Formal analysis, Investigation, Writing – review & editing. MD: Conceptualization, Funding acquisition, Project administration, Resources, Supervision, Writing – review & editing. YD: Conceptualization, Funding acquisition, Project administration, Resources, Supervision, Writing – review & editing.

## Funding

The author(s) declare that financial support was received for the research, authorship, and/or publication of this article. This research was funded by National Key R&D Program of China (Beijing, China; Grant No. 2023YFD1801400).

## Acknowledgments

The authors gratefully thank staff members at Henan Jinlu Special Breeding Ostrich Farm (Pinqing Yang, Jianmin Shi, Fuqiang Li, Yanqing Wang, and Lei Li) for their ongoing collaboration and help in caring for experimental animals as well as taking samples during this study.

## Conflict of interest

ML was employed by Henan Jinlu Special Breeding Farm.

The remaining authors declare that the research was conducted in the absence of any commercial or financial relationships that could be construed as a potential conflict of interest.

## Publisher's note



## Supplementary material

The Supplementary material for this article can be found online at: https://www.frontiersin.org/articles/10.3389/fvets.2024.1432269/full#supplementary-material

SUPPLEMENTARY FIGURE S1
**(A)** The sequence information of 12 fecal samples of both non-chicory (NC) and chicory (CC) groups. **(B)** Venn diagram for bacterial ASV/OTU distribution in the NC and CC fecal samples. **(C)** Rarefaction curves. **(D)** Accumulation curves. **(E)** Rank abundance curve.

SUPPLEMENTARY FIGURE S2
Significant alternations in the bacterial abundance at different classification levels in both non-chicory (NC) and chicory (CC) groups. All of the data represent means ± SD. *p < 0.05; **p < 0.01; ***p < 0.001, and **** p < 0.0001.

SUPPLEMENTARY FIGURE S3
Mean proportion (%) of predicted metabolic pathways of ileal bacterial species between non-chicory (NC) and chicory (CC) groups. The significant differences were observed at 95% confidence level and p < 0.05.

SUPPLEMENTARY TABLE S1
Raw data of weight gain of juvenile ostriches in the chicory (CC) forage supplementation experiment and data of weight gain, intestinal villi length, western blot (WB), and immunofluorescence analysis in the CA supplementation experiment.

SUPPLEMENTARY DATA SHEET S1
Original western blot (WB) images generated from the CA supplementation experiment show expressed TLR4/NF-κBp65 pathway-related proteins and tight junction (TJ) proteins in the ileal tissues.

# References

1. Cooper RG, Mahrose KMA, Horbańczuk JO, Villegas-Vizcaíno R, Kennou Sebei S, Faki Mohammed AE. The wild ostrich (*Struthio camelus*): a review. *Trop Anim Health Prod*. (2009) 41:1669–78. doi: 10.1007/s11250-009-9364-1

2. Videvall E, Song SJ, Bensch HM, Strandh M, Engelbrecht A, Serfontein N, et al. Early-life gut dysbiosis linked to juvenile mortality in ostriches. *Microbiome*. (2020) 8:147–13. doi: 10.1186/s40168-020-00925-7

3. Wang JX, Peng KM. Developmental morphology of the small intestine of African ostrich chicks. *Poult Sci*. (2008) 87:2629–35. doi: 10.3382/ps.2008-00163

4. Amado MF, Xavier DB, Boere V, Torres-Pereira C, McManus C, Bernal FEM. Behaviour of captive ostrich chicks from 10 days to 5 months of age. *Rev Bras Zootec*. (2011) 40:1613–8. doi: 10.1590/S1516-35982011000700029

5. Verwoerd DJ, Deeming DC, Angel CR, Perelman B. Rearing environments around the world In: DC Deeming, editor. The ostrich: biology, production, and health. Wallingford, Oxfordshire, UK: CABI Publishing (1999). 191–216.

6. Keokilwe L, Olivier A, Burger WP, Joubert H, Venter EH, Morar-Leather D. Bacterial enteritis in ostrich (*Struthio camelus*) chicks in the Western Cape Province, South Africa. *Poult Sci*. (2015) 94:1177–83. doi: 10.3382/ps/pev084

7. Samson J. Prevalent diseases of ostrich chicks farmed in Canada. *Can Vet J*. (1997) 38:425–8.

8. Marshall BM, Levy SB. Food animals and antimicrobials: impacts on human health. *Clin Microbiol Rev*. (2011) 24:718–33. doi: 10.1128/CMR.00002-11

9. Van Boeckel TP, Brower C, Gilbert M, Grenfell BT, Levin SA, Robinson TP, et al. Global trends in antimicrobial use in food animals. *Proc Natl Acad Sci U S A*. (2015) 112:5649–54. doi: 10.1073/pnas.1503141112

10. Yang L, Bajinka O, Jarju PO, Tan Y, Taal AM, Ozdemir G. The varying effects of antibiotics on gut microbiota. *AMB Express*. (2021) 11:116–3. doi: 10.1186/s13568-021-01274-w

11. Ahmad S, Yousaf MS, Tahir SK, Mustafa G, Majeed KA, Rashid MA, et al. Effects of co-supplementation of β-galacto-oligosaccharides and methionine on production performance, blood metabolites, and gut histomorphometry in broilers. *Pak Vet J*. (2022) 42:173–8. doi: 10.29261/pakvetj/2022.031

12. Khan I, Zaneb H, Masood S, Ashraf S, Rehman HF, Rehman HU, et al. Supplemental selenium nanoparticles-loaded to chitosan improves meat quality, pectoral muscle histology, tibia bone morphometry and tissue mineral retention in broilers. *Pak Vet J*. (2022) 42:236–40. doi: 10.29261/pakvetj/2022.007

13. Gul ST, Alsayeqh AF. Probiotics as an alternative approach to antibiotics for safe poultry meat production. *Pak Vet J*. (2022) 42:285–91. doi: 10.29261/pakvetj/2022.061

14. Widowati W, Prahastuti S, Hidayat M, Hasiana ST, Wahyudianingsih R, Afifah E, et al. Protective effect of ethanolic extract of jati belanda (*Guazuma ulmifolia* L.) by inhibiting oxidative stress and inflammatory processes in cisplatin-induced nephrotoxicity in rats. *Pak Vet J*. (2022) 42:376–82. doi: 10.29261/pakvetj/2022.050

15. Hussain K, Abbas A, Alanazi HAH, Alharbi AMA, Alaiiri AA, Rehman A, et al. Immunomodulatory effects of *Artemisia brevifolia* extract against experimentally induced coccidiosis in broiler chicken. *Pak Vet J*. (2023) 43:333–8. doi: 10.29261/pakvetj/2023.026

16. Prakoso YA, Babazadeh D, Wijayanti AD. Potency of desert rose (*Adenium obesum* (Forssk.) Roem. & Schult.) flower extract against artificially induced Furunculosis in Oranda goldfish (*Carassius auratus auratus*). *Pak Vet J*. (2023) 43:339–44. doi: 10.29261/pakvetj/2023.024

17. Perović J, Šaponjac VT, Kojić J, Krulj J, Moreno DA, García-Viguera C, et al. Chicory (*Cichorium intybus* L.) as a food ingredient-nutritional composition, bioactivity, safety, and health claims: a review. *Food Chem*. (2021) 336:127676. doi: 10.1016/j.foodchem.2020.127676

18. Nwafor IC, Shale K, Achilonu MC. Chemical composition and nutritive benefits of chicory (*Cichorium intybus*) as an ideal complementary and/or alternative livestock feed supplement. *Sci World J*. (2017) 2017:1–11. doi: 10.1155/2017/7343928

19. Ivarsson E, Liu HY, Dicksved J, Roos S, Lindberg JE. Impact of chicory inclusion in a cereal-based diet on digestibility, organ size and faecal microbiota in growing pigs. *Animal*. (2012) 6:1077–85. doi: 10.1017/S1751731111002709

20. Liu H, Ivarsson E, Dicksved J, Lundh T, Lindberg JE. Inclusion of chicory (*Cichorium intybus* L.) in pigs' diets affects the intestinal microenvironment and the gut microbiota. *Appl Environ Microbiol*. (2012) 78:4102–9. doi: 10.1128/AEM.07702-11

21. Niderkorn V, Martin C, Bernard M, Le Morvan A, Rochette Y, Baumont R. Effect of increasing the proportion of chicory in forage-based diets on intake and digestion by sheep. *Animal*. (2019) 13:718–26. doi: 10.1017/S1751731118002185

22. Morel I, Schmid E, Soney C, Aragon A, Dufey PA. Influence of ryegrass alone or blended with clover and chicory on feed intake and growth performance of steers. *Grassl Sci Eur*. (2014) 19:731–3. Available at: https://ira.agroscope.ch/en-US/publication/34204

23. Awad WA, Ghareeb K, Böhm J. Evaluation of the chicory inulin efficacy on ameliorating the intestinal morphology and modulating the intestinal electrophysiological properties in broiler chickens. *J Anim Physiol Anim Nutr*. (2011) 95:65–72. doi: 10.1111/j.1439-0396.2010.00999.x

24. Tufarelli V, Ghavami N, Nosrati M, Rasouli B, Kadim IT, Suarez Ramirez L, et al. The effects of peppermint (*Mentha piperita* L.) and chicory (*Cichorium intybus* L.) in comparison with a prebiotic on productive performance, blood constituents, immunity and intestinal microflora in broiler chickens. *Anim Biotechnol*. (2023) 34:3046–52. doi: 10.1080/10495398.2022.2130798

25. Liu Q, Hu Y, Cao Y, Song G, Liu Z, Liu X. Chicoric acid ameliorates lipopolysaccharide-induced oxidative stress via promoting the Keap1/Nrf2 transcriptional signaling pathway in BV-2 microglial cells and mouse brain. *J Agric Food Chem*. (2017) 65:338–47. doi: 10.1021/acs.jafc.6b04873

26. Liu Q, Fang J, Chen P, Die Y, Wang J, Liu Z, et al. Chicoric acid improves neuron survival against inflammation by promoting mitochondrial function and energy metabolism. *Food Funct*. (2019) 10:6157–69. doi: 10.1039/c9fo01417a

27. Li Z, Feng H, Han L, Ding L, Shen B, Tian Y, et al. Chicoric acid ameliorate inflammation and oxidative stress in lipopolysaccharide and d-galactosamine induced acute liver injury. *J Cell Mol Med*. (2020) 24:3022–33. doi: 10.1111/jcmm.14935

28. Ding H, Ci X, Cheng H, Yu Q, Li D. Chicoric acid alleviates lipopolysaccharide-induced acute lung injury in mice through anti-inflammatory and anti-oxidant activities. *Int Immunopharmacol*. (2019) 66:169–76. doi: 10.1016/j.intimp.2018.10.042

29. Liu L, Sui W, Yang Y, Liu L, Li Q, Guo A. Establishment of an enteric inflammation model in broiler chickens by oral administration with dextran sulfate sodium. *Animals*. (2022) 12:3552. doi: 10.3390/ani12243552

30. Gu YF, Chen YP, Jin R, Wang C, Wen C, Zhou YM. Dietary chitooligosaccharide supplementation alleviates intestinal barrier damage, and oxidative and immunological stress in lipopolysaccharide-challenged laying hens. *Poult Sci*. (2022) 101:101701. doi: 10.1016/j.psj.2022.101701

31. Kers JG, Saccenti E. The power of microbiome studies: some considerations on which alpha and beta metrics to use and how to report results. *Front Microbiol*. (2022) 12:796025. doi: 10.3389/fmicb.2021.796025

32. Plantinga AM, Wu MC. Beta diversity and distance-based analysis of microbiome data In: S Datta and S Guha, editors. Statistical analysis of microbiome data. Frontiers in probability and the statistical sciences. Cham: Springer (2021). 101–27.

33. Deeming DC. The ostrich biology. Production and health. Cambridge: Cambridge University Press (1999). 196 p.

34. The Macaulay Land Use Research Institute. (2003). Ostrich farming: a review and feasibility study of opportunities in the EU. Available at: https://macaulay.webarchive.hutton.ac.uk/livestocksystems/feasibility/ostrich.htm. (Accessed August 15, 2023).

35. Cloete SWP, Lambrechts H, Punt K, Brand Z. Factors related to high levels of ostrich chick mortality from hatching to 90 days of age in an intensive rearing system. *J S Afr Vet Assoc*. (2001) 72:197–202. doi: 10.4102/jsava.v72i4.652

36. Videvall E, Bensch HM, Engelbrecht A, Cloete S, Cornwallis CK. Coprophagy rapidly matures juvenile gut microbiota in a precocial bird. *Evol Lett*. (2023) 7:240–51. doi: 10.1093/evlett/qrad021

37. Niaki HD, Goli AA, Nakhaee P, Razmyar J. Determination of antimicrobial susceptibility of *Clostridium Perfringens* strains isolated from healthy and diseased ostriches (*Struthio camelus*). *J Poult Sci Avian Dis*. (2023) 1:28–36. doi: 10.61838/kman.jpsad.1.2.4

38. Huchzermeyer FW. Diseases of ostriches and other ratites. Onderstepoort: Agricultural Research Council, Onderstepoort Veterinary Institute (1998).

39. Videvall E, Song SJ, Bensch HM, Strandh M, Engelbrecht A, Serfontein N, et al. Major shifts in gut microbiota during development and its relationship to growth in ostriches. *Mol Ecol*. (2019) 28:2653–67. doi: 10.1111/mec.15087

40. Mushi EZ, Isa JFW, Chabo RG, Segaise TT. Growth rate of ostrich (*Struthio camelus*) chicks under intensive management in Botswana. *Trop Anim Health Prod*. (1998) 30:197–203. doi: 10.1023/a:1005067821642

41. Azam SM, Ali A, Kashif M, Khalid M, Rehman SU, Faizan M, et al. Effect of commercial & natural feeds on the growth performance of ostrich (*Struthio camelus*) in captivity. *Front Chem Sci*. (2022) 3:25–30. doi: 10.52700/fcs.v3i1.37

42. Liu HY, Ivarsson E, Jönsson L, Holm L, Lundh T, Lindberg JE. Growth performance, digestibility, and gut development of broiler chickens on diets with inclusion of chicory (*Cichorium intybus* L.). *Poult Sci*. (2011) 90:815–23. doi: 10.3382/ps.2010-01181

43. Heitmann S. MSc thesis. Stellenbosch: Stellenbosch University (2020) Available at: http://hdl.handle.net/10019.1/109458.

44. Adewole D, Akinyemi F. Gut microbiota dynamics, growth performance, and gut morphology in broiler chickens fed diets varying in energy density with or without bacitracin methylene disalicylate (BMD). *Microorganisms*. (2021) 9:787. doi: 10.3390/microorganisms9040787

45. Zafar H, Saier MH Jr. Gut Bacteroides species in health and disease. *Gut Microbes*. (2021) 13:1–20. doi: 10.1080/19490976.2020.1848158

46. Tannahill GM, Curtis AM, Adamik J, Palsson-McDermott EM, McGettrick AF, Goel G, et al. Succinate is an inflammatory signal that induces IL-1β through HIF-1α. *Nature*. (2013) 496:238–42. doi: 10.1038/nature11986

47. Watanabe Y, Nagai F, Morotomi M. Characterization of *Phascolarctobacterium succinatutens* sp. nov., an asaccharolytic, succinate-utilizing bacterium isolated from human feces. *Appl Environ Microbiol*. (2012) 78:511–8. doi: 10.1128/AEM.06035-11

48. Semova I, Carten JD, Stombaugh J, Mackey LC, Knight R, Farber SA, et al. Microbiota regulate intestinal absorption and metabolism of fatty acids in the zebrafish. *Cell Host Microbe*. (2012) 12:277–88. doi: 10.1016/j.chom.2012.08.003

49. Zhang X, Hu Y, Ansari AR, Akhtar M, Chen Y, Cheng R, et al. Caecal microbiota could effectively increase chicken growth performance by regulating fat metabolism. *Microb Biotechnol*. (2022) 15:844–61. doi: 10.1111/1751-7915.13841

50. Zhang T, Hu BW, Duan YH, Deng JP, Yin YL, Kong XF. Dietary chicory powder supplementation affects growth performance, carcass traits, and muscular profiles of amino acids and fatty acids in growing-finishing Xiangcun Black pigs. *J Appl Anim Res*. (2021) 49:46–52. doi: 10.1080/09712119.2021.1876702

51. Umami N, Rahayu ERV, Suhartanto B, Agus A, Suryanto E, Rahman MM. Effect of *Cichorium intybus* on production performance, carcass quality and blood lipid profile of hybrid duck. *Anim Biosci*. (2023) 36:84–97. doi: 10.5713/ab.22.0041

52. Tam JSY, Coller JK, Prestidge CA, Bowen JM. Investigation of TLR4 antagonists for prevention of intestinal inflammation. *Inflammation*. (2023) 46:103–14. doi: 10.1007/s10753-022-01714-0

53. Chen L, Dai M, Zuo W, Dai Y, Yang Q, Yu S, et al. NF-κB p 65 and SETDB1 expedite lipopolysaccharide-induced intestinal inflammation in mice by inducing IRF7/NLR-dependent macrophage M1 polarization. *Int Immunopharmacol*. (2023) 115:109554. doi: 10.1016/j.intimp.2022.109554

54. Zhuang S, Zhong J, Zhou Q, Zhong Y, Liu P, Liu Z. Rhein protects against barrier disruption and inhibits inflammation in intestinal epithelial cells. *Int Immunopharmacol*. (2019) 71:321–7. doi: 10.1016/j.intimp.2019.03.030

55. Guo S, Nighot M, Al-Sadi R, Alhmoud T, Nighot P, Ma TY. Lipopolysaccharide regulation of intestinal tight junction permeability is mediated by TLR4 signal transduction pathway activation of FAK and MyD88. *J Immunol*. (2015) 195:4999–5010. doi: 10.4049/jimmunol.1402598

56. Brandenburg K, Schromm AB, Weindl G, Heinbockel L, Correa W, Mauss K, et al. An update on endotoxin neutralization strategies in Gram-negative bacterial infections. *Expert Rev Anti-Infect Ther*. (2021) 19:495–517. doi: 10.1080/14787210.2021.1834847

57. Gilani S, Chrystal PV, Barekatain R. Current experimental models, assessment and dietary modulations of intestinal permeability in broiler chickens. *Anim Nutr*. (2021) 7:801–11. doi: 10.1016/j.aninu.2021.03.001

58. Anwar U, El-Kott AF, Bilal MQ, Riaz M, Khalid MF, Mustafa R, et al. Supplementation of xylanase levels in lower energy diets on digesta viscosity, blood metabolites and gut health of broiler. *Pak Vet J*. (2023) 43:351–5. doi: 10.29261/pakvetj/2023.033

59. Apperson KD, Cherian G. Effect of whole flax seed and carbohydrase enzymes on gastrointestinal morphology, muscle fatty acids, and production performance in broiler chickens. *Poult Sci*. (2017) 96:1228–34. doi: 10.3382/ps/pew371

60. Kuralkar P, Kuralkar SV. Role of herbal products in animal production—an updated review. *J Ethnopharmacol*. (2021) 278:114246. doi: 10.1016/j.jep.2021.114246

61. Rafeeq M, Rashid N, Tariq MM, Sheikh IS, Mustafa MZ, Shafee M, et al. Effect of herbal extract on the growth performance, serum biochemical composition, ileal histomorphology and immune response of broiler chickens. *Pak J Zool*. (2021) 53:1793–801. doi: 10.17582/journal.pjz/20200505070545

62. Mohammadi Z, Ghazanfari S, Moradi MA. Effect of supplementing clove essential oil to the diet on microflora population, intestinal morphology, blood parameters and performance of broilers. *Eur Poult Sci*. (2014) 78:1–11. doi: 10.1399/eps.2014.51

63. Redoy MRA, Shuvo AAS, Cheng L, Al-Mamun M. Effect of herbal supplementation on growth, immunity, rumen histology, serum antioxidants and meat quality of sheep. *Animal*. (2020) 14:2433–41. doi: 10.1017/S1751731120001196

frontiers | Frontiers in Veterinary Science

TYPE Original Research
PUBLISHED 15 October 2024
DOI 10.3389/fvets.2024.1441074



OPEN ACCESS

EDITED BY
Xianyao Li,
Shandong Agricultural University, China

REVIEWED BY
Wenlin Bai,
Shenyang Agricultural University, China
Xiaolong Kang,
Ningxia University, China

*CORRESPONDENCE
Hongmei Xiao
✉ lhtdyx@126.com

†These authors have contributed equally to this work

RECEIVED 30 May 2024
ACCEPTED 25 September 2024
PUBLISHED 15 October 2024

CITATION
Chang J, Meng F, Zhang R, Feng J, Liu Y, Zhang J, Liu Z, Liang J and Xiao H (2024) Screening and expression validation of key proteins for secondary hair follicle growth in cashmere goats based on iTRAQ quantitative proteomics technology.
*Front. Vet. Sci.* 11:1441074.
doi: 10.3389/fvets.2024.1441074



# Screening and expression validation of key proteins for secondary hair follicle growth in cashmere goats based on iTRAQ quantitative proteomics technology

Jiale Chang[1,2†], Fanhua Meng[1,2†], Ru Zhang[1,2†], Juan Feng[1,2], Yujing Liu[1,2], Junjie Zhang[1,2], Zhaomin Liu[1,2], Jiayue Liang[3] and Hongmei Xiao[1,2*]

[1]College of Life Sciences, Inner Mongolia Agricultural University, Hohhot, China, [2]Inner Mongolia Autonomous Region Key Laboratory of Biomanufacturing, Hohhot, China, [3]Institute of Microbiology, Chinese Academy of Sciences, Beijing, China

**Background:** The growth of secondary hair follicles (SHFs) in cashmere goats has periodic changes, including telogen, anagen, and catagen, during which proteins play important roles as the executor of life activities.

**Results:** In this study, the skin tissues of cashmere goats at three different growth stages of SHFs were collected for proteome sequencing and validation experiments. Through protein differential expression analysis and time series analysis, FKBP prolyl isomerase 10 (FKBP10) and fibrillin 2 (FBN2) were screened as the key proteins for SHF cycle growth of cashmere goats, and albumin (ALB), collagen type I alpha 1 chain (COL1A1) and elastin (ELN) were predicted to be their interacting proteins. The results of quantitative real-time PCR (qRT-PCR), western blot, and immunohistochemistry experiments showed that the mRNA and protein expression levels of FKBP10, FBN2, COL1A1, ELN and ALB were higher in anagen and lower in telogen. They were all highly expressed in the outer root sheath of SHFs in anagen.

**Conclusion:** FKBP10, FBN2, COL1A1, ELN, and ALB can promote the growth of SHFs in cashmere goats. This study lays the foundation for analyzing the growth cycle regulatory mechanism of SHFs in cashmere goats, and provides new ideas for further improving cashmere yield and quality.

KEYWORDS

**cashmere goat, secondary hair follicles, proteomics, western blot, immunohistochemistry, hair follicle cycle**

## 1 Introduction

Cashmere goat (*Capra hircus*) is an important economic breed with the characteristics of drought resistance, strong disease resistance and tolerance to roughage (1, 2). Its cashmere is used as the preferred high-end textile raw material because of its soft texture, good thermal performance and air permeability, and enjoys the reputation of "soft gold" (3). In recent years, with the rapid

development of the economy and the continuous reform and innovation of domestic cashmere products, it has become an inevitable trend to improve cashmere quality and yield (4). Cashmere goats have two different types of hair follicles. The primary hair follicles (PHFs) produce coarse hairs, which mainly provide mechanical protection for the animal bodies due to their thick and strong hair shaft. And SHFs produce cashmere, which have no medulla, are slender and soft and play a role in keeping animals warm (5, 6). SHF is a regenerative system with a complex developmental process, and its growth exhibits periodic changes with light intensity, which is divided into telogen, anagen, and catagen (7). Telogen is from February to March, anagen is from April to November, and catagen is from December to January of the following year (8). The structure of a hair follicle can be divided into five parts from bottom to top, including the hair bulb, keratin hyperplasia area, terminal sclerosis area, abscission area and funnel. The hair bulb surrounding the dermal papilla is the enlarged part of the end of the hair follicle (9). The hair papilla plays an important role in regulating the cyclical cycle of SHFs (10). In the early stage of hair follicle growth, dermal papilla cells proliferate and differentiate to form the inner root sheath and hair shaft. When hair follicles enter a vigorous growth period, their growth rate can reach the fastest. After anagen, all hair follicles enter catagen at similar times, and their activities gradually weaken over time (11). When hair follicles are ready to enter telogen from catagen, the inner root sheaths begin to undergo apoptosis. In telogen, the hair follicles are considered to be in a dormant state, and the hair shafts stop growing and begin to shed. Some studies have shown that telogen plays an important role in the hair follicle growth cycles, with its main function being to store energy, regulate and repair the skin microenvironment for hair follicle regeneration (12).

Proteome refers to the collection of all the corresponding proteins expressed in the genome, that is, the existence and activity of all proteins in cells, tissues, or organisms (13). Proteomics, which takes the proteome as the object, clarifies the expression and functional patterns of all proteins in organisms and has become a hot topic in life science in the post-genomic era. In order to explored the expression pattern of high mobility group nucleosome binding domain protein 1 (HMGN1) in hair follicles and whether the loss of HMGN1 can affect hair follicle development or cycle changes, Furusawa T. found that HMGN1 was expressed in the epidermal basal layer, outer root sheath and hair bulb in adult hair follicles, but not in the inner root sheath and hair shaft by proteomics technology. At the same time, he also found HMGN1 was expressed in some hair follicle stem cells (14). Yang et al. (15) screened for differentially expressed proteins in the skins of Yangtze River Delta white goats with type III and non type III wool, and identified four proteins. Among them, fibrinogen beta chain isoform 1 and ATP synthase beta subunit (ATB5B) were up-regulated in the skins with type III wool, while succinyl-CoA:3-ketoacid-coenzyme A transferase 1-mitochondrial-like and actin-cytoplasmic 1 (ACTB) were up-regulated in the skins with non type III wool, indicating that these four proteins play important roles in different aspects of hair follicle development. Through comprehensive analysis of cashmere goat skin transcriptome and proteome, Dai et al. (16) found that overexpression of thymosin beta 4 (Tβ4) in hair follicles could effectively increase cashmere yields. By the same method, Liu et al. (17) discovered that keratin (KRT) and collagen alpha families might play important roles in goat hair follicles and wool curvature development. Li et al. (18) confirmed that DSC2 gene is key to the woolly straight phenotype in goats through studying the differences of protein abundance in different fiber ranges from 18 sheep and goat wool samples. In the study on hair follicles in cashmere goats, Gao et al. (19) found that the expression levels of KRT1, KRT5, KRT25 and KRT71 were highest in anagen of hair follicles. In addition, studies have shown that *KRTAP28-1*, *KRTAP27-1*, *KRTAP24-1*, *KRTAP11-1*, *KRTAP15-1* and *KRTAP8-1* gene mutations are associated with cashmere fiber diameter (20–25), which has the value of molecular markers for improving cashmere diameter.

As a special biological resource, Albas white cashmere goats not only have delicious meat but are also recognized around the world for their unique cashmere. Many researchers try to understand the species at the molecular, cellular, and even individual levels, further improve its breeding, and expand the quantity and scale of breeding in order to improve cashmere yield and quality (26–29). Especially in recent years, many genes and proteins related to economic traits have been found through various omics analyses, which provide methods for the study on hair follicle growth and development in cashmere goats (30–33). However, research in the interactions between proteins regulating hair follicle growth and development, as well as the mechanisms related to hair follicle growth in cashmere goats, remains unresolved (34). In this study, skin samples of cashmere goats from three different periods were collected for proteome sequencing and validation experiments. Through sequencing data analysis, key proteins related to hair follicle growth of cashmere goats were screened, and their interacting proteins were predicted by bioinformatics methods. Meanwhile, the expression of key proteins and their interacting proteins was detected at the gene and protein levels by qRT-PCR, western blot, and immunohistochemistry technology. The purpose of this study was to lay the foundation for analyzing the regulation mechanism of SHF growth cycle of cashmere goats.

## 2 Methods

### 2.1 Animal and tissue collection

One centimeter square scapular skin samples of three 1.5-year-old Albas female cashmere goats with similar body weight and consistent feeding conditions according to standard cashmere goat husbandry practices were collected in anagen (September), catagen (December) and telogen (February) of SHFs. The skin samples from living body surface after hair removal and alcohol disinfection were collected by sterile surgical blades after the muscle tissue anesthetized with 1% pentobarbital sodium (Sinopharm Chemical Reagent Co., Ltd., China). Then Yunnan Baiyao powder (Yunnan

Abbreviations: FKBP10, FKBP prolyl isomerase 10; FBN2, Fibrillin 2; ALB, Albumin; COL1A1, Collagen type I alpha 1 chain; ELN, Elastin; qRT-PCR, Quantitative real-time PCR; iTRAQ/TMT, Isobaric tag for relative absolute quantitation/tandem mass tags; LC-MS/MS, Liquid chromatography-tandem mass spectrometry; PPI, Protein-protein interaction; BCA, Bicinchoninic acid; PVDF, Polyvinylidene fluoride; GAPDH, Glyceraldehyde-3-phosphate dehydrogenase; SHFs, Secondary hair follicles; PHFs, Primary hair follicles; GO, Gene Ontology; KEGG, Kyoto Encyclopedia of Genes and Genomes; BP, Biological process; MF, Molecular function; CC, Cellular component; STEM, Short Time-series Expression Miner; CE, Cell envelope; FKBPs, FK506-binding proteins; FBN, Fibrillar protein; FN, Fibronectin; CCA, Congenital contractural arachnodactyly; MD, Macular degeneration.

Baiyao Group Co., Ltd., China) was applied to the wound sites to stop bleeding. The samples are divided into three parts, one part of them was placed in 4% paraformaldehyde (biosharp, Anhui, China) for paraffin section preparation, and the other two parts were placed in liquid nitrogen for sequencing and subsequent molecular experiments. All sample collections were conducted in accordance with the International Guiding Principles for Biomedical Research Involving Animals and with the approval of the Experimental Animal Welfare and Ethics Committee of Inner Mongolia Agricultural University.

## 2.2 Paraffin section embedding

The fixed skin tissues in paraformaldehyde were taken out, washed with PBS, then soaked in 50% alcohol for 30 min, 70% alcohol for 1 h, 80% alcohol for 1 h, and 95% alcohol for 1 h, and dehydrated with anhydrous ethanol I and II for 2 h, respectively. The samples were soaked in xylene and anhydrous ethanol (1:1) for 1 h and in xylene and paraffin (1:1) at 37°C overnight. After transparency with xylene, the samples soaked in soft wax and hard wax at 52°C and 56°C for 2 h, respectively, and embedded for tissue sections. One part was used for HE staining to observe the quality of sections, and the other part was used for immunohistochemical detection and microscopy photographing.

## 2.3 HE staining

Paraffin sections were deparaffinized in xylene for 10 min, twice. They were then hydrated through 95, 85, and 75% ethanol, followed by rinsing with deionized water. After stained with hematoxylin (LEAGENE, Anhui, China) for 10 min, the sections were rinsed with deionized water again, followed by differentiation in 1% acid alcohol (LEAGENE, Anhui, China), and another rinsed with deionized water. Eosin (LEAGENE, Anhui, China) staining was performed for 10 min. The sections were dehydrated through graded alcohols: 80, 85, 95%, and absolute ethanol, and in xylene twice for 10 min each time. Finally, neutral gum was applied to the sections, which were allowed to dry before being examined under a microscope (Eclipse Ti2-U, Nikon, Tokyo, Japan).

## 2.4 Protein extraction

Appropriate amount of frozen skin samples was taken and transferred into 1.5 mL centrifuge tubes. Samples were lysed by adding RIPA Lysis Buffer (Beyotime, Shanghai, China) and protease inhibitor PMSF (Beyotime, Shanghai, China) included to achieve a final concentration of 1 mM. Samples were subjected to ultrasonication on ice using a power setting of 80 W with cycles of 1 s on and off, for a total duration of 3 min. The lysates were centrifuged at room temperature at 12,000 × g for 10 min. The supernatant was carefully collected and subjected to a second centrifugation step under the same conditions. The protein concentration of supernatant was measured by BCA Protein Assay Kit (Solarbio, Beijing, China) and stored at −80°C after subpacking.

## 2.5 Proteome sequencing and data analysis

The different period total sample protein extracted by protein concentration and SDS-PAGE detection, were subjected to trypsin digestion and isobaric tag for relative absolute quantitation/tandem mass tags (iTRAQ/TMT) labeling. Then an equal amount of each labeled sample was mixed and separated by chromatography. Finally, the three group samples (anagen, catagen, and telogen) with 3 biological replicates in each group were analyzed by liquid chromatography-tandem mass spectrometry (LC-MS/MS). Chromatographic conditions: samples were uploaded at a flow rate of 400 nL/min to an analytical column Acclaim PepMap RSLC, 75 μm × 25 cm (RP-C18 ionopticks, Thermo Fisher) for separation. Mobile phase A phase: $H_2O$-FA (99.9:0.1, v/v); mobile phase B phase: ACN-$H_2O$-FA (80:19.9:0.1, v/v/v). Gradient elution conditions: 0–27 min, 2–21% B; 27–37 min, 21–42% B; 37–40 min, 42–95% B; 40–44 min, 95% B. Mass spectrometry conditions: capillary voltage of 1.5 kV, drying gas temperature of 180°C, flow rate of 3.0 L/min, primary MS scanning range of 100–1,700 m/z, ion mobility range of 0.6–1.6, collision energy range of 20–59 eV.

Based on the reliable proteins obtained by LC-MS/MS detection and database (Maxquant 1.6.17.0) search and compute, visualization of protein results after quality assessment and data normalization, the differential proteins were screened, and the screening conditions were set as Foldchange ≥2 (up-regulated protein expression was greater than or equal to 2 times, or down-regulated protein expression was less than or equal to 0.5 times) and $p < 0.05$. Correlation analysis, expression pattern clustering heat map, and Venn analysis were performed in R (Version 4.1.0). Various annotation information was extracted, and protein functions were mined from databases (UniProt, KEGG, GO, KOG/COG, etc.). At the same time, Gene Ontology (GO) analysis and Kyoto Encyclopedia of Genes and Genomes (KEGG) analysis[1] of differential proteins obtained were performed. In the enrichment analysis, the Benjamini–Hochberg method was utilized for multiple test correction. The STRING (35)[2] was used to upload the differentially expressed proteins in different periods to the String database for analysis. The visual protein–protein interaction (PPI) network was created by Cytoscape (Version 3.8.2), and the time series analysis of protein expression was performed by STEM (Version 1.3.13).

## 2.6 qRT-PCR validation

Total RNA was extracted from frozen cashmere goat skin samples using TRIzon Reagent (CWBIO, Jiangsu, China). The concentration and quality of the total RNA were assessed using NanoDrop 1000 (Thermo, Massachusetts, United States). The RNA extracted was reverse-transcribed into cDNA by the PrimeScript™ RT Master Mix kit (TAKARA, Dalian, China). The mRNA coding region sequences of the genes were retrieved from NCBI database,[3] and the fluorescent quantitative specific primers of the genes were designed using Primer

1 https://cloud.oebiotech.com/#/bio/detail?number=7e90ec6d-9ef9-422a-8301-fc75b49970f3
2 https://string-db.org/
3 https://www.ncbi.nlm.nih.gov/

TABLE 1 Primer sequences of candidate and reference genes.

| Gene name | NCBI Reference Sequence | Primer sequences | | Product length (bp) | TM (°C) |
|---|---|---|---|---|---|
| *COL1A1* | XM_018064893.1 | F | GGTAGCCCTGGTGAAAATGGA | 196 | 60 |
| | | R | CTTCACCCTTAGCACCCACA | | |
| *ALB* | XM_005681744.2 | F | GCGCTGATTTCCCTCTATTCA | 1,910 | 60 |
| | | R | GCTGAGATGCTTGTGGTTGTG | | |
| *FKBP10* | XM_005694317.3 | F | ATGGAACAAGGAGGACACCG | 1,133 | 60 |
| | | R | TGATGAAGGTGGAAAACTCCTC | | |
| *FBN2* | XM_018050706.1 | F | GCGTTACTGCACTGATGTTGA | 885 | 60 |
| | | R | ATCCTGGCAAACCCTCTTGG | | |
| *ELN* | XM_018040738.1 | F | GGAAAGTGCCAGGAGTGGG | 253 | 60 |
| | | R | TAAGGCAGTCCATAGCCACC | | |
| *GAPDH* | XM_005680968.3 | F | CTTCAACAGCGACACTCACTCT | 122 | 60 |
| | | R | CCACCACCCTGTTGCTGTA | | |

5.0. The primer sequences are shown in Table 1. The relative expression levels of *ALB, COL1A1, FKBP10, ELN,* and *FBN2* genes were verified by qRT-PCR, and *GAPDH* (glyceraldehyde-3-phosphate dehydrogenase) was used as the reference gene. The reaction mix: TB Green Premix Ex Taq II (Tli RNaseH Plus) (2X) 10 µL, forward primer 0.8 µL, reverse primer 0.8 µL, cDNA 2 µL, and $ddH_2O$ 6.4 µL. Programs: initial denaturation (95°C 30 s), quantification (95°C 5 s, Tm 30 s) for a total of 45 cycles, melting (95°C 5 s, Tm 60 s, 95°C), and cooling (50°C 30 s).

## 2.7 Western blot

The target protein separated by SDS-PAGE electrophoresis was transferred to a polyvinylidene fluoride (PVDF) membrane soaked in methanol, and the blocking solution was added for shaking 1 h on a shaker. Then the PVDF membrane was washed with TBST 3 times. ALB, COL1A1, FKBP10, ELN, FBN2, and GAPDH were incubated overnight with primary antibodies (Bioss, Beijing, China). After PVDF membrane was washed with TBST 3 times again, the secondary antibody (GeneTex, United States) was added and incubated for 2 h. Followed by washing the PVDF membrane with TBST, and ECL luminescent solution (Servicebio, Wuhan, China) was applied to the membrane and imaged in an imaging device (ImageQuant LAS 500, GE Healthcare, Piscataway, New Jersey, United States).

## 2.8 Immunohistochemistry

Paraffin sections were baked at 65°C and then deparaffinized in xylene. They were subsequently hydrated through a graded series of ethanol: absolute ethanol, 95, 85, and 75% ethanol, followed by immersion in distilled water. The sections were then immersed in citrate buffer and microwaved for 8 min, followed by cooling the sections to room temperature. After cooling, they were washed with PBS, treated with 3% hydrogen peroxide for 10 min, and rinsed with PBS. The sections were incubated with 5% sheep serum at room temperature for 20 min. Primary antibody (Bioss, Beijing, China) was added, and the sections were incubated overnight at 4°C. After incubation, the sections were incubated with secondary antibody (GeneTex, United States) at 37°C in the dark for 30 min and washed with PBS. DAB working solution (Solarbio, Beijing, China) was added for color development. Counterstaining was performed with hematoxylin for 1–3 min, followed by washing with distilled water, differentiation with acid alcohol, and washing with PBS. They were then dehydrated through a graded series of ethanol: 70, 80, 90, 95%, and absolute ethanol. Sections are dipped twice in xylene. Neutral gum was applied to the sections, which were allowed to dry before examination under a microscope.

## 2.9 Statistical analysis

The relative expression levels of *ALB, COL1A1, FKBP10, ELN,* and *FBN2* genes were calculated using the $2^{-\Delta\Delta Ct}$ method. Data were analyzed using one-way ANOVA with SPSS (Version 25), followed by multiple comparisons using the Duncan method, and graphs were generated using GraphPad Prism (Version 9.5). $p < 0.05$ was considered statistically significant.

# 3 Results

## 3.1 Quality of tissue sections

The skin sections of Inner Mongolian Cashmere goats at different growth stages prepared were stained with hematoxylin and eosin (Figure 1). The growth cycles of PHFs in cashmere goats is different from that of the SHFs. In anagen, SHFs were round and full, indicating the active growth stage of the follicles. Dermal papillae were present in SHFs. In catagen, SHFs exhibited signs of atrophy. In telogen, further contraction of SHFs was observed, with reduced growth activity. The distribution of SHFs with clear outlines at different stages was suitable on the slices, showing that the section quality was better to can be used for subsequent experiments.

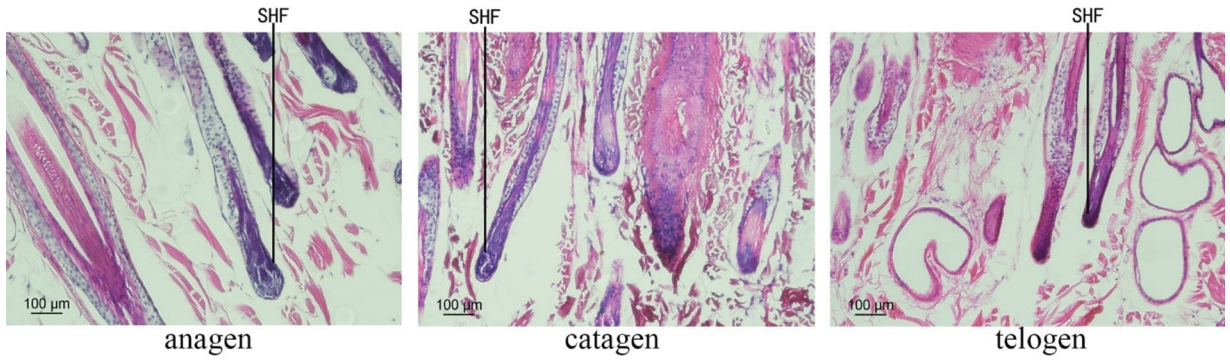


FIGURE 1
SHF morphological characteristics of cashmere goats.

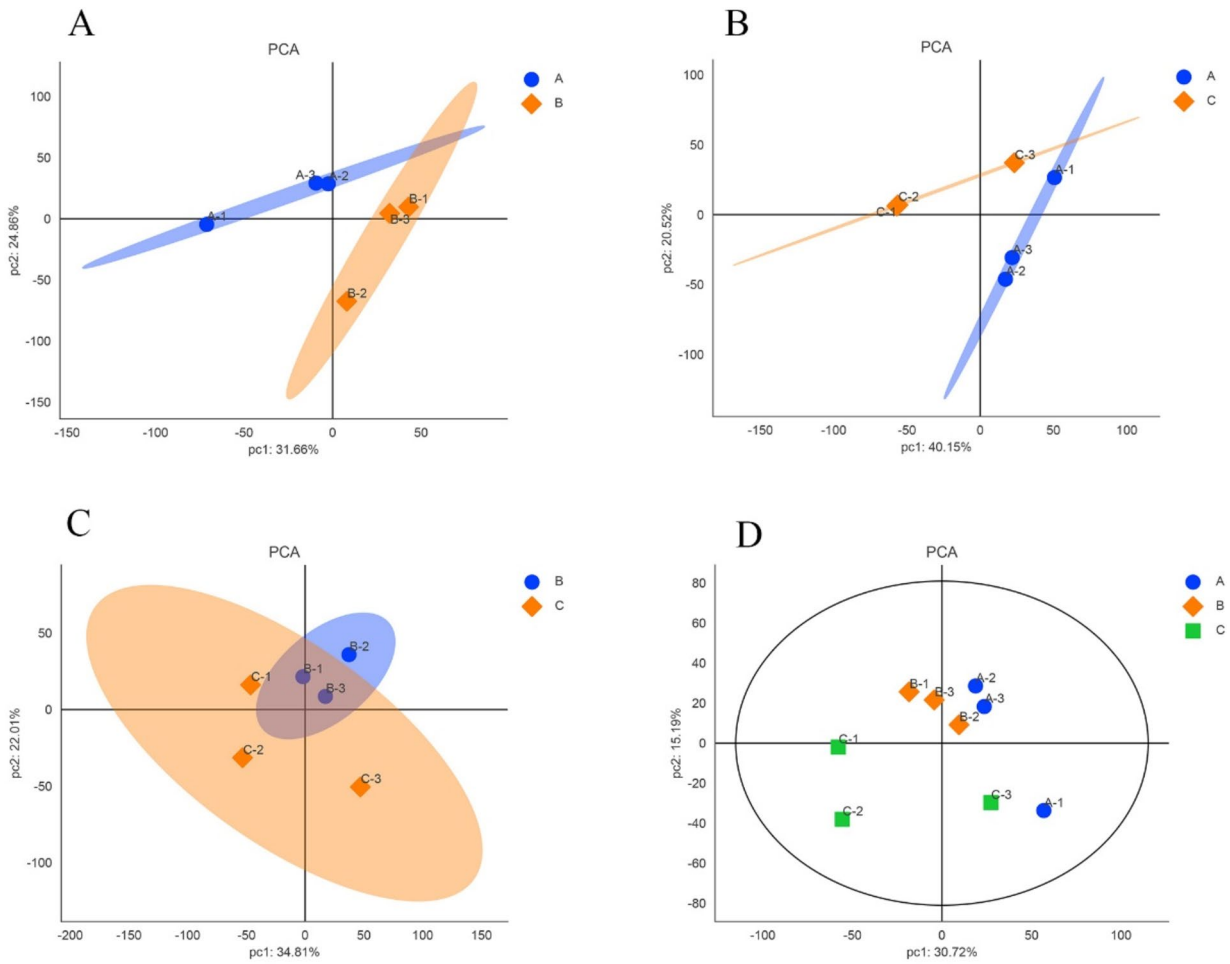


FIGURE 2
Principal component analysis of samples in different growth periods of SHFs in cashmere goats. **(A)** anagen and catagen **(B)** anagen and telogen **(C)** catagen and telogen **(D)** anagen, catagen and telogen. A, B, and C represent anagen, catagen, and telogen. In each figure, each point represents one replicate of an experimental group.

## 3.2 Principal component analysis

The expression levels of reliable proteins obtained from raw data through database retrieval and screening were subjected to principal component analysis (PCA). The PCA analysis results were shown in Figure 2. The more points clustered, the higher similarity between the samples, and the more points discrete, the lower similarity between the samples. As shown in Figures 2A,B, the confidence zones of the anagen samples and the other two period samples overlap less, and there are large differences between them. In Figure 2C, although there are

differences between the catagen and the telogen samples, the reason for the larger overlap between them comparing with the telogen and the anagen samples may be due to the short time interval between catagen and telogen. Figure 2D showed that the three samples in anagen and catagen were more concentrated, indicating that there is little difference within the group, and the samples showed better correlation and similar of protein composition. The three samples in telogen are relatively dispersed, which may be due to individual differences in telogen.

## 3.3 Differential protein screening and specificity analysis of cashmere goat SHFs at different growth stages

The proteins expressed in three different periods were screened separately. In anagen and catagen, there were 57 differentially expressed proteins, of which 24 were up-regulated proteins and 33 were down-regulated proteins. The significantly up-regulated proteins were KLK6, FBN2, GLYATL2, LOC102188300, CYP4X1, LOC102172669, etc., and the significantly down-regulated proteins were NAAA, QTRT1, A0A452G482, LGALS15, LOC102180520, BRAP, etc. (Figures 3A,D). In catagen and telogen, there were 31 differential proteins, of which 12 were up-regulated proteins and 19 were down-regulated proteins. The significantly up-regulated proteins were MBNL2, PLEKHF1, QTRT1, USP8, GTF2F1, ADD2, etc., and the significantly down-regulated proteins were NLGN2, TTC21B, GRM2, BRAP, GC, SYN1, etc. (Figures 3B,E). In anagen and telogen, there were 37 differentially expressed proteins, of which 19 were up-regulated proteins and 18 were down-regulated proteins. The significantly up-regulated proteins were LOC102172669, LOC108633164, KRT4, S100A7A, FBN2, CRNN, etc., and the significantly down-regulated proteins were A0A452FY47, LGALS15, TTC21B, POLR3GL, LGALS16, LOC102180520, etc. (Figures 3C,F).

The screened differentially expressed proteins in different periods were made into a Venn diagram (Figure 3G). Figure 3G shows that a total of 93 differential proteins were enriched in three periods. The largest number of differential proteins, 57, were found in anagen and catagen. The least number of differential proteins was found in catagen and telogen, with only 31. There were 31 differential proteins specific to anagen and catagen, 21 differential proteins specific to catagen and telogen, and only 12 differential proteins specific to anagen and telogen. Three differential proteins among anagen, catagen and telogen were screened, namely BRAP, MPO and LOC102180520.

## 3.4 Differential protein Gene Ontology and Kyoto Encyclopedia of Genes and Genomes analysis

In order to comprehensively and systematically describe the functions of differential proteins in cells and organisms, the GO entries corresponding to the number of differential proteins greater than 1 were screened through GO annotation. Analysis was performed according to biological process (BP), molecular function (MF), and cellular component (CC). GO terms were ranked from the largest to the smallest based on their-log10(*p*-value), and the top 10 terms within each category (biological process, molecular function, and cellular component) were selected. The differential proteins in growth phase and degenerative phase mainly involved in the biological process of cell adhesion; in the cellular component, they were enriched in the cytosol, extracellular region, and other components; in terms of molecular function, they mainly involved in calcium ion binding, carbohydrate binding, and transition metal ion binding (Figure 4A). The differentially expressed proteins in catagen and telogen mainly involved in four biological processes: endosome organization, positive regulation of canonical Wnt signaling pathway, positive regulation of transcription, and cell adhesion. In the cellular component, they mainly were enriched in the extracellular space; in terms of molecular function, they involved in metal ion binding and other functions (Figure 4B). The differential proteins in the growth phase and the resting phase mainly involved in the biological processes of peptide cross-linking and cell adhesion. In the cellular component, they mainly were enriched in extracellular region, cytosol, and other components; in terms of molecular function, they mainly involved in calcium ion binding, transition metal ion binding, etc. (Figure 4C). Through the analysis of the GO categories of differential proteins across three periods, it was discovered that these proteins were predominantly enriched in the functions related to cell adhesion, cytosol, extracellular region, calciumion binding and carbohydrate binding. Differential protein enrichment on cell adhesion indicates the importance of cell–cell interactions in the hair follicle growth cycles. Differential protein enrichment on the cytosol and extracellular region indicates the cytosol and extracellular region as crucial sites for signal transduction and material exchange during the hair follicle cycle transition. Differential protein enrichment on calciumion binding may shed light on the pivotal role of calcium signaling in regulating the hair follicle growth cycles. Furthermore, differential protein enrichment on carbohydrate binding suggests that carbohydrate may play a role in structural support and signal transduction in regulating the hair follicle growth cycles. This not only underscores the central role of these biological processes and functions in regulating the hair follicle growth cycles, but also hints at underlying mechanisms that persist throughout the lifespan of the hair follicle.

Pathway analysis of differential proteins was performed using the KEGG database, and the significance of differential protein enrichment in each pathway entry was calculated by hypergeometric distribution test. Pathways were ranked from the largest to the smallest based on their-log10(*p*-value), and the top 20 pathways were selected for analysis. In anagen and catagen, MPO, NCF1, THBS4, and NCF2 were enriched in the phagosome pathway. Proteins enriched in glycolysis/gluconeogenesis pathway were A0A452DP35, FBP2, and HK3; proteins enriched in the arachidonic acid metabolism pathway were ALOX15, LOC102172669, and LOC102187932 (Figure 4D). LOC102172488 and TF were enriched in the mineral absorption pathway in catagen and telogen; lOC102172488 and TF were enriched in the ferroptosis pathway. AGT and GRM2 were enriched in the phospholipase D signaling pathway. LOC102172488 and TF were enriched in the HIF-1 signaling pathway (Figure 4E). At the growing and resting stages, S100A7A and LOC108633164 were enriched by the IL-17 signaling pathway, and ALOX15 and LOC102172669 were enriched in the arachidonic acid metabolism pathway (Figure 4F).

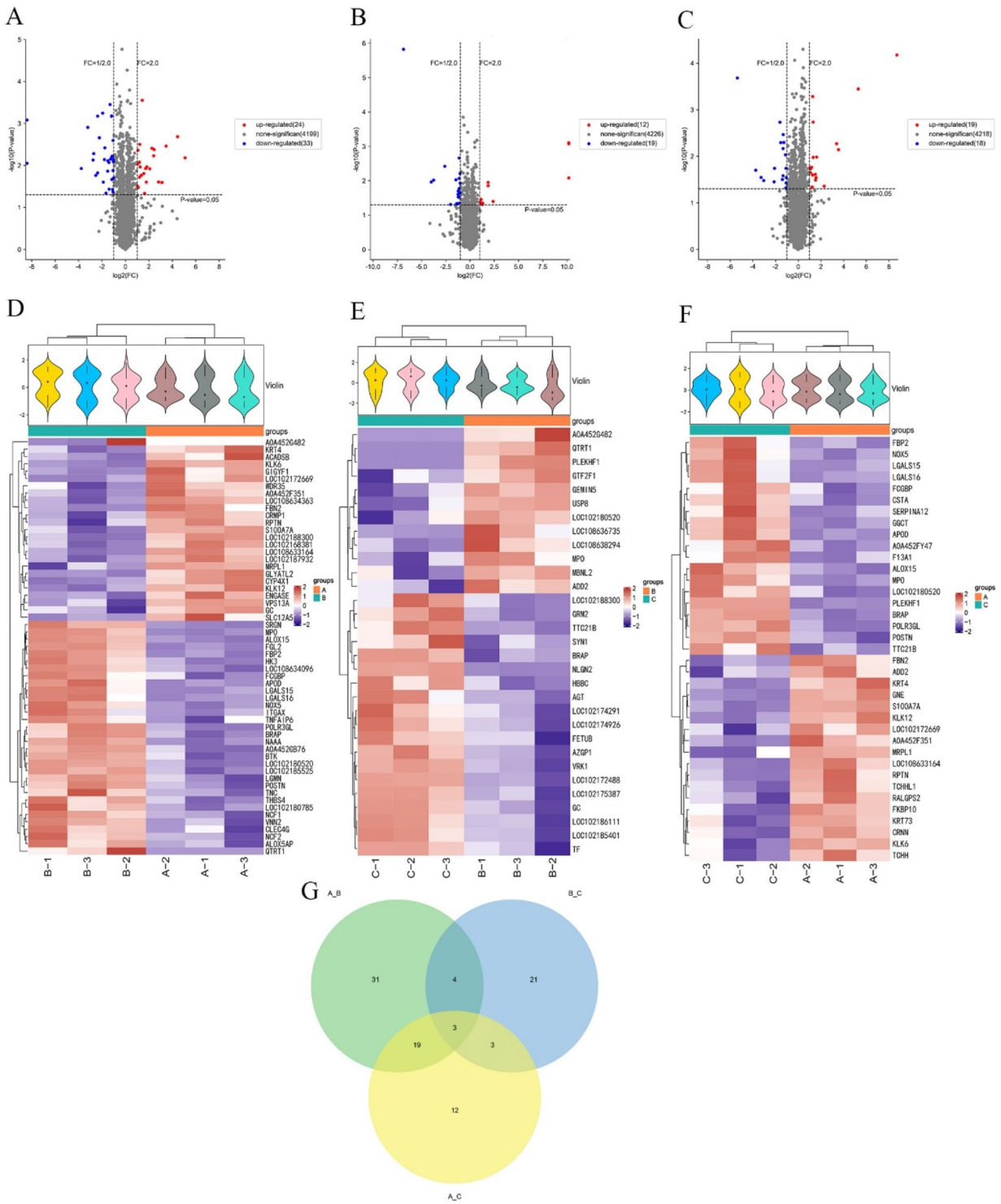


FIGURE 3
Screening of differential proteins in the skins of cashmere goats at different stages. **(A)** Volcano map of cashmere goat skins differential proteins in anagen and catagen. **(B)** Volcano map of cashmere goat skins differential proteins in catagen and telogen. **(C)** Volcano map of cashmere goat skins differential proteins in anagen and telogen. **(D)** Cashmere goat skins in anagen and catagen differential protein cluster analysis heat map. **(E)** Cashmere goat skins in catagen and telogen differential protein cluster analysis heat map. **(F)** Cashmere goat skins in anagen and telogen differential protein cluster analysis heat map. "+" represents the median. The vertical axis is the protein expression level, red indicates higher protein expression, and blue indicates lower protein expression. **(G)** Venn diagram of differential proteins. The numbers represent the number of differential proteins. A, B, and C represent anagen, catagen, and telogen.

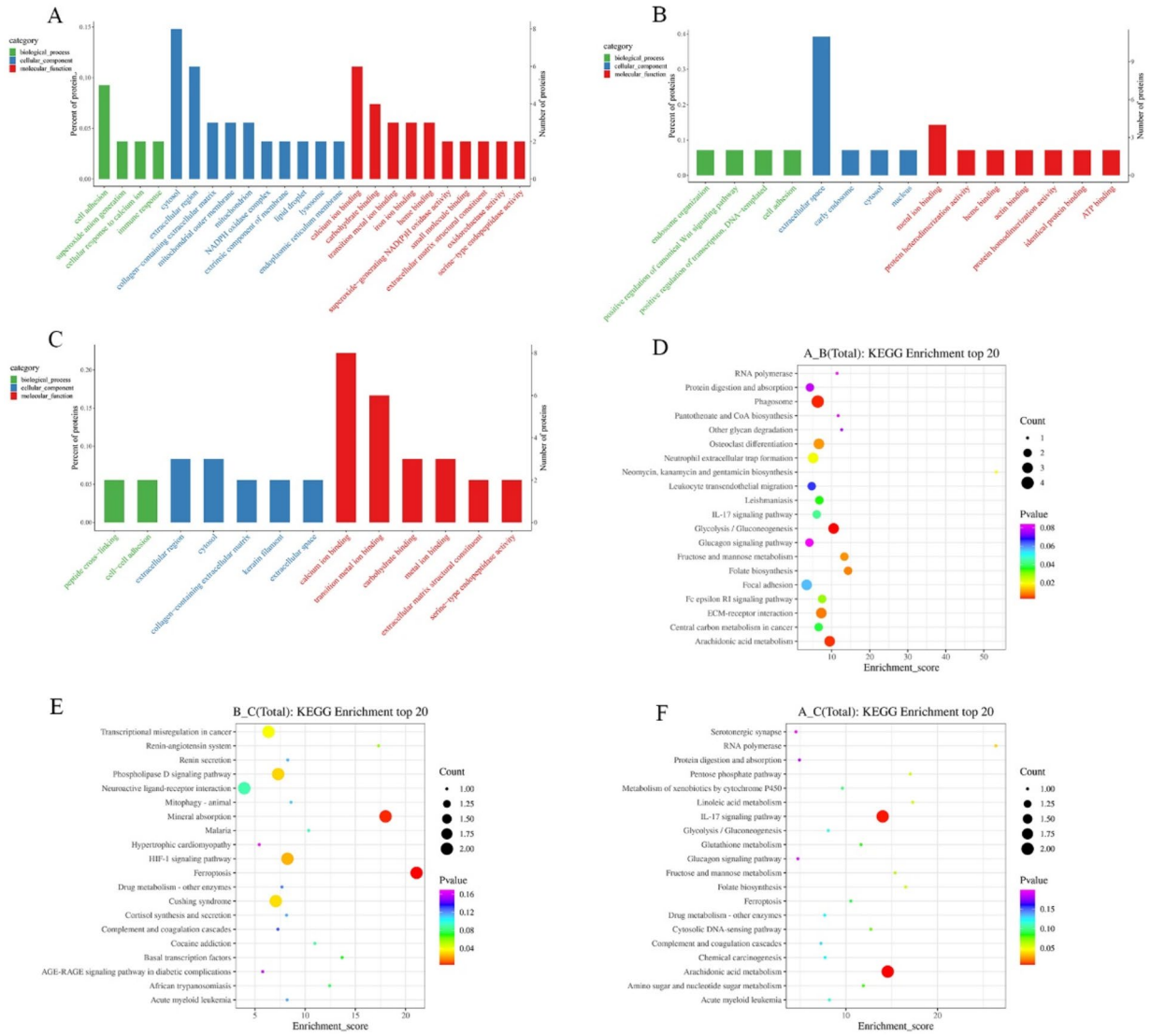


FIGURE 4
GO and KEGG enrichment analysis of differential proteins in different periods. **(A)** GO enrichment analysis in anagen and catagen. **(B)** GO enrichment analysis in catagen and telogen. **(C)** GO enrichment analysis in anagen and telogen. **(D)** KEGG enrichment analysis in anagen and catagen. **(E)** KEGG enrichment analysis in catagen and telogen. **(F)** KEGG enrichment analysis in anagen and telogen. The larger the bubble, the greater the number of differential proteins contained. The bubble color changes from red to green to blue-purple, and the smaller *p*-value, the greater the significance.

## 3.5 Differential protein PPI and time series analysis

The differential proteins were analyzed in the STRING database to obtain the interaction relationship of the differential proteins. Then the interaction network visualization map of the top 25 node proteins with node connectivity was drawn by the Python software package "network." There were 9 proteins up-regulated at the growth and regression stages, and they were LOC102172669, CYP4X1, ACADSB, A0A452F351, LOC102168381, KLK6, FBN2, RPTN, and CRMP1 according the interaction strength with other proteins. There were 16 down-regulated proteins, and the order of interaction with other proteins from strong to weak was NCF2, ALOX5AP, FGL2, NCF1, LOC102185525, ALOX15, SRGN, VNN2, BTK, LGMN, NOX5, FBP2, APOD, BRAP, FCGBP, and TNFAIP6 (Figure 5A). In telogen and catagen, 3 proteins up-regulated interacting with other proteins from strong to weak was QTRT1, ADD2, and USP8, and 11 proteins down-regulated interacting with other proteins from strong to weak were LOC102185401, FETUB, AGT, LOC102172488, TF, AZGP1, SYN1, NLGN2, GRM2, LOC102174926, and LOC102174291 (Figure 5B). At the growing and resting stages, 11 proteins up-regulated interacting with other proteins from strong to weak were CRNN, PPTN, TCHHL1, TCHH, KLK6, ADO2, FBN2, A0A452F351, KRT73, KLK12, and GNE. While 5 proteins were down-regulated, and the order of interaction with other proteins from strong to weak was APOD, GGCT, FBP2, CSTA, and FCG8P (Figure 5C).

Using Short Time-series Expression Miner (STEM) software, the time series analysis of differential protein expression in anagen,

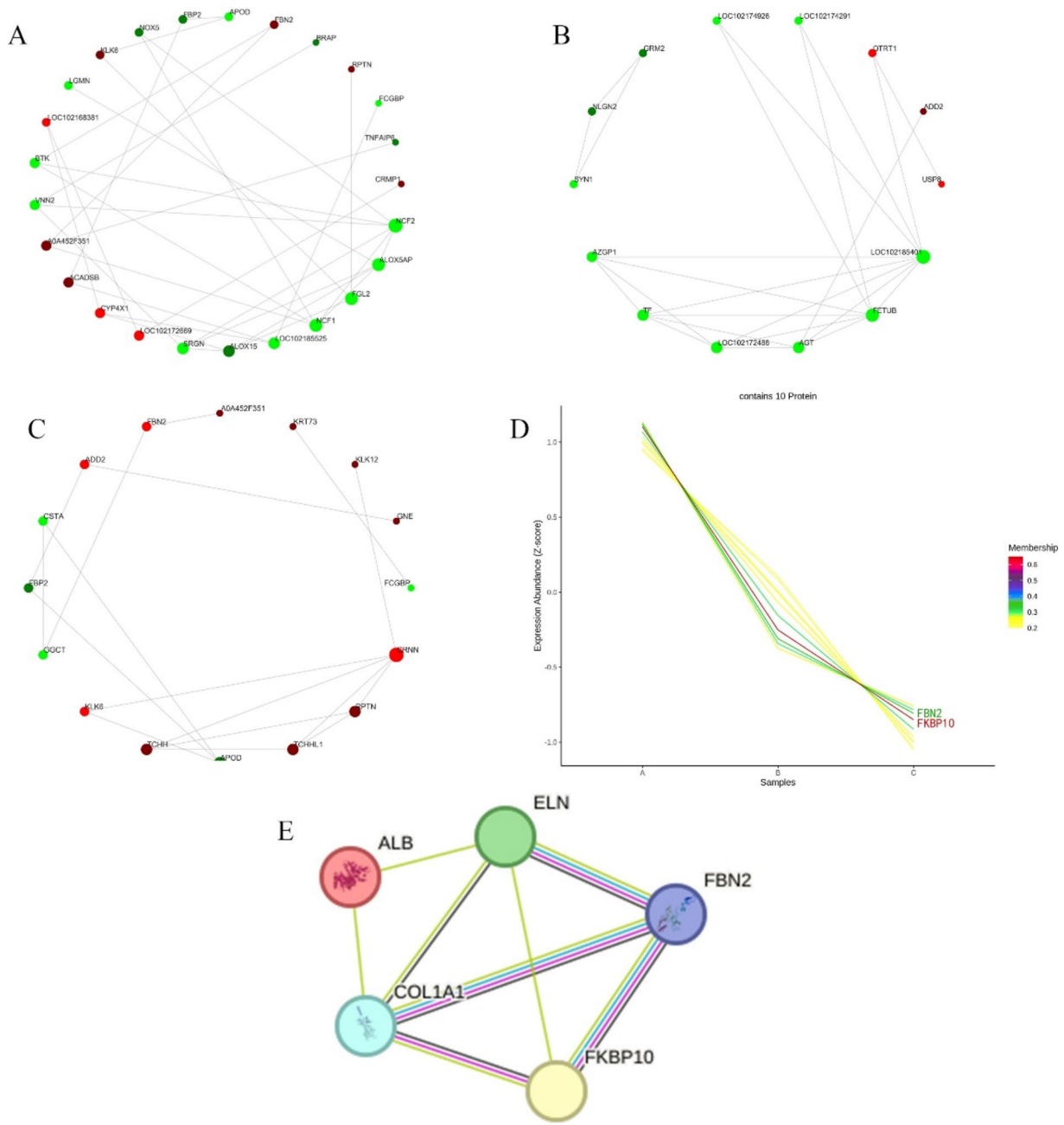


FIGURE 5
Differential protein interaction network and time sequence analysis. **(A)** Differential proteins interactions in anagen and catagen. **(B)** Differential protein interactions in catagen and telogen. **(C)** Differential protein interactions in anagen and telogen. In each figure, the red circle represents the up-regulated proteins; the green circle represents the down-regulated proteins; and the circle size represents the degree of connection. **(D)** Differential protein time series analysis. A, B, and C represent anagen, catagen, and telogen. Shades of color represent the degree of match. **(E)** Node proteins interaction network. Light blue and pink lines represent known interactions; blue comes from the selected database, and pink represents experimental determination; green, red, and dark blue lines represent predictive interactions; green represents gene neighborhoods; red represents gene fusion; and dark blue represents gene co-occurrence; the yellow line segment represents those mentioned in the literature; and the black line segment represents co-expression.

catagen and telogen was carried out, and then the corresponding change trend model was constructed. Cluster that matched the trend of highest expression during anagen, followed by the catagen, and lowest in telogen were selected, as shown in Figure 5D. The number of lines in Figure 5D represents the final number of proteins matched to this cluster. The membership value represents the degree of each protein fitting into this cluster. The larger membership values, the better fit. Finally, 10 proteins were screened, including FKBP10, FBN2, GNE, TCHH, KRT4, RALGPS2, TCHHL1, CRNN, KRT73 and GTF2F1.

10.3389/fvets.2024.1441074

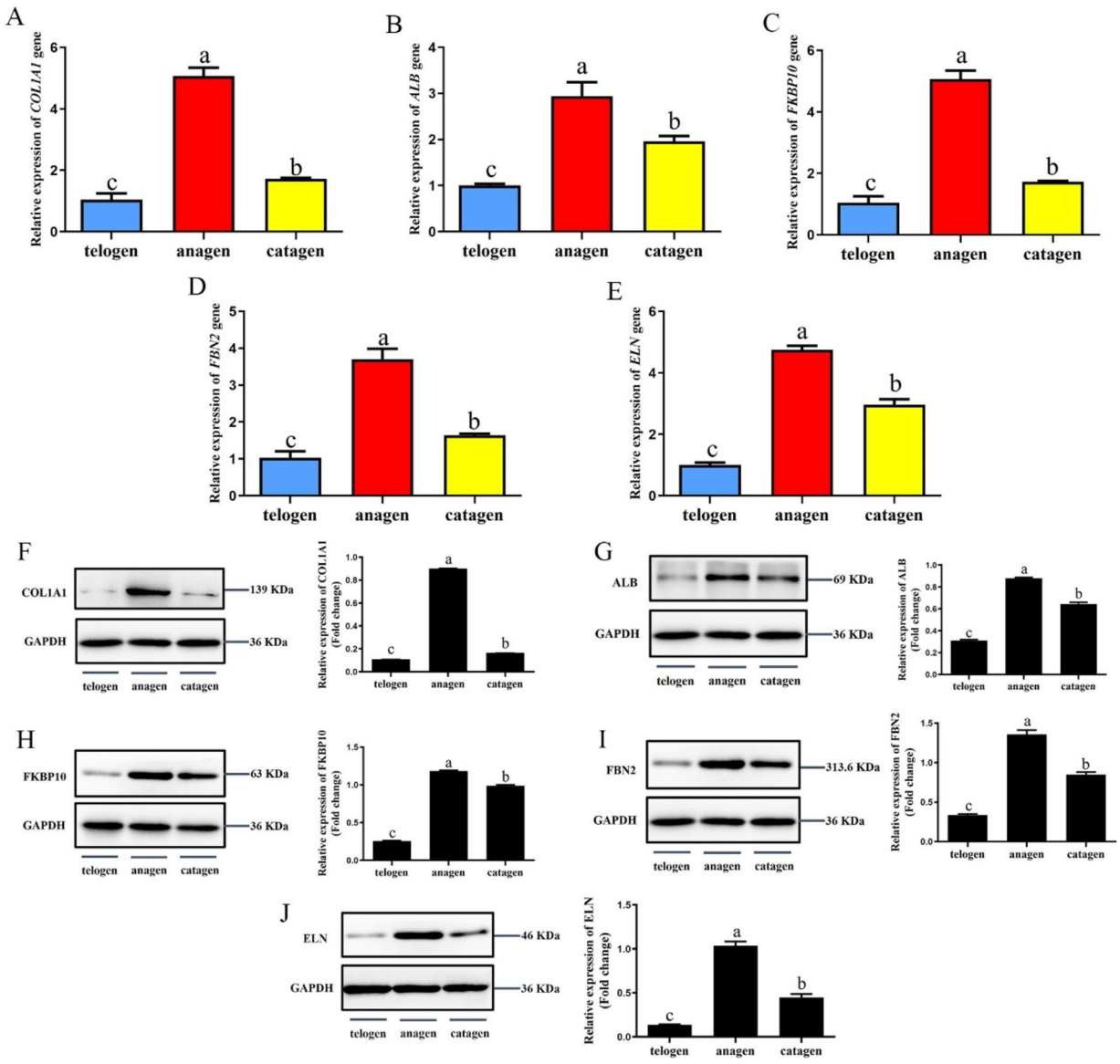


FIGURE 6
Expression of interaction proteins and their genes in the skins of SHFs in different growth periods. **(A)** The relative expression levels of *COL1A1* gene. **(B)** The relative expression levels of *ALB* gene. **(C)** The relative expression levels of *FKBP10* gene. **(D)** The relative expression levels of *FBN2* gene. **(E)** The relative expression levels of *ELN* gene. **(F)** COL1A1 expression and semi-quantitative analysis. **(G)** ALB expression and semi-quantitative analysis. **(H)** FKBP10 expression and semi-quantitative analysis. **(I)** FBN2 expression and semi-quantitative analysis. **(J)** ELN expression and semi-quantitative analysis.

## 3.6 Prediction of interaction proteins for key proteins

PPI analysis was performed on FKBP10 and FBN2 screened by the STRING online protein database. The number of protein network nodes was 5, and the average number of nodes was 3.2. The results showed that the interaction proteins of FKBP10 and FBN2 were COL1A1 and ELN. There is an interaction between FKBP10 and FBN2, and their homologues are co-expressed and interact with each other in other organisms. COL1A1 and FKBP10 are co-expressed in other organisms. COL1A1 interacts with both ELN and ALB (Figure 5E).

## 3.7 Expression of key proteins, interacting proteins, and their genes in SHF growth cycles

The relative expression levels of *COL1A1*, *ALB*, *FKBP10*, *FBN2*, and *ELN* genes in different growth cycles of cashmere goat SHFs were significantly different ($p < 0.05$) (Figures 6A–E). They were expressed highest in the growing period, followed by the degenerative period, and lowest in telogen.

The protein expression levels of COL1A1, ALB, FKBP10, FBN2, and ELN in skins was detected by western blot (Figures 6F–J). The results showed that the expression trend of these proteins in the skins

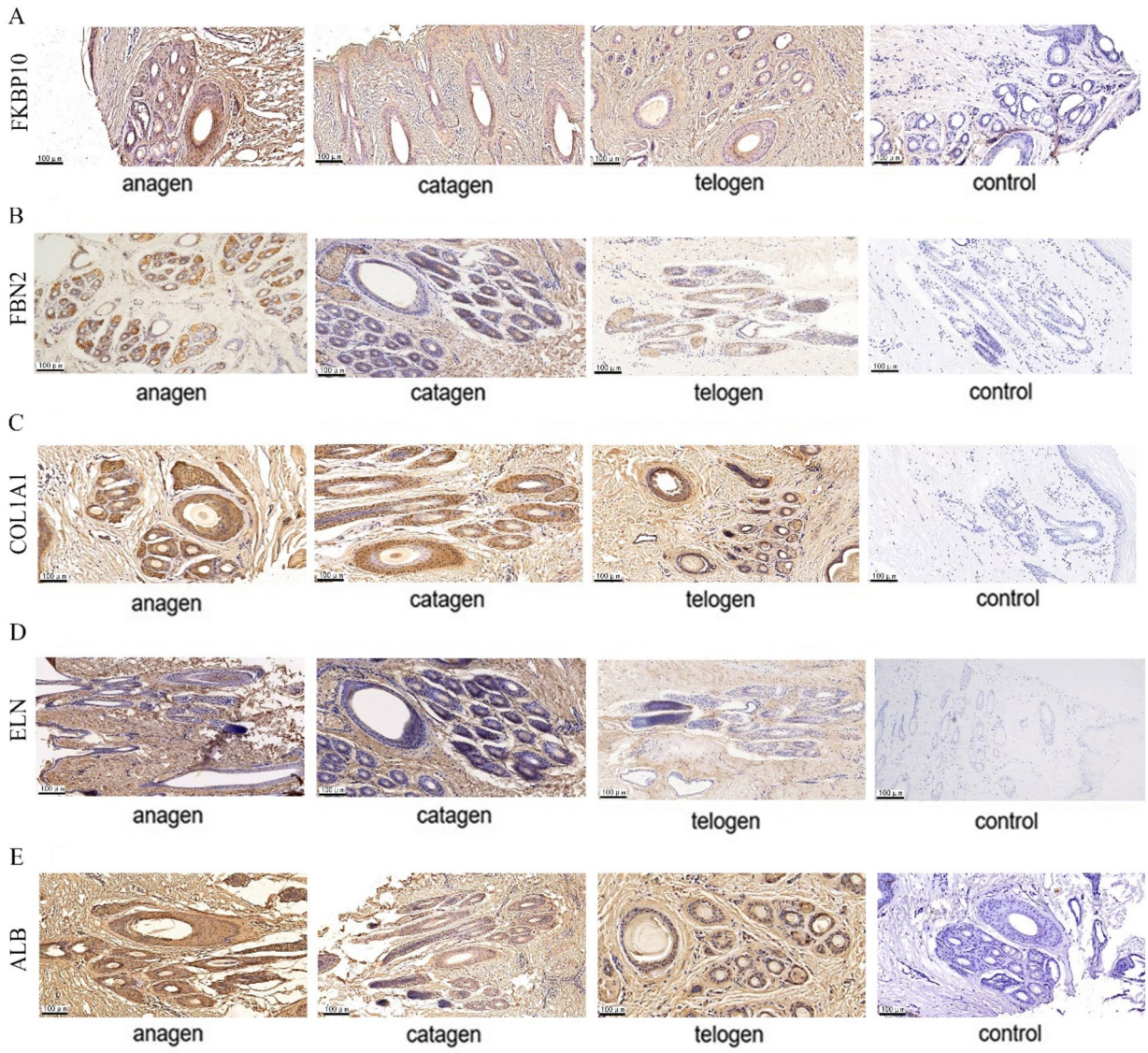


FIGURE 7
Five protein expression sites in SHFs at different growth stages. **(A)** FKBP10 immunohistochemistry **(B)** FBN2 immunohistochemistry **(C)** COL1A1 immunohistochemistry **(D)** ELN immunohistochemistry **(E)** ALB immunohistochemistry. Shades of brown indicate protein expression.

of different cashmere growth stages was consistent with the corresponding genes expression trend, and the protein expression level was the highest in the growth period, which was significantly higher than that in the regression period and telogen ($p < 0.05$).

## 3.8 The expression sites of key proteins and their interacting proteins in SHF growth cycles

The expression sites of FKBP10, FBN2, COL1A1, ELN, and ALB in SHFs was detected by immunohistochemistry. The signal intensity on the slices of different growth cycles was different.

FKBP10 and FBN2 were significantly expressed in the outer and inner root sheaths of SHF growth period, and their expression levels in the inner root sheath were higher than that in the outer root sheath, while the expression level of two proteins in the inner root sheath and outer root sheath was significantly reduced in the degeneration period and significantly higher than that in telogen (Figures 7A,B). COL1A1 was significantly expressed in the outer root sheath and inner root sheath during SHF growth period. During the degeneration period, the protein was expressed more in the outer root sheath and less in the inner root sheath. The expression in the inner root sheath and outer root sheath of SHFs during the resting period was significantly reduced (Figure 7C). ELN is expressed in the outer root sheath of SHFs during the growth period, and it is only expressed in a small amount in the outer root sheath during the degeneration period, and no expression in the inner root sheath and the outer root sheath of SHFs in telogen (Figure 7D). The expression of ALB in the outer root sheath and inner root sheath was obvious in SHF growth period, and the expression in the inner root sheath was more than that in the outer

root sheath. In catagen and telogen, ALB expression in the inner root sheath and outer root sheath was significantly reduced (Figure 7E).

In summary, these proteins are expressed in SHFs in different periods and highly expressed in the outer root sheath in anagen.

## 4 Discussion

The hair follicles of cashmere goats are divided into two types, namely PHFs and SHFs. SHFs produce unmyelinated cashmere, while PHFs produce medullated coarse hairs (36). Under the influence of *in vivo* and *in vitro* environments, as well as the skin microenvironment, hair follicles show strong self-regeneration ability and undergo periodic changes from anagen of rapid growth and development to catagen when hair follicle cells begin to apoptosis and then to telogen of a relatively static state (37). In anagen, SHFs are in an active stage of growth and development, and the length of fleece depends on the duration of this stage. The longer growth period, the longer the wool fiber produced by cashmere goats. In recent years, many researchers have utilized transcriptomics, genomics, and other omics approaches to investigate cashmere goat hair follicles. With the development of modern sequencing technologies, whole genome sequencing is able to examine sequence differences between populations, morphologies, and varieties of a large number of genes and gene families simultaneously (38). Li et al. (39) identified 135 genomic regions associated with cashmere fiber traits in cashmere goat populations through whole genome sequencing of 70 cashmere goats, including genes that may be involved in cashmere fiber production, such as *FGF5*, *SGK3*, *IGFBP7*, etc. Whole transcriptomics is becoming increasingly important due to the increasing research on non-coding RNAs and the boom in high-throughput sequencing. Liu et al. (40) used transcriptomic sequencing to study the mRNA-microRNA regulatory mechanisms of cashmere growth in cashmere goats under different photoperiods, revealing and validating the target relationships of differentially expressed genes and miRNAs. *BSDC1* and *RHBDF2* were targeted to miRNA-107-3p, and *ARSA* was targeted to miRNA-107-3p. *ALDH3A2* was targeted to miRNA-30b-3p. Xu et al. (41) adopted an integrated approach using transcriptomics, translatomics, proteomics, and metabolomics to identify substances associated with cashmere fineness, determining key regulators of cashmere fineness, including *PLA2G12A*, *KRT79*, and *prostaglandin B2*. During the periodic changes in hair follicle growth, many proteins involve in biological signal transduction, gene expression regulation, material and energy metabolism, cell cycle regulation, and other life activities through interactions with each other (16, 42–44). These proteins are trichohyalin (TCHH), KRT26, repetin (RPTN), cornulin (CRNN), tenascin-C (TNC), arachidonate-15-lipoxygenase (Alox15), SRY-box 18 (SOX18), matrix metalloproteinase-9 (MMP9), COL1A1, S100A7A etc. It is reported that TCHH was expressed in epithelial cells characterized by high mechanical strength, such as the inner root sheath cells of hair follicles. Its function was as an interfilament matrix protein by cross-linking with the head and tail ends of keratin intermediate filaments within the inner root sheath (45), and as a cross-linking enhancement protein, TCHH interacting with proteins such as RPTN, is crucial for the mechanical protection of the hair follicles. Through studying the expression patterns of specific genes of the hair follicles at different developmental stages in the inner root sheath of the embryonic of Tan sheep, Shi et al. (46) found that the expression level of *TCHH* gene was consistent with the pattern of wool crimping, and by affecting the morphology of the inner root sheath, it thereby affected the crimping of the wool of the beach sheep. Xu et al. (47) found that *KRT26* and *TCHH* genes were associated with cashmere fineness through studying the relationship between *KRT26* and *TCHH* gene polymorphisms and the production performance of Liaoning cashmere goat, which provided more theoretical basis for further research on cashmere fineness. *RPTN* involved in interactions with *TCHH* (48). *RPTN* was a member of the fusion protein family and is located on the epidermal differentiation complex on chromosome 1q21. The fusion protein family was associated with keratin intermediate filaments and is partially cross-linked to the cell envelope (CE) (49). In addition, CRNN of the fusion protein family is predominantly found in the upper spiny and granular layers of the epidermis and may be involved in the formation of the CE (50). Kim et al. (51) studied the anti-inflammatory role of *Alox15* in skin homeostasis. The authors knocked out *Alox15* in mice resulting in loss of hair follicle stem cells and an abnormal transition of dermal adipocytes to fibroblasts. Although the skin of *Alox15* knockout mice appeared to develop normally after birth, impaired skin barrier as well as hair loss was observed in adult mice. *TNC* was a marker for touch dome keratin-forming cells, which induced new hair follicles upon stimulation (52), and it was thought to be a regulator of WNT signaling in hairs and is required for Wnt/β-catenin signaling (53). SOX2 and SOX18 of SOX family proteins played important roles in determining hair follicle types, and Villani et al. (54) demonstrated that Sox18 regulates the normal differentiation of dermal papillae in all hair types. WNT5A and TNC are potential downstream effectors of SOX18 and were important for epidermal WNT signaling, and the expression of *WNT5A*, *MMP9* and *TNC* was significantly reduced in the skin of Sox18+/OP mice. Through RNA-seq of skin samples from E60 and E120 cashmere goat embryos as well as newly born cashmere goats, Gao et al. (55) showed that *TNC* was up-regulated as a key gene and expressed in HF initiation from E60 to E120. To explore the molecular mechanism of hair bending with growth, Liu et al. (17) identified *CRNN* and *TNC* as candidate genes for wool bending in Zhongwei goats. Tian et al. (56) showed hair growth is regulated by the *KRT4* gene interaction network in a study of vellus hair follicles in different seasons in Min pigs. Based on comprehensive analysis of the transcriptome and proteome of cashmere goat skins, Dai's et al. (16) showed that KRT4 and tβ 4 may interact to mediate extracellular signal regulated protein kinase (ERK) signaling pathway, thereby affecting hair growth, promoting SHF development, and improving cashmere production. *KRTs* family showed strong correlation throughout the hair follicle development cycle in yak, where *KRT4* was associated with cell cycle regulation, hair follicle development, and proliferation of keratin-forming cells (57). Wu et al. (7) examined mRNA, lncRNA and their candidate genes in SHF development and cycling. It was determined that *S100A7A* is a key gene with importance in hair follicle development and cycling in the Jiangnan cashmere goat.

In this study, not only TCHH, KRT4, RALGPS2, CRNN, ALOX15, TNC, MMP9 and other proteins were screened, but also FKBP10, FBN2, GNE, TCHH1, KRT73 and GTF2F1, etc. were

screened by analyzing the skin proteomics data of cashmere goats at different hair follicle growth stages. Therefore, we mainly verified the expression levels of FKBP10 and FBN2, and predicted their interaction proteins, ALB, COL1A1, and ELN. The experimental results were consistent with the sequencing results by qRT-PCR, western blot, and immunohistochemical verification at the gene and protein levels. They were highly expressed in the growth period of hair follicles, lowly expressed in telogen, and mainly expressed in the outer root sheath of SHFs. It shows that these five proteins promote hair follicle growth through different interactions. However, the specific way they interact in SHFs and their effects on hair follicle cells are still unclear. It is only found in the researches of others in other fields. FKBP10 is a member of the FK506-binding proteins (FKBPs). FKBPs are a class of highly homologous proteins widely expressed in eukaryotic cells that can assist transcription factors to regulate gene expression, participate in protein folding, modification, and transport, and have important functions. For example, studies on the relationship between *FKBP10* and *COL1A1* have shown that *FKBP10* silencing can significantly reduce the mRNA level of *COL1A1*. It is speculated that *FKBP10* silencing will change the quantity or cross-linking of extracellular matrix (58). Both of them can regulate Wnt/β-catenin and PI3K/AKT pathways related to cell proliferation and abnormal cell migration (59), promote the formation of cancer cells or participate in the occurrence of tumors through the interaction of cell adhesion molecules and receptors (60, 61), and regulate the fracture repair of osteoporosis (62). In the study of a mouse lung cancer model, it was found that the low expression of the FKBP10 protein could inhibit the occurrence of lung cancer. When endoplasmic reticulum stress occurred, FKBP10 protein was significantly down-regulated, and the expression of CyclinD1 protein decreased, which blocked the cell cycle and inhibited cell proliferation (63). ELN is an elastin, which is a common extracellular matrix component in connective tissue and plays an important role in maintaining tissue structure and function. The elastic fibers of skin tissue are loose network structures. The main components of elastic fibers are elastin and microfibers, and the formation of elastic fibers requires a variety of extracellular matrix proteins to be synthesized in a specific temporal and space order, while microfibers are composed of fibrillar protein (FBN), of which FBN2 is the main component (64, 65). In the early stage of tissue development, FBN1 and FBN2 synthesize microfiber bundles with a diameter of about 10 nm in the extracellular matrix in the form of N-terminal and C-terminal binding (66, 67), which is the basis for the final formation of the fiber bundle morphology of elastic fibers, binding to fibronectin (FN) and being fixed around the cell (68, 69). Mutations in the *FBN2* gene are closely related to hereditary connective tissue diseases, such as congenital contractural arachnodactyly (CCA), macular degeneration (MD), and myopathy, etc. (70). Studies have found that in the early stage of tissue development, the content of microfibers is high, and after tissue development, the content of ELN is also high, indicating that ELN can bind to FBN2 and participate in the assembly of microfibrils and the regulation of growth factors (71, 72). Due to it can participate in many physiological processes such as promoting extracellular matrix synthesis, cell proliferation, and migration (73–76), in recent years, through gene co-expression analysis and proteome sequencing of cashmere goats, *COL1A1* has been found to be associated with SHF growth (77, 78). It is believed that it can enhance the aggregation of dermal papilla cells and promote the growth of SHFs by affecting cell adhesion and movement (42). Cashmere fineness is a critical factor in determining cashmere quality. Wang et al. (28) used single-cell RNA sequencing to identify 13 skin cell types in Liaoning cashmere goats. Through cell trajectory analysis, the molecular changes during development were analyzed. SHF dermal papilla cells play a significant role in cashmere growth. It was found that COL1A1 is highly expressed in SHF dermal papilla cells. Zhao et al. (79) studied the molecular mechanism of hair follicle development through methylation and the whole transcriptome, proved the interaction between *E65*, *E85*, *E105*, and *E135* and DNA methylation, and studied the development stages and genes related to wool growth, laying a foundation for improving wool trait breeding.

In order to further understand the interaction between the five proteins and reveal their roles in the growth of cashmere goat hair follicles, the following experiments will be carried out through yeast two-hybrid and co-immunoprecipitation to explore the signaling pathways and interaction modes regulated by them. The function of the above proteins in secondary dermal papilla cells will be verified by overexpression and interference techniques.

## 5 Conclusion

Based on iTRAQ quantitative proteomics technology, we identified and screened differential proteins in skins of cashmere goat in anagen, catagen and telogen. There were 57 differential proteins screened in anagen and catagen, of which 24 were up-regulated and 33 were down-regulated in anagen. There were 31 differential proteins screened in catagen and telogen, of which 12 were up-regulated and 19 were down-regulated in catagen. There were 37 differential proteins screened in anagen and telogen, of which 19 were up-regulated and 18 were down-regulated in anagen. Through analysis, two key proteins and three interacting proteins of hair follicle growth in cashmere goats were identified, namely FKBP10, FBN2, COL1A1, ELN, and ALB. The expression levels of these five proteins in skins of cashmere goat were highest in anagen, followed by catagen, and lowest in telogen. They are highly expressed in the outer root sheath of SHFs during the growing period, which can promote the growth of SHFs.

## Data availability statement

Data during the current study are available from the corresponding author on reasonable request. Requests to access these datasets should be directed to Hongmei Xiao: lhtdyx@126.com.

## Ethics statement

The animal study was approved by Inner Mongolia Agricultural University Laboratory Animal Welfare and Ethics Committee. The

study was conducted in accordance with the local legislation and institutional requirements.

## Author contributions

JC: Conceptualization, Formal analysis, Methodology, Writing – original draft, Writing – review & editing. FM: Conceptualization, Methodology, Writing – original draft, Writing – review & editing. RZ: Conceptualization, Methodology, Writing – original draft, Writing – review & editing. JF: Conceptualization, Formal analysis, Writing – original draft. YL: Methodology, Writing – review & editing. JZ: Methodology, Writing – review & editing. ZL: Formal analysis, Writing – review & editing. JL: Formal analysis, Writing – review & editing. HX: Conceptualization, Resources, Writing – review & editing.

## Funding

The author(s) declare that financial support was received for the research, authorship, and/or publication of this article. This work was supported by National Natural Science Foundation of China (32160778 and 31860626), Science and Technology Major Project of Inner Mongolia Autonomous Region (RZ2200000003), Inner Mongolia Autonomous Region Directly Affiliated Universities Basic Scientific Research Fund-Young Teacher Research Capability Improvement Fund Project (BR220131).

## Acknowledgments

The authors thank the members of Inner Mongolia Autonomous Region Key Laboratory of Bio-Manufacturing, especially Dong Wang for his assistance in the tissue collection.

## Conflict of interest

The authors declare that the research was conducted in the absence of any commercial or financial relationships that could be construed as a potential conflict of interest.

## Publisher's note



## References

1. Zhao Q, Huang C, Chen Q, Su Y, Zhang Y, Wang R, et al. Genomic inbreeding and runs of homozygosity analysis of cashmere goat. *Animals*. (2024) 14:1246. doi: 10.3390/ani14081246

2. Chang L, Zheng Y, Li S, Niu X, Huang S, Long Q, et al. Identification of genomic characteristics and selective signals in Guizhou black goat. *BMC Genomics*. (2024) 25:164. doi: 10.1186/s12864-023-09954-6

3. Li J. Study on breeding methods in Inner Mongolia cashmere goats In: PhD dissertation. Beijing: China Agricultural University (2005) (in Chinese)

4. Zhao J. Screening and functional regulation network and verification of key proteins in the initiation of secondary hair follicle growth period in Liaoning cashmere goats In: MA thesis. Shenyang: Shenyang Agricultural University (2022) (in Chinese)

5. Bernard BA. The hair follicle enigma. *Exp Dermatol*. (2017) 26:472–7. doi: 10.1111/exd.13337

6. Ansari-Renani HR, Ebadi Z, Moradi S, Baghershah HR, Ansari-Renani MY, Ameli SH. Determination of hair follicle characteristics, density and activity of Iranian cashmere goat breeds. *Small Rumin Res*. (2010) 95:128–32. doi: 10.1016/j.smallrumres.2010.09.013

7. Wu C, Qin C, Fu X, Huang X, Tian K. Integrated analysis of lncRNAs and mRNAs by RNA-Seq in secondary hair follicle development and cycling (anagen, catagen and telogen) of Jiangnan cashmere goat (*Capra hircus*). *BMC Vet Res*. (2022) 18:167. doi: 10.1186/s12917-022-03253-0

8. Gong G, Fan Y, Yan X, Li W, Yan X, Liu H, et al. Identification of genes related to hair follicle cycle development in Inner Mongolia cashmere goat by WGCNA. *Front Vet Sci*. (2022) 9:894380. doi: 10.3389/fvets.2022.894380

9. Dai B, Sha RN, Yuan JL, Liu DJ. Multiple potential roles of thymosin B4 in the growth and development of hair follicles. *J Cell Mol Med*. (2021) 25:1350–8. doi: 10.1111/jcmm.16241

10. Luo Y, Hao F. Hair follicle growth cycle and dermal papilla. *Northwest Def Med J*. (2004) 25:287–9. (in Chinese). doi: 10.16021/j.cnki.1007-8622.2004.04.026

11. Lavker RM, Miller S, Wilson C, Cotsarelis G, Wei ZG, Yang JS, et al. Hair follicle stem cells: their location, role in hair cycle, and involvement in skin tumor formation. *J Invest Dermatol*. (1993) 101:16S–26S. doi: 10.1111/1523-1747.ep12362556

12. Geyfman M, Plikus MV, Treffeisen E, Andersen B, Paus R. Resting no more: re-defining telogen, the maintenance stage of the hair growth cycle. *Biol Rev Camb Philos Soc*. (2015) 90:1179–96. doi: 10.1111/brv.12151

13. Li L, Huang Z, Gu Y, Zhang J, Feng X, Wang Z. Advances in proteomics technology in animal science. *J Xichang Coll*. (2023) 37:1–5. (in Chinese). doi: 10.16104/j.issn.1673-1891.2023.01.001

14. Furusawa T, Ko JH, Birger Y, Bustin M. Expression of nucleosomal protein HMGN1 in the cycling mouse hair follicle. *Gene Expr Patterns*. (2009) 9:289–95. doi: 10.1016/j.gep.2009.03.002

15. Yang B, Cai MY, Li YJ, Zhang H, Cheng GH, Zhang JH, et al. Proteomic analysis identifies differentially expressed proteins participating in forming type iii brush hair in Yangtze River Delta white goat. *Gene Expr Patterns*. (2015) 14:323–38. doi: 10.4238/2015.January.23.6

16. Dai B, Liang H, Guo DD, Bi ZW, Yuan JL, Jin Y, et al. The overexpression of Tβ4 in the hair follicle tissue of Alpas cashmere goats increases cashmere yield and promotes hair follicle development. *Animals*. (2019) 10:75. doi: 10.3390/ani10010075

17. Liu Y, Ding Y, Liu Z, Chen Q, Li X, Xue X, et al. Integration analysis of transcriptome and proteome reveal the mechanisms of goat wool bending. *Front Cell Dev Biol*. (2022) 10:836913. doi: 10.3389/fcell.2022.836913

18. Li Y, Zhou G, Zhang R, Guo J, Li C, Martin G, et al. Comparative proteomic analyses using iTRAQ-labeling provides insights into fiber diversity in sheep and goats. *J Proteome*. (2018) 172:82–8. doi: 10.1016/j.jprot.2017.10.008

19. Gao L, Zhang Y, Zhang W, Wang Z, Nai R, Du C, et al. Analysis of protein expression profile of hair follicle cycle of Inner Mongolia cashmere goat. *J Agric Biotechnol*. (2014) 22:727–35. (in Chinese)

20. Jin M, Cao Q, Wang R, Piao J, Zhao F, Piao J. Molecular characterization and expression pattern of a novel keratin-associated protein 11.1 gene in the Liaoning cashmere goat (*Capra hircus*). *Asian Australas J Anim Sci*. (2017) 30:328–37. doi: 10.5713/ajas.16.0078

21. Zhao M, Zhou H, Hickford JGH, Gong H, Wang J, Hu J, et al. Variation in the caprine keratin-associated protein 15-1 (Kap15-1) gene affects cashmere fibre diameter. *Arch Anim Breed*. (2019) 62:125–33. doi: 10.5194/aab-62-125-2019

22. Wang J, Zhou H, Luo Y, Zhao M, Gong H, Hao Z, et al. Variation in the caprine Kap24-1 gene affects cashmere fibre diameter. *Animals*. (2019) 9:15. doi: 10.3390/ani9010015

23. Zhao M, Zhou H, Luo Y, Wang J, Hu J, Liu X, et al. Variation in the caprine keratin-associated protein 27-1 gene is associated with cashmere fiber diameter. *Genes*. (2020) 11:934. doi: 10.3390/genes11080934

24. Wang J, Zhou H, Hickford JGH, Zhao M, Gong H, Hao Z, et al. Identification of caprine Krtap28-1 and its effect on cashmere fiber diameter. *Genes*. (2020) 11:121. doi: 10.3390/genes11020121

25. Zhao M, Chen H, Wang X, Yu H, Wang M, Wang J, et al. aPCR-SSCP and DNA sequencing detecting two silent SNPs at KAP8.1 gene in the cashmere goat. *Mol Biol Rep*. (2009) 36:1387–91. doi: 10.1007/s11033-008-9325-1

26. Manlin W, Wenlei B, Xiyan H, Xu Z, Yanfeng W, Zhigang W. Molecular characterization and expression analysis of S6k1 in cashmere goats (*Capra hircus*). *Asian Australas J Anim Sci*. (2013) 26:1057–64. doi: 10.5713/ajas.2012.12710

27. Hui T, Zhu Y, Shen J, Bai M, Fan Y, Feng S, et al. Identification and molecular analysis of m$^6$A-circRNAs from from cashmere goat reveal their integrated regulatory network and putative functions in secondary hair follicle during anagen stage. *Animals*. (2022) 12:694. doi: 10.3390/ani12060694

28. Wang Z, Wang Y, Hui T, Chen R, Xu Y, Zhang Y, et al. Single-cell sequencing reveals differential cell types in skin tissues of Liaoning cashmere goats and key genes related potentially to the fineness of cashmere fiber. *Front Genet*. (2021) 12:726670. doi: 10.3389/fgene.2021.726670

29. Li J, Xing W, Gegen T, Zhang C, Ren Y, Yang C. Effect of fasted live-weight gain during the cashmere non-growing period on cashmere production performance and secondary hair follicle activity of cashmere goats. *Animals*. (2023) 13:3519. doi: 10.3390/ani13223519

30. Wu C, Ma S, Zhao B, Qin C, Wu Y, Di J, et al. Drivers of plateau adaptability in cashmere goats revealed by genomic and transcriptomic analyses. *BMC Genomics*. (2023) 24:428. doi: 10.1186/s12864-023-09333-1

31. Hu L, Wang J, Luo Y, Liu X, Li S, Hao Z, et al. Identification and characterization of circular RNAs (circRNAs) using RNA-Seq in two breeds of cashmere goats. *Genes*. (2023) 14:331. doi: 10.3390/genes14020331

32. Wu C, Xu Q, Li J, Qin C, Tulafu H, Liu W, et al. Regulation of cashmere fineness traits by noncoding RNA in Jiangnan cashmere goats. *BMC Genomics*. (2023) 24:604. doi: 10.1186/s12864-023-09531-x

33. Gao GZ, Hao F, Zhu L, Jiang GQ, Yan W, Liu J, et al. Combination of transcriptomics and proteomics reveals differentially expressed genes and proteins in the skin of EDAR gene-targeted and wildtype cashmere goats. *Animals*. (2023) 13:1452. doi: 10.3390/ani13091452

34. Bai Z, Xu Y, Gu M, Cai W, Zhang Y, Qin Y, et al. Proteomic analysis of coarse and fine skin tissues of Liaoning cashmere goat. *Funct Integr Genomics*. (2022) 22:503–13. doi: 10.1007/s10142-022-00856-6

35. String. String: functional protein association networks. Available from: https://string-db.org/ (Accessed August 27, 2022).

36. Yan W, Hao F, Zhe X, Wang Y, Liu D. Neural, adipocyte and hepatic differentiation potential of primary and secondary hair follicle stem cells isolated from Arbas cashmere goats. *BMC Vet Res*. (2022) 18:313. doi: 10.1186/s12917-022-03420-3

37. Wang M, Dai H, Sheng S, Liu Y, Zhang S, Bai W, et al. Discovery and functional analysis of secondary hair follicle miRNAs during annual cashmere growth. *Int J Mol Sci*. (2023) 24:1063. doi: 10.3390/ijms24021063

38. Chen Q, Chai Y, Zhang W, Cheng Y, Zhang Z, An Q, et al. Whole-genome sequencing reveals the genomic characteristics and selection signatures of Hainan black goat. *Genes*. (2022) 13:1539. doi: 10.3390/genes13091539

39. Li X, Su R, Wan W, Zhang W, Jiang H, Qiao X, et al. Identification of selection signals by large-scale whole-genome resequencing of cashmere goats. *Sci Rep*. (2017) 7:15142. doi: 10.1038/s41598-017-15516-0

40. Liu B, Zhao R, Wu T, Ma Y, Gao Y, Wu Y, et al. Transcriptomes reveal microRNAs and mRNAs in different photoperiods influencing cashmere growth in goat. *PLoS One*. (2023) 18:e0282772. doi: 10.1371/journal.pone.0282772

41. Xu Y, Zhang Y, Qin Y, Gu M, Chen R, Sun Y, et al. Multi-omics analysis of functional substances and expression verification in cashmere fineness. *BMC Genomics*. (2023) 24:720. doi: 10.1186/s12864-023-09825-0

42. Wang J, Sui J, Mao C, Li X, Chen X, Liang C, et al. Identification of key pathways and genes related to the development of hair follicle cycle in cashmere goats. *Genes*. (2021) 12:180. doi: 10.3390/genes12020180

43. Hu X, Hao F, Li X, Xun Z, Gao Y, Ren B, et al. Generation of VEGF Knock-in cashmere goat via the CRISPR/Cas9 system. *Int J Biol Sci*. (2021) 17:1026–40. doi: 10.7150/ijbs.55559

44. Chai Y, Sun Y, Liu B, Guo L, Liu Z, Zhou L, et al. Role of sulfur metabolism gene and high-sulfur gene expression in wool growth regulation in the cashmere goat. *Front Genet*. (2021) 12:715526. doi: 10.3389/fgene.2021.715526

45. Steinert PM, Parry DA, Marekov LN. Trichohyalin mechanically strengthens the hair follicle: multiple cross-bridging roles in the inner root sheath. *J Biol Chem*. (2003) 278:41409–19. doi: 10.1074/jbc.M302037200

46. Shi A, Lv J, Ma Q, Liu Z, Ma L, Zhou J, et al. Study on the expression patterns of inner root sheath-specific genes in tan sheep hair follicle during different developmental stages. *Gene*. (2024) 927:148751. doi: 10.1016/j.gene.2024.148751

47. Xu Y, Zhang X, Hui T, Sun J, Cai W, Lin G, et al. Association analysis for Snps of Krt26 and Tchh genes with cashmere production performance, body measurement traits and milk production traits in Liaoning cashmere goats. *Anim Biotechnol*. (2023) 34:698–708. doi: 10.1080/10495398.2021.1996386

48. Pośpiech E, Lee SD, Kukla-Bartoszek M, Karłowska-Pik J, Woźniak A, Boroń M, et al. Variation in the RPTN gene may facilitate straight hair formation in Europeans and East Asians. *J Dermatol Sci*. (2018) 91:331–4. doi: 10.1016/j.jdermsci.2018.06.003

49. Huber M, Siegenthaler G, Mirancea N, Marenholz I, Nizetic D, Breitkreutz D, et al. Isolation and characterization of human repetin, a member of the fused gene family of the epidermal differentiation complex. *J Invest Dermatol*. (2005) 124:998–1007. doi: 10.1111/j.0022-202X.2005.23675.x

50. Makino T, Mizawa M, Takemoto K, Shimizu T. Ultraviolet B irradiation increases the expression of cornulin and retepin in human skin xenotransplants. *Exp Dermatol*. (2024) 33:e15109. doi: 10.1111/exd.15109

51. Kim SN, Akindehin S, Kwon HJ, Son YH, Saha A, Jung YS, et al. Anti-inflammatory role of 15-lipoxygenase contributes to the maintenance of skin integrity in mice. *Sci Rep*. (2018) 8:8856. doi: 10.1038/s41598-018-27221-7

52. Nguyen MB, Flora P, Branch MC, Weber M, Zheng XY, Sivan U, et al. Tenascin-C expressing touch dome keratinocytes exhibit characteristics of all epidermal lineages. *Sci Adv*. (2024) 10:eadi5791. doi: 10.1126/sciadv.adi5791

53. Hendaoui I, Tucker RP, Zingg D, Bichet S, Schittny J, Chiquet-Ehrismann R. Tenascin-C is required for normal Wnt/β-catenin signaling in the whisker follicle stem cell niche. *Matrix Biol*. (2014) 40:46–53. doi: 10.1016/j.matbio.2014.08.017

54. Villani R, Hodgson S, Legrand J, Greaney J, Wong HY, Pichol-Thievend C, et al. Dominant-negative Sox18 function inhibits dermal papilla maturation and differentiation in all murine hair types. *Development*. (2017) 144:1887–95. doi: 10.1242/dev.143917

55. Gao Y, Wang X, Yan H, Zeng J, Ma S, Niu Y, et al. Comparative transcriptome analysis of fetal skin reveals key genes related to hair follicle morphogenesis in cashmere goats. *PLoS One*. (2016) 11:e0151118. doi: 10.1371/journal.pone.0151118

56. Tian M, He X, Wang W, Feng Y, Zhang D, Li Z, et al. Transcriptome analysis reveals genes contributed to min pig villi hair follicle in different seasons. *Vet Sci*. (2022) 9:639. doi: 10.3390/vetsci9110639

57. Bao Q, Zhang X, Bao P, Liang C, Guo X, Yin M, et al. Genome-wide identification, characterization, and expression analysis of keratin genes (KRTs) family in yak (*Bos grunniens*). *Gene*. (2022) 818:146247. doi: 10.1016/j.gene.2022.146247

58. Vollmann EH, Cao L, Amatucci A, Reynolds T, Hamann S, Dalkilic-Liddle I, et al. Identification of novel fibrosis modifiers by *in vivo* siRNA silencing. *Mol Ther Nucleic Acids*. (2017) 7:314–23. doi: 10.1016/j.omtn.2017.04.014

59. Liang X, Chai B, Duan R, Zhou Y, Huang X, Li Q. Inhibition of Fkbp10 attenuates hypertrophic scarring through suppressing fibroblast activity and extracellular matrix deposition. *J Invest Dermatol*. (2017) 137:2326–35. doi: 10.1016/j.jid.2017.06.029

60. Liang L, Zhao K, Zhu JH, Chen G, Qin XG, Chen JQ. Comprehensive evaluation of Fkbp10 expression and its prognostic potential in gastric cancer. *Oncol Rep*. (2019) 42:615–28. doi: 10.3892/or.2019.7195

61. Hagedorn M, Siegfried G, Hooks KB, Khatib AM. Integration of zebrafish fin regeneration genes with expression data of human tumors *in silico* uncovers potential novel melanoma markers. *Oncotarget*. (2016) 7:71567–79. doi: 10.18632/oncotarget.12257

62. Gao F, Xu F, Wu D, Cheng J, Xia P. Identification of novel genes associated with fracture healing in osteoporosis induced by Krm2 overexpression or Lrp5 deficiency. *Mol Med Rep*. (2017) 15:3969–76. doi: 10.3892/mmr.2017.6544

63. Ramadori G, Konstantinidou G, Venkateswaran N, Biscotti T, Morlock L, Galié M, et al. Diet-induced unresolved ER stress hinders KRAS-driven lung tumorigenesis. *Cell Metab*. (2015) 21:117–25. doi: 10.1016/j.cmet.2014.11.020

64. Zhang H, Apfelroth SD, Hu W, Davis EC, Sanguineti C, Bonadio J, et al. Structure and expression of fibrillin-2, a novel microfibrillar component preferentially located in elastic matrices. *J Cell Biol*. (1994) 124:855–63. doi: 10.1083/jcb.124.5.855

65. Corson GM, Chalberg SC, Dietz HC, Charbonneau NL, Sakai LY. Fibrillin binds calcium and is coded by cDNAs that reveal a multidomain structure and alternatively spliced exons at the 5′ end. *Genomics*. (1993) 17:476–84. doi: 10.1006/geno.1993.1350

66. Kielty CM, Wess TJ, Haston L, Ashworth JL, Sherratt MJ, Shuttleworth CA. Fibrillin-rich microfibrils: elastic biopolymers of the extracellular matrix. *J Muscle Res Cell Motil*. (2002) 23:581–96. doi: 10.1023/A:1023479010889

67. Ashworth JL, Kelly V, Wilson R, Shuttleworth CA, Kielty CM. Fibrillin assembly: dimer formation mediated by amino-terminal sequences. *J Cell Sci*. (1999) 112:3549–58. doi: 10.1242/jcs.112.20.3549

68. Beene LC, Wang LW, Hubmacher D, Keene DR, Reinhardt DP, Annis DS, et al. Nonselective assembly of fibrillin 1 and fibrillin 2 in the rodent ocular zonule and in cultured cells: implications for Marfan syndrome. *Invest Ophthalmol Vis Sci*. (2013) 54:8337–44. doi: 10.1167/iovs.13-13121

69. Giusti B, Pepe G. Fibrillins in tendon. *Front Aging Neurosci*. (2016) 8:237. doi: 10.3389/fnagi.2016.00237

70. Xu F, Jiang W, Zhang T, Jiang Q, Zhang R, Bi H. Fibrillin-2 gene mutations associated with hereditary connective tissue diseases. *Journal of Agricultural Biotechnology*. (2014) 22:727–35. (in Chinese). doi: 10.16288/j.yczz.19-052

71. Guo R. Bioinformatics analysis of albumin (Alb) gene in animals. *Heilongjiang Anim Sci Vet Med*. (2016):45–8. (in Chinese). doi: 10.13881/j.cnki.hljxmsy.2016.2081

72. Chuang VT, Kragh-Hansen U, Otagiri M. Pharmaceutical strategies utilizing recombinant human serum albumin. *Pharm Res*. (2002) 19:569–77. doi: 10.1023/a:1015396825274

73. Cao W, Feng Y. LncRNA XIST promotes extracellular matrix synthesis, proliferation and migration by targeting miR-29b-3p/COL1A1 in human skin fibroblasts after thermal injury. *Biol Res*. (2019) 52:52. doi: 10.1186/s40659-019-0260-5

74. Xie H, Zhang Q, Zhang N, Zhong Y, Xie M. Gene expression of Tp53, Col1a1 and Fn1 associated with nasopharyngeal carcinoma and their significance. *Genom Appl Biol*. (2022) 41:2029–38. (in Chinese). doi: 10.13417/j.gab.041.002029

75. Zhang H, Li X, Jia M, Ji J, Wu Z, Chen X, et al. Roles of H19/miR-29a-3p/COL1A1 axis in COE-induced lung cancer. *Environ Pollut*. (2022) 313:120194. doi: 10.1016/j.envpol.2022.120194

76. Wu W, Zheng L. Comprehensive analysis identifies Col1a1, Col3a1, and Postn as key genes associated with brain metastasis in patients with breast cancer. *Evid Based Complement Alternat Med*. (2022) 2022:7812218. doi: 10.1155/2022/7812218

77. Gong G, Fan Y, Li W, Yan X, Yan X, Zhang L, et al. Identification of the key genes associated with different hair types in the Inner Mongolia cashmere goat. *Animals*. (2022) 12. doi: 10.3390/ani12111456

78. Nai R. Mechanism analysis of vimentin and periodic growth of hair follicle in Inner Mongolia cashmere goat In: PhD dissertation. Inner Mongolia: Inner Mongolia Agricultural University (2018) (in Chinese)

79. Zhao B, Luo H, He J, Huang X, Chen S, Fu X, et al. Comprehensive transcriptome and methylome analysis delineates the biological basis of hair follicle development and wool-related traits in merino sheep. *BMC Biol*. (2021) 19:197. doi: 10.1186/s12915-021-01127-9

frontiers | Frontiers in Veterinary Science

TYPE Review
PUBLISHED 19 December 2024
DOI 10.3389/fvets.2024.1495010



OPEN ACCESS

EDITED BY
Izhar Hyder Qazi,
South China Agricultural University, China

REVIEWED BY
Abraham Loera Muro,
Centro de Investigación Biológica del Noroeste (CIBNOR), Mexico
Michael Lattorff,
University of KwaZulu-Natal, South Africa

*CORRESPONDENCE
Emma Allen-Vercoe
✉ eav@uoguelph.ca

RECEIVED 11 September 2024
ACCEPTED 05 December 2024
PUBLISHED 19 December 2024

CITATION
Mallory E, Freeze G, Daisley BA and Allen-Vercoe E (2024) Revisiting the role of pathogen diversity and microbial interactions in honeybee susceptibility and treatment of *Melissococcus plutonius* infection. *Front. Vet. Sci.* 11:1495010. doi: 10.3389/fvets.2024.1495010



# Revisiting the role of pathogen diversity and microbial interactions in honeybee susceptibility and treatment of *Melissococcus plutonius* infection

Elizabeth Mallory, Gwendolyn Freeze, Brendan A. Daisley and Emma Allen-Vercoe*

Department of Molecular and Cellular Biology, University of Guelph, Guelph, ON, Canada

European Foulbrood (EFB) is a severe bacterial disease affecting honeybees, primarily caused by the Gram-positive bacterium *Melissococcus plutonius*. Although the presence of *M. plutonius* is associated with EFB, it does not consistently predict the manifestation of symptoms, and the role of 'secondary invaders' in the disease's development remains a subject of ongoing debate. This review provides an updated synthesis of the microbial ecological factors that influence the expression of EFB symptoms, which have often been overlooked in previous research. In addition, this review examines the potential negative health consequences of prolonged antibiotic use in bee colonies for treating EFB, and proposes innovative and sustainable alternatives. These include the development of probiotics and targeted microbiota management techniques, aiming to enhance the overall resilience of bee populations to this debilitating disease.

KEYWORDS

**European foulbrood, *Melissococcus plutonius*, clonal complex, secondary invaders, microbial ecological interactions, probiotics**

## 1 Introduction

The pollination services of honeybees contributes to revenue of over USD $18 billion in crop production annually in the United States and more than 80% of all crops depend, to varying extents, on insect pollination (1, 2). Overall global honeybee numbers have grown since 1961, yet in that same time period, the area of insect pollinated crops has grown by more than 300%, highlighting the increased demand for such pollinators (2, 3). Over the past few decades, beekeepers from many nations around the world (including, for example, EU, Mexico, Canada, New Zealand and Iran) have experienced an alarming and continually increasing rate of honeybee mortality (4–6). In 2022–2023, total Canadian honeybee colony loss was estimated at 48%, over three times the approximate sustainable limit (5). Major colony losses have been attributed to a combinatorial effect of pesticide exposure, natural habitat loss, nutritional deficiencies, pathogen infection, and more (7). Due to the importance of honeybees to the environment and the agricultural system, researchers and industrialists seek strategies to reduce and treat the stressors challenging honeybees.

One stressor, European Foulbrood (EFB), is a major honeybee disease which affects larvae of managed Western and Asian honeybees (8). Despite the serious consequences of infection (larval mortality and subsequent colony population decline) this disease is poorly understood.

EFB is caused by the pathogenic bacterium, *Melissococcus plutonius*, where larvae become infected through oral ingestion via dietary contamination by asymptomatic worker bees. The pathogen then colonizes the larval gut, outcompeting the host for nutritional substrates, ultimately leading to host starvation. New evidence suggests *M. plutonius* crosses the host gut epithelium layer to cause septic infection (9). Infected larvae undergo a distinctive transformation, transitioning in color from a white to a yellow hue and manifesting a deflated appearance before succumbing to the infection. A colony affected by EFB experiences sporadic and irregular brood development, leading to diminished honey output, reduced pollination efficiency, and, in severe cases, complete colony collapse. For a beekeeper, the direct monetary impact of a single infected colony exhibiting mild disease is estimated to be ~ USD $215 in treatment and equipment replacement costs (10).

Due to its potential economic impact, and the ease of spread of the disease between hives, EFB is categorized as a reportable disease in many countries, as listed in the World Organization for Animal Health (WOAH). In terms of treatment for infected hives, beekeepers have rather limited options. Oxytetracycline, a broad-spectrum antibiotic that interferes with bacterial protein synthesis, has been used for years in many countries as both a treatment for, and a prophylactic against, infection. However, this antibiotic is associated with high rates of EFB recurrence (27%) and honeybee larval toxicity (11–13). In addition, despite strict adherence to current treatment guidelines by beekeepers, honeybee colonies continue to be commonly infected by *M. plutonius*, demonstrating an acute need for research to elucidate strategies for effective EFB treatment and eradication.

## 2 History, cultivation challenges, and pathogen diversity

Although *M. plutonius* was identified as the causative agent of EFB over 100 years ago, researchers have faced significant challenges in studying this pathogenic bacterium because of its fastidious growth requirements. Most *M. plutonius* strains require strict anaerobic conditions for growth as well as a culture medium containing specific nutrients (14). Although recent advances have been made with regard to improved isolation methods and media types, many strains of *M. plutonius* are still difficult to cultivate and tend to grow very poorly under laboratory conditions, thereby hindering research.

Further complicating matters is the fact that *M. plutonius* can often be detected in asymptomatic hives, suggesting that it is a common pathobiont of honeybees, i.e., its presence may not necessarily cause apparent signs of disease. It is been long speculated that the pathobiont behavior of *M. plutonius* is a result of distinct genetic determinants impacting virulence (15). Consistent with this, Arai et al. performed comparative characterization of 33 *M. plutonius* field isolates and identified two clear phenotypic groupings, denoted as 'typical' or 'atypical' based on their biochemical and culture characteristics relative to the features of the type strain, *M. plutonius* ATCC 35311 (Table 1). Using *in vitro* in larvae infection assays, it was found that atypical isolates caused higher mortality rates compared to typical isolates; specifically, atypical isolates killed between 70–90% of infected larvae within 5 days, whereas typical isolates killed less than 20% even when given the same infectious dose (16). From the limited number of studies that have been done, it can be surmised that typical strains have a wide variance in their infectious capabilities, whereas atypical isolates consistently cause high mortality (17).

TABLE 1 Phenotypic differences between typical and atypical *Melissococcus plutonius* as described in Arai et al. (2012) and Takamatsu (2023).

| | Typical | Atypical |
|---|---|---|
| Clonal Complex(es) | CC3, CC13 | CC12 |
| Oxygen Requirements | Strict anaerobe | Facultative anaerobe |
| Potassium Supplementation for Growth[a] | Required (K > Na) | Optional |
| Carbohydrate Utilization | Limited carbohydrate utilization profile | Wider carbohydrate utilization profile |
| Regions and Countries Prevalent | Widespread through all continents (except Antarctica) | Japan, Mexico, Canada, United Kingdom, Switzerland, USA |
| *In Vitro* Lethality | Low to high mortality (dependent on strain) | High mortality |

[a]Potassium supplementation in growth medium to achieve a K:Na ratio, where K > Na.

Genomic investigations have shown that *M. plutonius* strains can be grouped into three 'clonal' complexes of *M. plutonius* (CC3, CC12, and CC13; Table 1). CC12 strains are of particular interest due to their virulence and prevalence in certain regions, and all display 'atypical' characteristics (18). CC3 and CC13 strains, seen as more predominant, display the 'typical' phenotypic characteristics, such as required low sodium and high potassium growth conditions. A summation of this can be found in Table 1.

## 3 Geographic distribution of EFB and detection of antibiotic resistance

Some of the oldest and most well-documented reports of EFB come from Canada in the early 20th century. In 1916, the "Apiary Inspection in Ontario" indicated that out of 5,367 colonies inspected, a total of 1,387 colonies (~25%) displayed symptoms of EFB (19). Following the introduction of oxytetracycline in the 1940s, EFB either disappeared or dropped to undetectable levels in many regions, and when disease outbreaks did occur, they were generally considered self-limiting with clinical symptoms often found to resolve spontaneously (20, 21).

In the past several years, there has been a re-emergence of severe EFB outbreaks in several regions of the world including the US, Canada, and Switzerland (22–24). The extent of this re-emergence, however, is likely underestimated, since EFB symptoms can be ambiguous and the disease itself is reportable in many countries, as per its assignment in WOAH. In Canada, the increase in symptomatic EFB infections was first observed in 2019 in colonies used for commercial blueberry pollination (23, 25). The phenomenon was initially thought to be related to immune deficits of bees feeding on nutrient-poor blueberry pollen. However, colonies not necessarily exposed to blueberry crops have also been affected, for example, a three-year molecular survey conducted in Alberta recently detected EFB in over 30% of the province's colonies (10).

Insight regarding the prevalence of typical and atypical *M. plutonius* within hives can be gleaned from two studies using genetic surveillance. Arai et al. conducted random sampling of honeybee colonies across Japan and found that of infected colonies, 40% contained only typical *M. plutonius* strains, 6% contained only atypical *M. plutonius* strains and 54% were co-infected with both typical and atypical strains (26). De León-Door et al. confirmed similar findings (27). The higher proportion of co-infected hives suggests that atypical *M. plutonius* strains may gain an advantage when co-infecting with typical strains. Diverse, thorough sampling in regionally distinct areas is required to confirm this phenomenon. Additionally, further research is needed to elucidate why typical/atypical strain co-infections may be beneficial for disease progression.

Compared to other areas of the world (e.g., the United States Japan, Switzerland, and United Kingdom) (17, 28) there has been limited genetic investigation of the EFB strains present in Canada or their proportionality. One exception is the recent study by Thebeau et al., which assessed pathogenicity and determined clonal complex genotypes of 4 clinical *M. plutonius* isolates derived from EFB outbreaks in Saskatchewan, Alberta, and British Columbia (29). Notably, 75% of the *M. plutonius* isolates found were identified as CC12 strains that were highly pathogenic (associated with ~58–70% mortality of larvae) based on *in vitro* larval infection assays (note that the convention for the use of '*in vitro* larval' in this field tends to refer to studies of larvae within a lab environment).

One Canadian CC12 isolate, 2019 BC1, has displayed a minimum inhibitory concentration (MIC) of 16 µg/mL to oxytetracycline (30). This MIC is higher than the concentration used for standard EFB treatment, and therefore could constitute this strain as oxytetracycline resistant. In a later study by Takamatsu et al., 77 *M. plutonius* isolates from Japan were examined, revealing an additional four strains [comprising three CC3 and one CC12 strain(s)] resistant to oxytetracycline, based on MICs of 16 µg/mL (31). The emergence of oxytetracycline resistance in *M. plutonius* appears independent of clonal complex type, and dates to at least 2008 when the Japanese isolates were first isolated. Elucidation of the mechanism of resistance to oxytetracycline in *M. plutonius* is warranted to obtain a comprehensive understanding of its prevalence and risk and to explore potential avenues for intervention. Genome level analysis of *M. plutonius* isolates from EFB-infected hives sampled globally are needed in order to better understand the relationship between genetic diversity and virulence in this pathogen.

# 4 Virulence determinants of *Melissococcus plutonius*

## 4.1 Molecular determinants

As described above, *M. plutonius* isolates can be grouped into three clonal complexes with distinct phenotypic and genomic characteristics. Nonetheless, data collected from over 500 isolates across 18 countries show a lack of consensus with regard to pathogenicity of *M. plutonius* based solely on clonal complex genotype (32). These inconsistencies may be related to the acquisition by some strains of a virulence plasmid (pMP19) which encodes a putative ETX/MTX2 toxin family protein with insecticidal properties, provisionally named 'melissotoxin A'. For example, pMP19 positive CC3 strains produce mortality rates of >91% during larval infection assays (32). Demonstrating a causal link, Nakamura et al. showed that loss of the pMP19 plasmid abrogated pathogenicity and that larvae infected with pMP19-cured CC3 strains experienced only a 6% mortality rate (33). In the same study, pMP19 failed to explain the virulence of CC12, with both pMP19-positive and -negative strains resulting in up to 90–100% larval mortality rates (33). Given this extreme virulence combined with a lack of understanding of the underlying mechanisms, 'atypical' CC12 *M. plutonius* strains are considered the most dangerous strains which pose the greatest risk for severe EFB outbreaks.

Other genetic determinants have been proposed to play a role in virulence, such as the presence of the gene encoding tyrosine decarboxylase, a catalytic enzyme responsible for the conversion of tyrosine to tyramine and carbon dioxide (34). A buildup of tyramine has been linked to development of classic EFB symptoms in larvae (35). The tyrosine decarboxylase gene is present and functional in strains belonging to CC12 and CC3 only, and presents a compelling potential virulence determinant of these clonal complexes compared to CC13 (16, 36).

## 4.2 Interplay between 'secondary invaders' and EFB disease onset

EFB disease severity may be influenced by larval co-infection with so-called 'secondary invaders', i.e., other microbial species that can work in tandem with *M. plutonius* to cause symptoms. Several studies have focused on this phenomenon and the major findings can be found in Figure 1.

Originally, *Bacillus alvei* (since reclassified as *Paenibacillus alvei*) was indicated as the causal organism responsible for producing EFB, since this bacterial species was found abundantly in larvae with EFB symptoms (37). This finding was called into question by White, who proposed the causal organism of EFB as *M. plutonius* (38). More than four decades later, Bailey failed to reproduce EFB symptoms in larvae when using only pure cultures of *M. plutonius* (39), but later was the first to suggest that *M. plutonius* may not act alone to cause disease; *M. plutonius* was identified as the primary etiological agent of EFB in addition to a supplementary role of several other bacterial species, including *Enterococcus faecalis*, '*Achromobacter eurydice*', or *Paenibacillus alvei* (40). The source of these accomplice strains is not always clear, but several reports have suggested that *Paenibacillus* and *Enterococcus* spp. can be vectored by ectoparasites such as Varroa mites and small hive beetles (41–44). However, the roles and impact of *E. faecalis*, *A. eurydice* and *P. alvei* on EFB disease progression have been contentious, with contradictory evidence of their involvement.

Not discussed in detail in this review, confusion surrounding the actual identity of the proposed secondary invader first described as '*A. eurydice*' has been called into question, thus rendering past research regarding its role in EFB progression contentious. This controversy is discussed in depth in Erler et al. (45).

Testing the secondary invader hypothesis *in vitro* in larvae, Giersch et al. reported that the specific combination of *M. plutonius* and *P. alvei* field isolates derived from the same EFB infected colony could reliably produce symptoms characteristic of EFB (46). Furthermore, this combination increased mortality in lab-reared larvae when compared to monoculture infection with only

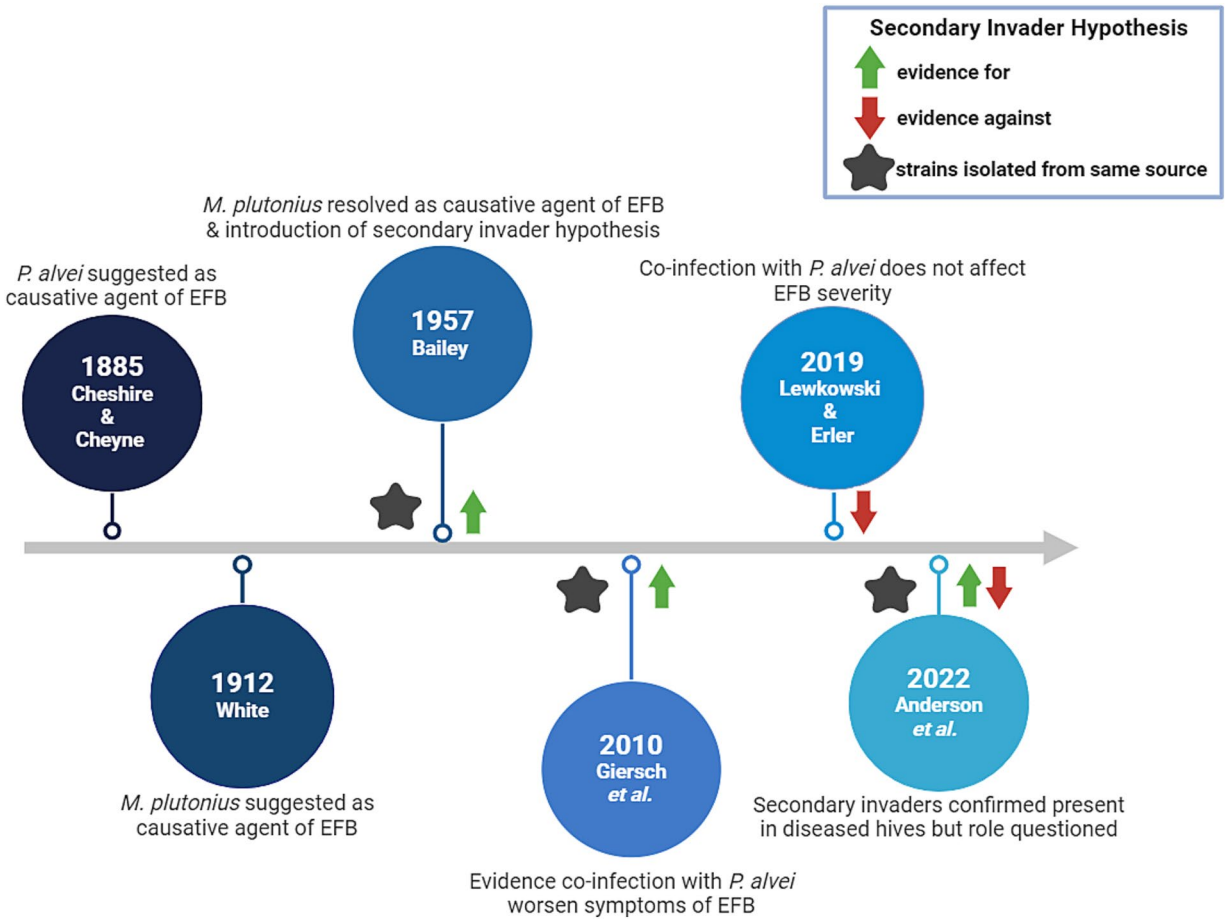


FIGURE 1
Timeline of major findings indicating the causative agents of EFB.

*M. plutonius* (46). Conversely, Lewkowski and Erler found no effect of experimental co-infection when using strains of *M. plutonius* 49.3 and *P. alvei* LMG 13253 in larvae *in vitro* (47). Anderson et al. confirmed that both *P. alvei* and *E. faecalis* were present in EFB diseased colonies, but did not necessarily find that the presence of one or both species correlated with disease progression (41). *In vitro* in larvae it has been shown that *E. faecalis* co-infection with *M. plutonius* did not result in more severe infection compared to each species alone, however this may have been because the strains used for this work were not isolated from a diseased colony (47). Analysis of the role of '*A. eurydice*' in EFB, has not been further investigated, to the best of our knowledge.

Although there has not been much work done to understand synergistic infections with multiple microbes in cases of EFB disease, the work that has been done offers some compelling evidence that in addition to *M. plutonius*, other microbes are involved. Whether microbial adaptation is required of *M. plutonius* in order to infect with a given secondary invader, or whether existing strain-level differences influence the likelihood of disease is undetermined.

The combined effects of primary and secondary pathogens, along with unknowns about clonal complex (CC3/CC12/CC13), create a complex web of interactions driving the probability of EFB disease incidence and severity that is yet to be fully deciphered. Unraveling this complexity will require comprehensive research but is necessary in order to devise effective EFB management strategies and ensure honeybee health and sustainability.

## 5 Use of honeybee symbionts in the development of alternative EFB treatments

### 5.1 Natural defense mechanisms of the honeybee gut microbiota

The adult honeybee gut microbiota is highly conserved and plays a pivotal role in nutrient absorption, detoxification, and immune system modulation (48). Although it also provides host benefits, the gut microbiota of honeybee larvae is more variable than that of adults, showing lower abundance of microbial species, and often the presence of environmental microbes (41). In terms of the role of the honeybee microbiota in EFB interactions, only a limited number of studies have been completed to date.

One study assessed the microbiomes of two types of adult worker bees derived from apiaries with clinical signs of EFB infection: a symptomatic type and an asymptomatic type (49). Unsurprisingly, there were large differences in the abundance of *M. plutonius* among the bees, with symptomatic bees harboring a 75-fold higher load of

*M. plutonius* compared to asymptomatic bees (49). However, significant differences in the abundance of other microbial taxa among the two types were also identified (49). Symptomatic bees not only possessed a higher incidence of *M. plutonius*, but also higher proportions of *Fructobacillus fructosus*, *Apilactobacillus kunkeei*, *Gilliamella apicola*, *Frischella perrara*, and *Bifidobacterium indicum* (49). Species of *Snodgrassella alvi*, *Lactobacillus melliventris, L. helsingborgensis* and *L. kullabergensis*, the latter 3 of which are lactic acid-producing bacteria (LAB), were found in higher abundance in worker bees from asymptomatic colonies compared to their counterparts and it is therefore possible that their presence plays a role in EFB disease protection or suppression, especially early on in development (49). It is notable that in a further study where microbiomes of larva were screened, LAB were also negatively associated with *M. plutonius* (50). In addition, the lack of a single acetic acid-producing bacterium (*Bombella apis*) was found to be uniquely associated with atypical EFB symptomatology (50).

Due to the correlative nature of typical microbiome research, results indicating the positive or negative correlation of a certain species with *M. plutonius* load is a cause-and-effect dilemma. One member being in higher abundance when *M. plutonius* levels are higher could indicate that this species is spurring growth of *M. plutonius*, or, the growth of that member could be a response to independent *M. plutonius* growth. As such, mechanistic microbiome research must be carried out to determine the nature of this correlation, through methods such as infection assays with individual gain or loss of specific microbiome members or crosswise microbiota transplants.

Overall, these results raise questions about whether symbiotic bacteria may play a central role in the promotion of colony health in the presence of *M. plutonius,* mitigating the risk of EFB development. While our understanding of bee microbiota ecology and interactions in EFB is still nascent, these findings suggest that certain beneficial bacteria may impede the colonization of *M. plutonius* and act as a natural barrier against infection. As such, the potential for harnessing certain beneficial microbes as prophylactics for EFB disease prevention is of interest.

## 5.2 Probiotics as a promising therapeutic alternative

The development of beneficial microbes as probiotics for use in hive management is a relatively new and expanding strategy for apiarists. Several groups have successfully identified honeybee-derived strains of LAB representative of *Lactobacillus*, *Apilactobacillus,* and *Pediococcus* spp. which were able to strongly inhibit *M. plutonius* growth *in vitro* (51–53). The mechanism(s) of this inhibition remains unexplored, however some LAB produce metabolites, such as organic acids, bacteriocins (a class of small antimicrobial peptides), or bacteriocin-like inhibitory substances (BLIS) that are known to inhibit pathogen growth. For example, it has been found that the cell-free supernatant of an isolate of *Apilactobacillus kunkeei* (formerly *Lactobacillus kunkeei*), thought to be one of the most abundant LAB species in honeybees, has growth inhibitory effects against *M. plutonius* (54). This finding was later confirmed by Zendo et al., who also demonstrated that the mechanism of *M. plutonius* growth inhibition was through the production of a bacteriocin, kunkecin A, by *A. kunkeei* (52). Additionally, a recent study by Leska et al. revealed that 55 out of 103 tested LAB strains showed antagonistic activity against *M. plutonius*, with one strain of *Ligilactobacillus salivarius* demonstrating the most notable growth inhibition among them (51). As well, the cell-free supernatant of *L. salivarius*, as well as strains of *Pediococcus parvulus* and *Levilactobacillus brevis* also notably inhibited *M. plutonius* growth (51). Mojgani et al. also found that the cell-free supernatants from LAB species *Lactobacillus acidophilus*, *Lacticaseibacillus rhamnosus*, *Lactiplantibacillus plantarum*, *Lactobacillus apis* and *Pediococcus acidilactici* potently inhibited *M. plutonius* growth, with the production of organic acids, bacteriocins or BLIS being proposed as critical mediators of this activity (53).

These results support microbiota associations and suggest that certain LAB may be prime probiotic candidates. However, each of these *in vitro* studies used a single *M. plutonius* strain as their test organism: the type strain ATCC 35311. Since (as described above) atypical *M. plutonius* strains have divergent virulence factors and culture requirements, the inhibitory activity seen with the type strain may not be generalizable to all EFB etiologic agents.

That said, two studies have screened honeybee-derived bacterial strains for antagonistic activity toward atypical *M. plutonius* strains. Wu et al. found that one *Lactobacillus* sp. strain (Acaj3) exhibited strong inhibitory activity against atypical *M. plutonius* (strain DAT 561) *in vitro* (55). In direct comparison with antibiotics, the same authors found that Acja3 was comparable to tetracycline in its antibacterial activity against *M. plutonius* and could reduce *in vitro* larval mortality by ~50% during infection assays. A notable advantage of some beneficial bacteria is their bactericidal properties (i.e., killing capacity) in comparison to tetracycline, which exerts bacteriostatic effects (i.e., growth inhibitory without killing) (56). Various *Bifidobacterium* spp. have also been investigated for their antagonism against two atypical *M. plutonius* strains (DAT 561 and DAT 351), and some were found to exhibit antagonistic effects against its growth (57).

To date, in total, only three *M. plutonius* strains (ATCC 35311, DAT 561, and DAT 351) have been tested for their direct inhibition by potential probiotic strains *in vitro*. As it is becoming clear that different *M. plutonius* strains can possess a multitude of different virulence factors and culture requirements, it is also becoming clear that there is a gap in knowledge about the likely applicability of these probiotic strains to protect against EFB disease in general. Furthermore, while work in the field shows intriguing results, future studies will be imperative to understand the effect of these candidate strains *in vivo*, especially to account for the impact of other gut microbial members and host-factors on probiotic efficacy.

In support of this, in the field, a recent study in Italy (979 colonies/22 apiaries) showed that *Lactiplantibacillus plantarum* LMG P-21806 treatment reduced EFB prevalence from 4.5 to 2.5% over a 6 month period *in vivo* (58). Another *in vivo* study in California (33 colonies/2 apiaries) indicated a three-strain lactobacilli consortium (LX3; composed of *Lactiplantibacillus plantarum* Lp39, *Lactobacillus rhamnosus* GR-1 and *Apilactobacillus kunkeei* BR-1) could reduce *M. plutonius* burden by five-fold over a 20 week period (59). This work is an especially promising start to understanding the role of probiotic treatment *in vivo*; however, future studies are required to better characterize these interactions and outcomes on EFB. Furthermore, since these studies utilized natural EFB infections, no genotype or *M. plutonius* strain information was provided, which is an area in need of further characterization.

TABLE 2 Candidate probiotics demonstrating strain-level *in vitro* or *in vivo* activity against select strains of *Melissococcus plutonius*.

| Strain(s) causing antagonism | *M. plutonius* strain(s) tested against | Basic methodology | Reference |
|---|---|---|---|
| *Ligilactobacillus salivarius* 9AN | ATCC 35311 (typical) | *in vitro* inhibition assay | (51) |
| *Apilactobacillus kunkeei* FF30-6 | ATCC 35311 (typical) | *in vitro* inhibition assay | (52) |
| *Lactobacillus acidophilus* ZN06<br>*Lactobacillus apis* ZN027<br>*Lacticaseibacillus rhamnosus* ZN012<br>*Lactiplantibacillus plantarum* ZN098 and ZN3b-ab<br>*Pediococcus acidilactici* ZN016 | ATCC 35311 (typical) | *in vitro* inhibition assay | (53) |
| *Lactobacillus apis* sp. nov. strain R4B$^T$ | ATCC 35311 (typical) | *in vitro* inhibition assay | (78) |
| *Lactiplantibacillus plantarum* strains:<br>LP 31, LP 42, LP 148 and LP 179<br>*Apilactobacillus kunkeei* strains:<br>ALK 181, ALK 222, ALK 268 and ALK 385 | ATCC 35311 (typical) | *in vitro* inhibition assay | (79) |
| *Bifidobacterium* sp.:<br>Acj BF1-Acj BF11 | DAT561 (atypical)<br>DAT351 (atypical) | *in vitro* inhibition assay | (57) |
| *Lactobacillus* sp. Acja3 | DAT561 (atypical) | *in vitro* inhibition assay<br>*in vitro* larval assay | (55) |
| *Lactiplantibacillus plantarum* LMG P-21806 | undetermined (natural infections, presumedly typical) | *in vivo* (field-level, observational) | (58) |
| LX3 Mixture: (*Lactiplantibacillus plantarum* Lp39, *Lactobacillus rhamnosus* GR-1 and *Apilactobacillus kunkeei* BR-1) | undetermined (natural infections, presumedly typical) | *in vivo* (field-level, observational) | (59) |

While the potential effectiveness of probiotic strains/treatments have been described for mitigating *M. plutonius* growth and honeybee disease, it should be noted that not all probiotics show equally promising results. In recent years, commercial bee probiotics (e.g., SuperDFM®-HoneyBee™, the most popular honeybee probiotic in the United States) have been found unable to colonize or restore/antibiotic rescue the honeybee gut microbiome (60–62).

A strong hypothesis regarding this discrepancy is due to the composition of probiotics, as commercial products are typically comprised of non-native microbiota that have a slim chance of establishment and subsequent survival in the honeybee gut (60–62). The efficacy of probiotics composed of a mixture of native bee microbiota, however, have been shown to colonize the honeybee gut with success and are a promising area of future work, which could potentially be applied in the treatment of EFB (62, 63). That said, it is important to consider that further *in vivo* work is imperative before drawing conclusions regarding the therapeutic use of probiotic strains for disease management in honeybees.

Additionally, the influence of geographic variation and environmental factors is crucial to the interpretation of research outcomes, and there is not enough data to evaluate this at present. This limitation leaves substantial gaps in our understanding of how probiotics interact with *M. plutonius* strains, both typical and atypical. Understanding these dynamics, and others, is essential for developing effective treatment strategies that can be adapted to diverse environmental conditions and regional characteristics. A summary of candidate species and tested strains discussed in this section are found in Table 2.

## 5.3 Other therapeutic alternatives to counteract EFB disease

There are several approaches currently used to try to control the incidence of EFB disease. Hygienic breeding techniques can generate bees that efficiently detect and remove dead and infected larvae, which is expected to reduce EFB spread. Palacio et al. found that colonies selectively bred for hygienic behavior experience diminished rates of EFB, yet Fowler et al. has since suggested that there was no effect of hygienic bee behavior on the development of EFB (64, 65). These conflicting studies may be a result of the rate at which a given *M. plutonius* strain is able to kill larvae. For example, CC12 strains tend to kill larvae before capping, whereas some CC3 *M. plutonius* can cause mortality at a slower rate such that larvae are capped before death (66); all honeybees will dispose of dead larvae in uncapped cells, suggesting that hygienic behavior would not be an advantage in infections caused by CC12 *M. plutonius* (67).

Some honeybee lines also naturally resist EFB, hinting at a potential for advancements in bee breeding, however the host genetic determinants of resistance are currently unknown (47, 68). Additionally, natural substances such as essential oils show antimicrobial properties against several microbes and parasites that cause various bee diseases, but these substances require careful use to avoid toxicity in the bees themselves, and to prevent the development of microbial resistance (69). In this respect, tea tree oil application has been shown to inhibit *M. plutonius in vitro* and was determined to be non-toxic to honeybee larvae at effective levels (70).

A proposed factor in the development and progression of EFB is malnutrition. As previously stated, a suggested mechanism of disease

involves host-pathogen competition for nutrients. During infection, malnutrition may also result from the immune system's energy demands, which divert resources away from nutrient uptake and metabolism (71). Pollen, a critical component of royal jelly and a key dietary addition during later larval development, may significantly influence disease outcomes. Outside the context of infection, larvae fed different pollen sources during the pre-pupal stage exhibit varying survival rates (72). Additionally, pollen type has been shown to affect pre-pupal weight, while pollen dose impacts development speed (72). These findings underscore the importance of pollen type for healthy larval development, even under normal conditions.

This evidence supports the notion that supplementing honeybee colonies with pollen or pollen substitutes could improve overall health and potentially reduce disease susceptibility, especially in colonies with insufficient pollen sources or storage. Researchers have demonstrated that pollen supplementation reduces *Nosema* spp. infestations in adult bees; however, it also shortens the bees' average lifespan (73). While this approach shows promise as a preventative measure, further research and refinement are needed to optimize its benefits. To our knowledge, no studies have directly examined the effects of pollen supplementation on *M. plutonius* infections.

Lastly, a treatment known as the 'shook swarm' method, involves transfer of EFB-infected adult bees to a new brood box supplemented with a sugar-oxytetracycline solution. This method results in decreased EFB symptoms and significantly reduces the reoccurrence rate compared to hygienic breeding, or the use of natural substances (11), although it runs the risk of contributing toward the development of antimicrobial resistance in bacteria associated with treated hives.

# 6 Areas requiring further research and future directions

## 6.1 Strain diversity and its role in disease progression

The escalating EFB crisis jeopardizes the honeybee population and, subsequently, their pollination services that contribute to agricultural efficiency. Partly attributed to the presence of atypical *M. plutonius* strains, EFB infections are becoming steadily more problematic and rising in occurrence. Although many atypical strains have been isolated from Japan, their presence has recently become apparent in other regions, including North America and Europe. Already determined to be phenotypically different in terms of growth requirements, the extent to which atypical strains differ in disease progression from their typical counterparts is still unclear. Continued genomic investigations of distinct strains *M. plutonius* strains, their associated virulence factors, and requirements for virulence expression need to be completed alongside confirmatory *in vitro* assays to clarify these discrepancies.

## 6.2 Defining the secondary invaders and their impact

Conflicting *in vitro* reports of the impact of secondary invaders could be explained by several different experimental factors which have been proposed to affect larval survival in other settings, such as: different larval rearing protocols (74), differing honeybee lineages with disparate innate resistance (68), or different experimental inoculation methods (75). To limit the impact of differing experimental design, future studies should look to incorporating a broader array of *M. plutonius* strains and using multiple larval rearing and larval inoculation protocols, akin to treatment groups. This would aid in determining whether virulence is indeed enhanced or remains unchanged in the presence of a variety of proposed secondary invaders, and not merely an effect of experimental design.

A further reason for the conflicting results so far seen between studies may be strain-specific co-adaptation within a given hive environment. For example, when *M. plutonius* and purported secondary invader strains were isolated from the same infected colony, synergism in EFB infection outcomes was seen; this was not repeated in a separate study using strains isolated from different sources (46, 47, 76). To determine this argument's validity, a co-infection study should be conducted using *M. plutonius*-secondary invader pairings from unrelated and single isolation source(s). Furthermore, whether *M. plutonius* genotype also plays a role in interactions with secondary invaders remains in question. To the extent of our knowledge, no research to date has comprehensively compared the interactions of different *M. plutonius* clonal complexes with secondary invader partners. Studying the role of genotype in these interactions may also explain discrepancies seen in work to date, and is an area requiring future research.

These contradictory findings could also be a result of the misidentification of the secondary invader itself. Giersch et al. indicated *P. alvei* identity via Gram stain and morphological comparison of vegetative cells and endospores, yet several *Paenibacillus* spp. are highly similar in these characteristics. For example, the recently-described species *Paenibacillus melissococcoides,* also isolated from a honeybee colony experiencing EFB, is closely related to *P. alvei* as determined through 16S rRNA gene sequence comparison, and also forms endospores (77). Therefore, it is possible that the secondary invader which produced EFB symptoms and increased virulence when co-infected with *M. plutonius* in Giersch et al.'s study may be representative of another *Paenibacillus* spp. such as *P. melissococcoides.* Detailed molecular investigation regarding the true identity of strains used in these studies, would help to resolve species and strain co-occurrence in EFB-infected larva.

## 6.3 Probiotic efficacy to emerging strains

Discoveries regarding the determinants of EFB disease can be used to inform future alternative treatments. Current treatment options for EFB, such as oxytetracycline application, pose several unacceptable limitations, particularly in an era of increasing antimicrobial resistance, and with a dawning understanding of the importance of the honeybee microbiome in health. In contrast, probiotic approaches offer exciting new avenues, with many potential benefits. However, only limited work on the effectiveness of probiotics against EFB disease has been undertaken, and there remains a critical gap in understanding probiotic efficacy against divergent *M. plutonius* strains. Going forward, probiotic efficacy studies in the treatment and prevention of EFB should encompass multiple *M. plutonius* strains, including representatives of typical and atypical strains to demonstrate applicability in the field. Moreover, when considering prophylactic

probiotic use in honeybees, developing researchers should aim to understand how these probiotics affect beneficial gut flora and as well as potential secondary invaders.

## Author contributions

EM: Conceptualization, Formal analysis, Investigation, Visualization, Writing – original draft. GF: Conceptualization, Formal analysis, Investigation, Writing – original draft. BD: Conceptualization, Supervision, Writing – review & editing. EA-V: Funding acquisition, Project administration, Supervision, Writing – review & editing.

## Funding

The author(s) declare that financial support was received for the research, authorship, and/or publication of this article. This work was supported by a Canadian Institutes of Health Research (CIHR) Banting Postdoctoral Fellowship Award (PDF-402947–2023, award to BAD) and Canada First Research Excellence Fund (CFREF) Food from Thought (FfT) Thematic III Research Grant (THE3-00525) to EA-V. EM and GF were supported by scholarships from Ontario Graduate Scholarships, respectively.

## Conflict of interest

EA-V is co-founder of NuBioyota, a company developing novel microbiome-based therapeutics for human use.

The remaining authors declare that the research was conducted in the absence of any commercial or financial relationships that could be construed as a potential conflict of interest.

## Publisher's note



## References

1. Khalifa SAM, Elshafiey EH, Shetaia AA, El-Wahed AAA, Algethami AF, Musharraf SG, et al. Overview of bee pollination and its economic value for crop production. *Insects*. (2021) 12:688. doi: 10.3390/insects12080688

2. Aizen MA, Harder LD. The global stock of domesticated honey bees is growing slower than agricultural demand for pollination. *Curr Biol*. (2009) 19:915–8. doi: 10.1016/j.cub.2009.03.071

3. Aizen MA, Garibaldi LA, Cunningham SA, Klein AM. Long-term global trends in crop yield and production reveal no current pollination shortage but increasing pollinator dependency. *Curr Biol*. (2008) 18:1572–5. doi: 10.1016/j.cub.2008.08.066

4. Gray A, Adjlane N, Arab A, Ballis A, Brusbardis V, Bugeja Douglas A, et al. Honey bee colony loss rates in 37 countries using the COLOSS survey for winter 2019–2020: the combined effects of operation size, migration and queen replacement. *J Apic Res*. (2023) 62:204–10. doi: 10.1080/00218839.2022.2113329

5. Ferland Julie, Wilson Geoff, Nasr Medhat. Canadian Association of Professional Apiculturists Statement on Honey Bee Wintering Losses in Canada (2022). Available from: https://capabees.com/shared/CAPA-Statement-on-Colony-Losses-2021-2022-FV.pdf (Accessed August 7, 2024).

6. Hristov P, Shumkova R, Palova N, Neov B. Factors associated with honey bee Colony losses: a Mini-review. *Vet Sci*. (2020) 7:166. doi: 10.3390/vetsci7040166

7. Daisley BA, Pitek AP, Mallory E, Chernyshova AM, Allen-Vercoe E, Reid G, et al. Disentangling the microbial ecological factors impacting honey bee susceptibility to *Paenibacillus larvae* infection. *Trends Microbiol*. (2023) 31:521–34. doi: 10.1016/j.tim.2022.11.012

8. Takamatsu D, Morinishi K, Arai R, Sakamoto A, Okura M, Osaki M. Typing of *Melissococcus plutonius* isolated from European and Japanese honeybees suggests spread of sequence types across borders and between different Apis species. *Vet Microbiol*. (2014) 171:221–6. doi: 10.1016/j.vetmic.2014.03.036

9. Takamatsu D, Sato M, Yoshiyama M. Infection of *Melissococcus plutonius* clonal complex 12 strain in European honeybee larvae is essentially confined to the digestive tract. *J Vet Med Sci*. (2016) 78:29–34. doi: 10.1292/jvms.15-0405

10. Laate E. Potential economic impact of European and American foulbrood on Alberta's beekeeping industry. Canada: agriculture and forestry, government of Alberta; (2020). Available from: https://open.alberta.ca/dataset/029a345b-8621-4986-ad78-7fc6ddcd8b17/resource/25f7b78d-a359-428c-9648-9175c3634720/download/af-potential-economic-impact-european-american-foulbrood-on-albertas-beekeeping-industry.pdf (Accessed August 7, 2024).

11. Budge GE, Barrett B, Jones B, Pietravalle S, Marris G, Chantawannakul P, et al. The occurrence of *Melissococcus plutonius* in healthy colonies of *Apis mellifera* and the efficacy of European foulbrood control measures. *J Invertebr Pathol*. (2010) 105:164–70. doi: 10.1016/j.jip.2010.06.004

12. Thompson HM, Waite RJ, Wilkins S, Brown MA, Bigwood T, Shaw M, et al. Effects of shook swarm and supplementary feeding on oxytetracycline levels in honey extracted from treated colonies. *Apidologie*. (2006) 37:51–7. doi: 10.1051/apido:2005058

13. Pettis JS, Kochansky J, Feldlaufer MF. Larval *Apis mellifera* L. (Hymenoptera: Apidae) mortality after topical application of antibiotics and dusts. *J Econ Entomol*. (2004) 97:171–6. doi: 10.1603/0022-0493-97.2.171

14. Djordjevic S, Noone K, Smith L, Hornitzky MAZ. Development of a hemi-nested PCR assay for the specific detection ofMelissococcus pluton. *J Apic Res*. (1998) 37:165–74. doi: 10.1080/00218839.1998.11100968

15. McKee BA, David Goodman R, Alan HM. The transmission of European foulbrood (*Melissococcus plutonius*) to artificially reared honey bee larvae (*Apis mellifera*). *J Apic Res*. (2004) 43:93–100. doi: 10.1080/00218839.2004.11101117

16. Arai R, Tominaga K, Wu M, Okura M, Ito K, Okamura N, et al. Diversity of *Melissococcus plutonius* from honeybee larvae in Japan and experimental reproduction of European foulbrood with cultured atypical isolates. *PLoS One*. (2012) 7:e33708. doi: 10.1371/journal.pone.0033708

17. Takamatsu D. Atypical *Melissococcus plutonius strains*: their characteristics, virulence, epidemiology, and mysteries. *J Vet Med Sci*. (2023) 85:880–94. doi: 10.1292/jvms.23-0180

18. Haynes E, Helgason T, Young JPW, Thwaites R, Budge GE. A typing scheme for the honeybee pathogen *Melissococcus plutonius* allows detection of disease transmission events and a study of the distribution of variants. *Environ Microbiol Rep*. (2013) 5:525–9. doi: 10.1111/1758-2229.12057

19. Pettit M. Outline of apiary inspection in Ontario. *J Econ Entomol*. (1916) 9:196–9. doi: 10.1093/jee/9.1.196

20. Bailey L, Locher N. Experiments on the etiology of European foul brood of the honeybee. *J Apic Res*. (1968) 7:103–7. doi: 10.1080/00218839.1968.11100197

21. Chopra I, Roberts M. Tetracycline antibiotics: mode of action, applications, molecular biology, and epidemiology of bacterial resistance. *Microbiol Mol Biol Rev*. (2001) 65:260. doi: 10.1128/mmbr.232.2.232-260.2001

22. Alburaki M, Abban SK, Evans JD, Chen YP. Occurrence and distribution of two bacterial brood diseases (American and European foulbrood) in US honey bee colonies and resistance to antibiotics from 2015 to 2022. *J Apic Res*. (2024) 63:701–10. doi: 10.1080/00218839.2024.2329854

23. Olmstead S, McCallum R, Shaw J. Evaluating the effect of feeding pollen substitute to honey bee colonies destined for wild blueberry pollination in Colchester County, Nova Scotia. Nova Scotia, Canada: Atlantic Tech Transfer Team for Apiculture; (2019). p. 1–4. Available from: https://www.perennia.ca/wp-content/uploads/2019/10/ATTTA-FactSheet-Oct-2019.pdf (Accessed August 1, 2024).

24. Roetschi A, Berthoud H, Kuhn R, Imdorf A. Infection rate based on quantitative real-time PCR Of*melissococcus plutonius*, the causal agent of European foulbrood, in honeybee colonies before and after apiary sanitation. *Apidologie*. (2008) 39:362–71. doi: 10.1051/apido:200819

25. Guarna M, Higo H, Foster L, Pernal S, Wolf VP. Bee health and blueberry pollination. *Hive Lights*. (2019) 32:14.

26. Arai R, Miyoshi-Akiyama T, Okumura K, Morinaga Y, Wu M, Sugimura Y, et al. Development of duplex PCR assay for detection and differentiation of typical and atypical *Melissococcus plutonius* strains. *J Vet Med Sci*. (2014) 76:491–8. doi: 10.1292/jvms.13-0386

27. de León-Door AP, Romo-Chacón A, Rios-Velasco C, Zamudio-Flores PB, Ornelas-Paz JJ, Acosta-Muñiz CH. Prevalence, typing and phylogenetic analysis of *Melissococcus plutonius* strains from bee colonies of the state of Chihuahua, Mexico. *J Invertebr Pathol*. (2018) 159:71–7. doi: 10.1016/j.jip.2018.10.006

28. Grossar D, Haynes E, Budge GE, Parejo M, Gauthier L, Charrière JD, et al. Population genetic diversity and dynamics of the honey bee brood pathogen *Melissococcus plutonius* in a region with high prevalence. *J Invertebr Pathol*. (2023) 196:107867. doi: 10.1016/j.jip.2022.107867

29. Thebeau JM, Liebe D, Masood F, Kozii IV, Klein CD, Zabrodski MW, et al. Investigation of *Melissococcus plutonius* isolates from 3 outbreaks of European foulbrood disease in commercial beekeeping operations in western Canada. *Can Vet J*. (2022) 63:935–42.

30. Masood F, Thebeau JM, Cloet A, Kozii IV, Zabrodski MW, Biganski S, et al. Evaluating approved and alternative treatments against an oxytetracycline-resistant bacterium responsible for European foulbrood disease in honey bees. *Sci Rep*. (2022) 12:5906. doi: 10.1038/s41598-022-09796-4

31. Takamatsu D, Yoshida E, Watando E, Ueno Y. Oxytetracycline resistance Of*melissococcus plutonius*strains in Japan. *J Apic Res*. (2024) 63:306–9. doi: 10.1080/00218839.2023.2213401

32. Grossar D, Kilchenmann V, Forsgren E, Charrière JD, Gauthier L, Chapuisat M, et al. Putative determinants of virulence in *Melissococcus plutonius*, the bacterial agent causing European foulbrood in honey bees. *Virulence*. (2020) 11:554–67. doi: 10.1080/21505594.2020.1768338

33. Nakamura K, Okumura K, Harada M, Okamoto M, Okura M, Takamatsu D. Different impacts ofpMP19on the virulence Of*melissococcus plutonius*strains with different genetic backgrounds. *Environ Microbiol*. (2020) 22:2756–70. doi: 10.1111/1462-2920.14999

34. Connil N, Le Breton Y, Dousset X, Auffray Y, Rincé A, Prévost H. Identification of the *Enterococcus faecalis* tyrosine decarboxylase operon involved in tyramine production. *Appl Environ Microbiol*. (2002) 68:3537–44. doi: 10.1128/AEM.68.7.3537-3544.2002

35. Kanbar G, Engels W, Nicholson GJ, Hertle R, Winkelmann G. Tyramine functions as a toxin in honey bee larvae during Varroa-transmitted infection by *Melissococcus pluton*. *FEMS Microbiol Lett*. (2004) 234:149–54. doi: 10.1111/j.1574-6968.2004.tb09526.x

36. Djukic M, Erler S, Leimbach A, Grossar D, Charrière JD, Gauthier L, et al. Comparative genomics and description of putative virulence factors of *Melissococcus plutonius*, the causative agent of European foulbrood disease in honey bees. *Gen Dent*. (2018) 9:419. doi: 10.3390/genes9080419

37. Cheshire FR, Watson Cheyne W. The Pathogenic History and History under Cultivation of a new Bacillus (*B. alvei*), the Cause of a Disease of the Hive Bee hitherto known as Foul Brood - Cheshire - 1885 - Journal of the Royal Microscopical Society - Wiley Online Library. (2024). Available from: https://onlinelibrary.wiley.com/doi/abs/10.1111/j.1365-2818.1885.tb05794.x (Accessed July 30, 2024).

38. White GF. The cause of European foul brood. U.S. government printing. *Office*. (1912) 157:24. doi: 10.5962/bhl.title.63494

39. Bailey L. The isolation and cultural characteristics of *Streptococcus pluton* and further observations on *bacterium eurydice*. *Microbiology*. (1957) 17:39–48.

40. Bailey L. The pathogenicity for honey-bee larvae of microorganisms associated with European foulbrood. *J insect pathol*. (1963) 5:198–205.

41. Anderson KE, Copeland DC, Erickson RJ, Floyd AS, Maes PC, Mott BM. A high-throughput sequencing survey characterizing European foulbrood disease and varroosis in honey bees. *Sci Rep*. (2023) 13:1162. doi: 10.1038/s41598-023-28085-2

42. Pakwan C, Kaltenpoth M, Weiss B, Chantawannakul P, Jun G, Disayathanoowat T. Bacterial communities associated with the ectoparasitic mites *Varroa destructor* and *Tropilaelaps mercedesae* of the honey bee (*Apis mellifera*). *FEMS Microbiol Ecol*. (2018) 94:fix160. doi: 10.1093/femsec/fix160

43. Hubert J, Erban T, Kamler M, Kopecky J, Nesvorna M, Hejdankova S, et al. Bacteria detected in the honeybee parasitic mite *Varroa destructor* collected from beehive winter debris. *J Appl Microbiol*. (2015) 119:640–54. doi: 10.1111/jam.12899

44. Huang Q, Lopez D, Evans JD. Shared and unique microbes between small hive beetles (*Aethina tumida*) and their honey bee hosts. *MicrobiologyOpen*. (2019) 8:e899. doi: 10.1002/mbo3.899

45. Erler S, Lewkowski O, Poehlein A, Forsgren E. The curious case of *Achromobacter eurydice*, a gram-variable pleomorphic bacterium associated with European foulbrood disease in honeybees. *Microb Ecol*. (2018) 75:1–6. doi: 10.1007/s00248-017-1007-x

46. Giersch T, Barchia I, Hornitzky M. Can fatty acids and oxytetracycline protect artificially raised larvae from developing European foulbrood? *Apidologie*. (2010) 41:151–9. doi: 10.1051/apido/2009066

47. Lewkowski O, Erler S. Virulence of *Melissococcus plutonius* and secondary invaders associated with European foulbrood disease of the honey bee. *Microbiology*. (2019) 8:e00649. doi: 10.1002/mbo3.649

48. Daisley BA, Chmiel JA, Pitek AP, Thompson GJ, Reid G. Missing microbes in bees: how systematic depletion of key symbionts erodes immunity. *Trends Microbiol*. (2020) 28:1010–21. doi: 10.1016/j.tim.2020.06.006

49. Erban T, Ledvinka O, Kamler M, Hortova B, Nesvorna M, Tyl J, et al. Bacterial community associated with worker honeybees (*Apis mellifera*) affected by European foulbrood. *PeerJ*. (2017) 5:e3816. doi: 10.7717/peerj.3816

50. Anderson K, Floyd A, Maes P, Mott B, Copeland D. Microbiomes associated with European foul brood disease, and idiopathic brood disease syndrome in honey bees. (2022). Available from: https://www.researchsquare.com/article/rs-1436205/v1 (Accessed June 13, 2024).

51. Leska A, Nowak A, Szulc J, Motyl I, Czarnecka-Chrebelska KH. Antagonistic activity of potentially probiotic lactic acid Bacteria against honeybee (*Apis mellifera* L.) pathogens. *Pathogens*. (2022) 11:1367. doi: 10.3390/pathogens11111367

52. Zendo T, Ohashi C, Maeno S, Piao X, Salminen S, Sonomoto K, et al. Kunkecin a, a new Nisin variant Bacteriocin produced by the Fructophilic lactic acid bacterium, *Apilactobacillus kunkeei* FF30-6 isolated from honey bees. *Front Microbiol*. (2020) 11:11. doi: 10.3389/fmicb.2020.571903

53. Mojgani N, Bagheri M, Moharrami M, Toutiaee S, Rousta HM. Bioactive metabolites from autochthonous lactic acid bacteria inhibit the growth Of*melissococcus plutonius*, causal agent of European foulbrood disease in honey bees. *Entomol Exp Appl*. (2023) 171:386–94. doi: 10.1111/eea.13295

54. Endo A, Salminen S. Honeybees and beehives are rich sources for fructophilic lactic acid bacteria. *Syst Appl Microbiol*. (2013) 36:444–8. doi: 10.1016/j.syapm.2013.06.002

55. Wu M, Sugimura Y, Iwata K, Takaya N, Takamatsu D, Kobayashi M, et al. Inhibitory effect of gut bacteria from the Japanese honey bee, *Apis cerana japonica*, against *Melissococcus plutonius*, the causal agent of European foulbrood disease. *J Insect Sci*. (2014) 14:129. doi: 10.1093/jis/14.1.129

56. Chukwudi CU. rRNA binding sites and the molecular mechanism of action of the Tetracyclines. *Antimicrob Agents Chemother*. (2016) 60:4433–41. doi: 10.1128/AAC.00594-16

57. Wu M, Sugimura Y, Takaya N, Takamatsu D, Kobayashi M, Taylor D, et al. Characterization of bifidobacteria in the digestive tract of the Japanese honeybee, *Apis cerana japonica*. *J Invertebr Pathol*. (2013) 112:88–93. doi: 10.1016/j.jip.2012.09.005

58. Pietropaoli M, Carpana E, Milito M, Palazzetti M, Guarducci M, Croppi S, et al. Use of *Lactobacillus plantarum* in preventing clinical cases of American and European foulbrood in Central Italy. *Appl Sci*. (2022) 12:1388. doi: 10.3390/app12031388

59. Daisley BA, Pitek AP, Chmiel JA, Al KF, Chernyshova AM, Faragalla KM, et al. Novel probiotic approach to counter *Paenibacillus larvae* infection in honey bees. *ISME J*. (2020) 14:476–91. doi: 10.1038/s41396-019-0541-6

60. Damico ME, Beasley B, Greenstein D, Raymann K. Testing the effectiveness of a commercially sold probiotic on restoring the gut microbiota of honey bees: a field study. *Probiotics & Antimicro Prot*. (2023). doi: 10.1007/s12602-023-10203-1

61. Anderson KE, Allen NO, Copeland DC, Kortenkamp OL, Erickson R, Mott BM, et al. A longitudinal field study of commercial honey bees shows that non-native probiotics do not rescue antibiotic treatment, and are generally not beneficial. *Sci Rep*. (2024) 14:1954. doi: 10.1038/s41598-024-52118-z

62. Motta EVS, Powell JE, Leonard SP, Moran NA. Prospects for probiotics in social bees. *Philosophical Trans Royal Society B: Biolog Sci*. (2022) 377:20210156. doi: 10.1098/rstb.2021.0156

63. Powell JE, Carver Z, Leonard SP, Moran NA. Field-realistic Tylosin exposure impacts honey bee microbiota and pathogen susceptibility, which is ameliorated by native gut probiotics. *Microbiol Spectr*. (2021) 9:e0010321. doi: 10.1128/Spectrum.00103-21

64. Palacio MA, Figini EE, Ruffinengo SR, Rodriguez EM, Del HML, Bedascarrasbure EL. Changes in a population Of*apis mellifera*l. Selected for hygienic behaviour and its relation to brood disease tolerance. *Apidologie*. (2000) 31:471–8. doi: 10.1051/apido:2000139

65. Fowler PD, Schroeder DC, Kevill JL, Milbrath MOG. No impact of hygienic behavior and viral coinfection on the development of European foulbrood in honey bee (*Apis mellifera*) colonies during blueberry pollination in Michigan. *J Insect Sci*. (2023) 23:21. doi: 10.1093/jisesa/iead094

66. Nakamura K, Yamazaki Y, Shiraishi A, Kobayashi S, Harada M, Yoshiyama M, et al. Virulence differences among *Melissococcus plutonius* strains with different genetic backgrounds in *Apis mellifera* larvae under an improved experimental condition. *Sci Rep*. (2016) 6:33329. doi: 10.1038/srep33329

67. Al Toufailia H, Evison SEF, Hughes WOH, Ratnieks FLW. Both hygienic and non-hygienic honeybee, *Apis mellifera*, colonies remove dead and diseased larvae from open brood cells. *Philos Trans R Soc Lond Ser B Biol Sci*. (2018) 373:20170201. doi: 10.1098/rstb.2017.0201

68. Ameline C, Beaurepaire A, Ory F, de La Harpe M, Dainat B, Dietemann V. Differential resistance across paternal genotypes of honey bee brood to the pathogenic Bacterium*melissococcus plutonius*. *J Appl Entomol*. (2023) 147:85–93. doi: 10.1111/jen.13087

69. Hýbl M, Bohatá A, Rádsetoulalová I, Kopecký M, Hoštičková I, Vaníčková A, et al. Evaluating the efficacy of 30 different essential oils against Varroa destructor and honey bee workers (*Apis mellifera*). *Insects*. (2021) 12:1045. doi: 10.3390/insects12111045

70. Santos RCV, Lopes LQS, Alves CFS, Fausto VP, Pizzutti K, Barboza V, et al. Antimicrobial activity of tea tree oil nanoparticles against American and European foulbrood diseases agents. *J Asia Pac Entomol*. (2014) 17:343–7. doi: 10.1016/j.aspen.2014.02.003

71. Arrese EL, Soulages JL. Insect fat body: energy, metabolism, and regulation. *Annu Rev Entomol*. (2010) 55:207–25. doi: 10.1146/annurev-ento-112408-085356

72. Pang C, Dong K, Guo Y, Ding G, Lu Y, Guo Z, et al. Effects of three types of pollen on the growth and development of honey bee larvae (Hymenoptera, Apidae). *Front Ecol Evol*. (2022) 10. doi: 10.3389/fevo.2022.870081

73. Lamontagne-Drolet M, Samson-Robert O, Giovenazzo P, Fournier V. The impacts of two protein supplements on commercial honey bee (*Apis mellifera*l.) colonies. *J Apic Res*. (2019) 58:800–13. doi: 10.1080/00218839.2019.1644938

74. Crailsheim K, Brodschneider R, Aupinel P, Behrens D, Genersch E, Vollmann J, et al. Standard methods for artificial rearing Of*apis mellifera*larvae. *J Apic Res*. (2013) 52:1–16. doi: 10.3896/IBRA.1.52.1.05

75. Brødsgaard CJ, Ritter W, Hansen H. Response of in vitro reared honey bee larvae to various doses of *Paenibacillus larvae larvae* spores. *Apidologie*. (1998) 29:569–78. doi: 10.1051/apido:19980609

76. Bellah H, Seiler NF, Croll D. Divergent outcomes of direct conspecific pathogen strain interaction and plant co-infection suggest consequences for disease dynamics. *Microbiol Spectrum*. (2023) 11:e0444322–2. doi: 10.1128/spectrum.04443-22

77. Ory F, Dietemann V, Guisolan A, von Ah U, Fleuti C, Oberhaensli S, et al. *Paenibacillus melissococcoides* sp. nov., isolated from a honey bee colony affected by European foulbrood disease. *Int J Syst Evol Microbiol*. (2023) 73:005829. doi: 10.1099/ijsem.0.005829

78. Killer J, Dubná S, Sedláček I, Švec P. Lactobacillus apis sp. nov., from the stomach of honeybees (*Apis mellifera*), having an in vitro inhibitory effect on the causative agents of American and European foulbrood. *Int J Syst Evol Microbiol*. (2014) 64:152–7. doi: 10.1099/ijs.0.053033-0

79. Iorizzo M, Ganassi S, Albanese G, Letizia F, Testa B, Tedino C, et al. Antimicrobial activity from putative probiotic lactic acid Bacteria for the biological control of American and European foulbrood diseases. *Vet Sci*. (2022) 9:236. doi: 10.3390/vetsci9050236

frontiers | Frontiers in Veterinary Science

TYPE Original Research
PUBLISHED 19 December 2024
DOI 10.3389/fvets.2024.1443856



OPEN ACCESS

EDITED BY
Izhar Hyder Qazi,
Shaheed Benazir Bhutto University of Veterinary & Animal Sciences, Pakistan

REVIEWED BY
Susumu Muroya,
Kagoshima University, Japan
Jana Frahm,
Friedrich-Loeffler-Institut, Germany
Yanfen Ma,
Ningxia University, China

*CORRESPONDENCE
Xiangfei Zhang
✉ zxfsicau@foxmail.com
Xiaolin Luo
✉ Luoxl2004@sina.com

RECEIVED 04 June 2024
ACCEPTED 07 October 2024
PUBLISHED 19 December 2024

CITATION
Shang K, Guan J, An T, Zhao H, Bai Q, Li H, Sha Q, Jiang M, Zhang X and Luo X (2024) Effects of perinatal nutrition supplementation and early weaning on serum biochemistry, metabolomics, and reproduction in yaks. *Front. Vet. Sci.* 11:1443856. doi: 10.3389/fvets.2024.1443856



# Effects of perinatal nutrition supplementation and early weaning on serum biochemistry, metabolomics, and reproduction in yaks

Kaiyuan Shang[1], Jiuqiang Guan[1], Tianwu An[1], Hongwen Zhao[1], Qin Bai[1], Huade Li[1], Quan Sha[1], Mingfeng Jiang[2], Xiangfei Zhang[1]* and Xiaolin Luo[1]*

[1]Sichuan Academy of Grassland Sciences, Chengdu, China, [2]College of Animal and Veterinary Sciences, Southwest Minzu University, Chengdu, China

The transition period is a crucial stage in the reproductive cycle for dams and is linked closely with postpartum recovery, reproduction performance, and health. The confronting problem in the yak industry is that transition yaks under a conventional grazing feeding regime endure nutritional deficiency since this period is in late winter and early spring of the Qinghai-Tibet Plateau with the lack of grass on natural pasture. Therefore, this study aimed to investigate the effects of perinatal nutritional supplementation and early weaning on serum biochemistry, reproductive performance, and metabolomics in transition yaks. Eighteen healthy yaks in late pregnancy (233.9 $\pm$ 18.3 kg, 2–4 parity) were randomly assigned to three groups: conventional grazing feeding (GF, $n$ = 6), additional nutrition supplementation (SF, $n$ = 6), and additional nutrition supplementation with early weaning (SW, $n$ = 6). Yaks in the GF, SF, and SW groups were free grazing on the same pasture in the daytime from –30 to 90 d relative to parturition. Yaks in SF and SW groups received total mixed ration supplementation in the barn during the night throughout the trial. Calves in the SW group were early weaned and separated from the dam at 60 d postpartum. Maternal body weight was measured at –30 and 90 d, and serum samples were collected to analyze serum biochemistry, hormones, and metabolomics at –15, 30, and 90 d relative to calving. In the SF and SW groups, yaks showed significantly higher body weight gain, serum glucose, globulin, and total protein concentrations. Lipid transportation molecules apolipoprotein B100 and very low-density lipoprotein of SF and SW yaks were significantly increased along with the decreased lipid mobilization products non-esterified fatty acid and β-hydroxybutyric acid when compared to GF yaks at –15 and 30 d. At 90 d, serum non-esterified fatty acid and β-hydroxybutyric acid levels were significantly lower in SW yaks than in SF ones, while apolipoprotein B100 and very low-density lipoprotein levels were significantly higher in SW yaks than in GF yaks. The serum levels of metabolic regulatory hormones, including insulin, leptin, and insulin-like growth factor I were significantly increased, and glucagon was significantly reduced in the SF and SW groups than in the GF group at –15 and 30 d. Among serum reproductive hormones, SF and SW yaks had significantly higher estradiol and progesterone concentrations than GF ones at –15 and 30 d. Follicle-stimulating and luteinizing hormone levels were increased in SW group than in SF and GF ones at 90 d. The calving rates in the following year were 0% (GF), 16.7% (SF), and 83.3% (SW), respectively. The serum metabolomics analysis revealed 848 metabolites in positive mode and 350 in negative mode. With the

perinatal nutritional supplementation, the lipid and energy metabolism of transition yaks were improved, meanwhile, lipid mobilization and estrogen production-related pathways were down-regulated. These data suggest that perinatal nutrition supplementation reduces body weight loss, improves glucose and lipid metabolic adaptation to the transition period, and improves yaks' reproductive performance. Additionally, the combination of early weaning and nutritional supplementation results in lower lipid mobilization and up-regulation of lipid transportation and reproductive hormone secretion, which may further contribute to postpartum recovery and acceleration of the reproductive cycle.

KEYWORDS

perinatal period, yak, nutritional supplementation, serum biochemistry, metabolomics

# 1 Introduction

Yak (*Bos grunniens*) is a predominant livestock species on the Qinghai-Tibet Plateau, providing local herders with the necessary producing and living materials (1, 2). Additionally, yaks in conventional grazing systems experience severe forage shortage during the winter season, which lasts 6–8 months per year and potentially leads to 25% body weight loss or even death (3). Yaks generally come into heat in July–August when pasture becomes abundant, and their gestation period is approximately 259 d (4). This reproductive characteristic places the yak in the winter with forage deficiency throughout late gestation and early lactation. The late gestation period, when the fetus develops rapidly, is critical for the dam and fetus. During this stage, the imbalance between the nutrition requirement of fetal development and inadequate nutrient intake can result in several issues. These problems comprise mobilization of maternal body reserves, loss of body condition and subsequent fertility, insufficient nutrients supply for the fetus, and the reduction of birth weight of calf (5). After parturition, a large amount of nutrients are also needed for milk synthesis in contrast to the lack of grass ingestion (6). Moreover, most calves are breastfed with dams and naturally weaned at about one year of age. Thus, most yaks fail to initiate the subsequent estrus in the calving year, leading to low reproductive efficiency, with calving intervals typically extending to two or even three years (7).

The perinatal period refers to the physiological stage of pregnant female animals from 28 d before to 28 d after parturition (8). This period is a crucial transitional phase during pregnancy that significantly influences fetal development, maternal health, and reproductive performance (9, 10). Research on dairy cows (11) has established that the demand for energy in the perinatal period increased dramatically due to the needs of pregnancy and lactation, while the dry matter intake of cows during this period is significantly reduced, resulting in an obstacle to energy supply. The dam in a negative energy balance (NEB) has to mobilize body reserve by lipid catabolism for maintenance metabolism, pregnancy, and lactation, which may produce plenty of ketone bodies and even cause ketosis. Previous reports (12, 13) on beef cattle demonstrated that early-weaned cows exhibit shorter postpartum intervals and higher conception rates than lactating cows. However, there is limited research on the effects of periparturient nutrition manipulation and early weaning on metabolic adaptation to the perinatal period and reproductive performance of yaks, which needs to be further investigated.

It was reported that serum metabolomics could be an effective research method for exploring the transition of nutrient metabolism in periparturient females (14, 15). However, metabolomics has barely been utilized to analyze the nutritional metabolism of perinatal yaks. This study assessed the impacts of nutritional supplementation and early weaning on maternal body weight change, serum biochemistry, hormone secretion, and serum metabolome in perinatal yaks, to explore feasible perinatal strategies to improve metabolic transition and reproductive performance.

# 2 Materials and methods

## 2.1 Experimental design and feeding management

The animal experiment of this research was approved by the Experimental Animal Ethics Committee of the Sichuan Academy of Grassland Sciences (Approval No. 20220012). It consisted of an adapting period of 10 days and an experimental period of 120 days. Eighteen healthy yaks in late-gestation (body weight 233.9 ± 18.3 kg, 2–4 parity) diagnosed with single calf were selected and randomly divided into three groups (1) conventional grazing feeding (GF), (2) grazing feeding with nutritional supplementation group (SF) and (3) grazing feeding with nutritional supplementation + early weaning group (SW), with six replicates ($n = 6$) in each group. Yaks were enrolled at −50 d before the expected parturition. Yaks in the GF, SF, and SW groups were grazing on the same grassland under the same management from −30 to 90 d relative to parturition, being released to pasture at 08:00 and returning to the barn at 18:00 daily. They were kept in individual stalls during the night (18:00–08:00). Yaks of SF and SW groups received total mixed ration (TMR) supplementation in the barn after daily grazing from −30 to 90 d. Calves were breastfed and naturally weaned postpartum without intervention for GF and SF yaks, while calves in the SW group were early weaned and separated from the dam at 60 d postpartum.

The supplemental TMR rations for SF and SW groups were formulated based on the estimation of grazing nutrients intake of experimental yaks in preliminary work, and to make up the gap between grazing ingestion and nutrition requirement according to the nutrition requirements of late pregnant and early lactating cattle in the "Feeding Standard of Beef Cattle in China (2004)." The ratio of concentrate to roughage of TMR was 45:55 in late gestation and

TABLE 1 Animal diet of supplemental feeding groups (DM basis).

| Ingredients (%) | Late pregnancy diet | Early lactation diet[a] |
|---|---|---|
| Oat hay | 55.00 | 50.00 |
| Corn | 21.55 | 27.82 |
| Wheat bran | 12.08 | 5.95 |
| Soybean meal | 2.13 | 4.01 |
| Rapeseed meal | 2.75 | 2.94 |
| Cottonseed meal | 1.37 | 1.73 |
| Fermentation concentrates | 2.29 | 3.05 |
| Rumen-protected fat | - | 1.09 |
| Active dry yeast | 0.13 | 0.14 |
| $CaHPO_4$ | 0.62 | 0.87 |
| $NaHCO_3$ | 0.57 | 0.74 |
| NaCl | 0.51 | 0.57 |
| Functional peptides | 0.49 | — |
| Rumen-protected glucose | — | 0.52 |
| Premix[b] | 0.51 | 0.57 |
| Nutrient levels[c] | | |
| NEmf (MJ/kg) | 4.81 | 5.32 |
| CP (%) | 11.71 | 11.98 |
| NDF (%) | 46.9 | 41.96 |
| ADF (%) | 27.93 | 25.9 |
| Ca (%) | 1.29 | 1.37 |
| P (%) | 0.58 | 0.57 |

[a]The late pregnancy diet and early lactation diet were fed to the yaks in SF and SW groups from −30 d to parturition and from parturition to 90 d postpartum, respectively.
[b]The per kg premix provided the following: VA 2,750,000 IU, $VD_3$ 750,000 IU, VE 14,500 IU, Cu 6,000 mg, Mn 20,000 mg, Zn 25,000 mg, I 240 mg, Se 140 mg, Co 190 mg.
[c]CP, crude protein; EE, ether extract; NDF, neutral detergent fiber; ADF, acid detergent fiber; Ca, calcium; P, phosphorus.

50:50 in early lactation, respectively (Table 1). The active dry yeast and functional peptides were purchased from Angel Yeast Co., Ltd. and Chengdu Mytech Biotech Co., Ltd., China. The nutrient levels of the milk replacer and starter diets for early-weaned calves are shown in Supplementary Table S1.

## 2.2 Sample collection and analysis

### 2.2.1 Production performance

The body weight of the experimental yaks were measured before morning feeding at the beginning of the trial and 90 d after calving to calculate the body weight change. The feed intake of TMR was recorded daily, and the feed amount offered to each yak was determined by the feed refusal of the previous day to target <10% refusal.

### 2.2.2 Serum biochemical

Blood samples were collected from the jugular vein of each yak into vacuum tubes before morning grazing (08:00) every 15 d until parturition in the prenatal stage. Samples close to −15 d relative to the actual calving date were selected as prepartum samples. Blood was harvested at 30 and 90 d after parturition during the postpartum stage. These samples were centrifuged at 3,500 rpm for 10 min to obtain serum, and aliquots of serum were stored at −80°C for subsequent analysis.

Glucose (GLU), cholesterol (CHO), triglyceride (TG), albumin (ALB), and total protein (TP) in serum samples at −15, 30, and 90 d were determined by an automatic biochemistry analyzer (BS360S, Shenzhen Mindray Co., Ltd., China) using corresponding reagents (Shenzhen Mindray Co., Ltd., China). Globulin (GLB) concentration was calculated as TP minus ALB. Enzyme-linked immunosorbent assay (ELISA) kits (Shanghai Enzyme-Linked Biotechnology Co., Ltd., China) were used to measure the serum apolipoprotein B100 (APOB100), very low-density lipoprotein (VLDL), and β-hydroxybutyric acid (BHBA) levels with a 96-well plate and microplate spectrophotometer (μQuant, BioTek Instruments, Inc., United States). Meanwhile, serum nonesterified fatty acid (NEFA) was analyzed using a commercial kit (E-BC-K013-M, Shanghai Elabscience Biotechnology Co., Ltd., China).

### 2.2.3 Metabolic regulation hormones

The measurements of serum insulin (INS), glucagon (GC), insulin-like growth factor I (IGF-I), and leptin (LEP) concentrations were also performed using commercial ELISA kits (Shanghai Elabscience Biotechnology Co., Ltd., China) with the same instrument.

### 2.2.4 Reproduction hormone and performance

The secretion levels of reproduction hormones, including estradiol ($E_2$), follicle-stimulating hormone (FSH), luteinizing hormone (LH), and progesterone (PROG), were measured in serum samples at −15, 30, and 90 d with ELISA kits purchased from the same company. The calving rate in the following year was recorded for all yaks.

## 2.3 Statistical analysis

Yaks were excluded from the trial if they received nutritional supplementation less than 30 days before parturition to ensure the nutrition supply covered the entire perinatal period. The experimental data, except metabolomics, were statistically analyzed using the general linear model (GLM) of SAS 9.4 (SAS Institute, Inc.). Student–Newman–Keuls (SNK) statements were constructed to compare experimental treatments (nutritional supplementation and early weaning). Significance was declared at $p \leq 0.05$, and trends were discussed when $0.05 < p \leq 0.10$.

## 2.4 Metabolomics analysis

### 2.4.1 LC-MS untargeted metabolomics procedures and parameters

Serum samples from all groups at −15, 30, and 90 d were selected for Liquid Chromatograph Mass Spectrometer (LC-MS) untargeted metabolomics analysis (Beijing Novogene Co., Ltd., China). After sample pretreatment, the supernatant was collected and injected for LC-MS analysis (16–18). The experimental parameters were as follows:

Chromatographic conditions: Hypesil Gold column (C18), column temperature of 40°C, injection flow rate of 0.2 mL/min,

TABLE 2 Effects of perinatal nutritional supplementation and early weaning on production performance of yaks.

| Item | Group[1] | | | SEM | *p*-value[2] |
|---|---|---|---|---|---|
| | GF | SF | SW | | |
| Initial body weight (kg) | 236.50 | 234.08 | 231.25 | 7.55 | 0.895 |
| Postpartum 90 d final weight (kg) | 238.08 | 248.08 | 251.92 | 8.46 | 0.539 |
| Body weight change (kg)[2] | 1.58$^{c}$ | 14.00$^{b}$ | 20.67$^{a}$ | 1.97 | <0.001 |
| Dry matter intake of supplemental feeding (kg) | — | 4.05 | 3.98 | 0.03 | 0.127 |

[1]Yaks in the GF, SF and SW groups were free grazing on the same pasture from −30 to 90 d relative to parturition, being released to pasture at 08:00 and returning to barn at 18:00. Yaks in SF and SW groups received total mixed ration supplementation in barn during the night (18:00–08:00) from −30 to 90 d. Calves in the SW group were early weaned and separated from the dam at 60 d postpartum.
[2]Values with different superscript letters in the same row indicate significant differences ($p < 0.05$), and the same superscript letter or no letter indicates no significant difference ($p > 0.05$). The same as below.

positive mode (mobile phase A: 0.1% formic acid, mobile phase B: methanol), and negative mode (mobile phase A: 5 mM ammonium acetate, pH 9.0 mobile phase B: methanol).

Mass spectrometry conditions: The scanning range was set from m/z 100 to 1,500. The ESI source settings were spray voltage: 3.5 kV, sheath gas flow rate: 35 psi, aux gas flow rate: 10 L/min, Capillary Temp: 320°C, S-lens RF level: 60, and Aux gas heater temperature: 350°C. Polarity was set to positive and negative. MS/MS secondary scans were conducted in a data-dependent manner.

### 2.4.2 Metabolomics data processing and statistical analyses

The metabolites were annotated using the Kyoto Encyclopedia of Genes and Genomes (KEGG) database,[1] the HMDB database,[2] and the LIPID Maps database.[3] Multivariate statistical analyses were conducted with metabolomics data processing software metaX (19). Data after conversion underwent principal component analysis (PCA) and partial least squares discriminant analysis (PLS-DA) to derive the variable importance in projection (VIP) values for each metabolite. The T-test was performed for statistical significance (*p*-value) and fold change (FC) between groups. Correlation analysis (Pearson coefficient) among metabolites and statistical significance were analyzed using R programming language. Statistical significance was defined as $p < 0.05$. Visualization utilized R's corrplot package for volcano plots and bubble plots.

# 3 Results

## 3.1 Production performance

There was no significant difference in the initial body weight of the yaks among the three groups ($p > 0.05$, Table 2). Significant treatment effects on body weight change were observed ($p < 0.05$), showing values of 1.58 kg, 14.00 kg, and 20.67 kg for GF, SF, and SW yaks, respectively. Additionally, the dry matter intake (DMI) of yaks between the SF and SW groups did not differ significantly ($p > 0.05$).

1 https://www.genome.jp/kegg/pathway.html
2 https://hmdb.ca/metabolites
3 http://www.lipidmaps.org/

TABLE 3 Effects of perinatal nutritional supplementation and early weaning on serum glucose and nitrogen metabolism related metabolites in yaks.

| Item[2] | Day relative to calving | Group[1] | | | SEM | *p*-value |
|---|---|---|---|---|---|---|
| | | GF | SF | SW | | |
| GLU (mmol/L) | −15 | 2.04$^{b}$ | 2.98$^{a}$ | 3.07$^{a}$ | 0.20 | 0.005 |
| | 30 | 1.90$^{b}$ | 2.67$^{a}$ | 2.63$^{a}$ | 0.14 | 0.002 |
| | 90 | 1.76$^{b}$ | 2.52$^{ab}$ | 3.21$^{a}$ | 0.24 | 0.004 |
| ALB (g/L) | −15 | 21.97 | 21.98 | 22.13 | 2.29 | 0.999 |
| | 30 | 19.37 | 22.18 | 21.57 | 1.46 | 0.396 |
| | 90 | 21.55 | 22.52 | 22.48 | 1.35 | 0.857 |
| GLB (g/L) | −15 | 29.10$^{b}$ | 34.68$^{a}$ | 34.00$^{a}$ | 1.55 | 0.047 |
| | 30 | 22.33$^{b}$ | 27.63$^{a}$ | 27.05$^{a}$ | 1.48 | 0.050 |
| | 90 | 22.47 | 23.82 | 20.15 | 0.97 | 0.060 |
| TP (g/L) | −15 | 51.07 | 56.67 | 56.13 | 3.22 | 0.432 |
| | 30 | 41.70$^{b}$ | 49.82$^{a}$ | 48.62$^{a}$ | 2.20 | 0.042 |
| | 90 | 44.02 | 46.33 | 42.63 | 1.74 | 0.375 |

[1]Yaks in the GF, SF and SW groups were free grazing on the same pasture from −30 to 90 d relative to parturition, being released to pasture at 08:00 and returning to barn at 18:00. Yaks in SF and SW groups received total mixed ration supplementation in barn during the night (18:00–08:00) from −30 to 90 d. Calves in the SW group were early weaned and separated from the dam at 60 d postpartum.
[2]GLU, glucose; ALB, albumin; GLB, globulin; TP, total protein.

## 3.2 Serum biochemistry

Regarding serum metabolites associated with glucose and nitrogen metabolism (Table 3), GLU and GLB levels were significantly elevated in SF and SW yaks at −15 and 30 d ($p < 0.05$). ALB levels did not differ significantly among treatments ($p > 0.05$). TP levels were significantly higher in the yaks received SF and SW treatments at 30 d than in the GF yaks ($p < 0.05$). GLU concentration exhibited significant differences between the SW and GF yaks at 90 d ($p < 0.05$), with nonsignificant differences between SF and SW.

Among the serum metabolites related to lipid metabolism (Table 4), serum TG levels significantly decreased in the yaks of the SF and SW groups at 30 d compared to those of GF ($p < 0.05$). Significantly increased prepartum and postpartum CHO concentrations in response to SF and SW treatments were observed ($p < 0.05$). Yaks in the SF and SW groups had significantly lower serum NFEA and BHBA levels than

TABLE 4 Effects of perinatal nutritional supplementation and early weaning on serum lipid metabolism related metabolites of yaks.

| Item[2] | Day relative to calving | Group[1] | | | SEM | *p*-value |
|---|---|---|---|---|---|---|
| | | GF | SF | SW | | |
| TG (mmol/L) | −15 | 0.2 | 0.24 | 0.23 | 0.02 | 0.538 |
| | 30 | 0.19$^{a}$ | 0.11$^{b}$ | 0.12$^{b}$ | 0.02 | 0.013 |
| | 90 | 0.15 | 0.12 | 0.12 | 0.01 | 0.305 |
| CHO (mmol/L) | −15 | 1.10$^{b}$ | 1.53$^{a}$ | 1.53$^{a}$ | 0.1 | 0.015 |
| | 30 | 0.79$^{b}$ | 1.07$^{a}$ | 1.12$^{a}$ | 0.09 | 0.034 |
| | 90 | 1.05$^{b}$ | 1.38$^{ab}$ | 1.73$^{a}$ | 0.11 | 0.004 |
| NEFA (mmol/L) | −15 | 1.50$^{a}$ | 1.21$^{b}$ | 1.20$^{b}$ | 0.02 | <0.001 |
| | 30 | 1.68$^{a}$ | 1.40$^{b}$ | 1.40$^{b}$ | 0.02 | <0.001 |
| | 90 | 1.59$^{a}$ | 1.43$^{b}$ | 1.28$^{c}$ | 0.03 | <0.001 |
| BHBA (μmol/L) | −15 | 469.63$^{a}$ | 337.22$^{b}$ | 307.40$^{b}$ | 26.55 | 0.003 |
| | 30 | 836.51$^{a}$ | 553.39$^{b}$ | 532.95$^{b}$ | 30.29 | <0.001 |
| | 90 | 636.55$^{a}$ | 463.55$^{b}$ | 283.38$^{c}$ | 26.05 | <0.001 |
| VLDL (mmol/L) | −15 | 26.43$^{b}$ | 31.81$^{a}$ | 31.21$^{a}$ | 0.91 | 0.002 |
| | 30 | 20.48$^{b}$ | 25.02$^{a}$ | 26.04$^{a}$ | 1.05 | 0.005 |
| | 90 | 21.86$^{b}$ | 25.47$^{ab}$ | 29.00$^{a}$ | 1.4 | 0.010 |
| APOB100 (μg/mL) | −15 | 31.90$^{b}$ | 42.49$^{a}$ | 41.03$^{a}$ | 1.82 | 0.002 |
| | 30 | 21.86$^{b}$ | 29.75$^{a}$ | 29.91$^{a}$ | 1.4 | 0.002 |
| | 90 | 22.78$^{b}$ | 26.48$^{b}$ | 34.08$^{a}$ | 1.73 | 0.002 |

[1]Yaks in the GF, SF and SW groups were free grazing on the same pasture from −30 to 90 d relative to parturition, being released to pasture at 08:00 and returning to barn at 18:00. Yaks in SF and SW groups received total mixed ration supplementation in barn during the night (18:00–08:00) from −30 to 90 d. Calves in the SW group were early weaned and separated from the dam at 60 d postpartum.

[2]TG, triglyceride; CHO, cholesterol; NEFA, nonesterified fatty acid; BHBA, β-hydroxybutyric acid; VLDL, very low-density lipoprotein; APOB100, apolipoprotein B100.

those in the GF group ($p < 0.05$), and there was a further significant reduction with SW yaks ($p < 0.05$). APOB100 and VLDL concentrations were significantly increased at −15 and 30 d ($p < 0.05$) in SF and SW yaks compared with GF ones. Furthermore, the differences in serum APOB100 and VLDL levels between SW and GF groups reached significant levels at 90 d postpartum ($p < 0.05$).

## 3.3 Metabolic regulation hormones

As for hormones associated with metabolic regulation (Table 5), serum INS, LEP, and IGF-I levels significantly increased in the SF and SW groups at −15 and 30 d ($p < 0.05$). In contrast, SF and SW yaks had significantly lower GC concentrations than GF ones ($p < 0.05$). At 90 d, serum INS and IGF-I levels were significantly higher in the SW group than in the GF ($p < 0.05$).

## 3.4 Reproductive hormones and reproduction rate for the next year

Significantly increased serum $E_2$ and PROG concentrations in response to SF and SW treatments were observed at −15 and 30 d (Table 6, $p < 0.05$). At 90 d postpartum, SW yaks had significantly greater $E_2$ and PROG levels than GF yaks ($p < 0.05$). With no difference among treatments at −15 and 30 d, the serum FSH and LH of yaks receiving SW treatment were elevated significantly compared to GF and SF at 90 d. Yaks in the GF, SF, and SW groups had calving rates of 0, 16.7, and 83.3% in the following year, respectively (Table 7).

## 3.5 Serum metabolomics analysis

### 3.5.1 PLS-DA analysis

The PLS-DA scatter plots of serum samples (Figure 1) exhibited high sample aggregation within each treatment group in positive and negative modes, indicating good repeatability. Additionally, differences among the groups were observed, suggesting that different experimental treatments significantly influenced the serum metabolome of periparturient yaks. In all datasets, $R^2Y > Q^2Y$ indicated a well-established model (20).

### 3.5.2 Results of differential metabolite screening

Thresholds were set at VIP >1.0, FC >1.2 or FC <0.833, and *p*-value <0.05 (21–23), and the number of differential metabolites screened is listed in Supplementary Figure S1 and Supplementary Table S2. Eight hundred forty-eight and Three hundred fifty significantly differential metabolites were identified in the positive and negative modes, respectively.

### 3.5.3 Analysis of the top 20 differential metabolites

The top 20 differential metabolites in the pairwise comparison of all treatments are illustrated in Figures 2–4.

Results showed an increase in lysphosphatidylcholine (LPC) (14:0, 19:0, 19:1) concentrations and decreased 3-acetoxyurs-12-en-23-oic acid, 2-isopropylmalate, and glycerol 1-hexadecanoate levels ($p < 0.05$) in SF yaks compared to GF yaks at −15 d. SF yaks had higher serum DL-m-tyrosine, 2-hydroxyphenylalanine, and 3-hydroxy-L-proline concentrations ($p < 0.05$) in amino acid metabolism than GF. Regarding the organic acid metabolism, 3-indoxyl sulfate and D-glucuronic acid concentrations significantly increased and reduced methyl eudesmate levels ($p < 0.05$) in the SF group than in GF. SF yaks reached a significant decrease in the levels of deoxyadenosine monophosphate (dAMP) ($p < 0.05$), an indicator of nucleotide metabolism. SF yaks had significantly elevated 15(R)-Lipoxin A4, androsterone, dehydroepiandrosterone, epitestosterone, and etiocholanolone levels, while estrone, 5-trans prostaglandin F2β, and bicyclo prostaglandin E2 concentrations were notably reduced ($p < 0.05$) in hormone and hormone derivative metabolism.

At 30 d, SF yaks had higher LPC 14:0, hexadecanedioic acid, and 10-hydroxydecanoic acid levels ($p < 0.05$), and lower phosphatidylcholine (PC) [(18:3/18:4), (20:5/22:6)], branched fatty acid esters of hydroxy fatty acids (FAHFAs) [(20:0/22:2), (18:1/19:2), (20:0/22:3), (20:0/20:2), (18:3/16:2), (18:1/20:3), (17:0/20:3), (18:0/20:2), (18:2/20:4)], and 15-Acetyldeoxynivalenol concentrations related to lipid metabolism compared to GF yaks ($p < 0.05$). Regarding amino acid metabolism, SF yaks had elevated DL-m-tyrosine and 2-hydroxyphenylalanine levels ($p < 0.05$) but lower L-(+)-citrulline, gamma-glutamylleucine, homoarginine, cinnamoylglycine, capryloylglycine, and N-acetyl glycine levels ($p < 0.05$). With respect

TABLE 5 Effects of perinatal nutritional supplementation and early weaning on serum hormones related to metabolism regulation in yaks.

| Item[2] | Day relative to calving | Group[1] | | | SEM | *p*-value |
|---|---|---|---|---|---|---|
| | | GF | SF | SW | | |
| INS (mIU/L) | −15 | 35.95$^{b}$ | 42.35$^{a}$ | 43.72$^{a}$ | 1.24 | 0.001 |
| | 30 | 30.62$^{b}$ | 37.32$^{a}$ | 38.50$^{a}$ | 1.74 | 0.013 |
| | 90 | 28.27$^{b}$ | 32.62$^{ab}$ | 36.06$^{a}$ | 1.45 | 0.010 |
| GC (pg/mL) | −15 | 226.30$^{a}$ | 188.37$^{b}$ | 184.26$^{b}$ | 9.36 | 0.014 |
| | 30 | 254.49$^{a}$ | 197.88$^{b}$ | 202.48$^{b}$ | 8.9 | 0.001 |
| | 90 | 194.92 | 187.88 | 180.00 | 10.59 | 0.628 |
| LEP (ng/mL) | −15 | 4.20$^{b}$ | 5.62$^{a}$ | 5.35$^{a}$ | 0.3 | 0.017 |
| | 30 | 4.07$^{b}$ | 5.04$^{a}$ | 5.10$^{a}$ | 0.28 | 0.040 |
| | 90 | 4.97 | 5.25 | 6.29 | 0.33 | 0.053 |
| IGF-I (ng/mL) | −15 | 202.31$^{b}$ | 280.79$^{a}$ | 285.24$^{a}$ | 11.64 | <0.001 |
| | 30 | 161.42$^{b}$ | 222.65$^{a}$ | 223.78$^{a}$ | 13.02 | 0.007 |
| | 90 | 199.62$^{b}$ | 235.29$^{b}$ | 285.29$^{a}$ | 12.85 | 0.002 |

[1]Yaks in the GF, SF and SW groups were free grazing on the same pasture from −30 to 90 d relative to parturition, being released to pasture at 08:00 and returning to barn at 18:00. Yaks in SF and SW groups received total mixed ration supplementation in barn during the night (18:00–08:00) from −30 to 90 d. Calves in the SW group were early weaned and separated from the dam at 60 d postpartum.

[2]INS, insulin; GC, glucagon; LEP, leptin; IGF-I, insulin-like factor I.

TABLE 6 Effects of perinatal nutritional supplementation and early weaning on serum reproductive hormones of yaks.

| Item[2] | Day relative to calving | Group[1] | | | SEM | *p*-value |
|---|---|---|---|---|---|---|
| | | GF | SF | SW | | |
| FSH (mIU/mL) | −15 | 2.71 | 3.14 | 3.03 | 0.4 | 0.781 |
| | 30 | 6.00 | 5.75 | 6.03 | 0.45 | 0.895 |
| | 90 | 8.01$^{c}$ | 9.65$^{b}$ | 11.45$^{a}$ | 0.47 | 0.001 |
| LH (mIU/mL) | −15 | 4.33 | 4.66 | 4.59 | 0.43 | 0.855 |
| | 30 | 6.94 | 7.45 | 7.58 | 0.49 | 0.636 |
| | 90 | 12.07$^{b}$ | 13.01$^{b}$ | 15.05$^{a}$ | 0.6 | 0.011 |
| $E_2$ (pg/mL) | −15 | 53.54$^{b}$ | 74.32$^{a}$ | 72.53$^{a}$ | 3.41 | 0.001 |
| | 30 | 17.99$^{b}$ | 24.79$^{a}$ | 27.46$^{a}$ | 2.02 | 0.016 |
| | 90 | 24.40$^{b}$ | 29.37$^{ab}$ | 35.13$^{a}$ | 2.78 | 0.049 |
| PROG (ng/mL) | −15 | 42.28$^{b}$ | 53.68$^{a}$ | 54.08$^{a}$ | 1.85 | <0.001 |
| | 30 | 15.43$^{b}$ | 23.41$^{a}$ | 24.91$^{a}$ | 1.35 | <0.001 |
| | 90 | 23.71$^{b}$ | 25.35$^{b}$ | 33.24$^{a}$ | 1.28 | <0.001 |

[1]Yaks in the GF, SF and SW groups were free grazing on the same pasture from −30 to 90 d relative to parturition, being released to pasture at 08:00 and returning to barn at 18:00. Yaks in SF and SW groups received total mixed ration supplementation in barn during the night (18:00–08:00) from −30 to 90 d. Calves in the SW group were early weaned and separated from the dam at 60 d postpartum.

[2]FSH, follicle stimulating hormone; LH, luteinizing hormone; $E_2$, estradiol; PROG, progesterone.

to organic acid metabolism, SF yaks showed higher tetranor-PGDM and oxohongdenafil levels than GF ($p < 0.05$). Additionally, riboflavin-5-phosphate concentrations were higher in the SF group ($p < 0.05$), while puromycin levels decreased ($p < 0.05$) involved in nucleotide metabolism. SF yaks had significantly higher 15(R)-lipoxin A4, androstenedione, dehydroepiandrosterone, and epitestosterone concentrations ($p < 0.05$) but lower 11-deoxy prostaglandin F1β, 2,3-dinor-11β-prostaglandin F2α, and 13,14-dihydro-15-keto prostaglandin A2 levels ($p < 0.05$) in hormone and hormone derivative metabolism than GF ones. Lastly, vitamin K2 levels were significantly higher in the SF group ($p < 0.05$).

At 90 d, regarding lipid metabolism, SF yaks showed significant increases in LPC 14:0, corchorifatty acid F, dodecanedioic acid, undecanedioic acid, 12-hydroxydodecanoic acid, and 10-hydroxydecanoic acid concentrations ($p < 0.05$), meanwhile, significant reduction in 15(S)-HpETE, FAHFAs [(20:0/20:2), (20:0/22:2), (20:0/22:3)], and 12(S)-HpETE levels when compared to the GF group ($p < 0.05$). Glu-Gln and L-Glutathione oxidized concentrations increased ($p < 0.05$) in the SF group in amino acid metabolism. SF yaks had elevated 2,3-dinor-TXB2 and tetranor-PGDM levels ($p < 0.05$) related to organic acid metabolism. Additionally, riboflavin-5-phosphate concentrations were higher ($p < 0.05$), while puromycin levels were lower ($p < 0.05$) in the SF group in nucleotide metabolism. In hormone and hormone derivative metabolism, the SF group showed a significant effect on higher androstenedione, dehydroepiandrosterone, epitestosterone, and 2-methoxyestradiol concentrations ($p < 0.05$) compared with the GF group, along with decreased levels of 11-deoxy prostaglandin F1β, 6-keto-prostaglandin f1alpha, prostaglandin E2, prostaglandin D2, 13,14-dihydro-15-keto prostaglandin A2, bicyclol prostaglandin E2, and lipoxin B4 ($p < 0.05$). Moreover, vitamin K2 levels were improved ($p < 0.05$) in the SF group in vitamin metabolism.

At 90 d, in the comparison between SW and GF groups, significant increases in serum LPC 14:0, corchorifatty acid F, suberic acid, dodecanedioic acid, undecanedioic acid, 12-hydroxydodecanoic acid, and 10-hydroxydecanoic acid concentrations involved in lipid metabolism ($p < 0.05$) were observed in SW group. In contrast, there were significant decreases in 15(S)-HETE, FAHFA [(20:0/22:2), (20:0/20:2), (20:0/22:3)], and 12(S)-HETE levels ($p < 0.05$). Glu-Gln and L-glutathione oxidized concentrations ($p < 0.05$) occurred with SW treatment in amino acid metabolism. SW yaks had significantly higher 2,3-Dinor-TXB2 and tetranor-PGDM levels ($p < 0.05$) related to organic acid metabolism. Additionally, riboflavin-5-phosphate levels increased ($p < 0.05$), while puromycin levels decreased ($p < 0.05$) regarding nucleotide metabolism in the SW group. With respect to hormone and hormone derivative metabolism, androsterone, dehydroepiandrosterone, and epitestosterone levels significantly increased ($p < 0.05$), and 11-deoxy prostaglandin F1β, prostaglandin E2, 2,3-dinor-11β-prostaglandin F2α, bicyclic prostaglandin E2, and 6-keto-prostaglandin f1alpha concentrations significantly decreased ($p < 0.05$) among yaks of SW group when compared with those of GF. Moreover, vitamin K2 levels were higher in the SW group ($p < 0.05$) than in the GF group.

At 90 d, serum PC [(18:3e/2:0), (17:0/18:1), (18:0e/14:1), (14:0e/18:0), (14:0e/22:3), (16:2e/18:0), (18:4e/2:0), (18:5/20:5), (18:1e/18:2), (22:3e/13:0)], LPC (12:1, 17:0, 22:6, 20:3, 18:0, 20:4), SM [(d14:0/18:1), (d25:3/16:2), (d14:0/22:2)], punicic acid, branched fatty acid esters of hydroxy fatty acids (FAHFAs) (18:2/18:3) and lysopc (12:1, 17:0) related to lipid metabolism levels were significantly elevated in SW yaks when compared to SF ones ($p < 0.05$). In contrast, octadecane tricarboxylic acid, oleoyl ethanamide, and 15(S)-HpEPE, corchorifatty acid F, LPC 16:0, pipecolic acid, and FAHFAs (14:0/6:0) concentrations were significantly lower ($p < 0.05$) in SW yaks. SW

TABLE 7 Effect of perinatal nutritional supplementation and early weaning on the calving rate of yaks in the following year.

| Item | Group[a] | | |
|---|---|---|---|
| | GF | SF | SW |
| Next-year calving rate (%) | 0 | 16.7 | 83.3 |

[a]Yaks in the GF, SF and SW groups were free grazing on the same pasture from −30 to 90 d relative to parturition, being released to pasture at 08:00 and returning to barn at 18:00. Yaks in SF and SW groups received total mixed ration supplementation in barn during the night (18:00–08:00) from −30 to 90 d. Calves in the SW group were early weaned and separated from the dam at 60 d postpartum.

group had significantly increased ornithine, L-cystine, N-acetylglycine, N-isobutyrylglycine, and 3-hydroxy-L-proline concentrations ($p < 0.05$) among amino acid metabolites. Meanwhile, N-phenylacetylglutamine, 4-hydroxyisoleucine, D-(−)-glutamine, prolylglycine, and calcium D-panthotenate levels were significantly reduced by SW treatment ($p < 0.05$). Terephthalic acid concentration was significantly lower in the SW group ($p < 0.05$). In nucleotide metabolism, significantly higher thymidine levels ($p < 0.05$) were observed in SW yaks than in SF yaks. A significant reduction of N4-acetylcysteine and β-nicotinamide mononucleotide levels in serum of SW yaks was detected ($p < 0.05$). As for hormone and hormone derivative metabolism, decreased β-estradiol-17β-glucuronide levels ($p < 0.05$) were observed for SW yaks compared to SF ones.

### 3.5.4 KEGG enrichment analysis

In the positive mode (Figures 5–7 and Table 8), four pathways were significantly enriched in the comparison between SF and GF groups at −15 d using KEGG, including steroid hormone biosynthesis [KEGG, map00140], prolactin signaling pathway [KEGG, map04917], aldosterone synthesis and secretion [KEGG, map04925], and ovarian steroidogenesis [KEGG, map04913]. In the steroid hormone biosynthesis pathway, androsterone and etiocholanolone were significantly increased in SF yaks ($p < 0.05$), and pregnenolone, cortodoxone, corticosterone, androstenedione, tetrahydrocorticosterone, estrone, and progesterone were significantly decreased ($p < 0.05$). In the prolactin signaling pathway, the SF treatment significantly reduced androstenedione, estrone, and progesterone levels ($p < 0.05$). The pregnenolone, corticosterone, and progesterone concentrations were significantly decreased in SF compared to GF yaks ($p < 0.05$) in the aldosterone synthesis and secretion pathway. In the ovarian steroidogenesis pathway, SF yaks had significantly decreased pregnenolone, androstenedione, estrone, and progesterone levels ($p < 0.05$).

At 30 d, SF yaks had one significantly enriched pathway for biosynthesis of unsaturated fatty acids [KEGG, map01040] in positive mode compared to GF groups. In this pathway, eicosapentaenoic, docosapentaenoic, and docosahexaenoic acid concentrations were significantly reduced in the SF group ($p < 0.05$).

At 90 d, two pathways were significantly enriched in the positive mode of the comparison between SF and GF groups, including serotonergic synapse [KEGG, map04726] and regulation of lipolysis in adipocytes [KEGG, map04923]. Significant reductions in serotonin (5-HT), prostaglandin E2, and prostaglandin J2 levels were observed in the serotonergic synaptic pathway in the comparison between the SF and GF groups ($p < 0.05$). Corticosterone, prostaglandin E2, and adenosine 5′-monophosphate concentration of SF yaks were significantly decreased in the regulation of lipolysis in the adipocytes pathway ($p < 0.05$).

One pathway significantly enriched in the positive mode of the comparison between the SW and GF groups at 90 d was the serotonergic synapse [KEGG, map04726], where the 5-HT, prostaglandin E2, and prostaglandin J2 metabolite concentrations were significantly decreased in SW yaks ($p < 0.05$). In the negative mode, the comparison between SW and SF groups at 90 d exhibited one significantly enriched pathway, that is, pyrimidine metabolism [KEGG, map00240], and we observed significantly increased thymidine and 2-deoxyuridine levels for SW yaks in this pathway ($p < 0.05$).

## 4 Discussion

In this study, we simulated the conventional grazing feeding regime of yaks by releasing all experimental yaks to pasture during the daytime (08:00–18:00) and keeping them in the barn at night (18:00–08:00) because this represents the typical and common grazing pattern on the Qinghai-Tibet Plateau (24). For a long time, in the conventional grazing regime, local herders let yaks graze daily and had to gather them back to the barn due to the cold temperature, frequent wolf attacks, and yak thieves at night. Under the same grazing condition, SF and SW groups were supplemented with additional TMR to compare adequate nutritional supply and inadequate nutrient ingestion in the conventional grazing of the GF group.

Body weight change is one of the most intuitive indicators for observing yaks' nutritional status and production performance. In the present study, the body weight of yaks in the SF and SW groups increased by 14.00 kg and 20.67 kg, significantly higher than the 1.58 kg GF group. Studies on dairy cows (11) and ewes (25) have found that periparturient energy requirement rises dramatically due to the demands of pregnancy and lactation and that dams are very likely to suffer NEB, leading to significant body weight loss. In that case, sufficient nutrient intake during the perinatal period can alleviate the weight loss. Lusby et al. (26) reported that cows gained more weight in the summer after early weaning. Our results also revealed that adequate nutrition supplementation during the perinatal period and early weaning strategies for yaks were conducive to their body condition recovery and the transition from late gestation to early lactation.

With respect to serum metabolite, in the prepartum period, the placenta transfers sugars such as GLU and fructose, lipids such as glycerol and free fatty acids (FFA), and free amino acids from the maternal to the fetus to supply energy, as well as fat and protein synthesis, by active transport and simple diffusion (27). In the postpartum period, mammary tissue requires large amounts of nutrients for the synthesis of milk components such as lactose, milk fat, and protein when lactation initiates after delivery (28). In the present study, GF yaks had significantly lower prepartum and postpartum serum GLU levels. It is speculated that due to the perinatal dam's nutrition requirement and the deficient nutrient ingestion from conventional grazing, GF yaks could not have sufficient VFAs substrates from ruminal fermentation for gluconeogenesis. In contrast, this study's significantly increased serum GLU levels in SF yaks enlightened us that perinatal nutritional supply provided more readily digestible carbohydrates for gluconeogenesis of transition yaks,

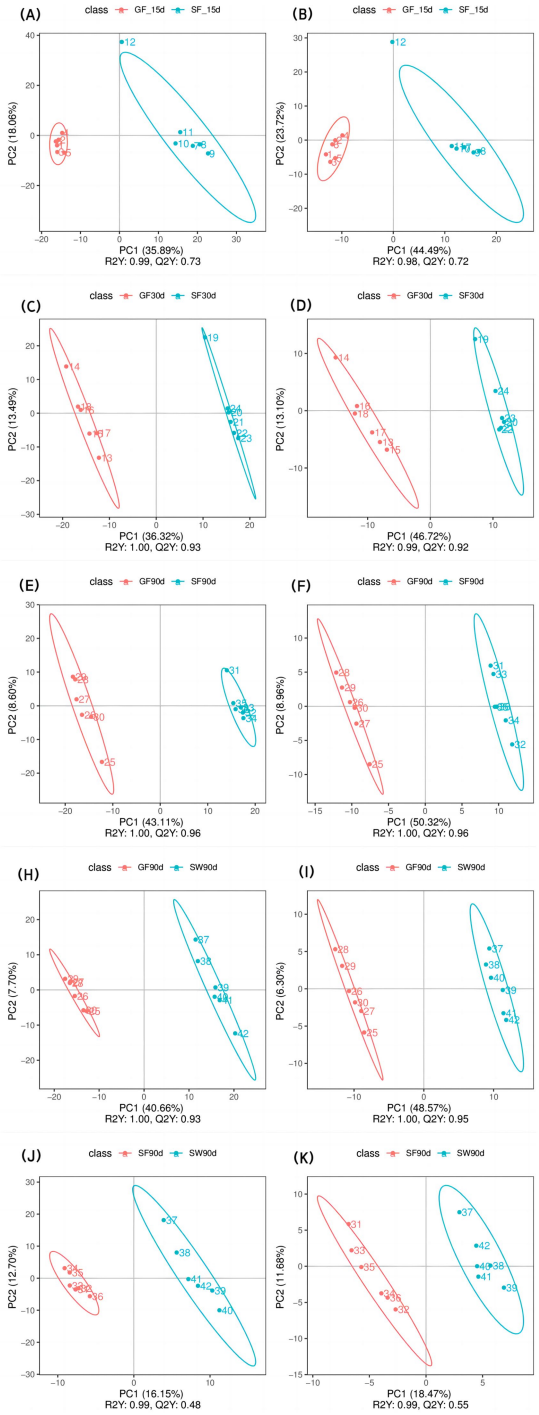


FIGURE 1
PLS-DA analysis of the effects of perinatal nutritional supplementation and early weaning on serum metabolomics in yaks. Yaks in the GF, SF and SW groups were free grazing on the same pasture from −30 to 90 d relative to parturition, being released to pasture at 08:00 and returning to barn at 18:00. Yaks in SF and SW groups received total mixed ration supplementation in barn during the night (18:00–08:00) from −30 to 90 d. Calves in the SW group were early weaned and separated from the dam at 60 d postpartum. (A,B) SF vs. GF in positive and negative modes at −15 d, (C,D) SF vs. GF in positive and negative modes at 30 d, (E,F) SF vs. GF in positive and negative modes at 90 d. (G,H) SW vs. GF in positive and negative modes at 90 d. (I,J) SW vs. SF in positive and negative modes at 90 d.

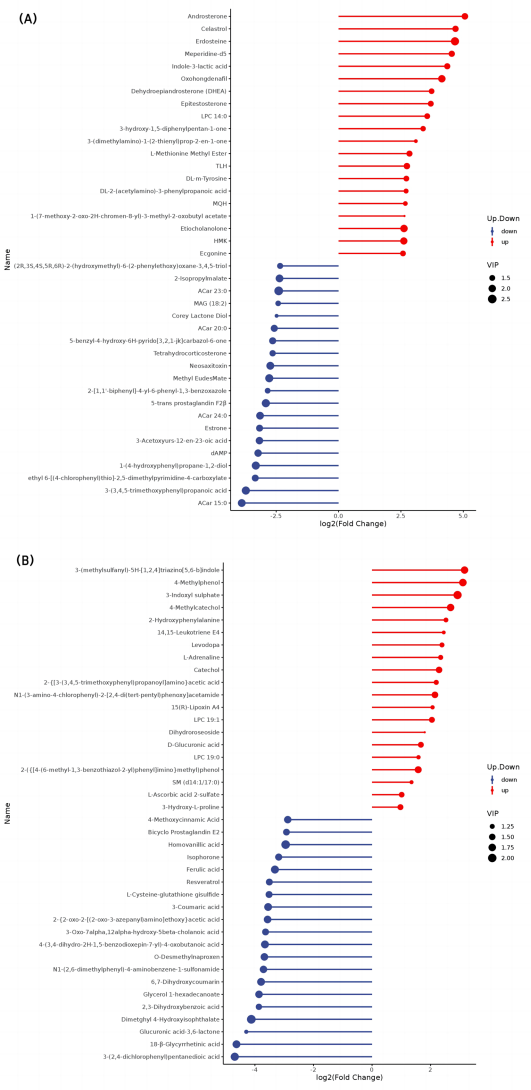


FIGURE 2
Stem map of the effects of perinatal nutritional supplementation and early weaning on serum metabolomics at −15 d relative to parturition. Yaks in the GF, SF and SW groups were free grazing on the same pasture from −30 to 90 d relative to parturition, being released to pasture at 08:00 and returning to barn at 18:00. Yaks in SF and SW groups received total mixed ration supplementation in barn during the night (18:00–08:00) from −30 to 90 d. Calves in the SW group were early weaned and separated from the dam at 60 d postpartum. (A,B) SF vs. GF in positive and negative modes at −15 d.

an indispensable substrate of lactose synthesis in milk (29). Furthermore, yaks displayed significantly high serum glucose without nutrient output of lactation after early weaning. Serum levels of TG, NEFA, and BHBA can be the indicators revealing lipid and energy metabolism in animals (30, 31). NEFA in the blood reflects the degree of lipid mobilization, while BHBA indicates the process of incomplete lipid oxidation (32). Studies on dairy cows (11, 33) showed that under insufficient nutrient intake and NEB conditions, adipose tissue was mobilized during late pregnancy and early lactation due to fetal development and lactation. Our results show that yaks in the GF group experienced nutritional deficiency, as reflected in significantly

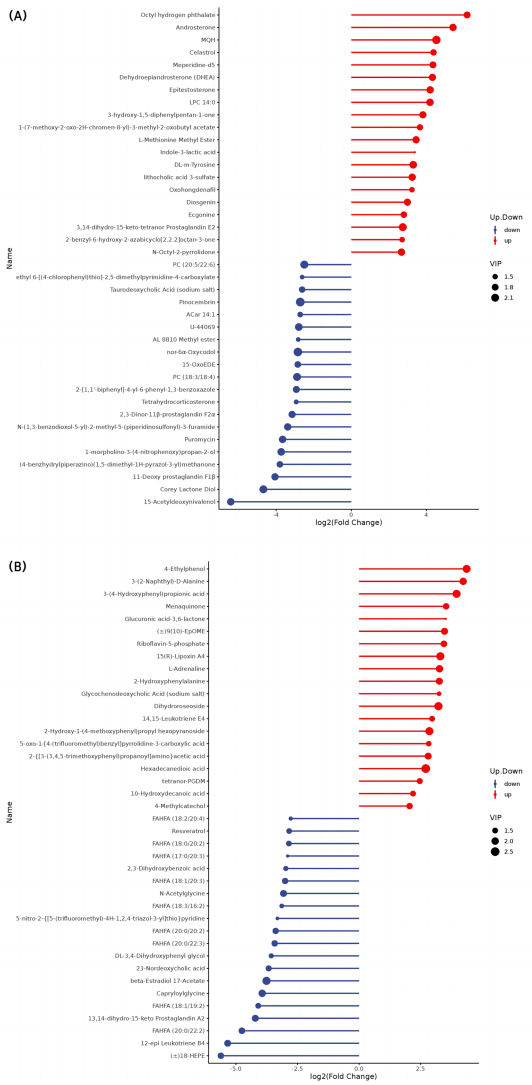


FIGURE 3
Stem map of the effects of perinatal nutritional supplementation and early weaning on serum metabolomics at 30 d relative to parturition. Yaks in the GF, SF and SW groups were free grazing on the same pasture from −30 to 90 d relative to parturition, being released to pasture at 08:00 and returning to barn at 18:00. Yaks in SF and SW groups received total mixed ration supplementation in barn during the night (18:00–08:00) from −30 to 90 d. Calves in the SW group were early weaned and separated from the dam at 60 d postpartum. (A,B) SF vs. GF in positive and negative modes at 30 d.

higher NEFA and BHBA and lower body weight. As discussed above, lipids also play a crucial role in fetal energy supply and synthesis processes in the prepartum period and milk fat synthesis during lactation (27, 28). Under conventional grazing conditions, perinatal yaks could not generate enough lipid through ruminal fermentation and *de novo* lipogenesis (34). Therefore, the maternal adipose tissue was mobilized and utilized to alleviated the NEB and support the lipids requirement during transition period, leading to the increased lipolysis products NEFA and BHBA levels in GF yaks. With the nutritional supplementation treatment, SF and SW yaks' nutrients intake increased, the NEB was thereby offset, favoring maternal pregnancy maintenance and perinatal transition. Supplementation and early weaning alleviated negative maternal energy balance and reduced lipid mobilization and ketone body when lactation was terminated. In the present study, the lipid transportation molecules APOB100 and VLDL of SF and SW yaks were significantly increased along with decreased lipid mobilization products NEFA and BHBA. The primary role of VLDL is to transport excess endogenous fatty acids (mostly TG) from the liver to provide energy to the tissues, which is crucial for lipid turnover and homeostasis (35). ApoB100, presents in every VLDL particle, is essential for VLDL structure and function (36). Elevated levels of serum APOB100 and VLDL indicate that nutritional supply and early weaning contributed to lipid transportation in periparturient yaks. In the postpartum period, we found that serum GLB and TP levels were significantly higher in SF and SW yaks compared to conventional grazing yaks, indicating the improvement of protein nutriture (37, 38) and hepatic function (39) of transition yaks with nutritional supplementation and early weaning treatment.

Regarding metabolic regulation hormones, it was demonstrated that improvement of nutritional supply contributed to decreased GC levels, reducing body lipid mobilization and promoting energy storage in the research on ewes (40). While poor nutritional status in yaks led to significantly reduced INS levels, and stimulation of body fat and glycogen breakdown (41). LEP, acting in the hypothalamus, regulates energy homeostasis and negatively correlates with serum NEFA and BHBA levels (42). IGF-I is structurally similar to INS (43) and performs a similar function in promoting the growth of animals. In our study, INS, LEP, and IGF-I levels were elevated in yaks who received nutrition supplementation during the perinatal transition. Increased INS levels are associated with nutritional and insulin resistance in late pregnancy and early lactation (44). Studies on dairy cows (45) have confirmed that cows at the end of gestation and early lactation experience a physiological state of high milk production and lipolysis, resulting in a physiological state of diminished biological effect of tissues on normal insulin doses (i.e., the onset of insulin resistance). Nutritional levels that may influence IGF-I secretion through insulin levels, fasting, malnutrition and food restriction have decreased plasma INS, IGF-I secretion, and IGF-I mRNA (46, 47). In contrast to the SF and SW yaks with nutrition supplementation, the GF yaks in our research with lower INS and IGF-I levels cohere with the previous studies. LEP levels were improved due to the enhanced maternal demand for milk fat synthesis (48). In transition yaks, an early weaning strategy elevated IGF-I levels. This result is consistent with the findings of early weaning on lactating Nellore cows (49), but the mechanism underlying the impact of early weaning on IGF-I secretion requires further study. With the increasing secretion of INS, LEP, and IGF-I involved in the regulation of nutritional metabolism, the anabolism of perinatal yaks with nutrition supplementation was potentially enhanced, and catabolism was downregulated following the results of body weight change.

Regarding reproduction, PROG positively correlates with litter size, milk yield, and body condition in dairy cows (50–52). Serum $E_2$ also responds to the high fertility of the dam and coordinates the cycle of endometrial proliferation, differentiation, shedding, and regeneration (53–56). The significantly increased secretion of reproductive hormones $E_2$ and PROG levels in SF and SW yaks imply that nutritional supplementation is beneficial in maintaining pregnancy and reproductive performance in periparturient yaks (57). Early weaning with a nutritional supplementation strategy further increased the serum FSH, LH, and PROG after weaning, which

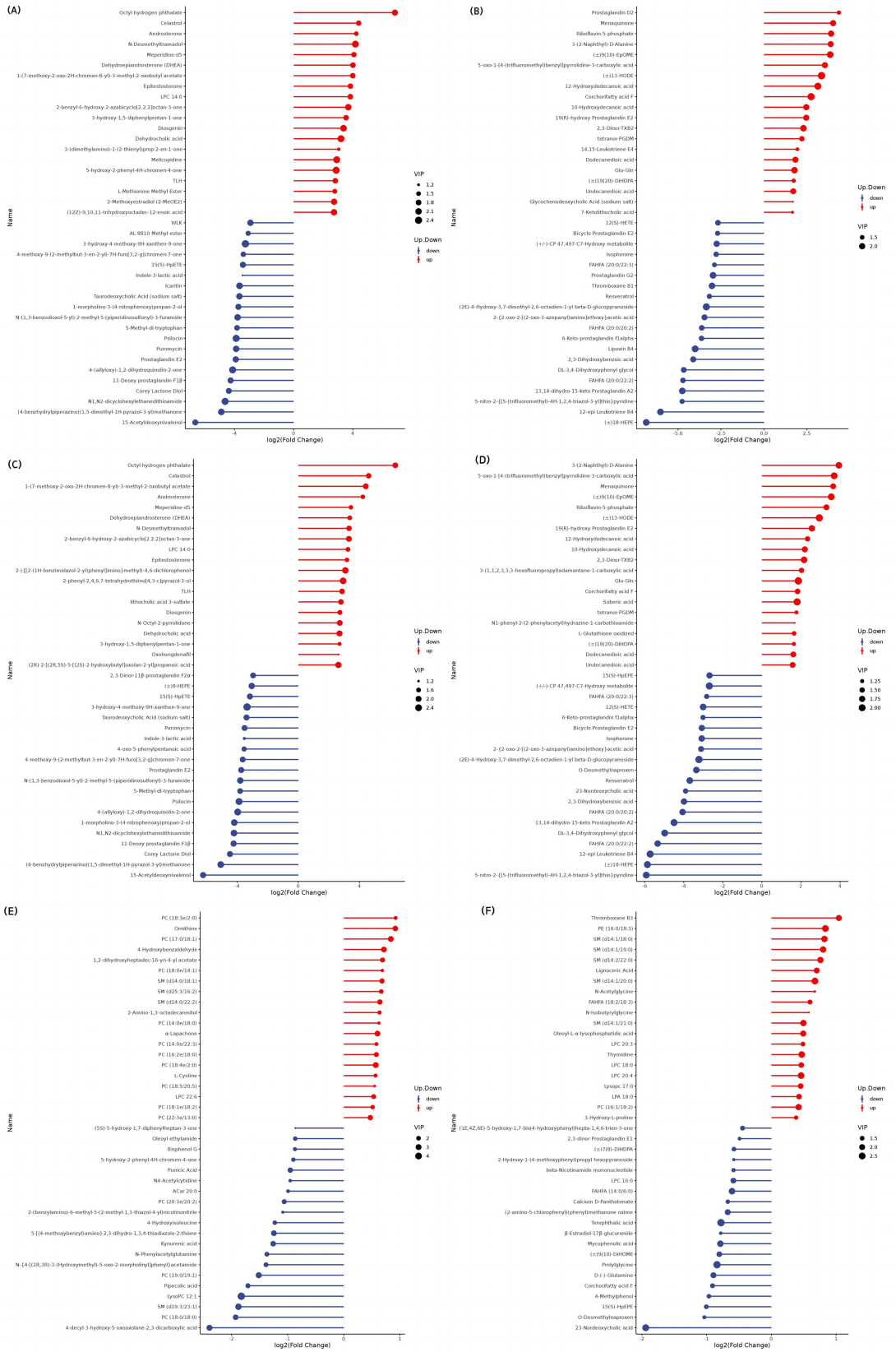


FIGURE 4
Stem map of the effects of perinatal nutritional supplementation and early weaning on serum metabolomics at 90 d relative to parturition. Yaks in the GF, SF and SW groups were free grazing on the same pasture from −30 to 90 d relative to parturition, being released to pasture at 08:00 and returning to barn at 18:00. Yaks in SF and SW groups received total mixed ration supplementation in barn during the night (18:00–08:00) from −30 to 90 d. Calves in the SW group were early weaned and separated from the dam at 60 d postpartum. (A,B) SF vs. GF in positive and negative modes at 90 d. (C,D) SW vs. GF in positive and negative modes at 90 d. (E,F) SW vs. SF in positive and negative modes at 90 d.

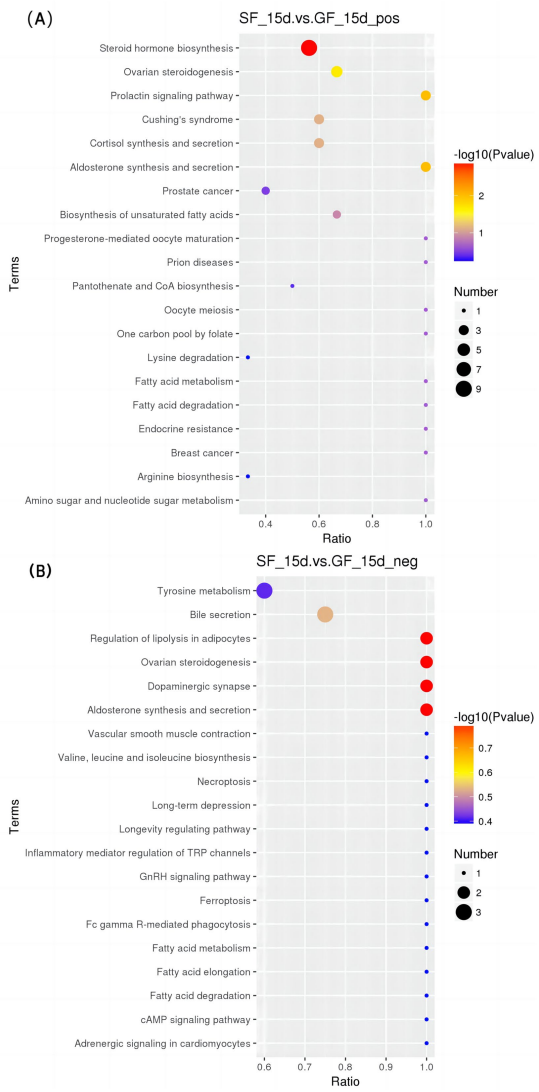


FIGURE 5
KEGG bubble diagram of the enriched pathways at −15 d relative to parturition. Yaks in the GF, SF and SW groups were free grazing on the same pasture from −30 to 90 d relative to parturition, being released to pasture at 08:00 and returning to barn at 18:00. Yaks in SF and SW groups received total mixed ration supplementation in barn during the night (18:00–08:00) from −30 to 90 d. Calves in the SW group were early weaned and separated from the dam at 60 d postpartum. (A,B) SF vs. GF in positive and negative modes at −15 d.


FIGURE 6
KEGG bubble diagram of the enriched pathways at 30 d relative to parturition. Yaks in the GF, SF and SW groups were free grazing on the same pasture from −30 to 90 d relative to parturition, being released to pasture at 08:00 and returning to barn at 18:00. Yaks in SF and SW groups received total mixed ration supplementation in barn during the night (18:00–08:00) from −30 to 90 d. Calves in the SW group were early weaned and separated from the dam at 60 d postpartum. (A,B) SF vs. GF in positive and negative modes at 30 d.

potentially promotes maturation and ovulation of the oocytes (58) and accelerates the next reproductive cycle, in accordance with the findings from a study on early weaning in beef cattle (59). The calving rate in the following year is considered a reliable indicator for evaluating the impact of perinatal nutrition supplementation and early weaning on the reproductive performance of yaks (60). The calving rates in the following year were 0% (GF), 16.7% (SF), and 83.3% (SW) in the present study. Adequate nutrition ingestion during the peripartum period was conducive to the recovery of the reproductive system, and an early weaning strategy can further expedite the reproductive cycle of yaks.

Metabolomic analysis identified differential metabolites associated with lipid metabolism, including lysophosphatidylcholine (LPC), phosphatidylcholine (PC), and branched fatty acid esters of hydroxy fatty acids (FAHFAs). PC is one of the major components of biofilms (61), and LPC is a metabolite produced by the enzymatic digestion of PC (62), which has a strong emulsifying capacity. Reportedly, LPC can enhance the uptake and utilization of glucose and effectively reduce blood glucose levels (61, 63, 64). Haetinger et al. (65), Papadopoulos et al. (66), and Boontiam et al. (67) have shown that LPC improves energy and nutrient utilization, especially lipid and protein digestibility, thus promotes production performance and gut health. However, studies on PC and LPC in ruminants are still scarce. Our experiment revealed a significant increase in LPC levels in SF yaks at −15 and 30 d. We speculated that the elevated serum levels of LPC are one of the reasons for elevated serum concentrations of INS. LPC can

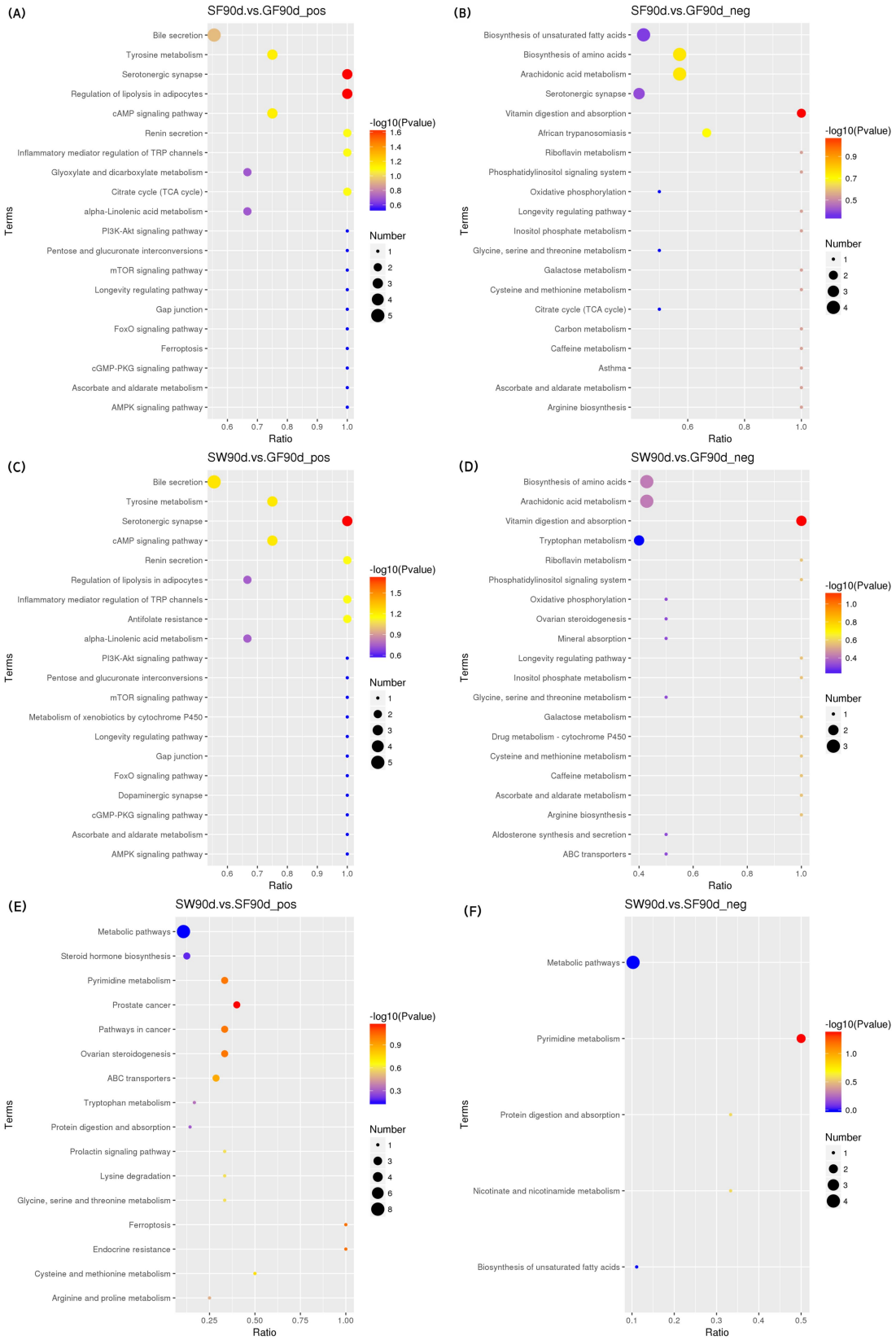


FIGURE 7
KEGG bubble diagram of the enriched pathways at 90 d relative to parturition. Yaks in the GF, SF and SW groups were free grazing on the same pasture from −30 to 90 d relative to parturition, being released to pasture at 08:00 and returning to barn at 18:00. Yaks in SF and SW groups received total mixed ration supplementation in barn during the night (18:00–08:00) from −30 to 90 d. Calves in the SW group were early weaned and separated from the dam at 60 d postpartum. (A,B) SF vs. GF in positive and negative modes at 90 d. (C,D) SW vs. GF in positive and negative modes at 90 d. (E,F) SW vs. SF in positive and negative modes at 90 d.

TABLE 8 Significantly enriched metabolic pathways and significantly different metabolites in each pathway.

| Item[a] | Mode | Metabolic pathways | Significantly different metabolites | *p*-value |
|---|---|---|---|---|
| SF15d vs. GF15d | Positive | Steroid hormone biosynthesis | Pregnenolone↓; Etiocholanolone↑; Cortodoxone↓; Corticosterone↓; Androsterone↑; Androstenedione↓; Tetrahydro corticosterone↓; Estrone↓; Progesterone↓ | 0.001 |
| | | Prolactin signaling pathway | Androstenedione↓; Estrone↓; Progesterone↓ | 0.010 |
| | | Aldosterone synthesis and secretion | Pregnenolone↓; Corticosterone↓; Progesterone↓ | 0.010 |
| | | Ovarian steroidogenesis | Pregnenolone↓; Androstenedione↓; Estrone↓; Progesterone↓ | 0.022 |
| SF30d vs. GF30d | Positive | Biosynthesis of unsaturated fatty acids | Eicosapentaenoic acid↓; Docosapentaenoic acid↓; Docosahexaenoic acid↓ | 0.025 |
| SF90d vs. GF90d | Positive | Serotonergic synapse | Serotonin↓; Prostaglandin E2↓; Prostaglandin J2↓ | 0.023 |
| | | Regulation of lipolysis in adipocytes | Corticosterone↓; Prostaglandin E2↓; Adenosine 5′-monophosphate↓ | 0.023 |
| SW90d vs. GF90d | Positive | Serotonergic synapse | Serotonin↓; Prostaglandin E2↓; Prostaglandin J2↓ | 0.018 |
| SW90d vs. SF90d | Negative | Pyrimidine metabolism | Thymidine↑; 2-Deoxyuridine↑ | 0.043 |

[a]Yaks in the GF, SF and SW groups were free grazing on the same pasture from −30 to 90 d relative to parturition, being released to pasture at 08:00 and returning to barn at 18:00. Yaks in SF and SW groups received total mixed ration supplementation in barn during the night (18:00–08:00) from −30 to 90 d. Calves in the SW group were early weaned and separated from the dam at 60 d postpartum.

stimulate INS secretion through the protein kinase a (PKA)-related signaling pathway (68), thereby regulating glucose metabolism. In fat turnover metabolism, hepatic fat is transported in the form of PC, which is then transported by VLDL (69). Finally, PC generates glycerophosphatidylcholine (GPC) by activating phospholipase A2 and lysophosphatidylcholinesterase (70). At 90 d, SW yaks exhibited higher PC and LPC levels than SF yaks. This result implies that early weaning strategy facilitated the synthesis of PC and LPC, accelerated hepatic lipid turnover metabolism, reduced hepatic lipid accumulation, and thus improved the liver health in postpartum yaks. Our observation is consistent with previous findings showing significantly increased levels of ApoB100 in SW yaks compared to SF yaks at 90 d. In this study, serum of various FAHFA levels was notably reduced in SF yaks compared to GF yaks at −15, 30, and 90 d. FAHFAs constitute a novel class of biologically active lipid molecules discovered by Yore et al. (71) through lipidomic analysis. The FAHFAs family comprises a range of fatty acids (FA) and hydroxylated fatty acids (HFA). Within this family, FAHFA with identical FA and HFA compositions can generate ester bond position isomers resulting from variations in the positions of their ester bonds (71). Previous studies (72) have reported the presence of FAHFAs in both free and bound forms within the organism, with the initial discovery of bound FAHFAs occurring in TG. The reduction in FAHFA levels may correlate with the decrease in serum TG concentration after the treatment of SF. The impact of nutritional supplementation on perinatal serum FAHFA concentrations in our research is in accordance with the results obtained by Brezinova et al. (73), showing the negative correlation between nutritional levels and FAHFAs concentrations in maternal milk. Furthermore, FAHFAs [(18:2/18:3), (14:0/6:0)] in the SW group were significantly lower than those in the SF group at 90 d. With the previous observation that the lipid mobilization products NEFA and BHBA concentrations were also significantly reduced, it is inferred that early weaning had a contributory effect on the energy balance of the periparturient yaks. Consequently, the adipose mobilization of SW yaks was relieved, with decreasing levels of FAHFAs in the serum. The metabolism of milk protein synthesis rises once cows enter lactation, during which there is a significant increase in the demand for amino acids in the milk glands (74). During lactation, phenylalanine is a potentially limiting amino acid after methionine and lysine in milk (75). The serum metabolomics analysis also revealed, in comparison with GF yaks, the DL-m-tyrosine was significantly higher in SF yaks at −15 and 30 d, suggesting that periparturient nutritional supplementation may be able to improve the periparturient transition of yaks through the modulation of the protein turnover metabolism. Previous study reported that tyrosine has a function in relieving stress and fatigue (76). Yak dams with better nutritional supplementation in late pregnancy and early lactation had a higher level of tyrosine synthesis to reduce stress around parturition.

Our results exhibited three pathways related to lipid metabolism after KEGG pathways enrichment: biosynthesis of unsaturated fatty acids, serotonergic synapse, and regulation of lipolysis in adipocytes. At 30 d, the concentrations of significantly different metabolites, eicosapentaenoic, docosapentaenoic, and docosahexaenoic acids in the serum metabolome of SF yaks were significantly lower in the unsaturated fatty acid biosynthesis pathway as compared with those of GF yaks. This result enlightened us that yaks with nutritional supplementation had down-regulation of unsaturated fatty acid biosynthesis, which may contribute to more energy available for the demand of early lactating yaks and alleviate lipid mobilization. Serotonin (5-HT) is a neurotransmitter associated with feed intake and lipid metabolism (77, 78). It is reported that the down-regulation of 5-HT synthesis decreased lipogenesis, increased brown fat thermogenesis, and reduced body fat storage (79). In addition, hepatic gluconeogenesis could be promoted by 5-HT via 5-HT 2B receptors in hepatocytes (80). At 90 d, the 5-HT content in the serotonergic synapse pathway was reduced in the SF group compared with the GF group. The perinatal yaks benefited from nutrition supplementation through higher fat utilization, instead of lipogenesis, under the regulation of decreased 5-HT, in contrast, yaks responded to conventional grazing feeding with improved hepatic gluconeogenesis, which resulted from the greater 5-HT in order to maintain blood glucose level. TG in white adipose tissue (WAT) is the main energy reserve of the organism (81). Corticosterone regulates adipocyte

lipolysis by acting on a glycoprotein-like phospholipase structural domain protein 2 (82). During energy deprivation, WAT undergoes a shift toward greater net rates of lipolysis, which can be defined as the hydrolysis of TG to generate fatty acids (FAs) and glycerol into the vasculature for utilization by other tissues as energy substrates (83). At 90 d postpartum, we observed decreased corticosterone, prostaglandin E2, and adenosine 5′-monophosphate concentrations in the regulation of lipolysis in adipocytes pathway in the SF group when compared with the GF group, corresponding to significantly lower NEFA and BHBA levels. Thus, nutrition supplementation for perinatal yaks reduced body fat mobilization by relieving NEB and down-regulating TG catabolic activity in regulating lipolysis in the adipocyte pathway (83). Overall, periparturient nutrient supplementation improved the nutritional status of yaks and consequent inhibition of lipid mobilization. The biosynthesis of unsaturated fatty acids and the regulation of lipolysis in adipocyte pathways involved in lipid metabolism were down-regulated by nutritional supply, which was also reflected in decreases of intermediate products of lipid metabolism, as well as the decreased lipolysis products NEFA and BHBA.

In the steroid hormone biosynthesis pathway, corticosterone tetrahydrocorticosterone levels were significantly reduced in SF yaks when compared to GF ones at −15 d. Based on the studies in poultry (84, 85), the decrease in corticosterone and tetrahydrocorticosterone concentrations likely indicates that periparturient stress is alleviated in yaks under nutritional supplementation. Meanwhile, the differential metabolites of androstenedione, dehydroepiandrosterone, and epitestosterone concentrations in serum hormones and hormone derivatives significantly increased in the SF group compared with the GF group at −15, 30, and 90 d. The better nutritional status of the yak dam could participate in the regulation of the immune, metabolism, and reproduction systems by stimulating the secretion of androsterone and dehydroepiandrosterone (86), reducing the deposition of lipids through the enhancement of hepatic lipid oxidation and inhibition of lipid synthesis in the liver (87, 88). Furthermore, we identified two reproductive-related metabolic pathways at −15 d, the prolactin signaling pathway and ovarian steroidogenesis, using KEGG pathway enrichment analysis. The ovarian steroidogenic pathway involves the transportation of cholesterol (CHO) to the inner mitochondrial membrane, where it is converted to pregnenolone. Pregnenolone is then transformed into progesterone, followed by conversion to 17α-hydroxy pregnenolone. This compound is further metabolized into dehydroepiandrosterone and then into androstenedione. Finally, androstenedione is converted to $E_2$ (89). PROG is involved in the prolactin signaling pathway, generating androstenedione. This conversion occurs through the action of 17α-monooxygenase and 17α-hydroxyprogesterone deacetylase. Subsequently, androstenedione is metabolized via the estrogen signaling pathway to produce $E_2$ (90, 91). SF yaks exhibited lower pregnenolone, androstenedione, estrone, and PROG concentrations in the ovarian steroidogenesis pathway, as well as significantly reduced androstenedione, estrone, and progesterone levels in the prolactin signaling pathway compared to GF yaks. Interestingly, serum biochemistry showed that the serum CHO, PROG and E2 levels increased with nutritional supplementation during the perinatal period. We speculated that improved nutritional intake in SF yaks may contribute to better maintenance of pregnancy and higher reproductive hormone levels, thus the demands of PROG and $E_2$ reduced, resulting in down-regulation of the above pathways and decreased concentrations of intermediary metabolites. From the point of view of GF yaks, serum levels of TP, TG, and the reproductive hormones PROG and $E_2$ were significantly lower, and the fat mobilization products NEFA and BHBA were significantly increased. Serum Biochemistry, reproductive hormones, and metabolomics results provided the evidence that yaks in late gestation maintain pregnancy and ensure fetal development (57), probably through up-regulating the biological process of $E_2$ and PROG production in the prolactin signaling pathway and ovarian steroidogenesis pathway and lipid mobilization for energy supply (89) when perinatal nutrition and pregnant status are poor.

## 5 Conclusion

These results demonstrated that yaks in conventional grazing system had poor recovery and adaptation to transition period because of nutrition deficiency. Perinatal nutrition supplementation contributed to body condition recovery and improved glucose and nitrogen metabolism of yaks under the regulation of increased INS, LEP, and IGF-I secretion. The lipid metabolism of periparturient yaks benefited from the nutrition supplementation, which also promoted the maintenance of pregnancy and the recovery of the reproductive system after parturition by stimulating the secretion of the reproductive hormones $E_2$ and PROG. The early weaning strategy (60 d) combined with nutritional supplementation further improved postpartum recovery and lipid metabolism adaptation to the transition period. It subsequently accelerated the reproductive cycle by enhancing the reproductive hormones FSH and LH secretion of transition yaks.

## Data availability statement

The data presented in the study are deposited in Figshare database, DOI: 10.6084/m9.figshare.27894057. https://figshare.com/s/143f6db2b15d789daea9.

## Ethics statement

The animal studies were approved by Experimental Animal Ethics Committee of the Sichuan Academy of Grassland Science Institute (Approval No. 20220012). The studies were conducted in accordance with the local legislation and institutional requirements. Written informed consent was obtained from the owners for the participation of their animals in this study.

## Author contributions

KS: Data curation, Investigation, Methodology, Software, Writing – original draft, Writing – review & editing. JG: Validation, Writing – review & editing. TA: Conceptualization, Investigation, Validation, Writing – review & editing. HZ: Formal analysis, Supervision, Validation, Writing – review & editing. QB: Validation, Visualization, Writing – review & editing. HL: Conceptualization, Methodology, Supervision, Writing – review & editing. QS: Formal analysis, Supervision, Visualization, Writing – review & editing. MJ: Project administration, Writing – review & editing. XZ: Funding acquisition,

Methodology, Project administration, Writing – review & editing. XL: Funding acquisition, Methodology, Project administration, Writing – review & editing.

## Funding

The author(s) declare that financial support was received for the research, authorship, and/or publication of this article. This study was funded by the National Key Research Project (2022YFD1302103), the Innovation Team of Forestry and Grassland Sciences in Sichuan Province, Basic Scientific Research Project in Sichuan (Evaluation on the effect of introduction of Maiwa yak and its offspring performance) and the CARS-37.

## Acknowledgments

The authors express our appreciation to the Beijing Novogene Co., Ltd. (Beijing, China) for running the metabolomic analysis and providing helpful insight and guidance for the statistical analysis.

## Conflict of interest

The authors declare that the research was conducted in the absence of any commercial or financial relationships that could be construed as a potential conflict of interest.

## Publisher's note



## Supplementary material

The Supplementary material for this article can be found online at: https://www.frontiersin.org/articles/10.3389/fvets.2024.1443856/full#supplementary-material

## References

1. Guo X, Long R, Kreuzer M, Ding L, Shang Z, Zhang Y, et al. Importance of functional ingredients in yak milk-derived food on health of Tibetan nomads living under high-altitude stress: a review. *Crit Rev Food Sci Nutr*. (2014) 54:292–302. doi: 10.1080/10408398.2011.584134

2. Ren M, Yang F, Gou JM, Wang PX, Zou M, Zhong XH, et al. First detection and molecular identification of *Entamoeba* in yaks from China. *Acta Parasitol*. (2021) 66:264–70. doi: 10.1007/s11686-020-00258-3

3. Long RJ, Zhang DG, Wang X, Hu ZZ, Dong SK. Effect of strategic feed supplementation on productive and reproductive performance in yak cows. *Prev Vet Med*. (1999) 38:195–206. doi: 10.1016/S0167-5877(98)00125-1

4. Iqbal Yatoo M, Shabir M, Kubrevi SS, Dar RA, Angmo K, Kanwar MS, et al. A study on biological rhythms of Himalayan yaks. *Biol Rhythm Res*. (2020) 51:1087–94. doi: 10.1080/09291016.2019.1579883

5. Lopreiato V, Mezzetti M, Cattaneo L, Ferronato G, Minuti A, Trevisi E. Role of nutraceuticals during the transition period of dairy cows: a review. *J Anim Sci Biotechnol*. (2020) 11:96. doi: 10.1186/s40104-020-00501-x

6. Huang B, Khan MZ, Kou X, Chen Y, Liang H, Ullah Q, et al. Enhancing metabolism and milk production performance in periparturient dairy cattle through rumen-protected methionine and choline supplementation. *Metabolites*. (2023) 13:1080. doi: 10.3390/metabo13101080

7. Zi XD. Reproduction in female yaks (*Bos grunniens*) and opportunities for improvement. *Theriogenology*. (2003) 59:1303–12. doi: 10.1016/S0093-691X(02)01172-X

8. Sharma N, Singh NK, Singh OP, Pandey V, Verma PK. Oxidative stress and antioxidant status during transition period in dairy cows. *Asian Australas J Anim Sci*. (2011) 24:479–84. doi: 10.5713/ajas.2011.10220

9. Esposito G, Irons PC, Webb EC, Chapwanya A. Interactions between negative energy balance, metabolic diseases, uterine health and immune response in transition dairy cows. *Anim Reprod Sci*. (2014) 144:60–71. doi: 10.1016/j.anireprosci.2013.11.007

10. Garverick HA, Harris MN, Vogel-Bluel R, Sampson JD, Bader J, Lamberson WR, et al. Concentrations of nonesterified fatty acids and glucose in blood of periparturient dairy cows are indicative of pregnancy success at first insemination. *J Dairy Sci*. (2013) 96:181–8. doi: 10.3168/jds.2012-5619

11. White HM. The role of TCA cycle anaplerosis in ketosis and fatty liver in periparturient dairy cows. *Animals*. (2015) 5:793–802. doi: 10.3390/ani5030384

12. Bellows RA, Short RE, Urick JJ, Pahnish OF. Effects of early weaning on postpartum reproduction of the dam and growth of calves born as multiples or singles. *J Anim Sci*. (1974) 39:589–600. doi: 10.2527/jas1974.393589x

13. Laster DB, Glimp HA, Gregory KE. Effects of early weaning on postpartum reproduction of cows. *J Anim Sci*. (1973) 36:734–40. doi: 10.2527/jas1973.364734x

14. Kenéz Á, Dänicke S, Rolle-Kampczyk U, von Bergen M, Huber K. A metabolomics approach to characterize phenotypes of metabolic transition from late pregnancy to early lactation in dairy cows. *Metabolomics*. (2016) 12:165. doi: 10.1007/s11306-016-1112-8

15. Luo ZZ, Shen LH, Jiang J, Huang YX, Bai LP, Yu SM, et al. Plasma metabolite changes in dairy cows during parturition identified using untargeted metabolomics. *J Dairy Sci*. (2019) 102:4639–50. doi: 10.3168/jds.2018-15601

16. Want EJ, Masson P, Michopoulos F, Wilson ID, Theodoridis G, Plumb RS, et al. Global metabolic profiling of animal and human tissues via UPLC-MS. *Nat Protoc*. (2013) 8:17–32. doi: 10.1038/nprot.2012.135

17. Want EJ, O'Maille G, Smith CA, Brandon TR, Uritboonthai W, Qin C, et al. Solvent-dependent metabolite distribution, clustering, and protein extraction for serum profiling with mass spectrometry. *Anal Chem*. (2006) 78:743–52. doi: 10.1021/ac051312t

18. Barri T, Dragsted LO. UPLC-ESI-QTOF/MS and multivariate data analysis for blood plasma and serum metabolomics: effect of experimental artefacts and anticoagulant. *Anal Chim Acta*. (2013) 768:118–28. doi: 10.1016/j.aca.2013.01.015

19. Wen B, Mei Z, Zeng C, Liu S. metaX: a flexible and comprehensive software for processing metabolomics data. *BMC Bioinformatics*. (2017) 18:183. doi: 10.1186/s12859-017-1579-y

20. Xiong QQ, Shen TH, Zhong L, Zhu CL, Peng XS, He XP, et al. Comprehensive metabolomic, proteomic and physiological analyses of grain yield reduction in rice under abrupt drought-flood alternation stress. *Physiol Plant*. (2019) 167:564–84. doi: 10.1111/ppl.12901

21. Heischmann S, Quinn K, Cruickshank-Quinn C, Liang LP, Reisdorph R, Reisdorph N, et al. Exploratory metabolomics profiling in the kainic acid rat model reveals depletion of 25-hydroxyvitamin D3 during epileptogenesis. *Sci Rep*. (2016) 6:31424. doi: 10.1038/srep31424

22. Haspel JA, Chettimada S, Shaik RS, Chu JH, Raby BA, Cernadas M, et al. Circadian rhythm reprogramming during lung inflammation. *Nat Commun*. (2014) 5:4753. doi: 10.1038/ncomms5753

23. Sreekumar A, Poisson LM, Rajendiran TM, Khan AP, Cao Q, Yu J, et al. Metabolomic profiles delineate potential role for sarcosine in prostate cancer progression. *Nature*. (2009) 457:910–4. doi: 10.1038/nature07762

24. Shah AM, Bano I, Qazi IH, Matra M, Wanapat M. "The yak"—a remarkable animal living in a harsh environment: an overview of its feeding, growth, production performance, and contribution to food security. *Front Vet Sci*. (2023) 10:1086985. doi: 10.3389/fvets.2023.1086985

25. Gao F, Hou XZ, Liu YC, Wu SQ, Ao CJ. Effect of maternal under-nutrition during late pregnancy on lamb birth weight. *Asian Australas J Anim Sci*. (2008) 21:371–5. doi: 10.5713/ajas.2008.70187

26. Lusby KS, Wettemann RP, Turman EJ. Effects of early weaning calves from first-calf heifers on calf and heifer performance. *J Anim Sci*. (1981) 53:1193–7. doi: 10.2527/jas1981.5351193x

27. Long NM, Vonnahme KA, Hess BW, Nathanielsz PW, Ford SP. Effects of early gestational undernutrition on fetal growth, organ development, and placentomal composition in the bovine. *J Anim Sci*. (2009) 87:1950–9. doi: 10.2527/jas.2008-1672

28. Cant JP, Trout DR, Qiao F, Purdie NG. Milk synthetic response of the bovine mammary gland to an increase in the local concentration of arterial glucose. *J Dairy Sci*. (2002) 85:494–503. doi: 10.3168/jds.S0022-0302(02)74100-3

29. Threadgold LC, Kuhn NJ. Monosaccharide transport in the mammary gland of the intact lactating rat. *Biochem J*. (1984) 218:213–9. doi: 10.1042/bj2180213

30. Stanley CC, Williams CC, Jenny BF, Fernandez JM, Bateman HG, Nipper WA, et al. Effects of feeding milk replacer once versus twice daily on glucose metabolism in Holstein and Jersey calves. *J Dairy Sci*. (2002) 85:2335–43. doi: 10.3168/jds.S0022-0302(02)74313-0

31. Luke TDW, Pryce JE, Wales WJ, Rochfort SJ. A tale of two biomarkers: untargeted $^{1}$H NMR metabolomic fingerprinting of BHBA and NEFA in early lactation dairy cows. *Metabolites*. (2020) 10:247. doi: 10.3390/metabo10060247

32. Ospina PA, Nydam DV, Stokol T, Overton TR. Evaluation of nonesterified fatty acids and beta-hydroxybutyrate in transition dairy cattle in the northeastern United States: critical thresholds for prediction of clinical diseases. *J Dairy Sci*. (2010) 93:546–54. doi: 10.3168/jds.2009-2277

33. Zhang X, Glosson KM, Bascom SS, Rowson AD, Wang Z, Drackley JK. Metabolic and blood acid-base responses to prepartum dietary cation-anion difference and calcium content in transition dairy cows. *J Dairy Sci*. (2022) 105:1199–210. doi: 10.3168/jds.2021-21191

34. Tom WA, Judy JV, Kononoff PJ, Fernando SC. Influence of empirically derived filtering parameters, ASV, and OTU pipelines on assessing rumen microbial diversity. *J Dairy Sci*. (2024). 28:S0022-0302(24)00961-5. doi: 10.3168/jds.2023-24479

35. Heeren J, Scheja L. Metabolic-associated fatty liver disease and lipoprotein metabolism. *Mol Metab*. (2021) 50:101238. doi: 10.1016/j.molmet.2021.101238

36. Segrest JP, Jones MK, De Loof H, Dashti N. Structure of apolipoprotein B-100 in low density lipoproteins. *J Lipid Res*. (2001) 42:1346–67. doi: 10.1016/S0022-2275(20)30267-4

37. Molefe K, Mwanza M. Serum biochemistry in cows of different breeds presented with reproductive conditions. *Onderstepoort J Vet Res*. (2019) 86:e1–7. doi: 10.4102/ojvr.v86i1.1742

38. Graugnard DE, Bionaz M, Trevisi E, Moyes KM, Salak-Johnson JL, Wallace RL, et al. Blood immunometabolic indices and polymorphonuclear neutrophil function in peripartum dairy cows are altered by level of dietary energy prepartum. *J Dairy Sci*. (2012) 95:1749–58. doi: 10.3168/jds.2011-4579

39. Zhang X, Liu T, Hou X, Hu C, Zhang L, Wang S, et al. Multi-channel metabolomics analysis identifies novel metabolite biomarkers for the early detection of fatty liver disease in dairy cows. *Cells*. (2022) 11:2883. doi: 10.3390/cells11182883

40. ThanThan S, Saito T, Yannaing S, Zhao H, Nakashima K, Kuwayama H. Glucagon-like peptide-1 inhibits insulinotropic effects of oxyntomodulin and glucagon in cattle. *Domest Anim Endocrinol*. (2012) 42:155–64. doi: 10.1016/j.domaniend.2011.11.004

41. Mayer JP, Zhang F, DiMarchi RD. Insulin structure and function. *Biopolymers*. (2007) 88:687–713. doi: 10.1002/bip.20734

42. Avondo M, Di Trana A, Valenti B, Criscione A, Bordonaro S, De Angelis A, et al. Leptin gene polymorphism in goats fed with diet at different energy level: effects on feed intake, milk traits, milk fatty acids composition, and metabolic state. *Animals*. (2019) 9:424. doi: 10.3390/ani9070424

43. Laron Z. IGF-1 and insulin as growth hormones. *Novartis Found Symp*. (2004) 262:56–77. doi: 10.1002/0470869976.ch5

44. Alegría KG, Gaona RC, Terranova MV, Hernández EA. Insulin resistance indexes of grazing cows and mineral or vitamin supplementation under tropical conditions. *Open Vet J*. (2021) 11:587–97. doi: 10.5455/OVJ.2021.v11.i4.8

45. Chirivi M, Rendon CJ, Myers MN, Prom CM, Roy S, Sen A, et al. Lipopolysaccharide induces lipolysis and insulin resistance in adipose tissue from dairy cows. *J Dairy Sci*. (2022) 105:842–55. doi: 10.3168/jds.2021-20855

46. Buonomo FC, Baile CA. Influence of nutritional deprivation on insulin-like growth factor I, somatotropin, and metabolic hormones in swine. *J Anim Sci*. (1991) 69:755–60. doi: 10.2527/1991.692755x

47. Thissen JP, Ketelslegers JM, Underwood LE. Nutritional regulation of the insulin-like growth factors. *Endocr Rev*. (1994) 15:80–101. doi: 10.1210/edrv-15-1-80

48. Casabiell X, Piñeiro V, Tomé MA, Peinó R, Diéguez C, Casanueva FF. Presence of leptin in colostrum and/or breast milk from lactating mothers: a potential role in the regulation of neonatal food intake. *J Clin Endocrinol Metab*. (1997) 82:4270–3. doi: 10.1210/jcem.82.12.4590

49. Nishimura TK, da Silva AG, Abitante G, Dahlen CR, Goulart RS, Zamudio GDR, et al. Effects of early weaning on the reproductive performance of suckled Nelore cows in the subsequent breeding season. *J Anim Sci*. (2023) 101:101. doi: 10.1093/jas/skad330

50. Madureira AML, Burnett TA, Borchardt S, Heuwieser W, Baes CF, Vasconcelos JLM, et al. Plasma concentrations of progesterone in the preceding estrous cycle are associated with the intensity of estrus and fertility of Holstein cows. *PLoS One*. (2021) 16:e0248453. doi: 10.1371/journal.pone.0248453

51. Sartori R, Haughian JM, Shaver RD, Rosa GJ, Wiltbank MC. Comparison of ovarian function and circulating steroids in estrous cycles of Holstein heifers and lactating cows. *J Dairy Sci*. (2004) 87:905–20. doi: 10.3168/jds.S0022-0302(04)73235-X

52. Wiltbank M, Lopez H, Sartori R, Sangsritavong S, Gümen A. Changes in reproductive physiology of lactating dairy cows due to elevated steroid metabolism. *Theriogenology*. (2006) 65:17–29. doi: 10.1016/j.theriogenology.2005.10.003

53. Hewitt SC, Carmona M, Foley KG, Donoghue LJ, Lierz SL, Winuthayanon W, et al. Peri- and postpubertal estrogen exposures of female mice optimize uterine responses later in life. *Endocrinology*. (2020) 161:bqaa081. doi: 10.1210/endocr/bqaa081

54. Vasquez YM. Estrogen-regulated transcription: mammary gland and uterus. *Steroids*. (2018) 133:82–6. doi: 10.1016/j.steroids.2017.12.014

55. Miyamoto T, Shiozawa T. Two-sided role of estrogen on endometrial carcinogenesis: stimulator or suppressor? *Gynecol Endocrinol*. (2019) 35:370–5. doi: 10.1080/09513590.2018.1549219

56. Fitzgerald HC, Dhakal P, Behura SK, Schust DJ, Spencer TE. Self-renewing endometrial epithelial organoids of the human uterus. *Proc Natl Acad Sci USA*. (2019) 116:23132–42. doi: 10.1073/pnas.1915389116

57. Constantin NT, Bercea-Strugariu CM, Bîrțoiu D, Posastiuc FP, Iordache F, Bilteanu L, et al. Predicting pregnancy outcome in dairy cows: the role of IGF-1 and progesterone. *Animals*. (2023) 13:1579. doi: 10.3390/ani13101579

58. Scaramuzzi RJ, Baird DT, Campbell BK, Driancourt MA, Dupont J, Fortune JE, et al. Regulation of folliculogenesis and the determination of ovulation rate in ruminants. *Reprod Fertil Dev*. (2011) 23:444–67. doi: 10.1071/RD09161

59. De Castro T, Ibarra D, Rodriguez M, Valdez L, Benquet N, Rubianes E. Resumption of postpartum ovarian cyclicity after different suckling manipulation treatments in primiparous beef cows. *Anim Prod Sci*. (2011) 51:111–4. doi: 10.1071/AN10108

60. Favero RJ, Faulkner DB, Nash TG, Kesler DJ. Effect of norgestomet treatment after insemination on the calving rate of postpartum suckled beef cows. *J Anim Sci*. (1995) 73:3230–4. doi: 10.2527/1995.73113230x

61. Bellot PENR, Moia MN, Reis BZ, Pedrosa LFC, Tasic L, Barbosa F, et al. Are phosphatidylcholine and lysophosphatidylcholine body levels potentially reliable biomarkers in obesity? A review of human studies. *Mol Nutr Food Res*. (2023) 67:e2200568. doi: 10.1002/mnfr.202200568

62. Xing JJ, van Heugten E, Lit DF, Touchette KJ, Coalson JA, Odgaard RL, et al. Effects of emulsification, fat encapsulation, and pelleting on weanling pig performance and nutrient digestibility. *J Anim Sci*. (2004) 82:2601–9. doi: 10.2527/2004.8292601x

63. Overton HA, Fyfe MC, Reynet C. GPR119, a novel G protein-coupled receptor target for the treatment of type 2 diabetes and obesity. *Br J Pharmacol*. (2008) 153:S76–81. doi: 10.1038/sj.bjp.0707529

64. Xu J, Zhang K, Qiu B, Liu J, Liu X, Yang S, et al. Decreased hyocholic acid and lysophosphatidylcholine induce elevated blood glucose in a transgenic porcine model of metabolic disease. *Metabolites*. (2022) 12:1164. doi: 10.3390/metabo12121164

65. Haetinger VS, Dalmoro YK, Godoy GL, Lang MB, de Souza OF, Aristimunha P, et al. Optimizing cost, growth performance, and nutrient absorption with a bio-emulsifier based on lysophospholipids for broiler chickens. *Poult Sci*. (2021) 100:101025. doi: 10.1016/j.psj.2021.101025

66. Papadopoulos GA, Poutahidis T, Chalvatzi S, Di Benedetto M, Hardas A, Tsiouris V, et al. Effects of lysolecithin supplementation in low-energy diets on growth performance, nutrient digestibility, viscosity and intestinal morphology of broilers. *Br Poult Sci*. (2018) 59:232–9. doi: 10.1080/00071668.2018.1423676

67. Boontiam W, Hyun YK, Jung B, Kim YY. Effects of lysophospholipid supplementation to reduced energy, crude protein, and amino acid diets on growth performance, nutrient digestibility, and blood profiles in broiler chickens. *Poult Sci*. (2019) 98:6693–701. doi: 10.3382/ps/pex005

68. Soga T, Ohishi T, Matsui T, Saito T, Matsumoto M, Takasaki J, et al. Lysophosphatidylcholine enhances glucose-dependent insulin secretion via an orphan G-protein-coupled receptor. *Biochem Biophys Res Commun*. (2005) 326:744–51. doi: 10.1016/j.bbrc.2004.11.120

69. Ridgway ND. The role of phosphatidylcholine and choline metabolites to cell proliferation and survival. *Crit Rev Biochem Mol Biol*. (2013) 48:20–38. doi: 10.3109/10409238.2012.735643

70. Milkevitch M, Shim H, Pilatus U, Pickup S, Wehrle JP, Samid D, et al. Increases in NMR-visible lipid and glycerophosphocholine during phenylbutyrate-induced apoptosis in human prostate cancer cells. *Biochim Biophys Acta*. (2005) 1734:1–12. doi: 10.1016/j.bbalip.2005.01.008

71. Yore MM, Syed I, Moraes-Vieira PM, Zhang T, Herman MA, Homan EA, et al. Discovery of a class of endogenous mammalian lipids with anti-diabetic and anti-inflammatory effects. *Cell*. (2014) 159:318–32. doi: 10.1016/j.cell.2014.09.035

72. McLean S, Davies NW, Nichols DS, Mcleod BJ. Triacylglycerol estolides, a new class of mammalian lipids, in the paracloacal gland of the brushtail possum (*Trichosurus vulpecula*). *Lipids*. (2015) 50:591–604. doi: 10.1007/s11745-015-4025-9

73. Brezinova M, Kuda O, Hansikova J, Rombaldova M, Balas L, Bardova K, et al. Levels of palmitic acid ester of hydroxystearic acid (PAHSA) are reduced in the breast milk of obese mothers. *Biochim Biophys Acta*. (2018) 1863:126–31. doi: 10.1016/j.bbalip.2017.11.004

74. Elsaadawy SA, Wu Z, Bu D. Feasibility of supplying ruminally protected lysine and methionine to periparturient dairy cows on the efficiency of subsequent lactation. *Front Vet Sci*. (2022) 9:892709. doi: 10.3389/fvets.2022.892709

75. Yeo JM, Knight CH, Nevison IM, Chamberlain DG. Effects of amino acid nutrition on the responses of dairy cows to milking more frequently with or without injection of growth hormone. *J Dairy Sci*. (2003) 86:2409–15. doi: 10.3168/jds.S0022-0302(03)73835-1

76. Brady K, Brown JW, Thurmond JB. Behavioral and neurochemical effects of dietary tyrosine in young and aged mice following cold-swim stress. *Pharmacol Biochem Behav*. (1980) 12:667–74. doi: 10.1016/0091-3057(80)90146-X

77. Brodie BB, Shore PA. A concept for a role of serotonin and norepinephrine as chemical mediators in the brain. *Ann N Y Acad Sci*. (1957) 66:631–42. doi: 10.1111/j.1749-6632.1957.tb40753.x

78. Engel M, Smidt MP, van Hooft JA. The serotonin 5-HT3 receptor: a novel neurodevelopmental target. *Front Cell Neurosci*. (2013) 7:76. doi: 10.3389/fncel.2013.00076

79. Oh CM, Namkung J, Go Y, Shong KE, Kim K, Kim H, et al. Regulation of systemic energy homeostasis by serotonin in adipose tissues. *Nat Commun*. (2015) 6:6794. doi: 10.1038/ncomms7794

80. Sumara G, Sumara O, Kim JK, Karsenty G. Gut-derived serotonin is a multifunctional determinant to fasting adaptation. *Cell Metab*. (2012) 16:588–600. doi: 10.1016/j.cmet.2012.09.014

81. Kalderon B, Mayorek N, Berry E, Zevit N, Bar-Tana J. Fatty acid cycling in the fasting rat. *Am J Physiol Endocrinol Metab*. (2000) 279:E221–7. doi: 10.1152/ajpendo.2000.279.1.E221

82. Widmaier EP, Margenthaler J, Sarel I. Regulation of pituitary-adrenocortical activity by free fatty acids *in vivo* and *in vitro*. *Prostaglandins Leukot Essent Fatty Acids*. (1995) 52:179–83. doi: 10.1016/0952-3278(95)90019-5

83. Duncan RE, Ahmadian M, Jaworski K, Sarkadi-Nagy E, Sul HS. Regulation of lipolysis in adipocytes. *Annu Rev Nutr*. (2007) 27:79–101. doi: 10.1146/annurev.nutr.27.061406.093734

84. Sharma D, Cornett LE, Chaturvedi CM. Corticosterone- or metapyrone-induced alterations in adrenal function and expression of the arginine vasotocin receptor VT2 in the pituitary gland of domestic fowl, *Gallus gallus*. *Gen Comp Endocrinol*. (2009) 161:208–15. doi: 10.1016/j.ygcen.2008.12.019

85. Hu Y, Sun Q, Liu J, Jia Y, Cai D, Idriss AA, et al. In ovo injection of betaine alleviates corticosterone-induced fatty liver in chickens through epigenetic modifications. *Sci Rep*. (2017) 7:40251. doi: 10.1038/srep40251

86. Frye CA. Neurosteroids' effects and mechanisms for social, cognitive, emotional, and physical functions. *Psychoneuroendocrinology*. (2009) 34:S143–61. doi: 10.1016/j.psyneuen.2009.07.005

87. Mastrocola R, Aragno M, Betteto S, Brignardello E, Catalano MG, Danni O, et al. Pro-oxidant effect of dehydroepiandrosterone in rats is mediated by PPAR activation. *Life Sci*. (2003) 73:289–99. doi: 10.1016/S0024-3205(03)00287-X

88. Tagliaferro AR, Davis JR, Truchon S, Van Hamont N. Effects of dehydroepiandrosterone acetate on metabolism, body weight and composition of male and female rats. *J Nutr*. (1986) 116:1977–83. doi: 10.1093/jn/116.10.1977

89. Drummond AE. The role of steroids in follicular growth. *Reprod Biol Endocrinol*. (2006) 4:16. doi: 10.1186/1477-7827-4-16

90. Bouilly J, Sonigo C, Auffret J, Gibori G, Binart N. Prolactin signaling mechanisms in ovary. *Mol Cell Endocrinol*. (2012) 356:80–7. doi: 10.1016/j.mce.2011.05.004

91. Grattan DR, Kokay IC. Prolactin: a pleiotropic neuroendocrine hormone. *J Neuroendocrinol*. (2008) 20:752–63. doi: 10.1111/j.1365-2826.2008.01736.x

frontiers | Frontiers in Veterinary Science

TYPE Original Research
PUBLISHED 22 January 2025
DOI 10.3389/fvets.2024.1497115



OPEN ACCESS

EDITED BY
Izhar Hyder Qazi,
South China Agricultural University, China

REVIEWED BY
Lei Deng,
Harvard Medical School, United States
Chao Xu,
Jilin Agricultural University, China

*CORRESPONDENCE
Xiaolan Feng
✉ 13896737996@163.com
Yongjiang Wu
✉ wyongjang@163.com

†These authors have contributed equally to this work

RECEIVED 16 September 2024
ACCEPTED 18 December 2024
PUBLISHED 22 January 2025

CITATION
Xie S, Yang Q, Ying Z, Cai M, Fan W, Gao H, Feng X and Wu Y (2025) Dietary supplementation with *Epimedium* contributes to the improvement of hormone levels, gut microbiota, and serum metabolite composition in the Chinese forest musk deer (*Moschus berezovskii*).
*Front. Vet. Sci.* 11:1497115.
doi: 10.3389/fvets.2024.1497115



# Dietary supplementation with *Epimedium* contributes to the improvement of hormone levels, gut microbiota, and serum metabolite composition in the Chinese forest musk deer (*Moschus berezovskii*)

Shan Xie[1,2†], Qinlin Yang[3†], Zaixiang Ying[1,2], Mingcheng Cai[1], Wenqiao Fan[1], Hanyu Gao[1,2], Xiaolan Feng[3*] and Yongjiang Wu[1*]

[1]College of Smart Agriculture, Chongqing University of Arts and Sciences, Yongchuan, China, [2]College of Biology and Food Engineering, Chongqing Three Gorges University, Wanzhou, China, [3]Chongqing Institute of Medicinal Plant Cultivation, Nanchuan, China

The Chinese forest musk deer (*Moschus berezovskii*) is a small ruminant animal with special economic value. It is listed as a National Level I key protected species in China. However, these animals are prone to stress responses in captive environments. *Epimedium*, a traditional Chinese herb with aphrodisiac and anti-stress properties, may have potential benefits for the health of the captive Chinese forest musk deer, though its efficacy requires further investigation. This study aimed to evaluate the effects of dietary supplementation with *Epimedium* on the hormone levels, gut microbiota composition, and serum metabolism of the Chinese forest musk deer. The fourteen adult male Chinese forest musk deer with similar initial body weights (7.0 $\pm$ 0.3 kg) and an average age of 4.5 years were randomly divided into two groups, each containing seven animals. The control group was fed a standard diet without *Epimedium*, while the *Epimedium* group received the standard diet supplemented with 15 g *Epimedium* /kg DM. The results indicated that the inclusion of *Epimedium* in the diet increased dry matter intake (DMI) and improved the ratio of feed to gain (F/G), with an increase in fecal testosterone levels ($p < 0.05$). 16S rDNA sequencing analysis revealed that *Epimedium* enhanced the richness and diversity of the gut microbiota in the Chinese forest musk deer, increasing the relative abundance of beneficial bacteria such as Firmicutes, while reducing the relative abundance of the potentially pathogenic Proteobacteria ($p < 0.05$). A widely targeted metabolomics analysis identified 25 differential metabolites between the two groups. Significant alterations were observed in key metabolic pathways related to lipid metabolism, hormone regulation, and antioxidation, such as ovarian steroidogenesis, tyrosine metabolism, and glycerophospholipid metabolism. Furthermore, correlation analysis between gut microbiota and serum differential metabolites showed that the relative abundances of *Clostridia_vadinBB60_group* and *UCG-010* were positively correlated with anserine and 7-ketocholesterol, respectively ($p < 0.05$). In conclusion, *Epimedium* positively influenced feed intake and hormone levels in the Chinese forest musk deer by modulating gut microbiota composition and serum metabolism.

KEYWORDS

***Epimedium*, *Moschus berezovskii*, hormone levels, gut microbiota, serum metabolism**

# 1 Introduction

The Chinese forest musk deer (*Moschus berezovskii*), also known as the dwarf musk deer, is a rare and endangered species primarily found in the mountain forests of Sichuan, Gansu, and Shaanxi provinces in China (1). This animal is highly valued for its unique musk gland, which secretes musk, a substance of significant economic and medicinal importance in fields such as medicine, perfumery, and cosmetics (2, 3). However, the artificial breeding of the Chinese forest musk deer is fraught with considerable challenges. Due to their inherently timid and solitary nature (4), it is particularly difficult to meet their growth and reproductive requirements in captive environments (5). This adversity directly compromises the health of the Chinese forest musk deer and the quality of the musk they produce (6, 7). Compared to their wild counterparts, the captive Chinese forest musk deer are more susceptible to various health issues, including diarrhea, pneumonia, and malnutrition (8, 9). Therefore, the conservation of this rare species and the enhancement of its health status are of paramount importance.

Nutritional supplementation is a critical method for improving animal health and survival capabilities (10). For wildlife, appropriate nutritional interventions can significantly enhance physiological functions and increase resistance to adverse environmental conditions. *Epimedium*, a traditional Chinese medicinal herb, is extensively utilized in traditional Chinese medicine (TCM) due to its significant bioactive properties, including anti-inflammatory, antioxidant, and hormone-regulating effects. It is particularly recognized for its potential to modulate sexual function and enhance physical strength (11–13). For the Chinese forest musk deer, hormonal levels are critical indicators of health and reproductive capacity (14). Abnormal hormonal levels can result in reproductive disorders, delayed growth and development, and other health issues (15). The primary bioactive compounds in *Epimedium*, particularly icariin, are believed to effectively promote testosterone and sperm production, thereby improving reproductive function and overall health status (16). Additionally, flavanols extracted from *Epimedium* have been shown to enhance sexual function by stimulating Leydig cells in the testes, leading to increased secretion of testosterone and other androgens (17).

The gut microbiota is an essential component of animal health, playing critical roles in nutrient absorption, immune regulation, and disease prevention (18, 19). Flavonoids and other bioactive compounds in *Epimedium* improve digestive absorption and immune status by modulating the composition and function of the gut microbiota (20). Incorporating *Epimedium* into broiler diets can modulate the abundance of beneficial bacteria, such as *Lactobacillus*, improve gut microbiota composition, and increase the concentration of metabolites like lactic acid and short-chain fatty acids, thereby enhancing metabolic function (21). *Epimedium* can also improve the health status of rats by regulating lipid metabolism, energy metabolism, and amino acid metabolism. This helps to reduce the levels of harmful metabolites in the blood while increasing the levels of beneficial metabolites (22). Additionally, the flavonoids in *Epimedium* can enhance the activity of antioxidant enzymes such as superoxide dismutase (SOD) and glutathione peroxidase (GSH-Px) (23). These enzymes play a crucial role in scavenging free radicals and protecting cells from oxidative damage. These characteristics make *Epimedium* a promising natural feed additive, suitable for use in livestock and poultry farming, offering an effective solution for improving animal health and economic efficiency.

In view of this, the present study aims to explore the potential effects of *Epimedium* as a dietary supplement on the gut microbiota composition, serum metabolic components, and hormone levels in the Chinese forest musk deer. The results could provide new scientific evidence for enhancing the health and hormonal regulation of the captive Chinese forest musk deer.

# 2 Materials and methods

## 2.1 Experimental design

The experiment was conducted at the Chinese forest musk deer breeding base of the Institute of Medicinal Plant Cultivation in Chongqing, China. The fourteen adult male Chinese forest musk deer with similar initial body weights (7.0 ± 0.3 kg) and an average age of 4.5 years were randomly divided into two groups, each containing seven animals. The CK group was fed a standard diet without the addition of *Epimedium*, while the EPI group received the standard diet supplemented with 15 g *Epimedium* /kg DM. The composition and nutritional levels of the standard feed are shown in Table 1. All the Chinese forest musk deer were housed individually, and the environmental conditions, including temperature, humidity, and management methods, were kept identical for both groups. One week before the trial, the ventilation equipment was thoroughly inspected

TABLE 1 Composition and nutrient levels of the basal diet (DM basis) %.

| Items | Content |
|---|---|
| Ingredients | |
| Leaves of *Pittosporum truncatum Pritz* | 50.00 |
| Corn | 30.00 |
| Soybean meal | 11.80 |
| wheat bran | 3.50 |
| Corn germ meal | 2.40 |
| NaCl | 0.30 |
| $CaHPO_4$ | 0.50 |
| Limestone | 0.50 |
| Premix[a] | 1.00 |
| Total | 100.00 |
| Nutrient levels | |
| Dry matter | 73.50 |
| Metabolic energy/(MJ /kg)[b] | 8.24 |
| Crude protein | 10.64 |
| Neutral detergent fiber | 30.23 |
| Acid detergent fiber | 15.26 |
| Calcium | 0.57 |
| Phosphorus | 0.31 |

[a]The premix provided the following per kg of the diet: VA 7000 IU, VD 1800 IU, VE 40 IU, Cu 12 mg, Fe 60 mg, Mn 50 mg, Zn 40 mg, I 1.0 mg, Se 0.27 mg, Co 0.3 mg.
[b]Metabolic energy is the calculated value, while the rest are measured values.

to ensure proper functioning, and the pens were meticulously cleaned and disinfected. Daily management during the trial period was conducted according to the protocol, with feeding scheduled at 3:00 PM each day. The pre-trial period lasted 7 d, followed by a formal trial period of 30 d.

## 2.2 Sample collection

During the trial period, the remaining feed was weighed daily using an electronic scale before feeding to calculate the dry matter intake (DMI). Given that the Chinese forest musk deer are classified as a national first-grade protected animal in China, they are highly sensitive to external environments and prone to stress reactions, which can even lead to death. Growth performance and serum metabolomics analyses require direct manipulation of the animals, including procedures such as weighing and blood collection, which can induce stress in the Chinese forest musk deer. Therefore, in this experiment, we selected only the three Chinese forest musk deer per group for these operations to minimize potential impacts on other individuals and ensure the smooth progression and safety of the experiment. On days 1 and 30 of the trial, the three randomly selected Chinese forest musk deer from each group were weighed after a 12 h fasting period to determine the average daily gain (ADG). On the final day of the trial, the three Chinese forest musk deer from each group were randomly selected for blood collection. The blood samples were placed in coagulation-promoting tubes and centrifuged at 3000 rpm for 10 min at 4°C to collect the serum. All serum samples were stored at −80°C for subsequent analysis. On the same day, fresh fecal samples were collected from all the 14 Chinese forest musk deer, placed in sterile centrifuge tubes, and rapidly frozen in liquid nitrogen. These samples were then stored at −80°C for 16S rDNA sequencing of the gut microbiome.

## 2.3 Fecal hormone level analysis

The levels of testosterone, estradiol, and progesterone in the fecal were measured using enzyme-linked immunosorbent assay (ELISA) kits. These kits were purchased from Quanzhou Ruixin Biotechnology Co., Ltd.

## 2.4 Fecal microbiota profiling

The total DNA of fecal bacteria was extracted using the E.Z.N.A. Soil DNA Kit (Omega Bio-tek, Inc., United States). Concentration and quality of the genomic DNA were checked by NanoDrop 2000 spectrophotometer (Thermo Scientific Inc., United States). The V3–V4 regions of the bacterial 16S rDNA gene were amplified using universal primers 338F (5'-ACTCCTACGGGA-GGCAGCAG-3′) and 806R (5'-GGACTACHVGGGTWTCTAAT-3′). The universal primers with barcode sequences were synthesized and the amplification was carried out on an ABI 9700 PCR instrument (Applied Biosystems, Inc., United States). After purifying the PCR amplification products, the concentration was measured, and high-throughput sequencing was performed on the Illumina Novaseq sequencing platform.

Sequencing data were processed using Pear software (24) (version 0.9.6) for sequence assembly, filtering, and chimera removal, resulting in optimized sequences. High-quality sequences were clustered into OTUs using Vsearch software (25) (version 2.7.1) with a sequence similarity threshold of 99%. Species classification for each OTU was determined by aligning the sequences with the Silva138 database (26) using the BLAST algorithm (27). Alpha and Beta diversity analyses were performed based on OTU and abundance data using QIIME2 software (28) (version 2024.2). Species composition bar plots were generated using R project (29) (version 3.6.0) based on species annotation and relative abundance results. LEfSe analysis was conducted using Python software (version 2.7) (30). The sequencing was conducted at Beijing Allwegene Technology Co., Ltd.

## 2.5 Determination of serum metabolites

The sample stored at −80°C refrigerator was thawed on ice and vortexed for 10 s. 50 μL of serum sample and 300 μL of extraction solution (ACN: Methanol = 1:4, V/V) containing internal standards were added into a 2 mL microcentrifuge tube. The sample was vortexed for 3 min and then centrifuged at 12000 rpm for 10 min (4°C). 200 μL of the supernatant was collected and placed in −20°C for 30 min, and then centrifuged at 12000 rpm for 3 min (4°C). A 180 μL aliquots of supernatant were transferred for LC–MS analysis. The relative concentrations of serum metabolites were analyzed using an LC-ESI-MS/MS system (UPLC, ExionLC AD, https://sciex.com.cn/; MS, QTRAP® System, https://sciex.com/). After the analysis, the raw data obtained were imported into Progenesis QI software (31) (version 3.0) for data preprocessing, which was used for subsequent analysis.

Metabolite information was obtained by annotating the database using HMDB[1] and Metlin.[2] Partial least squares discriminant analysis (PLS-DA) was performed using R project. For two-group analysis, differential metabolites were determined by Variable Importance in Projection (VIP > 1) and *p*-value (*p*-value <0.05, *t*-test). Identified metabolites were annotated using the KEGG Compound database[3], and the annotated metabolites were then mapped to the KEGG Pathway database.[4] The analysis was conducted at Beijing Allwegene Technology Co., Ltd.

## 2.6 Correlation analysis between rumen microbiota and serum metabolite profiles

Correlation analysis was performed between differential microbiota and metabolites. The spearman correlation coefficients between microbiome and metabolite data were calculated using the psych package in the R project. Correlation heatmaps were generated using the heatmap package.

1 https://hmdb.ca/
2 https://metlin.scripps.edu/
3 http://www.kegg.jp/kegg/compound/
4 http://www.kegg.jp/kegg/pathway.html

TABLE 2 Growth performance of the Chinese forest musk deer.

| Item | CK | EPI | *p*-value |
|---|---|---|---|
| Initial BW, kg | 6.91 ± 0.24 | 7.31 ± 0.53 | 0.685 |
| Final BW, kg | 7.15 ± 0.18 | 7.91 ± 0.29 | 0.089 |
| ADG, kg | 0.09 ± 0.06 | 0.02 ± 0.01 | 0.090 |
| DMI, g/d | 99.48 ± 3.13 | 110.55 ± 2.86 | 0.012 |
| F/G | 1.70 ± 0.26 | 0.74 ± 0.05 | 0.024 |

DMI, dry matter intake; Initial BW, initial body weight; Final BW, final body weight; ADG, average daily gain; F/G, the ratio of feed to gain; EPI, *Epimedium* group; CK, control group; The statistical results are shown as means ± SEM.

TABLE 3 Fecal hormone levels in the Chinese forest musk deer.

| Item | CK | EPI | *p*-value |
|---|---|---|---|
| Progesterone, ng/mL | 5.37 ± 0.30 | 6.29 ± 0.16 | 0.055 |
| Estradiol, pg./g | 892.51.68 ± 51.04 | 1012.16 ± 58.95 | 0.200 |
| Testosterone, ng/g | 2.57 ± 0.29 | 3.68 ± 0.21 | 0.037 |

EPI, *Epimedium* group; CK, control group; The statistical results are shown as means ± SEM.

## 2.7 Statistical analysis

All data were analyzed using independent sample *t*-tests, and the results are presented as mean ± standard error of the mean (SEM). Experimental data with $p < 0.05$ were considered statistically significant.

# 3 Results

## 3.1 The effects of *Epimedium* on growth performance and hormone levels in the Chinese forest musk deer

As shown in Table 2, compared to the CK group, the final BW and ADG tended to increase in the EPI group ($p < 0.1$). The DMI and F/G in the EPI group were higher than those in the CK group ($p < 0.05$), indicating that dietary supplementation with *Epimedium* significantly increased the feed intake and feed conversion ratio in the Chinese forest musk deer. As shown in Table 3, *Epimedium* supplementation increased fecal testosterone levels in the Chinese forest musk deer ($p < 0.05$). Compared to the CK group, the progesterone levels in the fecal samples of the EPI group showed a trend towards increase ($p < 0.1$). Although there were slight increases in estradiol levels, these changes were not statistically significant. This suggests that *Epimedium* can effectively regulate hormone levels in the Chinese forest musk deer.

## 3.2 Gut microbiome 16S rDNA sequencing analysis

### 3.2.1 The effects of *Epimedium* on the abundance and diversity of gut microbiota

As shown in Figure 1A, the EPI group had 1,124 unique operational taxonomic units (OTUs), while the CK group had 908 unique OTUs. Both groups shared 2,919 OTUs. The alpha diversity indices of 14 samples were calculated using the QIIME2 software (Supplementary Table S1). Compared to the CK group, the Chao1 and Observed species indices of the EPI group were slightly higher, but the differences were not statistically significant (Figures 1C,D). Additionally, the Shannon index in the EPI group showed a trend towards increased values, although the change in the PD_whole_tree index was not significant (Figures 1E,F). Beta diversity analysis revealed that the samples from the CK and EPI groups tended to cluster internally, with distinct separation between the groups, indicating significant differences in the gut microbiota composition between the two groups (Figure 1B).

### 3.2.2 The effects of *Epimedium* on the gut microbiota composition

A total of 21 phylum, 33 class, 68 order, 117 family, and 258 genus were identified across both groups. As shown in Figure 2A, at the phylum level, the gut microbiota of the Chinese forest musk deer was primarily composed of Bacteroidetes, Firmicutes, and Proteobacteria, with Firmicutes being the dominant phylum. After dietary supplementation with *Epimedium*, the relative abundance of Firmicutes in the EPI group was higher compared to that in the control group, while the relative abundance of Proteobacteria was lower in the EPI group than in the control group ($p < 0.05$). Notably, Firmicutes are considered beneficial bacteria, whereas Proteobacteria are viewed as potential pathogens, indicating that *Epimedium* supplementation may have improved the gut microbiota composition of the Chinese forest musk deer. At the genus level, the relative abundance of *Ruminobacter* and *UCG-005* decreased, while the relative abundance of the beneficial genus *Bacteroides* increased in the EPI group compared to the CK group (Figure 2B).

### 3.2.3 Gut microbiota differential species analysis

Linear discriminant analysis Effect Size (LEfSe) analysis revealed significantly dominant species in both groups. As shown in Figure 3A, 8 clades were found to have higher abundances in the CK group, while 12 clades were more abundant in the EPI group. The differences in the abundances of various microbial taxa between the CK and EPI groups are depicted in Figure 3B. In the CK group, the most significant difference was observed for the genus *Succinivibrio*, whereas in the EPI group, the classes *Clostridia* and Firmicutes, as well as the order *Oscillospirales*, exhibited notable differences. Among these, *Clostridia* and Firmicutes showed the greatest intergroup differences, with LDA scores greater than 4. Firmicutes is a critical component of the normal gut microbiota, playing a significant role in maintaining intestinal health and helping to prevent diarrhea and other gastrointestinal diseases.

### 3.2.4 Prediction of gut microbial functions

Prediction of the metabolic functions of the gut microbiota revealed a relatively high abundance of functional genes associated with thiamine metabolism, nicotinate and nicotinamide metabolism, amino sugar and nucleotide sugar metabolism, and RNA polymerase (Figure 4). Differential analysis using a *t*-test identified 12 pathways with significant differences in related genes between the two groups. Compared to the CK group, the EPI group exhibited enhanced pathways in gut microbiota, including ubiquinone and other terpenoid-quinone biosynthesis, glutathione metabolism, and nicotinate and nicotinamide metabolism ($p < 0.05$). Conversely, pathways such as thiamine metabolism, starch and sucrose metabolism, and methane metabolism were significantly reduced in the EPI group ($p < 0.05$). The functional gene classification of the gut microbiota primarily involved energy metabolism, antioxidant protection, and DNA repair.

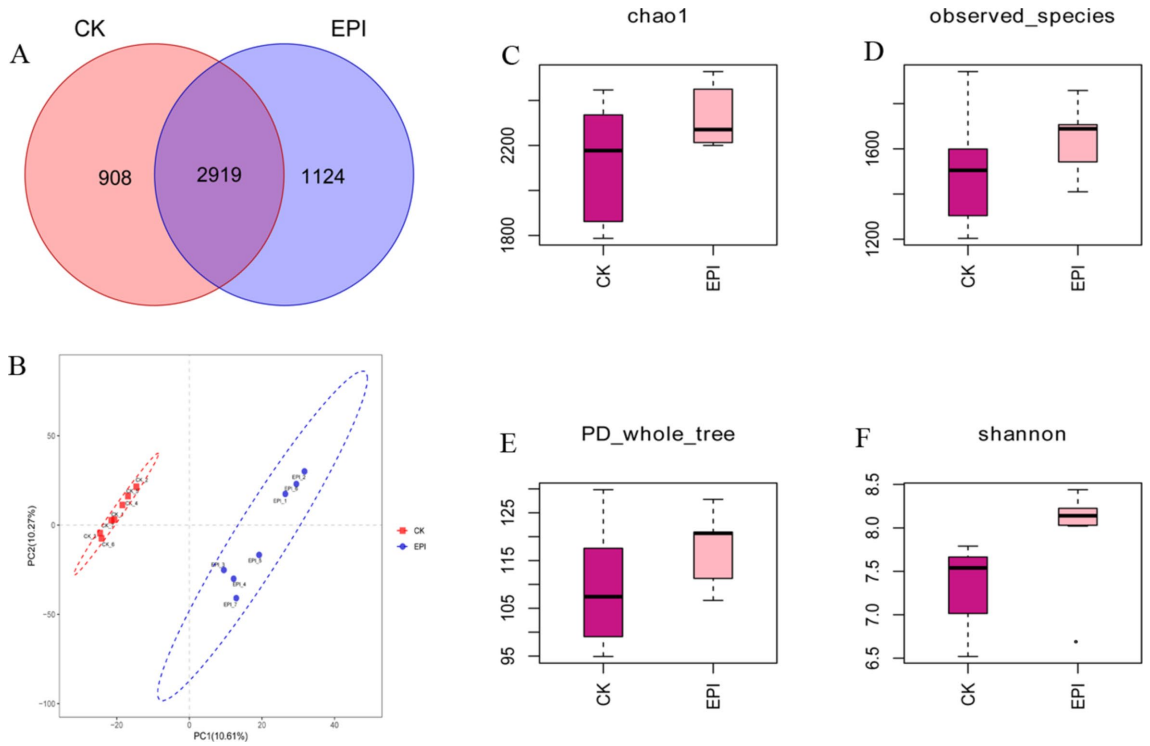


FIGURE 1
Comparison of gut microbial diversity between the two groups. The Venn diagram shows the number of shared or unique OTUs **(A)**. PLS-DA analysis based on OTUs **(B)**. Box plot of Chao1 index **(C)**. Box plot of observed species index **(D)**. Box plot of PD_whole_tree index **(E)**. Box plot of Shannon index **(F)**. EPI, *Epimedium* group; CK, control group.

## 3.3 Serum widely targeted metabolomics analysis

### 3.3.1 Serum metabolite multivariate statistical analysis

As shown in Figure 5A, there is a clear separation of metabolites between the two experimental groups, with a well-defined clustering pattern, indicating significant differences between the metabolites of the EPI group and those of the CK group. To assess the presence of overfitting in the PLS-DA model, permutation tests were conducted for statistical validation of the PLS-DA model. $R^2Y$ and $Q^2$ represent the explanatory and predictive abilities within the PLS-DA model, respectively, with values closer to 1 indicating greater stability and reliability of the model. With $R^2Y = 0.998$ and $Q^2 = 0.632$, the model demonstrates good predictive ability and reliable results (Figure 5B).

### 3.3.2 Serum differential metabolites

Through a combination of univariate statistical analysis and multivariate statistical analysis methods, we screened for differential metabolites between the groups. The screening criteria used were a $p$-value $<0.05$ & VIP $\geq 1$. The results of the screening were visualized in a volcano plot, revealing a total of 25 differential metabolites, with 11 metabolites being upregulated and 14 metabolites being downregulated (Figure 6A). In addition, hierarchical clustering analysis of the differential metabolites showed that the serum differential metabolites were distinct between the groups, as shown in Figure 6B. Red indicates an increase in the relative content of substances, while green indicates a decrease in the relative content of substances. The intra-group clustering of the CK group and the EPI group was ideal. Compared with the CK group, the expression levels of anserine, 2-hydroxy estrone, and estrone were upregulated in the EPI group, while the expression levels of nicotinamide-n-oxide, asn-met, and salidroside were downregulated (Table 4). Dietary supplementation with *Epimedium* led to significant changes in the serum metabolism of the Chinese forest musk deer.

### 3.3.3 Serum metabolic pathways

Based on the differential metabolites identified, KEGG pathway enrichment analysis was performed, and the enriched pathways were visually represented in bar charts and bubble plots. The pathways with significantly different metabolisms were selected based on the significance index $p$-value. The KEGG results showed that the differential metabolites between the CK and EPI groups were annotated into five categories of metabolic pathways, with metabolic pathways and glycerophospholipid metabolism being the most significantly enriched (Figure 7A). Additionally, KEGG pathway enrichment analysis indicated that the major metabolic pathways altered in the EPI group compared to the CK group included glycerophospholipid metabolism, tyrosine metabolism, nicotinate and nicotinamide metabolism, ovarian steroidogenesis, and beta-alanine metabolism (Figure 7B). Among these, glycerophospholipid metabolism and tyrosine metabolism were the most significantly altered pathways, suggesting that the supplementation of *Epimedium* might have had a notable impact on metabolic pathways related to lipid metabolism and hormone regulation.

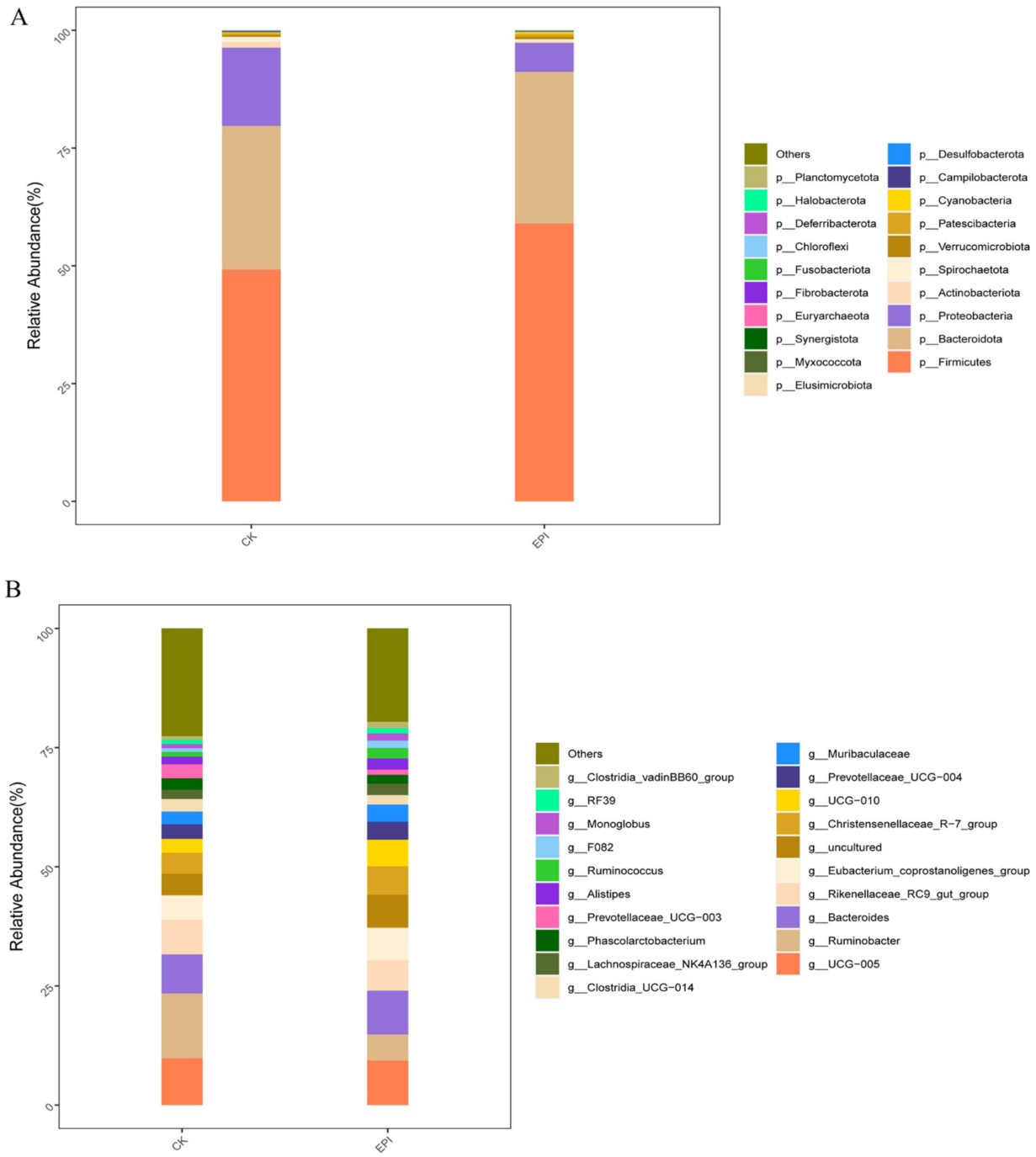


FIGURE 2
Effects of *Epimedium* on gut microbial community. Phylum–level **(A)**. Genus–level **(B)**. EPI, *Epimedium* group; CK, control group.

## 3.4 Correlation analysis for differential microbes and metabolites

Through Pearson correlation analysis, it was found that there was a correlation between differential metabolites and differential bacterial genera. As shown in Figure 8, the *Clostridia_vadinBB60_group* exhibits a positive correlation with anserine and N(alpha)-acetyl-epsilon-(2-propenal) lysine, and a negative correlation with N-acetyl-L-leucine and N-methyl-2-pyridone-5-carboxamide ($p < 0.05$). Similarly, *UCG-010* shows a positive correlation with 7-ketocholesterol and ethyl-dodecanoate, while displaying a negative correlation with N6, N6, N6-trimethyl-l-lysine ($p < 0.05$).

# 4 Discussion

*Epimedium* possesses various bioactive properties, and its appropriate supplementation as a feed additive can effectively enhance feed utilization rates in animals, thereby significantly improving economic benefits (32). In this study, compared to the CK group,

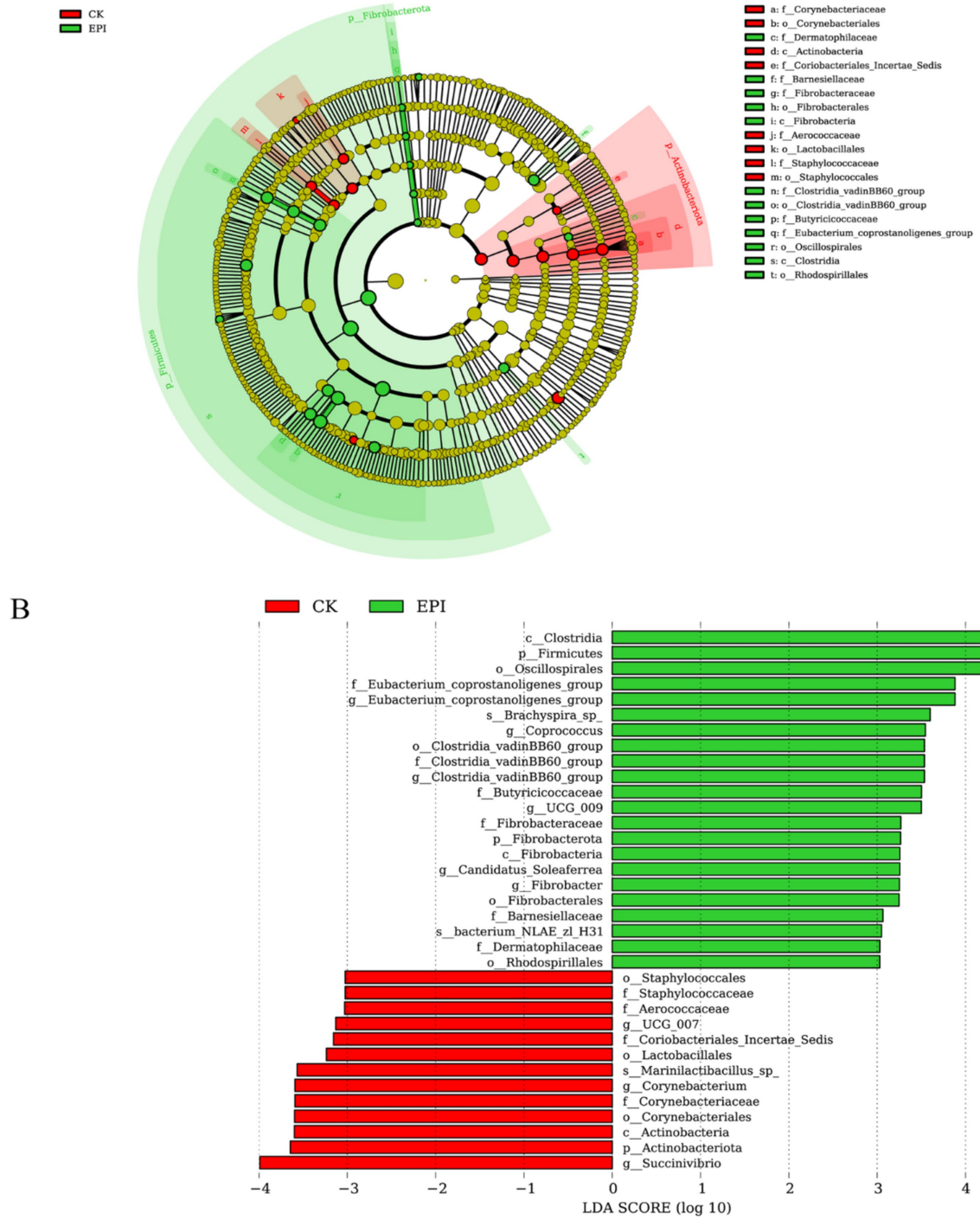


FIGURE 3
LEfSe cladogram comparing microbial communities between two groups **(A)**. The red represents CK, and the green represents EPI. Significantly different bacterial taxa identified by the linear discriminant analysis effect size **(B)**. Bacteria with an LDA score > 3 are considered to be significantly discriminative. The red represents CK, and the green represents EPI. CK, control group; EPI, *Epimedium* group.

dietary supplementation with *Epimedium* increased feed intake and feed conversion ratio in the experimental group, with a trend towards increased ADG. Zhang et al. (21) found that adding *Epimedium* to the diet improved intestinal function and gut microbiota in broilers, significantly increasing ADG and enhancing growth performance. This effect is attributed to the flavonoids in *Epimedium*, which can promote the secretion of digestive enzymes, enhancing the digestion and absorption of nutrients in the feed, thereby improving feed efficiency and promoting animal growth (33, 34). *Epimedium* leaves can enhance testosterone production in rat Leydig cells by regulating

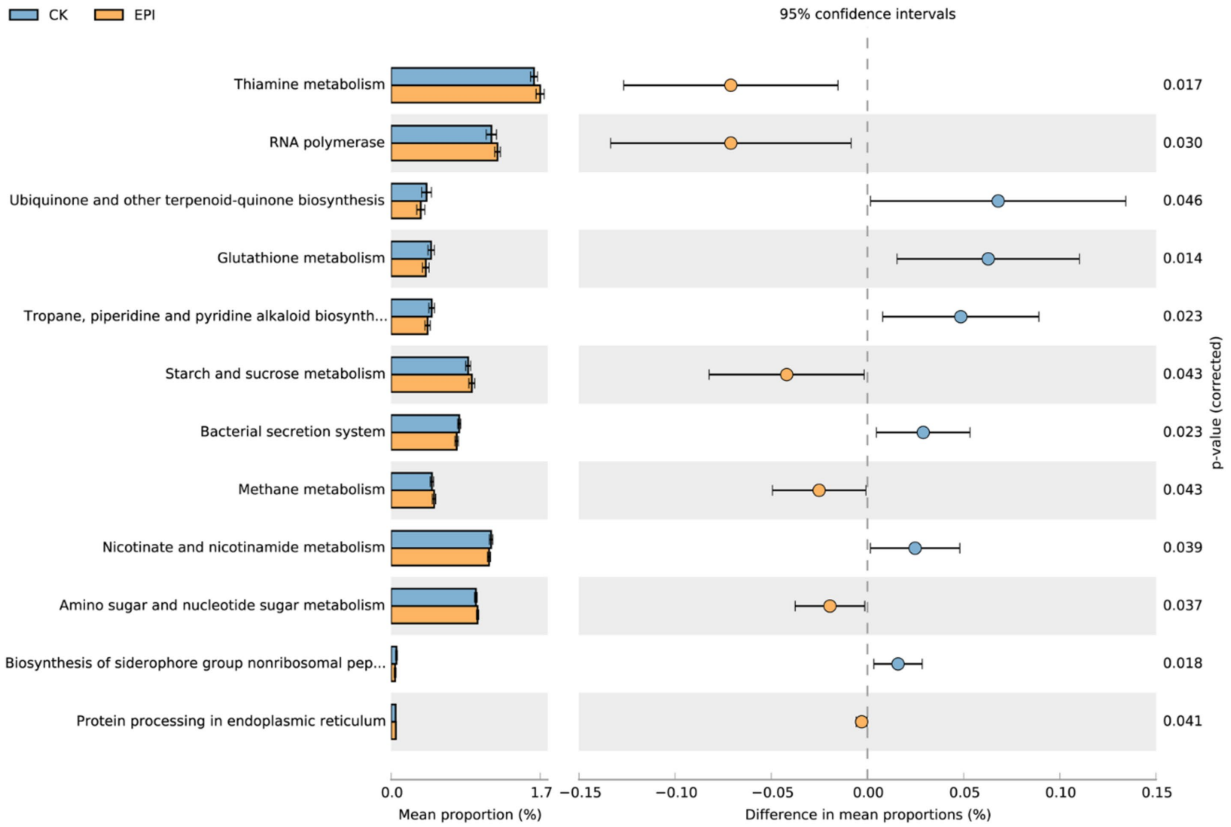


FIGURE 4
Microbial functional analysis. The blue represents CK, and the yellow represents EPI. CK, control group; EPI, *Epimedium* group.

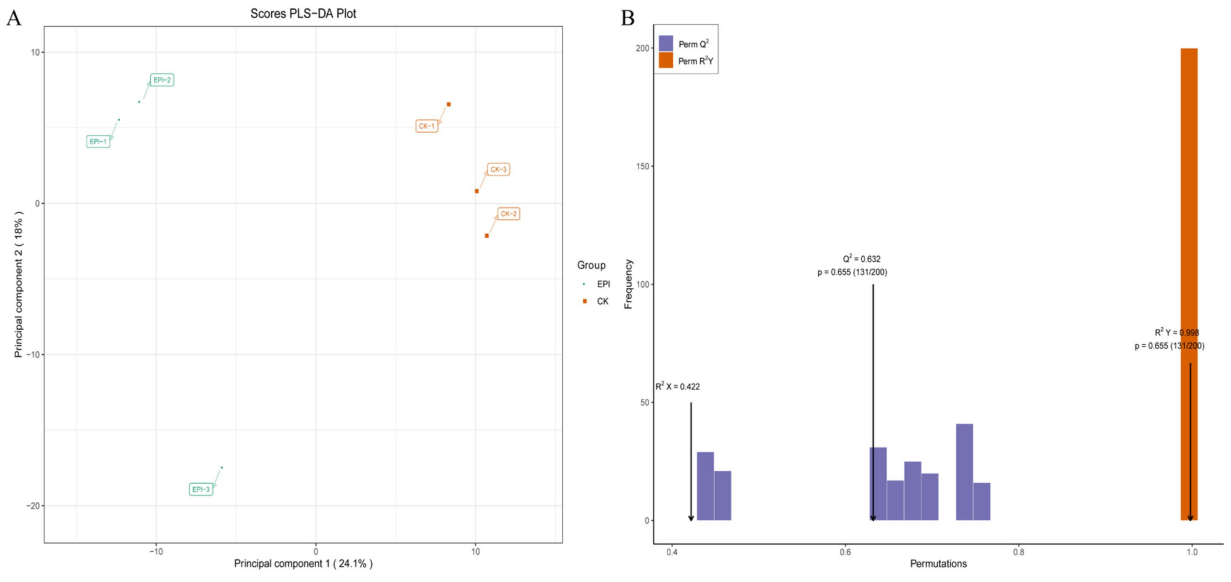


FIGURE 5
PLS-DA score plot for the CK and EPI groups **(A)**. The yellow represents CK, and the green represents EPI. PLS-DA model validation plot **(B)**. CK, control group; EPI, *Epimedium* group.

the expression of steroidogenic enzymes (35). Research has shown that polyphenolic compounds in *Epimedium* significantly elevate levels of reproductive hormones such as testosterone and luteinizing hormone in albino rats, while significantly reducing levels of progesterone and estradiol (36). However, in our study, we found that adding *Epimedium* to the diet increased fecal testosterone levels, but

10.3389/fvets.2024.1497115

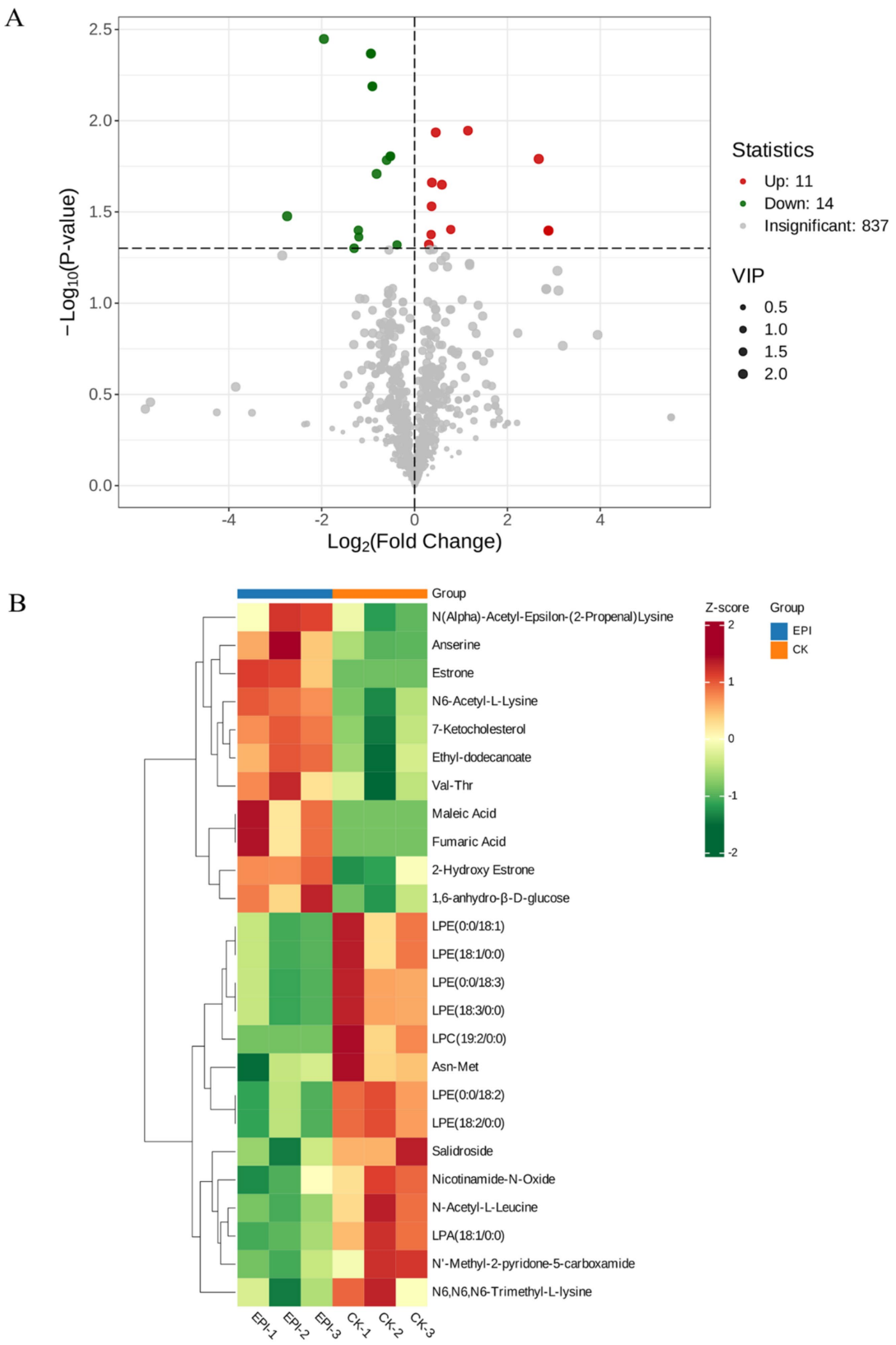


FIGURE 6
Volcano plot of intergroup differential metabolites **(A)**. The red represents significantly upregulated metabolites, green represents significantly downregulated metabolites, and gray represents non-significantly changed metabolites. The size of the dots represents the VIP value. Heatmap of clustering analysis of gut differential metabolites **(B)**. The color blocks at different positions represent the relative expression levels of the corresponding metabolites at those locations. CK, control group; EPI, *Epimedium* group.

TABLE 4 Partial information on differential metabolites.

| Name | Vip | *p*-value | Up/Down | Cas |
|---|---|---|---|---|
| Ethyl-dodecanoate | 1.91 | 0.029 | Up | 106-33-2 |
| N6, N6, N6-Trimethyl-L-lysine | 1.71 | 0.048 | Down | – |
| 7-Ketocholesterol | 2.01 | 0.022 | Up | 566-28-9 |
| Nicotinamide-N-Oxide | 1.80 | 0.039 | Down | 1986-81-8 |
| Anserine | 2.02 | 0.022 | Up | 584-85-0 |
| 2-Hydroxy Estrone | 1.92 | 0.047 | Up | 362-06-1 |
| N(Alpha)-Acetyl-Epsilon-(2-Propenal) Lysine | 1.77 | 0.042 | Up | 99124-74-0 |
| Asn-Met | 1.65 | 0.043 | Down | – |
| Salidroside | 1.89 | 0.016 | Down | 10338-51-9 |
| Estrone | 2.16 | 0.016 | Up | 53-16-7 |

Vip, variable importance in projection; Up/Down, levels of metabolites adjusted upward/downward; Cas, Chemical Abstracts Service.

had no effect on progesterone and estradiol levels. This may be due to the unique digestive system and physiological characteristics of musk deer, which make their metabolic mechanisms significantly different from those of mice. Additionally, the experimental conditions in our study (such as housing environment, diet, sample processing, etc.) may differ from those in mouse experiments. These differences in conditions may have affected the measurement of progesterone levels. These findings suggest that *Epimedium* has a positive impact on increasing feed intake and regulating hormone levels in the Chinese forest musk deer, thereby effectively maintaining overall health. The yield of musk is closely related to fluctuations in hormone levels (14). Studies have indicated that quercetin can promote musk secretion by regulating the hormone production (such as testosterone and estradiol) in the Chinese forest musk deer (37). Additionally, administering exogenous testosterone during the non-secretory season can also promote musk secretion in the Chinese forest musk deer (38, 39). In this study, the level of testosterone increased after the addition of *Epimedium*, hypothesizing that *Epimedium* may increase musk yield by influencing hormone levels. Future studies should consider to provide a more comprehensive assessment of the benefits of *Epimedium* supplementation in the Chinese forest musk deer.

The diversity of gut microbiota is associated with the host's health status, and *Epimedium* can effectively improve animal health by modulating the composition of the gut microbiota (40). In this study, after adding *Epimedium* to the Chinese forest musk deer diet, the Chao1 index, observed species index, and Shannon index in the EPI group were all higher than in the CK group, but these differences did not reach statistical significance. This may indicate that the addition of *Epimedium* has a positive effect on the richness and diversity of the Chinese forest musk deer gut microbiota, but this effect was not detected significantly due to the limited sample size or experimental conditions. According to the annotation results, the main bacterial phyla in the gut of the Chinese forest musk deer are Bacteroidetes, Firmicutes, and Proteobacteria, with Firmicutes being the dominant phylum, which is consistent with previous research findings (41, 42). Firmicutes is one of the main microbiota in the gut of ruminants, capable of producing short-chain fatty acids (SCFAs) such as acetic acid, propionic acid, and butyric acid through fermentation (43). These SCFAs play a crucial role in maintaining gut health and amino acid metabolism. Additionally, ecological biotherapy strategies enriched with Firmicutes can be used to prevent or treat colitis, demonstrating potential anti-inflammatory properties (44). In contrast, Proteobacteria are considered potentially harmful microbiota, as their increased relative abundance is associated with various gut diseases and inflammatory bowel diseases (45). They are present in lower amounts in the gut of healthy animals (46). Abnormal growth of Proteobacteria may represent an imbalance in the gut microbiota and could serve as a potential marker for disease risk (47). After adding *Epimedium* to the Chinese forest musk deer diet, the relative abundance of Firmicutes in the EPI group was higher than in the control group, while the relative abundance of Proteobacteria was lower. This indicates that *Epimedium* has a positive effect on regulating the composition of the musk deer gut microbiota. At the genus level, the dominant microbiota in the gut is *Bacteroides*. We found that the relative abundance of *Bacteroides* in the EPI group was higher than that in the CK group. Studies have demonstrated that an increase in the abundance of *Bacteroides* species can reduce lipopolysaccharide (LPS) levels and inhibit immune responses, thereby preventing the onset of cardiovascular diseases in humans (48). *Bacteroides* can effectively degrade polysaccharides, providing essential nutrients for other gut microbiota, which promotes symbiotic relationships and synergistic interactions among gut microbiota (49). In conclusion, we hypothesize that *Epimedium* has potential benefits in regulating the gut microbiota of the Chinese forest musk deer by increasing the abundance of beneficial bacteria and reducing the abundance of harmful bacteria, thereby maintaining the stability of the gut microbiome composition. Although we minimized the impact of parasites on the gut microbiota of the Chinese forest musk deer through regular health checks and preventive treatment with anti-parasitic drugs, recent studies have shown that parasitic infections can affect the composition and function of the gut microbiota (50). These findings suggest that future research should further investigate the interaction between parasitic infections and the gut microbiota to achieve a more comprehensive understanding of the various factors influencing the health of the Chinese forest musk deer.

In this study, the overall composition of serum metabolites showed differences. A total of 25 differential metabolites were detected in the serum. We found that dietary supplementation with *Epimedium* may impact metabolic pathways involved in lipid metabolism, antioxidation, and hormone regulation. *Epimedium* is believed to help increase sex hormone levels and effectively improve sexual function (51). Fluctuations in sex hormone levels can affect the estrous cycle and reproductive capacity of animals (52). Estrone may indirectly influence the behavior of the male Chinese forest musk deer during

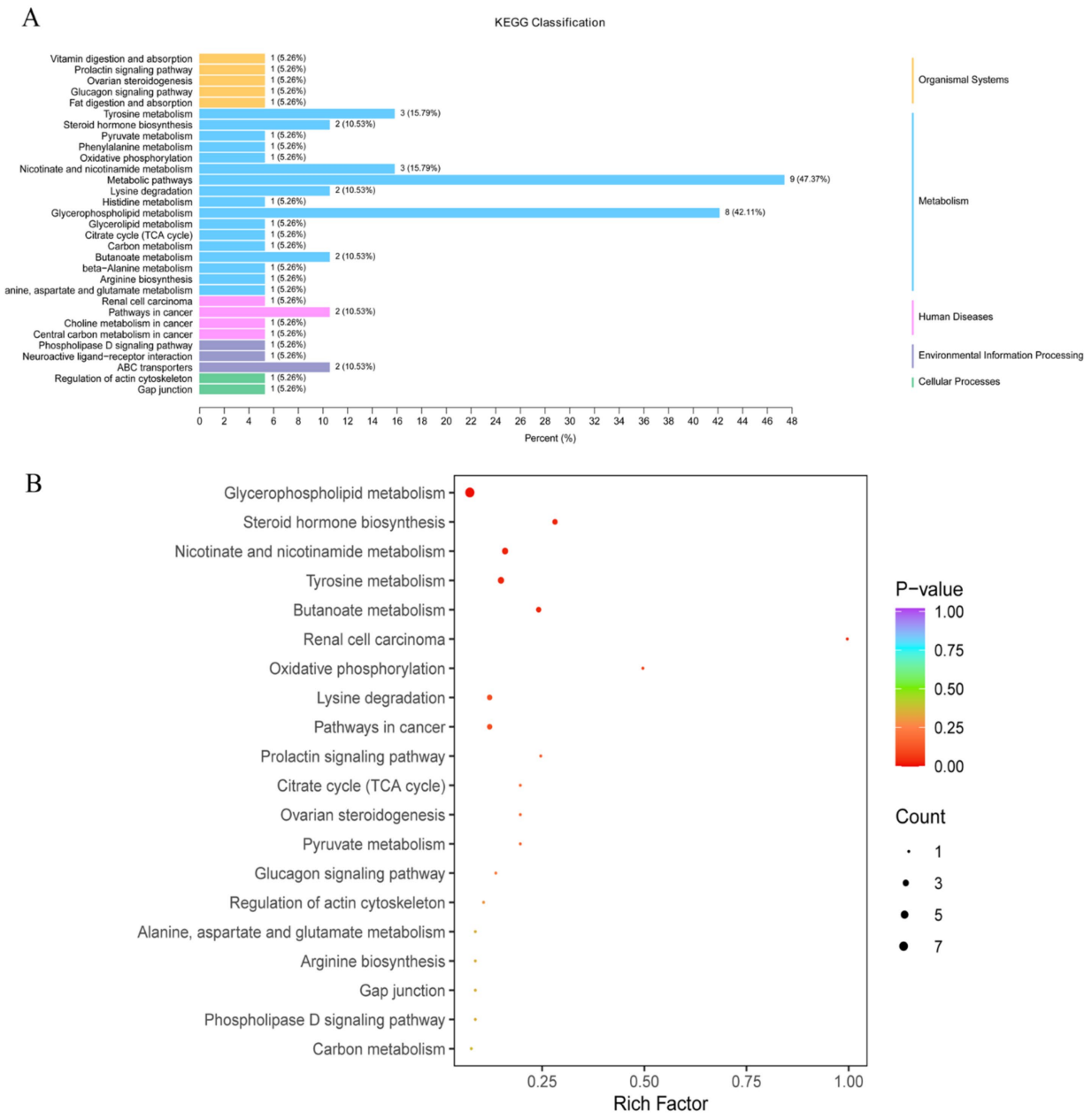


FIGURE 7
Differential metabolite pathway classification diagram **(A)**. The color represents the *p*-value of the enrichment analysis, with a deeper red color indicating a more significant degree of enrichment. Enrichment plot of differential metabolite pathways **(B)**. The color of the bubble represents the *p*-value of the enrichment analysis, with a deeper red color indicating a more significant degree of enrichment. The size of the dots represents the number of differential metabolites enriched in that pathway. CK, control group; EPI, *Epimedium* group.

the breeding season, promoting musk secretion (53). Additionally, sex hormones such as testosterone, estrogen, and cortisol play a significant role in determining the composition of musk (39). In this experiment, compared to the CK group, the levels of estrone and 2-hydroxy estrone in the EPI group increased, which positively impacted the ovarian steroidogenesis and prolactin signaling pathways. Anserine, a natural compound found in animal tissues, has been shown to effectively reduce oxidative stress-induced damage by regulating antioxidant-related signaling pathways such as Keap1-Nrf2 and JNK-Caspase-3, thereby exerting antioxidant effects (54, 55). Chen et al. (56) found that anserine can increase the activity of serum superoxide dismutase and reduce levels of malondialdehyde, alkaline phosphatase, and alanine aminotransferase, thereby alleviating hyperuricemia in rats. In this experiment, anserine levels increased and were enriched in histidine metabolism and beta-alanine metabolism pathways. Histidine metabolism, a critical amino acid metabolic process, plays a vital role in protein synthesis, neurotransmitter function, and the immune system, and has a positive impact on appetite regulation (57, 58). *β*-Alanine can combine with L-histidine to form carnosine, a compound with antioxidant properties that can neutralize free radicals and reduce oxidative stress-induced damage to muscle cells (59, 60). Glycerophospholipid metabolism involves various enzymes and

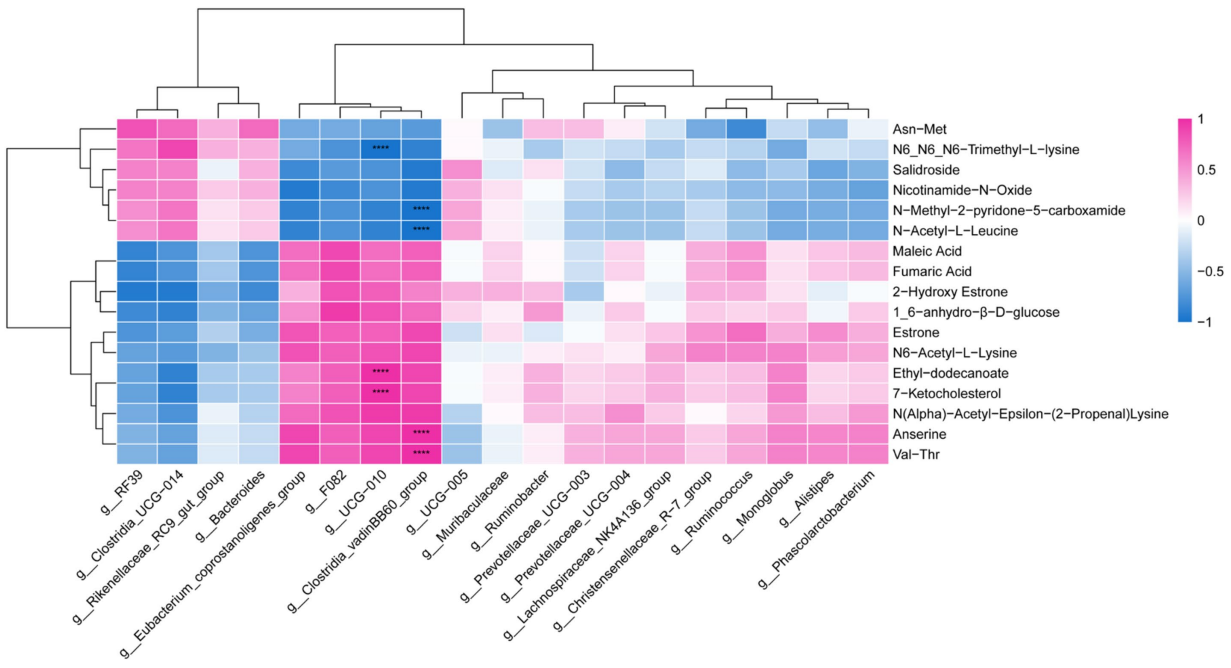


FIGURE 8
Microbiome-metabolome correlation heatmap. **** $p < 0.0001$. Red represents a positive correlation, and blue represents a negative correlation.

metabolic pathways that regulate lipid synthesis and degradation, thereby influencing cellular lipid balance and metabolism. The products of glycerophospholipid metabolism can affect the body's immune response by modulating the synthesis and release of inflammatory mediators (61). In summary, *Epimedium* may positively influences related metabolic pathways by regulating the production of key metabolites, effectively increasing hormone levels and antioxidant capacity. This contributes to the stabilization of metabolic and physiological functions in the Chinese forest musk deer.

Correlation analysis revealed associations between *Clostridia_vadinBB60_group* and *UCG-010* with different metabolites. We found that *Clostridia_vadinBB60_group* was positively correlated with anserine. As a beneficial bacterium, *Clostridia_vadinBB60_group* can effectively degrade complex organic compounds such as cellulose, hemicellulose, and polysaccharides, producing SCFAs like acetate, butyrate, and propionate, which play a crucial role in host energy supply, gut health, and microbial balance (62–64). This is particularly important in ruminant production, where it contributes to improving feed conversion efficiency (65). Dietary supplementation of *Epimedium*, the level of anserine increased, which may be related to the increased abundance of *Clostridia_vadinBB60_group* in this study. Further experiments are needed to verify this hypothesis by vitro culture and mechanistic studies. *UCG-010* is widely present in the intestines of animals, particularly within the digestive systems of ruminants, where it plays a significant role in the gut microbiota by breaking down complex carbohydrates, thereby effectively promoting nutrient absorption (66, 67). In this study, *UCG-010* was found to be positively correlated with 7-ketocholesterol. After adding the diet with *Epimedium*, the relative abundance of *UCG-010* increased, which may affect the metabolism of 7-ketocholesterol, predicting it may affect the metabolism of 7-ketocholesterol. Further research is needed to focus on clarifying their regulation relationship and systematic mechanism.

In this study, only a small number of the Chinese forest musk deer samples ($n = 3$) were used for growth performance and metabolomics analysis, which is directly related to the rarity and protected status of this species. The limited number of animals included in our study may introduce biases. Specifically, the small sample size may not fully capture the natural variability within the species, potentially affecting the robustness of our statistical analyses. Due to insufficient statistical power, true biological effects may be overlooked. Furthermore, the limited representation of the Chinese forest musk deer population may not adequately reflect the complexity and diversity of their biological systems, leading to an incomplete understanding of the underlying mechanisms. To address these limitations, future studies should aim to replicate our findings with larger and more diverse sample sizes. This would enhance the reliability and validity of the results, allowing for a more comprehensive exploration of the relevant biological pathways. However, given the conservation status and ethical considerations associated with studying the Chinese forest musk deer, alternative approaches such as non-invasive sampling methods or collaborations with multiple research institutions may be necessary to effectively increase the sample size.

## 5 Conclusion

Dietary supplementation with *Epimedium* may increase the feed intake and feed conversion ratio of the Chinese forest musk deer, and positively influence their hormone levels, particularly with an observed increase in testosterone levels. Additionally, *Epimedium* may enhance the richness and diversity of the gut microbiota in the Chinese forest musk deer and altered serum metabolism, including amino acid metabolism, lipid metabolism, and energy metabolism. In summary, appropriate supplementation of *Epimedium* may contribute

to the improvement of hormone levels, gut microbiota, and serum metabolite composition in the Chinese forest musk deer.

## Data availability statement

The data presented in the study are deposited in the NCBI repository, accession number PRJNA1195406.

## Ethics statement

The animal study was approved by Ethics Committee of Chongqing University of Arts and Sciences (approval number, CQWLDF0031). The study was conducted in accordance with the local legislation and institutional requirements.

## Author contributions

SX: Conceptualization, Data curation, Formal analysis, Writing – original draft. QY: Conceptualization, Data curation, Formal analysis, Writing – original draft. ZY: Methodology, Writing – original draft. MC: Visualization, Writing – original draft. WF: Visualization, Writing – original draft. HG: Methodology, Writing – original draft. XF: Conceptualization, Funding acquisition, Project administration, Writing – review & editing. YW: Conceptualization, Funding acquisition, Project administration, Writing – review & editing.

## Funding

The author(s) declare that financial support was received for the research, authorship, and/or publication of this article. This research was supported by the China Postdoctoral Science Foundation in China (2023M740414), the Chongqing Natural Science Foundation in China (CSTB2022NSCQ-MSX1098), the Traditional Chinese Medicine Research Project of Chongqing Science and Technology Bureau and Health Commission in China (2023MSXM181), the Project of Science and Technology Research Program of Chongqing Education Commission in China (KJQN202001312), the Chongqing Basic Research Projects in China (2024jbky-05), the Youth Project of Science and Technology Research Program of Chongqing Education Commission in China (KJQN202201350), and the Tower Foundation Program of Chongqing University of Arts and Sciences in China (R2022YS08).

## Conflict of interest

The authors declare that the research was conducted in the absence of any commercial or financial relationships that could be construed as a potential conflict of interest.

## Publisher's note

All claims expressed in this article are solely those of the authors and do not necessarily represent those of their affiliated organizations, or those of the publisher, the editors and the reviewers. Any product that may be evaluated in this article, or claim that may be made by its manufacturer, is not guaranteed or endorsed by the publisher.

## Supplementary material

The Supplementary material for this article can be found online at: https://www.frontiersin.org/articles/10.3389/fvets.2024.1497115/full#supplementary-material

## References

1. Feng H, Feng T, Mo Y, Sun S, Wang L, Lu C, et al. Integrated multi-omics analysis reveals insights into Chinese Forest musk deer (*Moschus Berezovskii*) genome evolution and musk synthesis. *Front cell. Dev Biol.* (2023) 11:11. doi: 10.3389/fcell.2023.1156138

2. Liu K, Xie L, Deng M, Zhang X, Luo J, Li X. Zoology, chemical composition, pharmacology, quality control and future perspective of musk (*Moschus*): a review. *Chin Med.* (2021) 16:46. doi: 10.1186/s13020-021-00457-8

3. Gong R, Song S, Ai Y, Wang S, Dong X, Ren Z, et al. Exploring the growing Forest musk deer (*Moschus Berezovskii*) dietary protein requirement based on gut microbiome. *Front Microbiol.* (2023) 14:1124163. doi: 10.3389/fmicb.2023.1124163

4. Feng H, Wang L, Cao F, Ma J, Tang J, Feng C, et al. Forest Musk Deer (*Moschus Berezovskii*) in China: research and protection. *J Vertebr Biol.* (2023) 72:72. doi: 10.25225/jvb.22067

5. Zhao Y, Wang J, Li Y, Zhou M, Weladji RB, Bonoan JT, et al. Temporal pattern of parturition in captive alpine musk deer (*Moschus Sifanicus*). *Biologia.* (2020) 75:259–66. doi: 10.2478/s11756-019-00293-0

6. Qi W-H, Li J, Zhang X-Y, Wang Z-K, Li X-X, Yang C-Z, et al. The reproductive performance of female Forest musk deer (*Moschus Berezovskii*) in captivity. *Theriogenology.* (2011) 76:874–81. doi: 10.1016/j.theriogenology.2011.04.018

7. Cai Y, Yang J, Wang J, Yang Y, Fu W, Zheng C, et al. Changes in the population genetic structure of captive Forest musk deer (*Moschus Berezovskii*) with the increasing number of generation under closed breeding conditions. *Animals.* (2020) 10:255. doi: 10.3390/ani10020255

8. Tian Q, Zhou X, Cheng J, Luo Y, Dai L, Zhao W, et al. Genome sequence of lung pathogenic *Escherichia Coli* O78, a chimeric strain isolated from pneumonia Forest musk deer. *Genes Genom.* (2017) 39:805–15. doi: 10.1007/s13258-017-0545-4

9. Li Y, Hu X, Yang S, Zhou J, Qi L, Sun X, et al. Comparison between the fecal bacterial microbiota of healthy and diarrheic captive musk deer. *Front Microbiol.* (2018) 9:300. doi: 10.3389/fmicb.2018.00300

10. Montout L, Poullet N, Bambou J-C. Systematic review of the interaction between nutrition and immunity in livestock: effect of dietary supplementation with synthetic amino acids. *Animals.* (2021) 11:2813. doi: 10.3390/ani11102813

11. Zhuang W, Sun N, Gu C, Liu S, Zheng Y, Wang H, et al. A literature review on *Epimedium*, a medicinal plant with promising slow aging properties. *Heliyon.* (2023) 9:e21226. doi: 10.1016/j.heliyon.2023.e21226

12. Liu S-P, Li Y-F, Zhang D, Li C-Y, Dai X-F, Lan D-F, et al. Pharmacological actions of the bioactive compounds of *Epimedium* on the male reproductive system: current status and future perspective. *Asian J Androl.* (2024) 26:1–10. doi: 10.4103/aja20248

13. Bi Z, Zhang W, Yan X. Anti-inflammatory and Immunoregulatory effects of icariin and Icaritin. *Biomed Pharmacother.* (2022) 151:151. doi: 10.1016/j.biopha.2022.113180

14. Tang Z-S, Liu Y-R, Lv Y, Duan J-A, Chen S-Z, Sun J, et al. Quality markers of animal medicinal materials: correlative analysis of musk reveals distinct metabolic changes induced by multiple factors. *Phytomedicine.* (2018) 44:258–69. doi: 10.1016/j.phymed.2018.03.008

15. Xu Q, Wells CC, Garman JH, Asico L, Escano CS, Maric C. Imbalance in sex hormone levels exacerbates diabetic renal disease. *Hypertension*. (2008) 51:1218–24. doi: 10.1161/hypertensionaha.107.100594

16. Szabo R, Racz CP, Dulf FV. Bioavailability improvement strategies for icariin and its Derivates: a review. *Int J Mol Sci*. (2022) 23:7519. doi: 10.3390/ijms23147519

17. Zhang Y, Zhang C, Li Z, Zeng C, Xue Z, Li E, et al. New 8-Prenylated quercetin glycosides from the flowers of *Epimedium* Acuminatum and their testosterone production-promoting activities. *Front Chem*. (2022) 10:10. doi: 10.3389/fchem.2022.1014110

18. Lee W-J, Hase K. Gut microbiota-generated metabolites in animal health and disease. *Nat Chem Biol*. (2014) 10:416–24. doi: 10.1038/nchembio.1535

19. Chen S, Luo S, Yan C. Gut microbiota implications for health and welfare in farm animals: a review. *Animals*. (2022) 12:93. doi: 10.3390/ani12010093

20. Li B, Xiang T, Bindawa Isah M, Chen C, Zhang X. In vitro simulated saliva, gastric, and intestinal digestion followed by Faecal fermentation reveals a potential modulatory activity of *Epimedium* on human gut microbiota. *J Pharm Biomed Anal*. (2024) 245:116151. doi: 10.1016/j.jpba.2024.116151

21. Zhang J, Yu H, Zhang H, Zhao Q, Si W, Qin Y, et al. Dietary *Epimedium* extract supplementation improves intestinal functions and alters gut microbiota in broilers. *J Anim Sci Biotechnol*. (2023) 14:14. doi: 10.1186/s40104-022-00812-1

22. Pan S, Chen A, Han Z, Wang Y, Lu X, Yang Y. 1h Nmr-based Metabonomic study on the effects of *Epimedium* on glucocorticoid-induced osteoporosis. *J Chromatogr B*. (2016) 1038:118–26. doi: 10.1016/j.jchromb.2016.10.015

23. Yang X-H, Li L, Xue Y-B, Zhou X-X, Tang J-H. Flavonoids from *Epimedium* Pubescens: extraction and mechanism, antioxidant capacity and effects on cat and Gsh-Px of *Drosophila Melanogaster*. *PeerJ*. (2020) 8:e8361. doi: 10.7717/peerj.8361

24. Zhang J, Kobert K, Flouri T, Stamatakis A. Pear: a fast and accurate Illumina paired-end read merger. *Bioinformatics*. (2014) 30:614–20. doi: 10.1093/bioinformatics/btt593

25. Rognes T, Flouri T, Nichols B, Quince C, Mahe F. Vsearch: a versatile open source tool for metagenomics. *PeerJ*. (2016) 4:e2584. doi: 10.7717/peerj.2584

26. Pruesse E, Quast C, Knittel K, Fuchs BM, Ludwig W, Peplies J, et al. Silva: a comprehensive online resource for quality checked and aligned ribosomal Rna sequence data compatible with arb. *Nucleic Acids Res*. (2007) 35:7188–96. doi: 10.1093/nar/gkm864

27. Ye J, McGinnis S, Madden TL. Blast: improvements for better sequence analysis. *Nucleic Acids Res*. (2006) 34:W6–9. doi: 10.1093/nar/gkl164

28. Hall M, Beiko RG. 16s Rrna gene analysis with Qiime2. *Methods Mol Biol*. (2018) 1849:113–29. doi: 10.1007/978-1-4939-8728-3_8

29. Copeland WK, Krishnan V, Beck D, Settles M, Foster JA, Cho K-C, et al. Mcagui: microbial community analysis R-graphical user Interface (Gui). *Bioinformatics*. (2012) 28:2198–9. doi: 10.1093/bioinformatics/bts338

30. Segata N, Izard J, Waldron L, Gevers D, Miropolsky L, Garrett WS, et al. Metagenomic biomarker discovery and explanation. *Genome Biol*. (2011) 12:R60. doi: 10.1186/gb-2011-12-6-r60

31. Liao J, Zhang Y, Zhang W, Zeng Y, Zhao J, Zhang J, et al. Different software processing affects the peak picking and metabolic pathway recognition of metabolomics data. *J Chromatogr A*. (2023) 1687:1687. doi: 10.1016/j.chroma.2022.463700

32. Zhang X, Zhou S, Liang Y, Xie G, Zhu M, Wang Z, et al. Effects of Astragalus, Epimedium, and Fructus Ligustri Lucidi extractive on antioxidant capacity, production performance, and immune mechanism of breeding pigeons under stress. *Poult Sci*. (2023) 102:102350. doi: 10.1016/j.psj.2022.102350

33. Guo Y, Li Y, Zhang S, Wu X, Jiang L, Zhao Q, et al. The effect of Total flavonoids of Epimedium on granulosa cell development in laying hens. *Poult Sci*. (2020) 99:4598–606. doi: 10.1016/j.psj.2020.05.032

34. Liu J, Yan P, Li Y, Yu J, Huang Y, Bai R, et al. Gut microbiota and serum metabolome reveal the mechanism by which Tcm polysaccharides alleviate Salpingitis in laying hens challenged by Bacteria. *Poult Sci*. (2024) 103:103288. doi: 10.1016/j.psj.2023.103288

35. Sun X, Li Y, Li J, Liang H, Zhang J, Chen X, et al. Bioactive metabolites reveal the therapeutic consistency of Epimedii folium from multi-plant sources for the treatment of kidney-Yang deficiency. *J Ethnopharmacol*. (2024) 319:319. doi: 10.1016/j.jep.2023.117215

36. Munir N, Mahmood Z, Yameen M, Mustafa G. Therapeutic response of Epimedium Gandiflorum's different doses to restore the antioxidant potential and reproductive hormones in male albino rats. *Dose-Response*. (2020) 18:1559325820959563. doi: 10.1177/1559325820959563

37. Bo X, Chen J, Mu J, Dong X, Ren Z, Liu J, et al. Quercetin promotes the secretion of musk by regulating the hormone level and microbial structure of Forest musk deer. *Integr Zool*. (2024) 19:596–611. doi: 10.1111/1749-4877.12763

38. Jie H, Feng X-L, Zhao G-J, Zeng D-J, Zhang C-L, Chen Q. Research Progress on musk secretion mechanism of Forest musk deer. *Zhongguo Zhong Yao Za Zhi*. (2014) 39:4522–5.

39. Fang M, Zhang M, Shi M, Zhang T, Qi L, Yu J, et al. Sex hormones play roles in determining musk composition during the early stages of musk secretion by musk deer (*Moschus Berezovskii*). *Endocr J*. (2018) 65:1111–20. doi: 10.1507/endocrj.EJ18-0211

40. Jin Q, Cheng L, Zhu Y, Zhao X, Zhang W, Gao X, et al. Immune-related effects of compound Astragalus polysaccharide and sulfated Epimedium polysaccharide on newborn piglets. *Anim Biotechnol*. (2021) 34:508–19. doi: 10.1080/10495398.2021.1979022

41. Jiang Y, Han X, Li M, Feng N, Yang P, Zhao H, et al. Changes in the gut microbiota of Forest musk deer (*Moschus Berezovskii*) during ex situ conservation. *Front Microbiol*. (2022) 13:13. doi: 10.3389/fmicb.2022.969593

42. Hu X, Liu G, Li Y, Wei Y, Lin S, Liu S, et al. High-throughput analysis reveals seasonal variation of the gut microbiota composition within Forest musk deer (*Moschus Berezovskii*). *Front Microbiol*. (2018) 9:9. doi: 10.3389/fmicb.2018.00009

43. Kapoor P, Tiwari A, Sharma S, Tiwari V, Sheoran B, Ali U, et al. Effect of anthocyanins on gut health markers, Firmicutes-Bacteroidetes ratio and short-chain fatty acids: a systematic review via Meta-analysis. *Sci Rep*. (2023) 13:1729. doi: 10.1038/s41598-023-28764-0

44. Natividad JM, Pinto-Sanchez MI, Galipeau HJ, Jury J, Jordana M, Reinisch W, et al. Ecobiotherapy rich in Firmicutes decreases susceptibility to colitis in a humanized Gnotobiotic mouse model. *Inflamm Bowel Dis*. (2015) 21:1883–93. doi: 10.1097/mib.0000000000000422

45. Chen G, Hu P, Xu Z, Peng C, Wang Y, Wan X, et al. The beneficial or detrimental fluoride to gut microbiota depends on its dosages. *Ecotoxicol Environ Saf*. (2021) 209:111732. doi: 10.1016/j.ecoenv.2020.111732

46. Rizzatti G, Lopetuso LR, Gibiino G, Binda C, Gasbarrini A. Proteobacteria: a common factor in human diseases. *Biomed Res Int*. (2017) 2017:1–7. doi: 10.1155/2017/9351507

47. Shin N-R, Whon TW, Bae J-W. Proteobacteria: microbial signature of Dysbiosis in gut microbiota. *Trends Biotechnol*. (2015) 33:496–503. doi: 10.1016/j.tibtech.2015.06.011

48. Yoshida N, Yamashita T, Kishino S, Watanabe H, Sasaki K, Sasaki D, et al. A possible beneficial effect of *Bacteroides* on Faecal lipopolysaccharide activity and cardiovascular diseases. *Sci Rep*. (2020) 10:13009. doi: 10.1038/s41598-020-69983-z

49. Cheng J, Hu J, Geng F, Nie S. Bacteroides utilization for dietary polysaccharides and their beneficial effects on gut health. *Food Sci Hum Wellness*. (2022) 11:1101–10. doi: 10.1016/j.fshw.2022.04.002

50. Deng L, Chen S, Meng W, Zhou Z, Liu H, Zhong Z, et al. Changes in gut microbiota composition associated with the presence of enteric Protist Blastocystis in captive Forest musk deer (*Moschus Berezovskii*). *Microbiol Spectr*. (2022) 10:e0226921. doi: 10.1128/spectrum.02269-21

51. Huo S, Li Y, Guo Y, Zhang S, Li P, Gao P. Improving effects of *Epimedium* flavonoids on the selected reproductive features in layer hens after forced molting. *Poult Sci*. (2020) 99:2757–65. doi: 10.1016/j.psj.2019.12.053

52. Wang Y, Yang P, Chen T, Hu J, An X, Yao C, et al. Analysis and comparison of blood metabolome of Forest musk deer in musk secretion and non-secretion periods. *Sci Rep*. (2024) 14:16980. doi: 10.1038/s41598-024-67981-z

53. Yi L, Dalai M, Su R, Lin W, Erdenedalai M, Luvsantseren B, et al. Whole-genome sequencing of wild Siberian musk deer (*Moschus Moschiferus*) provides insights into its genetic features. *BMC Genomics*. (2020) 21:108. doi: 10.1186/s12864-020-6495-2

54. Chen M, Luo J, Ji H, Song W, Zhang D, Su W, et al. The preventive mechanism of anserine on Tert-butyl Hydroperoxide-induced liver injury in L-02 cells via regulating the Keap1-Nrf2 and Jnk-Caspase-3 signaling pathways. *Mar Drugs*. (2023) 21:477. doi: 10.3390/md21090477

55. Kasamatsu S, Komae S, Matsukura K, Kakihana Y, Uchida K, Ihara H. 2-Oxo-imidazole-containing dipeptides play a key role in the antioxidant capacity of imidazole-containing dipeptides. *Antioxidants*. (2021) 10:1434. doi: 10.3390/antiox10091434

56. Chen M, Ji H, Song W, Zhang D, Su W, Liu S. Anserine beneficial effects in Hyperuricemic rats by inhibiting Xod, regulating uric acid transporter and repairing Hepatorenal injury. *Food Funct*. (2022) 13:9434–42. doi: 10.1039/d2fo01533a

57. Moro J, Tome D, Schmidely P, Demersay T-C, Azzout-Marniche D. Histidine: a systematic review on metabolism and physiological effects in human and different animal species. *Nutrients*. (2020) 12:1414. doi: 10.3390/nu12051414

58. Holecek M. Histidine in health and disease: metabolism, physiological importance, and use as a supplement. *Nutrients*. (2020) 12:848. doi: 10.3390/nu12030848

59. Kopec W, Jamroz D, Wiliczkiewicz A, Biazik E, Pudlo A, Korzeniowska M, et al. Antioxidative characteristics of chicken breast meat and blood after diet supplementation with carnosine, L-histidine, and B-alanine. *Antioxidants*. (2020) 9:1093. doi: 10.3390/antiox9111093

60. Qi B, Wang J, Hu M, Ma Y, Wu S, Qi G, et al. Influences of Beta-alanine and L-histidine supplementation on growth performance, meat quality, carnosine content, and Mrna expression of carnosine-related enzymes in broilers. *Animals*. (2021) 11:2265. doi: 10.3390/ani11082265

61. Zhu Q, Wu Y, Mai J, Guo G, Meng J, Fang X, et al. Comprehensive metabolic profiling of inflammation indicated key roles of Glycerophospholipid and arginine metabolism in coronary artery disease. *Front Immunol*. (2022) 13:13. doi: 10.3389/fimmu.2022.829425

62. Xiao S-S, Mi J-D, Mei L, Liang J, Feng K-X, Wu Y-B, et al. Microbial diversity and community variation in the intestines of layer chickens. *Animals*. (2021) 11:840. doi: 10.3390/ani11030840

63. Harrison CA, Laubitz D, Ohland CL, Midura-Kiela MT, Patil K, Besselsen DG, et al. Microbial Dysbiosis associated with impaired intestinal Na+/H+ exchange accelerates and exacerbates colitis in ex-germ free mice. *Mucosal Immunol*. (2018) 11:1329–41. doi: 10.1038/s41385-018-0035-2

64. Zhang J, Shi H, Wang Y, Cao Z, Yang H, Li S. Effect of limit-fed diets with different forage to concentrate rations on fecal bacterial and archaeal community composition in Holstein heifers. *Front Microbiol*. (2018) 9:9. doi: 10.3389/fmicb.2018.00976

65. Fonseca PAS, Lam S, Chen Y, Waters SM, Guan LL, Canovas A. Multi-breed host rumen epithelium transcriptome and microbiome associations and their relationship with beef cattle feed efficiency. *Sci Rep*. (2023) 13:16209. doi: 10.1038/s41598-023-43097-8

66. Han X, Lei X, Yang X, Shen J, Zheng L, Jin C, et al. A metagenomic insight into the hindgut microbiota and their metabolites for dairy goats fed different rumen degradable starch. *Front Microbiol*. (2021) 12:12. doi: 10.3389/fmicb.2021.651631

67. Li B, Yin W, Lei M, Wang X, Yang Y, Zhang C, et al. Exploring the Digesta- and mucosa-associated microbial community dynamics in the rumen and hindgut of goats from birth to adult. *Front Microbiol*. (2023) 14:1190348. doi: 10.3389/fmicb.2023.1190348

frontiers | Frontiers in Plant Science

TYPE Original Research
PUBLISHED 28 February 2025
DOI 10.3389/fpls.2025.1517050



OPEN ACCESS

EDITED BY
Solomon Abate Mekonnen,
Ethiopian Institute of Agricultural Research, Ethiopia

REVIEWED BY
Sileshi Andualem,
Bahir Dar University, Ethiopia
Lingaiah Kusuma,
Central Sericultural Research & Training Institute (CSRTI), India

*CORRESPONDENCE
Izhar Hyder Qazi
vetdr_izhar@yahoo.com
Jiping Liu
liujiping@scau.edu.cn

RECEIVED 25 October 2024
ACCEPTED 16 January 2025
PUBLISHED 28 February 2025

CITATION
Huang X, Yuan T, Huang Y, Qazi IH and Liu J (2025) Analysis of causal pathogens of mulberry bacterial blight in samples collected from eight provinces of China using culturomics and metagenomic sequencing methods.
*Front. Plant Sci.* 16:1517050.
doi: 10.3389/fpls.2025.1517050



# Analysis of causal pathogens of mulberry bacterial blight in samples collected from eight provinces of China using culturomics and metagenomic sequencing methods

Xinpeng Huang, Ting Yuan, Yuxin Huang, Izhar Hyder Qazi* and Jiping Liu*

Guangdong Provincial Key Lab of Agro-Animal Genomics and Molecular Breeding, College of Animal Science, South China Agricultural University, Guangzhou, Guangdong, China

Mulberry bacterial blight (MBB) is a complex and one of the devastating diseases of mulberry that causes serious reduction in the yield and quality of mulberry. In recent years, the transformation of sericulture industry, mulberry production system, and increasing seedling trade have resulted in the spread of MBB to different parts of China, posing a major economic threat to the farmers and industry. This study investigated the occurrence of MBB in eight provinces of China during years 2023 and 2024. The MBB disease samples were collected and the composition of the MBB pathogenic microbiome was analyzed by combining culturomics and metagenomic sequencing methods. A total of 498 bacterial strains were isolated and identified through culturomics, and then 109 suspected pathogen strains were preliminarily screened based on metagenomic sequencing data. Finally, 10 pathogens including, *Pseudomonas syringae, P. fulva, P. fluorescens, Pantoea ananatis, Pectobacterium parvum, P. carotovorum, Flavobacterium fluviale, Citrobacter portucalensis, Klebsiella grimontii, Stenotrophomonas maltophilia*, were identified through Koch's postulates. Based on the distribution pattern of pathogens and the changes in the microbiome community of mulberry following infection with *P. syringae*, we infer that *P. syringae*, and *P. fulva* are important pathogens of MBB. In addition, based on the analysis of meteorological data, different bacteria showed adaptability to different environments, leading to differences in the pathogens of MBB under different climate conditions and latitudes. The data presented herein provides a foundation for understanding the occurrence, spatial distribution and pathogenic mechanism of MBB and its major pathogens.

KEYWORDS

**bacterial blight, climate, culturomics, distribution, metagenomics, mulberry**

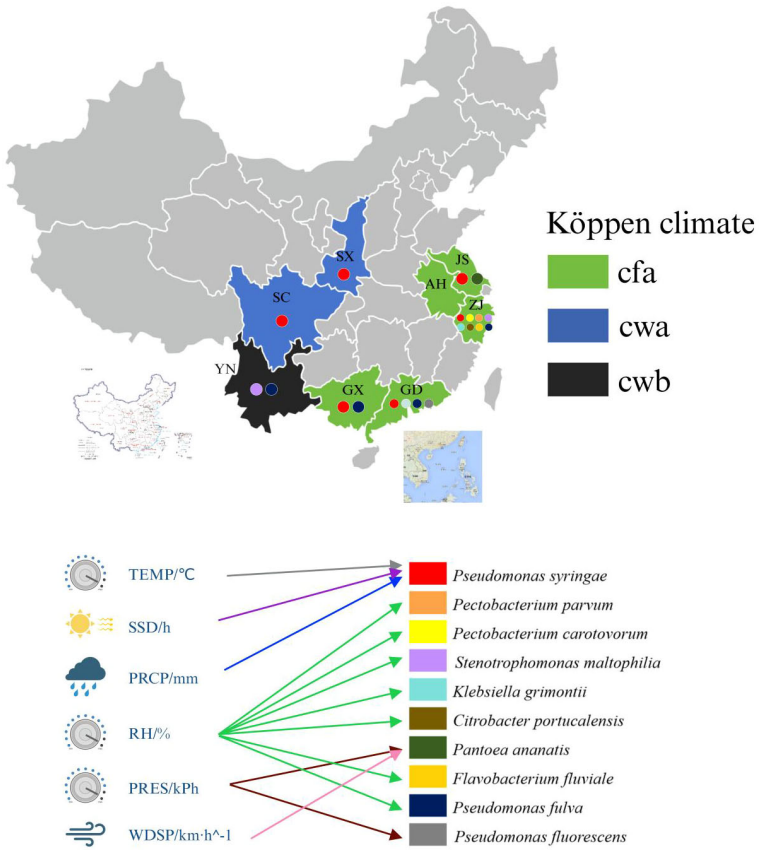


GRAPHICAL ABSTRACT
Cfa: Humid subtropical climate. Cwa: Dry-winter humid subtropical climate. Cwb: Dry-winter subtropical highland climate. SX: Shaanxi province. SC: Sichuan province. YN: Yunnan province. GD: Guangdong province. ZJ: Zhejiang province. JS: Jiangsu province. AH: Anhui province. GX: Guangxi Zhuang autonomous region. TEMP: Monthly average temperature. SSD: Sunshine duration. PRCP: Monthly total precipitation. RH: Relative humidity. WDSP: Wind direction speed. PRES: Station pressure. Arrows indicate positive correlation.

## 1 Introduction

Mulberry is an important economic crop that has been cultivated and used in sericulture in China for over 5000 years (Chen et al., 2022). The stability of the global silk supply chain is highly reliant on healthy growth of mulberry production systems (Memete et al., 2022). In recent years, mulberry bacterial blight (MBB) has emerged as one of the major diseases affecting the growth, yield, and quality of mulberry (Xie et al., 2017). The occurrence of MBB has been reported in several countries including China, India, Iran, Pakistan, Indonesia, and Poland, among others (Krawczyk and Łochyńska, 2020). Although, MBB has been reported in many provinces and different agro-climatic conditions in China, the estimation of its exact economic impact is difficult due to the complexities of cropping practices and sericulture industry itself. However, the estimated direct economic losses are huge in areas where intensive sericulture/moriculture is practiced (Liu Jiping, personal communication).

At present, *Pseudomonas syringae* is generally considered as the main causal pathogen of MBB (Akhtar and Sarwar, 1988; Krawczyk and Łochyńska, 2020). To date, over 50 pathovars of *P. syringae* have been reported worldwide, which are pathogenic to over 180 plant species, including mulberry trees (Krawczyk and Łochyńska, 2020). *P. syringae* can spread through wind and rain. After attachment to the host surface, it quickly causes necrotic spots on the leaves and shoots, causing serious damage to plant health (Donati et al., 2020). Importantly, available evidence shows the diversity of causal pathogens of the MBB, as several other pathogens including *Achromobacter xylosoxidans* (Oksel et al., 2024), *P. oryzihabitans* (Huai et al., 2023), *Xanthomonas phaseoli* (Zárate-Chaves et al., 2024), and *Klebsiella oxytoca* (Huang et al., 2024) have been reported to cause bacterial blight in plants. On the other hand, we now know that bacterial diseases in plants can be caused by co-infection of multiple bacterial species. For instance, recently it was shown that *K. michiganensis* (Luo et al., 2022), *Ralstonia pseudosolanacearum* (Li et al., 2024), *Pantoea ananatis* (Yuan et al., 2023a) can all cause bacterial wilt disease in mulberry trees. In light of this evidence, it is important to investigate the diversity of the causal pathogens of bacterial blight disease of mulberry.

At present, the strategies for prevention and control of MBB are still limited, therefore, research on the diversity of its pathogenic microbiome is very critical for understanding the disease itself. With

the rapid development of molecular sequencing technology, metagenomic sequencing and other omics tools are now gaining popularity in the field of plant pathogen diagnosis (Melcher et al., 2014). Compared with the traditional culture-dependent technique, these molecular methods not only provide advantage of simultaneous detection of multiple pathogens, but they are also useful in studying the diversity, structure and composition of the entire plant-associated microbiome in a given sample (Roman-Reyna and Crandall, 2024). These methods also allow exploration and prediction of novel genes and metabolic pathways implicated in pathogenesis of plant diseases (Roman-Reyna and Crandall, 2024). Genomic information can be obtained directly from environmental samples, and many uncultured microbial species can be identified (Xu et al., 2018). Although, genomic analysis-based methods provide rich data, and that the technological advancement has made it possible to extract DNA/RNA from environmental samples with reduced contamination and improved purity, these methods come with some technical limitations. Restrictions in sequencing methods, gene assembly with the risk of chimaera production, and inadequate quality/availability of annotated genes and gene families in the databases are some of the key limitations that lead to genes of unknown functions and consequently to unknown taxa (Sarhan et al., 2019). These problems can easily lead to bias in researchers' analysis of the microbial samples and incorrect functional prediction of microbial genes. Culturomics, developed by Jean-Christophe Lagier et al. (2015), refers to a high-throughput culture method for obtaining a variety of pure bacterial cultures under different culture conditions. It has now been used to explore microbial communities and gene functions in samples from human (Lagier et al., 2018), animals (Wang et al., 2021), plants (Li et al., 2023) and environment (Sun et al., 2023). Metagenomic sequencing and culturomics are complementary approaches that can be used in combination to explore the true picture of microbial communities in a given sample (Ji et al., 2024). There are recent studies in which combined metagenomic sequencing and culture-dependent methods were employed to identify the causal pathogens and disease diagnosis in plants (Zhang et al., 2023; Yuan et al., 2023b).

At present, the MBB research mainly focuses on pathogen identification and patho-biology, preliminary exploration of disease mechanisms, and disease prevention and control (Huang et al., 2024; Baharuddin, 1997; Krawczyk and Łochyńska, 2020). However, as the global climate outlook and agricultural practices are changing, it is likely that new pathways for pathogen transmission may continue to emerge (Rosario et al., 2020). Given the complexity of sericulture and mulberry production systems, it becomes necessary to conduct more in-depth research on the causal pathogens of MBB and their transmission mechanism. It is said that, among non-human factors, meteorological factors play a key role in the spread of pathogens, as microorganisms, including bacteria, can exist stably in aerosols and can spread from place to place with atmospheric movement (Fröhlich-Nowoisky et al., 2016; Jung et al., 2018). Therefore, in this context, it is important to study the driving factors of MBB transmission, especially meteorological factors. Such studies are expected to help us understand the disease to a greater extent, and will certainly provide basis for the development and implementation of measures for the prevention and control of MBB.

In the present study, the MBB disease samples were collected from eight provinces in China including Guangdong, Jiangsu, Zhejiang, Sichuan, Shaanxi, Yunnan, Anhui, and Guangxi Zhuang Autonomous Region. The samples were analyzed for microbiome composition and diversity in the disease samples through combined metagenomic sequencing and culturomics methods. The suspected pathogens were screened out, and pathogenicity tests were performed on mulberry to verify the Koch's postulates. The screened pathogenic strains were combined with their distribution patterns in the samples to determine the main causal pathogen of MBB. Then, the pathogens of MBB in combination with the local meteorological data (15 days before and after the sample collection) were analyzed to draw a potential relationship between each pathogen and relevant meteorological factors. Finally, the selected primary pathogens were re-inoculated into mulberry. Following exhibition of typical symptoms, mulberry plants were used for metagenomic sequencing to investigate the changes in the diversity of pathogens in the disease samples. The results of this study provide a reasonable basis for the focused research on the prevention and control of MBB, and will also contribute to the sustainable development of the global silk industry.

## 2 Materials and methods

The entire experimental flow of this study is presented in the form of schematic as Figure 1.

### 2.1 Metagenomics-based detection of MBB field disease samples

#### 2.1.1 Locations and sample material

The MBB samples were collected from 16 different locations in eight provinces of China. The selection of these regions was based on the fact that these provinces are sericulture intensives regions in China and reportedly contributed to 91.39% of the total sericulture production in 2023[1]. These provinces cover three different types of Köppen climate (see Table 1; Figure 2).

Accordingly, field investigations were extended to 16 diverse locations including Hangzhou City, Zhejiang (P1-P8); Hai'an City (S1, HA); Sheyang City (S3, S4, S6); Dongtai City (S2); Suining City (S5) and Dafeng (DF) City, Jiangsu; Hefei City, Anhui (X); Ankang City, Shaanxi (T1); Puer City, Yunnan (U); Nanchong City, Sichuan (R1-R2); Yingde City (ZA1-5); Yunfu City (Y); Zhongshan City (ZA6); Guangzhou City (ZC, ZD, ZK and ZL), Guangdong; Mashan City (W); Huanjiang, City (A), Guangxi. Based on the source location, the collected samples were divided into eight groups, and named as GX (W and A), GD (ZA6, ZC, ZD, ZK, ZL, ZA1-5 and Y), ZJ (P1-P8), SC (R1-R2), JS (DF, HA, S1, S2, S3, S4, S5 and S6), YN (U), AH (X), SX (T1).

Detailed information of all samples and collection sites is shown in Table 1, and Figures 2, 3. A five-point sampling method was used to randomly survey 30 mulberry trees in the local mulberry fields

1 Statistical data from Ministry of Commerce, People's Republic of China, https://www.mofcom.gov.cn/).

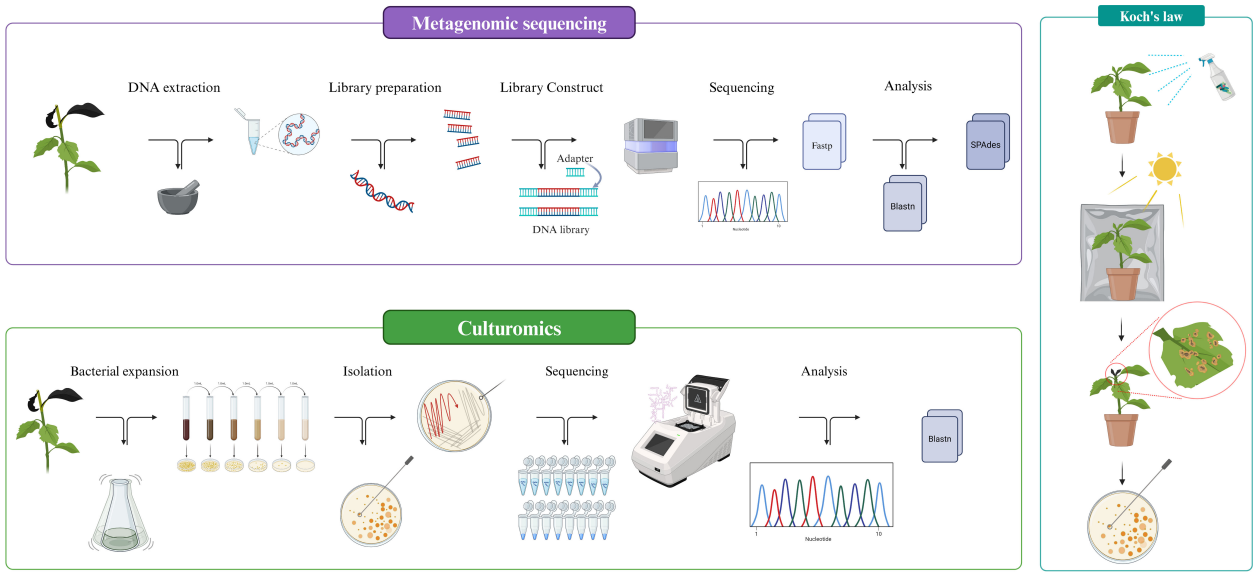


FIGURE 1
Experimental flowchart.

where samples were collected. The number of mulberry trees showing MBB symptoms and the number of healthy mulberry trees were counted to calculate the morbidity (Table 1). The diseased parts of mulberry trees were collected with ethanol-disinfected scissors, and placed into zip lock PE bags, and kept in a refrigerator at 4°C until used for the bacterial isolation. The collected MBB disease samples were washed with soapy water, disinfected with 75% ethanol, and then rinsed with sterile water for at least three times. Then the samples were frozen (-80°C) in sterile bags for further analysis. Climate type of the sampling sites were determined according to the Köppen climate classification (Table 1). At the same time, the meteorological data including Temperature (TEMP), Precipitation (PRCP), Relative humidity (RH), Wind direction speed (WDSP), Station pressure (STP) of all sample collection sites (15 days before and after the sampling period) were recorded (Table 1). Meteorological data was downloaded from the open data platform of the National Meteorological Information Center, China Meteorological Administration via its Application Programming Interface (http://data.cma.cn).

### 2.1.2 Cultivation of mulberry for replanting

The mulberry tree variety Qiangsang No. 1 (*Morus alba* var. *multicaulis*) was used for grafting in this experiment. The plant material was sourced from the mulberry research station of the South China Agricultural University, China (113. 35°E, 23. 16°N).

## 2.2 Metagenomic sequencing

### 2.2.1 DNA extraction, metagenomic sequencing, assembly, read quality control and processing

The samples (Table 1; MBB sample S1) collected from Jiangsu province exhibiting typical symptoms of the MBB disease were used for metagenomic sequencing. As per the instructions of the bacterial genomic DNA extraction kit (CW0552, CoWin Biosciences), the diseased-healthy junction area of the diseased sample was cut and used for total DNA extraction. The extracted total DNA was quality controlled by agarose gel electrophoresis, and the qualified DNA was stored at -20°C. The qualified DNA samples were randomly broken into fragments of about 350 bp in length using a Covaris ultrasonic crusher (Covaris, USA) to construct a small fragment genomic DNA library. The library construction process was carried out according to the instructions of the VAHTSTM Universal DNA Library Prep Kit for Illumina® Library Construction Kit. Following library construction, quality control was performed using RT-qPCR and Agilent 2100 Bioanalyzer (Agilent Technologies, USA). The DNA library that passed the quality inspection was sequenced on the Illumina Novaseq6000 (Illumina, USA) high-throughput sequencing platform, using the sequencing strategy PE150 (Pair-End 150). To ensure the accuracy and reliability of subsequent analysis and test results, the sequencing data was subjected to further statistical screening. These checks included sequencing data volume, quality index, and GC ratio distribution. The data from the Illumina high-throughput sequencing platform was converted into raw reads using CASAVA software. Then the adapter sequences and low-quality sequences in the raw data were filtered to ensure the quality of the data analysis. The raw sequences were filtered to obtain high-quality clean reads. When the N content in any read exceeded 10% of the base number of the read, the paired reads were removed. When the number of low-quality (Q<=5) bases in any sequencing read exceeded 50% of the base number of the read, the paired reads were removed. Sequence assembly was performed using SPAdes v. 3. 5. 0 software (Bankevich et al., 2012).

### 2.2.2 Annotation of metagenomic data

Using the BLASTn (v2. 5. 0+) alignment strategy (Zhang et al., 2000), sequencing tags were aligned against the bacterial and fungal

TABLE 1 Information of sample source and collection locations.

| Sample code | Date | Location | | | TEMP (°C) | SSD (h) | PRCP (mm) | RH (%) | WDSP (km/h) | PRES (hPa) | K ö ppen climate | Mor* (%) | Season | Cultivar | Species | Symptom |
|---|---|---|---|---|---|---|---|---|---|---|---|---|---|---|---|---|
| | | Region | | Latitude and longitude | | | | | | | | | | | | |
| X | 2024.8.18 | AH | Hefei | 117.37°E,31.53°N | 30.5 | 13.28 | 65.9 | 79.87 | 6.1 | 998.19 | Cwa | 16.67 | summer | Qiang Sang NO.1 | Morus multicaulis Perr. | terminal bud curl |
| ZA1-5 | 2024.3.11 | GD | Yingde | 113.41°E,24.18°N | 18 | 12.01 | 10.9 | 77.18 | 5.8 | 1008.59 | Cfa | 6.67 | spring | Yuesang11 | *M. atropurpurea* | terminal bud black |
| ZA6 | 2024.3.13 | GD | Zhongshan | 113.46°E,22.41°N | 20 | 12.02 | 16 | 78.76 | 9.5 | 1000.46 | Cfa | 6.67 | spring | Sha2xLun109 | *M. atropurpurea* | terminal bud black |
| ZC | 2024.3.19 | GD | Zengcheng | 113.81°E,23.26°N | 19.5 | 12.02 | 7 | 77.36 | 6.59 | 1012.55 | Cfa | 50.00 | spring | Shengxiansang | M. multicaulis Perr. | terminal bud black |
| ZD | 2024.3.19 | GD | Zengcheng | 113.81°E,23.26°N | 19.5 | 12.02 | 7 | 77.36 | 6.59 | 1012.55 | Cfa | 63.33 | spring | Da10 | *M. atropurpurea* | terminal bud black |
| ZK | 2024.3.19 | GD | Zengcheng | 113.81°E,23.26°N | 19.5 | 12.02 | 7 | 77.36 | 6.59 | 1012.55 | Cfa | 50.00 | spring | Kangqing10 | *M. atropurpurea* | terminal bud black |
| ZL | 2024.3.19 | GD | Zengcheng | 113.81°E,23.26°N | 19.5 | 12.02 | 7 | 77.36 | 6.59 | 1012.55 | Cfa | 43.33 | spring | Lunbai10 | M. alba L. | terminal bud black |
| Y | 2024.3.30 | GD | Yunan | 111.54°E,23.23°N | 20.1 | 12.02 | 17.9 | 79.36 | 5.37 | 1007.29 | Cfa | 16.67 | spring | Qiang Sang NO.1 | M. multicaulis Perr. | terminal bud black |
| A | 2023.10.15 | GX | Huanjiang | 108.26°E,24.83°N | 21 | 12.83 | 1.2 | 70 | 3.1 | 985.95 | Cfa | 10.00 | autumn | Gui Sang12 | M. atropurpurea Roxb. | terminal bud black |
| W | 2024.8.13 | GX | Mashan | 108.20°E,23.73°N | 28.5 | 12.92 | 155.2 | 84.24 | 5.14 | 980.13 | Cfa | 6.67 | summer | Guisang12 | M. atropurpurea Roxb. | terminal bud black |
| DF | 2023.5.19 | JS | Dafeng | 120.56°E,33.36°N | 18 | 14.16 | 40.6 | 69 | 3.1 | 985.95 | Cfa | 73.33 | summer | Qiang Sang NO.1 | M. multicaulis Perr. | terminal bud black |
| HA | 2023.5.29 | JS | Haian | 120.47°E,32.53°N | 20 | 14.17 | 24 | 70 | 3.45 | 998.67 | Cfa | 96.67 | summer | Qiang Sang NO.1 | M. multicaulis Perr. | terminal bud black |
| S2 | 2024.6.11 | JS | Dongtai | 120.07°E,32.33°N | 25 | 14.27 | 222.1 | 74.42 | 6.32 | 1006.27 | Cfa | 73.33 | summer | Yu71-1 | M. multicaulis Perr. | terminal bud black |
| S3 | 2024.6.11 | JS | Sheyang | 119.67°E,34.07°N | 24 | 14.35 | 92.4 | 76.26 | 9.89 | 1006.59 | Cfa | 70.00 | summer | Yu71-1 | M. multicaulis Perr. | terminal bud black |
| S4 | 2024.6.11 | JS | Sheyang | 119.67°E,34.07°N | 24 | 14.35 | 92.4 | 76.26 | 9.89 | 1006.59 | Cfa | 73.33 | summer | Xuan792 | M. multicaulis Perr. | terminal bud black |
| S5 | 2024.6.11 | JS | Suining | 114.80°E,34.18°N | 27 | 14.37 | 59.5 | 60.3 | 7.23 | 1002.83 | Cfa | 73.33 | summer | Qiang Sang NO.1 | M. multicaulis Perr. | terminal bud black |

*(Continued)*





10.3389/fpls.2025.1517050

10.3389/fpls.2025.1517050

TABLE 1 Continued

| Sample code | Date | Location | | | TEMP (°C) | SSD (h) | PRCP (mm) | RH (%) | WDSP (km/h) | PRES (hPa) | K ö ppen climate | Mor* (%) | Season | Cultivar | Species | Symptom |
|---|---|---|---|---|---|---|---|---|---|---|---|---|---|---|---|---|
| | | | Region | Latitude and longitude | | | | | | | | | | | | |
| S1 | 2024.6.9 | JS | Haian | 120.47°E,32.53°N | 25 | 14.25 | 248.7 | 75.3 | 9.17 | 1005.91 | Cfa | 80.00 | summer | Yu71-1 | M. multicaulis Perr. | terminal bud black |
| S6 | 2024.8.14 | JS | Sheyang | 119.67°E,34.07°N | 29.5 | 13.37 | 170.2 | 83.78 | 7.12 | 1004.96 | Cfa | 63.33 | summer | Yu71-1 | M. multicaulis Perr. | terminal bud black |
| R1-R2 | 2024.5.27 | SC | Nanchong | 105.86°E,30.74°N | 23 | 13.71 | 45.4 | 74.45 | 6.41 | 969.38 | Cwa | 40.00 | summer | Qiang Sang NO.1 | M. multicaulis Perr. | terminal bud black |
| T1 | 2024.7.3 | SX | Ankang | 108.51°E,32.89°N | 27.5 | 14.05 | 249 | 86.49 | 5.56 | 939.68 | Cwa | 60.00 | summer | Nongsang14 | M. multicaulis Perr. | terminal bud black |
| U | 2024.7.25 | YN | Puer | 100.82°E,23.09°N | 27.5 | 13.47 | 249.2 | 84.01 | 4.92 | 877.37 | Cwb | 10.00 | summer | Qiang Sang NO.1 | M. multicaulis Perr. | terminal bud black |
| P1-P8 | 2024.4.20 | ZJ | Hangzhou | 118.21°E,29.11°N | 18.5 | 12.89 | 103.3 | 80.03 | 6.17 | 1006.55 | Cfa | 96.67 | spring | Qiang Sang NO.1 | M. multicaulis Perr. | terminal bud black |

TEMP, Monthly average temperature; SSD, Sunshine duration; PRCP, Monthly total precipitation; RH, Relative humidity; WDSP, Wind direction speed; PRES, Station pressure; SX, Shaanxi province; SC, Sichuan province; YN, Yunnan province; GD, Guangdong province; ZJ, Zhejiang province; JS, Jiangsu province; AH, Anhui province; GX, Guangxi Zhuang autonomous region; Cfa, Humid subtropical climate; Cwa, Dry-winter humid subtropical climate; Cwb, Dry-winter subtropical highland climate; Mor., Morbidity%;

databases in the National Center for Biotechnology Information (NCBI, http://ftp.ncbi.nlm.nih.gov/) nt database. Based on multiple dimensions such as sequence alignment similarity, alignment length, and sequence integrity, the optimal alignment results were selected through a similarity evaluation algorithm to annotate the tag sequences, and the microbial diversity in the samples was analyzed. The abundance of species was calculated based on the sequencing depth and assembly length of the sequence tags. The MEGAN software (Version 6. 20. 0) was used to visualize the microbial species and quantities (Huson et al., 2016). High-abundance microbial species in MBB samples were screened and preliminarily identified as pathogens.

### 2.2.3 Screening and annotation of suspected pathogens

Based on the high-throughput sequencing data assembly and experimental verification results, the complete rRNA sequence was obtained. The rRNA sequence was annotated using blastn. Based on the rRNA sequences of closely related species in the nt database, the length and GC ratio of the 16S/18S, ITS1, 23S/28S, ITS2, and 5S intervals were counted respectively. With 250 bp as the statistical threshold, the GC ratio distribution of the sequence was counted and the GC ratio distribution map was drawn by sliding 10 bp each time. The rDNA sequences of species with high percent identity to the alignment results were downloaded from the NCBI for phylogenetic tree construction. MUSCLE v. 3. 8. 31 software (Edgar, 2004) was used for sequence alignment between multiple species. jModelTest2. 1. 7 was used to test the nucleic acid model of the selected sequence DNA (Posada, 2008). The substitution model with the smallest AIC (Akaike Information Criterion) value was taken as the optimal phylogenetic tree substitution model. The phylogenetic tree was constructed using the RAxML8. 1. 5 software (Stamatakis, 2014), using the ML method (maximum likelihood) with the bootstrap value set to 1000.

## 2.3 Culturomics

### 2.3.1 Isolation and culture

As described in our previous publication Yuan et al. (2023a); the stems of mulberry plants with typical bacterial blight symptoms were selected (Figure 3; Table 1) and washed with soapy water and then rinsed with tap water for five min. Tissue blocks of approximately 0. 5 cm×0. 5 cm×0. 5 cm were cut at the junction of diseased and healthy portion. Blocks were disinfected with 75% ethanol for 30 s, soaked in 0. 1% mercuric chloride for five minutes, rinsed with sterile water for three times, and dried using sterile filter paper. After drying, tissue block were cut into pieces under sterile conditions and put into a conical bottle containing sterile saline in the constant temperature shaker (Shanghai bluepard instruments Co., ltd) at 28°C and 180 rpm, separating fluid sample at 2h and 12h. Three technical replicates were used for each mulberry sample. To increase the opportunity of isolating the diverse bacteria, a culturomics strategy was devised. This strategy included two different culture media (described below) used for the bacterial isolation. After shaking, samples were subjected to a 10 fold gradient dilution, and

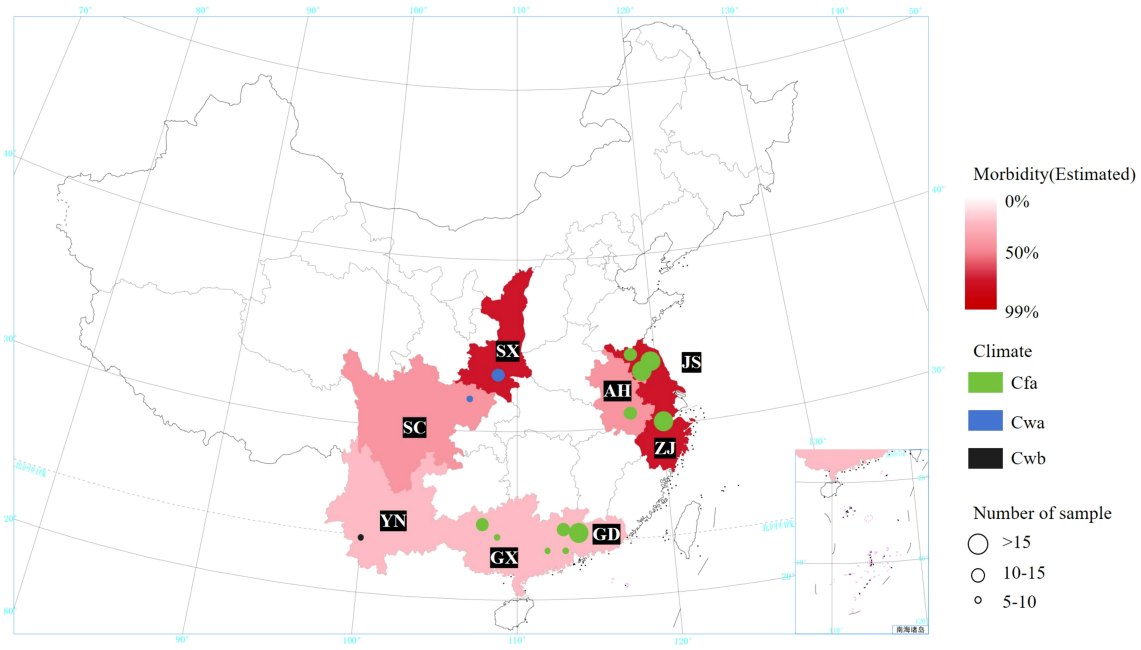


FIGURE 2
Information on Mulberry Bacterial Blight samples and collection locations. SX, Shaanxi province; SC, Sichuan province; YN, Yunnan province; GD, Guangdong province; ZJ, Zhejiang province; JS, Jiangsu province; AH, Anhui province; GX, Guangxi Zhuang autonomous region. Cfa, Humid subtropical climate; Cwa, Dry-winter humid subtropical climate; Cwb, Dry-winter subtropical highland climate.

then 100μL aliquots from $1 \times 10^4$ to $1 \times 10^8$ gradient were taken and coated on the Luria Bertani (LB) agar medium (Peptone 10g·$L^{-1}$, Yeast Extract 5g·$L^{-1}$, NaCl 5g·$L^{-1}$, D-Glucose 1g·$L^{-1}$, Agar 18g·$L^{-1}$, pH 7. 0) and Nutrient agar (NA) medium (Peptone 10g·$L^{-1}$, Beef Extract 3g·$L^{-1}$, NaCl 5g·$L^{-1}$, Agar 18g·$L^{-1}$, pH 7. 0) (Sarkar et al., 2022). At least three technical replicates were used for each gradient on different culture media.

### 2.3.2 Purification and cryopreservation of bacterial cultures

As previously described by Singh et al., 2017, colonies were picked from primary isolation media once every two days, for eight days, and subcultured onto new plates. All isolated strains were subcultured in the LB agar medium until they grew well. Colony morphology, texture, color and consistency were comprehensively assessed to ensure that only pure cultures of a single bacterial species were present on each medium. Pure cultures were stored on plates and agar slants for short periods, and colonies were also placed in sterile 30% glycerol and stored at −80°C for future use (Vanneste et al., 2013).

### 2.3.3 Bacterial 16S rRNA identification

Nucleic acids were extracted from pure cultures of the bacterial strains using a modified CTAB method. The *16S rDNA* was then amplified by PCR using bacterial 16S universal primers 27F (5'-AGAGTTTGATCCTGGCTCAG-3') and 1492R (5'-GGTTACCTTGTTACGACTT-3') (Weisburg et al., 1991). The PCR reaction system (25 μL) comprised of 2x Taq MIX 12. 5 μL (Genesand Biotech Co., Ltd), forward primer 1 μL, reverse primer1 μL, template DNA 1 μL, and dd $H_2O$. The PCR (Takara Bio Inc. Japan) reaction conditions were as follows: denaturation at 94°C for 5 min, followed by 33 cycles of: denaturation at 94°C for 30 s, annealing at 55°C for 30 s, extension at 72°C for 90 s, final extension at 72°C for 10 min. The PCR amplification products were subjected to analysis via 1. 2% agarose gel electrophoresis to confirm the size of the target amplicons. After gel extraction, the fragments were purified and sent to Sangon Biotech (Shanghai) Co., Ltd. for bidirectional sequencing. The obtained *16S rRNA* gene sequences were then assembled and submitted to the NCBI for BLAST analysis to facilitate identification of bacterial species (Ye et al., 2006). Phylogenetic trees were constructed using ML (maximum likelihood) method (MEGA 11 software) (Shen et al., 2002). Finally, based on the BLAST alignment results, strains with percent identity between 95% and 97%, query cover between 95% and 100%, were preliminarily identified at the genus level, while those with percent identity between 97% and 100%, query cover between 99% and 100%, were preliminarily identified at the species level (Gilbert et al., 2010).

## 2.4 Pathogenicity testing of pathogenic bacteria

As described by Chen et al. (2021), the species or genus of each isolate were initially identified based on the *16s rRNA* comparison

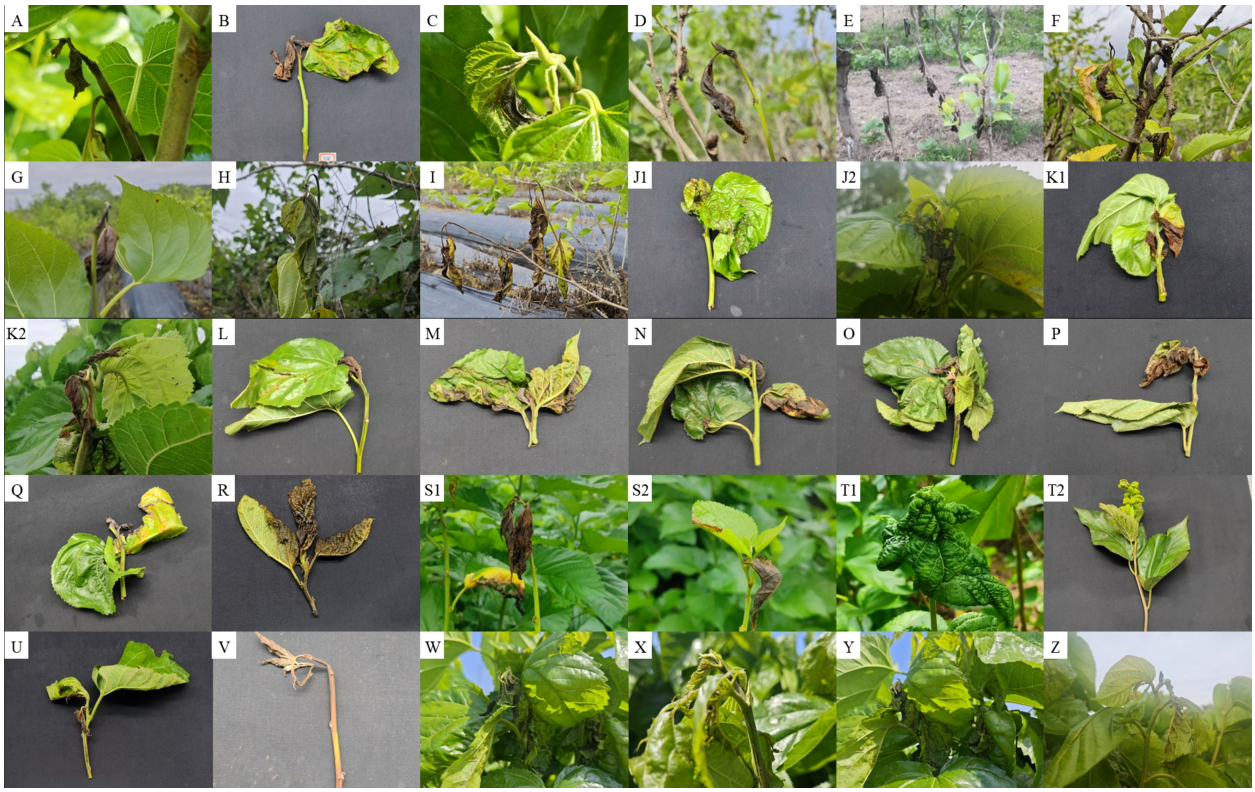


FIGURE 3
Samples of Mulberry bacterial blight collected from different locations. **(A)** Hai'an, Jiangsu sample (HA). **(B)** Dafeng, Jiangsu sample (DF). **(C)** Huanjiang, Guangxi sample (A). **(D)** Qingyuan, Guangdong sample (ZA1-5). **(E)** Zhongshan, Guangdong sample (ZA6). **(F–I)** Zengcheng, Guangdong sample (ZC). **(J1, J2)** Hangzhou, Zhejiang sample (P1-P8). **(K1, K2)** Nanchong, Sichuan sample (R1-R2). **(L)** Yancheng, Jiangsu sample (S1). **(M)** Nantong, Jiangsu sample. **(N)** Dongtai, Jiangsu sample (S2). **(O, P)** Sheyang, Jiangsu sample (S3, S4). **(Q)** Ankang, Shanxi sample (T1). **(R)** Puer, Yunnan sample (U). **(S1, S2)** Mashan, Guangxi sample (W). **(T1, T2)** Hefei, Anhui sample (X). **(U)**, Sheyang, Jiangsu sample (S6). **(V)** Yunan, Yunfu sample(Y). **(W)** Haining, Zhejiang sample (P1-P8). **(X)** Yancheng, Jiangsu sample (S5). **(Y)** Fuyang, Anhui sample (ZD). **(Z)** Hanyin Shanxi sample (ZL).

results. Bacterial colony composition of samples were identified using metagenomic and culturomics results. Bacteria that co-appeared in the results of the two identification methods were initially screened and tentatively designated as suspected pathogenic bacteria. In addition, the pathogens of several common plant diseases were screened out based on existing literature reports (Luo et al., 2022; Yuan et al., 2023a; Popović et al., 2021). The bacteria were selected according to the principle of taking at least two strains from each different sample as biological replicates, and the pathogenicity test was performed. Briefly, pure cultures of all suspected pathogenic bacteria were incubated overnight in the LB liquid culture medium, centrifuged at 5000 rpm for three min to collect the bacterial cells, then diluted with sterile water to $1\times10^7$.

Healthy mulberry plants were taken and the inoculation site was selected at the surface of the branch between 2-3 true leaves below the top bud. The selected inoculation site was disinfected with 75% alcohol, then 500 μL of bacterial suspension was slowly injected into the plant tissue with a sterile syringe, and inoculation site was wrapped the with sterile gauze. The samples were placed in a constant temperature and light incubator at 28°C, RH 85-95%, and 12h: 12h light cycle. The sterile water injection was used as the control (CK) group. Three technical replicates were used for each strain.

The disease situation was observed and the disease index (Di) was calculated after three days (Krawczyk and Łochyńska, 2020). The Di was calculated as follows:

$$D_i = \sum \frac{D_l * N_d}{N_t * N_s}$$

Di: Disease Index
Dl: Disease Level
Nd: number of disease tender leaves
Nt: number of total tender leaves
Ns: number of biological replicates

After the bacteria were re-inoculated, the samples that showed symptoms of disease were isolated and cultured to observe whether the bacteria inoculated in the sample could be re-isolated. The re-isolated bacteria were molecularly identified based on 16s rDNA, as mentioned in 2. 3. 1 to 2. 3. 3 of materials and methods. For clarity. the pathogens isolated/identified through the pathogenicity test were named as the "isolated" group. The phylogenetic tree including all pathogens was constructed using ML method (MEGA11 software).

## 2.5 Metagenomic sequencing of re-inoculated samples

Upon exhibition of typical symptoms, samples from two experimental groups were collected, including re-inoculated samples with *P. syringae* strain AHDX and re-inoculated samples with *P. syringae* strain ZJDX. The samples re-inoculated with *P. syringae* strain AHDX were designated as AHHG, and those re-inoculated with *P. syringae* strain ZJDX were designated as ZJHG. One group in which sterile water was inoculated to mulberry samples was designated as control (CK). For each group, three technical replicates were used, totaling nine samples. Metagenomic sequencing was performed to observe the microbial composition of the samples. The steps were essentially the same as described in 2. 2.

## 2.6 Correlation analysis between pathogenic bacteria and meteorological factors

As per the method of Rosario et al. (2020), Shapiro Wilk's test was applied to evaluate the normality of the data. The data on bacterial isolation showed non-normal distribution, so the relationship between meteorological factors and bacteria was studied using the Spearman rank correlation test.

## 2.7 Data statistics, processing, and visualization

The data were prepared via Microsoft Excel 2019 (Microsoft, USA). The normalized abundances of bacteria at the species-level were analyzed via SPSS software (v21. 0), and the results were visualized with Origin 2024b. Heatmap visualization of the pathogenic bacteria and meteorological data was performed via the "heatmap" package in R software (v4. 3. 2). Alpha diversity was calculated using the picante package, PcoA analysis and sample significance tests were conducted using the vegan package, the Welch's t-test was employed for T-tests. PLS-DA analysis was performed using the mixOmics package, and ggpubr was used for plotting. Phylogenetic tree construction was performed using MEGA11 and iqtree2 software, using the ML method. The refinement of the evolutionary tree was completed using the iTol online (https://itol.embl.de/) website (Letunic and Bork, 2016).

# 3 Results

## 3.1 Metagenomic sequencing results of MBB samples

### 3.1.1 Sequencing results and quality control checks

The metagenomic sequencing yielded raw data of 4737133500 bp sequence, 31580890 reads, with a GC content of 52. 55%. Q30 and Q20 were both greater than 90%, indicating that sequencing results were of good quality and reliable. After quality control, clean data of 4477161900 bp was obtained, with a total of 29847746 reads. The GC content was 52. 72%, and Q20 and Q30 were both greater than 90%. To eliminate the influence of the host genome, mulberry genome GCA_012066045. 3 and OP161261. 1 were used as host controls (Jiao et al., 2020). After removing the influence of host genomes from clean data, a total of 6312994 reads were removed, accounting for 21. 15% of the total clean data. After the above quality control, 23534752 reads were finally obtained, including the longest fragment of 284255 bp, the shortest fragment of 56 bp, an average fragment length of 459bp, N50 345, L50 1727, and a GC content of 52. 48% (Supplementary Table 1).

### 3.1.2 Sequence tag annotation, diversity analysis, and screening of suspected pathogens

After annotation, it was observed that the microbial composition of the samples was at the phylum and genus levels. The relative abundance of Proteobacteria was the highest at the phylum level (99. 83%) (Figure 4A), and *Pseudomonas* spp. was the highest at the genus level (99. 24%) (Figure 4B). Based on the analysis of microbial species and quantity, combined with the examination of symptoms and relevant information, it was preliminarily determined that the suspected causal pathogen of MBB was *Pseudomonas* spp. (Figure 4C). The complete ribosome sequence of the suspected pathogenic bacteria was assembled from metagenomic data, and the total length of the ribosome sequence of the *Pseudomonas* spp. was approximately 5251bp, with a GC ratio of 52. 24% (Supplementary Table 2). The length information of the 16S/18S, ITS1, 23S/28S, ITS2, 5S/5. 8 intervals is shown in the Supplementary Figure 1. Based on *16Sr RNA* sequence alignment and construction of evolutionary tree, it was found that it clustered with *P. syringae*, suggesting that the suspected pathogens were all *P. syringae* (Figure 4D).

## 3.2 Culturomics results

### 3.2.1 Bacterial isolation

A total of 103 samples were collected from 26 different times, locations or species in 20 different areas of eight provinces, and a total of 498 bacterial strains were isolated by culturomics. They were distributed in four phyla, six classes, 11 orders, 18 families and 48 genera (Table 2). At the phylum level, Proteobacteria was the most dominant community in all samples (410/502), and *Pseudomonas* spp. was the most frequently isolated genus at the genus level (138/410). Firmicutes was the second most dominant bacterial group, and at the genus level, *Paenibacillus* spp. showed the highest isolation frequency of 33/52. A total of 23 bacterial strains were isolated from *Actinobacteria* spp. *Curtobacterium* spp. and *Microbacterium* spp. were the two genera with the highest isolation frequency of 4/23, both of which were from Microbacteriaceae. In addition, we also isolated 13 strains of Bacteroidetes, with *Flavobacterium* spp. being the most abundant genus (9/13) (Table 2).

### 3.2.2 Assessment of climate type of sample site and sample alpha diversity

We used the Köppen climate classification to estimate the climate types of the eight sample source regions. There were four

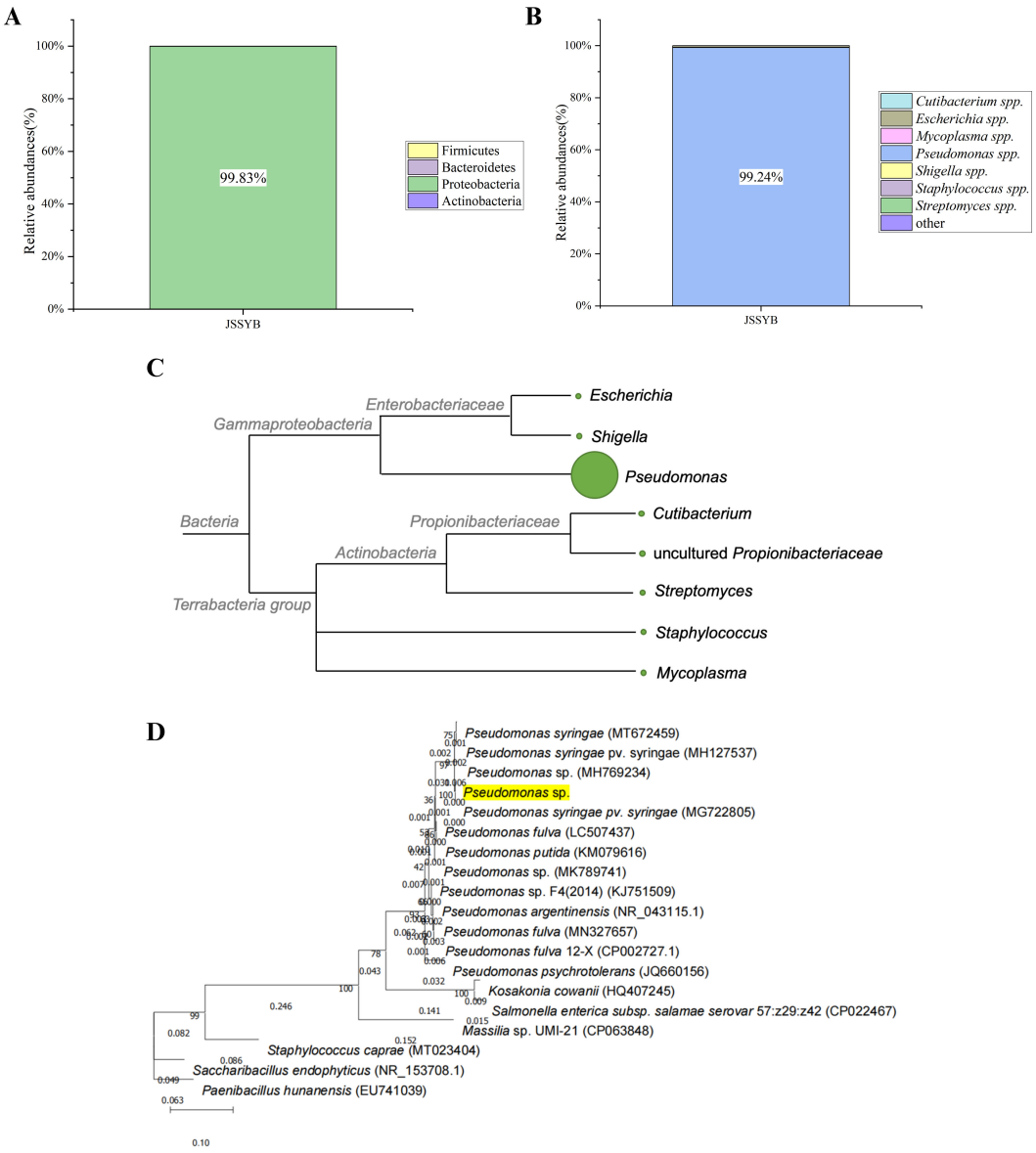


FIGURE 4
Metagenomic sequencing results of mulberry bacterial blight sample S1. **(A)** Relative abundance of bacteria at the phylum level. **(B)** Relative Abundance of Bacteria at the genus Level. **(C)** Cluster tree representing genetic relationships, with circle size indicating relative abundance of the genus. **(D)** Phylogenetic Tree based on rRNA (5S, 16S, 28S).

groups (GX, GD, ZJ, and JS) of Cfa type, three groups (SC, SX, and AH) of Cwa type, and one group (YN) of Cwb type. As for the alpha diversity, it was found that the Shannon index of the Cfa type climate sample community was greater than that of the Cwa and Cwb types, while the Simpsen index of Cfa was greater than that of Cwb and Cwa types (Table 3; Figure 2).

### 3.2.3 Bacterial community composition of samples

The bacterial community composition of eight samples was calculated at the phylum and genus levels. At the phylum level, Proteobacteria was the most dominant community in each group (Figure 5A). Except for the GX and AH samples, *Pseudomonas* spp. was the most frequently identified genus in other samples. The most frequently identified genus in GX samples was *Bacillus* spp. (8/32; 25.00%), and the most frequently identified genus in AH samples was *Enterobacter* spp. (4/17; 23.53%) (Figure 5B). Overall, *Pseudomona* spp., *Pantoea* spp., and *Enterobacter* spp. were the most frequently identified genera in each group, and *Pseudomona* spp. co-appeared in eight groups (Figure 5D). The relative abundance bubble chart also showed that *Pseudomonas* spp., *Pantoea* spp., and *Enterobacter* spp. are widely present in each group (Figure 5C). At the family level, except for *Pseudomonas* spp. from Pseudomonadales, the other three genera were all from Enterobacterales (Table 2).

10.3389/fpls.2025.1517050

TABLE 2 Cumulative list of taxonomic information of culturable bacteria from mulberry bacterial blight samples.

| Phyla | Classes | Orders | Families | General |
|---|---|---|---|---|
| Actinobacteria (23) | Actinobacteridae (23) | Actinomycetales (23) | Microbacteriaceae (19) | Cellulomonas *spp.* (2) |
| | | | | Curtobacterium *spp.* (4) |
| | | | | Gottfriedia sp. (1) |
| | | | | Leucobacter *spp.* (2) |
| | | | | Mammaliicoccus *spp.* (2) |
| | | | | Microbacterium spp. (4) |
| | | | | Niallia *sp.* (1) |
| | | | | Priestia *spp.* (3) |
| | | | Micrococcaceae (1) | Brevibacterium *sp.* (1) |
| | | | Nocardioidaceae (1) | Nocardioides *sp.* (1) |
| | | | Propionibacteriaceae (2) | Luteococcus spp. (2) |
| Bacteroidetes (13) | Flavobacteria (13) | Flavobacteriia (12) | Flavobacteriaceae (12) | Chryseobacterium *spp.* (3) |
| | | | | Flavobacterium *spp.* (9) |
| | | Rhodobacterales (1) | Alcaligenaceae (1) | Atlantibacter *sp.* (1) |
| Firmicutes (52) | Bacilli (52) | Bacillales (50) | Bacillaceae (15) | Bacillus *spp.* (11) |
| | | | | Exiguobacterium *sp.* (1) |
| | | | | Saccharibacillus *spp.* (3) |
| | | | Paenibacillaceae (34) | Paenibacillus *spp.* (33) |
| | | | | Paenimyroides sp. (1) |
| | | | Staphylococcaceae (1) | Staphylococcus *sp.* (1) |
| | | Lactobacillales (2) | Streptococcaceae (2) | Lactococcus sp. (1) |
| | | | | Aerococcus *sp.* (1) |
| Proteobacteria (410) | Alphaproteobacteria (3) | Rhizobiales (3) | Methylobacteriaceae (1) | Methylorubrum *sp.* (1) |
| | | | Rhizobiaceae (2) | Agrobacterium *spp.* (2) |
| | Betaproteobacteria (10) | Burkholderiales (10) | Comamonadaceae (10) | Comamonas *spp.* (7) |
| | | | | Paracidovorax *spp.* (3) |
| | Gammaproteobacteria (397) | Enterobacterales (233) | Enterobacteriaceae (233) | Buttiauxella *spp.* (6) |
| | | | | Citrobacter *spp.* (10) |
| | | | | Cnuibacter *sp.* (1) |
| | | | | Enterobacter *spp.* (35) |
| | | | | Erwinia *spp.* (6) |
| | | | | Escherichia *spp.* (4) |
| | | | | Klebsiella *spp.* (7) |
| | | | | Kosakonia *spp.* (43) |
| | | | | Kluyvera *spp.* (13) |
| | | | | Leclercia *spp.* (8) |
| | | | | Lelliottia *spp.* (3) |
| | | | | Pantoea *spp.* (74) |
| | | | | Pectobacterium *spp.* (11) |

*(Continued)*

TABLE 2 Continued

| Phyla | Classes | Orders | Families | General |
|---|---|---|---|---|
| | | | | Pseudescherichia *spp.* (2) |
| | | | | Rahnella *spp.* (9) |
| | | | | Yersinia sp. (1) |
| | | Pseudomonadales (143) | Moraxellaceae (5) | Acinetobacter *spp.* (5) |
| | | | Pseudomonadaceae (138) | Pseudomonas *spp.* (138) |
| | | Sphingomonadales (2) | Sphingomonadaceae (2) | Sphingomonas spp. (2) |
| | | Xanthomonadales (19) | Xanthomonadaceae (19) | Pseudoxanthomonas *spp.* (2) |
| | | | | Stenotrophomonas *spp.* (15) |
| | | | | Xanthomonas *spp.* (2) |

The numbers within parentheses indicate the quantity of culturable bacteria strains belonging to this classification.

### 3.2.4 Screening and distribution of suspected pathogens

To further screen the MBB pathogenic bacteria, we compared the culture group isolation and identification results with the metagenomic sequencing results at the species level. Six common bacterial species, including *P. syringae, P. fulva, P. oryzihabitans, P. fluorescens, P. viridiflava, and E. coli* were found to be common (Figure 6A). In this experiment, based on comprehensive consideration about the isolation frequency, relative abundance and previously reported genera/species of pathogenic bacteria, we screened 109 strains of suspected pathogenic bacteria, including 27 species from 12 genera, and analyzed their distribution in each group. We found that there were no species that appeared in common in the eight groups (Figure 6B). The top three most widespread species appearing in all groups were *P. syringae, P. fulva* and *P. agglomerans* (Figures 6C, D).

### 3.2.5 Pathogenicity tests of suspected pathogens

To further verify the pathogenicity of all suspected pathogens, we conducted pathogenicity tests on Qiangsang No. 1 mulberry to verify Koch's postulates. The pathogenicity test results showed that from 27 suspected pathogenic bacterial species tested, the disease index of 10 species was significantly higher than that of the blank control ($P$<0. 05). These species included *P. syringae, P. fulva, P. fluorescens, Pectobacterium carotovorum, P. parvum, Stenotrophomonas maltophilia, K. grimontii, C. portucalensis, P. ananatis*, and *F. fluviale*, (Figure 7A). It was found that *P. carotovorum* was the most virulent strain (Figure 7B). The phylogenetic tree of the 10 pathogenic bacteria was constructed. They were found to be distributed in two Phyla (Bacteroidetes, Proteobacteria) and classified into the same species as the respective pathogens of the re-inoculated groups. (Figure 8).

### 3.2.6 Distribution of pathogens, correlation analysis between meteorological factors and pathogens

In order to analyze whether these 10 pathogens were widely distributed, the distribution of 10 pathogens in samples from the eight provinces was statistically analyzed. Briefly, *P. syringae* was isolated from samples from six provinces with a frequency of 75% (6/8). *P. fulva* was isolated from samples from four provinces with a frequency of 50% (4/8). *P. ananatis* and *S. maltophilia* were isolated from samples from two provinces with a frequency of 25% (2/8). *P. fluorescens, P. parvum, F. fluviale, C. portucalensis, K. grimontii* and *P. carotovorum* were only isolated from samples from one province, with a frequency of 12.5% (1/8) *F. fluviale*, *C. portucalensis*, and *K. grimentii* were only distributed in the cwa climate region, and only *P. syringae* was found in the cwb climate region (Figures 9A, B).

TABLE 3 Diversity profile of the Mulberry Bacterial Blight wilt communities in mulberry.

| | Province/Location | | | | | | | | Climate type | | |
|---|---|---|---|---|---|---|---|---|---|---|---|
| | GX | GD | ZJ | SC | JS | YN | AH | SX | Cfa | Cwa | Cwb |
| Number of isolates | 32 | 106 | 178 | 25 | 104 | 24 | 17 | 12 | 420 | 54 | 24 |
| Number of genera | 12 | 19 | 20 | 4 | 10 | 9 | 17 | 3 | 41 | 17 | 10 |
| Shannon | 3. 19 | 3. 30 | 3. 81 | 1. 62 | 2. 08 | 2. 66 | 3. 38 | 1. 19 | 2. 71 | 2. 06 | 1. 84 |
| Simpson | 0. 89 | 0. 87 | 0. 90 | 0. 65 | 0. 70 | 0. 83 | 0. 94 | 0. 53 | 0. 88 | 0. 80 | 0. 83 |
| Pielou's evenness | 0. 89 | 0. 78 | 0. 88 | 0. 81 | 0. 63 | 0. 84 | 0. 94 | 0. 75 | 0. 73 | 0. 74 | 0. 84 |
| Berger-Parker | 4. 00 | 4. 82 | 4. 34 | 2. 08 | 2. 60 | 3. 00 | 4. 25 | 1. 50 | 3. 89 | 2. 45 | 3. 00 |

SX, Shaanxi province; SC, Sichuan province; YN, Yunnan province; GD, Guangdong province; ZJ, Zhejiang province; JS, Jiangsu province; AH, Anhui province; GX, Guangxi Zhuang autonomous region; Cfa, Humid subtropical climate; Cwa, Dry-winter humid subtropical climate; Cwb, Dry-winter subtropical highland climate.

10.3389/fpls.2025.1517050

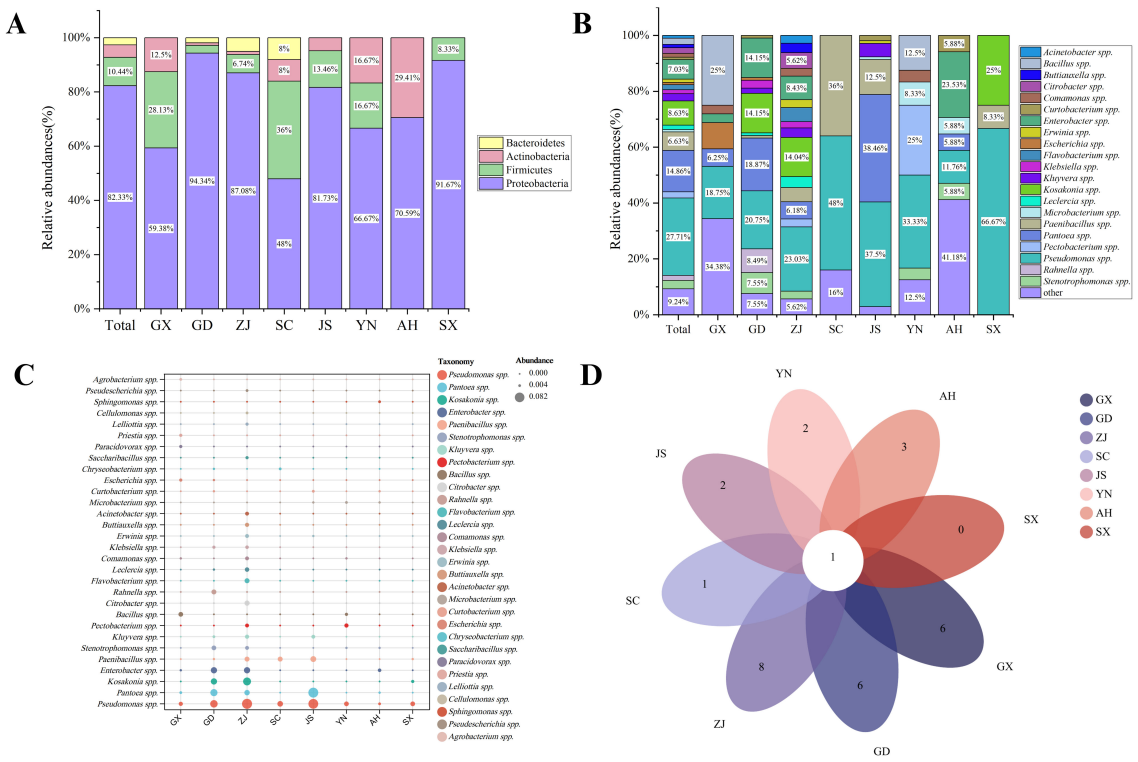


FIGURE 5
Results of bacterial communities isolated by culturomics. **(A)** Culturomics analysis of microbial composition of mulberry bacterial blight samples at the phylum level. **(B)** Culturomics analysis of microbial composition of mulberry bacterial blight samples at the genus levels. **(C)** Distribution of isolated bacteria across samples from eight different locations. **(D)** Venn analysis of the common and unique bacteria in samples from eight different locations.

In this analysis, the distribution result of the above 10 bacteria in samples from different regions was combined with the local meteorological data to calculate the Spearman rank correlation test. As shown in the heatmap (Figure 9C), the occurrence of *P. syringae* was positively correlated with PRCP, WDSP, and TEMP, and was extremely significantly positively correlated with SSD ($P<0.01$). The occurrence of *P. fulva* was only positively correlated with RH, not correlated with PRES and PRCP, negatively correlated with TEMP and SSD, and significantly negatively correlated with WDSP. *P. fluorescens* was positively correlated ($P>0.05$) with PRES, and had no correlation or negative correlation ($P>0.05$) with the other environmental factors. The occurrence of *P. ananatis* was positively correlated with PRES and WDSP, and negatively correlated with RH, PRCP, and TEMP. The occurrence of *P. parvum, F. fluviale, C. portucalensis, K. grimontii, P. carotovorum, S. maltophilia* was positively correlated with RH and PRCP (Figure 9C).

## 3.3 Results of metagenomic sequencing of re-inoculated samples

The read numbers in the raw data were between 13247304 and 32796380, and the base numbers were between 1987095600 and 4919457000 bp. After quality control, clean data was obtained, with read numbers between 12769796-31651202 and base numbers between 1915469400 and 4747680300bp. The Q30 and Q20 of all samples were greater than 90%, indicating good sequencing quality. The data of all samples are listed in Supplementary Table 4.

Analysis of the bacterial community composition of CK, AHHG, and ZJHG groups revealed that Proteobacteria was the most dominant bacterial group in all samples. Compared with CK samples, the relative abundance of Proteobacteria decreased in AHHG and ZJHG samples, while the relative abundance of Firmicutes and Actinobacteria increased (Figure 10A). The relative changes in abundance of bacterial composition at the genus level between CK, AHHG, and ZJHG showed a decrease in *Klebsiella* spp. and *Stenotrophomonas* spp., and an increase in *Pseudomonas.* spp. (Figure 10B).

To screen the changes in bacterial distribution in samples after MBB pathogen re-inoculation, we analyzed the common bacterial species in the CK, AHHG, ZJHG, and isolated groups. As shown in the Venn diagram (Figure 11A), a total of 66 bacterial species were found common in AHHG and ZJHG groups, five bacterial species were common in AHHG, ZJHG, and isolated groups. Meanwhile, there were nine bacterial species that only appeared in the CK group. The PCoA analysis was used to compare the similarities or differences between the CK and AHHG and ZJHG groups. The results showed that the bacterial communities between healthy and infected mulberry plants were different, and there were obvious changes at the species-level composition after *P. syringae* strain AHDX, and *P. syringae* strain ZJDX infection (Figure 11B). The results of PLS-DA analysis showed a significant difference in the bacterial composition between the CK and AHHG groups. There

10.3389/fpls.2025.1517050

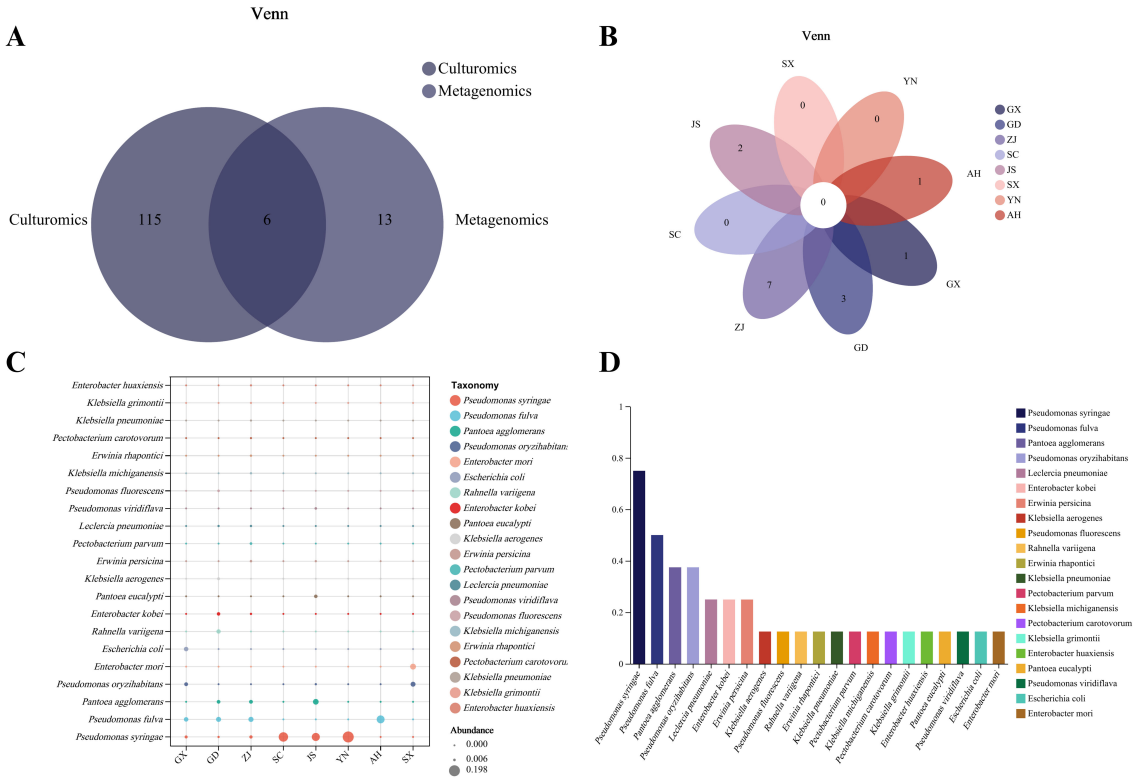


FIGURE 6
Results of metagenomic sequencing and culturomics. **(A)** Venn analysis of metagenomic sequencing and culturomics isolation and identification results. **(B)** Venn analysis of the presence of suspected pathogens in various isolated samples. **(C)** Relative abundance distribution of suspected pathogens in each sample. **(D)** Isolation rate of suspected pathogens in each sample.

was a significant difference in the bacterial composition between the CK and ZJHG groups. There was also a significant difference in the bacterial composition between ZJHG and AHHG groups (Figure 11C). Non-metric multidimensional scaling (NMDS) analysis showed that the CK, AHHG, and ZJHG groups clustered in a separate cluster (Figure 11D).

The Student's *t* test (*t* test) showed changes in several pathogenic bacteria in the control and re-inoculated groups. The statistical analysis showed that the relative abundance of *P. syringae*, and *P. fluorescens* increased significantly ($P$ <0. 01) in the AHHG group compared to the CK group after infection (Figure 12A). Based on the color schemes, it was observed that the relative abundance of *P. fulva, C. portucalensis*, and *K. grimonti* increased, but the changes were not significant ($P$>0. 05) (Figure 12B). Following ZJHG infection, compared with the CK group, the relative abundance of *P. syringae*, *P. fluorescens*, increased significantly ($P$<0. 05) (Figure 12C). The relative abundance of *P. fulva*, *P. carotovorum*, *P. ananatis*, *K. grimonti* also increased but these changes were not significant ($P$>0. 05) (Figure 12D).

## 4 Discussion

In the present study, we used combined high-throughput metagenomic sequencing, culturomics, and pathogenicity test (validation by the Koch's postulates) approaches to analyze the bacterial community composition and diversity in MBB samples collected from different field locations in the eight provinces of China. Based on the omics results and screening of suspected pathogens through pathogenicity test and changes in distribution pattern, *P. syringae*, and *P. fulva* were inferred to be important causal pathogens of MBB in samples analyzed. In addition, microbiome and meteorological data were further analyzed to draw a potential relationship between key causal pathogens and relevant meteorological factors. The identified pathogens showed adaptability to different environments, and that the changes in distribution of causal pathogens of MBB were linked with different climatic conditions of the studied locations.

The MBB samples collected from Jiangsu province showing typical disease samples were used for high-throughput metagenomic sequencing. We found that the microbiome of MBB samples was dominated by bacteria, while eukaryotes (fungi) only accounted for a small proportion (data not shown) of the sequences related to the known taxonomic groups. Given that the classification methods used for identification of microbial community composition based on metagenomic sequencing are based on reference uploaded sequence annotations, and that the reference genomes for most eukaryotes are not available (Bulgarelli et al., 2015), therefore, eukaryote (fungi) sequences weren't taken into the account. Consistent to finding of our study, a previous study (Xu et al., 2018) using metagenomic sequencing to

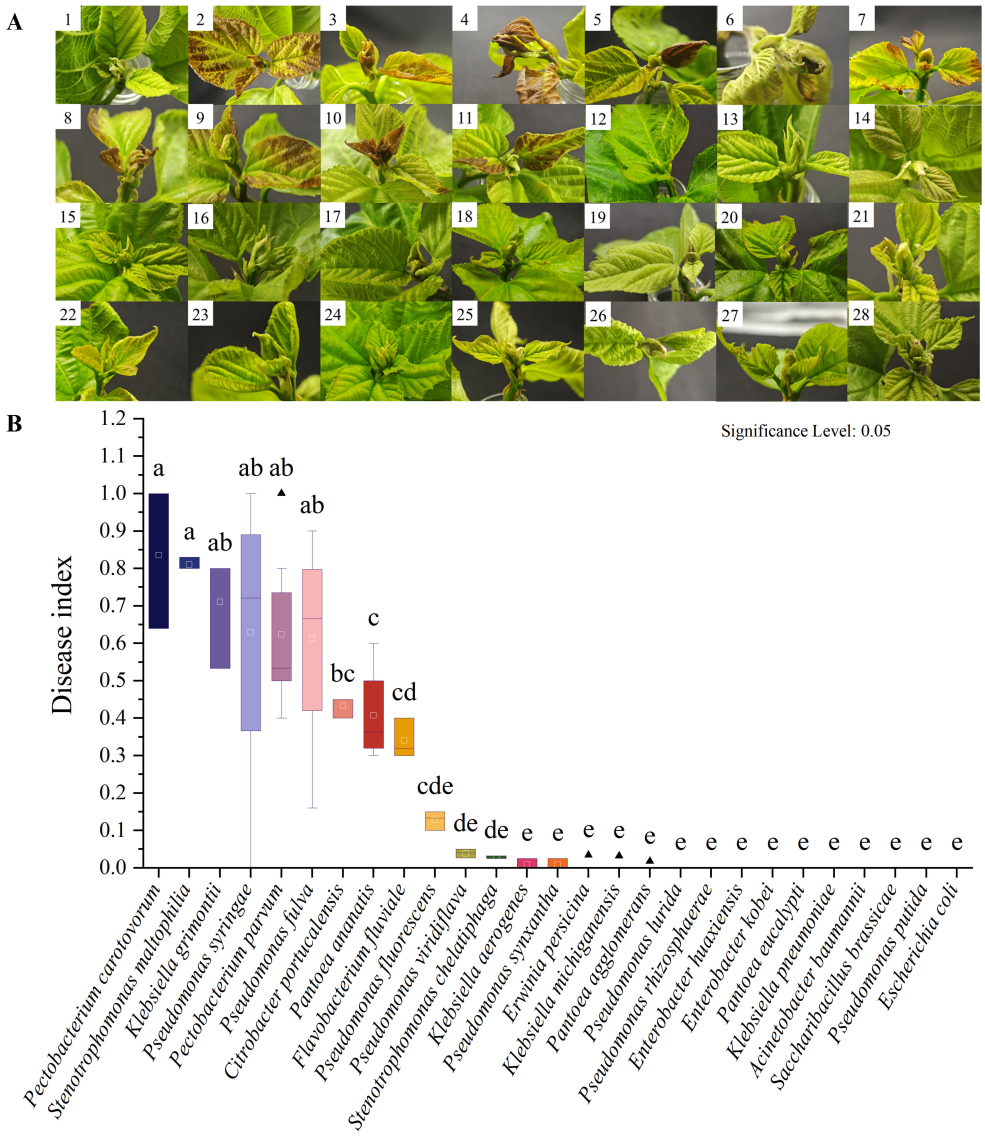


FIGURE 7
Results of pathogen verification by pathogenicity test. **(A)** Pathogenicity test results for 27 suspected pathogens. 1: CK. 2: *P. syringae* R2-2. 3: *P. fulva* P1-2-1. 4: *P. carotovorum* P7-24-3. 5: *P. fluorescens* ZA4-12. 6: *P. parvum* P7-2-5. 7: *F. fluviale* P5-24-1. 8: *C. portucalensis* P7-24-9. i: *K. grimontii* P7-24-8. 10: *S. maltophilia* P4-2-9. 11: *P. ananatis* ZA1-2. 12: *Pseudomonas lurida* P4-2-4. 13: *Pseudomonas rhizosphaerae* P2-24-16. 14: *Enterobacter huaxiensis* P7-2-2. 15: *P. agglomerans* ZA2-2. 16: *Klebsiella aerogenes* ZA4-8. 17: *Enterobacter kobei* ZK11. 18: *Pseudomonas synxantha* P4-24-1. 19: *Pantoea eucalypti* S1-1. 20: *Erwinia persicina* S1-10. 21: *P. viridiflava* S2-16. 22: *Klebsiella pneumoniae* P8-24-10. 23: *Acinetobacter baumannii* P8-24-12. 24: Saccharibacillus brassicae P8-24-13. 25: *Pseudomonas putida* P3-24-9. 26: *K. michiganensis* P3-24-13. 27: *Stenotrophomonas chelatiphaga* P4-2-10. 28: *E. coli* ZD6. **(B)** Disease index results for 27 suspected pathogens.

analyze the microbiome of the citrus rhizosphere, reported that 99. 55% of the non-redundant genes were assigned to prokaryotic (bacteria and archaea), while only 0.17% of the non-redundant genes were annotated as eukaryotic (fungi, protozoa, algae, and plants).

In recent times, high-throughput omics techniques like metagenomic sequencing are increasingly used in the field of plant disease/pathogen research (Tyler et al., 2009). It is said that the "rare" biosphere is actively attracted by specific environments, and may play an important role despite their low abundance (Hartmann and Six, 2023). While the vast majority of microorganisms (bacteria and archaea) referred to as "microbial dark matter" still remains underexplored, the refined high-throughput culturomics techniques have the capacity to illumine the previously unculturable bacterial species (Dickson, 2017). However, use of culturomics is relatively new and substantially lagging behind in plant microbiome research (Sarhan et al., 2019).

It is no surprise that the reduced cost and the level of sequence coverage of samples are the key driving factors for use of these techniques in future studies on complex plant pathogens. Indeed, previously, metagenomic sequencing has been used to study microbial diversity of plant pathogens and to determine causal pathogens of highly destructive plant diseases (Yuan et al., 2023a; Chen et al., 2021). For instance, metagenomic sequencing was used to evaluate the microbial diversity in the phloem of citrus infected

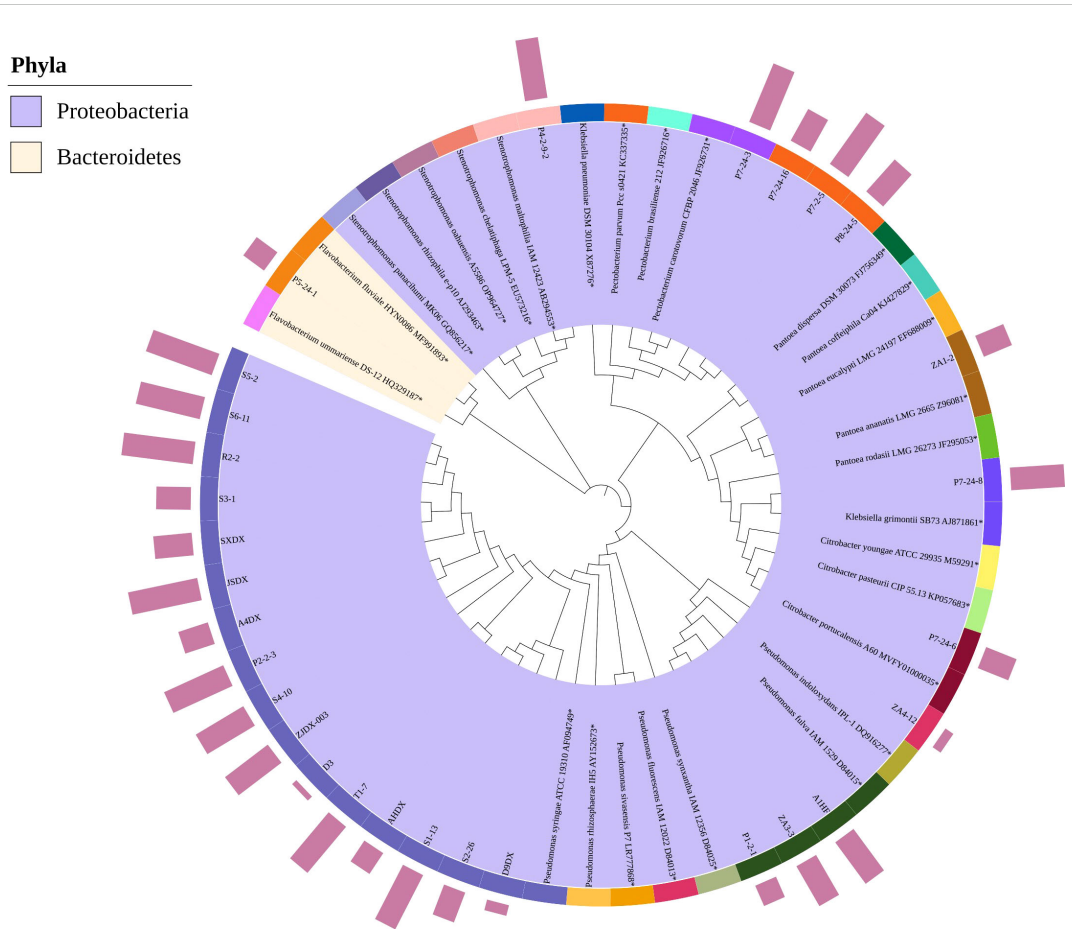


FIGURE 8
Phylogenetic tree of 10 causal pathogenic bacteria of mulberry bacterial blight. The inner circle represents the branching topology of the phylogenetic tree, and the second circle indicates the strain numbers. *Represents the type strain of this species. The color in the second circle denotes the phylum-level classification of the strain, the third circle represents the species-level classification, and the bar chart in the fourth circle indicates the pathogenicity of the strain as tested in this study.

with Huanglongbing (HLB) disease (Tyler et al., 2009). Based on annotation results of metagenomic data, *Candidatus* Liberibacter asiaticus was confirmed to be the causal agent of this disease (Tyler et al., 2009). In the present study, the proportion of Proteobacteria in the MBB field samples at the phylum level reached 99. 83%, and *Pseudomonas* spp. also showed a high relative abundance of 99. 24% at the genus level. This finding was consistent with the previous reports from Turkey (Sahin et al., 1999) and Poland (Krawczyk and Łochyńska, 2020), in which *Pseudomonas syringae* was identified as the causal agent of MBB in mulberry plants. We assembled the rRNA sequences of *Pseudomonas* spp. in diseased samples to construct an evolutionary tree, and found that it clustered with *P. syringae* on the same branch. Therefore, based on these results and verification by pathogenicity test, we inferred that *P. syringae* and other *Pseudomonas* spp. are possibly the main causal pathogens of MBB in samples analyzed in the present study.

The bacterial strains obtained through culturomics are suitable for studying bacteria at the strain level (Zhao et al., 2024). In order to improve the sensitivity and accuracy of detection of pathogenic bacteria, we used culturomics technique alongside metagenomic sequencing and classical culture-dependent approaches. This combined approach provided a more comprehensive understanding of the causal pathogens of MBB samples collected from different study locations. Consistent with the metagenomic results, we were able to isolate and identify a large number of bacteria belonging to the phylum Proteobacteria and Firmicutes and Actinobacteria using culturomics technique. While the frequency of isolation of Bacteroidetes was lower, it was consistent with previously reported results (Anteneh et al., 2022; Singh et al., 2017). In slight contrast to the metagenomic sequencing results, the relative abundance of Proteobacteria decreased at the phylum level, while the relative abundance of Firmicutes, Actinobacteria, and Bacteroidetes increased. Previous research on plant-associated microbial community composition has shown that the plant microbial colonization has tissue preference (Edwards et al., 2015). Given that MBB causes lesions in the terminal buds, it is possible that the microbial communities in the samples analyzed in this study maybe similar to the plant phyllosphere microbiome. Tellingly, this microbiome is considered to be more adapted to the environment inside the plant tissues (Leach et al., 2017), and being quite labile to UV radiation, temperature, and sensitivity to drying and dehydration (Bringel and Couée, 2015). We speculate that many other bacteria belonging to Proteobacteria might be present in the samples but they cannot be isolated under the current culture conditions, or they exist

10.3389/fpls.2025.1517050

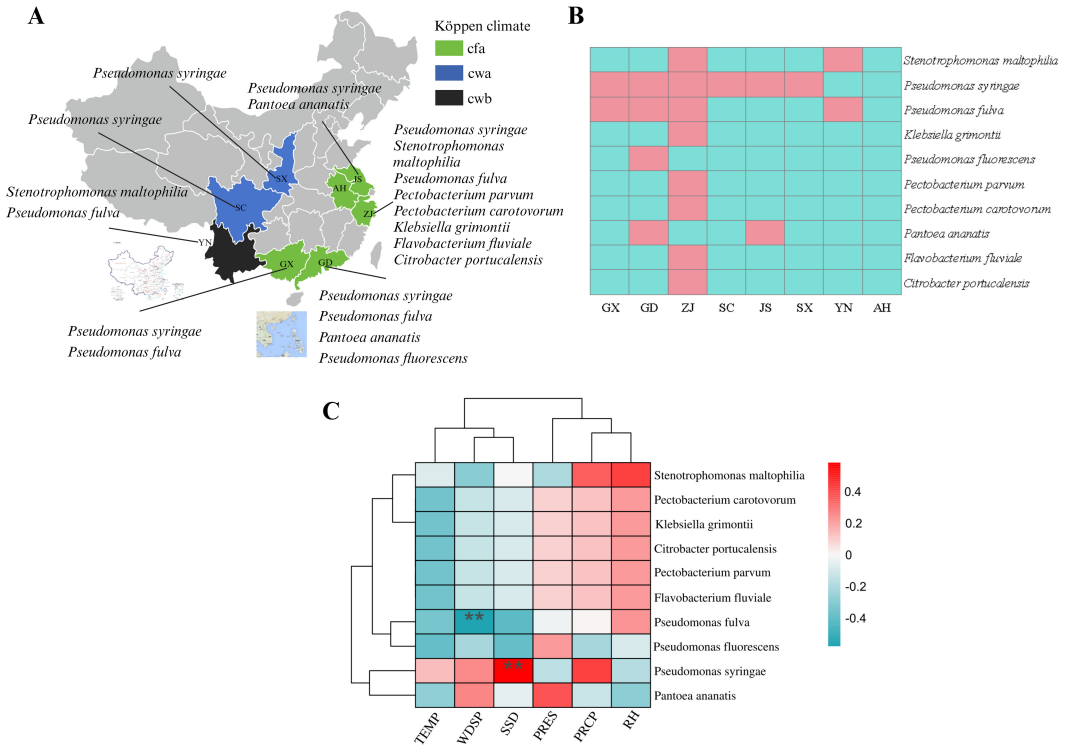


FIGURE 9
Distribution of pathogen and correlation analysis between meteorological factors and pathogens. **(A)** Pathogen distribution in different locations. Cfa, Humid subtropical climate; Cwa, Dry-winter humid subtropical climate; Cwb, Dry-winter subtropical highland climate. **(B)** Heatmap of distribution of 10 pathogenic bacteria in the sample. Red: existence in the sample, blue: non-existent in the sample. **(C)** Heatmap of pathogenic bacteria and local environmental factors. TEMP, Monthly average temperature; SSD, Sunshine duration; PRCP, Monthly total precipitation; RH, Relative humidity; WDSP, Wind direction speed; PRES, Station pressure. Red:, positively correlated, blue: negative correlation. **highly significant correlation ($P$<0. 01).

in the viable but nonculturable (VBNC) state. It is also possible that the critical factors affecting the cultivation of uncultured plant bacteria and suitable culture/media conditions are not known. Therefore, further research and understanding is required to develop strategies employing multiple and customized media to isolate the diverse bacterial communities.

We compared the results of metagenomic sequencing and culturomics, and identified 10 pathogens (*P. syringae, P. fulva, P. fluorescens, P. ananatis, P. parvum, P. carotovorum, F. fluviale, C. portucalensis, K. grimontii, S. maltophilia*) that were able to infect mulberry and caused typical MBB symptoms, as verified through the Koch's postulates. Interestingly, most of these bacteria are reported to be common foliar bacteria that cause serious plant diseases, for example, tomato bacterial speck disease (Elsharkawy et al., 2023; Huot et al., 2017), bacterial canker of kiwifruit (Pei et al., 2023), hazelnut decline disease (Lamichhane et al., 2016), and mulberry bacterial blight (Krawczyk and Łochyńska, 2020). Consistent with the previous studies, we reconfirmed that *P. syringae* is indeed the key

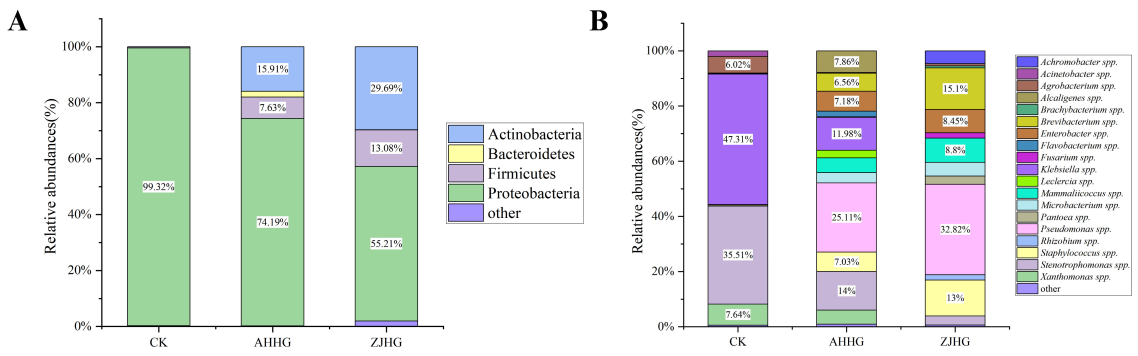


FIGURE 10
Colony composition of control (CK) and re-inoculated samples at the phylum level **(A)** and genus level **(B)**.

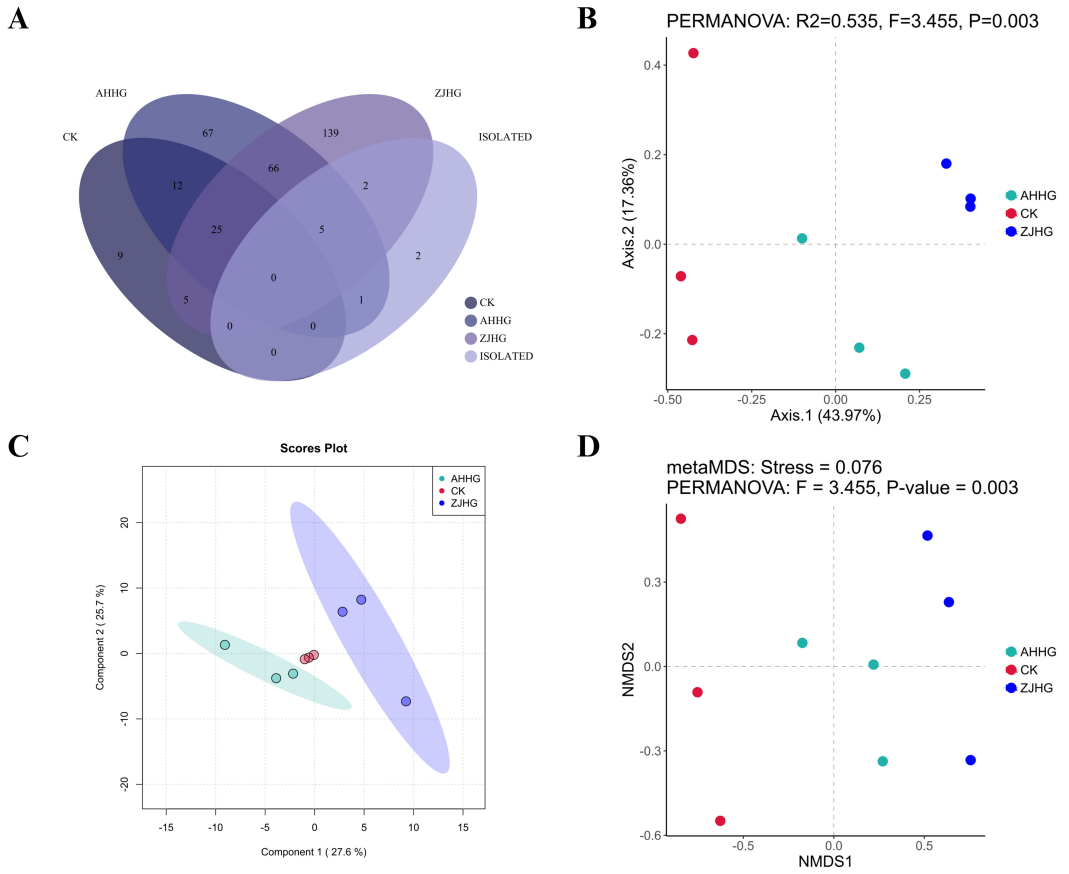


FIGURE 11
The metagenomic sequencing results of the re-inoculated samples. **(A)** Venn diagram showing the bacterial distribution at the species level between the control (CK) and the cultured metagenomics-separated results (isolated group), as well as the re-inoculated samples AHHG and ZJHG. **(B)** Principal Co-ordinates Analysis (PCoA) of CK and the re-inoculated samples AHHG and ZJHG. **(C)** Partial Least Squares-Discriminant Analysis (PLS-DA) of the CK and re-inoculated samples AHHG and ZJHG. **(D)** Non-metric Multidimensional Scaling (NMDS) analysis of CK and the re-inoculated samples AHHG and ZJHG. Note: the isolated groups refers to the pathogens identified through the pathogenicity test (see sub-section 3.2.5) i.e., *Pseudomonas syringae, P. fulva, P. fluorescens, Pantoea ananatis, Pectobacterium parvum, P. carotovorum, Flavobacterium fluviale, Citrobacter portucalensis, Klebsiella grimontii, Stenotrophomonas maltophilia*.

causal pathogen of MBB (Akhtar and Sarwar, 1988; Krawczyk and Łochyńska, 2020). Similarly, *P. fulva* has been isolated from bananas (Zhang et al., 2022), *Capsicum annuum L.* bacterial disease (Sheng et al., 2017) and Zanthoxylum black rot (Liu, 2020) disease samples. It has also been reported as an opportunistic human pathogen causing infections such as urinary sepsis (Stark, 2022), bacteremia (Uddin et al., 2018), and wound infections (Cobo et al., 2016). *P. carotovorum* has a global distribution and a wide host range, causing blackleg and tuber soft rot in cruciferous plants and potatoes grown in temperate climates (Czajkowski et al., 2014). *P. parvum* has been reported to infect potatoes and cause bacterial soft rot, limiting yield and quality, thus affecting global food security (Wang et al., 2022). We have recently reported *P. ananatis* as one of several causal pathogens of mulberry bacterial wilt (Yuan et al., 2023a). However, none of the above bacteria have been reported to cause MBB.

*S. maltophilia* is a common pathogen in nosocomial infections that can cause skin infections in human (Zhong et al., 2023). *C. portucalensis* (Sellera et al., 2022) and *F. fluviale* (Kämpfer et al., 2012) have been reported as common opportunistic pathogens in air or water and have the potential to become bacteria of public health concern worldwide. Although, these bacteria have not yet been reported as the causal pathogens of mulberry diseases, there is considerable value in studying them, as mulberry and its byproducts are commonly used in human food chain and pharmaceutical industry (Gao et al., 2024; Zhao et al., 2023). Within Enterobacteriaceae, a large group of soft rot Enterobacteriaceae (SRE) bacteria causes blackleg wilt and soft rot diseases in a wide range of important plants worldwide (Pritchard et al., 2016). *Pectobacterium* spp., a sub-group in the SRE, are recognized as the most significant bacterial plant pathogens in terms of economic and yield losses they cause (Pritchard et al., 2016). In the present study, we found that *P. carotovorum* had stronger virulence and caused more serious terminal bud black blight in mulberry than other pathogens under similar conditions. However, *P. carotovorum* was only isolated in one sample. We speculate that, although *P. carotovorum* is one of the important causal pathogens of MBB causing serious blight symptoms, it is possible that its spread to

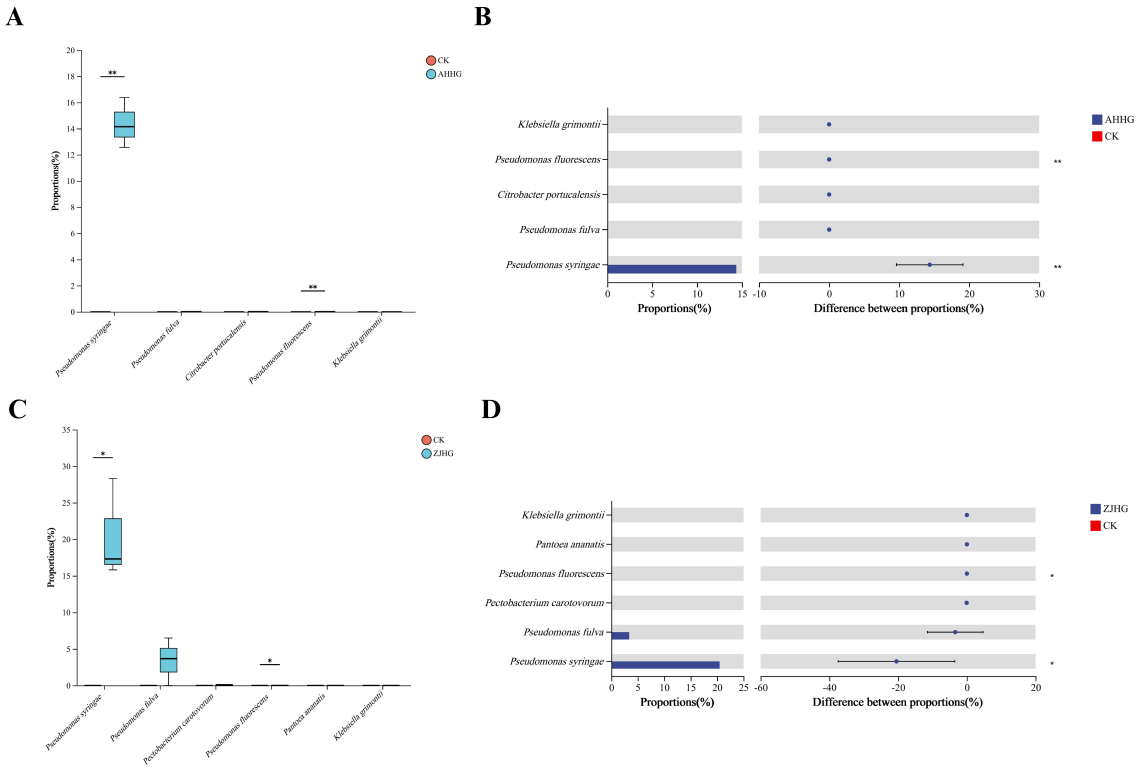


FIGURE 12
Welch's t-test of control (CK) against the re-inoculated samples AHHG **(A, B)** and ZJHG **(C, D)**. **(A, C)** The box plots show the relative abundance values of species level that significantly changed relative to the CK in re-inoculated samples on the x-axis, with the y-axis representing the relative abundance values. The box plots display the distribution of expression values or abundance for each feature name across different groups, with different colors representing different groups. **(B, D)** The bar chart on the left shows the average relative abundance of species across different groups on the x-axis, with the y-axis representing different features, and different colors representing different groups. The dot-line plot on the right indicates the difference in average relative abundance of species between the two groups within the specified confidence interval. The value corresponding to the dot represents the difference in average relative abundance, with the dot color indicating the group with the larger abundance. The I-shaped interval above the dot represents the upper and lower limits of the difference. *significant correlation (P<0. 05). **highly significant correlation (P<0. 01).

other sampling locations covered in the present study might have been prevented by the fact that it is more adapted to temperate climate zones.

In order to draw a relationship between pathogen distribution, community composition, and relevant metrological factors, we performed the Spearman correlation coefficient analysis to study the distribution of 10 suspected bacterial pathogens of MBB in samples collected from different locations in relation to the local meteorological data of 15 days before and after sampling. The results of the correlation analysis between occurrence of *P. syringae* and meteorological factors suggested that MBB caused by *P. syringae* may occur in summer season with long and rainy days, and that wind and precipitation might help its spread. This is supported by an evidence on bacterial canker of kiwifruit caused by *Pseudomonas syringae* pv. Actinidiae (Donati et al., 2020). It was argued that the bacterial colonization is affected by environmental factors, and that the disease incidence requires a combination of mild temperature and leaf wetness (Donati et al., 2020). Interestingly, in the present study, among all suspected pathogenic bacteria, only *P. syringae* was positively correlated with TEMP, suggesting that it may be more sensitive to environmental temperature. This is also consistent with the report that *P. syringae* has ice nucleation activity (INA) function and can produce ice nucleation proteins to induce ice crystals (Du et al., 2017). Meanwhile, the occurrence of *P. fulva* and *P. fluorescens* was not correlated or negatively correlated with five of the six meteorological factors covered in the present research. This finding suggested that *P. fluorescens* and *P. fulva* might be conditional pathogens endogenous to mulberry or inherent in the air and soil. We argue that these bacteria could cause infection and lead to mulberry blight under specific/favorable changes in conditions i.e., *P. fluorescens* under dry conditions and *P. fulva* under wet conditions. The occurrence of *P. ananatis* was positively correlated with PRES and WDSP, and negatively correlated with RH, PRCP, and TEMP. High-pressure air masses have high density and small gas expansion, which are often accompanied by low temperatures and dryness. We therefore speculate that *P. ananatis* infection is likely to occur in low temperature and dry conditions, environment or season, and wind is also conducive to the spread of *P. ananatis*. The occurrence of *P. parvum, P. carotovorum, F. fluviale, C. portucalensis, K. grimontii* and *S. maltophilia* were all positively correlated with RH and PRCP, suggesting that these

pathogens are more adapted to humid and wet environments. Given that the correlation between the pathogen distribution and meteorological factors studied in the present study was based on statistical analysis, therefore, further experimental validation of these relationships may be carried out in the future works. Future research should also focus on exploring the precise mechanistic basis by which these meteorological factors influence the distribution of the causal pathogens of MBB, their virulence and transmission dynamics in different agro-climatic conditions. Studies addressing the evolutionary significance of the identified pathogens in specific areas of adaptation are particularly required to gain more insight in this regard.

Combined metagenomic sequencing and conventional culture methods are presently seen as the "best practice" for the diagnosis of pathogenic microorganisms. Chen et al. (2021) compared the results of metagenomic sequencing and conventional culture methods for diagnosing human infectious pathogens, and reported a highly consistent result between both methods. In the present study, the results of metagenomic sequencing and isolation culture methods were also highly consistent and showed that *P. syringae* and *P. fulva* were widely distributed in the samples. These pathogens also showed high virulence when artificially inoculated in mulberry plants, and therefore, they were considered as the main causal pathogen of MBB. However, further focused studies are still required for confirmation and to gain detailed understanding.

The composition of plant microbial communities is influenced by cooperation, competition, and interactions among countless microbial members. These microbial members as a whole affect plant health (Gao et al., 2021). Interestingly, when we re-inoculated the pathogenic bacteria *P. syringae* to mulberry, the microbial community changed. Infection with MBB pathogens led by *P. syringae* affected the composition of mulberry endophyte community. In support of this, we argue that the increase in the relative abundance of pathogenic bacteria might be proportional to the increase in the endophytic bacteria. However, we currently don't have concrete evidence to support this notion. We believe that these pathogenic strains may have formed a certain ecological niche in mulberry, posing a threat to overall plant health.

Although, the diversity of experimental methods used in this study helped us report more shared genera between metagenomic sequencing and culturomics, these methods also have limitations. We know that despite obvious advantages of metagenomic technology, its effectiveness is highly dependent on the complexity and biomass of the community, sequencing technology and reference database used. It is therefore possible that certain specific taxa, (e.g. with low abundance) might have been omitted (Li et al., 2023 and references therein). Although culturomics is now seen as an important tool to provide comprehensive insight on the diversity of previously unculturable microbes, it is often considered as a labor/resource-intensive method. Generation of comprehensive strain collections through culturomics is still an unresolved challenge, as it may omit the specific target groups of importance within the microbial community (Li et al., 2023 and references therein).

Tellingly, metagenomics- and Culturomics-based studies have the potential to contribute to agricultural sustainability (Clagnan et al., 2024), we therefore believe that the results presented herein could provide a valuable resource for building climate-smart and resource-efficient mulberry production systems. These results could also serve as a baseline for developing and implementing sustainable approaches like nature-based biological control and integrated pest management to combat pathogens in mulberry production systems. However, if we are to build practically improved mulberry production, future research needs to bridge the experimental data and field application.

## 5 Conclusions

In the present study, we surveyed and collected MBB disease samples in silkworm rearing areas in eight provinces of China, and conducted a comprehensive and in-depth analysis of the potential causal pathogens of MBB. Through combined metagenomic and culturomics techniques, we screened and identified several suspected causal bacterial pathogens of MBB. Based on verification results of pathogenicity test, 10 pathogens including *P. syringae P. fulva, P. fluorescens, P. ananatis, P. parvum, P. carotovorum, F. fluviale, C. portucalensis, K. grimontii and S. maltophilia* were identified as potential causal agents, with *P. syringae* and *P. fulva* being identified as the key pathogens of MBB. Combining the result of isolation of pathogenic bacteria with the meteorological factors, it was found that different bacteria adapt to different environmental conditions, leading to differences in the pathogenic bacteria of MBB in mulberry fields in different climate types and different latitudes. Future focused studies on the causal pathogens of MBB are required to gain insight on the precise infection mechanisms of these pathogenic strains and how they interact/behave in different environments and metrological factors.

## Data availability statement

The datasets presented in this study can be found in online repositories. The names of the repository/repositories and accession number(s) can be found in the article/Supplementary Material. The raw metagenomic data obtained in this study has been deposited in the National Center for Biotechnology Information (NCBI) GenBank under BioProject number: PRJNA1177990. The genome sequence of pure culture bacteria obtained through isolation and cultivation in this study has been deposited at NCBI GenBank under BioProject number PQ454732-PQ455177.

## Author contributions

XH: Conceptualization, Data curation, Formal analysis, Investigation, Methodology, Writing – original draft. TY: Conceptualization, Data curation, Methodology, Writing – original draft. YH: Investigation, Methodology, Writing – original draft. IQ: Formal analysis, Supervision, Validation, Writing – original draft, Writing – review & editing. JL: Conceptualization, Funding acquisition, Project administration, Resources, Supervision, Validation, Writing – original draft, Writing – review & editing.

## Funding

The author(s) declare financial support was received for the research, authorship, and/or publication of this article. The research was financially supported by the Earmarked Fund of the China Agriculture Research System (CARS-18-ZJ0304).

## Acknowledgments

We express our gratitude to Prof. Weijia from Zhejiang Academy of Agricultural Sciences and Dr. Tianyue from Jiangsu University of Science and Technology for their assistance during the experiment. We thank all lab mates who supported during this project but are not listed as co-authors.

## Conflict of interest

The authors declare that the research was conducted in the absence of any commercial or financial relationships that could be construed as a potential conflict of interest.

## Generative AI statement

The author(s) declare that no Generative AI was used in the creation of this manuscript.

## Publisher's note

All claims expressed in this article are solely those of the authors and do not necessarily represent those of their affiliated organizations, or those of the publisher, the editors and the reviewers. Any product that may be evaluated in this article, or claim that may be made by its manufacturer, is not guaranteed or endorsed by the publisher.

## Supplementary material

The Supplementary Material for this article can be found online at: https://www.frontiersin.org/articles/10.3389/fpls.2025.1517050/full#supplementary-material

## References

Akhtar, M. A., and Sarwar, M. (1988). Mulberry germplasm resistance to bacterial blight(Pseudomonas syringaepv. mori) in Pakistan. *Trop. Pest Manage.* 34, 227–228. doi: 10.1080/09670878809371246

Anteneh, Y. S., Yang, Q., Brown, M. H., and Franco, C. M. (2022). Factors affecting the isolation and diversity of marine sponge-associated bacteria. *Appl. Microbiol. Biotechnol.* 106 (4), 1729–1744. doi: 10.1007/s00253-022-11791-8

Baharuddin, (1997). "Characteristics of Pseudomonas syringae pv. mori, Causal Agent of Bacterial Blight of Mulberry (Morus Spp.) in Indonesia," in *Developments in Plant Pathology* (Springer Netherlands, Dordrecht), 548–552.

Bankevich, A., Nurk, S., Antipov, D., Gurevich, A. A., Dvorkin, M., Kulikov, A. S., et al. (2012). SPAdes: A new genome assembly algorithm and its applications to single-cell sequencing. *J. Comput. Biol.* 19 (5), 455–477. doi: 10.1089/cmb.2012.0021

Bringel, F., and Couée, I. (2015). Pivotal roles of phyllosphere microorganisms at the interface between plant functioning and atmospheric trace gas dynamics. *Front. Microbiol.* 06, 486. doi: 10.3389/fmicb.2015.00486

Bulgarelli, D., Garrido-Oter, R., Münch, P. C., Weiman, A., Dröge, J., Pan, Y., et al. (2015). Structure and function of the bacterial root microbiota in wild and domesticated barley. *Cell Host Microbe* 17 (3), 392–403. doi: 10.1016/j.chom.2015.01.011

Chen, H., Li, J., Yan, S., Sun, H., Tan, C., Liu, M., et al. (2021). Identification of pathogen(s) in infectious diseases using shotgun metagenomic sequencing and conventional culture: a comparative study. *PeerJ* 9, e11699. doi: 10.7717/peerj.11699

Chen, T., Shuang, F.-F., Fu, Q.-Y., Ju, Y. X., Zong, C. M., Zhao, W. G., et al. (2022). Evaluation of the chemical composition and antioxidant activity of mulberry (Morus alba L.) fruits from different varieties in China. *Molecules* 27 (9), 2688. doi: 10.3390/molecules27092688

Clagnan, E., Costanzo, M., Visca, A., Di Gregorio, L., Tabacchioni, S., Colantoni, E., et al. (2024). Culturomics-and metagenomics-based insights into the soil microbiome preservation and application for sustainable agriculture. *Front. Microbiol.* 15, 1473666. doi: 10.3389/fmicb.2024.1473666

Cobo, F., Jiménez, G., Rodríguez-Granger, J., and Sampedro, A. (2016). Posttraumatic skin and soft-tissue infection due to *Pseudomonas fulva*. *Case Reports Infectious Dis* 2016, 8716068. doi: 10.1155/2016/8716068

Czajkowski, R., Pérombelon, M. C. M., Jafra, S., Lojkowska, E., Potrykus, M., van der Wolf, J., et al. (2015). Detection, identification and differentiation of Pectobacterium and Dickeya species causing potato blackleg and tuber soft rot: a review. *Ann. Appl. Biol.* 166 (1), 18–38. doi: 10.1111/aab.2015.166.issue-1

Dickson, I. (2017). Culturomics: illuminating microbial dark matter. *Nat. Rev. Gastroenterol. Hepatol.* 14, 3–3. doi: 10.1038/nrgastro.2016.189

Donati, I., Cellini, A., Sangiorgio, D., Vanneste, J. L., Scortichini, M., Balestra, G. M., et al. (2020). Pseudomonas syringae pv. actinidiae: Ecology, Infection Dynamics and Disease Epidemiology. *Microb. Ecol.* 80 (1), 81–102. doi: 10.1007/s00248-019-01459-8

Du, R., Du, P., Lu, Z., Ren, W., Liang, Z., Qin, S., et al. (2017). Evidence for a missing source of efficient ice nuclei. *Sci. Rep.* 7, 39673. doi: 10.1038/srep39673

Edgar, R. C. (2004). MUSCLE: multiple sequence alignment with high accuracy and high throughput. *Nucl. Acids Res.* 32, 1792–1797. doi: 10.1093/nar/gkh340

Edwards, J., Johnson, C., Santos-Medellín, C., Lurie, E., Podishetty, N. K., Bhatnagar, S., et al. (2015). Structure, variation, and assembly of the root-associated microbiomes of rice. *Proc. Natl. Acad. Sci. U. S. A.* 112 (8), E911–E920. doi: 10.1073/pnas.1414592112

Elsharkawy, M. M., Khedr, A. A., Mehiar, F., El-Kady, E. M., Alwutayd, K. M., and Behiry, S. I. (2023). Rhizobacterial colonization and management of bacterial speck pathogen in tomato by pseudomonas spp. *Microorganisms* 11 (5), 1103. doi: 10.3390/microorganisms11051103

Fröhlich-Nowoisky, J., Kampf, C. J., Weber, B., Huffman, J. A., Pöhlker, C., Andreae, M. O., et al. (2016). Bioaerosols in the Earth system: Climate, health, and ecosystem interactions. *Atmos. Res.* 182, 346–376. doi: 10.1016/j.atmosres.2016.07.018

Gao, M., Xiong, C., Gao, C., Tsui, C. K. M., Wang, M. M., Zhou, X., et al. (2021). Disease-induced changes in plant microbiome assembly and functional adaptation. *Microbiome* 9 (1), 1–18. doi: 10.1186/s40168-021-01138-2

Gao, Q., Chen, N., Li, B., Zu, M., Ma, Y., Xu, H., et al. (2024). Natural lipid nanoparticles extracted from Morus nigra L. leaves for targeted treatment of hepatocellular carcinoma via the oral route. *J. Nanobiotechnol.* 22 (1), 4. doi: 10.1186/s12951-023-02286-3

Gilbert, J. A., Field, D., Swift, P., Thomas, S., Cummings, D., Temperton, B., et al. (2010). The taxonomic and functional diversity of microbes at a temperate coastal site: A 'Multi-omic' Study of seasonal and diel temporal variation. *PloS One* 5 (11), e15545. doi: 10.1371/journal.pone.0015545

Hartmann, M., and Six, J. (2023). Soil structure and microbiome functions in agroecosystems. *Nat. Rev. Earth Environ.* 4, 4–18. doi: 10.1038/s43017-022-00366-w

Huai, T., Zhao, J., Zhang, X., He, H., Zhu, X., Ma, H., et al. (2023). First report of pseudomonas oryzihabitans causing walnut leaf spot disease in China. *Plant Dis.* 108), 514. doi: 10.1094/PDIS-08-23-1634-PDN

Huang, Y., Wei, J., Liu, P., Zhu, Y., Lin, T., Lv, Z., et al. (2024). Identification of mulberry bacterial blight caused by klebsiella oxytoca in Bazhong, Sichuan, China. *Phyton* 93 (8), 1995–2008. doi: 10.32604/phyton.2024.052353

Huot, B., Castroverde, C. D. M., Velásquez, A. C., Hubbard, E., Pulman, J. A., Yao, J., et al. (2017). Dual impact of elevated temperature on plant defence and bacterial virulence in Arabidopsis. *Nat. Commun.* 8 (1), 1808. doi: 10.1038/s41467-017-01674-2

Huson, D. H., Beier, S., Flade, I., Górska, A., El-Hadidi, M., Mitra, S., et al. (2016). MEGAN community edition - interactive exploration and analysis of large-scale microbiome sequencing data. *PloS Comput. Biol.* 12 (6), e1004957. doi: 10.1371/journal.pcbi.1004957

Ji, C., Guo, J., Ma, Y., Xu, X., Zang, T., Liu, S., et al. (2024). Application progress of culturomics in the isolated culture of rhizobacteria: A review. *J. Agric. Food Chem.* 72 (14), 7586–7595. doi: 10.1021/acs.jafc.3c08885

Jiao, F., Luo, R., Dai, X., Liu, H., Yu, G., Han, S., et al. (2020). Chromosome-Level Reference Genome and Population Genomic Analysis Provide Insights into the Evolution and Improvement of Domesticated Mulberry (Morus alba). *Mol. Plant* 13 (7), 1001–1012. doi: 10.1016/j.molp.2020.05.005

Jung, T., Pérez-Sierra, A., Durán, A., Horta Jung, M., Balci, Y., and Scanu, B. (2018). Canker and decline diseases caused by soil- and airborne Phytophthora species in forests and woodlands. *Persoonia* 40, 182–220. doi: 10.3767/persoonia.2018.40.08

Kämpfer, P., Lodders, N., Martin, K., and Avendaño-Herrera, R. (2012). Flavobacterium Chilense sp. nov. and Flavobacterium araucananum sp. nov., isolated from farmed salmonid fish. *Int. J. Syst. Evol. Microbiol.* 62 (Pt 6), 1402–1408. doi: 10.1099/ijs.0.033431-0

Krawczyk, K., and Łochyńska, M. (2020). Identification and characterization of Pseudomonas syringae pv. mori affecting white mulberry (Morus alba) in Poland. *Eur. J. Plant Pathol.* 158, 281–291. doi: 10.1007/s10658-020-02074-x

Lagier, J.-C., Hugon, P., Khelaifia, S., Fournier, P. E., La Scola, B., and Raoult, D. (2015). The rebirth of culture in microbiology through the example of culturomics to study human gut microbiota. *Clin. Microbiol. Rev.* 28 (1), 237–264. doi: 10.1128/CMR.00014-14

Lagier, J. C., Dubourg, G., Million, M., Cadoret, F., Bilen, M., Fenollar, F., et al. (2018). Culturing the human microbiota and culturomics. *Nature Reviews. Microbiology* 16, 540–550. doi: 10.1038/s41579-018-0041-0

Lamichhane, J. R., Bartoli, C., and Varvaro, L. (2016). Extensive field survey, laboratory and greenhouse studies reveal complex nature of pseudomonas syringae-associated hazelnut decline in central Italy. *PloS One* 11, e0147584. doi: 10.1371/journal.pone.0147584

Leach, J. E., Triplett, L. R., Argueso, C. T., and Trivedi, P. (2017). Communication in the phytobiome. *Cell* 169 (4), 587–596. doi: 10.1016/j.cell.2017.04.025

Letunic, I., and Bork, P. (2016). Interactive tree of life (iTOL) v3: an online tool for the display and annotation of phylogenetic and other trees. *Nucleic Acids Res.* 44, W242–W245. doi: 10.1093/nar/gkw290

Li, P., Wang, S., Liu, M., Dai, X., Shi, H., Zhou, W., et al. (2024). Antibacterial Activity and Mechanism of Three Root Exudates from Mulberry Seedlings against Ralstonia pseudosolanacearum. *Plants* 13 (4), 482. doi: 10.3390/plants13040482

Li, C., Wu, Y., Li, L., Zhao, C., Li, B., Wu, Y., et al. (2023). Different techniques reveal the difference of community structure and function of fungi from root and rhizosphere of Salvia miltiorrhiza Bunge. *Plant Biol. J.* 25 (6), 848–859. doi: 10.1111/plb.13556

Liu, Z. (2020). Research of Pathogen ldentification, Detection, and Drug Resistant of Bacterial Black Rot on Zanthoxylum armatum. (Harbin City, Heilongjiang Province, China: Northeast Forestry University).

Luo, L., Huang, Y., and Liu, J. (2022). Genome sequence resources of klebsiella michiganensis AKKL-001, which causes bacterial blight of mulberry. *MPMI* 35, 349–351. doi: 10.1094/MPMI-09-21-0222-A

Melcher, U., Verma, R., and Schneider, W. L. (2014). Metagenomic search strategies for interactions among plants and multiple microbes. *Front. Plant Sci.* 5, 1–5. doi: 10.3389/fpls.2014.00268

Memete, A. R., Timar, A. V., Vuscan, A. N., Miere Groza, F., Venter, A. C., and Vicas, S. I. (2022). Phytochemical composition of different botanical parts of morus species, health benefits and application in food industry. *Plants* 11 (2), 152. doi: 10.3390/plants11020152

Oksel, C., Avin, F. A., Liyanapathiranage, P., Shreckhise, J., and Baysal-Gurel, F. (2024). First Report of Achromobacter xylosoxidans Causing Bacterial Stem and Leaf Blight on Cyrilla arida in Tennessee and the United States. *Plant Dis.* 4, 1094. doi: 10.1094/PDIS-01-24-0005-PDN

Pei, Y., Ma, L., Zheng, X., Yao, K., Fu, X., Chen, H., et al. (2023). Identification and Genetic Characterization of Pseudomonas syringae pv. Actinidiae from Kiwifruit in Sichuan, China. *Plant Dis.* 107 (10), 3248–3258. doi: 10.1094/PDIS-01-23-0005-RE

Popović, T., Menković, J., Prokić, A., Zlatković, N., and Obradović, A. (2021). Isolation and characterization of Pseudomonas syringae isolates affecting stone fruits and almond in Montenegro. *J. Plant Dis. Prot.* 128 (2), 391–405. doi: 10.1007/s41348-020-00417-8

Posada, D. (2008). jModelTest: phylogenetic model averaging. *Mol. Biol. Evol.* 25, 1253–1256. doi: 10.1093/molbev/msn083

Pritchard, L., Glover, R. H., Humphris, S., et al. (2016). Genomics and taxonomy in diagnostics for food security: soft-rotting enterobacterial plant pathogens. *Anal. Methods* 8, 12–24. doi: 10.1039/C5AY02550H

Roman-Reyna, V., and Crandall, S. G. (2024). Seeing in the dark: a metagenomic approach can illuminate the drivers of plant disease. *Front. Plant Sci.* 15, 1405042. doi: 10.3389/fpls.2024.1405042

Rosario, D. K. A., Mutz, Y. S., Bernardes, P. C., and Conte-Junior, C. A. (2020). Relationship between COVID-19 and weather: Case study in a tropical country. *Int. J. Hyg. Environ. Health* 229, 113587. doi: 10.1016/j.ijheh.2020.113587

Sahin, F., Kotan, R., and Dönmez, M. F. (1999). First Report of Bacterial Blight of Mulberries Caused by Pseudomonas syringae pv. mori in the Eastern Anatolia Region of Turkey. *Plant Dis.* 83, 1176–1176. doi: 10.1094/PDIS.1999.83.12.1176B

Sarhan, M. S., Hamza, M. A., Youssef, H. H., Patz, S., Becker, M., ElSawey, H., et al. (2019). Culturomics of the plant prokaryotic microbiome and the dawn of plant-based culture media – A review. *J. Adv. Res.* 19, 15–27. doi: 10.1016/j.jare.2019.04.002

Sarkar, S., Kamke, A., Ward, K., Hartung, E., Ran, Q., Feehan, B., et al. (2022). Culturomics of Andropogon gerardii rhizobiome revealed nitrogen transforming capabilities of stress-tolerant Pseudomonas under drought conditions. *Cold Spring Harbor Lab*. doi: 10.1101/2022.07.18.500515

Sellera, F. P., Fernandes, M. R., Fuga, B., Fontana, H., Vásquez-Ponce, F., Goldberg, D. W., et al. (2022). Phylogeographical landscape of citrobacter portucalensis carrying clinically relevant resistomes. *Microbiol. Spectr.* 10 (2), e01506-21. doi: 10.1128/spectrum.01506-21

Shen, W., Zhao, G., Zhu, B., Xu, A., and Zhong, Y. (2002). Phylogenetic analyses of homologous amino acid sequences of five conserved genes in bacteria. *J. Genet. Mol. Biol.* 13 (2), 108–118. doi: 10.30047/JGMB.200206.0006

Sheng, Q., Luo, M., Guan, J., Zhang, X., and Zhang, C.. (2017). Characterization of Pseudomonas fulva as a new pathogen of pepper leaf spot isolated from Xinjiang in China. *J. Plant Prot.* 44, 260–268. doi: 10.13802/j.cnki.zwbhxb.2017.2015180

Singh, A. K., Sharma, R. K., Sharma, V., Singh, T., Kumar, R., and Kumari, D. (2017). Isolation, morphological identification and *in vitro* antibacterial activity of endophytic bacteria isolated from Morus nigra (Mulberry) leaves. *J. Anim. Rese.* 7 (1), 155. doi: 10.5958/2277-940X.2017.00022.5

Stamatakis, A. (2014). RAxML version 8: a tool for phylogenetic analysis and post-analysis of large phylogenies. *Bioinformatics* 30, 1312–1313. doi: 10.1093/bioinformatics/btu033

Stark, J. (2022). First case of non-traumatic community-acquired Pseudomonas fulva infection. *Indian J. Med. Microbiol.* 40 (2), 317–318. doi: 10.1016/j.ijmmb.2021.12.010

Sun, Y., Liu, Y., Li, J., Tan, Y., An, T., Zhuo, M., et al. (2023). Characterization of lung and oral microbiomes in lung cancer patients using culturomics and 16S rRNA gene sequencing. *Microbiol. Spectr.* 11 (3), e00314-23. doi: 10.1128/spectrum.00314-23

Tyler, H. L., Roesch, L. F. W., Gowda, S., Dawson, W. O., and Triplett, E. W. (2009). Confirmation of the sequence of 'Candidatus liberibacter asiaticus' and assessment of microbial diversity in huanglongbing-infected citrus phloem using a metagenomic approach. *MPMI* 22 (12), 1624–1634. doi: 10.1094/MPMI-22-12-1624

Uddin, F., Roulston, K., McHugh, T. D., Khan, T. A., and Sohail, M. (2018). Bacteremia in a human caused by an XDR strain of Pseudomonas fulva. *J. Infect. Dev. Ctries.* 12 (7), 597–599. doi: 10.3855/jidc.10326

Vanneste, J. L., Yu, J., Cornish, D. A., Tanner, D. J., Windner, R., Chapman, J. R., et al. (2013). Identification, Virulence, and Distribution of Two Biovars of Pseudomonas syringaepv. actinidiae in New Zealand. *Plant Dis.* 97 (6), 708–719. doi: 10.1094/PDIS-07-12-0700-RE

Wang, J., Han, W., Pirhonen, M., Pan, Y., Zhang, D., Zhao, D., et al. (2022). High-quality complete genome resource of pectobacterium parvum isolate FN20211 causing aerial stem rot of potato. *MPMI* 35 (6), 488–491. doi: 10.1094/MPMI-01-22-0009-A

Wang, X., Howe, S., Wei, X., Deng, F., Tsai, T., Chai, J., et al. (2021). Comprehensive cultivation of the swine gut microbiome reveals high bacterial diversity and guides bacterial isolation in pigs. *mSystems* 6 (4), 00477–00421. doi: 10.1128/msystems.00477-21

Weisburg, W. G., Barns, S. M., Pelletier, D. A., and Lane, D. J. (1991). 16S ribosomal DNA amplification for phylogenetic study. *J. Bacteriol.* 173 (2), 697–703. doi: 10.1128/jb.173.2.697-703.1991

Xie, J., Shu, P., Strobel, G., Chen, J., Wei, J., Xiang, Z., et al. (2017). Pantoea agglomerans SWg2 colonizes mulberry tissues, promotes disease protection and seedling growth. *Biol. Control.* 113, 9–17. doi: 10.1016/j.biocontrol.2017.06.010

Xu, J., Zhang, Y., Zhang, P., Trivedi, P., Riera, N., Wang, Y., et al. (2018). The structure and function of the global citrus rhizosphere microbiome. *Nat. Commun.* 9 (1), 4894. doi: 10.1038/s41467-018-07343-2

Ye, J., McGinnis, S., and Madden, T. L. (2006). BLAST: improvements for better sequence analysis. *Nucl. Acids Res.* 34, W6–W9. doi: 10.1093/nar/gkl164

Yuan, T., Huang, Y., Luo, L., Wang, J., Li, J., Chen, J., et al. (2023a). Complete genome sequence of pantoea ananatis strain LCFJ-001 isolated from bacterial wilt mulberry. *Plant Dis.* 107, 2500–2505. doi: 10.1094/PDIS-10-22-2473-A

Yuan, T., Qazi, I. H., Yang, P., Zhang, X., Li, J., and Liu, J. (2023b). Analysis of endophytic bacterial flora of mulberry cultivars susceptible and resistant to bacterial wilt using metagenomic sequencing and culture-dependent approach. *World J. Microbiol. Biotechnol.* 39, 163. doi: 10.1007/s11274-023-03599-z

Zárate-Chaves, C. A., Moufid, Y., López, C. E., Bernal, A. J., Szurek, B., and Yánez, J. M. (2024). First Report of Cassava Bacterial Blight Caused by Xanthomonas phaseoli pv. manihotis in the Amazonian Forest of Ecuador. *Plant Dis.* 108, 1879. doi: 10.1094/PDIS-10-23-2111-PDN

Zhang, L., Cao, Q., Ruan, W., Guo, Y., Zhuang, Y., Li, Y., et al. (2023). Culturomics and Amplicon-Based Metagenomic Insights into the Bacteria of Soils with High Yield of Oryza sativa L. subsp. Japonica. *Agronomy (Basel)* 13 (12), 2867. doi: 10.3390/agronomy13122867

Zhang, N., He, J., Muhammad, A., and Shao, Y. (2022). CRISPR/cas9–mediated genome editing for pseudomonas fulva, a novel pseudomonas species with clinical, animal, and plant–associated isolates. *IJMS* 23 (10), 5443. doi: 10.3390/ijms23105443

Zhang, Z., Schwartz, S., Wagner, L., and Miller, W. (2000). A greedy algorithm for aligning DNA sequences. *J. Computational Biol.: J. Computational Mol. Cell Biol.* 7 (1-2), 203–214. doi: 10.1089/10665270050081478

Zhao, Q., Wang, Z., Wang, X., Yan, X., Guo, Q., Yue, Y., et al. (2023). The bioaccessibility, bioavailability, bioactivity, and prebiotic effects of phenolic compounds from raw and solid-fermented mulberry leaves during *in vitro* digestion and colonic fermentation. *Food Res. Int.* 165, 112493–112493. doi: 10.1016/j.foodres.2023.112493

Zhao, L., Zhang, S., Xiao, R., Zhang, C., Lyu, Z., and Zhang, F. (2024). Diversity and Functionality of Bacteria Associated with Different Tissues of Spider Heteropoda venatoria Revealed through Integration of High-Throughput Sequencing and Culturomics Approaches. *Microb. Ecol.* 87 (1), 67. doi: 10.1007/s00248-024-02383-2

Zhong, L., Li, H., and Zhang, J. (2023). Disseminated Stenotrophomonas maltophilia skin infection. *Acad. Dermatol. Venereol.* 37 (6), e806–e807. doi: 10.1111/jdv.18902

frontiers | Frontiers in Veterinary Science

TYPE Original Research
PUBLISHED 16 April 2025
DOI 10.3389/fvets.2025.1553218



OPEN ACCESS

EDITED BY
Ling Tian,
South China Agricultural University, China

REVIEWED BY
Maria Giovanna Ciliberti,
University of Foggia, Italy
Francesca Arfuso,
University of Messina, Italy

*CORRESPONDENCE
Giovanni Buonaiuto
✉ giovanni.buonaiuto@unibo.it

RECEIVED 30 December 2024
ACCEPTED 20 March 2025
PUBLISHED 16 April 2025

CITATION
Fusaro I, Parrillo S, Buonaiuto G, Prasinou P, Gramenzi A, Bucci R, Cavallini D, Carosi A, Carluccio A and De Amicis I (2025) Effects of hemp-based polyunsaturated fatty acid supplementation on membrane lipid profiles and reproductive performance in Martina Franca jacks.
*Front. Vet. Sci.* 12:1553218.
doi: 10.3389/fvets.2025.1553218



# Effects of hemp-based polyunsaturated fatty acid supplementation on membrane lipid profiles and reproductive performance in Martina Franca jacks

Isa Fusaro[1], Salvatore Parrillo[1], Giovanni Buonaiuto[2]*, Paraskevi Prasinou[1], Alessandro Gramenzi[1], Roberta Bucci[1], Damiano Cavallini[2], Alessia Carosi[1], Augusto Carluccio[1] and Ippolito De Amicis[1]

[1]Department of Veterinary Medicine, University of Teramo, Teramo, Italy, [2]Department of Veterinary Medical Science, Alma Mater Studiorum, University of Bologna, Bologna, Italy

This study evaluates the impact of dietary supplementation with hemp-based polyunsaturated fatty acids (PUFAs) on the membrane lipid profiles and reproductive performance of Martina Franca jacks. Over a 90-day period, twelve donkeys were divided into a treatment group receiving hemp oil and a control group on a standard diet. Semen and blood samples were collected and analyzed at multiple time points for lipid composition and reproductive parameters. Results revealed that sperm motility improved significantly, increasing from 92.61% in the control group to 96.63% by Day 60 in the treatment group ($p = 0.05$). Normal sperm morphology also showed a significant enhancement, rising from 96.58% in the control group to 98.85% by Day 60 ($p = 0.04$). Conversely, gel-free semen volume decreased significantly in the treatment group, from 64.17 mL in the control group to 28.20 mL at Day 60 ($p < 0.0001$). Lipidomic analyses indicated an increased proportion of omega-3 PUFAs, such as eicosapentaenoic acid (EPA; 0.08% in the control group to 0.20% by Day 60, $p < 0.0001$), in sperm membranes, alongside a reduction in the peroxidation index (264.11 in the control group to 86.53 in the treatment group, $p < 0.0001$). These changes suggest improved membrane fluidity and oxidative stability. These findings underscore the potential of hemp oil as a dietary supplement to enhance reproductive outcomes in donkeys, with broader implications for livestock management.

KEYWORDS

**semen quality, lipidomic, antioxidants, cannabidiol, industrial hemp, donkey nutrition**

## 1 Introduction

In recent decades, increasing consumer awareness of social and environmental issues has driven a growing demand for more sustainable animal products. As a result, the livestock sector, has adopted more efficient resource management strategies, particularly regarding soil and water. Among the various approaches explored to reduce the environmental impact of animal production, the inclusion of sustainable feed ingredients has gained considerable

interest (1, 2). One crop that has received attention for its sustainability potential is hemp [*Cannabis sativa*; (3)].

Hemp is an annual angiosperm belonging to the Cannabaceae family (4). While the terms "hemp" and "cannabis" are often used interchangeably; "hemp" generally refers to the plant when cultivated for industrial, textile, or culinary purposes (5). In contrast, "cannabis" is commonly associated with the plant's therapeutic or psychoactive properties (6). Currently, hemp cultivation falls into two distinct categories (7). The first is industrial hemp, characterized by a tetrahydrocannabinol (THC) content of less than 0.2% (8). The second is medical cannabis, which is cultivated under strict quality standards for therapeutic use. Hemp has a wide range of domestic and industrial applications, as extensively documented in previous reviews [e.g., (9–11)]. In medicine, cannabis is employed for its therapeutic potential in treating various conditions in both humans and animals (12–14). According to the European Food Safety Authority (EFSA), hemp seeds and hempseed meal can be included in the diets of various animal species, though the recommended inclusion rates vary depending on species-specific metabolic needs (15). Hemp oil serves as a dietary supplement due to its high EFA content. Research on hemp supplementation in livestock has demonstrated beneficial effects on both animal health and productivity (16–19), yet studies specifically investigating equids remain scarce. Notably, the limited research available has focused primarily on horses, often examining the plant's pharmaceutical applications (20, 21) or its use as a bedding material (22) rather than as a nutritional supplement.

Equids' diets are traditionally based on forages, often supplemented with compound feedstuffs (23, 24). Certain equine categories, including those used for meat production, intense physical work (e.g., racehorses, draft donkeys), or breeding, require high-energy diets rich in grains (25, 26). However, excessive starch intake has been linked to metabolic disorders such as gastrointestinal disturbances (27, 28) and laminitis (29), which can compromise both performance and welfare. To mitigate these risks, lipid supplementation has emerged as a viable alternative energy source (30). Among the fat sources used in equine nutrition, vegetable oils have gained increasing due to their positive effects on diet palatability, general health, and animal welfare. Rich in PUFAs and precursors of the omega-3 and omega-6 series, vegetable oils contribute to improved metabolic efficiency and overall physiological function. Consequently, their use in equine diets has become increasingly popular (31, 32). Corn, soybean, and canola oils are among the most frequently incorporated lipid sources, either as feed supplements or as top-dress additives for grains (31, 33). Despite the growing interest in alternative lipid sources, no studies to date have investigated the effects of hemp supplementation on the reproductive performance of donkey stallions.

In recent decades, donkey farming has attracted growing interest from both researchers and consumers, largely due to the recognized health benefits of donkey milk (34, 35). The rediscovery of its nutritional and therapeutic properties has played a key role in preserving preservation and, in some cases, restoring several native donkey breeds (36, 37). Additionally, policies promoting farm diversification and supporting the conservation of local animal populations have further encouraged the expansion of donkey farming. These animals are particularly well-suited to marginal areas that would otherwise be unsuitable for other types of livestock production (38). The increasing demand for donkey-derived products has led many farmers to expand their herds and adopt modern technologies, including milking systems (35). In this context, developing strategies to enhance the reproductive performance of donkeys is crucial to ensuring sustainable herd growth and the long-term viability of these animals. Currently, one of the most commonly used breeds for milk production is the Martina Franca donkey (38). Native to the rural areas of the Apulia region in Italy, this breed is characterized by its tall stature, exceptional robustness, and docile temperament (39). These traits have contributed to its expansion beyond its region of origin, with increasing presence in central and northern Italy (40).

This study represents the first investigation into the effects of hemp-based polyunsaturated fatty acid supplementation on the membrane lipid profiles and reproductive performance of Martina Franca jacks.

## 2 Materials and methods

The study was conducted at the experimental stables of the University of Teramo, located in Bellante (Teramo, Italy), over a period of 90 days. Ethical approval for the experimental procedures was obtained from the Ethical Animal Care and Use Committee of the University of Teramo (Protocol No. 18532 of 28/06/2022), and all activities were carried out in accordance with Directive 2010/63/EU.

### 2.1 Animals and diets

Twelve Martina Franca donkey jack (average age: 7 ± 3 years; mean body weight: 333 ± 51 kg) were enrolled in this study. Prior to the study, the donkeys underwent a comprehensive clinical examination to confirm they were in good health status. Additionally, inclusion criteria required a favorable body condition score (BCS; average 2.8 ± 0.4), assessed by visual appraisal and palpation was obtained independently by two technicians, but final classification was decided by consensus if there was any discrepancy, and the maintenance of optimal health throughout the trial period. To ensure this, the animals were monitored weekly by trained personnel who assessed various health indicators. These assessments included physical condition, skin cleanliness, eye health (evaluating for sunken or dull eyes, and the tendency to keep eyes closed or partially closed), salivation, ear positioning during inspection, and respiratory patterns (such as tachypnea, hyperpnea, or dyspnea). Additionally, feed and water intake, social interactions (e.g., signs of fleeing or hiding), the presence of stereotypies or aggression, posture, lameness or uncoordinated movements, and the presence of skin or ocular lesions were all evaluated. The presence of blood in the feces, fecal consistency, and cleanliness of the stall were also assessed. Each of these criteria was scored on a scale from 1 to 6, with 1 indicating abnormal or pathological conditions and 6 indicating normal conditions.

All jacks were housed in individual paddocks (each at least 160 $m^2$) with appropriate shelter, water troughs, and feeders. For the experimental trial, the animals were divided into two groups: the treatment group (TRT) and the control group (CTR). Each donkey had free access to an *ad libitum* amount (41) of clean drinking water throughout the study. The donkeys were fed according to the nutritional requirements outlined in the Nutrient Requirements of Horses (42), taking into account their weight, age, and activity level.

The trial lasted for 3 months, during which the stallions received an isoproteic diet. The treatment group's diet was enriched with hemp oil, while the control group did not receive this supplement. All animals had *ad libitum* access to mixed hay (2% of body weight), and complete feed was provided twice daily. The ingredients of the complete feed are listed in Table 1. To minimize the risk of colic and ensure the animals' welfare, dietary changes were introduced gradually over a 15-day period, allowing a smooth transition to the new feeding regime (43, 44). During this period, animals were closely monitored for any signs of digestive discomfort or behavioral changes, and no adverse effects were observed. This approach was aligned with ethical guidelines for animal welfare in nutritional trials.

## 2.2 Sampling operations

### 2.2.1 Feed sampling and chemical analysis

During the experimental period, hays and feed samples were collected once a week for qualitative and chemical-nutritional evaluation. Additionally, the quality of the hay was assessed following the guidelines of Cavallini et al. (23) to ensure the absence of molds and spores. All collected samples were immediately transported to the laboratory for dry matter (DM) and chemical analysis, using detailed methodologies for feed analysis previously published by other authors (45, 46).

### 2.2.2 Semen sampling and analysis

Each stallion selected for this research project had been approved for assisted reproduction and had previously participated in breeding programs. As a result, the donkeys underwent a training protocol for semen collection procedures. Semen was collected weekly using a Missouri artificial vagina, with each stallion assigned a specific device at the start of the breeding season. During collection, an in-line gel filter (Minitüb, Tiefenbach, Germany) was used, and a jenny in natural or induced estrus was present to stimulate the stallion's copulatory response. After collection, semen samples were promptly sent at room temperature to the laboratory, located in the same facility, for semen analysis. The total semen volume (vol. tot) was measured using a graduated cylinder immediately after collection, while the gel-free volume (vol. gf) was determined by filtering the sample through sterile gauze into a graduated test tube. Sperm concentration (conc.) and the proportion of nonviable spermatozoa (death) were assessed using an automated sperm counting system [Nucleo-Counter SP 100TM, ChemoMetec, Allerod, Denmark; (47)]. Motility parameters (total and progressive motility) and sperm morphology (morph.) were evaluated with a computer-assisted semen analysis system (CASA IVOS II, Hamilton Thorne, Beverly, MA, United States), following the standardized settings provided by the manufacturer, as described by Contri et al. (48). To analyze the semen lipidomic profile, sperm cells were separated from the seminal plasma through two consecutive centrifugations (2,500 rpm for 10 min). After removing the seminal plasma, the cells were washed with PBS (0.5 mL, pH 7.8) twice (2,500 rpm × 5 min each). The sperm cells were then resuspended in pure water (18 mQ) to achieve a concentration of $6 \times 10^6$ cells per mL. This suspension was used to extract membrane lipids, employing a 2:1 chloroform mixture as the organic phase, following the Folch method (49). The organic layer was subsequently extracted, and the sample was dried under vacuum.

TABLE 1 Ingredients (kg/head/day) and chemical composition of the experimental feeds.

| | CTR | TRT |
|---|---|---|
| Oat meal | 0.64 | 0.64 |
| Faba bean meal | 0.20 | 0.20 |
| Soybean hulls | 0.66 | 0.66 |
| Hemp oil | 0.00 | 0.08 |
| Min-vit supplement | 0.06 | 0.06 |

### 2.2.3 Blood sampling and analysis

Blood samples (1 mL each) were collected every 15 days. The samples were drawn from the jugular vein by a trained technician and collected in tubes containing ethylenediaminetetraacetic acid (EDTA) as a tripotassium salt. To analyze the erythrocyte lipidomic profile, erythrocytes were isolated from whole blood collected in EDTA tubes. The procedure for membrane lipidome analysis was conducted as previously outlined by Prasinou et al. (50). In brief, starting with a 1 mL whole blood sample, erythrocytes were separated from plasma by two consecutive centrifugations (3,000 g × 5 min, each), followed by a washing step with phosphate buffer (0.5 mL) two times (3,000 g × 5 min, each) and finally obtaining the erythrocyte membrane pellet by centrifugation (15,000 g × 15 min). The resulting pellet was then resuspended in pure water and used for phospholipid extraction using a 2:1 chloroform mixture as the organic phase, following the same methodology as described for the semen lipidomic analysis.

### 2.2.4 Gas chromatography

To assess the effectiveness of the lipid extraction, thin layer chromatography (TLC) was carried out using a chloroform/methanol/water solvent system (65:25:4) as described by Fuchs et al. (51). The extracted phospholipids were then transesterified at room temperature for 10 min using 0.5 M KOH in methanol to produce the corresponding fatty acid methyl esters (FAMEs). This chemical conversion was performed according to established protocols, with careful monitoring to prevent oxidative or degradative reactions that could alter the fatty acid profile. Each sample was analyzed in duplicate, with the entire procedure repeated twice to ensure the accuracy and reliability of the results.

Initially, gas chromatography (GC) analysis was conducted on commercially available reference standards for each of the 9 selected fatty acids. Calibration curves for quantitative analysis were generated for each chromatogram peak, as illustrated in Prasinou et al. (52). The FAME mixture obtained from both sperm and erythrocyte membrane pellets was dissolved in 20 µL of n-hexane, and 1 µL of this solution was directly injected into an Agilent 7890B GC system equipped with a flame ionization detector and a DB-23 (50%-Cyanopropyl)-methylpolysiloxane capillary column (60 m, 0.25 mm i.d., 0.25 µm film thickness). The GC temperature program started at 165°C, maintained for 3 min, followed by a gradual increase of 1°C/min until reaching 195°C, which was held for 40 min. The temperature was then increased by 10°C/min up to 240°C and held for 10 min. Hydrogen was used as the carrier gas, with a constant pressure of 16.482 psi. FAMEs were identified by comparing their retention times with those

of standard references, which were either commercially sourced or synthesized.

## 2.3 Statistical analysis

The effects of hemp-based polyunsaturated fatty acid supplementation on the semen parameters, membrane lipid profiles, and reproductive performance in Martina Franca jacks were evaluated across different time points: Day 15 (D15), Day 45 (D45), and Day 60 (D60). The normal distribution of the data was tested by the Shapiro–Wilk normality test according to Ferlizza et al. (53). Measurements were not normally distributed, and they were therefore normalized by Box–Cox transformation as reported in Dini et al. (54). Repeated-measures linear mixed-effects models were constructed as previously (55) according to the sampling time points performed. Model fixed effect was the group while each subject was the experimental unit. After the analysis, normal distribution of the data was checked again for the resulting residuals. A bivariate matrix with Pearson correlation was calculated to evaluate the relationship between ration and or semen and or blood parameters, according to Bordin et al. (56).

# 3 Results

Regarding semen parameters (Table 2), the gel-free volume of semen showed a significant decrease following supplementation. The control group (CTR) exhibited a gel-free volume of 64.17 mL, which significantly reduced to 45.18 mL at D15 and remained stable at 45.90 mL by D45. A further reduction was observed at D60, with the volume reaching 28.20 mL ($p < 0.0001$). Sperm concentration also demonstrated a significant decline, starting from 632.89 million/mL in the control group and decreasing to 371.69 million/mL at D15 and 343.10 million/mL at D45. By D60, the concentration showed a slight recovery to 407.28 million/mL; however, it remained significantly lower than the control ($p < 0.0001$). These changes suggest a notable impact of the hemp oil supplementation on semen volume and concentration. Sperm motility displayed a different trend, with a slight increase from the control value of 92.61 to 95.08% at D15, and a further improvement to 96.63% by D60 ($p = 0.05$). Progressive motility, however, did not show significant changes across the supplementation periods. Normal morphology of the sperm significantly improved from 96.58% in the control group to 98.12% at D15, remained consistent at 96.26% at D45, and further increased to 98.85% by D60 ($p = 0.04$).

The membrane lipid profiles of spermatozoa (Table 3) revealed significant changes in fatty acid composition. The proportion of C18:0 decreased significantly from 10.06% in the control group to 7.88% at D45, with a partial recovery to 9.14% at D60 ($p = 0.001$). In contrast, the proportion of C18:2 9c 12c significantly increased from 4.54% in the control group to 5.63% at D45 and 5.97% at D60 ($p = 0.003$). Moreover, the EPA content showed a significant increase after supplementation, rising from 0.08% in the control group to 0.16% at D45 and 0.20% at D60 ($p < 0.0001$). Significant alterations were also observed in the overall lipid profile indices. The ω3/(ω3 + ω6) ratio and the unsaturation index both decreased significantly after 45 days of supplementation, with the unsaturation index dropping from 233.53 in the control group to 87.65 at D45 ($p < 0.0001$). The peroxidation index also showed a significant reduction, suggesting decreased susceptibility to lipid peroxidation ($p < 0.0001$).

In erythrocyte membrane lipid profiles (Table 4), the study found that the level of C16:0 significantly decreased from 10.79% in the control group to 9.27% at D45 ($p = 0.05$). Similarly, the proportion of C18:1 9c increased significantly from 29.39% in the control group to 32.28% at D60 ($p = 0.001$). The ω6/ω3 ratio showed a significant increase from 211.63 in the control group to 259.22 at D60 ($p = 0.03$). The Pearson correlation coefficients among semen parameters are presented in Table 5. Gel-free volume was strongly positively correlated with total volume ($r = 0.82$), indicating a substantial relationship between these variables. Weak to negligible correlations were observed between concentration and other parameters, including total volume ($r = 0.05$) and gel-free volume ($r = 0.23$). Motility showed a weak negative correlation with gel-free volume ($r = -0.06$) and concentration ($r = -0.11$), while progressive motility displayed a modest positive correlation with gel-free volume ($r = 0.37$). Dead percentage exhibited weak negative correlations with total volume ($r = -0.22$) and gel-free volume ($r = -0.30$). A strong positive correlation was noted between motility and normal morphology ($r = 0.80$).

Significant correlations were observed between dietary fatty acid profiles and spermatozoa membrane glycerophospholipids (Table 6). Among the most relevant associations, PUFA balance ω3/(ω3 + ω6) ($r = 0.53$, $p = 0.01$) showed the highest positive correlations, while the ω6/ω3 ratio was negatively correlated ($r = -0.49$, $p = 0.01$). For erythrocyte membrane glycerophospholipids (Table 7), stearic acid (C18:0, $r = 0.50$, $p = 0.01$), and PUFA ($r = 0.98$, $p = 0.01$) exhibited strong positive correlations with dietary fatty acids, whereas EPA

TABLE 2 Semen parameters of Martina Franca jacks after different timepoints[a] of inclusion of hemp oil.

| Item | CTR | D15 | D45 | D60 | SEM | *p*-value |
|---|---|---|---|---|---|---|
| Total volume (mL) | 79.17 | 72.97 | 68.98 | 64.77 | 5.91 | 0.19 |
| Gel-free volume (mL) | 64.17$^{A}$ | 45.18$^{B}$ | 45.90$^{B}$ | 28.20$^{C}$ | 5.50 | <0.0001 |
| Concentration (mln/mL) | 632.89$^{A}$ | 371.69$^{B}$ | 343.10$^{B}$ | 407.28$^{B}$ | 50.74 | <0.0001 |
| Dead (%) | 12.61 | 13.16 | 11.08 | 14.06 | 2.11 | 0.56 |
| Motility (%) | 92.61$^{B}$ | 95.08$^{AB}$ | 93.06$^{B}$ | 96.63$^{A}$ | 1.18 | 0.05 |
| Progressive Motility (%) | 65.89$^{A}$ | 66.66$^{AB}$ | 67.38$^{B}$ | 63.64$^{A}$ | 2.49 | 0.62 |
| Normal morphology (%) | 96.58$^{B}$ | 98.12$^{AB}$ | 96.26$^{B}$ | 98.85$^{A}$ | 0.77 | 0.04 |

[a]D15: results after 15 days of inclusion; D45: results after 45 days of inclusion; D60: results after 15 days of inclusion.
$^{A,B,C}$ Least squares means with different superscript letters within a row are significantly different ($p < 0.05$).

TABLE 3 Fatty acids (% of the Found μg/mL) of spermatozoa membrane glycerophospholipids after different timepoints[a] of inclusion of hemp oil.

| FAME (%μg/mL) | D0 | D15 | D45 | D60 | SEM | *p*-value |
|---|---|---|---|---|---|---|
| C14:0 | 4.51 | 4.16 | 4.81 | 4.54 | 0.27 | 0.45 |
| C16:0 | 30.45 | 30.19 | 30.76 | 29.15 | 0.83 | 0.50 |
| C16:1 9c | 0.13 | 0.10 | 0.10 | 0.10 | 0.03 | 0.81 |
| C18:0 | 10.06$^{A}$ | 11.08$^{A}$ | 7.88$^{B}$ | 9.14$^{AB}$ | 0.51 | 0.001 |
| C18:1 9c | 2.73 | 2.80 | 2.79 | 3.21 | 0.18 | 0.19 |
| C18:1 11c | 3.32$^{AB}$ | 2.81$^{B}$ | 3.68$^{AB}$ | 3.95$^{A}$ | 0.25 | 0.03 |
| C18:2 9c, 12c | 4.54$^{B}$ | 4.37$^{B}$ | 5.63$^{AB}$ | 5.97$^{A}$ | 0.32 | 0.003 |
| C20:3 8c, 11c, 14c | 2.13 | 2.28 | 2.15 | 2.06 | 0.18 | 0.88 |
| C20:4 5c, 8c, 11c, 14c | 6.54 | 5.81 | 5.10 | 5.38 | 0.53 | 0.19 |
| EPA | 0.08$^{B}$ | 0.07$^{B}$ | 0.16$^{A}$ | 0.20$^{A}$ | 0.01 | <0.0001 |
| DPA n-6 | 27.63$^{A}$ | 27.77$^{A}$ | 29.67$^{A}$ | 29.36$^{A}$ | 0.70 | 0.04 |
| DHA | 7.78$^{AB}$ | 8.59$^{A}$ | 7.16$^{AB}$ | 6.80$^{B}$ | 0.43 | 0.04 |
| SFA | 45.10 | 45.55 | 43.53 | 42.89 | 0.80 | 0.07 |
| MUFA | 6.20$^{AB}$ | 5.70$^{B}$ | 6.56$^{AB}$ | 7.27$^{A}$ | 0.32 | 0.02 |
| ω3 | 7.85 | 8.66 | 7.33 | 6.99 | 0.43 | 0.07 |
| ω6 | 40.96$^{BC}$ | 40.24$^{C}$ | 42.57$^{AB}$ | 42.86$^{A}$ | 0.71 | 0.04 |
| PUFA | 48.80$^{A}$ | 48.82$^{A}$ | 20.10$^{B}$ | 20.36$^{B}$ | 0.85 | <0.0001 |
| SFA/MUFA | 7.57$^{A}$ | 8.09$^{A}$ | 6.79$^{AB}$ | 5.99$^{B}$ | 0.43 | 0.01 |
| ω6/ω3 | 5.44 | 4.86 | 5.90 | 6.26 | 0.35 | 0.07 |
| ω3/(ω3 + ω6) | 16.00$^{B}$ | 17.66$^{B}$ | 36.83$^{A}$ | 34.52$^{A}$ | 1.33 | <0.0001 |
| Unsaturation Index | 233.53$^{A}$ | 234.90$^{A}$ | 87.65$^{B}$ | 88.18$^{B}$ | 3.52 | <0.0001 |
| Peroxidation Index | 264.11$^{A}$ | 267.66$^{A}$ | 87.51$^{B}$ | 86.53$^{B}$ | 4.07 | <0.0001 |

[a]D15: results after 15 days of inclusion; D45: results after 45 days of inclusion; D60: results after 15 days of inclusion.
$^{A,B,C}$ Least squares means with different superscript letters within a row are significantly different ($p < 0.05$).

($r = -0.78$, $p = 0.01$) and the PUFA balance ω3/(ω3 + ω6) ($r = -0.91$, $p = 0.01$) showed negative correlations. The relationships between semen parameters and spermatozoa membrane fatty acids (Table 8) revealed that PUFA, along with the unsaturation index (UI) and peroxidation index (PI), were correlated with sperm concentration (ranging from $r = 0.48$ to $r = 0.69$, $p < 0.05$). For erythrocyte membrane fatty acids (Table 9), stearic acid (C18:0) was positively correlated with gel-free volume ($r = 0.63$, $p < 0.05$). PUFA, UI, and PI exhibited strong associations with sperm concentration (ranging from $r = 0.44$ to $r = 0.69$, $p < 0.05$). Finally, comparative analyses of fatty acid profiles between spermatozoa and erythrocyte membrane glycerophospholipids (Tables 10–12) showed that ω3 levels in spermatozoa were positively correlated with PUFA levels in erythrocytes ($r = 0.53$, $p < 0.05$).

## 4 Discussions

This study represents the first investigation into the effects of hemp-based PUFA supplementation on membrane lipid profiles and reproductive performance in Martina Franca jacks. The findings provide novel insights into the interaction between diet and reproductive function, supporting the hypothesis that dietary modulation of fatty acid profiles can influence reproductive health. While the role of nutrition in regulating female reproductive function is well-documented and widely recognized [e.g., the effects of sudden changes in body condition in dairy cows; (57)], its significance for male fertility is equally substantial, as highlighted by several studies [e.g., (58–60)].

The effect of diet on sperm quality is shaped by both quantitative and qualitative aspects, including the macronutrient composition (primarily fats) and the specific proportions of carbohydrates, proteins, and fatty acids (61). Among these, fatty acids play a crucial role in sperm physiology by regulating membrane fluidity, acrosome reaction, motility, and viability (62). Sperm membrane lipids are fundamental for preserving structural integrity and facilitating membrane fusion events during fertilization (11, 62, 63). Notably, PUFAs are especially important, as they integrate into the sperm plasma membrane, enhancing its flexibility, preserving functional stability, and increasing the osmotic resistance of the acrosome membrane. Additionally, they provide a protective effect against physiological stressors and thermal fluctuations during cryopreservation (62, 64). Several studies have demonstrated that optimal PUFA levels in semen extenders can enhance sperm antioxidant capacity, improve DNA integrity (65), and mitigate oxidative stress (66). These findings underscore the potential of dietary interventions, particularly through PUFA supplementation, to support sperm function and overall reproductive efficiency. However, excessive intake of high-calorie diets, particularly those rich in SFAs and trans fats, can have a detrimental effect on sperm quality, primarily by increasing oxidative stress—a key factor contributing to reproductive dysfunction (67, 68). Conversely, adequate antioxidant

10.3389/fvets.2025.1553218

TABLE 4 Fatty acids (% of the Found μg/mL) of erythrocyte membrane glycerophospholipids after different timepoints[a] of inclusion of hemp oil.

| FAME (%μg/mL) | D0 | D15 | D45 | D60 | SEM | *p*-value |
|---|---|---|---|---|---|---|
| C16:0 | 10.79$^{A}$ | 9.60$^{AB}$ | 9.27$^{B}$ | 9.36$^{B}$ | 0.47 | 0.05 |
| C16:1 9c | 0.89 | 0.83 | 0.91 | 1.10 | 0.10 | 0.31 |
| C18:0 | 9.28 | 8.22 | 9.07 | 8.53 | 0.42 | 0.12 |
| C18:1 9c | 29.39$^{B}$ | 28.73$^{B}$ | 28.39$^{B}$ | 32.28$^{A}$ | 0.61 | 0.001 |
| C18:1 11c | 0.89 | 0.85 | 1.01 | 0.99 | 0.06 | 0.09 |
| C18:2 9c, 12c | 46.35$^{B}$ | 49.57$^{A}$ | 49.45$^{A}$ | 45.77$^{B}$ | 0.72 | 0.001 |
| C20:3 8c, 11c, 14c | 0.16$^{B}$ | 0.17$^{AB}$ | 0.20$^{A}$ | 0.19$^{AB}$ | 0.01 | 0.03 |
| C20:4 5c, 8c, 11c, 14c | 1.51 | 1.79 | 1.41 | 1.37 | 0.12 | 0.09 |
| EPA | 0.18$^{AB}$ | 0.21$^{A}$ | 0.18$^{AB}$ | 0.16$^{B}$ | 0.01 | 0.01 |
| DHA | 0.05$^{A}$ | 0.04$^{AB}$ | 0.04$^{AB}$ | 0.03$^{B}$ | 0.01 | 0.05 |
| SFA | 19.99$^{A}$ | 17.74$^{B}$ | 18.34$^{AB}$ | 17.87$^{B}$ | 0.70 | 0.02 |
| MUFA | 31.35$^{B}$ | 30.43$^{B}$ | 30.32$^{B}$ | 34.47$^{A}$ | 0.73 | 0.01 |
| ω3 | 0.23$^{A}$ | 0.25$^{A}$ | 0.22$^{AB}$ | 0.20$^{B}$ | 0.01 | 0.01 |
| ω6 | 48.01$^{B}$ | 51.54$^{A}$ | 51.05$^{A}$ | 47.32$^{B}$ | 0.79 | 0.001 |
| PUFA | 48.25$^{B}$ | 51.80$^{A}$ | 51.26$^{A}$ | 47.52$^{B}$ | 0.80 | 0.001 |
| SFA/MUFA | 0.64$^{A}$ | 0.59$^{AB}$ | 0.60$^{AB}$ | 0.52$^{B}$ | 0.03 | 0.03 |
| ω6/ω3 | 211.63$^{B}$ | 208.37$^{AB}$ | 239.06$^{AB}$ | 259.22$^{A}$ | 14.00 | 0.03 |
| ω3/(ω3 + ω6) | 0.48$^{A}$ | 0.48$^{AB}$ | 0.42$^{AB}$ | 0.41$^{B}$ | 0.02 | 0.02 |
| Unsaturation Index | 132.26$^{B}$ | 138.66$^{A}$ | 136.66$^{AB}$ | 133.36$^{B}$ | 1.50 | 0.004 |
| Peroxidation Index | 54.97$^{B}$ | 59.46$^{A}$ | 57.60$^{AB}$ | 53.72$^{B}$ | 1.09 | 0.003 |

[a]D15: results after 15 days of inclusion; D45: results after 45 days of inclusion; D60: results after 15 days of inclusion.
$^{A,B,C}$ Least squares means with different superscript letters within a row are significantly different ($p < 0.05$).

TABLE 5 Pearson correlations between semen parameters.

| | Total volume | Gel-free volume | Concentration | Motility | Progressive Motility | Dead % | Normal morphology |
|---|---|---|---|---|---|---|---|
| Total volume | | | | | | | |
| Gel-free volume | 0.82* | | | | | | |
| Concentration | 0.05 | 0.23 | | | | | |
| Motility | −0.03 | −0.06 | −0.11 | | | | |
| Progressive Motility | 0.32* | 0.37* | −0.19 | 0.10 | | | |
| Dead % | −0.22 | −0.30* | −0.12 | −0.12 | −0.07 | | |
| Normal morphology | −0.16 | −0.18 | 0.05 | 0.80* | 0.04 | 0.02 | |

*<0.05.

intake has been shown to play a protective role in mitigating male infertility (61). Various dietary compounds, including polyphenols, carotenoids, and vitamins, contribute significantly to this effect by modulating mitochondrial function, maintaining the balance of reactive oxygen species, and enhancing mitochondrial biogenesis (62, 69–71).

In this study, the inclusion of hemp oil in the diet of Martina Franca jacks significantly influenced semen quality parameters and the lipid profiles of spermatozoa and erythrocyte membranes. These changes likely reflect the incorporation of PUFAs from hemp oil into cellular lipid matrices, a process essential for maintaining cellular function and membrane fluidity. Mammals, including equids, cannot synthesize PUFAs and must obtain them from dietary sources (72). Equine spermatozoa, like those of other mammals, contain high proportions of PUFAs, particularly DHA (omega-3) and docosapentaenoic acid [DPA, omega-6; (73)]. These findings indicate that hemp oil supplementation significantly impacts the lipid composition and oxidative stability of sperm membranes. Since PUFAs are critical for sperm function (74, 75), numerous studies have explored the potential of dietary interventions to enhance male fertility. Over the past decade, research has increasingly focused on using nutritional supplements to improve equine semen quality (76), with various nutraceuticals demonstrating potential benefits (77). The present study highlights the importance of nutraceuticals in optimizing sperm production and functionality in donkeys.

TABLE 6 Pearson correlations between fatty acid profile in diet and fatty acids of spermatozoa membrane glycerophospholipids.

| | Ration | *p*-value |
|---|---|---|
| 16:00 | 0,3,713 | 0,03 |
| 16:1 9c | −0,2,524 | 0,16 |
| 18:00 | 0,0538 | 0,77 |
| 18:1 9c | −0,2,638 | 0,14 |
| 18:1 11c | −0,3,799 | 0,03 |
| 18:2 9c, 12c | 0,0072 | 0,97 |
| 20:3 8c, 11c, 14c | −0,3,472 | 0,05 |
| 20:4 5c, 8c, 11c, 14c | 0,3,324 | 0,06 |
| EPA | 0,4,044 | 0,02 |
| DHA | 0,3,932 | 0,02 |
| SFA | 0,2,745 | 0,12 |
| MUFA | −0,3,024 | 0,09 |
| ω3 | 0,4,852 | 0,01 |
| ω6 | 0,0442 | 0,81 |
| PUFA | 0,0505 | 0,78 |
| SFA/MUFA | 0,3,388 | 0,05 |
| ω6/ω3 | −0,4,918 | 0,01 |
| PUFA balance ω3/(ω3 + ω6) | 0,5,256 | 0,01 |
| UI | −0,0413 | 0,82 |
| PI | 0,1,556 | 0,39 |

TABLE 7 Pearson correlations between fatty acid profile in diet and fatty acids of erythrocyte membrane glycerophospholipids.

| | Ration | *p*-value |
|---|---|---|
| 14:00 | −0,1796 | 0,25 |
| 16:00 | 0,0799 | 0,61 |
| 16:1 9c | 0,1,011 | 0,52 |
| 18:00 | 0,503 | 0,01 |
| 18:1 9c | −0,2,104 | 0,18 |
| 18:1 11c | −0,3,995 | 0,01 |
| 18:2 9c, 12c | −0,5,531 | 0,01 |
| 20:3 8c, 11c, 14c | 0,0766 | 0,63 |
| 20:4 5c, 8c, 11c, 14c | 0,2,995 | 0,05 |
| EPA | −0,7,761 | 0,01 |
| DPA n-6 | −0,4,014 | 0,01 |
| DHA | 0,378 | 0,01 |
| SFA | 0,393 | 0,01 |
| MUFA | −0,4,057 | 0,01 |
| ω3 | 0,3,497 | 0,02 |
| ω6 | −0,4,266 | 0,01 |
| PUFA | 0,9,849 | 0,01 |
| SFA/MUFA | 0,4,571 | 0,01 |
| ω6/ω3 | −0,3,682 | 0,01 |
| PUFA balance ω3/(ω3 + ω6) | −0,9,104 | 0,01 |
| UI | 0,9,903 | 0,01 |
| PI | 0,9,913 | 0,01 |

The addition of hemp oil had a pronounced effect on several semen quality parameters. The observed results align with previous on Martina Franca jacks conducted in Italy (47, 78). These studies, involving a similar number of animals and age range (7 animals, 4–10 years old), differed primarily in the number of ejaculates analyzed (35–364 ejaculates vs. 144 ejaculates in the present study). Over time, total and gel-free semen volumes decreased, possibly indicating a concentration effect in which volume is reduced while motility and morphology remains stable or improves. Specifically, motility and normal morphology percentages showed slight improvements, with a statistically significant increase in normal morphology, suggesting enhanced sperm health and viability. Few studies have investigated the influence of dietary n-3 PUFAs on equine reproductive performance, and none have specifically evaluated such supplementation in donkey diets. The reduction in semen concentration over time may suggest a trade-off between semen volume and sperm quality, where the nutritional benefits of hemp oil prioritize sperm viability over quantity. While several studies have reported beneficial effects of n-3 PUFA supplementation on sperm concentration in various species – including boars (79), rams (80), roosters (81), and humans (82, 83) – findings are inconsistent across different studies [e.g., (80, 84)]. Such discrepancies may be attributed to variations in dietary PUFA sources and levels, subject characteristics, or experimental conditions.

In this study, PUFA supplementation altered semen quality parameters as early as 15 days after the start of supplementation. The observed improvement in sperm motility is likely linked to modifications in sperm membrane composition induced by dietary PUFA supplementation (85). PUFAs enhance sperm flexibility, compressibility, deformability, and elasticity, ultimately improving membrane fluidity (74). This mechanistic pathway may explain the positive effects of dietary lipid supplementation on sperm motility. Similarly, the enhancement of sperm viability observed in this study is probably related to the antioxidant defense system of semen (86). The ability to counteract lipid peroxidation is crucial for maintaining sperm viability, as oxidative stress can compromise membrane integrity and cellular function (87). While no studies have specifically examined PUFA supplementation in donkeys, mixed results have been reported in horses. For example, Rodrigues et al. (76) found no changes in fresh semen quality after supplementing the diets of ten Mangalarga Marchador stallions with 150 mL of linseed-based PUFA oil. However, Brinsko et al. (88) and Elhordoy et al. (89) reported improved semen quality after cooling and post-thawing when DHA was added to stallions' diets. The lipid composition of sperm membranes plays a crucial role in determining their functional properties. In this study, the observed improvement in semen quality may be attributed to modifications in the lipid profile of sperm plasma membranes. Previous research (62, 90) has highlighted DHA's role in enhancing membrane resistance to osmotic stress, a key factor in maintaining sperm viability, particularly in cryopreservation contexts. PUFAs contribute to the structural integrity of sperm membranes by preserving the optimal fluidity required for fusion events during

10.3389/fvets.2025.1553218

TABLE 8 Pearson correlation between semen parameters and fatty acids (% of the Found μg/mL) of spermatozoa membrane glycerophospholipids.

| | Total volume | Gel-free volume | Concentration | Motility | Progressive Motility | Dead % | Normal morphology |
|---|---|---|---|---|---|---|---|
| C14:0 | −0.18 | −0.13 | −0.08 | −0.04 | −0.01 | 0.02 | 0.07 |
| C16:0 | 0.16 | 0.15 | 0.03 | −0.30* | 0.04 | 0.08 | −0.27 |
| C16:1 9c | 0.02 | 0.02 | −0.04 | 0.05 | −0.05 | −0.16 | 0.09 |
| C18:0 | 0.39* | 0.47* | 0.24 | 0.43* | 0.33* | −0.20 | 0.32* |
| C18:1 9c | 0.01 | −0.06 | −0.03 | 0.27 | −0.13 | −0.10 | 0.23 |
| C18:1 11c | −0.24 | −0.22 | −0.06 | 0.29* | −0.16 | 0.00 | 0.22 |
| C18:2 9c, 12c | −0.37* | −0.49* | −0.20 | −0.04 | −0.24 | 0.26 | −0.18 |
| C20:3 8c, 11c, 14c | 0.00 | 0.01 | −0.07 | −0.25 | −0.18 | 0.10 | −0.17 |
| C20:4 5c, 8c, 11c, 14c | 0.04 | 0.11 | 0.05 | −0.26 | −0.06 | −0.11 | −0.20 |
| EPA | −0.17 | −0.37* | −0.32* | 0.27 | 0.02 | 0.11 | 0.17 |
| DPA n-6 | −0.18 | −0.24 | −0.09 | 0.19 | 0.03 | 0.00 | 0.32* |
| DHA | 0.01 | 0.05 | 0.05 | −0.16 | −0.06 | −0.02 | −0.27 |
| SFA | 0.38* | 0.44* | 0.17 | −0.02 | 0.27 | −0.05 | −0.04 |
| MUFA | −0.19 | −0.22 | −0.07 | 0.39* | −0.21 | −0.07 | 0.32* |
| ω3 | 0.00 | 0.03 | 0.03 | −0.15 | −0.06 | −0.02 | −0.26 |
| ω6 | −0.35* | −0.41* | −0.18 | −0.08 | −0.18 | 0.09 | 0.04 |
| PUFA | 0.46* | 0.68* | 0.48* | −0.28 | 0.22 | −0.17 | −0.24 |
| SFA/MUFA | 0.25 | 0.33* | 0.11 | −0.28 | 0.23 | 0.02 | −0.20 |
| ω6/ω3 | −0.13 | −0.17 | 0.01 | 0.08 | −0.07 | 0.06 | 0.25 |
| Unsaturation Index | 0.47* | 0.69* | 0.48* | −0.27 | 0.22 | −0.19 | −0.22 |
| Peroxidation Index | 0.47* | 0.69* | 0.48* | −0.26 | 0.23 | −0.19 | −0.22 |

*<0.05.

TABLE 9 Pearson correlation between semen parameters and fatty acids (% of the Found μg/mL) of erythrocyte membrane glycerophospholipids.

| | Total volume | Gel-free volume | Concentration | Motility | Progressive motility | Dead % | Normal morphology |
|---|---|---|---|---|---|---|---|
| C16:0 | −0.02 | 0.29 | 0.49* | −0.11 | 0.04 | −0.14 | −0.05 |
| C16:1 9c | −0.15 | −0.09 | 0.11 | 0.20 | 0.03 | 0.12 | 0.12 |
| C18:0 | 0.46* | 0.63* | 0.14 | −0.07 | 0.14 | −0.21 | −0.15 |
| C18:1 9c | 0.13 | 0.10 | −0.19 | 0.00 | 0.21 | 0.28 | −0.18 |
| C18:1 11c | 0.12 | 0.05 | −0.09 | 0.15 | 0.08 | 0.07 | −0.05 |
| C18:2 9c, 12c | −0.28 | −0.44* | −0.10 | 0.04 | −0.21 | −0.06 | 0.18 |
| C20:3 8c, 11c, 14c | −0.35* | −0.57* | −0.30 | 0.08 | −0.26 | 0.17 | 0.23 |
| C20:4 5c, 8c, 11c, 14c | 0.05 | −0.05 | −0.12 | 0.06 | −0.17 | −0.02 | 0.19 |
| EPA | −0.22 | −0.20 | 0.01 | −0.17 | −0.13 | −0.19 | −0.02 |
| DHA | −0.11 | −0.16 | 0.00 | −0.38* | −0.23 | 0.08 | −0.13 |
| SFA | 0.28 | 0.57* | 0.37* | −0.10 | 0.12 | −0.22 | −0.13 |
| MUFA | 0.10 | 0.08 | −0.16 | 0.04 | 0.20 | 0.28 | −0.15 |
| ω3 | −0.21 | −0.22 | 0.01 | −0.29 | −0.20 | −0.11 | −0.07 |
| ω6 | −0.25 | −0.42* | −0.11 | 0.05 | −0.21 | −0.06 | 0.19 |
| PUFA | −0.26 | −0.42* | −0.11 | 0.04 | −0.22 | −0.06 | 0.19 |
| SFA/MUFA | 0.17 | 0.43* | 0.44* | −0.10 | −0.01 | −0.34* | 0.01 |
| ω6/ω3 | 0.08 | −0.05 | −0.10 | 0.34* | 0.08 | 0.22 | 0.23 |
| ω3/(ω3 + ω6) | −0.09 | 0.00 | 0.08 | −0.37* | −0.11 | −0.10 | −0.20 |
| Unsaturation Index | −0.26 | −0.48* | −0.22 | 0.07 | −0.20 | 0.05 | 0.19 |
| Peroxidation Index | −0.20 | −0.36* | −0.13 | 0.04 | −0.22 | −0.05 | 0.20 |

*<0.05.

TABLE 10 Pearson correlation between fatty acids (% of the Found μg/mL) of spermatozoa membrane glycerophospholipids.

| | C14 | C16 | C16:1 9c | C18 | C18:1 9c | C18:1 11c | C18:2 9c, 12c | C20:3 8c, 11c, 14c | C20:4 5c, 8c, 11c, 14c | EPA | DPA n-6 | DHA | SFA | MUFA | ω3 | ω6 | PUFA | UI | PI |
|---|---|---|---|---|---|---|---|---|---|---|---|---|---|---|---|---|---|---|---|
| C14 | 0.07 | | | | | | | | | | | | | | | | | | |
| C16 | −0.27 | −0.33* | | | | | | | | | | | | | | | | | |
| C16:1 9c | 0.09 | 0.03 | −0.08 | | | | | | | | | | | | | | | | |
| C18 | 0.32* | −0.18 | −0.24 | 0.07 | | | | | | | | | | | | | | | |
| C18:1 9c | 0.23 | −0.22 | −0.22 | 0.09 | 0.23 | | | | | | | | | | | | | | |
| C18:1 11c | 0.22 | 0.15 | −0.50* | 0.00 | −0.08 | 0.00 | | | | | | | | | | | | | |
| C18:2 9c, 12c | −0.18 | −0.01 | −0.16 | 0.07 | −0.41* | −0.13 | 0.27 | | | | | | | | | | | | |
| C20:3 8c, 11c, 14c | −0.17 | −0.01 | 0.18 | −0.14 | −0.37* | −0.15 | −0.15 | 0.12 | | | | | | | | | | | |
| C20:4 5c, 8c, 11c, 14c | −0.20 | −0.24 | −0.10 | 0.20 | 0.04 | −0.09 | −0.01 | 0.05 | 0.06 | | | | | | | | | | |
| EPA | 0.17 | 0.10 | −0.05 | −0.02 | −0.14 | 0.02 | 0.13 | 0.32* | −0.18 | −0.19 | | | | | | | | | |
| DPA n-6 | 0.32* | 0.34* | −0.48* | −0.13 | −0.10 | 0.11 | 0.17 | −0.16 | −0.17 | −0.49* | 0.17 | | | | | | | | |
| DHA | −0.27 | 0.11 | −0.07 | −0.11 | −0.16 | −0.13 | −0.09 | −0.01 | −0.03 | −0.14 | −0.19 | −0.16 | | | | | | | |
| SFA | −0.04 | −0.18 | 0.77* | −0.02 | 0.38* | −0.12 | −0.53* | −0.44* | −0.07 | −0.15 | −0.12 | −0.47* | −0.15 | | | | | | |
| MUFA | 0.32* | 0.01 | −0.54* | 0.14 | 0.07 | 0.57* | 0.82* | 0.15 | −0.22 | −0.04 | 0.11 | 0.19 | −0.15 | −0.50* | | | | | |
| ω3 | −0.26 | 0.11 | −0.08 | −0.11 | −0.17 | −0.13 | −0.08 | 0.01 | −0.04 | −0.15 | −0.13 | −0.15 | 1.00* | −0.16 | −0.15 | | | | |
| ω6 | 0.04 | 0.15 | −0.59* | 0.01 | −0.38* | −0.06 | 0.26 | 0.42* | 0.20 | 0.27 | 0.15 | 0.53* | −0.27 | −0.82* | 0.18 | −0.26 | | | |
| PUFA | −0.24 | −0.12 | 0.00 | 0.10 | 0.45* | −0.18 | −0.18 | −0.41* | −0.03 | 0.43* | −0.65* | −0.39* | 0.22 | 0.28 | −0.24 | 0.19 | −0.31* | | |
| UI | −0.22 | −0.11 | 0.00 | 0.10 | 0.47* | −0.16 | −0.18 | −0.45* | −0.06 | 0.39* | −0.65* | −0.36* | 0.24 | 0.29* | −0.23 | 0.20 | −0.33* | −0.26 | |
| PI | −0.22 | −0.11 | 0.01 | 0.09 | 0.48* | −0.16 | −0.19 | −0.47* | −0.07 | 0.37* | −0.65* | −0.35* | 0.25 | 0.31* | −0.24 | 0.21 | −0.35* | −0.27 | |

*<0.05.





10.3389/fvets.2025.1553218

TABLE 11 Pearson correlation between fatty acids of erythrocyte membrane glycerophospholipids.

| | C16:0 | C16:1 9c | C18:0 | C18:1 9c | C18:1 11c | C18:2 9c,12c | C20:3 8c, 11c, 14c | C20:4 5c, 8c, 11c, 14c | EPA | DHA | SFA | MUFA | ω3 | ω6 | PUFA | UI |
|---|---|---|---|---|---|---|---|---|---|---|---|---|---|---|---|---|
| C16:0 | | | | | | | | | | | | | | | | |
| C16:1 9c | 0.46* | | | | | | | | | | | | | | | |
| C18:0 | 0.35* | 0.03 | | | | | | | | | | | | | | |
| C18:1 9c | −0.04 | 0.29 | 0.19 | | | | | | | | | | | | | |
| C18:1 11c | 0.08 | 0.19 | 0.12 | 0.38* | | | | | | | | | | | | |
| C18:2 9c, 12c | −0.51* | −0.46* | −0.67* | −0.75* | −0.35* | | | | | | | | | | | |
| C20:3 8c, 11c, 14c | −0.49* | −0.20 | −0.67* | −0.42* | −0.24 | 0.70* | | | | | | | | | | |
| C20:4 5c, 8c, 11c, 14c | −0.36* | −0.31 | −0.35* | −0.49* | −0.45* | 0.55* | 0.74* | | | | | | | | | |
| EPA | −0.04 | −0.09 | −0.33* | −0.42* | −0.41* | 0.40* | 0.57* | 0.52* | | | | | | | | |
| DHA | −0.17 | −0.31 | −0.29 | −0.36* | −0.19 | 0.42* | 0.46* | 0.43* | 0.33* | | | | | | | |
| SFA | 0.80* | 0.28 | 0.85* | 0.10 | 0.12 | −0.72* | −0.71* | −0.43* | −0.24 | −0.28 | | | | | | |
| MUFA | 0.03 | 0.41* | 0.19 | 0.99* | 0.44* | −0.78* | −0.43* | −0.52* | −0.43* | −0.39* | 0.14 | | | | | |
| ω3 | −0.11 | −0.20 | −0.38* | −0.48* | −0.40* | 0.49* | 0.64* | 0.59* | 0.91* | 0.69* | −0.31 | −0.50* | | | | |
| ω6 | −0.52* | −0.46* | −0.67* | −0.75* | −0.38* | 1.00* | 0.74* | 0.63* | 0.43* | 0.44* | −0.73* | −0.78* | 0.52* | | | |
| PUFA | −0.51* | −0.46* | −0.67* | −0.75* | −0.38* | 1.00* | 0.75* | 0.63* | 0.44* | 0.44* | −0.72* | −0.78* | 0.53* | 1.00* | | |
| UI | −0.65* | −0.42* | −0.78* | −0.56* | −0.33* | 0.95* | 0.82* | 0.68* | 0.43* | 0.44* | −0.87* | −0.59* | 0.52* | 0.96* | 0.96* | |
| PI | −0.51* | −0.45* | −0.64* | −0.74* | −0.43* | 0.95* | 0.81* | 0.78* | 0.51* | 0.49* | −0.71* | −0.77* | 0.61* | 0.98* | 0.98* | 0.96* |

*<0.05.





10.3389/fvets.2025.1553218

TABLE 12 Pearson correlation between fatty acids (% of the Found μg/mL) of spermatozoa membrane glycerophospholipids and fatty acids of erythrocyte membrane glycerophospholipids.

| | C14 | C16 | C16:1 9c | C18 | C18:1 9c | C18:1 11c | C18:2 9c, 12c | C20:3 8c, 11c, 14c | C20:4 5c, 8c, 11c, 14c | EPA | DPA n-6 | DHA | SFA | MUFA | ω3 | ω6 | PUFA | UI | PI |
|---|---|---|---|---|---|---|---|---|---|---|---|---|---|---|---|---|---|---|---|
| C16:0 | −0.10 | −0.03 | −0.02 | 0.41* | −0.05 | −0.25 | −0.24 | 0.08 | 0.16 | −0.45* | −0.22 | 0.15 | 0.26 | −0.24 | 0.13 | −0.23 | 0.47* | 0.47* | 0.48* |
| C16:1 9c | −0.28 | 0.04 | −0.11 | 0.13 | 0.21 | −0.25 | 0.13 | 0.18 | −0.10 | −0.04 | −0.18 | 0.21 | 0.05 | −0.09 | 0.21 | −0.15 | −0.04 | −0.05 | −0.04 |
| C18:0 | −0.13 | −0.06 | 0.21 | 0.32* | 0.24 | −0.16 | −0.27 | −0.09 | 0.31 | −0.30 | −0.19 | 0.00 | 0.14 | 0.02 | −0.01 | −0.15 | 0.42* | 0.43* | 0.42* |
| C18:1 9c | −0.01 | −0.11 | 0.11 | 0.03 | 0.17 | 0.12 | 0.23 | −0.02 | −0.04 | −0.02 | −0.15 | 0.12 | −0.11 | 0.21 | 0.12 | −0.08 | 0.14 | 0.13 | 0.13 |
| C18:1 11c | −0.17 | 0.19 | −0.05 | 0.09 | −0.04 | 0.14 | 0.16 | −0.28 | −0.23 | 0.04 | −0.07 | −0.09 | 0.22 | 0.09 | −0.09 | −0.23 | −0.16 | −0.16 | −0.15 |
| C18:2 9c, 12c | 0.14 | 0.10 | −0.14 | −0.32* | −0.24 | 0.10 | 0.07 | 0.00 | −0.13 | 0.33* | 0.27 | −0.16 | −0.09 | −0.07 | −0.15 | 0.23 | −0.44* | −0.44* | −0.44* |
| C20:3 8c, 11c, 14c | 0.11 | 0.08 | −0.19 | −0.38* | 0.02 | 0.22 | 0.08 | 0.14 | −0.29 | 0.32* | 0.22 | −0.05 | −0.17 | 0.18 | −0.03 | 0.11 | −0.59* | −0.58* | −0.58* |
| C20:4 5c, 8c, 11c, 14c | 0.07 | −0.09 | −0.04 | −0.05 | 0.09 | 0.12 | −0.18 | 0.17 | −0.11 | 0.03 | 0.17 | 0.01 | −0.12 | 0.15 | 0.01 | 0.06 | −0.10 | −0.09 | −0.09 |
| EPA | −0.13 | 0.01 | −0.07 | −0.17 | −0.05 | 0.00 | −0.25 | 0.16 | 0.15 | −0.14 | 0.07 | 0.18 | −0.17 | −0.04 | 0.17 | 0.09 | 0.01 | 0.02 | 0.03 |
| DHA | 0.03 | 0.32* | −0.05 | −0.17 | −0.05 | −0.24 | −0.23 | 0.09 | 0.22 | −0.05 | −0.20 | 0.08 | 0.23 | −0.23 | 0.07 | −0.16 | 0.02 | 0.03 | 0.03 |
| SFA | −0.14 | −0.05 | 0.12 | 0.44* | 0.13 | −0.25 | −0.31 | −0.01 | 0.29 | −0.45* | −0.25 | 0.09 | 0.24 | −0.12 | 0.06 | −0.22 | 0.54* | 0.54* | 0.55* |
| MUFA | −0.06 | −0.09 | 0.08 | 0.05 | 0.18 | 0.08 | 0.24 | −0.01 | −0.07 | −0.02 | −0.17 | 0.14 | −0.08 | 0.18 | 0.14 | −0.10 | 0.11 | 0.11 | 0.10 |
| ω3 | −0.08 | 0.14 | −0.07 | −0.21 | −0.06 | −0.10 | −0.29 | 0.16 | 0.21 | −0.13 | −0.03 | 0.17 | −0.03 | −0.13 | 0.16 | 0.00 | 0.02 | 0.03 | 0.03 |
| ω6 | 0.13 | 0.08 | −0.14 | −0.31 | −0.21 | 0.11 | 0.05 | 0.02 | −0.14 | 0.31 | 0.27 | −0.15 | −0.10 | −0.05 | −0.14 | 0.22 | −0.43* | −0.43* | −0.42* |
| PUFA | 0.13 | 0.09 | −0.14 | −0.31 | −0.21 | 0.11 | 0.04 | 0.02 | −0.14 | 0.31 | 0.27 | −0.15 | −0.10 | −0.05 | −0.13 | 0.22 | −0.42* | −0.42* | −0.42* |
| UI | 0.14 | 0.06 | −0.14 | −0.36 | −0.17 | 0.18 | 0.12 | 0.04 | −0.20 | 0.36* | 0.28 | −0.12 | −0.17 | 0.04 | −0.10 | 0.23 | −0.48* | −0.48* | −0.47* |
| PI | 0.12 | 0.05 | −0.12 | −0.27 | −0.14 | 0.12 | −0.02 | 0.07 | −0.13 | 0.25 | 0.26 | −0.11 | −0.11 | 0.00 | −0.10 | 0.19 | −0.37* | −0.36* | −0.36* |

*<0.05.





10.3389/fvets.2025.1553218

fertilization. According to Rodrigues et al. (76), PUFAs modulate the phase transition temperature of sperm membranes, delaying their transition from a liquid to a crystalline state. A higher PUFA content increases membrane flexibility, extending the duration in which cellular components remain in a liquid state and reducing the risk of ice crystal formation (91). This property enhances sperm resilience to sudden temperature fluctuations during freezing and thawing, ultimately improving post-thaw viability (76).

However, as noted by Van Tran et al. (92), the mechanisms of action of these molecules vary across species, leading to contrasting results. This variability poses challenges in interpreting the findings, particularly given the limited research on dietary additives' effects on donkey semen quality. Studies in other species support the benefits of PUFA supplementation. For instance, Khoshvaght et al. (93) reported improved semen quality and sperm cryosurvival in Holstein bulls following supplementation with 3.5% fish oil. Similar findings have been reported in stallions (94) and Nili-Ravi buffalo bulls (95). These effects are often attributed to increased DHA content in sperm plasma membranes, which enhances sperm motility and morphology (96, 97). DHA and EPA are associated with enhanced membrane fluidity and sperm functionality (98). In particular, Khoshvaght et al. (93) proposed that increased incorporation of DHA into plasma membrane phospholipids, particularly in the sperm tail, may improve motility. This hypothesis is supported by Connor et al. (99), who reported that DHA is predominantly localized in the tail region of primate sperm. A high DHA content in the sperm tail appears to be critical for flagellar function and movement, both of which are essential for motility.

Conversely, an elevated ω6/ω3 ratio has been associated with increased oxidative stress and lipid peroxidation in sperm membranes. Excessive ω6 fatty acids, particularly arachidonic acid, contribute to reactive oxygen species production, negatively impacting sperm motility and viability. Adjusting dietary intake to favor ω3 fatty acids may mitigates oxidative damage and improve reproductive outcomes (100). In the present study, the observed decrease in SFAs and increase in monounsaturated fatty acids (MUFAs) suggest a shift toward greater membrane fluidity, which is consistent with improved sperm parameters. Similarly, lipidomic analysis of erythrocyte membranes revealed a comparable trends, with reduced SFAs and increased MUFAs contributing to enhanced membrane fluidity and deformability. Despite a slight reduction in ω3 PUFAs, the overall unsaturation index remained stable, indicating preserved membrane functionality. Additionally, the downward trend in the peroxidation index suggests reduced oxidative susceptibility, which may confer benefits to both erythrocyte and spermatozoa membranes. These findings align with previous studies emphasizing the pivotal role of dietary fatty acid composition in reproductive health (98).

## 5 Conclusion

This study provides novel insights into the effects of hemp oil supplementation on reproductive performance in Martina Franca jacks. The incorporation of omega-3 PUFAs into sperm and erythrocyte membranes enhances cellular functionality while reducing oxidative stress, ultimately contributing to improved sperm motility and morphology. These findings suggest that dietary hemp oil supplementation may serve as an effective strategy for enhancing reproductive efficiency in donkey breeding programs. Future research should investigate the long-term effects and optimal supplementation levels to support broader applications in equine and livestock reproduction.

## Data availability statement

The raw data supporting the conclusions of this article will be made available by the authors, without undue reservation.

## Ethics statement

The animal study was approved by Ethical Animal Care and Use Committee of the University of Teramo. The study was conducted in accordance with the local legislation and institutional requirements.

## Author contributions

IF: Conceptualization, Funding acquisition, Project administration, Resources, Supervision, Visualization, Writing – review & editing. SP: Formal analysis, Investigation, Visualization, Writing – review & editing. GB: Data curation, Validation, Visualization, Writing – original draft, Writing – review & editing. PP: Data curation, Formal analysis, Methodology, Software, Visualization, Writing – review & editing. AG: Conceptualization, Resources, Supervision, Validation, Visualization, Writing – review & editing. RB: Data curation, Formal analysis, Investigation, Methodology, Validation, Visualization, Writing – review & editing. DC: Data curation, Formal analysis, Methodology, Software, Validation, Visualization, Writing – original draft. AlC: Formal analysis, Investigation, Visualization, Writing – review & editing. AuC: Conceptualization, Resources, Supervision, Visualization, Writing – review & editing. IA: Data curation, Formal analysis, Investigation, Methodology, Visualization, Writing – review & editing.

## Funding

The author(s) declare that financial support was received for the research and/or publication of this article. This work has been funded by the European Union -NextGeneration EU, Mission 4, Component 1, under the Italian Ministry of University and Research (MUR) National.

## Conflict of interest

The authors declare that the research was conducted in the absence of any commercial or financial relationships that could be construed as a potential conflict of interest.

The author(s) declared that they were an editorial board member of Frontiers, at the time of submission. This had no impact on the peer review process and the final decision.

## Generative AI statement

The authors declare that no Gen AI was used in the creation of this manuscript.

## Publisher's note



## References

1. Vastolo A, Serrapica F, Cavallini D, Fusaro I, Atzori AS, Todaro M. Editorial: Alternative and novel livestock feed: reducing environmental impact. *Front Vet Sci*. (2024) 11:1441902. doi: 10.3389/fvets.2024.1441905

2. Gasparini M, Brambilla G, Menotta S, Albrici G, Avezzù V, Vitali R, et al. Sustainable dairy farming and fipronil risk in circular feeds: insights from an Italian case study. *Food Addit Contam Part A*. (2024) 41:1582–93. doi: 10.1080/19440049.2024.2414954

3. Kaur G, Kander R. The sustainability of industrial hemp: a literature review of its economic, environmental, and social sustainability. *Sustain For*. (2023) 15:6457. doi: 10.3390/su15086457

4. Small E, Cronquist A. A practical and natural taxonomy for Cannabis. *Taxon*. (1976) 25:405–35. doi: 10.2307/1220524

5. Rehman M, Fahad S, Du G, Cheng X, Yang Y, Tang K, et al. Evaluation of hemp (*Cannabis sativa* L.) as an industrial crop: a review. *Environ Sci Pollut Res*. (2021) 28:52832–43. doi: 10.1007/s11356-021-16264-5

6. Yano H, Fu W. Hemp: a sustainable plant with high industrial value in food processing. *Food Secur*. (2023) 12:651. doi: 10.3390/foods12030651

7. Pollio A. The name of cannabis: a short guide for nonbotanists. *Cannabis Cannabinoid Res*. (2016) 1:234–8. doi: 10.1089/can.2016.0027

8. Hazekamp A, Tejkalová K, Papadimitriou S. Cannabis: from cultivar to chemovar II—a metabolomics approach to cannabis classification. *Cannabis Cannabinoid Res*. (2016) 1:202–15. doi: 10.1089/can.2016.0017

9. Aloo SO, Mwiti G, Ngugi LW, Oh D-H. Uncovering the secrets of industrial hemp in food and nutrition: the trends, challenges, and new-age perspectives. *Crit Rev Food Sci Nutr*. (2024) 64:5093–112. doi: 10.1080/10408398.2022.2149468

10. Dudziec P, Warmiński K, Stolarski MJ. Industrial hemp as a multi-purpose crop: last achievements and research in 2018−2023. *J Nat Fibers*. (2024) 21:2369186. doi: 10.1080/15440478.2024.2369186

11. Santos TF, Santos CM, Aquino MS, Suyambulingam I, Hussein EK, Verma A, et al. Towards sustainable and ecofriendly polymer composite materials from bast fibers: a systematic review. *Eng Res Express*. (2024) 6:012501. doi: 10.1088/2631-8695/ad2640

12. Callaway J. Hempseed as a nutritional resource: an overview. *Euphytica*. (2004) 140:65–72. doi: 10.1007/s10681-004-4811-6

13. Fallahi S, Bobak Ł, Opaliński S. Hemp in animal diets—Cannabidiol. *Animals*. (2022) 12:2541. doi: 10.3390/ani12192541

14. Marliani G, Vaccari L, Cavallini D, Montesano CS, Buonaiuto G, Accorsi PA. Assessing the effectiveness of cannabidiol additive supplementation on canine behavior and cortisol levels. *Heliyon*. (2024) 10:e31345. doi: 10.1016/j.heliyon.2024.e31345

15. FEEDAP. Scientific opinion on the safety of hemp (*Cannabis genus*) for use as animal feed. *EFSA J*. (2011) 9:2011. doi: 10.2903/j.efsa.2011.2011

16. Palade LM, Habeanu M, Marin DE, Chedea VS, Pistol GC, Grosu IA, et al. Effect of dietary hemp seed on oxidative status in sows during late gestation and lactation and their offspring. *Animals*. (2019) 9:194. doi: 10.3390/ani9040194

17. Kanbur G. Growth-depressing effect of dietary hempseed oil on broiler performance in the starting period and alterations in meat oxidation, serum parameters and abdominal fatty acids*. *Anim Sci Paper Rep*. (2022) 40:203–16.

18. Halle I, Schöne F. Influence of rapeseed cake, linseed cake and hemp seed cake on laying performance of hens and fatty acid composition of egg yolk. *J Verbr Lebensm*. (2013) 8:185–93. doi: 10.1007/s00003-013-0822-3

19. Skřivan M, Englmaierová M, Vít T, Skřivanová E. Hempseed increases gamma-tocopherol in egg yolks and the breaking strength of tibias in laying hens. *PLoS One*. (2019) 14:e0217509. doi: 10.1371/journal.pone.0217509

20. St Blanc MP, Chapman AM, Keowen ML, Garza F, Liu C-C, Gray L, et al. Effects of a supplement containing cannabidiol (CBD) on sedation and ataxia scores and health. *J Equine Vet Sci*. (2022) 117:104085. doi: 10.1016/j.jevs.2022.104085

21. Interlandi C, Tabbì M, Di Pietro S, D'Angelo F, Costa GL, Arfuso F, et al. Improved quality of life and pain relief in mature horses with osteoarthritis after oral transmucosal cannabidiol oil administration as part of an analgesic regimen. *Front Vet Sci*. (2024) 11:1341396. doi: 10.3389/fvets.2024.1341396

22. Bambi G, Rossi G, Barbari M. Comparison between different types of bedding materials for horses. *Agron Res*. (2018) 16:646–55. doi: 10.15159/AR.18.124

23. Cavallini D, Penazzi L, Valle E, Raspa F, Bergero D, Formigoni A, et al. When changing the hay makes a difference: a series of case reports. *J Equine Vet Sci*. (2022) 113:103940. doi: 10.1016/j.jevs.2022.103940

24. Raspa F, Tarantola M, Muca E, Bergero D, Soglia D, Cavallini D, et al. Does feeding management make a difference to behavioural activities and welfare of horses reared for meat production? *Animals*. (2022) 12:740. doi: 10.3390/ani12141740

25. Fayt J, Dotreppe O, Hornick JL, Istasse L. Spelt, an ancient cereal and first pressure linseed oil as ingredients of compound feedstuffs for modern horse feeding. *J Anim Physiol Anim Nutr*. (2008) 92:303–9. doi: 10.1111/j.1439-0396.2007.00772.x

26. Raspa F, Vervuert I, Capucchio MT, Colombino E, Bergero D, Forte C, et al. A high-starch vs. high-fibre diet: effects on the gut environment of the different intestinal compartments of the horse digestive tract. *Vet Res*. (2022) 18:89. doi: 10.1186/s12917-022-03289-2

27. Clarke LL, Roberts MC, Argenzio RA. Feeding and digestive problems in horses. Physiologic responses to a concentrated meal. *Vet Clin North Am Equine Pract*. (1990) 6:433–50. doi: 10.1016/s0749-0739(17)30550-3

28. Raspa F, Valle E, Ozella L, Bergero D, Tarantola M, Necci A, et al. Horse welfare in semi-extensive system: establishing a welfare protocol and comparing pasture and stable farming systems. *Ital J Anim Sci*. (2024) 23:1057–68. doi: 10.1080/1828051X.2024.2382271

29. Ralston SL. Hyperglycemia/hyperinsulinemia after feeding a meal of grain to young horses with osteochondritis dissecans (OCD) lesions. *Pferdeheilkunde*. (1996) 12:320–2. doi: 10.21836/PEM19960332

30. Geelen SN, Jansen WL, Geelen MJ, Sloet van Oldruitenborgh-Oosterbaan MM, Beynen AC. Lipid metabolism in equines fed a fat-rich diet. *Int J Vitam Nutr Res*. (2000) 70:148–52. doi: 10.1024/0300-9831.70.3.148

31. Williams T, Rude B, Liao S, Mochal-King C, Nicodemus M. Effects of fat supplementation on plasma glucose, insulin and fatty acid analysis in ponies maintained on a forage-based diet. *J Anim Physiol Anim Nutr*. (2018) 102:1069–76. doi: 10.1111/jpn.12905

32. Piccione G, Arfuso F, Fazio F, Bazzano M, Giannetto C. Serum lipid modification related to exercise and polyunsaturated fatty acid supplementation in jumpers and thoroughbred horses. *J Equine Vet Sci*. (2014) 34:1181–7. doi: 10.1016/j.jevs.2014.07.005

33. Williams T, Rude B, Liao S, Mochal-King C, Nicodemus M. Effects of feeding fat on nutrient digestion in cannulated ponies fed a forage diet. *Anim Husb Dairy Vet Sci*. (2017) 1:116. doi: 10.15761/AHDVS.1000116

34. Cavallarin L, Giribaldi M, Soto-Del Rio M, De Los D, Valle E, Barbarino G, et al. A survey on the milk chemical and microbiological quality in dairy donkey farms located in North Western Italy. *Food Control*. (2015) 50:230–5. doi: 10.1016/j.foodcont.2014.08.019

35. Papademas P, Mousikos P, Aspri M. Valorization of donkey milk: technology, functionality, and future prospects. *JDS Commun*. (2022) 3:228–33. doi: 10.3168/jdsc.2021-0175

36. Monti G, Bertino E, Muratore MC, Coscia A, Cresi F, Silvestro L, et al. Efficacy of donkey's milk in treating highly problematic cow's milk allergic children: an in vivo and in vitro study. *Pediatr Allergy Immunol*. (2007) 18:258–64. doi: 10.1111/j.1399-3038.2007.00521.x

37. Martini M, Altomonte I, Licitra R, Salari F. Nutritional and nutraceutical quality of donkey milk. *J Equine Vet Sci*. (2018) 65:33–7. doi: 10.1016/j.jevs.2017.10.020

38. Bragaglio A, Romano E, Cutini M, Nannoni E, Mota-Rojas D, Claps S, et al. Study on the suitability of life cycle assessment for the estimation of donkey milk environmental impact. *Animal*. (2024) 18:101057. doi: 10.1016/j.animal.2023.101057

39. De Berardinis A, Bucci R, De Amicis I, Del Signore F, Parrillo S, Massirio I, et al. Phenotypic characterization of the Martina Franca donkey: an endangered Italian donkey breed. *Animals*. (2024) 14:1950. doi: 10.3390/ani14131950

40. Banca Dati Nazionale (BDN). Anagrafe Zootecnica. Metadata. (2022). Available online at: https://www.vetinfo.it (Accessed August 15, 2024).

41. Greppi M, Bordin C, Raspa F, Maccone E, Harris P, Ellis AD, et al. Feeding behaviour related to different feeding devices. *J Anim Physiol Anim Nutr*. (2024) 108:1393–404. doi: 10.1111/jpn.13977

42. Nutrient requirements of horses. *Sixth revised* ed. Washington, DC: National Academies Press (2007).

43. Spadari A, Gialletti R, Gandini M, Valle E, Cerullo A, Cavallini D, et al. Short-term survival and postoperative complications rates in horses undergoing colic surgery: a multicentre study. *Animals*. (2023) 13:1107. doi: 10.3390/ani13061107

44. Raspa F, Chessa S, Bergero D, Sacchi P, Ferrocino I, Cocolin L, et al. Microbiota characterization throughout the digestive tract of horses fed a high-fiber vs. a high-starch diet. *Front Vet Sci*. (2024) 11:1386135. doi: 10.3389/fvets.2024.1386135

45. Felini R, Cavallini D, Buonaiuto G, Bordin T. Assessing the impact of thermoregulatory mineral supplementation on thermal comfort in lactating Holstein cows. *Vet Anim Sci*. (2024) 24:100363. doi: 10.1016/j.vas.2024.100363

46. Koakoski DL, Bordin T, Cavallini D, Buonaiuto G. A preliminary study of the effects of gaseous ozone on the microbiological and chemical characteristics of whole-plant corn silage. *Fermentation*. (2024) 10:398. doi: 10.3390/fermentation10080398

47. Bucci R, De Amicis I, Parrillo S, Robbe D, Carluccio A. Evaluation of testicular volume and correlation with sperm production in Martina Franca donkeys: a parameter to consider when approving breeding jacks. *Animals*. (2023) 13:3619. doi: 10.3390/ani13233619

48. Contri A, De Amicis I, Veronesi MC, Faustini M, Robbe D, Carluccio A. Efficiency of different extenders on cooled semen collected during long and short day length seasons in Martina Franca donkey. *Anim Reprod Sci*. (2010) 120:136–41. doi: 10.1016/j.anireprosci.2010.02.018

49. Folch J, Lees M, Stanley GHS. A simple method for the isolation and purification of total lipides from animal tissues. *J Biol Chem*. (1957) 226:497–509. doi: 10.1016/S0021-9258(18)64849-5

50. Prasinou P, Crisi PE, Chatgilialoglu C, Di Tommaso M, Sansone A, Gramenzi A, et al. The erythrocyte membrane lipidome of healthy dogs: creating a benchmark of fatty acid distribution and interval values. *Front Vet Sci*. (2020) 7:502. doi: 10.3389/fvets.2020.00502

51. Fuchs B, Süß R, Teuber K, Eibisch M, Schiller J. Lipid analysis by thin-layer chromatography—a review of the current state. *J Chromatogr A*. (2011) 1218:2754–74. doi: 10.1016/j.chroma.2010.11.066

52. Prasinou P, De Amicis I, Fusaro I, Bucci R, Cavallini D, Parrillo S, et al. The lipidomics of spermatozoa and red blood cells membrane profile of Martina Franca donkey: preliminary evaluation. *Animals*. (2023) 13:8. doi: 10.3390/ani13010008

53. Ferlizza E, Fasoli S, Cavallini D, Bolcato M, Andreani G, Isani G. Preliminary study on urine chemistry and protein profile in cows and heifers. *Pak Vet J*. (2020) 40:413–8. doi: 10.29261/pakvetj/2020.067

54. Dini FM, Jacinto JGP, Cavallini D, Beltrame A, Del Re FS, Abram L, et al. Observational longitudinal study on *toxoplasma gondii* infection in fattening beef cattle: serology and associated haematological findings. *Parasitol Res*. (2024) 123:169. doi: 10.1007/s00436-024-08189-y

55. Raspa F, Schiavone A, Pattono D, Galaverna D, Cavallini D, Vinassa M, et al. Pet feeding habits and the microbiological contamination of dog food bowls: effect of feed type, cleaning method and bowl material. *BMC Vet Res*. (2023) 19:261. doi: 10.1186/s12917-023-03823-w

56. Bordin C, Raspa F, Greppi M, Harris P, Ellis AD, Roggero A, et al. Pony feeding management: the role of morphology and hay feeding methods on intake rate, ingestive behaviors and mouth shaping. *Front Vet Sci*. (2024) 11:1332207. doi: 10.3389/fvets.2024.1332207

57. Buonaiuto G, Visentin G, Costa A, Niero G, Degano L, Cavallini D, et al. The effect of first-lactation calving season, milk production, and morphology on the survival of Simmental cows. *Animal*. (2024) 18:101128. doi: 10.1016/j.animal.2024.101128

58. Nassan FL, Chavarro JE, Tanrikut C. Diet and men's fertility: does diet affect sperm quality? *Fertil Steril*. (2018) 110:570–7. doi: 10.1016/j.fertnstert.2018.05.025

59. Castellini C, Mattioli S, Signorini C, Cotozzolo E, Noto D, Moretti E, et al. Effect of dietary n-3 source on rabbit male reproduction. *Oxidative Med Cell Longev*. (2019) 2019:3279670. doi: 10.1155/2019/3279670

60. Skoracka K, Eder P, Łykowska-Szuber L, Dobrowolska A, Krela-Kaźmierczak I. Diet and nutritional factors in male (in)fertility—underestimated factors. *J Clin Med Res*. (2020) 9:1400. doi: 10.3390/jcm9051400

61. Mattioli S, Angelucci E, Dal Bosco A, Signorini C, Sylla L, Bosa L, et al. Pro-atherogenic and pro-oxidant diets influence semen and blood traits of rabbit bucks. *Antioxidants*. (2023) 12:1880. doi: 10.3390/antiox12101880

62. Yuan C, Wang J, Lu W. Regulation of semen quality by fatty acids in diets, extender, and semen. *Front Vet Sci*. (2023) 10:1119153. doi: 10.3389/fvets.2023.1119153

63. Collodel G, Castellini C, Lee JC-Y, Signorini C. Relevance of fatty acids to sperm maturation and quality. *Oxidative Med Cell Longev*. (2020) 2020:7038124. doi: 10.1155/2020/7038124

64. Strzezek J, Fraser L, Kuklińska M, Dziekońska A, Lecewicz M. Effects of dietary supplementation with polyunsaturated fatty acids and antioxidants on biochemical characteristics of boar semen. *Reprod Biol*. (2004) 4:271–87.

65. Kiernan M, Fahey AG, Fair S. The effect of the in vitro supplementation of exogenous long-chain fatty acids on bovine sperm cell function. *Reprod Fertil Dev*. (2013) 25:947–54. doi: 10.1071/RD12204

66. Huang A, Isobe N, Obitsu T, Yoshimura Y. Expression of lipases and lipid receptors in sperm storage tubules and possible role of fatty acids in sperm survival in the hen oviduct. *Theriogenology*. (2016) 85:1334–42. doi: 10.1016/j.theriogenology.2015.12.020

67. Crean AJ, Senior AM. High-fat diets reduce male reproductive success in animal models: a systematic review and meta-analysis. *Obes Rev*. (2019) 20:921–33. doi: 10.1111/obr.12827

68. Kujoana TC, Mabelebele M, Sebola NA. Role of dietary fats in reproductive, health, and nutritional benefits in farm animals: a review. *Open Agric*. (2024) 9:244. doi: 10.1515/opag-2022-0244

69. Merino O, Sánchez R, Gregorio MB, Sampaio F, Risopatrón J. Effect of high-fat and vitamin D deficient diet on rat sperm quality and fertility. *Theriogenology*. (2019) 125:6–11. doi: 10.1016/j.theriogenology.2018.09.030

70. Torres-Arce E, Vizmanos B, Babio N, Márquez-Sandoval F, Salas-Huetos A. Dietary antioxidants in the treatment of male infertility: counteracting oxidative stress. *Biology*. (2021) 10:241. doi: 10.3390/biology10030241

71. Pellegrino FJ, Corrada Y, Picco SJ, Relling AE, Risso A. Association between dietary polyunsaturated fatty acids and their concentration in blood plasma, red blood cell, and semen of dogs. *Open Vet J*. (2023) 13:348–51. doi: 10.5455/OVJ.2023.v13.i3.11

72. Bazzano M, Laus F, Spaterna A, Marchegiani A. Use of nutraceuticals in the stallion: effects on semen quality and preservation. *Reprod Domest Anim*. (2021) 56:951–7. doi: 10.1111/rda.13934

73. Wolkmer P, Stumm AMG, Borges LFK, Ferreira EPT, Favaretto B, Siqueira LC. Plasma lipid peroxidation as a marker for seminal oxidative stress in stallion. *J Agric Sci*. (2019) 11:p401. doi: 10.5539/jas.v11n6p401

74. Speake BK, Surai PK, Rooke JA, Vriese SD, Christophe AB. Regulation of avian and mammalian sperm production by dietary fatty acids. In: SR De Vriese and AB Christophe, editors. *Male Fertility and Lipid Metabolism*. Champaign: AOCS Press. (2003):96–117.

75. Wathes DC, Abayasekara DRE, Aitken RJ. Polyunsaturated fatty acids in male and female reproduction 1. *Biol Reprod*. (2007) 77:190–201. doi: 10.1095/biolreprod.107.060558

76. Rodrigues PG, de Moura RS, Rocha LGP, Bottino MP, Nichi M, Maculan R, et al. Dietary polyunsaturated fatty acid supplementation improves the quality of stallion cryopreserved semen. *J Equine Vet Sci*. (2017) 54:18–23. doi: 10.1016/j.jevs.2016.08.007

77. Díaz Rojas E, Carrillo Moreno DI, Contreras Villarreal V, Arellano Rodríguez F, Alvarado Espino AS, Ángel GO. Effect of nutraceutical supplementation on semen quality in stallions. *Vet Med Sci*. (2023) 9:2600–5. doi: 10.1002/vms3.1289

78. Carluccio A, Contri A, Amendola S, De Angelis E, De Amicis I, Mazzatenta A. Male isolation: a behavioral representation of the pheromonal "female effect" in donkey (*Equus asinus*). *Physiol Behav*. (2013) 118:1–7. doi: 10.1016/j.physbeh.2013.04.005

79. Estienne MJ, Harper AF, Crawford RJ. Dietary supplementation with a source of omega-3 fatty acids increases sperm number and the duration of ejaculation in boars. *Theriogenology*. (2008) 70:70–6. doi: 10.1016/j.theriogenology.2008.02.007

80. Fair S, Doyle DN, Diskin MG, Hennessy AA, Kenny DA. The effect of dietary n-3 polyunsaturated fatty acids supplementation of rams on semen quality and subsequent quality of liquid stored semen. *Theriogenology*. (2014) 81:210–9. doi: 10.1016/j.theriogenology.2013.09.002

81. Blesbois E, Lessire M, Grasseau I, Hallouis JM, Hermier D. Effect of dietary fat on the fatty acid composition and fertilizing ability of fowl semen. *Biol Reprod*. (1997) 56:1216–20. doi: 10.1095/biolreprod56.5.1216

82. Attaman JA, Toth TL, Furtado J, Campos H, Hauser R, JorgeE C. Dietary fat and semen quality among men attending a fertility clinic. *Hum Reprod*. (2012) 27:1466–74. doi: 10.1093/humrep/des065

83. Esmaeili V, Shahverdi AH, Moghadasian MH, Alizadeh AR. Dietary fatty acids affect semen quality: a review. *Andrology*. (2015) 3:450–61. doi: 10.1111/andr.12024

84. Aydin R, Cook ME. The effect of dietary conjugated linoleic acid on egg yolk fatty acids and hatchability in Japanese quail. *Poult Sci*. (2004) 83:2016–22. doi: 10.1093/ps/83.12.2016

85. Safari Asl R, Shariatmadari F, Sharafi M, Karimi Torshizi MA, Shahverdi A. Improvements in semen quality, sperm fatty acids, and reproductive performance in aged Ross breeder roosters fed a diet supplemented with a moderate ratio of n-3: n-6 fatty acids. *Poult Sci*. (2018) 97:4113–21. doi: 10.3382/ps/pey278

86. Agradi S, Sulce M, Menchetti L, Vigo D, Castrica M, Barbato O, et al. Dietary supplementation with n-3 polyunsaturated fatty acids: effects on reproductive and productive performance and meat quality in rabbit breeding. *Animal Nutr*. (2023) 14:70–8. doi: 10.1016/j.aninu.2023.03.009

87. Patricio A, Cruz DF, Silva JV, Padrão A, Correia BR, Korrodi-Gregório L, et al. Relation between seminal quality and oxidative balance in sperm cells. *Acta Urol Portuguesa*. (2016) 33:6–15. doi: 10.1016/j.acup.2015.10.001

88. Brinsko SP, Varner DD, Love CC, Blanchard TL, Day BC, Wilson ME. Effect of feeding a DHA-enriched nutriceutical on the quality of fresh, cooled and frozen stallion semen. *Theriogenology*. (2005) 63:1519–27. doi: 10.1016/j.theriogenology.2004.07.010

89. Elhordoy DM, Cazales N, Costa G, Estévez J. Effect of dietary supplementation with DHA on the quality of fresh, cooled and frozen stallion semen. *Anim Reprod Sci*. (2008) 107:319. doi: 10.1016/j.anireprosci.2008.05.096

90. Silva PFN, Gadella BM. Detection of damage in mammalian sperm cells. *Theriogenology*. (2006) 65:958–78. doi: 10.1016/j.theriogenology.2005.09.010

91. Díaz R, Torres MA, Bravo S, Sanchez R, Sepúlveda N. Determination of fatty acid profile in ram spermatozoa and seminal plasma. *Andrologia*. (2016) 48:723–6. doi: 10.1111/and.12506

92. Van Tran L, Malla BA, Kumar S, Tyagi AK. Polyunsaturated fatty acids in male ruminant reproduction — a review. *Asian Australas J Anim Sci*. (2017) 30:622–37. doi: 10.5713/ajas.15.1034

93. Khoshvaght A, Towhidi A, Zare-shahneh A, Noruozi M, Zhandi M, Dadashpour Davachi N, et al. Dietary n-3 PUFAs improve fresh and post-thaw semen quality in Holstein bulls via alteration of sperm fatty acid composition. *Theriogenology*. (2016) 85:807–12. doi: 10.1016/j.theriogenology.2015.10.023

94. Harris MA, Baumgard LH, Arns MJ, Webel SK. Stallion spermatozoa membrane phospholipid dynamics following dietary n-3 supplementation. *Anim Reprod Sci*. (2005) 89:234–7.

95. Shah SMH, Ali S, Zubair M, Jamil H, Ahmad N. Effect of supplementation of feed with flaxseed (*Linum usitatissimum*) oil on libido and semen quality of Nilli-Ravi buffalo bulls. *J Anim Sci Technol*. (2016) 58:25. doi: 10.1186/s40781-016-0107-3

96. Nissen HP, Kreysel HW. Polyunsaturated fatty acids in relation to sperm motility. *Andrologia*. (1983) 15:264–9. doi: 10.1111/j.1439-0272.1983.tb00374.x

97. Zalata AA, Christophe AB, Depuydt CE, Schoonjans F, Comhaire FH. The fatty acid composition of phospholipids of spermatozoa from infertile patients. *Mol Hum Reprod*. (1998) 4:111–8. doi: 10.1093/molehr/4.2.111

98. Safarinejad MR, Hosseini SY, Dadkhah F, Asgari MA. Relationship of omega-3 and omega-6 fatty acids with semen characteristics, and anti-oxidant status of seminal plasma: a comparison between fertile and infertile men. *Clin Nutr*. (2010) 29:100–5. doi: 10.1016/j.clnu.2009.07.008

99. Connor WE, Lin DS, Wolf DP, Alexander M. Uneven distribution of desmosterol and docosahexaenoic acid in the heads and tails of monkey sperm. *J Lipid Res*. (1998) 39:1404–11. doi: 10.1016/s0022-2275(20)32521-9

100. Liu Q, Zhou Y-F, Duan R-J, Wei H-K, Peng J, Jiang S-W. Dietary n-6: n-3 ratio and vitamin E improve motility characteristics in association with membrane properties of boar spermatozoa. *Asian J Androl*. (2017) 19:223. doi: 10.4103/1008-682X.17044

# Frontiers in Veterinary Science

**Transforms how we investigate and improve animal health**

The third most-cited veterinary science journal, bridging animal and human health with a comparative approach to medical challenges. It explores innovative biotechnology and therapy for improved health outcomes.

---

## Discover the latest Research Topics

See more →

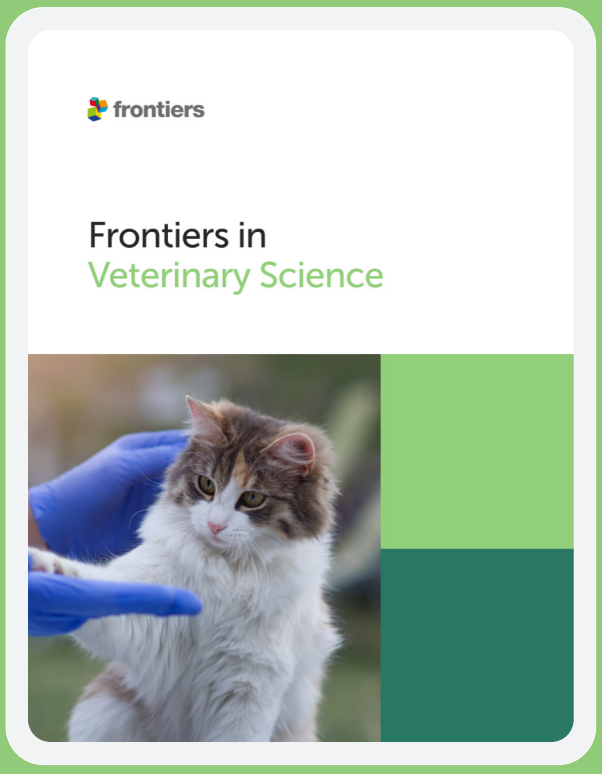


**Frontiers**

Avenue du Tribunal-Fédéral 34
1005 Lausanne, Switzerland
frontiersin.org

**Contact us**

+41 (0)21 510 17 00
frontiersin.org/about/contact